MINISTRY OF ENERGY AND MINES

www.empr.gov.bc.ca/geology

GEOLOGICAL FIELDWORK 2011

A SUMMARY OF FIELD ACTIVITIES AND CURRENT RESEARCH

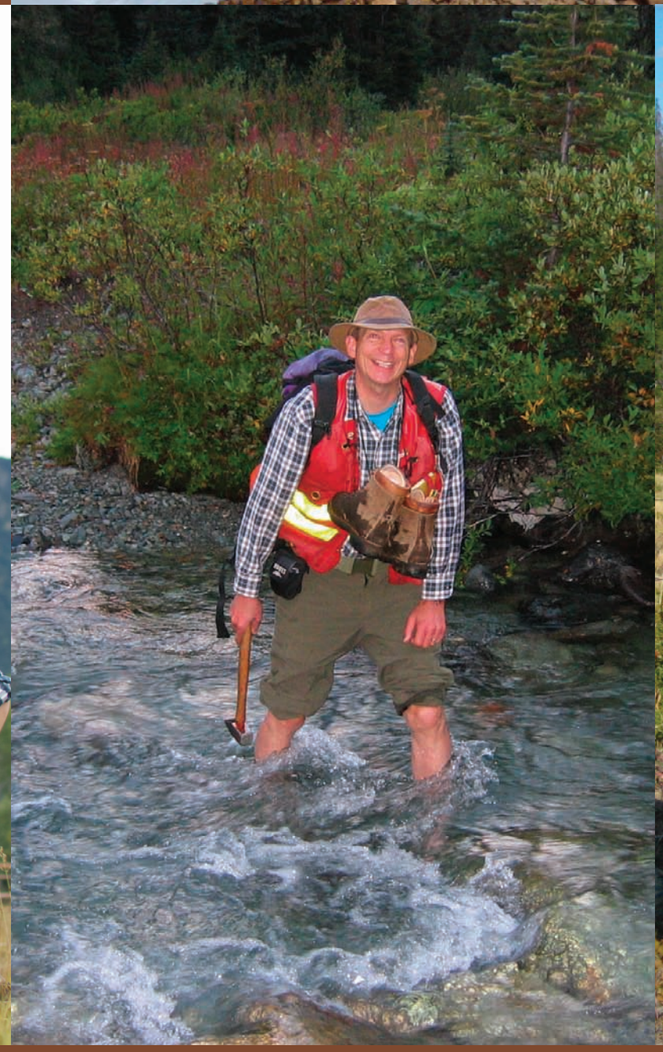

Paper 2012-1

GEOLOGICAL FIELDWORK 2011

A Summary of Field Activities and Current Research

Ministry of Energy and Mines
British Columbia Geological Survey

Paper 2012-1

Ministry of Energy and Mines
Mines and Mineral Resources Division
British Columbia Geological Survey

Parts of this publication may be quoted or reproduced if source and authorship are acknowledged.
The following is the recommended format for referencing individual works contained in this publication:

Nelson, J.L., Diakow, L.J., Mahoney, J.B., van Staal, C., Pecha, M., Angen, J.J., Gehrels, G. and Lau, T. (2012): North Coast Project: Tectonics and Metallogeny of the Alexander Terrane, and Cretaceous Sinistral Shearing of the Western Coast Belt ; *in* Geological Fieldwork 2011, *BC Ministry of Energy and Mines*, Paper 2012-1, pages 157-180.

COVER PHOTO: *Left – Dave Lefebure (retiring Chief Geologist) crossing creek in the Johanson Lake area*

Right – Steve Rowins (new Chief Geologist) in the Merritt gold camp with Charlie Blackburn

BACK PHOTO: *Jim Logan's Dease Lake mapping crew*

This publication is also available, free of charge, as colour digital files, in Adobe Acrobat® PDF format, from the BC Ministry of Energy and Mines website at:

http://www.empr.gov.bc.ca/Mining/Geoscience/PublicationsCatalogue/Fieldwork

British Columbia Cataloguing in Publication Data

Main entry under title:

Geological Fieldwork: - 1974 -

Annual.

Issuing body varies

Vols. For 1978-1996 issued in series: Paper / British Columbia. Ministry of Energy, Mines and Petroleum Resources; vols for 1997-1998, Paper / British Columbia. Ministry of Employment and Investment; vols for 1999-2004, Paper / British Columbia Ministry of Energy and Mines; vols for 2005- , Paper / British Columbia Ministry of Energy, Mines and Petroleum Resources.

Includes Bibliographical references.

ISSN 0381-243X=Geological Fieldwork

1. Geology - British Columbia - Periodicals. 2. Mines and mineral resources - British Columbia - Periodicals. 3. Geology - Fieldwork - Periodicals. 4. Geology, Economic - British Columbia - Periodicals. 5. British Columbia. Geological Survey Branch - Periodicals. I. British Columbia. Geological Division. II. British Columbia. Geological Survey Branch. III. British Columbia. Geological Survey Branch. IV. British Columbia. Dept. of Mines and Petroleum Resources. V. British Columbia. Ministry of Energy, Mines and Petroleum Resources. VI. British Columbia. Ministry of Employment and Investment. VII. British Columbia Ministry of Energy and Mines. VIII. Series: Paper (British Columbia. Ministry of Energy, Mines and Petroleum Resources). IX. Series: Paper (British Columbia. Ministry of Employment and Investment). X. Series: Paper (British Columbia Ministry of Energy and Mines). XI. Series: Paper (British Columbia Ministry of Energy, Mines and Petroleum Resources).

QE187.46 622.1'09711 C76-083084-3 (Rev.)

VICTORIA
BRITISH COLUMBIA
CANADA

JANUARY 2012

TABLE OF CONTENTS

FOREWORD

Geological Fieldwork 2011

This is the thirty-seventh edition of **Geological Fieldwork**, a volume of high quality peer-reviewed technical papers that presents the results of field surveys and geoscience research conducted by the **British Columbia Geological Survey** (BCGS) in 2011. Collectively, these papers demonstrate the breadth of staff expertise and our many research partners highlight the organization's collaborative nature. The release of new geoscience data about British Columbia is a key activity of the BCGS and it leads to mineral tenure acquisition and increased mineral exploration activity in the Province. This activity, in turn, directly aids in the discovery of new mines that provide significant economic benefits to all British Columbians. Most articles are contributions by Survey staff to the understanding of the geology, geochemistry, and mineral deposits of the Province. The volume also includes several contributions from other professional geoscientists that contain new data of interest to the exploration community.

Early in 2011, the government of British Columbia reorganized the natural resource sector ministries again and the BCGS moved to the expanded Ministry of Energy and Mines (MEM) from the Ministry of Forests, Mines and Lands (MFML). This latter Ministry was merged with the Ministry of Natural Resource Operations (MNRO) to become the Ministry of Forests, Lands and Natural Resource Operations (MFLNRO). The BCGS also underwent several staff changes in 2011 including the retirement of Dr. David Lefebure as Chief Geologist after many years of dedicated service. He was replaced by Dr. Stephen Rowins, who joined the BCGS in 2009 as the Director of Cordilleran Geoscience.

British Columbia Geological Survey Successes

- The BCGS, in partnership with Geoscience BC, undertook a major bedrock mapping and mineral assessment project in the Dease Lake area. The project is part of the larger QUEST-Northwest initiative, a program launched by Geoscience BC in early 2011 to stimulate mineral exploration along the Highway 37 corridor.
- A series of five new 1:50 000 scale geoscience maps covering northern Vancouver Island were released.
- Release of the entire Regional Geochemical Survey (RGS) database of 61 425 samples as Geofile 2011-7.
- The third season of the North Coast Edges project, jointly delivered with the Geological Survey of Canada (GSC), focused on regional-scale mapping along the Grenville Channel between Porcher Island and Klemtu.
- The third year of the Iskut River Edges project followed up on previous summer programs with mapping in the Hoodoo Mountain area north of the Rock and Roll volcanogenic massive sulphide deposit.
- The second year of the Kutcho Creek project, a two-year partnership with the GSC and Kutcho Mining Corp. focused on mapping the western portion of the Kutcho assemblage.
- A multi-year province-wide study of specialty (rare) metals continued under the renewed Targeted Geoscience Initiative program (TGI-4) of the GSC.
- Started a TGI-4 project in collaboration with the GSC and the University of British Columbia targeting potential "orogenic" Ni-Cu-PGE systems in British Columbia.
- Our online interface MapPlace and its supporting site is used 24 hours a day, 7 days a week, by the global exploration community.
- The Property File database now features more than 31 100 documents online.
- MINIFLE continues to improve with 300 MINFILE occurrences updated and 100 new ones identified.
- Staff of the BC Mineral Development Office in Vancouver hosted international investor delegations and participated in the Asia Investment Mission to Hong Kong, China and India.
- Survey geologists were key presenters at conferences and workshops including Roundup, KEG, GACMAC, CIM, Goldschmidt, NWMA, Minerals South, Yukon Geoscience Forum, Minerals North, and the Smither's Rock Talk.

Stephen M. Rowins
Chief Geologist & Executive Director
British Columbia Geological Survey

British Columbia Geological Survey Activities in 2011

by S.M. Rowins[1], L. Jones[1] and B. Madu[1]

INTRODUCTION

The British Columbia Geological Survey (BCGS) had another busy and productive year in 2011. It continued to play a leading role in the creation of a vibrant, safe, and sustainable mining industry in British Columbia by providing world-class geoscience expertise and data to government, industry, and the general public. These various groups use our expertise and data in different ways, but a common goal of all groups is to see the province position itself as a preferred destination for investment by the mineral exploration and mining industry. In the unpredictable world of today, the responsiveness of the BCGS to adapt to changing global market conditions (*i.e.* commodity scarcity) and government priorities is a clear advantage to the BC exploration and mining community. The variety of BCGS geoscience projects reported on in this volume highlights the organization's effort to deploy its people and resources in geoscience activities that deliver maximum return to the province. There are longer papers describing final results from multi-year field mapping programs, and shorter papers presenting preliminary results from projects initiated less than a year ago. A hallmark of the Survey is its ability to consistently deliver standardized high quality geological maps, geoscience reports, and online interactive geoscience databases in a very short timeframe. All geoscience products are made available online via MapPlace, the award-winning internet portal of the BCGS.

British Columbia's mineral exploration and mining industry continued to perform well and helped lead the economic recovery in BC. The total value of solid mineral production for 2010 was $7 billion and mineral exploration spending was $322 million, more than double the $154 million spent in 2009. It is anticipated that similar, if not stronger, numbers are expected for 2011. Nevertheless, core funding levels for the BCGS in 2011 were similar to those in 2010 and 2009. This resulted in the BCGS continuing to focus on creating new geoscience products in partnerships with universities, industry, and other public geoscience agencies. The BCGS continued its long collaboration with the Geological Survey of Canada (GSC) by participating in five joint field projects in 2011. Three field mapping projects were delivered as part of the GSC's Geo-mapping for Energy and Minerals (GEM) program. This was the third and final year of fieldwork these mapping projects. A four-year "specialty metals" project that started in 2010 under the auspices of the GSC's renewed Targeted Geoscience Initiative program (TGI-4) hit full stride in 2011. This specialty metals project is a national initiative with significant leadership provided by George Simandl of the BCGS. Its overall objective is to develop new exploration methodologies and technologies in the search for specialty metals. Specialty metals are important in the manufacturing of automobiles and many high-tech products such as cell phones and computers. Another, new, TGI-4 collaborative project between the BCGS and The University of British Columbia started over the summer and targeted Ni-Cu-PGE deposits associated with ultramafic intrusions in BC's orogenic belts. These "orogenic" Ni-Cu-PGE deposits are poorly understood and new models are needed.

Another important BCGS partnership included Geoscience BC (GBC). In 2011, the BCGS and GBC undertook a major collaborative bedrock mapping project in the Dease Lake area of northwestern BC. This area is highly prospective for porphyry Cu-Au, polymetallic skarn, epithermal Au, and orogenic (mesothermal) Au vein styles of mineralization. The project is part of the larger QUEST-Northwest initiative, a GBC program launched in early 2011 to stimulate mineral exploration in the northwestern part of the province along Highway 37. Finally, as in past years, university students were employed as co-op interns and geoscience assistants throughout the year. Their help with the delivery of our field programs and work on improving our digital geoscience databases is greatly appreciated.

BCGS FIELD ACTIVITIES

A main priority of the BCGS is to generate new geoscience data and products, including bedrock and surficial geology maps and targeted mineral deposit studies. The locations of the 2011 field projects are shown in Figure 1. Projects are typically chosen with the objective of helping to diversify local economies by attracting mineral exploration activity that may lead to the opening of new mines. In many parts of the province, mineral exploration and mining are essential drivers of

[1] *British Columbia Geological Survey, Victoria, BC*

This publication is also available, free of charge, as colour digital files in Adobe Acrobat® PDF format from the BC Ministry of Energy and Mines website at http://www.empr.gov.bc.ca/Mining/Geoscience/PublicationsCatalogue/Fieldwork.

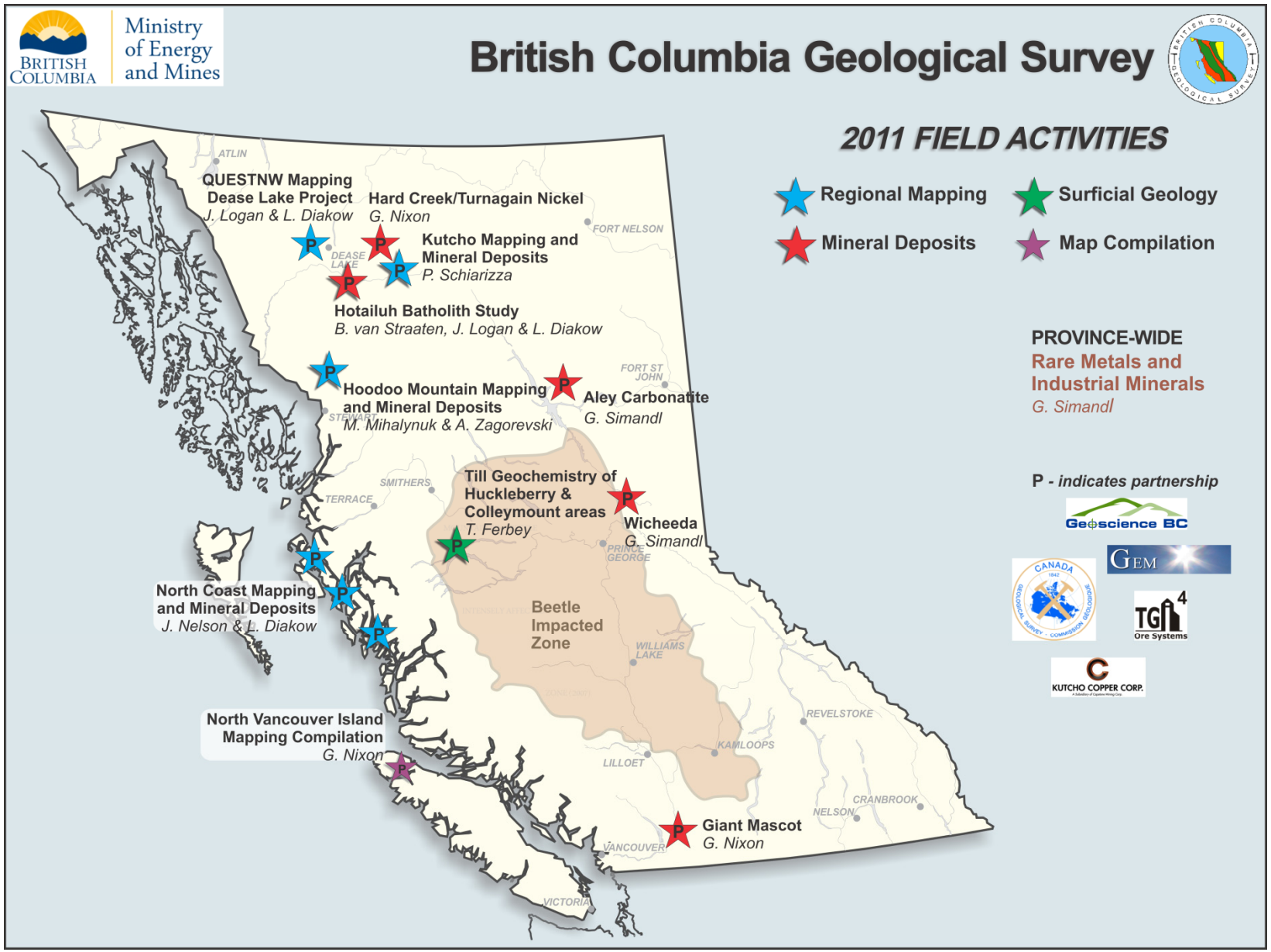

Figure 1. British Columbia Geological Survey 2011 field project areas.

local employment and tax revenue. These activities also directly support the development of regional infrastructure.

Multi-year field mapping studies (Figure 1) concluded in the North Coast (Nelson *et al.*, this volume; Angen *et al.*, this volume), the Hoodoo Mountain area north of the Iskut River (Mihalynuk *et al.*, this volume; Zagorevski *et al.*, this volume), and the Kutcho Creek area near the Kutcho Creek volcanogenic massive sulphide (VMS) deposit (Schiarizza, this volume). New field mapping projects started in the northwestern part of the province at Dease Lake (Logan *et al.*, this volume; Moynihan and Logan, this volume; Iverson *et al.*, this volume) and the Hotailuh batholith (van Straaten *et al.*, this volume). Several short trips by Graham Nixon to North Vancouver Island, which hosts the past-producing Island Copper mine, facilitated the release of five new 1:50 000 scale regional geology maps for that area.

In addition to these 2011 mapping projects, several other mineral deposit-related studies were undertaken. These include age determinations of potentially Cu (Mo) and Au prospective volcanic rocks near Ootsa Lake and Francois Lake in west-central BC (Ferbey and Diakow, this volume), new Mineral Deposit Profiles for sedimentary phosphate deposits (Simandl *et al.*, this volume) and carbonate-hosted, nonsulphide Zn (hypogene) deposits (Paradis and Simandl, this volume), and an investigation of metallic minerals in hand-panned black sands from creeks in the Atlin placer gold camp (Hora *et al.*, this volume). A study by Fajber and Simandl (this volume) evaluated the suitability of portable x-ray fluorescence (XRF) instruments for determining rare earth element (REE) abundances in sedimentary phosphate deposits. Finally, Soloviev (this volume) investigates the composition of granitic rocks - the Hellroaring Creek stock - associated with rare metal mineralization in southeastern BC.

Ongoing Projects

Edges – Modeling the Evolution of the Northern Cordillera Resource Environment from the Edges of Exotic Terranes

Edges is a highly focused multi-year geological mapping initiative involving formal collaboration between the Government of Canada, the Province of British Columbia, the Yukon Territory, Geoscience BC, the United States Geological Survey, and the Alaska Division of Geological and Geophysical Surveys. It began field operations in 2009 in British Columbia and will last until 2013. It is a key project in the Federal GEM program (Geoscience for Energy and Minerals). Support is being contributed by all participating agencies.

The ultimate goal of the initiative is to improve the effectiveness of resource exploration and discovery in the northern Cordillera by outlining resource-rich environments in British Columbia, the Yukon, and Alaska. The geological targets are the exotic outer terranes with their enclosed pre-accretionary syngenetic and epigenetic deposits and the metal-rich Triassic through Paleogene magmatic arcs and associated accretion zones that resulted from interaction of the terranes with the western margin of ancient North America. The target areas include parts of northern and central British Columbia where the geological map base is either several decades out of date or at insufficiently large scale to evaluate mineral potential using modern tectonic interpretations.

North Coast Partnership Project (Edges)

JoAnne Nelson and Larry Diakow, along with colleagues from the GSC, the University of Wisconsin at Eau Claire, the University of Arizona, and the University of Waterloo returned from a successful third field season mapping along the northern coastal region of BC (Figure 1). The first two years involved detailed mapping on and near Porcher Island in 2009 and near Klemtu in 2010. In this final field season, the focus was (1) to complete regional-scale geological coverage of the intervening area from Grenville Channel to northern Princess Royal Island, in order to update the provincial geological map for all of north coastal British Columbia, and (2) to address problems and questions arising from mapping and U-Pb isotopic results obtained from earlier fieldwork. A two-year sub-project was started by Joel Angen (his M.Sc. thesis) on the structural geology of Porcher Island. In 2011, the mapping team:

- Discovered new VMS showings on southern Kennedy Island (Figure 2).
- Collected sulphide samples for Pb isotopic analysis from the Pitt showing on Pitt Island. This is the only previously documented VMS occurrence in the southern Alexander terrane of BC.
- Documented and sampled a previously unrecognized late Paleozoic volcano-sedimentary unit east of the northern Grenville and Telegraph channels.
- Traced out the Grenville Channel fault for 300 km along strike.
- Investigated a Caledonian-age deformational event that probably marked the amalgamation of pericratonic and primitive arc elements within the composite Alexander terrane.

Iskut River Partnership Project (Edges)

Mitch Mihalynuk and Alex Zagorevski of the GSC returned to the Coast Belt of northwest BC and mapped the Hoodoo Mountain area immediately north of the Iskut River and the Rock and Roll VMS deposit. This was the third field season of an Edges partnership between the GSC and the BCGS. The Hoodoo Mountain area is located between the Galore Creek porphyry copper-gold

Figure 2. Cees van Staal (GSC) trying to remove the "Hard Case" showing he discovered on Kennedy Island.

deposit and the past-producing gold deposits of the Bronson Camp. Mapping in 2010 lead to the discovery of numerous copper-gold occurrences with similarities to the porphyry-style mineralization at Galore Creek (Figure 1). New mapping in 2011 extended the geological relationships, established in 2010, to the west. Project highlights include the recognition that the axis of the magmatic arc responsible for the Late Triassic and Early Jurassic strata lies in the eastern map sheet 104B/14E. Another finding was that north-trending regional folds may affect the Verrett-Iskut fault and, importantly, the location of the potentially offset host-rocks for the Rock and Roll VMS deposit. The project team also analyzed a large suite of Mississippian to Pliensbachian volcanic and hypabyssal rocks to test the usefulness of whole-rock geochemistry to discriminate petrographically similar rock sequences in the Hoodoo Mountain area.

Kutcho Partnership Project (Edges)

The Kutcho project is a two-year bedrock mapping program initiated by the BCGS in 2010 in partnership with the Geological Survey of Canada (Edges project) and Kutcho Mining Corp. (formerly Capstone Mining Corporation). The aim of this project, lead by Paul Schiarizza, is to gain a better understanding of, and provide more detailed geological maps for, the Permo-Triassic Kutcho assemblage, which hosts the Kutcho Creek volcanogenic massive sulphide deposit (Figure 1). In 2011, another 200 square kilometres of the Kutcho assemblage was mapped. Only a few minor base metal occurrences are currently known in the Kutcho district, but newly identified zones of pyritic quartz-sericite schist indicate that parts of the map area have potential for future base metal discoveries.

North Vancouver Island Regional Mapping Project

A series of five new 1:50 000 scale geoscience maps covering northern Vancouver Island were released by Graham Nixon and colleagues in 2011 (Figure 1). Several field trips to northern Vancouver Island in 2011 permitted final touches to be made to the maps prior to their release. North Vancouver Island is prospective for porphyry, skarn, and epithermal styles of mineralization and hosts the past-producing Island Copper mine. Together, these five maps provide a revised Early Mesozoic stratigraphic framework and Mesozoic-Tertiary plutonic history for southern Wrangellia (Figure 3).

Specialty Metals TGI-4 Partnership Project

The BCGS and GSC began collaborating on a multi-year province-wide study of specialty or rare metals in 2010. The term "specialty metals" refers mainly to uncommon, nonferrous metals used in small quantities, typically <150 000 tonnes/year, or derived from geographically restricted areas. The Specialty Metals TGI-4 Program is studying ore deposits in terms of geological setting, mineralizing processes, applied mineralogy, exploration methods, and metallurgical constraints. The results will address some of the major knowledge gaps related to these deposits and are expected to help the Canadian mining industry tap domestic sources of rare metals. George Simandl of the BCGS is leading the BC component of the Specialty Metals TGI-4 program. In 2011, his team conducted a series of field examinations of various specialty metal properties throughout BC (Figure 1). The results were released in numerous publications and presented at conferences in Canada and overseas. A study by Robert Fajber and George Simandl on the effectiveness of portable hand-held x-ray fluorescence (XRF) analyzers in measuring lanthanides and Y concentrations in sedimentary phosphate deposits will be of particular interest to the mineral exploration industry.

Major New Projects

Dease Lake Mapping Project (QUEST-Northwest)

The BCGS's Dease Lake Mapping Project is part of GBC's larger QUEST-Northwest initiative, a program launched in 2011 to stimulate exploration in the northwestern part of the province along Highway 37

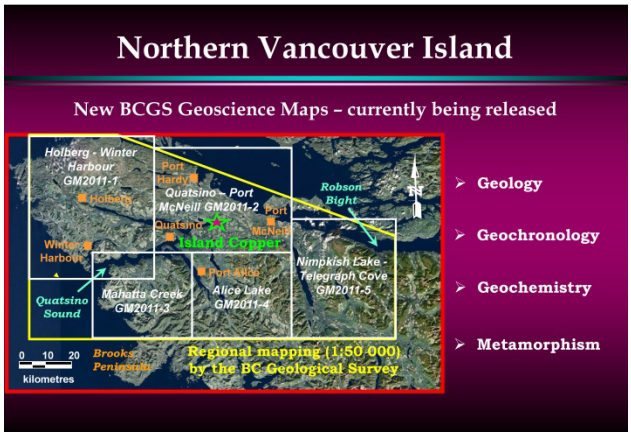

Figure 3. Series of five newly released 1:50 000 scale geoscience maps covering northern Vancouver Island.

(Figure 1). The Dease Lake area is highly prospective and proximal to the large porphyry Cu-Au deposits at Red Chris and Schaft Creek. Geoscience BC has committed $3.25 million in funding for high resolution airborne magnetic surveys, the collection of new regional stream sediment data, reanalysis of stream sediment samples, and the regional bedrock mapping done by the BCGS. The BCGS bedrock mapping program is complementary to the regional geophysical and geochemistry programs directly administered by GBC. Collectively, these programs will provide detailed, high quality geoscience data to aid mineral exploration in this highly prospective part of the province.

The Dease Lake Mapping project is lead by Jim Logan and Larry Diakow of the BCGS. Bram van Straaten and David Moynihan were Senior Geoscience Associates and selectively mapped and evaluated the mineral potential of the Hotailuh batholith and Snow Peak pluton, respectively. A group of enthusiastic summer students served as Geoscience Assistants on the project (Figure 4). Four field-based studies were completed within a 70 km radius of the community of Dease Lake. Collectively, these studies make up the Dease Lake Mapping Project. They include:

1. Dease Lake regional bedrock mapping conducted by Jim Logan, Larry Diakow, and David Moynihan;
2. Geological mapping and sampling of the Hotailuh batholith in order to understand its magmatic evolution and mineral potential. Bram van Straaten and a field assistant spent nine weeks visiting 331 field stations and collecting 134 samples for laboratory study and analysis. The 2011 study focused on mapping within the Gnat Pass area and seven smaller areas to the east. The field areas were chosen for their mineral occurrences and suitability for understanding the internal geology and external contact relationships for various phases of the batholith;
3. A focused study of the magmatic evolution and emplacement history of the Mo-bearing Snow Peak pluton. Preliminary results show that the Snow Peak pluton records Early Paleocene magmatism and associated Mo+/-Au and W mineralization that is about 10 Ma younger than other similar (?) plutons of the Surprise Lake Plutonic Suite of northern British Columbia and Yukon. This younger magmatic epoch may be the plutonic equivalent of the volcanic Carmacks Group exposed further to the north.
4. A study by Olivia Iverson and colleagues to establish the depositional environments, age, and lithogeochemical characteristics of the Late Triassic Tsaybahe and Stuhini group magmatic arc. New U-Pb detrital zircon data reveal that rocks previously assigned to the Triassic Stuhini Group are actually Middle Jurassic in age. They have been reassigned to the Hazelton Group. This implies that the Hotailuh thrust mapped in the present study area does not, in fact, exist.

Figure 4. Dease Lake field crew preparing traverse routes before helicopter set-outs.

Orogenic Ni-Cu-PGE TGI-4 Partnership Project

The BCGS (Graham Nixon), GSC (Doreen Ames), and the University of British Columbia (James Scoates) started the first year of a collaborative partnership examining the potential for "orogenic" Ni-Cu-PGE deposits associated with supra-subduction zone ultramafic-mafic intrusions exclusive of ophiolites and accreted large igneous provinces (*e.g.*, Wrangellia). The aim of the project is to establish mineral deposit models and exploration criteria for two poorly understood magmatic sulphide deposits in BC: (1) Giant Mascot – BC's only past-producing Ni mine (1958-74); and (2) the Turnagain Alaskan-type intrusion, which has a large resource of low-grade Ni and Co (Figure 1).

MAPPLACE AND DATABASE ACTIVITIES

MapPlace

Since 1995, the advanced web service of MapPlace has provided industry and government agencies with comprehensive tools and open geoscience data to aid in the discovery of mineral potential in BC. The mineral industry recognizes MapPlace as innovative and indispensable with unique and interactive web-based applications and tools to assist in decision-making for investment. MapPlace continues to provide clients with efficiencies in research time, data costs and analysis. Data themes and applications available on MapPlace include mineral potential, bedrock and surficial geology, publications, mineral and petroleum tenure, MINFILE, assessment reports, geochemistry, and geophysical surveys. Yao Cui and Pat Desjardins contributed geomatic expertise to MapPlace enhancements and the integration of servers. Major technical advances have taken place

since the inception of MapPlace 15 years ago, including growing databases, adding better servers, increasing bandwidth and using affordable advanced database software. Pat and co-op student Thomas Edgehill, while working with the next generation of Autodesk MapGuide®, are reviewing data modeling and architecture aspects to provide continued efficient delivery of data for the exploration community.

Property File, MINFILE, ARIS and RGS

During 2011, Property File, a collection of an estimated 98 000 unique industry documents and maps, continued to grow. As of December 2011, more than 31 100 Property File documents were available online, including 393 Falconbridge documents, 2710 Cyprus-Anvil documents, 330 Chevron documents, 618 Placer Dome documents, 2209 Rimfire documents, 2974 Mine Plans, more than 13 533 Library File items, and 7377 recently posted Tom Schroeter Project files. Another recent addition includes 879 RGS maps showing original locations of geochemical samples. Property File documents are retrieved through the search application (propertyfile.gov.bc.ca) or through links from MINFILE (minfile.ca). Kirk Hancock is the Property File contact and is currently accepting donations.

MINFILE contains geological, positional and economic information on more than 12 500 metallic, industrial mineral and coal mines, deposits and occurrences in BC. The BCGS has been allocated extra funding to update 2000 of the most critical records and add 400 new discoveries through the review of mineral assessment reports, recent publications, press releases and company websites. Sarah Meredith-Jones is the MINFILE contact and this year she approved the update of 300 occurrences and the addition of 100 new occurrences.

Users can now access more than 31 600 company mineral assessment reports using the online ARIS database. More than $1.8 billion of exploration expenditures has been recorded in assessment reports since 1947. In the past year, the value of expenditures on exploration programs reported was $86.3 million. The mining industry is encouraged to submit assessment reports in digital form to the Mineral Titles Branch. Benefits include higher quality line-work; more efficient digital reports; quicker approval; and lower costs for printing, mailing, storage, scanning and processing. During this year, 751 reports were submitted, of which 704 were approved. Of these, 616 or 85% were submitted digitally. This is up 65% from the previous year. Of these reports, 165 or 23% were sent back for amendments. Allan Wilcox and Ted Fuller work with clients to approve reports. The four most common reasons reports are returned are not enough detail in the cost statement, geochemical values were not plotted, full-scale geophysical maps were not included, and drillholes were submitted with missing cross sections and without proper scales.

Laura de Groot continues to manage 11 000 webpages and keeps staff on track with database management plans and needs. Website improvements include the addition of all new publications including 67 geological publications related to oil and gas activity and a listing of industrial minerals by commodity. The geosciences publications catalogue now has 4055 entries. CanGeoRef, a subscription-based bibliographic database of Canadian geoscience literature, was launched in September 2011. This database contains more than 200 000 entries from across the country, with gaps in grey literature having been filled for Alberta, Manitoba and Ontario. British Columbia is currently being updated.

The Regional Geochemical Survey (RGS) program covers roughly 75% of the province with stream sediment and stream water sampling at an average sample density of one sample per 13 km^2. Samples have been collected since the 1970s at a total estimated cost of $25 million. The most recent release of the entire RGS database of 61 425 samples was published as GeoFile 2011-7. The original hardcopy maps annotated with sample locations, labels and notes are an invaluable source for validating the positional accuracy of the sample locations and resolving issues of uncertainty in locations. Yao Cui managed the retrieval of the 900 original hardcopy NTS maps. Geoscience BC provided funding for the scanning to preserve this treasure of maps, which are now available as PDF documents through Property File. Yao would like to acknowledge assistance from Graham Green, Pat Desjardins and Wayne Jackaman for the retrieval of the maps, and Victoria Francis for quality assurance. Purple Rock Inc. indexed the collection, which was scanned by Camirage Imaging Services Inc.

During the past year, Kirk Hancock and Sarah Meredith-Jones provided mineral resource assessments of different areas of BC for the Ministry of Aboriginal Relations and Reconciliation to assist with treaty negotiations and other government business. Staff worked with the Mineral Policy and Regional Geology staff to develop economic and social assessments and exploration activity products.

BC's Digital Bedrock Geology Map: BCGeology Map

The province's digital geology map is essential for mineral exploration and assessing mineral potential. To facilitate the update and data integration of digital geological maps, Yao Cui continues the development of a Geology Operational Database Environment (GODE) to improve the efficiency of data maintenance and to enhance data quality. Certain components of GODE have already been completed, including the system architecture, data models, best practices, data quality assurance policies and rules, and some applications. The corporate spatial databases for GODE have been implemented in Microsoft® SQL Server 2008 (R2) to store source maps, archives and corporate resources. The spatial databases were also prototyped in

PostgreSQL/PostGIS. Upon completion, the GODE, together with Geology Application Database Environment (GADE), will result in all future provincial geological mapping products being available as online, digitally seamless geospatial databases. Pat Desjardins, Tian Han and students are working with Yao on this project.

The development of GODE has proven to be beneficial. One of the first results is a custom-built application for BCGS staff to retrieve styled TRIM topographic base maps stored in the corporate spatial database. When an area is selected in the province, with a single mouse click, up to hundreds of TRIM map sheets with typical topographic features can be retrieved in minutes, saving days of work to manually locate the TRIM maps on a file server, convert the GIS data format, transform the map projection, merge the map sheets and finally style the geographic features (Figure 5).

The development of GODE also helps to drive recent data quality-assurance work on the province-wide geological contact and fault line-work that has not been previously published. Two co-op students, Graham Green and Victoria Francis, contributed to the development and testing of data quality-assurance methodology, sequence-of-data processing and a test-run of recently compiled data quality rules for geological contacts and faults. The geological contact and fault line-work will become the base of future updates and to derive updated bedrock polygons.

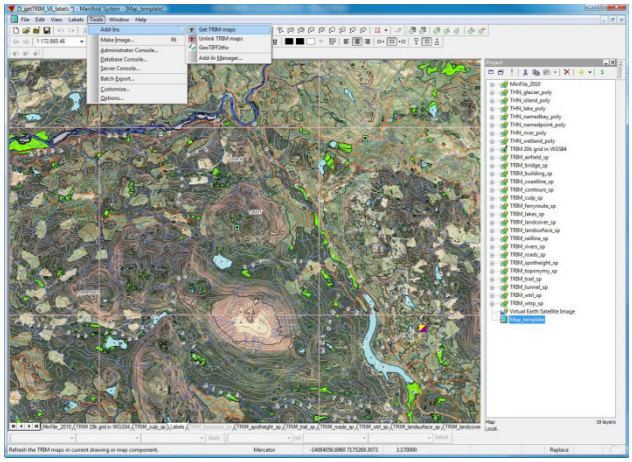

Figure 5: Instant access of styled TRIM topographic base maps (vector layers) and geoscience data stored in spatial databases.

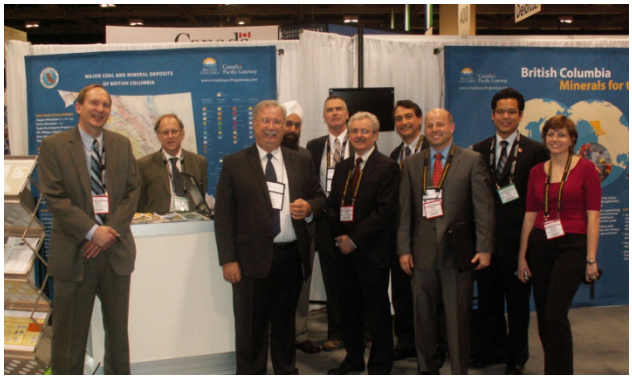

Figure 6. "Team BC" promoting the province's mineral resources to the world at the PDAC in Toronto, March 2011.

TECHNICAL MARKETING

Conferences and Workshops

Staff participated in numerous conferences and workshops during 2011, as organizers, speakers and attendees. Highlights from conferences and meetings included:

- presentations by JoAnne Nelson, Paul Schiarizza, and Mitch Mihalynuk at the Mineral Exploration Roundup 2011 in Vancouver;
- participation in the Prospectors and Developer's Association of Canada (PDAC) convention in Toronto by hosting a Ministry booth on the trade show floor and helping host an Asian investor luncheon (Figure 6);
- presentations by BCGS geoscientists at the 2011 KEG annual meeting in Kamloops;
- Yao Cui presented "Visualization of Geoscience Data from Multiple Sources" and Larry Jones presented an update of the BCGS at Minerals South in Kimberly during November 2011;
- a presentation by Bruce Madu on the activities of the BCGS at the NWMA's convention in Reno in December;
- presentations by George Simandl on BC specialty metals at the 2011 GACMAC meeting in Ottawa and at the 2011 Goldschmidt meeting in Prague, Czech Republic.
- presentation by Steve Rowins on Archean porphyry Au-Cu deposits at the 2011 GACMAC meeting in Ottawa;
- presentations by Jim Logan and Paul Schiarizza at the "Exploration Undercover Workshop" in Vancouver, October 12-14;
- Bruce Madu provided key leadership and technical expertise to the Premiers 2011 Asian Investment Mission and coincident annual mining events in Beijing, Tianjin and Hong Kong (Figure 7);
- Bruce Madu delivered high-level information for an inaugural mining and exploration session as part of the Premier's Mission in Delhi, India and supported the signing of an MOU between BC and India pertaining in some aspects to the exchange of geoscience expertise;
- public lecture by JoAnne Nelson at the Yukon Geoscience Forum in Whitehorse in November;

The Cordilleran Tectonics Workshop (CTW) is being organized by the BCGS and the Pacific Section of the Geological Association of Canada (the "GAC-PAC").

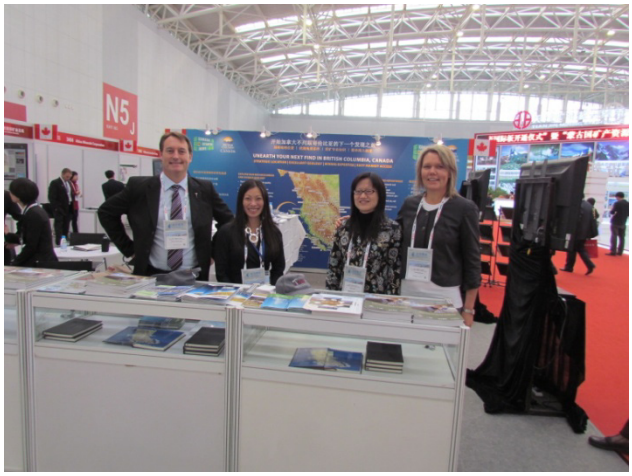

Figure 7. Bruce Madu, Janet Cho, Jin Xiuzhen (translator) and Tracey Sexton (AMEBC) ready to promote British Columbia's mineral resources at the China Mining Expo in Tianjin, China, November 2011 (photo courtesy of AMEBC).

This year it will be held at the Harbour Towers Hotel in Victoria, BC, February 24-26, 2012.

Earthbound Lectures

The BCGS hosts lectures throughout the year under the banner "Earthbound". Invited speakers in 2011 included:

1. February 25: **Jim Lewis** (Policy and Sustainability Branch, Mines and Mineral Resources Division, MEM) - Atlin-Taku Land Use Plan: A Social-Economic Assessment Method Based on GSB Mineral Potential Assessments.
2. March 18: **Tony Wass** (Ocean Floor Geophysics) - Dragon's Den: Exploration for Seafloor Massive Sulphides near Okinawa.
3. April 1: **JoAnne Nelson** (BCGS) - The Sinistral Side of the Mid-Cretaceous Gold Story.
4. May 18: **Steve Rowins** (BCGS) - Genesis of the oldest porphyry Au-Cu deposit in the Superior Province: The Troilus mine, Quebec.
5. September 30: **Mitch Mihalynuk** (BCGS) - Hooped in the Hoodoo Map Area.
6. October 7: **JoAnne Nelson** (BCGS) - Fishy Goings-on on the BC North Coast.
7. October 14: **Graham Nixon** (BCGS) - TGI-4: Ni-Cu-PGE and NVI update.
8. October 21: **Yao Cui** (BCGS) - Geology Operational Database Environment (GODE): progress and future.
9. November 4: **Paul Schiarizza** (BCGS) - The Kutcho Assemblage, Eastern King Salmon Allochthon.
10. November 18: **Fil Ferri** (Geoscience and Strategic Initiatives Section, MEM) - Geological Studies in the Toad River (094N) Map Area.

Publications

During the past year, the BCGS published *Geological Fieldwork 2011*; seven Open File maps and reports; five Geoscience Maps; twelve GeoFile maps, reports and data files; and four Information Circulars. Staff also provided contributions to the Canadian Journal of Earth Sciences' Mountain Pine Beetle Special Issue.

With the Regional Geologists as principal authors, the BCGS published *Exploration and Mining in British Columbia 2011* and *British Columbia Mines and Mineral Exploration Overview 2011* and coordinated articles on provincial industry activities in the other external publications.

All geoscience publications are available online at the BCGS website: www.empr.gov.bc.ca/geology.

BC MINERAL DEVELOPMENT OFFICE

The role of the BC Mineral Development Office (MDO) in Vancouver is to promote investment in the province's mineral exploration and mining industry, both domestically and internationally. This includes delivering a multifaceted technical campaign to highlight the province's superior coal and mineral potential, renowned geoscience database and expertise, and attractive business climate. The MDO interacts with decision-makers in industry, including executive management, geologists and prospectors, and forms part of the wider marketing efforts of government. The MDO also hosts incoming national and international companies and government representatives, and provides leadership for government trade missions.

Examples of MDO activities in the past year include acting as a key player to profile information on BC's mineral resources, investment procedures and specific mineral commodities to Asian investors, including the Asia Investment Mission to Hong Kong, China and India; preparing articles on BC's mineral resources and exploration and mining activity for numerous ministry and industry publications to promote the province; profiling BC mineral industry investment opportunities at numerous conferences, including the Mineral Exploration Roundup, the Prospectors and Developers Association of Canada (PDAC) Convention, the China Mining Conference and the KEG annual meeting; responding on a daily basis to requests for assistance from prospectors, geologists, companies and the public; working on various land-use issues, including those associated with referrals from Mineral Titles; delivering presentations to mining associations where possible; and updating publications such as Gold in BC, Copper in BC, and Opportunities to Explore – British Columbia Mining and Minerals.

Marketing Coal and Minerals to Asia-Pacific Region

Government continued an active Asia-Pacific marketing strategy to attract direct investment from Asia

in BC exploration and mining projects. The BC Jobs Plan specifically highlights the opportunities that the mining industry presents for growing the economy and creating more employment throughout the province. Asian countries are leading consumers of the province's coal and metal ores, and have a record of investment in BC's minerals industry. Key selling points are BC's rich geology, expert geoscience information, interactive online databases, continuing demand for commodities such as copper and coal, a Pacific Rim gateway, modern infrastructure and a skilled workforce. The BCGS provides marketing agencies with most of the technical expertise and professional delegates for international presentations and meetings with Asian companies. It is the point of contact for incoming international investors through the BC Mineral Development Office in Vancouver.

Regional Geologists

Regional Geologists are a vital component of government's ability to provide detailed geological knowledge of the region in which they live and work, and gather information on industry exploration and mining activity. The regional geologists remain in the Ministry of Forests, Land and Natural Resource Operations as part of government's consolidation of the natural resource agencies. There has been a significant turnover of staff recently and new staff is on board or incoming for several regions. Exciting times are ahead as all staff get into the field to visit many of the new projects in their regions.

Regional Geologist	Office	Region
Jeff Kyba	Smithers	Northwest
Paul Jago	Prince George	North-Central and Northeast
Jim Britton	Kamloops	South-Central
Dave Grieve	Cranbrook	Southeast
Bruce Northcote	Vancouver	Southwest

The MDO works closely with the regional geologists in attracting investment to BC and in preparing various publications.

STAFF UPDATE

Numerous staff changes occurred again in 2011 (Figure 8). Steve Rowins is the new Chief Geologist and Executive Director of the BCGS, replacing Dave Lefebure who retired in October 2011 after more than 25 years of service with the BC government. Steve, who joined the Survey in 2009, was previously the Director of Cordilleran Geoscience. Tian Han joined the BCGS in November 2011 as the new Senior Digital Information Geoscientist. He brings with him extensive knowledge of database and application development, mapping using remote sensing techniques, and geospatial data modeling and management. In January 2012, Alexei Rukhlov joined the Survey as the Provincial or Senior Geochemist. He replaced Ray Lett, who retired to a busy life of consulting in 2010. Kirk Hancock temporarily headed the MDO in

Figure 8. Staff of the British Columbia Geological Survey in 2011.

Vancouver as its Acting Director until the fall of 2011, when Bruce Madu arrived by sled from Kamloops. Bruce was the successful candidate for the vacant Director position. Bruce was previously the Regional Geologist in Kamloops. Another geoscientist stepping up into more of leadership role included JoAnne Nelson. She was promoted in the fall to the new Northern BC Manager and Senior Geologist in the Cordilleran Geoscience Section. She is also a co-author of the new edition of the bestselling book, *Geology of British Columbia*, published by Greystone Books. Melanie Mitchell returned from maternity leave to her position as the administrative assistant with the BCGS in February 2011.

Other good news was that three of the five Regional Geologists positions were finally filled in 2011: Jeff Kyba replaced the retired Paul Wojdak in the Smithers office in October 2011; Jim Britton replaced Bruce Madu in the Kamloops office in September 2011; and Paul Jago replaced John DeGrace in the Prince George office in January 2012.

The BC Jobs Plan, announced September 22, 2011, commits all Natural Resource Sector Agencies, including MEM, to a number of initiatives in support of economic development and job creation. The BCGS will be trying to fill four temporary positions until March 2013. These include a Senior Coal Geologist, a Marketing and Publications Geologist, a GIS Geologist and an Administrative Assistant for the Vancouver office.

NEED MORE INFORMATION? WANT TO COMMENT?

BCGS staff has considerable expertise and welcome the chance to share it. Our contact list is online at: http://www.empr.gov.bc.ca/Mining/Geoscience/Staff/Pages/default.aspx.

We always appreciate your input regarding our many programs and activities. To learn about new publications, data releases and upcoming events, join the BCGS release notification list by emailing Geological.Survey@gov.bc.ca or call (250) 952-0429.

Irarsite (IrAsS), Osarsite (OsAsS) and Gold from Placer Black Sands, Ruby Creek and Wright Creek, Atlin, British Columbia

by Z.D. Hora[1], E. Pivec[2] and A. Langrova[3]

KEYWORDS: Placer mineralogy, platinum group elements, PGE, osarsite, irarsite, osmium, iridium, placer gold, pure gold rims

INTRODUCTION

Atlin gold placers have been known to contain a wide variety of metallic minerals for almost one hundred years. T.L. Gledhill (1921) lists among others iridosmine, cassiterite, wolframite, magnetite, native gold, copper, bismuth, chalcopyrite, pyrite, amalgam and mercury. Some mineral relationships observed from black sands of Feather Creek were published recently by Sack and Mihalynuk (2004). For this study, three samples of about 10 grams each comprising 2 mm hand-panned black sand were provided by M. Mihalynuk from Ruby, Wright and Feather creeks. The samples were observed under the microscope and analyzed by the electron microprobe. The results are presented below.

GEOLOGY

The Atlin placer camp, located on the east side of Atlin Lake, is underlain by the northern Cache Creek terrane (Figure 1). In the Atlin area, this terrane consists of oceanic sedimentary strata of Mississippian to Jurassic age, ophiolitic rocks of Late Permian to Triassic age, and Middle Jurassic, Cretaceous and Tertiary plutons (Sack and Mihalynuk, 2004) (Figure 2). Valleys originally cut deep into bedrock, are now fluvially modified and filled by glacial and glaciofluvial deposits. Some of the placer deposits may be interglacial in age but most are probably preglacial (Levson, 1992). Postglacial placers are reworked, mostly deeply buried, original fluvial placers and are usually less productive. The original gravels rich in gold are characteristically oxidized and red in colour, deposited locally on altered bedrock (Levson, 1992) or on a bouldery till (Sack and Mihalynuk, 2004).

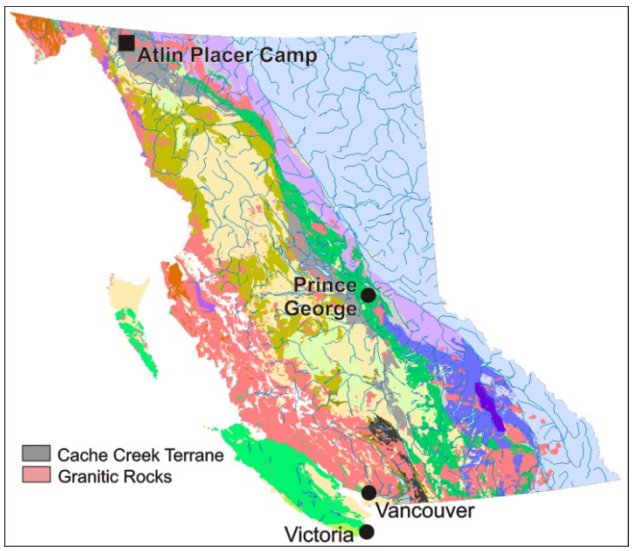

Figure 1. Location of study area.

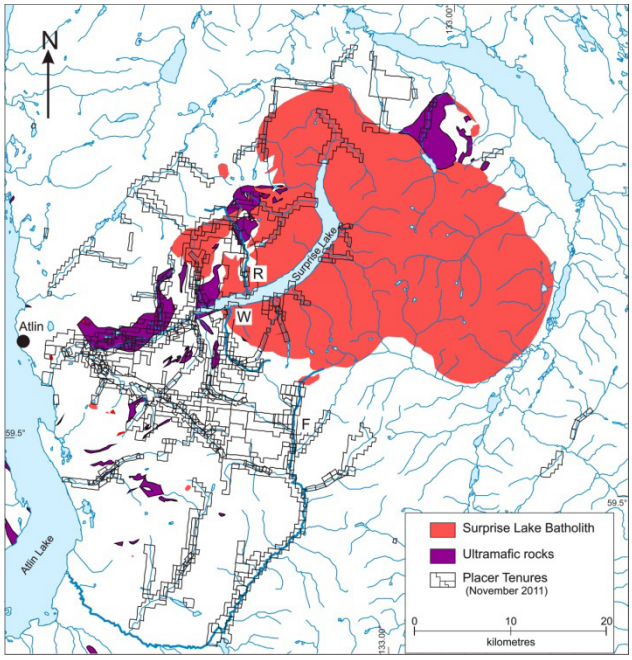

Figure 2. Map of the Atlin placer camp with placer tenures as of November 2011. Creeks discussed in the text : R=Ruby Creek, W=Wright Creek, F=Feather Creek.

[1] *British Columbia Geological Survey, Victoria, BC (retired)*
[2] *Institute of Geology, Academy of Sciences of the Czech Republic (retired)*
[3] *Institute of Geology, Academy of Sciences of the Czech Republic*

This publication is also available, free of charge, as colour digital files in Adobe Acrobat® PDF format from the BC Ministry of Energy and Mines website at http://www.empr.gov.bc.ca/Mining/Geoscience/PublicationsCatalogue/Fieldwork.

SAMPLE PREPARATION AND ANALYTICAL PROCEDURES

After microscopic examination, a small part of each black sand sample was cemented by synthetic resin, cut and made into polished sections to undergo electron probe analysis. This study focused on platinoids and gold.

Mineral analyses were made with a CAMECA SX-100 electron probe using the wavelength dispersive technique. The beam diameter was 2 μm with an accelerating potential of 20 kV. A beam current of 6 μA was measured on a Faraday cup. A counting time of 10 s was used for all elements. The standards employed were : sphalerite (S Kα), FeS_2 (Fe Kα), GaAs (As Lα), and 100% metals for Rh Lα, Os Mα, Ru Lα, Ni Kα, Re Mα, Pt Mβ, Ir Mβ. Correcting for overlapping peaks were made for Os Mα (Re Mβ1) and Rh Lα (Ir L13). The data were reduced using the ϕ(ρz) Merlet correction procedure.

Sample mineralogy

A fairly complex Ruby Creek composition of black sand has been published by Gledhill (1921). Our cursory examination confirmed the presence of gold, magnetite, wolframite and cassiterite. Iridosmine described by Gledhill was not detected. Wright Creek sample contains frequent small grains of magnetite, different shades of brown particles of iron oxides, pyrite, and relatively large particles of bright yellow gold. Feather Creek sample is dominated by magnetite, with some pyrite of silvery bluish colour. Compound gold-cassiterite grains described by Sack and Mihalynuk (2004) were not found.

Particles of gold are very common in Ruby Creek. A single silvery grain contains a suite of PGE with As and S. This irregularly-rounded grain (400 by 300 μm in size) is light grey in reflected light with metallic lustre. Its shape and texture are shown in Figure 3 a, b, c. The analytical results are listed in Table 1 and location of analytical points in Figure 3. The grain is an intimate intergrowth of two minerals. The lighter colour matrix is irarsite (Ir,Ru,Rh,Pt)AsS, with many irregular inclusions of darker osarsite (Os,Ru)AsS. The mottled pattern is most probably a result of immiscibility between a cubic structure of irarsite with its isomorphic Rh and Pt phases and monoclinic osarsite with its isomorphic Ru member. The results of 15 analytical points is in agreement with this interpretation. As shown in Table 1, the Pt and Rh values are higher in irarsite, while Ru values are high in osarsite.

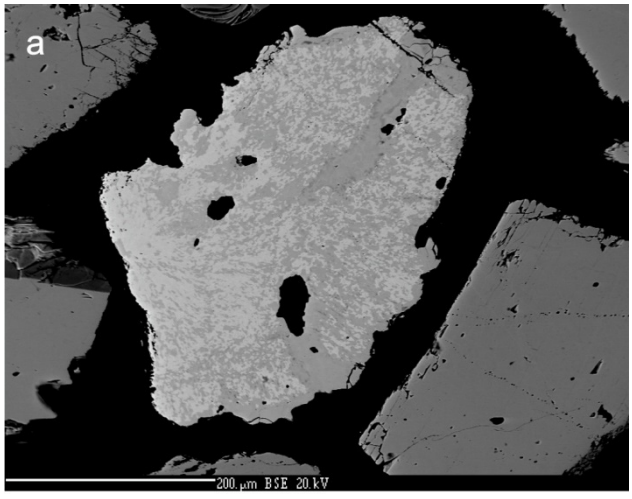

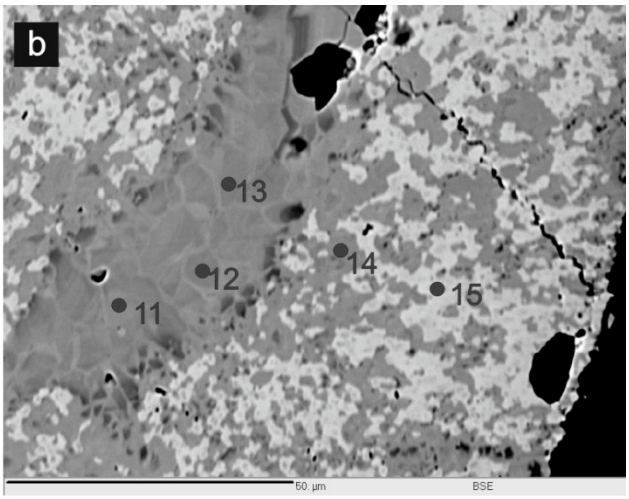

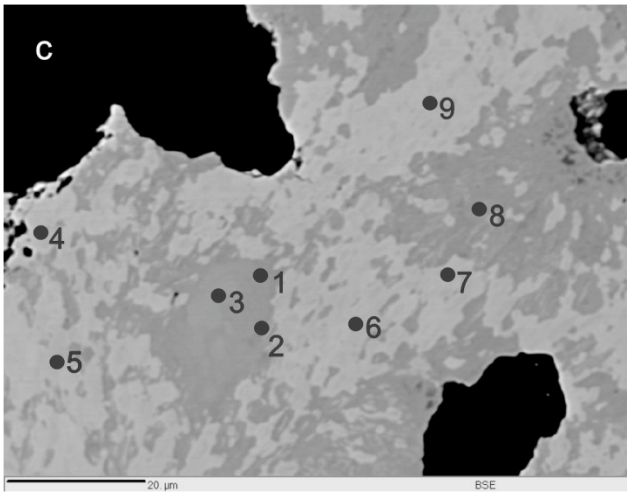

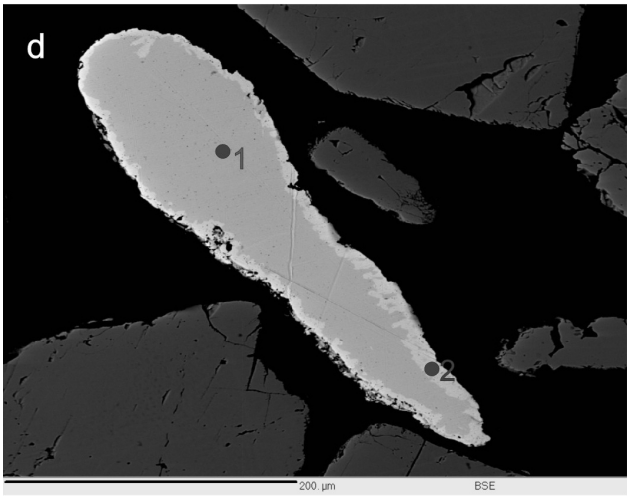

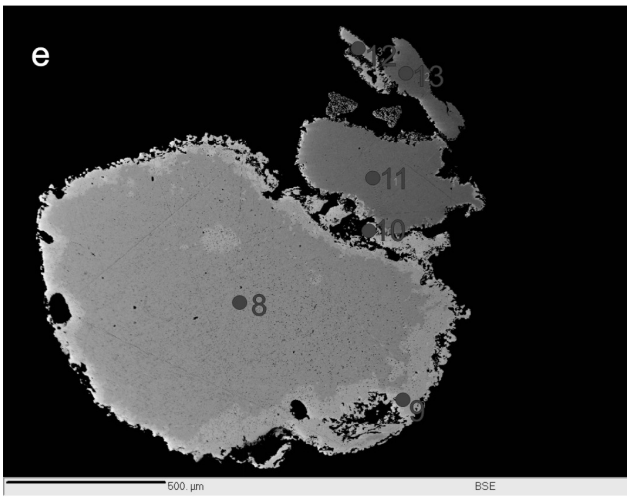

Figure 3. Scanning electron microscope photomicrographs showing: (a) a PGE grain, Ruby Creek; scale bar 200 µm. (b) analytical points of osarsite-rich detail, Ruby Creek; scale bar 50 µm; points correspond to analytical data in Table 1. (c) the osarsite–irarsite intergrowth texture, Ruby Creek; scale bar 20 µm. (d) an electrum grain with gold rim, Ruby Creek; scale bar 200 µm; analytical points 3–7 are outside the field of view; points correspond to analytical data in Table 2. (e) electrum grains with gold rim, Wright Creek; scale bar 500 µm.

The logical source of this mineral is the Atlin ophiolitic terrane with its ultramafic to mafic rocks. The high Ru content in osarsite is in agreement with conclusions of Barkov *et al.* (2005, 2007) based on a study of PGE metals and alloys which also included samples from the Atlin area. While irarsite is a relatively common component in both PGE placer and lode deposits in general, the osarsite occurrences are known from few placers worldwide.

Little particles of gold are a common component of samples from both Ruby and Wright Creeks. It is present in irregular, rounded grains of electrum (22 to 31 % of Ag) up to 100µm in size, with irregular, thin (up to 5µm) rims of high purity gold (Table 2). Such rims are known from numerous sites around the globe and there are two different interpretations for their origin. Knight *et al.* (1999) presents a well documented case linking placer gold with rims to its identified bedrock sources in Klondike District, Yukon. The interpretation of high purity rims has been linked to removal of Ag, Hg and Cu from the gold. The particle shape and width of the rim depends on the distance of transport from the primary source. The authors suggest that the rim may thicken in

Table 1. Electron probe analyses of osarsite and irarsite from Ruby Creek compared to composition of international standards.

Osarsite (Os,Ru)AsS, Ruby Creek, Atlin area, British Columbia

AP	As	Ir	Ru	Pt	Rh	S	Os	Fe	Ni	Re	wt.%
A	30.6	2	18.1	0.4	0.2	11.5	35.6		0.9		99.3
1	28.02	2.92	12.61	0	0.18	11.3	45.75	0	0.02	0	100.8
2	27.77	2.51	13.25	0	0.21	11.24	45.82	0	0.02	0	100.8
3	28.61	3.31	14.57	0	0.4	11.29	42.39	0.03	0.08	0	100.7
8	29.05	4.5	12.9	0	0.29	11.1	42.07	0	0.14	0.05	100.1
11	29.68	2.29	15.04	0	0.21	11.19	42.08	0.03	0.1	0.02	100.6
12	30.37	3.03	17.55	0	0.2	11.18	37.83	0.09	0.19	0.02	100.5
13	29.11	2.33	16.43	0	0.15	11.46	39.68	0.02	0.22	0.12	99.52
14	29.23	3.22	15.53	0	0.1	11.22	39.92	0.06	0.07	0.01	99.36

Irarsite (Ir,Ru,Rh,Pt)AsS , Ruby Creek, Atlin area, British Columbia

AP	As	Ir	Ru	Pt	Rh	S	Os	Fe	Ni	Re	wt.%
B	26.0	43.5	5.5	11.7	7.4	9.6					103.7
4	24.32	49.84	2.06	5.98	0.81	11.24	2.57	0	1.02	0	97.84
5	23.93	49.51	3.05	7.31	1.15	11.82	1.62	0.03	0.77	0	99.19
6	25.01	49.1	3.02	7.45	1.05	11.47	1.86	0	0.77	0.22	99.95
7	24.79	49.64	2.61	7.36	1.11	10.85	1.74	0	0.7	0	98.8
9	24.75	51.32	2.35	6.7	0.87	11.28	1.69	0.01	0.94	0	99.91
10	24.51	48.99	2.9	6.96	0.98	11.86	2.3	0.06	0.94	0.02	99.52
15	25.87	48.47	2.85	7.5	1.05	11.23	2.12	0	0.72	0	99.81

Remarks:

A - analytical data from Snetsinger (1972), Gold Bluff, California (+Pd 0.6)

B - analytical data from Johan *et al.* (2000), Papua New Guinea (+Cu 0.6, Pd 0.4)

AP - analytical points

Table 2. Electron probe analyses of electrum and gold grain rims from Ruby and Wright creeks.

Gold grains from placers in Atlin area, British Columbia

AP	Ag	Au	wt.%
1	27.40	71.96	99.36
2*	2.50	96.77	99.27
3	33.83	66.76	100.6
4*	2.29	99.84	102.1
5	22.66	77.94	100.6
6	22.51	79.01	101.5
7*	1.93	98.71	100.6
8	13.09	86.43	99.52
9*	0.01	98.13	98.14
10*	1.25	72.74	73.99
11	24.65	75.65	100.3
12	30.78	69.88	100.7
13	31.01	69.32	100.3

Remarks:
Points 1-7 - Ruby Creek
* rims
Points 8-13 - Wright Creek
AP - analytical points

dormant placers while getting removed by abrasion in active placers.

A different interpretation is presented by Groen *et al.* (1990), Eyles (1990), Eyles and Kocsis (1989) and Bakos, at al. (2004). The origin of gold rims is explained as a result of a supergene gold mobility as a thiosulphate ion under basic to neutral conditions. Also, humic acids in the presence of dense vegetation enable gold mobility in subsurface waters. Under favourable conditions, such as change in pH or temperature, the gold may precipitate. Such precipitation could be triggered by the presence of older gold grains, detrital organics, or newly formed iron sulphides.

The main gold-bearing gravels in both Wright and Ruby Creeks are described as heavily oxidized rusty coloured, strongly cemented, iron and manganese oxide rich gravels deposited on bedrock (Levson, 1992) or on a glacial till (Sack and Mihalynuk, 2004). Such a heavily oxidized environment suggests that the gold rims may be a product of supergene gold mobility such as suspected for the Cariboo Mining District by Eyles (1990), or the Danube River placers in Slovakia by Bakos *et al.* (2004).

The bedrock source for Atlin gold still remains to be identified. However, the distribution of placer streams on all sides of the Surprise Lake batholith, the coarsest placer gold recovered primarily from streams located along its margins and association of some gold grains with cassiterite suggest that a link between placer gold and the Surprise Lake batholith may exist (Sack and Mihalynuk, 2004).

ACKNOWLEDGMENTS

This contribution to the Atlin placer camp database benefited from a number of stimulating discussions with and help from Z. Johan, M. Mihalynuk and G. Nixon; K. Hancock assisted with figures 1 and 2, J. Jabůrkova helped with sample preparation and J. Pávková provided technical assistance. G. Nixon's editorial comments are greatly appreciated.

REFERENCES

Bakos, F., Chovan, M. and collective (2004): Gold in Slovakia; *Slovensky skauting*, Bratislava, Slovak Republic, pages 231–237; In Slovak with English abstracts.

Barkov, A.Y., Fleet, M.A., Nixon, G.T. and Levson, V.M. (2005): Platinum-group minerals from five placer deposits in British Columbia, Canada; *The Canadian Mineralogist*, Volume 43, pages 1687–1710.

Barkov, A.Y., Martin, R.F., Fleet, M.E., Nixon, G.T. and Levson, V.M.(2007): New data on associations of platinum-group minerals in placer deposits of British Columbia, Canada; *Mineralogy and Petrology*, Volume 75, pages 1-21.

Eyles, N. (1990): Post-depositional nugget accretion in Cenozoic placer gold deposits, Cariboo mining district, British Columbia (93 A,B,G,H) ; *BC Ministry of Energy, Mines and Petroleum Resources*, Exploration in British Columbia 1989, pages 147–169.

Eyles, N. and Kocsis S.P.(1989): Sedimentological controls on gold distribution in Pleistocene placer deposits of the Cariboo mining district, British Columbia; in Geological Fieldwork 1988, *BC Ministry of Energy, Mines and Petroleum Resources*, Paper 1989-1, pages 377–385.

Gledhill, T.L. (1921): Iridosmine crystals from Ruby Creek, Atlin district, B.C.; *University of Toronto studies*, Geological series number 12, pages 40–42.

Groen, J.C., Craig, J.R. and Rimstidt, J.D. (1990): Gold-rich rim formation on electrum grains in placers; *Canadian Mineralogist*, Volume 28, pages 207–228.

Kaspar, J., Hudec, I., Schiller, P., Cook, G.B., Kitzinger, A. and Wölfl, E. (1972): A contribution to the migration of gold in the biosphere of the humid mild zone; *Chemical Geology*, Volume 10, pages 299–305.

Knight, J.B., Morison, S.R. and Mortensen, J.K. (1999): The relationship between placer gold particle shape, rimming, and distance of fluvial transport as exemplified by gold from the Klondike District, Yukon Territory, Canada; *Economic Geology*, Volume 94, pages 635–648.

Johan, Z., Slansky, E. and Kelly, D. (2000): Platinum nuggets from the Kompiam area, Enga Province, Papua New Guinea: evidence for an Alaskan-type complex; *Mineralogy and Petrology*, Volume 68, pages 159–176.

Levson, V.M. (1992): Quaternary geology of the Atlin area (104N/11W, 12E); *BC Ministry of Energy and Mines*, Paper 1992-1, pages 375–390.

Mihalynuk, M.G., Ambrose, T.K., Devine, F.A.M. and Johnston, S.T. (2011): Atlin placer gold nuggets containing mineral and rock matter: implications for lode gold exploration; in Geological Fieldwork 2010, *BC Ministry of Energy, Mines and Petroleum Resources*, Paper 2011-1, pages 56–72.

Sack, P.J. and Mihalynuk, M.G. (2004): Proximal gold-cassiterite nuggets and composition of the Feather Creek placer gravels: clues to a lode source near Atlin, B.C.; in Geological Fieldwork 2003, *BC Ministry of Energy, Mines and Petroleum Resources*, Paper 2004–1, pages 147-161.

Snetsinger, K.G. (1972): Osarsite, a new osmium-ruthenium sulfarsenide from California; *The American Mineralogist*, Volume 57, pages 1029–1036.

Dease Lake Geoscience Project, Part IV: Tsaybahe Group: Lithological and Geochemical Characterization of Middle Triassic Volcanism in the Stikine Arch, North-Central British Columbia

by O. Iverson[1], J.B. Mahoney[1] and J.M. Logan[2]

KEYWORDS: QUEST-Northwest mapping, Geoscience BC, Triassic stratigraphy, Stuhini, Tsaybahe, volcanic geochemistry, detrital zircon geochronometry, Stikine terrane

INTRODUCTION

The Tsaybahe group study is one of four integrated projects that comprise the British Columbia Geological Survey Dease Lake Geoscience Project (Logan *et al.*, 2012), which is itself part of Geoscience BC's QUEST-Northwest initiative, a program initiated in 2011 to stimulate exploration in the northwestern part of the province along Highway 37 (Figure 1). Geoscience BC has committed $3.25 million in funding to provide two high-resolution (with a line spacing of 250 m) airborne magnetic surveys (Simpson, 2012), a collection of data on new regional stream sediments and a reanalysis of stream sediment samples (Jackaman, 2012) and new bedrock mapping and related studies (Logan *et al.*, this volume; van Straaten *et al.*, this volume; Moynihan and Logan, this volume; this study). Collectively, these programs provide detailed, high-quality geoscience data that is intended to enhance metallic mineral exploration in an area of prospective geology adjacent to Highway 37, near Dease Lake, in northern British Columbia.

The Dease Lake study area is situated within the Stikine terrane, an extensive subduction-generated island arc magmatic system responsible for recurring calcalkaline and/or alkaline plutonic events and associated Cu-Au mineralization, mainly during the Late Triassic and Early Jurassic. Previous mapping in the area identified two Triassic volcanic-sedimentary assemblages, the Stuhini and Tsaybahe groups (Anderson, 1981, 1983; Read, 1984, Read and Psutka, 1990; Gabrielse, 1998; Evenchick and Thorkelson, 2005). The Stuhini Group is a Late Triassic assemblage that is characterized by pyroxene porphyry breccias, volcaniclastic rocks, and

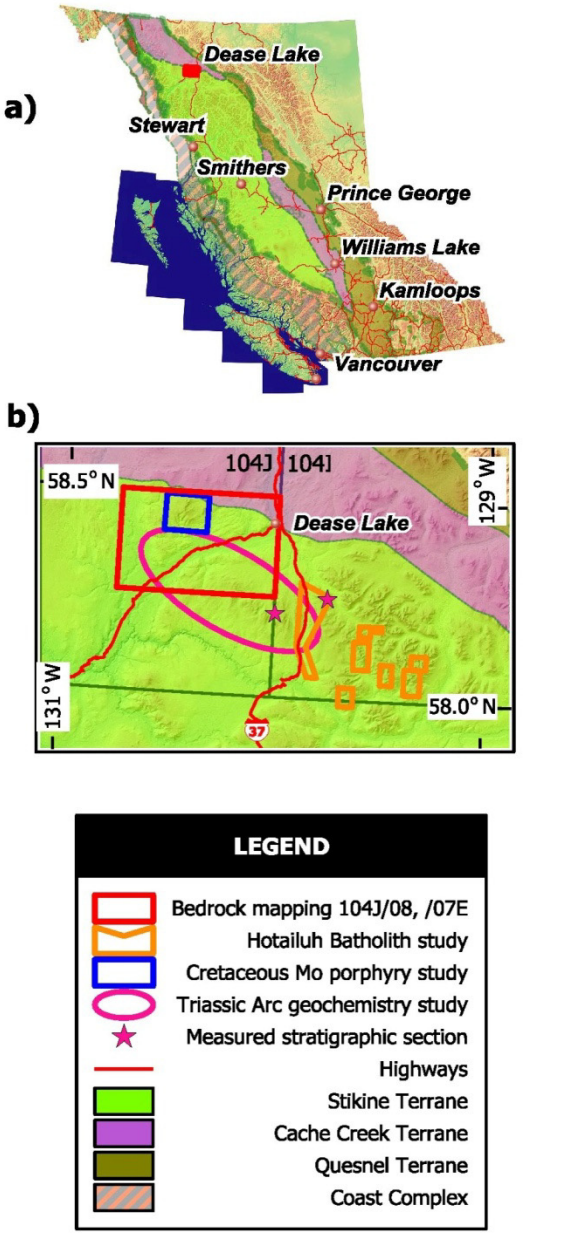

Figure 1. Location of the QUEST-Northwest mapping - British Columbia Geological Survey Dease Lake Geoscience Project on the (a) BC terrane map (after Massey *et al.*, 2005); (b) detailed view straddles NTS 104J and NTS 104I 1:250 000 map areas at Dease Lake, showing the location of the Tsaybahe Group lithological and geochemistry study.

[1] *University of Wisconsin at Eau Claire, WI, United States*
[2] *British Columbia Geological Survey, Victoria, BC*

This publication is also available, free of charge, as colour digital files in Adobe Acrobat® PDF format from the BC Ministry of Energy and Mines website at http://www.empr.gov.bc.ca/Mining/Geoscience/PublicationsCatalogue/Fieldwork.

basalt flows (Anderson, 1983). The underlying Early to Middle Triassic Tsaybahe group was defined by Read (1984) as a succession of cherty volcanic-rich sediments and crowded augite porphyry breccias containing Early and Middle Triassic fossils. The two units are strikingly similar in terms of lithology and are difficult to differentiate in the field.

This project is designed to compare and contrast the lithostratigraphic features, detrital zircon geochronology, and volcanic geochemistry of the Stuhini and Tsaybahe groups, thereby providing insight into the stratigraphic relationships and tectonic evolution of this part of the Stikine terrane. This paper reports the initial results of the senior authors B.Sc. thesis project currently underway at the University of Wisconsin–Eau Claire under the supervision of Professor J.B. Mahoney.

OBJECTIVES

Regional geologic mapping and tectonic reconstructions require accurate differentiation of the Stuhini and Tsaybahe successions in the field. The Dease Lake area is characterized by poor outcrop exposure making the accurate differentiation of the Stuhini and Tsaybahe groups more challenging. This project focuses on two well-exposed stratigraphic sections including a section north of the Cake Hill pluton, first described by Anderson (1981, 1983), and a second section on the north flank of Thenatlodi Mountain, mapped by Read (1984; Figure 1).

The stratified rocks north of the Cake Hill pluton have a complex history of age assignment. Anderson (1981, 1983) mapped these augite porphyry-bearing strata as the Late Triassic Stuhini Group in the upper plate of the Hotailuh thrust fault, which was interpreted to structurally overly a thin section of Lower Jurassic strata unconformably overlying the Late Triassic Cake Hill pluton. Subsequent work (Gabrielse, 1998) suggested that this strata was stratigraphically correlative with the informal Middle Triassic Tsaybahe group, a succession of volcanic and sedimentary rocks containing abundant coarse pyroxene porphyry breccias and Early and Middle Triassic fossils exposed to the west in Gnat Pass and further south in the Stikine River (Read, 1984; Read and Psutka, 1990). This stratigraphic and age uncertainty is the rationale behind the present investigation.

Definitive lithologic characteristics identified in these sections will be used as a reference for comparison to younger Stuhini assemblage. Analytical methods include detailed stratigraphy and sedimentology, petrography, detrital zircon geochronology, and whole rock geochemistry of the volcanogenic intervals.

Measured Sections

The stratigraphic section adjacent to the north margin of the Cake Hill pluton is located about 5 km east of Gnat Pass (NTS 104I/05, Figure 1). It was initially described by Anderson (1981, 1983; section 714) as a 1 km thick, north-dipping succession in the hangingwall of the Hotailuh fault. Anderson (1981) interpreted the rocks to be the Late Triassic Stuhini Group in thrust contact with a thin sliver of Toarcian sedimentary rocks overlying the Late Triassic Cake Hill pluton.

In this investigation, the section was subdivided into five members (Figures 2, 3). The lowest, first member (~320 m) is characterized by gray, thin to medium bedded, medium grained volcanic lithic arenite with abundant sedimentary structures including Ta-Te Bouma sequences and syndepositional folds (Figure 4a), intercalated with lesser white plagioclase porphyry volcanic pebble conglomerate, siltstone and minor argillite. Henderson and Perry (1981) describe a rich biota of Early Toarcian bryozoan, scleractinid corals, ammonites, foraminifera and pelecypods from arenaceous carbonate beds in the lower portion of the section, which was inferred to lie below the Hotailuh fault. The first member coarsens upward gradationally into the second member (~250 m) which consists of medium to thick bedded, medium to coarse grained tuffaceous volcanic lithic arenite intercalated with granule to pebble volcanic conglomerate with minor, yet distinctive, light gray siliceous ash tuff beds (Figure 4b). This member fines upwards into medium bedded siltstone of the third member (~170 m) that is intruded by augite and bladed plagioclase porphyry dikes and sills at low angles to the bedding. The intrusions have chilled margins and contain rare chloritic and calcsilicate xenoliths of country rock. The third member has an abrupt upper contact with volcanic rocks of the fourth member (~60 m), which consists of monomict, boulder conglomerate with clasts of plagioclase-rich, augite porphyritic basalt (Figure 4c). The fourth member grades upward into the fifth member (~200+ m) that is composed of locally columnar jointed augite porphyry flows and volcanic breccias characterized by angular, lapilli to block-sized augite porphyry fragments (Figure 4d). The fifth member elsewhere apparently forms extensive massifs (*e.g.* Thenatlodi Mountain and areas to the southeast) and isolated knobs throughout the map area.

A second stratigraphic section containing similar stratigraphy was examined on the north flank of Thenatlodi Mountain located approximately 14 km southwest of the previous stratigraphic section (NTS 104J/01, Figure 1). This section is intruded by a northwest trending biotite-hornblende quartz monzonite apophysis from the Three Sisters pluton (*ca.* 170 Ma), which interrupts stratigraphic continuity and apparently removes significant intervals of the stratigraphy. However, the Thenatlodi section is interpreted to be stratigraphically correlative with the section north of the Cake Hill pluton, as it contains lithologically similar strata with the same stratigraphic architecture. Unlike the Cake Hill section, the Thenatlodi section contains a lowermost member (~200+ m) characterized by argillite, siltstone, and carbonate intervals.

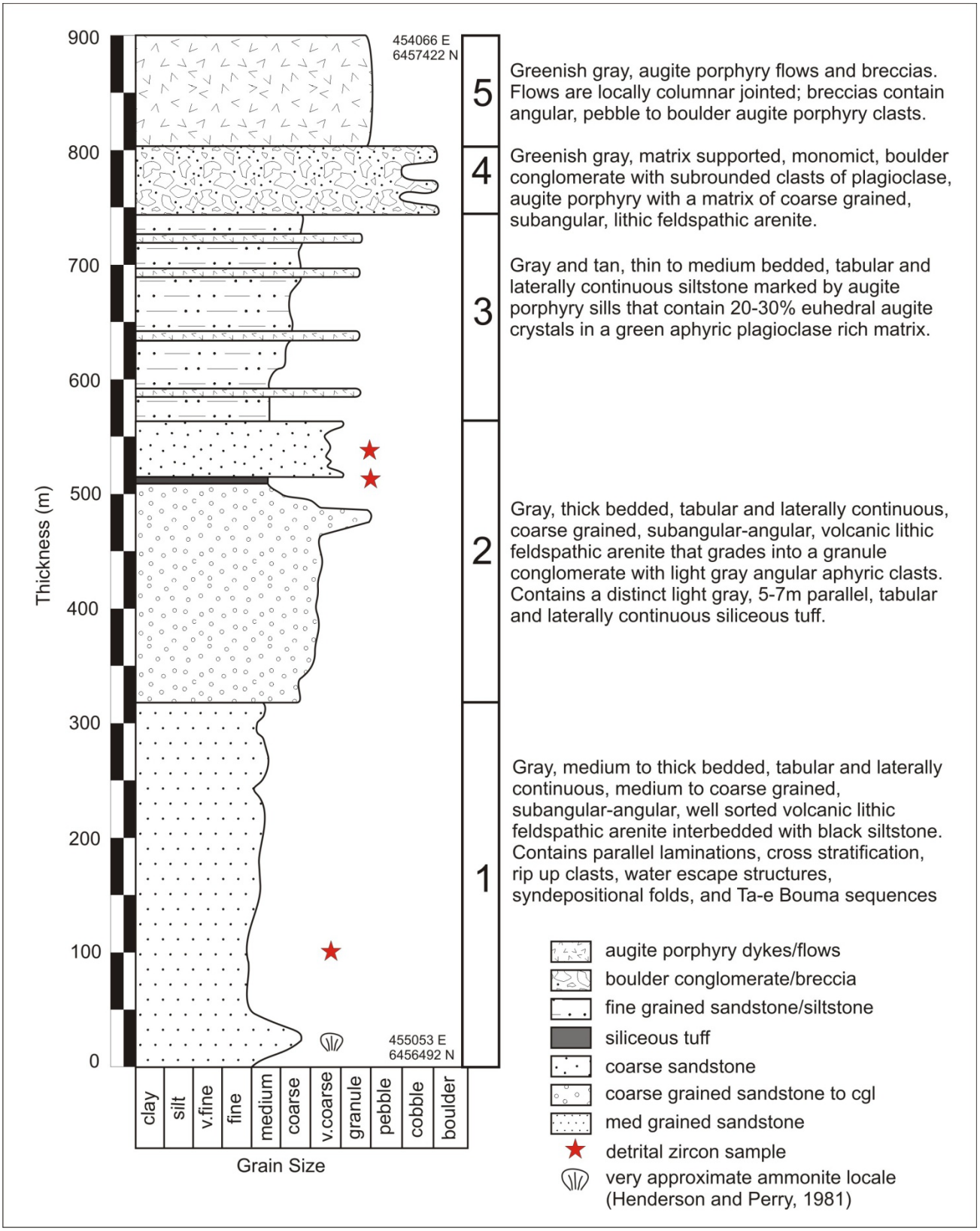

Figure 2. Schematic stratigraphic column for sedimentary and volcanic rocks overlying Cake Hill pluton measured east of Gnat Pass.

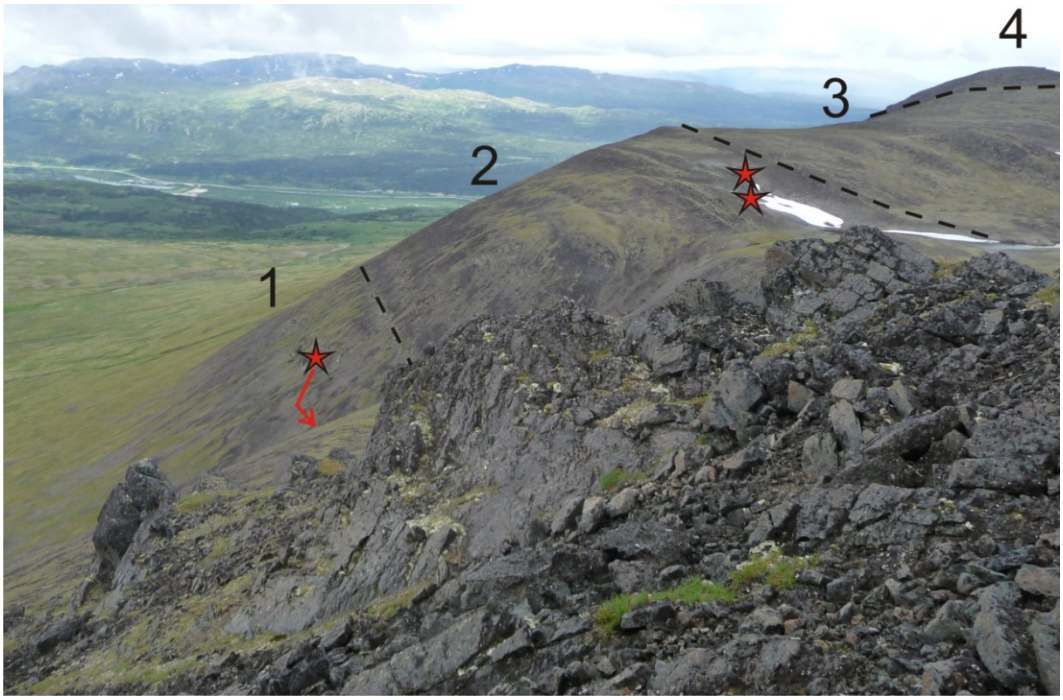

Figure 3. View looking west across the trace of the reference section north of Cake Hill pluton. Gnat Pass and Highway 37 are visible in the background. Down-faulted pyroxene porphyritic breccia of member 4 occupies foreground. Red stars show approximate location of detrital zircon sample sites.

Figure 4. Sedimentary characteristics of the measured section located north of Cake Hill pluton. (a) soft sediment deformation and basal scour features common in the thin-bedded intervals of Member 1. (b) thin to medium bedded, medium to coarse grained volcanic lithic arenite of Member 2, note distinct light grey siliceous tuff interbeds. (c) monomict volcanic (augite porphyry) boulder conglomerate of Member 4. (d) angular volcanic breccia within Member 5. Note reaction rims on volcanic clasts, indicating elevated temperatures during deposition.

Detrital Zircon Geochronology

Detrital zircon samples were collected from the section north of the Cake Hill pluton (n=3) and from the section on Thenatlodi Mountain (n=2). Relatively homogenous, medium to coarse grained volcanic lithic arenite was targeted, along with a quartz-bearing siliceous tuff located in the upper portion of the first reference section (member 3; ~520 m; Figure 2). Zircon was separated at the University of Wisconsin-Eau Claire and analyzed by LA-ICPMS at the LaserChron laboratory at the University of Arizona. Both samples from the Thenatlodi Mountain section were barren; however, all three samples from the section north of the Hotailuh fault yielded sufficient zircon for analysis.

The zircon populations from all three samples contained bimodal peaks; Middle to Late Triassic (*ca.* 220-230 Ma) and Early to Middle Jurassic (*ca.* 170-185 Ma; Figure 5). The presence of Early to Middle Jurassic detrital zircons within strata believed to be Triassic in age requires significant structural and stratigraphic revision of previous interpretations. These volcanic and sedimentary rocks are much younger than originally interpreted, and are correlative with the Early to Middle Jurassic Hazelton Group, not the Triassic Tsaybahe or Stuhini groups. This age assignment indicates that the Hotailuh thrust fault is not required because the entire section is an upright stratigraphic sequence of Early to Middle Jurassic strata unconformably overlying the Cake Hill pluton.

Stratigraphic similarities between these strata and those exposed on Thenatlodi Mountain suggest that the Hazelton Group is much more widespread than previously interpreted in the region.

Geochemistry

Whole rock geochemical analyses, including major, trace and select REE analyses, are in progress on volcanogenic rocks from the measured sections and collections made during the regional bedrock mapping program (Logan *et al.*, this volume). The primary objective is to compare and contrast the geochemical character of pyroxene porphyritic volcanic rocks in the region now recognized to include; Middle Jurassic Hazelton as well as Early-Middle and Late Triassic Tsaybahe and Stuhini groups respectively.

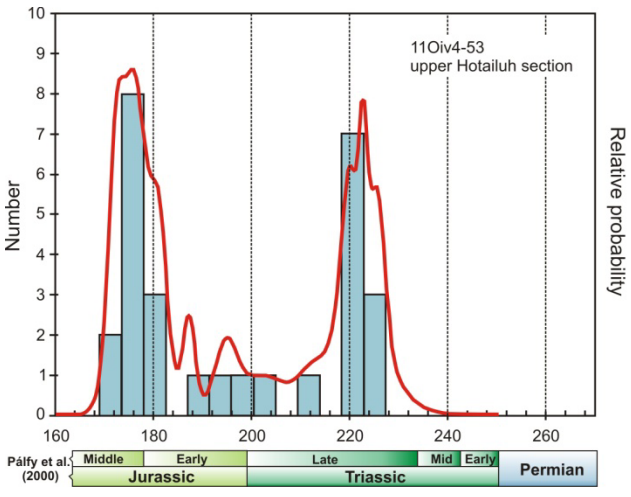

Figure 5. Detrital zircon populations for sample 11Oiv4-53 collected from quartz-bearing tuff of horizon 2 (see Figures 2 and 3).

CONCLUSIONS

Detrital zircon populations from a sedimentary dominated volcaniclastic section east of Gnat Pass indicate the strata are much younger than previously realized. Here, Early to Middle Jurassic rocks nonconformably overly the Late Triassic Cake Hill pluton in a north dipping, upright, bedded section which eliminates the necessity for the Hotailuh fault.

ACKNOWLEDGMENTS

Geoscience BC provided financial support for the field and analytical programs, and salary support for O. Iverson and the field assistants. Jan Anderson and Dempsey Callison are also thanked for providing great meals and courteous assistance at the ranch. The staff at the Arizona LaserChron Center provided expert guidance and camaraderie, as always.

REFERENCES

Anderson, R.G. (1981): Satellitic stocks, volcanic and sedimentary stratigraphy and structure around the northern and western margins of the Hotailuh Batholith, north-central British Columbia; in Current Research, Part A, *Geological Survey of Canada*, Paper 80-1A, pages 37-40.

Anderson, R.G. (1983): Geology of the Hotailuh Batholith and surrounding volcanic and sedimentary rocks, north-central British Columbia; unpublished Ph.D. thesis, *Carleton University*, 669 pages.

Evenchick, C.A. and Thorkelson, D.J. (2005): Geology of the Spatsizi River map area, north-central British Columbia; *Geological Survey of Canada*, Bulletin 577, 276 pages.

Gabrielse, H. (1998): Geology of Cry Lake and Dease Lake map areas, north-central British Columbia; *Geological Survey of Canada*, Bulletin 504, 147 pages.

Henderson, C.M and Perry, D.G. (1981): A Lower Jurassic heteroporid bryozoans and associated biota, Turnagain Lake, British Columbia; *Canadian Journal of Earth Sciences*, Volume 18, p. 457-468.

Jackaman, W. (2012): QUEST-Northwest Project: new regional geochemical survey and sample reanalysis data (NTS 104F, G, H, I, J), northern British Columbia; in Geoscience BC Summary of Activities 2011, *Geoscience BC*, Report 2012-1.

Logan, J.M., Moynihan, D.P. and Diakow, L.J. (2012): Dease Lake Geoscience Project, Part I: Geology and Mineralization of the Dease Lake (104J/8) and east-half of the Little Tuya River (104J/7E) map sheets, Northern British Columbia; this volume.

Logan, J.M., Diakow, L.J., van Straaten, B.I., Moynihan, D.P. and Iverson, O. (2012): QUEST-Northwest Mapping: BC

Geological Survey Dease Lake Geoscience Project (NTS 104J, 104I), Northern British Columbia; in Geoscience BC Summary of Activities 2011, *Geoscience BC*, Report 2012-1.

Massey, N.W.D., MacIntyre, D.G., Desjardins, P.J. and Cooney, R.T. (2005): Digital Geology Map of British Columbia: Whole Province, *BC Ministry of Energy, Mines and Petroleum Resources*, Geofile 2005-1.

Moynihan, D.P. and Logan, J.M. (2012): Dease Lake Geoscience Project, Part III: Age, Emplacement and Mineralization of the Cretaceous Snow Peak pluton; this volume.

Palfy, J., Smith, P.L. and Mortensen, J.K. (2000): A U-Pb ^{40}Ar-^{39}Ar time scale for the Jurassic; *Canadian Journal of Earth Sciences*, Volume 37, page 923-944.

Read, P.B. (1984): Geology Klastline River (104G/16E), Ealue Lake (104H/13W), Cake Hill (104I/4W), and Stikine Canyon (104J/1E), British Columbia; *Geological Survey of Canada*, Open File 1080.

Read, P.B. and Psutka, J.F. (1990): Geology of Ealue Lake east-half (104H/13E) and Cullivan Creek (104H/14) map areas, British Columbia; *Geological Survey of Canada*, Open File 2241.

Simpson, K.A. (2012): QUEST-Northwest: Geoscience BC's new minerals project in northwest British Columbia (104G, 104J, parts of NTS 104A, B, F, H, I, K, 103O, P); in Geoscience BC Summary of Activities 2011, *Geoscience BC*, Report 2012-1.

van Straaten, B.I., Logan, J.M. and Diakow, L.J. (2012): Dease Lake Geoscience Project, Part II: Initial investigations into the Mesozoic magmatic history and metallogeny of the Hotailuh batholith and surrounding volcanic and sedimentary rocks, northern Stikine terrane; this volume.

Dease Lake Geoscience Project, Part I: Geology and Mineralization of the Dease Lake (NTS 104J/08) and East-Half of the Little Tuya River (NTS 104J/07E) Map Sheets, Northern British Columbia

by J.M. Logan[1], D.P. Moynihan[2] and L.J. Diakow[1]

KEYWORDS: QUEST-Northwest mapping, Geoscience BC, regional bedrock mapping, integrated multi-disciplinary studies, geochemistry, copper-gold metallogeny, molybdenite, Triassic, Jurassic and Cretaceous plutonism, Tsaybahe, Stuhini, target generation, GIS

INTRODUCTION

The British Columbia Geological Survey's Dease Lake Geoscience Project is part of Geoscience BC's QUEST-Northwest initiative, a program launched in 2011 to stimulate exploration in the north western part of the province along Highway 37 (Figure 1). Geoscience BC has committed $3.25 million in funding for two high resolution (250 m line-spaced) airborne magnetic surveys, collection of new regional stream sediments data, reanalysis of stream sediment samples and the bedrock mapping described in this paper. The 2011 program of bedrock mapping and mineral deposit studies undertaken by the British Columbia Geological Survey is complementary to the geophysical and geochemical programs directly administered through Geoscience BC (Jackaman, 2012; Simpson, 2012). Collectively these programs will provide detailed, high quality geoscience data that is intended to enhance metallic mineral exploration in an area of prospective geology.

The Dease Lake study area is situated within the Stikine terrane, an extensive subduction-generated island arc magmatic system responsible for recurring calcalkaline and/or alkaline plutonic events and associated Cu-Au mineralization, mainly during Late Triassic and Early Jurassic time. Prospective Mesozoic volcanic rocks exposed around the margins of the Bowser Basin form an arcuate belt containing porphyry deposits that include KSM (MINFILE 104B 103), Galore Creek (MINFILE 104G 090) and Shaft Creek (MINFILE 104G 015) deposits to the west, and the Kemess deposits

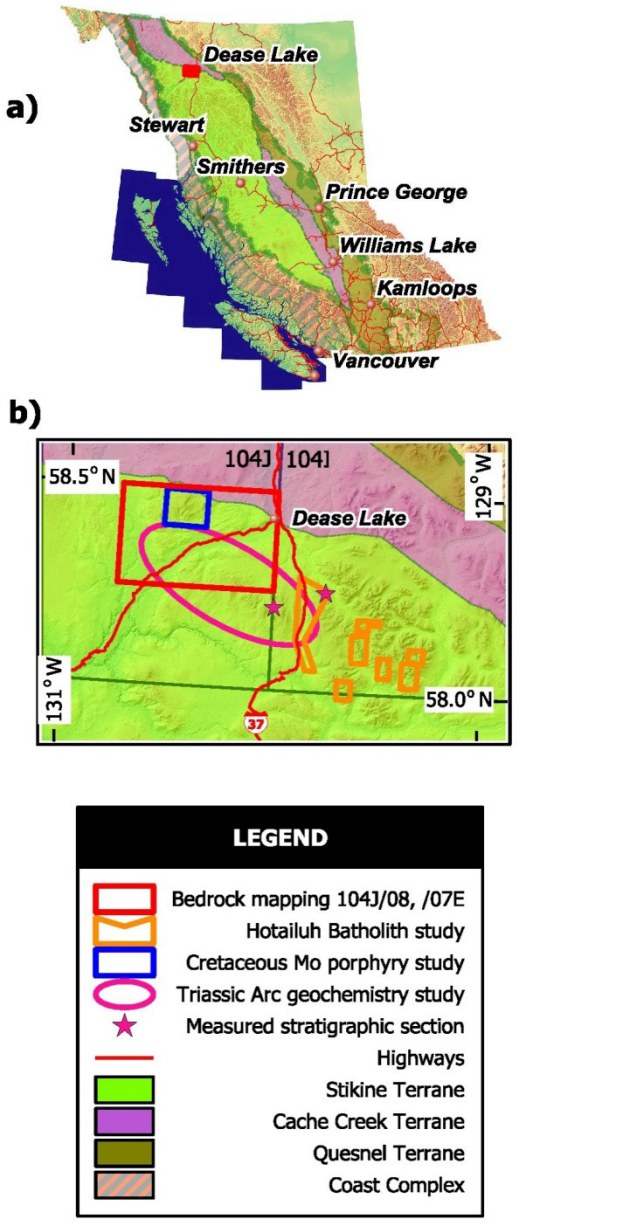

Figure 1. Location of the QUEST-Northwest mapping: British Columbia Geological Survey Dease Lake Geoscience Project on the a) BC terrane map (after Massey *et al.*, 2005); b) Detailed view straddles NTS 104J and NTS 104I 1:250 000 map areas at Dease Lake, showing the locations of the bedrock mapping study (NTS 104J/08, 07E), the Hotailuh batholith study, theSnow Peak pluton study and the Triassic arc geochemistry study.

[1] *British Columbia Geological Survey, Victoria, BC*
[2] *Department of Geosciences, University of Calgary, Calgary, AB*

This publication is also available, free of charge, as colour digital files in Adobe Acrobat® PDF format from the BC Ministry of Energy and Mines website at http://www.empr.gov.bc.ca/Mining/Geoscience/PublicationsCatalogue/Fieldwork.

(MINFILE 094E 094) to the east. The Dease Lake study area is located at the apex of this arcuate belt, immediately north of the Red Chris Cu-Au porphyry deposit (MINFILE 104H 005) and adjacent to the Hotailuh batholith, a large composite intrusive complex similar in age to the intrusions hosting porphyry mineralization at the Galore and Shaft Creek deposits.

Numerous small plutons intrude mainly Late Triassic arc stratigraphy in the Dease Lake area. Neither the plutons nor the volcano-sedimentary rocks have undergone a thorough regional geological re-evaluation for mineral potential since being mapped by the Geological Survey of Canada in the late 1970s and early 1980s (Gabrielse *et al.*, 1980; Anderson 1983, 1984). Modern detailed bedrock mapping is essential to characterize time–space relationships of this arc segment, which will allow an improved assessment of the potential for mineralization, comparison with mineralized arc segments elsewhere, and integration with the airborne magnetic program. In addition, the project will provide supplementary databases including rock geochemical classification, magnetic susceptibility and geochronology. These data will integrate with regional stream geochemical survey data and airborne geophysics to ensure cost effective exploration targeting for porphyry-style mineralization.

In 2011, the British Columbia Geological Survey completed four field-based geology studies located within a 70 km radius of the Dease Lake community (Figure 1). The four components, which collectively make up the Dease Lake Geoscience Project are:

- Dease Lake regional bedrock mapping
- Hotailuh batholith: intrusive phases, ages and related mineralization
- Snow Peak pluton: age, emplacement and molybdenum mineralization
- Tsaybahe group: lithological and geochemical characterization of Middle Triassic volcanism.

DEASE LAKE REGIONAL BEDROCK MAPPING

The main component of the Dease Lake Geoscience Project consisted of systematic regional bedrock mapping of the Dease Lake (NTS 104J/08) and the east half of Little Tuya River (NTS 104J/07) map sheets, with the following objectives:

1) Publish 1:50 000 scale geological maps for NTS 104J/07 east half and 104J/08, a cumulative area of 1275 km^2, located immediately west of Dease Lake;
2) Determine U-Pb and $^{40}Ar/^{39}Ar$ ages for layered and intrusive rock units as well as mineralized rocks in order to constrain magmatic and mineralizing events;
3) Establish the geological controls on mineralization, and compare these with regional metallogenic epochs between 220 and 190 Ma [*i.e.* Late Triassic (Cu-Mo±Au), Late Triassic to Early Jurassic (Cu-Au-Ag) and Cretaceous to Tertiary (Cu-Mo-W)], related to alkaline and calcalkaline plutonism elsewhere in Stikinia;
4) Determine the history of magmatism, tectonism and mineralization in the Dease Lake transect for comparison to other parts of the Stikine magmatic arc system.

This paper reports the preliminary results of this field mapping. Bedrock mapping traverses were helicopter supported and completed by three 2-person mapping teams over the course of nine weeks between late June and August.

PREVIOUS WORK AND REGIONAL GEOLOGY

Kerr (1925; 1948) carried out the earliest geological bedrock mapping surveys in the area around Dease Lake. Systematic regional mapping by the Geological Survey of Canada began in 1956 with Operation Stikine, a reconnaissance mapping program covering four adjoining 1:250 000 map sheets in northwestern British Columbia (Geological Survey of Canada, 1957). Mapping and thematic studies conducted between 1956 and 1991 in the NTS 104I and 104J map areas are summarized by Gabrielse (1998). Most relevant to the current study is Anderson's work on the Hotailuh and Stikine batholiths (1983; 1984) and, more recently, 1:250 000 scale geological mapping of the Iskut River area (Anderson, 1993). Read of Geotex Consultants Ltd. (Vancouver, British Columbia) has conducted detailed mapping for the Geological Survey of Canada in the Stikine Canyon area (Read, 1983, 1984; Read and Psutka, 1990). Regional mapping projects by the British Columbia Geological Survey include work to the south by Ash *et al.* (1997) around Tatogga Lake and further west by Brown *et al.* (1996) in the Stikine River area.

The Dease Lake map area (NTS 104J/08, 07E) straddles the early Middle Jurassic thrust-imbricated boundary between the Cache Creek and Stikine terranes (Figure 2). The boundary between the terranes is marked by the south-vergent King Salmon fault (KFS). North of the KSF, the King Salmon allochthon (Cache Creek terrane) comprises oceanic basalt, siliciclastic rocks and limestone of Carboniferous to Early Jurassic age (Figures 2, 3). In places, the fault zone is marked by serpentinized ultramafic rocks and zones of listwanite alteration. The latter are dun to orange weathering foliated zones containing various amounts of chrome-rich mica, quartz veining and often pyrite.

The structurally lowest panel of the King Salmon allochthon consists of massive metabasite, tuff and limestone of presumed Carboniferous-Permian age. Structurally overlying this panel, to the west of the south

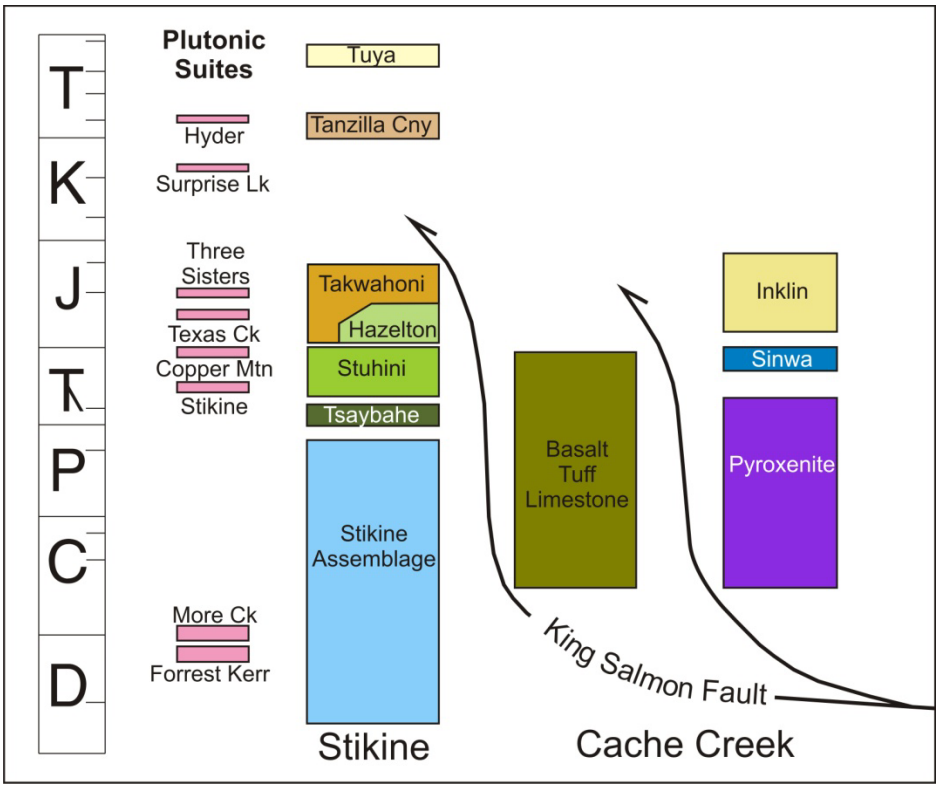

Figure 2. Schematic stratigraphic, plutonic and structural relationships for Stikine and Cache Creek terrane rocks within the map area (Abbreviations: Ck, creek; Cny, canyon; Mtn, mountain).

end of Dease Lake, are a large pyroxenite body and three west trending large outcrops of recrystallized massive limestone correlated with the Upper Triassic Sinwa limestone (Gabrielse, 1998). Apparently overlying these units are fine grained, foliated Jurassic clastic sediments of the Inklin Formation. The Inklin Formation underlies the northeastern part of the map area, which includes the southeastern margin of the Whitehorse Trough (Figure 2).

At this latitude, the Stikine terrane comprises three overlapping island arc successions; the Stikine assemblage, and the Stuhini and Hazleton groups that span 200 Ma from Devonian to Middle Jurassic. Their genetically related plutonic suites include the Devono-Carboniferous Forrest Kerr suite, the Late Triassic Stikine and Copper Mountain suites, the Early Jurassic Texas Creek suite and the Middle Jurassic Three Sisters suite (Anderson, 1983, 1993; Brown *et al.*, 1996; Logan *et al.*, 2000). These plutonic suites are the roots of cospatial arc rocks exposed along the Stikine arch, an east-trending area of uplifted Jurassic and older rocks that bound the northern margin of the Bowser Basin. Long-lived arc magmatism in the Stikine arch has produced diverse styles of magmatism (calcalkaline and alkaline) and large Cu–Au–Ag±Mo mineral deposits associated with some intrusive centres (*i.e.*, KSM, Snip [MINFILE 104B 004], Galore Creek, Schaft Creek and Kemess).

Paleozoic to Late Triassic sedimentary, volcanic and plutonic arc rocks of the Stikine terrane underlie the majority of the study area. Early Jurassic sedimentary rocks of the Takwahoni Formation overlie the Stikine terrane and comprise the immediate footwall to the King Salmon fault. An equidimensional latest Cretaceous/Palaeocene granodiorite body intrudes the Early Jurassic Takwahoni sedimentary rocks and columnar basalts of the Miocene to Pliocene Tuya Formation unconformably cap some of the highest peaks in the area. Preserved beneath these young basalts in the southwest corner of the map are lower Tertiary coal-bearing sedimentary rocks of the Tanzilla Canyon Formation.

Cache Creek terrane

MISSISSIPPIAN TO PERMIAN CACHE CREEK COMPLEX

Metabasalt, serpentinite, tuffaceous greenstone, limestone and minor chert comprise a fault bounded lozenge at the base of the King Salmon allochthon that extends 15 km east from Snow Peak pluton to Tatsho Creek. These rocks were assigned to the Cache Creek complex (Monger, 1975; Gabrielse, 1998). The trace of the northern faulted margin is marked by isolated outcrops of listwanite altered serpentinite along its length. The location of the southern fault is poorly constrained other than at its eastern end where it rejoins the northern fault and at its western end on the north-trending hillside east of Snow Peak pluton.

Dark green coloured, aphyric to locally fine pyroxene porphyritic, massive to weakly foliated metabasalt dominates the package. Vague pillowed forms were

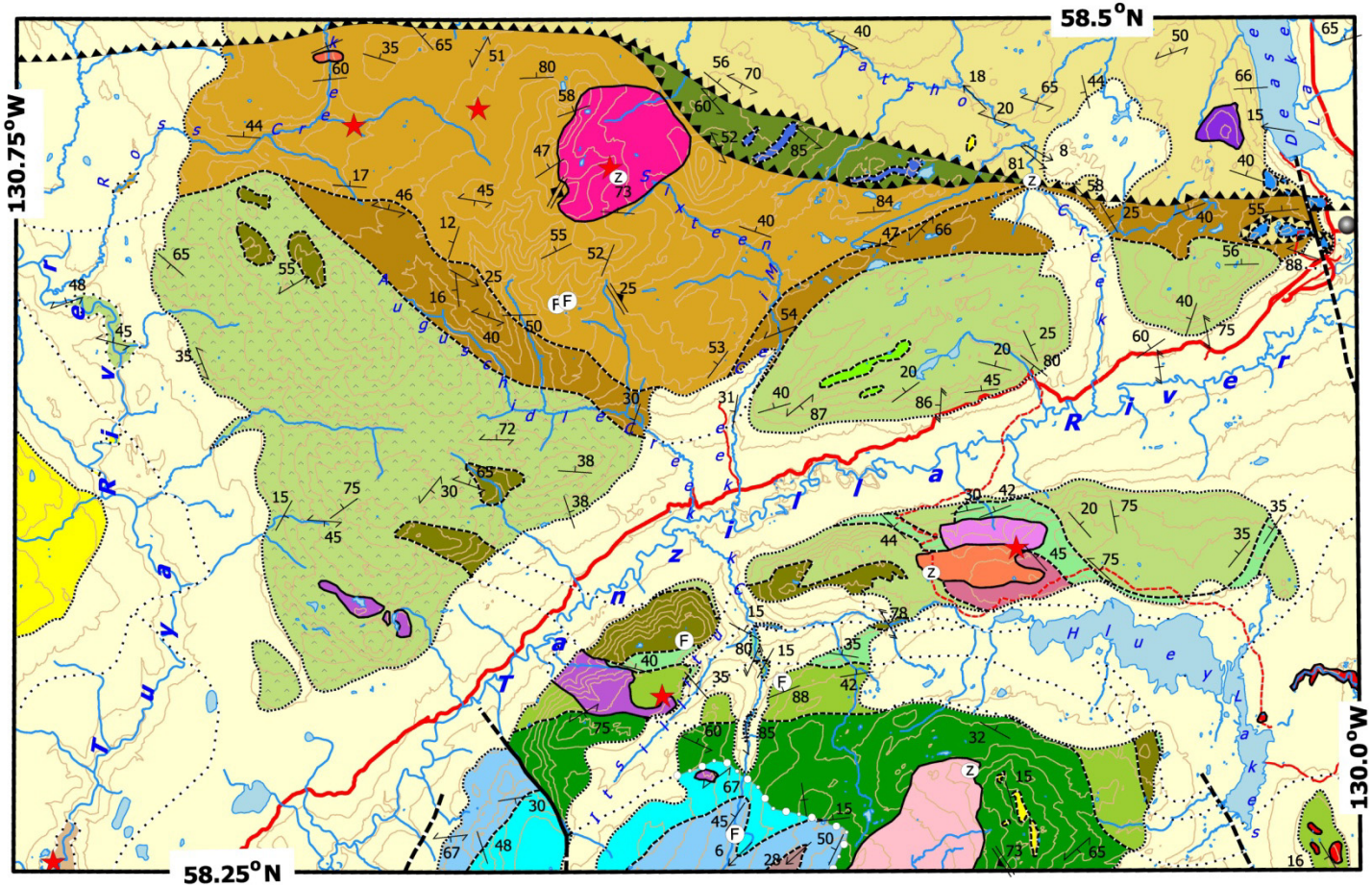

Figure 3. Generalized geology of the Dease Lake (NTS 104J/08) and east half of the Little Tuya River (NTS 104J/07E) map areas, including work by Ryan (1991) and Gabrielse (1998). Abbreviations: congl, conglomerate; sndst, sandstone; slstn, siltstone; mudstn, mudstone; crse, coarse; plag, plagioclase; px, pyroxene; brcc, breccia; xstl, crystal; hnbl, hornblende; qtz, quartz; bio, biotite; monzn, monzonite Symbols: F; fossil location, Z; U-Pb, zircon sample location.

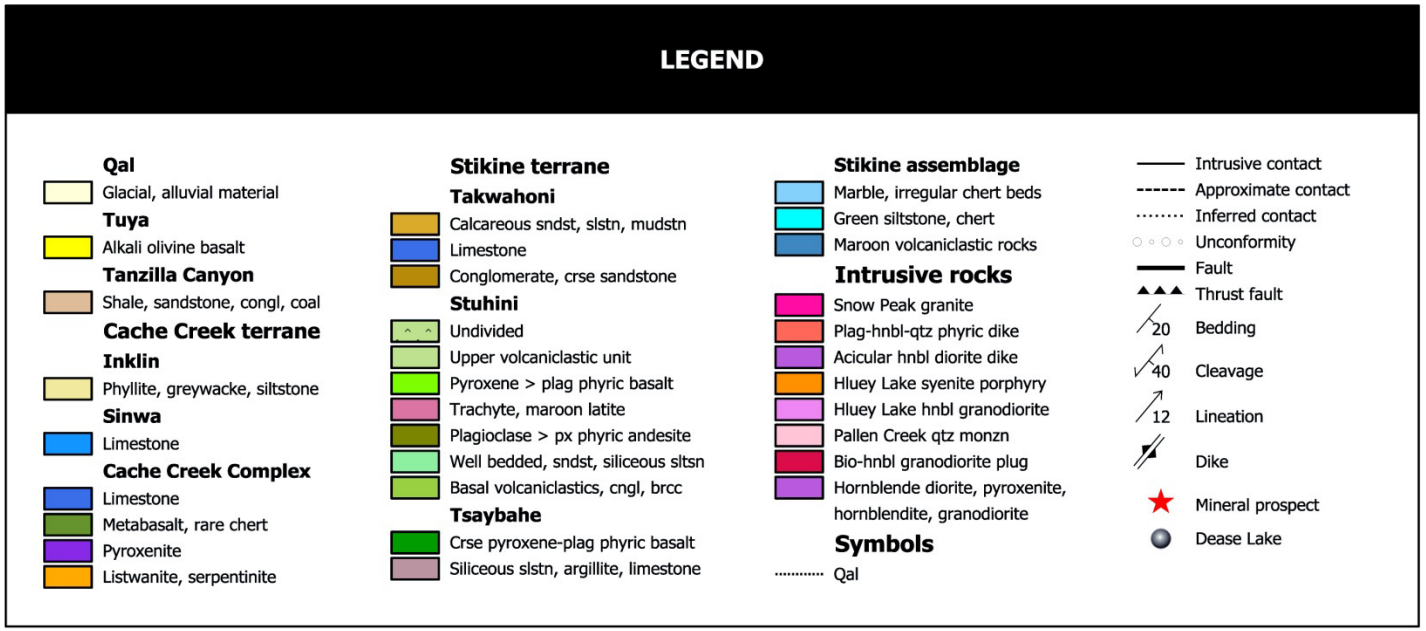

Figure 3. Continued.

noted. Locally pink-grey and black cherty alteration defined the margins of pillow tubes, but more often alteration masked the primary textures of the basalts. Commonly the metabasalt is microfractured and filled by chlorite, epidote, quartz, calcite, pyrite and locally hematite. Small bodies of dark green polished serpentinite are also present. The basalts are interleaved with schistose metavolcanics and greenstone which pass upwards into stratigraphically overlying limestone more than 50 metres thick. The limestone is medium bedded and recrystallized. It varies from white, grey to black and weathers smoke grey; it is thinly foliated and often layered with yellow weathering thin cherty horizons. Overlying the limestone and interlayered with it are thinly foliated, cherty lapilli to block mafic tuffs. These basalts are bleached, pyritized and silicified to a pale grey colour and comprise at least an 80 m-thick section which structurally overlies the limestone.

Whole rock chemical analysis from one sample of metabasalt plots in the subalkaline basalt field on major oxide and trace element rock classification diagrams and as a E-MORB on tectonic discrimination diagrams. Two limestone samples were collected and submitted to the Geological Survey of Canada, Vancouver for conodont extraction and identification. Results are pending.

LATE TRIASSIC SINWA FORMATION

The type section for the Sinwa Formation is 200 km northwest of Dease Lake in the Tulsequah map area (NTS 104K). There the Sinwa limestone is overlain by Lower Jurassic clastic metasedimentary rocks of the Inklin Formation in the hangingwall of the King Salmon Fault (Souther, 1971) and as such belongs to the Cache Creek complex. In the Dease Lake map area, Upper Triassic limestone designated as Sinwa Formation (Gabrielse, 1989) forms isolated high-standing white bluffs west of the community of Dease Lake. These limestones comprise two generally west-trending belts that are interpreted to be part of the Cache Creek complex and occupy a similar structural position above the King Salmon fault. The southernmost Sinwa limestone exposures are interpreted to represent a klippe of Cache Creek rocks preserved on top of the Takwahoni Formation conglomerates. Contact relationships between the Sinwa limestone and clastic rocks of the Inklin and Takwahoni formations in this area are equivocal. Alternate interpretations for the distribution of Late Triassic limestone outcrops south of the King Salmon fault are that they represent large olistostromes of Late Triassic Sinwa within the Takwahoni Formation or are Stuhini basement rocks. Thick accumulations of Stuhini limestone was not encountered during the present mapping so the latter interpretation is thought to be less likely.

In the Dease Lake map area, the Sinwa Formation consists of grey and white massive recrystallized limestone that weathers to a light grey or brownish colour. It forms large rounded, generally structureless massifs that locally are foliated and rarely thinly laminated. Typically, the limestone is a light brown amorphous rock cut by a dense stockwork of white calcite veinlets.

Few fossils have been recovered from the Sinwa Formation. However a hexacoral *Isastrea vancouverensis*, characteristic of the Upper Triassic Coral Reef Fauna of western North America was collected by Kerr approximately 2 km southwest of Dease Lake (Gabrielse, 1998).

EARLY JURASSIC INKLIN FORMATION

The Inklin Formation comprises interbedded phyllite and phyllitic greywacke, with minor limestone and conglomerate. It weathers recessively, and is only well exposed in stream cut-banks along Tatsho Creek, and along the shoreline of Dease Lake.

The phyllite is medium grey to black, and varies from homogeneous to laminated. It is well cleaved throughout, generally phyllitic, but slaty in places. Locally it contains concretions that are wrapped by the cleavage and limonitic spots are also abundant in places. Grey phyllite is generally non-calcareous, but there are some minor, cm-scale grey limy phyllite and banded argillic limestone layers.

The phyllitic greywacke, which is commonly calcareous, contains mostly sand-sized detrital grains wrapped by a wispy recrystallized phyllitic matrix. It is generally medium sand-sized, but coarser layers up to granule conglomerate are present. The greywacke is typically green-grey coloured and well cleaved, with abundant limonite spots. Graded bedding is locally developed and some of the coarser layers contain abundant black cm-scale mud rip-up clasts (Figure 4). Calcareous phyllitic greywacke locally contains abundant tremolite in clots up to 1 cm long. Tremolite is aligned parallel to the foliation and defines a mineral lineation. In rare instances, phyllitic greywacke contains lenses and thin continuous layers (up to 8 cm thick) of streaky white and grey recrystallized limestone.

Greywacke and phyllitic greywacke commonly form rhythmically layered sequences, with cm-scale alternations between the two rock types. In Tatsho Creek and at Dease Lake, the two rock types are present in roughly sub-equal proportions. Elsewhere, the unit is characterized by phyllite-rich intervals with subordinate greywacke. Phyllitic greywacke layers are typically 1-10 cm thick, but in rare instances greater than 1 m.

Age constraints for the Inklin are limited to areas as far away as Atlin Lake (NTS 104 N) where fossils of possibly Hettangain, but certainly Early Sinemurian to Late Toarcian ages have been identified (H.W. Tipper; in Gabrielse, 1998).

INTRUSIVE ROCKS

Ultramafic Rocks

West of the south end of Dease Lake there is a 2.2 km^2 ultramafic body of variably serpentinized, dun-

Figure 4. Lithologies in the Inklin Formation. a) Cm-scale alternations of dark phyllite and greenish coloured greywacke. b) Lenses of limestone within a calcareous greywacke (tremolite-bearing) layer.

weathering, chrome spinel-bearing peridotite. On weathered surfaces the peridotite is characterized by resistive equant pyroxene grains between 3 and 5 millimetres in a recessively weathering serpentine-altered olivine groundmass. The main body of peridotite is thoroughly serpentinized along its' southern margin and is cross cut by closely spaced orthogonal sets of serpentine veinlets throughout (Figure 5). Magnetic susceptibility values are 2 orders of magnitude higher (>100) on the serpentinized southern margin compared with those in the centre of the body, In thin section the rock contains 70-75% fractured and serpentine-altered subhedral olivine, large poikilitic orthopyroxene crystals characterized by deformation lamellae (25%) and approximately 5-10% subhedral clinopyroxene crystals. Large (1.0 mm) orange coloured idiomorphic crystals of spinel are conspicuous and form up to 1.5%.

In addition to peridotite, Gabrielse (1998) distinguished a coarse grained to pegmatitic unit of gabbro along the southeastern end of the intrusion, which also crops out along the lake shore as several small listwanite-altered exposures approximately 800 m north (Logan *et al.*, 2012b).

Figure 5. Serpentinized peridotite (Zn 9, UTM 437542E, 6480783N).

Serpentinite / Listwanite

A number of small ultramafic bodies occur along the trace of the King Salmon fault. These bodies, up to 100 m thick, consist of serpentinite that has been variably altered to listwanite. The listwanite comprises an orange weathered fine grained yellowish aggregate of white silica, talc, iron carbonate and diagnostic fuchsite that has replaced the primary mineralogy and textures of the protolith (Gabrielse, 1998). One of the best exposures of listwanite occurs where the fault crosses Tatsho Creek. At this location well-foliated listwanite in the hangingwall of the fault has been intruded by a nonfoliated hornblende-plagioclase porphyry dike with a preliminary U-Pb age of 155.2 ±1 Ma.

Stikine terrane

PERMIAN AND OLDER (?) STIKINE ASSEMBLAGE

The oldest rocks in the map area comprise Permian and older carbonate, siliceous siltstones and volcaniclastic rocks of the Late Paleozoic Stikine assemblage (Brown *et al.*, 1991; Gunning *et al.*, 1994; Logan *et al.*, 2000). They crop out within a northeast trending structural culmination in the southwest corner of the map area.

Maroon and light green coloured, foliated volcaniclastic rocks comprise the stratigraphically lowest unit beneath the Permian limestone. Fragments of vesicular, lapilli-size aphyric maroon basalt and intermediate plagioclase phyric andesitic basalt sit in a calcareous crystal-ash matrix. Overlying the volcaniclastic rocks is a section of pale grey, green and maroon siltstone and well bedded grey and black chert. Only a few outcrops of each of these units were encountered during mapping.

Thick accumulations of Paleozoic limestone are a diagnostic feature of the Early Permian sections of the Stikine assemblage in northwestern Stikine terrane. White and buff weathering, medium to thickly bedded limestone, thin to medium thickly bedded, buff-coloured

limestone with thin phyllitic partings, limestone with black or yellow chert nodules and interbedded chert layers form the west-facing cliffs above the Tanzilla River in the southwest corner of the map and in the headwaters of Itsillitu Creek (Figure 3). These lithologies are correlative with Early Permian Ambition Formation that crops out 140 km south in the type section at Scud River (Gunning *et al.*, 1994).

Fusulinid packstone from well bedded and deformed limestone outcropping near Itsillitu Creek were collected and submitted for identification to the Geological Survey of Canada, Calgary. The fossils were identified as schwagerinid fusulinaceans of Early or Middle Permian age and the limestone was correlated with the Ambition Formation (Bamber, 2011). Conodonts from this same limestone but collected approximately 700 m south of the map boundary (Geological Survey of Canada location C-87099) are Early Permian, Artinskian age (M. Orchard, in Gabrielse, 1998).

EARLY TO MIDDLE TRIASSIC TSAYBAHE GROUP

In the vicinity of the Stikine canyon, the "Tsaybahe group" (Read, 1984; Read and Psutka, 1990) was named informally for sedimentary and volcanic rocks characterized by abundant coarse pyroxene porphyry breccias and Early and Middle Triassic fossils. They distinguished it from the Stuhini Group which they characterized as being primarily sedimentary and Late Triassic in age. Subsequent workers (Gabrielse, 1998, Evenchick and Thorkelson, 2005) could not distinguished the volcanic and sedimentary rocks of the "Tsaybahe" from those of the Stuhini Group on a regional basis and therefore assigned all Triassic units to the Stuhini Group.

In this study we have retained the Tsaybahe nomenclature as defined by Read (1984) to include a two-fold sedimentary package and an overlying characteristic coarse grained crowded pyroxene porphyry breccia unit. The sedimentary packages consist of a siliceous siltstone, argillite and limestone unit and overlying pyroxene and plagioclase crystal-rich volcanic sandstone and siltstone unit. These are intruded by pyroxene porphyritic dikes and sills, and abruptly overlain by coarse breccias of the same composition.

Tsaybahe Sedimentary Rocks

Dark grey chert and interbedded siliceous argillite overlie Early Permian limestone in a southwest plunging, west dipping overturned syncline centered on the southern boundary of the study area (Figure 3). Fossil control is lacking but the lithology and stratigraphic position suggest that these sediments are likely Early-Middle Triassic Tsaybahe sedimentary rocks. They include deformed, grey and purplish coloured, 10 cm-thick bedded chert separated by 2 cm thick cleaved mudstone and siltstone beds. Along strike are purple slates, rusty fine sandstone and chert interbedded with thinly laminated green limestone.

Limestone was sampled and submitted to the Geological Survey of Canada, Vancouver for conodont extraction and identification; results are pending.

Tsaybahe Volcanic Breccias

Unconformably overlying the foliated limestone, chert and metavolcanic rocks of Late Paleozoic age and the lower chert and siliceous argillaceous sedimentary units are coarse pyroxene volcaniclastic and breccia units of the Tsaybahe. This unit is characterized by thick accumulations (200-270 m), of crowded augite porphyritic basalt breccia and volcanic-derived clastic rocks exposed at the tops of the ridges in the southern part of the map. In hand sample the rock contains 3-5 mm, dark green euhedral pyroxene phenocrysts (20-30%) and 1-2 mm, stubby white plagioclase laths (5-20%) within an aphanitic, often vesicular or amygdaloidal green or orange-weathering matrix (Figure 6).

Early work on adjoining map sheets to the south (Read, 1983 and 1984) reported Early and Middle Triassic paleontologic ages from cherty sedimentary rocks and from limestone horizons within coarse pyroxene breccia units of the "Tsaybahe group". However, no direct age constraints are known for the pyroxene breccias in the current study area.

LATE TRIASSIC STUHINI GROUP

A volcaniclastic dominated sequence of mafic to intermediate volcanic rocks assigned to the Late Triassic Stuhini Group underlies the central third of the study area. They overlie, apparently unconformably, the Early to Middle Triassic sedimentary and volcanic rocks of the Tsaybahe group to the south and are overlain unconformably (?) by quartz-bearing polylithic conglomerates and sandstones of the Early Jurassic Takwahoni Formation to the north.

The Stuhini Group in the study area is dominated by coarse to medium grained, massive to medium bedded volcaniclastic rocks (>60%), roughly equal proportions of augite dominated (10%) and plagioclase dominated (10%)

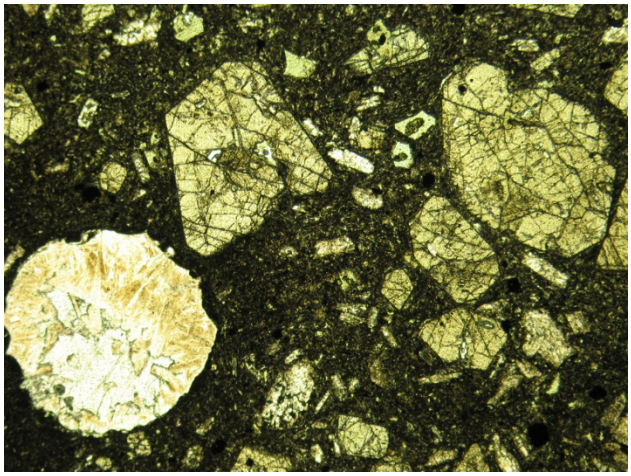

Figure 6. Photomicrograph of vesicular crowded pyroxene porphyritic basalt. Field of view = 3 mm. Plane-polarized light.

coherent flows and breccias with the remainder comprising fine grained siliceous siltstone and sandstone (10%) and an areally restricted unit of trachyte, and maroon latite. The units trend generally west to northwesterly, dip and face to the north. Because cleavage development and major folding was not observed, the succession is assumed to young northwards.

The Stuhini Group has been subdivided into six map units. From oldest to youngest these are: (1) a basal volcaniclastic unit of mixed, massive to thickly bedded reworked volcanic rocks and rare basalt flows that generally fine upwards into, (2) a well-bedded section of sandstone-siltstone with Upper Triassic (?) bivalves. Units 1 and 2 are overlain by, (3) a thick package of coarse plagioclase porphyritic andesitic basalt flows and subordinate clastic rocks and (4) isolated, thin units of alkalic, sparse K-feldspar phyric latite and maroon basalt. Unit 5 is pyroxene±plagioclase porphyritic monomict flow breccia and rarely pillowed basalt that are interlayered within, (6) an upper unit of massive volcaniclastic rocks containing plagioclase and pyroxene-phyric basalt clasts.

Unit 1 - Basal Volcaniclastic Rocks

Reworked volcaniclastic units derived from mafic to intermediate volcanism comprise the basal and the uppermost units of the Stuhini Group in the map area. Pale orange weathering, volcaniclastic deposits of the basal unit are exposed in a narrow west-trending belt north of the crowded pyroxene breccias of the Tsaybahe group. This unit includes thick, massive clast and matrix-supported lapilli and block breccias containing abundant clasts of green pyroxene porphyry, with sparse clasts of maroon pyroxene porphyry and pale grey limestone. These coarse deposits, which are typically 1-10 m thick are interlayered with volcanic granule conglomerates, 30 cm thick volcanic sandstone layers and rare thin layers (<10 cm) layers of well bedded fine-grained sandstone/siltstone. Clasts and matrix are almost identical in their composition. Parts of the unit are dominated by thick (1-3 m) beds of weakly graded granule conglomerate to medium grained volcanic sandstone, which comprise almost exclusively of fresh detrital pyroxene and plagioclase crystals.

Unit 2 - Well-Bedded Sandstone-Siltstone

Gradationally overlying the basal volcaniclastic unit are green, grey and black coloured, medium bedded to thinly laminated volcanic sandstone, siliceous siltstone and siliceous tuff. This generally fining upwards sequence of epiclastic volcanic material is characterized by its overall well-bedded nature, relative continuity and ~400 m thickness. The rocks display normal grading in the sandstone-siltstone couplets and load casts that indicate the north-dipping section is upright facing. Parallel, planar bedding laminations characterized the finer grained units. On the ridge above Tanzilla River the well-bedded section is cut by pyroxene porphyry and plagioclase porphyry dikes oriented roughly orthogonal to bedding. Similar fine grained bedded horizons occur throughout the Stuhini section but are typically only 1-10s of metres thick, discontinuous or display chaotic bedding attitudes suggestive of slumping. A particularly thick and continuous horizon of these fine grained, well bedded rocks within the upper volcaniclastic rocks of unit 6 is exposed along the Hluey Lake Road (Figure 3).

Unit 3 - Plagioclase Porphyritic Basalt

Orange weathering massive outcrops of plagioclase-phyric basalt define a 2 km wide westerly trending belt separating the basal volcaniclastic units from the upper volcaniclastic unit. The unit can be traced from south of Hluey Lakes into Hluey Creek, across the Tanzilla River and in isolated outcrops another 10 km northwest towards the Stuhini-Takwahoni unconformity (Figure 3). The basalts contain abundant white to cream coloured, 2-8 mm euhedral plagioclase phenocrysts, sometimes glomeroporphyritic, in a fine grained green matrix (Figure 7). Intergrown plagioclase and clinopyroxene form the matrix, and sparse pyroxene phenocrysts are also locally present. Minor interlayers of reworked pyroxene porphyry breccia are also contained within this unit. The plagioclase porphyry flows are generally coherent, unlike fragment-rich breccia deposits of the monolithic pyroxene porphyries elsewhere.

Immediately south of Ross Creek is a distinctive trachytic plagioclase porphyritic basalt characterized by glassy 4-7 mm euhedral plagioclase crystals (5-7%) within a very fine grained dark matrix that locally is glassy green and characterized by spherulitic devitrification textures. This unit was collected, and submitted for U-Pb, zircon age dating but did not contain sufficient zircons.

Unit 4 - K-feldspar Porphyritic Latite

A distinctive package of salmon pink weathering porphyritic latite, trachyte, and maroon weathering basalt and epiclastic rocks crop out northwest of Hluey Lakes along the Hluey Lake service road adjacent to the pink weathering syenite porphyry. Unit 4 rocks comprise the

Figure 7. Plagioclase porphyry basalt (Zn 9, UTM 417135E, 6464463N).

immediate country rock to the monzosyenite and (?) granodiorite phases of the Hluey Lake pluton. The rocks are characteristically potassic and mineralogically similar to the intrusive syenite phase of the pluton (Figures 8a, b). They include maroon-coloured basalt/latite with abundant calcite-filled vesicles, and phenocrysts of plagioclase, K-feldspar and biotite in an aphanitic matrix.

Porphyritic flows contain sparse mm-scale K-feldspar and biotite phenocrysts that locally display trachytic flow textures in the pink to brown coloured aphanitic matrix. The maroon rocks surrounding the Hluey Lake syenite are friable and variably altered by introduction of potassium and iron carbonate likely from the syenite. It is uncertain whether the alkaline character of these rocks is primary and they are extrusive equivalent rocks to the intrusion or can be attributed entirely to alteration from the syenite. Orthoclase and biotite porphyritic breccias/diatremes are well known Upper Triassic porphyry Cu-Au mineralized intrusive centres in this part of Stikinia (Logan *et al.*, 2000).

Unit 5 - Coherent Pyroxene Porphyritic Basalt

Pyroxene porphyritic basalt flows, breccias and volcaniclastic rocks are the hallmark of the Stuhini Group in northwestern Stikinia (Souther, 1971, 1972; Anderson, 1993; Gabrielse, 1998; Logan *et al.*, 2000) and these rock types are widely developed in the study area. Coherent flow units are often complexly interlayered with identical coarse pyroxene porphyritic clastic and reworked epiclastic units and could generally not be mapped separately. Where distinguished, single flow units are commonly from 5 to 12 m thick, with massive interiors and flow top breccias. Basalt types include; those with subequal amounts of pyroxene and plagioclase phenocrysts to those which contain pyroxene >>plagioclase phenocrysts. The former is characterized by typically quite small (~1-2 mm), sub-equal proportions of green or black pyroxene and white plagioclase laths in a fine grained green matrix. The pyroxene porphyry flows consists of typically 2-8 mm euhedral augite phenocrysts in a fine grained green matrix.

Unit 6 - Pyroxene and Plagioclase-Phyric Volcaniclastic Rocks

A ~450 m thick sequence of orange weathering pyroxene and plagioclase porphyry clast-dominated volcaniclastic succession with minor basalt flows underlies the area east of Sixteen Mile Creek and north of the Tanzilla River. Massive, cliff-forming units of chaotic, non-graded matrix-supported cobble to pebble-size volcanic conglomerate comprise the majority of outcrops (Figure 9). Metre-thick beds of pyroxene and plagioclase crystal-rich sandstone and siltstone occur throughout the package, as evidenced by bedding measurements (Figure 3). Many of the sandstones contain fresh, euhedral vitreous pyroxene and plagioclase crystals, making some of them difficult to distinguish from igneous rocks. Pyroxene porphyry basalt flows of unit 5 comprise a minor component of the section. The pyroxene phenocrysts within the porphyry clasts and fragments which dominate the volcaniclastic units are commonly 4-8 mm and much coarser than the 1-2 mm pyroxene phenocrysts in many of the porphyry flows.

The Stuhini rocks in the Dease Lake and Little Tuya River map areas form part of a continuous belt that is poorly dated and occupy the northern flank of the Stikine arch (Gabrielse, 1998). Correlative lithologies exposed in the Stikine River to the south indicate Late Triassic, Carnian to Norian ages (Read, 1983; 1984). Two new macrofossil collections from the basal volcaniclastic and the well bedded siliceous siltstone units within the map area contain *Spiriferinid* brachiopod (?) and *Posidoniid* bivalves, probably *Halobia* that suggest a probable Late Triassic, but possibly as old as Middle Triassic age (Poulton, 2011). A single detrital zircon sample was collected from medium-grained sandstone of the upper Stuhini volcaniclastic member exposed along the Hluey Lake road. Results are pending. In addition, limestone horizons were collected for conodont studies and age determinations from unit 1 and unit 2. These have been submitted to the Geological Survey of Canada, Vancouver for identification.

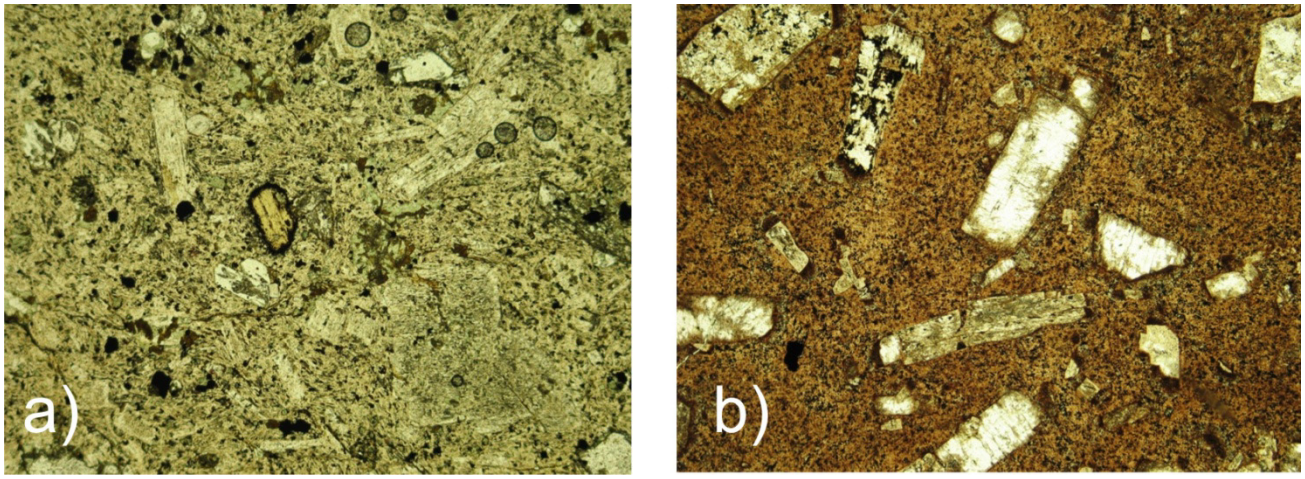

Figure 8. Photomicrographs of a) Maroon basalt/latite of Stuhini Unit 4 with phenocrysts of plagioclase, K-feldspar and biotite in an aphanitic matrix. b) K-feldspar, biotite porphyritic monzosyenite of Hluey Lake pluton. Field of view = 3mm. Plane-polarized light.

Figure 9. Weakly stratified matrix-supported augite porphyry volcanic clast-dominated conglomerate of Unit 6, upper volcaniclastic rocks, Stuhini Group (Zn 9, UTM 433593E, 6467919N).

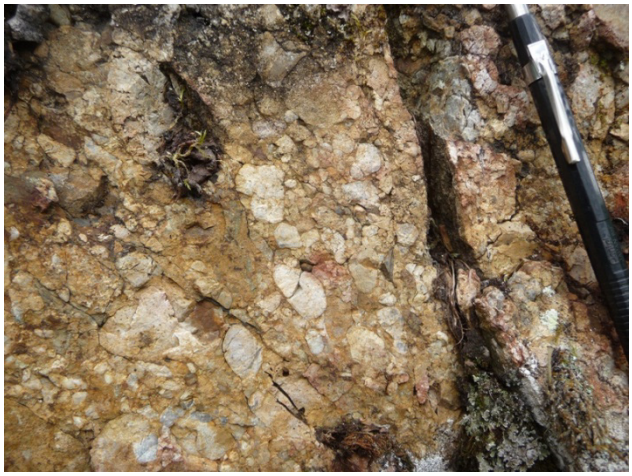

Figure 10. Well rounded, poorly sorted quartz, granitic and aphyric chert grey and green volcanic granule conglomerate of the Takwahoni Formation (Zn 9, UTM 433563E, 6478435N).

EARLY JURASSIC TAKWAHONI FORMATION

Clastic sedimentary rocks assigned to the Takwahoni Formation underlie an east trending and narrowing belt in the northern part of the map area that apparently pinches out against the Gnat Pass fault at the community of Dease Lake. East of the fault, the section comprises a five km wide belt of rocks that has been traced southeastward for more than 90 km (Gabrielse, 1998). In both cases these rocks occupy the immediate footwall to the King Salmon thrust fault.

The Takwahoni Formation consists mainly of an upper dark grey fine-grained sandstone-siltstone unit, and a lower coarse grained conglomerate-dominated unit with subordinate sandstone and siltstone layers. These are locally separated by a narrow discontinuous grey micritic limestone and orange brown weathering calcareous sandstone units.

The structural and stratigraphic lowest Takwahoni rocks are massive clast and matrix-supported polylithic conglomerate and coarse feldspathic, quartz-bearing sandstone that overlie volcaniclastic rocks of the upper Stuhini Group. The conglomerate forms positive topographic relief and cliff exposures within Auguschilde and Sixteen Mile creek drainages. It is generally polylithic with cobble to pebble-sized clasts of coarse-grained granite, hornblende quartz porphyry, aphyric grey and green volcanic rocks, argillite, chert and recrystallized limestone (Figure 10). Some of the clasts contain evidence for ductile deformation prior to their deposition.

In general, the sandstones are well sorted arenaceous rocks dominated by feldspar and variable amounts of quartz and lithic clasts and carbonate, clay and silica cement. In many rocks in the lower part of the formation quartz is a minor constituent. Thick bedded sandstones display sharp upper and lower planar contacts with 1-2 cm thick alternating parallel laminated pale grey-green and black siltstone and mudstone. Primary sedimentary structures within the latter include load casts, flaser bedding, cross and wavy laminated bedforms, and contorted bedding. Subordinate beds of granule to cobble conglomerate within the sandstone contain subrounded to subangular clasts of granite, limestone, volcanic clasts, laminated black mudstone chips, vein quartz, and sparse very fine grained, emerald-coloured clasts. Some of the conglomerate has a limy matrix.

Thermally altered fine clastic rocks comprising the upper Takwahoni Formation display a mauve coloration and locally contain fine shreds of secondary biotite, with cordierite developed adjacent to the Snow Peak pluton (see Moynihan and Logan, this volume).

An Early Jurassic age for the Takwahoni Formation is provided by a rich ammonite fauna of Sinemurian age contained within a basal conglomerate and shale-tuff unit located east of the McBride River (Tipper, in Gabrielse, 1998). Overlying this unit is a younger succession of interbedded greywacke and shale, with thin interbeds of polylithic pebble conglomerate of Pliensbachian age (Tipper, 1978). Limestone clasts collected from nearby but separate locations in the Takwahoni Formation approximately 5 and 5.1 km south of Snow Peak contain ichthyoliths and conodonts of Late Triassic, Norian age that have been correlated with the Sinwa Formation (Orchard, in Gabrielse, 1998). A single detrital zircon sample was collected from the coarse conglomerate member of the basal Takwahoni Formation exposed in Sixteen Mile Creek. Results are pending.

EOCENE TANZILLA CANYON FORMATION

Poorly consolidated Lower Tertiary sedimentary rocks of the Tanzilla Canyon Formation crop out in the southwestern corner of the map along the Tuya and Little Tuya rivers and further south along the Tanzilla River (Ryan, 1991; Gabrielse, 1998). The sediments are poorly consolidated conglomerate, sandstone and mudstone that comprise a stratigraphic section approximately 500-600 m

thick. The lower 200-300 m consists of mudstones and sandstones in the west and sandstones and chert-pebble conglomerate in the east and contains high volatile B bituminous coal in a seam 5-30 m thick. The lower unit is overlain by an upper unit at least 300 m thick of volcanic pebble-conglomerate, sandstone and volcanic rocks (Ryan, 1991).

Palynology (Vincent, 1979; De Nys, 1980) indicates the coal-bearing rocks as not younger than Early Eocene and no older than Paleocene (Ryan, 1991) which is age equivalent to the Brothers Peak Formation of the Sustut Group (Eisbacher, 1974). However, due to the fault-controlled nature of the basin (Tuya basin) and its' locally derived sediment, Yorath (1991) assigned these rocks to the Sifton assemblage.

MIOCENE–PLEISTOCENE TUYA FORMATION

The map area abuts against the eastern flank of the Miocene to Pleistocene Level Mountain shield volcano. Isolated outcrops of alkali basalts associated with this edifice crop out along the Tuya River and overlie one of the highest peaks in the southern part of the map area. In the latter area, the basalt is distributed across the peak in six isolated outcrops. It varies from 50-75 m thick and is columnar jointed with vertical to reclined dipping orientations (Figure 11). The basalt is grey to brown and contains mm-size phenocrysts of yellowish green olivine and vitreous plagioclase phenocrysts within a fine grained plagioclase, pyroxene, olivine-rich trachytic matrix. Whole rock chemical analysis from a sample of columnar basalt plots in the alkali basalt field on major oxide and trace element rock classification diagrams.

Whole rock potassium-argon ages for the Level Mountain volcanic rocks range from 14.9 to 5.3 Ma (Hamilton, 1984; in Gabrielse, 1998).

Intrusive rocks

Regionally, three distinct plutonic suites comprise the Hotailuh batholith (Anderson, 1983) and characterize

Figure 11. Columnar basalts of the Miocene to Pliocene Tuya Formation. View towards west from 6 km southwest of Hluey Lakes on top of repeater hill (Zn 9, UTM 431065E, 6458474N).

magmatism along the Stikine arch (Anderson, 1984; van Straaten *et al.*, this volume). They include the Late Triassic Stikine (Cake Hill, Beggerlay Creek and Gnat Lake plutons), the Early Jurassic Texas Creek (McBride River pluton) and the Middle Jurassic Three Sisters (Three Sisters pluton, Anderson, 1983; Anderson and Bevier, 1990) suites. The ~2300 km^2 Hotailuh batholith adjoins the southeast corner of the map area and many of the small satellite plutons that intrude the mainly Late Triassic arc stratigraphy in the Dease Lake map area are thought by corollary to have ages similar to these three main plutonic suites.

Preliminary U-Pb crystallization ages for the Pallen Creek pluton attests to this but ages for the Hluey Lake pluton and a hornblende plagioclase porphyry dike that cross cuts the King Salmon Fault returned ages that are not commonly reported from the Stikine arch. These preliminary ages were acquired by Laser Ablation ICP-MS analyses of zircons at the University of Washington (pers. comm., Paul O'Sullivan, 2011). Complete data sets, techniques and finalized ages will be reported elsewhere.

LATE TRIASSIC

Late Triassic ultramafic, mafic and granitic rocks of the Gnat Lakes, Beggerlay and Cake Hill plutons comprise the majority of the Hotailuh batholith (*e.g.* van Straaten *et al.*, this volume). However, Late Triassic intrusive rocks have not been recognized in the current study area.

EARLY JURASSIC (?)

A series of small to medium sized mafic intrusions define a 16 km long southeast trending corridor that straddles the Tanzilla River approximately 30 km southwest of the community of Dease Lake. The intrusions vary in size from less than 0.5 to 6 km^2 in area. They are coarse to medium grained bodies comprised of pyroxenite, hornblende gabbro or more often diorite to monzodiorite that locally was intruded and veined by leucocratic hornblende monzonite to granodiorite phases. A similar mafic-ultramafic dike is intruded into the Takwahoni Formation west of Snow Peak. The largest body crops out on a north-facing slope above the Tanzilla River. This unit has some of the highest magnetic susceptibility measurements in the map area and a mean value of 92.6 ±43 x 10^{-3} S.I. units.

Hornblende separates from the diorite have been submitted to Pacific Centre for Isotopic and Geochemical Research (PCIGR) at the Department of Earth and Ocean Sciences, University of British Columbia for $^{40}Ar/^{39}Ar$ step-heating analyses to determine cooling ages of the intrusion. Results are pending.

MIDDLE JURASSIC

The Pallen Creek pluton is a homogeneous biotite-hornblende-quartz monzonite to monzodiorite locally containing K-feldspar megacrysts (Anderson, 1980; this

study). The northwest (this study) and northeast (Anderson, 1980) sides of the pluton are characterized by a more mafic, hornblende diorite marginal phase that is intruded by the main quartz monzodiorite phase. The main quartz monzonite unit has moderate magnetic susceptibility measurements with a mean value of 32.5 ±3.4 x 10^{-3} S.I. units.

K-Ar cooling ages from hornblende (197 ±18 Ma and 165 ±8 Ma) and from biotite (145 ±7 Ma) have a substantial range (Wanless *et al.*, 1972; Stevens *et al.*, 1982), but a new U-Pb crystallization age determined by Laser Ablation ICP-MS analyses of zircons from a sample of K-feldspar porphyritic biotite hornblende monzodiorite taken at the north end of the pluton gave a Middle Jurassic, Bajocian age of 173.6 ±0.7 Ma (personal communication, Paul O'Sullivan, 2011). This age suggests that the Pallen Creek pluton is part of the Three Sisters plutonic suite.

EARLY CRETACEOUS

A 4 by 2 km east trending composite intrusion located northwest of Hluey Lakes on the north-facing cliffs above the Tanzilla River was described by Gabrielse (1998) and grouped with the Early to Middle Jurassic plutonic rocks of the region. The Hluey Lake pluton is a composite body comprised of at least two main lithologies. A medium grained homogeneous biotite hornblende granodiorite with minor inclusions of hornblende diorite comprises the older northern part of the pluton. It is equigranular, locally weakly foliated (eastern exposures) and consists of 2 mm subhedral white plagioclase, interstitial K-feldspar, euhedral 2-4 mm hornblende crystals and anhedral crystal aggregates of biotite. Magnetite is common and accompanies mineralization and alteration.

Intruding the granodiorite and comprising the southern portion is a pink weathering monzonite to syenite porphyry. The potassic phase comprises massive, equigranular (2-4 mm) phases and K-feldspar ±plagioclase and biotite porphyritic (5-10 mm) phases characterized by a fine-grained salmon pink K-feldspar matrix (Figures 8, 12). Aligned plagioclase and K-feldspar phenocrysts locally define trachytic textures in the porphyry. Abundant fine-grained dikes (?) with sparse K-feldspar phenocrysts intrude the hornblende diorite. This unit has moderate magnetic susceptibility measurements with a mean value of 33.4 ±22.8 x 10^{-3} S.I. units.

The K-feldspar biotite porphyritic monzonite was collected and submitted for isotopic age determinations. Preliminary Laser Ablation U-Pb zircon geochronology suggests there are two separate age populations. The majority of the zircons (n=45) gave a Middle Jurassic, Bathonian age of 164.9 ±0.8 Ma, similar to dating by van Straaten (this volume) of the Three Sisters potassic phase. However, 10% of the data (n=5) indicate a separate thermal event in the Early Cretaceous *ca.* 127.7 ±2.0 Ma (personal communication, Paul O'Sullivan, 2011).

Figure 12. Pink K-feldspar, plagioclase, biotite porphyritic monzosyenite of Hluey Lake pluton. Salmon pink matrix comprised of fine grained matrix K-feldspar. Note rounded monzodiorite xenolith.

Biotite from the monzonite has been submitted to PCIGR at the Department of Earth and Ocean Sciences, University of British Columbia for $^{40}Ar/^{39}Ar$ step-heating analyses to determine the cooling age of this phase. Results are pending.

LATE CRETACEOUS TO EARLY PALEOCENE

The Snow Peak pluton is a steep sided 15 km^2 equidimensional body that was intruded into Early Jurassic rocks of the Takwahoni Formation in the Late Cretaceous/Palaeocene (Gabrielse, 1998; Moynihan and Logan, this volume). The intrusion is a biotite hornblende monzodiorite to granodiorite with equigranular and locally K-feldspar porphyritic textures. Molybdenum mineralisation is developed along west-northwest trending brittle fracture planes in the central part of the pluton. A conspicuous, rusty weathering contact metamorphic aureole developed within the slate, siltstone and sandstone of the fine-grained member of the Takwahoni Formation. This hornfelsed zone extends for 2-3 km outwards from the contact of the intrusion coincident with a roughly circular magnetic high on the first vertical derivative magnetic map.

Magnetic susceptibility measurements of samples from the Snow Peak pluton indicate two populations. The higher readings have a mean value of 28.3 ±6.9 x 10^{-3} S.I. units and the lower population a mean value of 1.3 ±0.01 x 10^{-3} S.I. units. The variability has no spatial association or zonation.

A K-Ar cooling age of 73.5 ±4.2 Ma for hornblende from the Snow Peak granite was reported by Stevens *et al.* (1982). A sample collected during regional mapping has a Laser Ablation U-Pb zircon crystallization age of 64.4 ±0.5 Ma as reported by Moynihan and Logan (this volume).

MINOR HYPABYSSAL PLUTONS AND DIKES

Metre-wide, mafic pyroxene±plagioclase and bladed plagioclase±pyroxene porphyry dikes and acicular hornblende porphyry dikes intrude stratified rocks as young as late Triassic. The acicular hornblende porphyry dikes are preferentially oriented northwesterly.

A cream to white coloured, crowded biotite plagioclase porphyry plug is exposed along Ross Creek in the northwest corner of the map. It is a medium grained locally porphyritic biotite quartz diorite (Gabrielse, 1998). Mineralogically it is similar and probably genetically related to the hornblende-plagioclase±quartz porphyritic dike swarm that cross cut the Takwahoni sedimentary rocks in the area. The biotite phenocrysts have been altered and replaced by chlorite and the plagioclase intensely sericitized.

Quartz-hornblende-plagioclase porphyry (QFP) dikes and sills crosscut folded and penetratively deformed sedimentary rocks of the Takwahoni Formation in the vicinity of Snow Peak (Moynihan and Logan, this volume). Field relations indicate that the dike swarm is crosscut by the Early Paleocene Snow Peak pluton and is therefore older than 64.4 ±0.5 Ma. A lower age constraint for emplacement of these post-tectonic dikes is evident in Ross Creek where they can be seen crosscutting footwall Takwahoni Formation and hangingwall serpentinite of the King Salmon Fault. Southwest-directed motion was active between early Toarcian and middle Bajocian (Tipper, 1978), suggesting intrusion was after ~170 Ma.

Similar white weathering hornblende-bearing quartz plagioclase porphyries are located in the eastern portion of the map area. At one location well-foliated listwanite in the hangingwall of the fault has been intruded by a nonfoliated hornblende-plagioclase porphyry dike with a preliminary U-Pb age of 155.2 ±1 Ma (personal communication, Paul O'Sullivan, 2011).

STRUCTURE AND METAMOPRPHISM

The King Salmon fault is the dominant structure in the area, oriented approximately east it marks the boundary between the Cache Creek and Stikine terranes. The trace of the fault is marked by a number of small ultramafic bodies (listwanite and/or serpentinite) that range in size from 10s to 100s of metres. Rocks to the north of the KSF are penetratively foliated and have undergone extensive metamorphic recrystallization. Actinolite+epidote+plagioclase assemblages in metabasite suggest greenschist facies conditions during deformation.

In contrast, penetrative fabrics are only sporadically developed in Mesozoic units to the south and the rocks have not been fully metamorphically recrystallized. In general, rocks retain their primary volcanic/sedimentary textures, with metamorphic mineral growth restricted to grain boundaries, veins and heavily altered areas. Epidote-quartz veins are widespread and mafic phenocrysts have been variable replaced by epidote and/or chlorite.

Structures in each of the units are described below, in order of decreasing age. Equal area lower hemisphere stereonet projections of the structural data from the Paleozoic Stikine assemblage, Tsaybahe/Stuhini groups, Takwahoni and Inklin formations is presented in Figure 13.

Paleozoic Rocks/Lower Tsaybahe sediments

Southwest-trending folds are outlined by Paleozoic stratigraphy in the area west of the Pallen Creek pluton. The Paleozoic rocks are penetratively deformed, with a northwest-dipping foliation and southwest plunging stretching lineation. Locally, the foliation is overprinted by Z-folds with southwest-plunging axes (Figure 14). These minor folds may be parasitic with respect to larger structures but this was not definitively established. The map-scale folds appear to be truncated by the Paleozoic-Tsaybahe Group unconformity and overlying rocks are not penetratively deformed.

Stuhini Group

Bedding in the Stuhini Group dips predominantly north (Figure 13b), but like the overlying Takwahoni Formation, bedding and stratigraphic contacts are affected by map scale, upright, north-trending folds. Penetrative fabrics are almost completely absent from rocks of the Stuhini Group, though in rare instances a semi-penetrative, north dipping scaly fabric was observed in fine grained volcaniclastic rocks.

Takwahoni Formation

Rocks belonging to the Takwahoni Formation are generally unfoliated, but a mostly north dipping phyllitic foliation is locally developed in fine grained and limy lithologies. In a conglomerate close to the base of the formation, limestone clasts are also flattened parallel to the matrix foliation.

Bedding dips approximately towards the north (NW to NE), but there is considerable variation due to the effects of two phases of folding (Figure 13c). The first phase produced folds trending roughly east, but these have only been observed in the northern part of the formation around Snow Peak (Moynihan and Logan, 2012).

Second phase folds trend approximately north, have steeply dipping axial planes and are generally gentle-open. Metre-scale folds are locally evident (Figure 15), but this fold generation manifests itself primarily in map-scale deflections of bedding and stratigraphic contacts with fold wavelengths of 100s of metres to several kilometres (Figure 3).

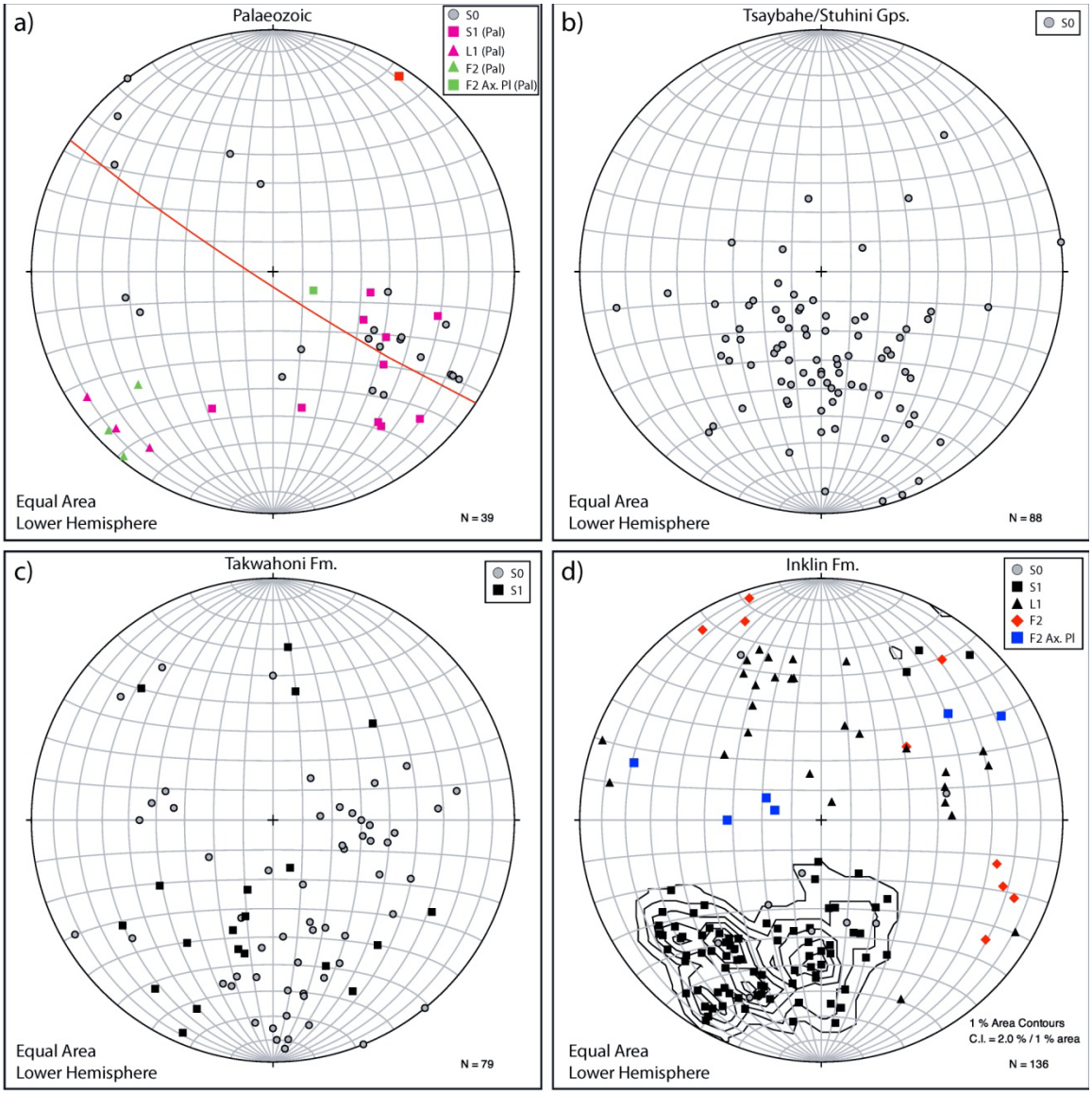

Figure 13. Equal area lower hemisphere stereonet projections of structural data from the Dease Lake and Little Tuya River map areas. a) Paleozoic Stikine assemblage rocks, b) Tsaybahe/Stuhini groups, c) Takwahoni Formation, d) Inklin Formation. The labels S_1(Pal) *etc.* refer to structures that are restricted to Palaeozoic rocks. In a), L_1(Pal) includes intersection and stretching lineations. In d), L_1 includes minor fold axes and intersection lineations.

Inklin Formation

A penetrative tectonic fabric is well developed throughout the Inklin Formation (Figure 13d). Cleavage (S_1) dips mostly to the north and northeast at variable angles and is axial planar to folds that range from open to almost isoclinal. Stretching lineations, defined by aligned metamorphic minerals and stretched limonite spots, plunge approximately down the dip of S_1. The orientation of fold axes (F_1) and intersection lineations (L_1) varies widely, from subhorizontal to steeply pitching, implying the presence of curvilinear fold hinges.

In outcrops in the northern part of the area, intersection lineations have approximately constant orientations over exposed areas 100s of metres long; however, the orientations of fold axes/intersection lineations are more variable in outcrops close to the trace of the King Salmon fault. For example, on Tatsho Creek many folds are tighter than those observed further north (Figures 16a, b). In these outcrops, a relationship was noted between the orientation of fold axes/intersection lineations, and the angle between bedding (S_0) and cleavage (S_1). In places where a high angle between bedding and cleavage is preserved, intersection lineations plunge gently, whereas rocks with subparallel S_0/S_1 have steeply pitching fold axes and intersection lineations. This relationship between fold orientation and tightness suggest that variation in the orientation of folds reflects tightening and rotation of fold hinges towards the stretching lineation during progressive deformation.

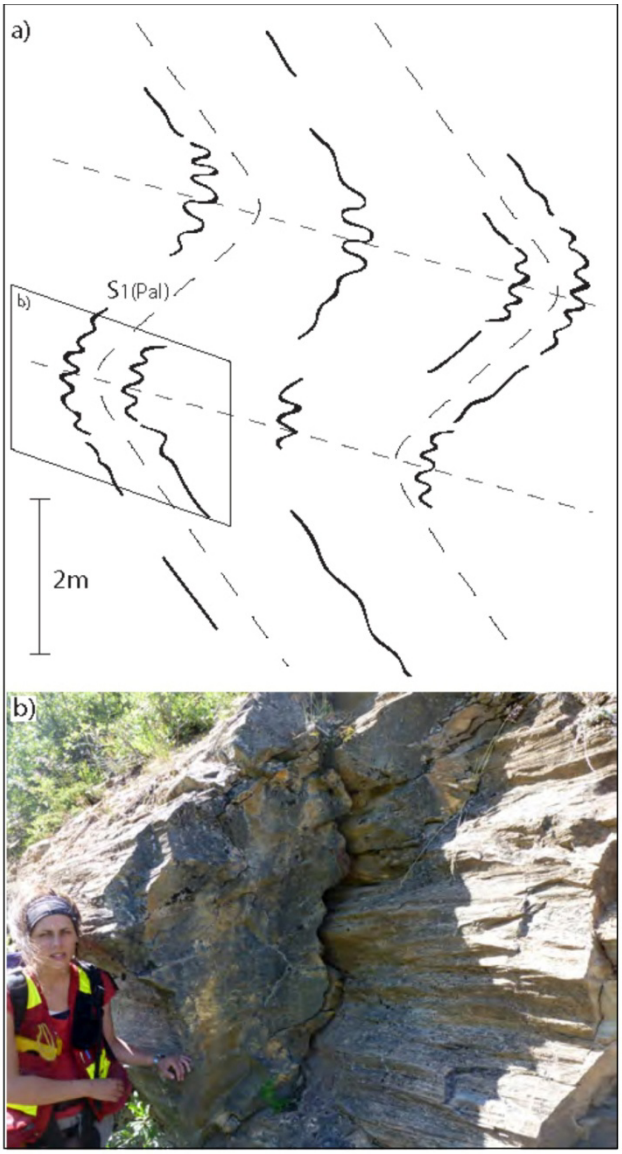

Figure 14. Sketch and matching photograph of (F_2Pal) Z-fold affecting Palaeozoic limestone in upper Itsillitu Creek. Sketch viewed down-plunge towards the southwest (approximately 225°).

The contrast with structures in the Inklin Formation observed further north suggests an increase in strain towards the King Salmon fault.

The dominant cleavage (Sn) in the Inklin Formation is widely overprinted by sets of conjugate kink-bands (F_2) with gently plunging chevron kink axes (Figures 16d, e). Millimetre to centimetre-scale kink bands are commonly visible, and larger scale kinks can be inferred from variations in the orientation of S_1 between outcrops. Locally, the hinge zones of kink folds are marked by minor faults.

Listwanite and mafic rocks of Cache Creek

Outcrops of listwanite along the trace of the KSF are massive to foliated. The foliation dips moderately steeply towards the north, parallel to foliation in the adjacent Inklin Formation. The foliation in the listwanite is locally

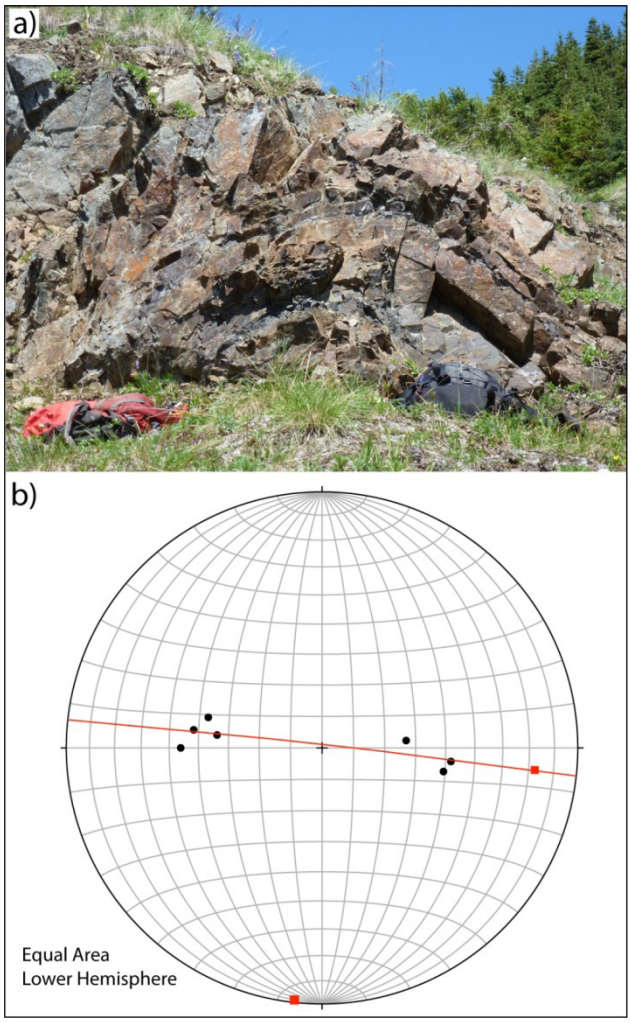

Figure 15. a) North-trending fold in the Takwahoni Formation south of Snow Peak. b) Equal area lower hemisphere stereonet projection of poles to bedding.

tightly folded around gently plunging axes, with axial planes parallel to the overall orientation of the foliation (Figure 17). Metabasaltic rocks on the north side of the KSF are also foliated, whereas limestone of the Sinwa Formation is mostly thoroughly recrystallized and massive. Rare darker argillaceous layers within the mainly white limestone define a weak wavy foliation.

The metabasalts are massive competent units and rarely possess a well developed penetrative foliation, however the overlying block and lapilli tuff breccia unit is well foliated. The foliation dips moderately steeply to the north with trends that swing northwesterly to follow the trace of the fault.

Summary

Penetrative deformation is largely restricted to Paleozoic rocks and to the region north of the KSF, whereas the whole area was affected by late east-west shortening. It appears that folding and penetrative deformation in the Paleozoic rocks (termed D_1PAL) predated deposition of Mesozoic units. Although this is based on limited data from a small part of the map sheet it

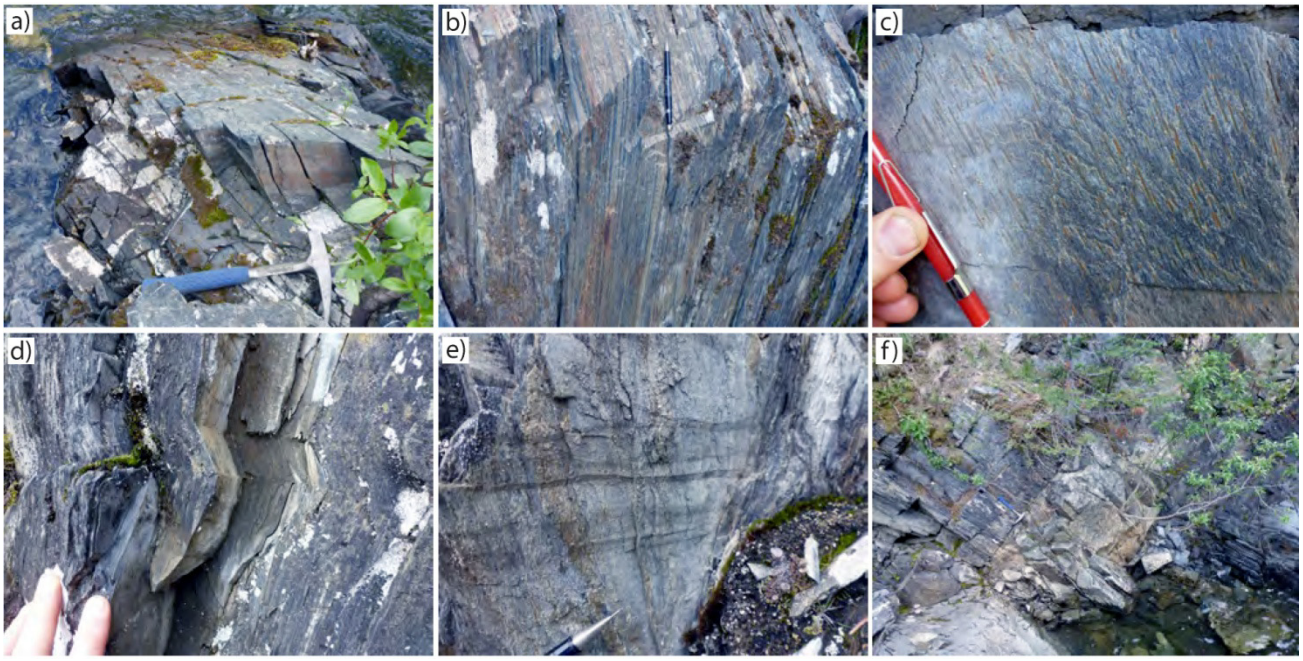

Figure 16. Structures in the Inklin Formation. a) Open fold with axial planar cleavage, northern Tatsho Creek. b) Parallel bedding and cleavage in outcrop close to the trace of the KSF. c) Stretching lineation in phyllite defined by elongate limonite aggregates. d) Profile view of kink fold (F_2) with subhorizontal axial plane overprinting the phyllitic foliation. e) F_2 kink folds viewed looking onto the S_1 surface. f) Diorite dike crosscutting phyllite of the Inklin Formation, northern Tatsho Creek.

Figure 17. a) Conspicuous green Cr-rich sheet silicate in listwanite along the trace of the KSF, Tasho Creek. b) North-dipping foliation in listwanite along the trace of the KSF, Tatsho Creek. The foliation is parallel to that in the adjacent Inklin Formation. c) Tight fold with gently plunging axis in listwanite on Tatsho Creek. The axial plane is parallel to the north-dipping foliation that is developed throughout the outcrop.

corroborates similar conclusion made by Read *et al.* (1983) for a late Permian or Early Triassic deformation and metamorphic event.

Post Triassic-pre Early Jurassic regional deformation is marked by the angular unconformity separating Late Triassic Stuhini Group from the Early Jurassic Hazelton Group in the Unuk River (Henderson *et al.*, 1992), Schaft Creek (Logan and Drobe, 1993), Strata Creek (Brown *et al.*, 1996) and Stikine River (Read, 1984). In addition, Early Jurassic granitic boulder conglomerates and sandstones nonconformably overlie late Triassic plutons of the Hotailuh batholith (Anderson, 1983).

However, the earliest Cordilleran deformation event which produced penetrative deformation (D_1) in the Cache Creek terrane, in the adjacent Takwahoni Formation and juxtaposed these units along the KSF was during the Middle Jurassic (Gabrielse, 1998). This area forms part of the south-vergent fold and thrust belt that formed during amalgamation of the Cache Creek and Stikine terranes in the Middle Jurassic (Gabrielse, 1998; Mihalynuk *et al.*, 2004).

The age of the north-trending folds that give rise to map-scale undulations in stratigraphy has not been established in the map area. Late north-trending folds in the Inklin Formation were identified by Gabrielse (1998) in the Dome Mountain area to the east. Ryan (1991) described north-trending folds in the Tuya River basin, to the west of the mapped area. These folds, which may be correlative with those observed, affect Tertiary sedimentary rocks.

MINERALIZATION

Metallic mineral occurrences within the map area include two alkalic porphyry Cu-Au prospects located south of the Tanzilla River in massive volcaniclastic rocks of the Stuhini Group. A porphyry Mo-Cu-W prospect (Mack; MINFILE 104J 014) within the Cretaceous Snow Peak pluton that intruded Takwahoni strata near the headwaters of Sixteen Mile Creek. Ag–Pb–Zn±Au quartz vein showing (Mac; MINFILE 104J 064) is associated with dikes cutting Takwahoni sedimentary rocks west of the Mack prospect. The Hu alkalic porphyry Cu-Au prospect (MINFILE 104J 013) is associated with an east-trending multiphase monzosyenite-granodiorite intrusion adjacent to the Hleuy Lake hydroelectric power station. The Tan showing (MINFILE 104J 036) is related to a southeast-trending composite pyroxenite-hornblendite-monzonite body (Table 1).

Geochemical rock samples (n=15) characterizing alteration and base and precious metal mineralization were collected during the course of mapping. These were analysed for 41 elements by Inductively Coupled Mass Spectrographic analyses (ICP-MS) and Au by fire assay fusion and ICP-ES at Acme Labs in Vancouver, British Columbia. The concentrations of Au plus a number of selected intrusive-related mineralization pathfinder elements from these samples are tabulated together with their location information in Table 2.

Regional Lithogeochemical Sampling

The King Salmon fault is characterized along its length by pods of carbonate altered ultramafic rocks that consist of a listwanite assemblage of rusty orange quartz-talc-carbonate-chrome bearing sheet silicate (mariposite or fuchsite) and locally iron sulphides. Listwanite alteration is structurally controlled along faults and fracture systems that provide pathways for CO_2-rich fluids and this alteration is well known for its association with lode gold mineralization (Ash and Arksey, 1990; Dubé and Gosselin, 2007). Grab samples of listwanite alteration were collected from three separate outcrops exposed along the King Salmon fault (Figure 3). As expected, geochemical analyses returned high Ni, Co and Cr values characteristic of ultramafic rocks and in addition elevated Sb and As values, however precious and base metal values are low to below detection levels at all three sites (11JLO8-65, 12-105 and 29-296-3; Table 2).

Hu, Huey (MINFILE 104J 013)

The Hu is located on the Tanzilla Plateau approximately 2 km northwest of Hluey Lakes. It extends northward onto the steep north-facing slope of the Tanzilla River. The area is underlain by well bedded sedimentary rocks, massive volcaniclastic rocks and maroon basalt and latite of the Stuhini Group that was intruded by a hornblende biotite granodiorite and younger pink weathering variably textured porphyritic biotite monzosyenite. The monzosyenite intrudes and alters the granodiorite along the northeastern contact exposed in Stain Creek. The granodiorite and syenite were assigned an Early to Middle Jurassic age by Gabrielse (1998), however other workers (Sellmer, 1973; Kasper, 1991) thought these intrusions were older and correlated them with the Late Triassic to Middle Jurassic Hotailuh batholith (Anderson, 1983). The Huey syenite is mineralogically similar and likely correlative with the potassic phase of the Three Sisters pluton (see van Straaten, this volume).

The most favourable alteration and mineralization on the Hu property is exposed along Stain Creek where monzosyenite and granodiorite have intruded sedimentary and volcanic rocks of the Stuhini Group. Alteration, including K-feldspar and carbonate are concentrated along northeast trending brittle faults and the intrusive contact between monzosyenite and granodiorite. Grab samples from an altered mineralized syenite (11JLO28-285) and pyritized hornblende granodiorite (11JLO-28-287) returned elevated Cu values only for the former (Table 2). Although, chip samples as high as 1.7 g/t Au, 6.9g/t Ag and 0.03% Cu and grab samples 1.3 g/t Au, 5.6g/t Ag and 0.03% Cu are known from this area (Kasper, 1991). Fractured, heavily altered and chalcopyrite mineralized argillite and maroon volcaniclastic rocks occur north and south of the monzosyenite (11DMO33-284 and 35-309; Table 2). This mineralization includes chalcopyrite-bearing quartz-carbonate veins and replacement sulphides in laminated siltstones.

Table 1. MINFILE BC mineral occurrences for Dease Lake NTS 104J/08 and the east-half of Little Tuya River NTS 104J/07 map areas.

MINFILE NO	NAME	STATUS	ZONE	UTMN	UTME	COMMODITIES	DEPOSIT TYPE
104J 013	HU, HUEY	PROS	9	6467707	430291	Cu, Au, Mo	Alkalic porphyry Cu-A
104J 014	MACK, SNOW PEAK	PROS	9	6480395	417285	Mo, Cu, Au, Wo	Porphyry Mo
104J 036	TAN	SHOW	9	6463105	418615	Cu	Alkalic porphyry Cu-A
104J 064	MAC	SHOW	9	6482412	413015	Au, Ag, Zn, Pb, Cu	Polymetallic veins
104J 154	BUD	ANOM	9	6481956	408947	Au	-
104J 041	TATSHO MOUNTAIN	SHOW	9	6477888	439393	LS	Limestone
104J 044	TUYA RIVER	PROS	9	6457905	398643	CL	Bituminous coal

Table 2. Selected elements from Inductively Coupled Mass Spectrographic analyses (ICPMS) of samples collected in the Dease Lake area.

Sample Number	Location		Lab Number	Ag	As	Au	Ba	Bi	Cd	Ce	Co	Ca	Cr	Cu	Fe	K	Mn	Mo	Ni	Pb	S	Sb	Sn	Th	W	Y	Zn	Zr
	UTM Zone 9		Detection Limit	0.1	1	2	1	0.1	0.1	1	0.2	0.01	1	0.1	0.01	0.01	1	0.1	0.1	0.1	0.1	0.1	0.1	0.1	0.1	0.1	1	0.1
	UTME	UTMN	Measure unit	PPM	PPM	PPB	PPM	PPM	PPM	PPM	PPM	%	PPM	PPM	%	%	PPM	PPM	PPM	PPM	%	PPM	PPM	PPM	PPM	PPM	PPM	PPM
OIV-3-38	428828	6E+06	62149	<0.1	2	3	308	<0.1	0.2	10	39.5	8.16	204	102	6.56	1.42	1485	3.1	43.2	5.8	1.5	0.1	0.6	0.7	<0.1	12.9	80	27
JLO-8-65	436103	6E+06	62145	<0.1	82	<2	7	<0.1	<0.1	<1	56.4	0.29	831	4.6	3.13	<0.01	499	0.2	1132	0.2	<0.1	8.9	<0.1	<0.1	0.3	0.2	28	<0.1
JLO-12-105	423171	6E+06	62146	0.2	64	4	87	<0.1	0.2	<1	54.4	0.22	883	6.6	4.21	0.27	735	<0.1	824	0.7	<0.1	5	<0.1	<0.1	0.2	0.5	26	<0.1
LDI-19-164a	424421	6E+06	62147	<0.1	31	21	64	0.2	0.2	70	48	3.66	173	39	6.44	1.08	581	0.3	131	4.6	2.7	1.4	2.9	2.2	0.4	19.6	56	95
LDI-19-164b	424421	6E+06	62148	<0.1	3	14	141	0.2	0.3	80	42.1	9.71	139	41.7	7.56	3.54	737	<0.1	115	4.8	2.4	1.4	3.1	2.7	0.3	29.2	77	44
JLO-24-244-2	417876	6E+06	62150	<0.1	3	7	566	<0.1	<0.1	11	27.4	5.34	12	158.1	6.64	1.2	1377	0.3	9.6	1.1	<0.1	0.6	0.6	0.7	0.5	15.7	62	44
JLO-24-249	417295	6E+06	62151	<0.1	7	<2	170	<0.1	0.2	14	21.5	9.34	71	113.4	4.95	0.48	1167	1.7	20	1.2	0.6	0.2	0.5	1	1.7	19.2	77	46
JLO-28-285	430650	6E+06	62152	<0.1	10	21	1490	0.1	0.2	84	17.2	3.21	17	1216.6	6.13	4.22	533	6.7	7.3	2.9	<0.1	2	2.2	22	1.7	23.5	36	278
JLO-28-287	430492	6E+06	62153	<0.1	13	4	199	0.1	0.1	65	24.1	3.1	17	127	6.18	3.78	995	1.8	8.2	7	1.3	2	1.9	13.5	1	22.2	32	104
JLO-29-296-3	431174	6E+06	62154	<0.1	108	<2	47	<0.1	0.1	<1	58.5	7.21	971	9.7	4.06	0.01	685	0.6	1208	0.1	<0.1	7.6	<0.1	<0.1	0.9	0.3	35	0.5
JLO32-319	451832	6E+06	62156	0.6	5	41	510	0.1	0.2	16	7.5	0.48	32	7221.4	1.26	5.76	221	16.7	3.7	6.9	0.5	1	0.6	1.8	0.6	7.8	32	24
DMO-6-49	415975	6E+06	62157	0.1	26	<2	20	<0.1	0.1	5	5.8	12.5	15	37.6	3.63	0.03	877	0.2	4.8	0.9	<0.1	0.2	0.3	0.3	0.5	8.4	27	23
JLO50-501 (BLK)	-	-	62158	<0.1	<1	<2	3	0.1	<0.1	<1	0.8	<0.01	215	17.3	0.35	<0.01	15	0.2	6.4	0.7	<0.1	<0.1	0.2	<0.1	<0.1	0.2	1	<0.1
DMO-33-284	427351	6E+06	62159	0.3	81	10	18	0.3	<0.1	7	141	10.5	116	1120.9	16.1	0.03	2709	1.8	61.5	9.7	4.8	6.5	1.1	1	0.4	24.5	41	70
DMO-35-309	430125	6E+06	62160	<0.1	7	7	338	0.5	<0.1	30	19.8	3.78	86	>10000.0	6.66	1.51	1090	0.8	5.8	2	1.3	5.9	1	1.5	12	18.7	12	48
DMO-35-309Dup	430125	6E+06	62155	<0.1	9	9	192	0.6	<0.1	28	20.4	3.42	82	>10000.0	6.87	1.46	1098	0.9	5	1.6	1.5	5.8	0.9	1.4	14	18.1	13	45
Reference Materials																												
STD OREAS24P	-	-	STD	<0.1	2	-	271	<0.1	0.2	36	45.7	6.01	196	45.3	7.22	0.66	1075	1.1	137	3.2	<0.1	0.3	1.5	2.8	0.4	20.3	108	134
STD OREAS45C	-	-	STD	0.1	10	-	272	0.2	0.1	52	97.8	0.46	925	591.2	18.5	0.34	1113	2.6	302	25	<0.1	0.8	3	10.7	1.2	12.1	79	173
Blank	-	-	BLK	<0.1	<1	<2	<1	<0.1	<0.1	<1	<0.2	<0.01	<1	<0.1	<0.01	<0.01	<1	<0.1	<0.1	<0.1	<0.1	<0.1	<0.1	<0.1	<0.1	<0.1	<1	<0.1

Tan showing (MINFILE 104J 036)

At the Tan showing a large gossan has developed within cherty siltstone and fine sandstone of the well bedded sedimentary unit of the Stuhini Group adjacent to its northwest trending faulted (?) contact with the composite pyroxenite-hornblendite-monzonite pluton. Grab samples from weakly altered and mineralized volcanic rocks were collected in the vicinity of the Tan showing. One comprised a plagioclase phyric basaltic andesite (11JLO24-244-2) the other an aphyric mafic lapilli tuff (11JLO24-249), both samples contained disseminated pyrite and chalcopyrite but returned low metal values (Table 2).

Mac (MINFILE 104J 064)

The Mac showing is located approximately 3 km west of Snow Peak pluton on the edge of a circular magnetic high centered on the intrusion. The magnetic high extends several kilometres beyond the intrusion and is interpreted to reflect pyrrhotite within hornfelsed country rock developed peripheral to the intrusion and evident on the first vertical derivative of the total field magnetic. Mineralization at the Mac is quartz vein hosted and associated with easterly trending quartz feldspar porphyry (QFP) dike swarms which are common in the area. These dikes and presumably the mineralization at the Mac predate intrusion of the Snow Peak pluton and development of the hornfels. Pyrite, galena, chalcopyrite ±galena, sphalerite and tetrahedrite in decreasing order of abundance are reported to occur within the quartz veins and as selvages in altered country rock. ICP-ES analyses of quartz veins and mineralized QFP dikes returned elevated base and precious metal values and up to 26.8 g/t Au and 137.1 g/t Ag from grab samples (Swenson, 2006).

Mack (MINFILE 104J 014)

Late Cretaceous Mo and Cu-Mo mineralization is a well-established Cordilleran-wide metallogenic event. Porphyry Mo±Au, W mineralization is present in the Cretaceous Snow Peak pluton (Gabrielse, 1998) and is described in a separate paper by Moynihan and Logan (this volume).

Coal and Limestone

Along Tuya Creek, at the southwestern margin of the map (Figure 3) from 5 to 30 m of high volatile B bituminous coal occurs within the Lower Tertiary, Paleocene sediments of the Tuya River coal basin (Ryan, 1991). The Tuya River (MINFILE 104J 044) prospect was not visited during the current mapping program.

Massive white limestone (Tatsho Mountain, MINFILE 104J 041) forms a west-trending ridge that overlooks the community of Dease Lake north of the airport. The white weathering limestone massif extends for approximately 2.5 km westward towards Tatsho Mountain and is correlated with the Upper Triassic Sinwa Formation.

PRELIMINARY OBSERVATIONS AND CONCLUSIONS

Polydeformed phyllite, greenstone and Early Permian limestone of the Stikine assemblage are overlain by less deformed Early to Middle Triassic cherty sediments and crowded pyroxene porphyry basalt breccias that pass up section through a dominantly volcaniclastic sequence of the Late Triassic Stuhini Group. A progression from proximal volcanic to distal epiclastic rocks northwards is similar to the facies changes observed for Triassic rocks in the Tulsequah map area (Monger, 1980).

Preliminary Laser Ablation U-Pb zircon ages have identified some Late Jurassic and Early Cretaceous thermal events not previously recognized in rocks of the Stikine arch.

Recognition that not all pyroxene porphyritic basalts are Middle or Late Triassic in age, but can comprise identical thick sections in the Jurassic (Brown *et al.*, 1996; Iverson *et al.*, this volume) requires careful mapping and age dating.

The British Columbia Geological Survey Dease Lake Geoscience Project is part of the new QUEST-Northwest Mapping initiative by Geoscience BC. The bedrock mapping project reported on here is one of 4 field-based integrated research projects designed to investigate the stratigraphy, magmatic evolution and metallogeny along the Stikine Arch in the vicinity of Dease Lake. The results of the mapping project will be released as a British Columbia Geological Survey Open File Map and a Geoscience BC publication.

ACKNOWLEDGMENTS

The authors acknowledge contributions from many people regarding various aspects of this study. Discussions with G. Nixon of the British Columbia Geological Survey and B. Anderson of the Geological Survey of Canada where important at the inception stage and ongoing phases of the study and are much appreciated. Capable and enthusiastic assistance throughout the 2011 field season was provided by O. Iverson, M. Hogg, T. McCarron and C. Young. The cooperation and free discussion of geological ideas with various mineral exploration companies made this study possible from its earliest stage. Safe and courteous flying by Pacific Northwest Helicopters in Dease Lake was the norm and much appreciated.

Patricia McIntosh is thanked for opening her home and ranch for the team's use during the summer mapping project and for providing two gracious hosts; cook, J. Anderson and bull cook and local historian D. Callison.

Geoscience BC provided financial support for the field and analytical programs, and salary support for B.I. van Straaten, D. Moynihan, O. Iverson and the field assistants.

REFERENCES

Anderson, R.G. (1980): Satellitic stocks, volcanic and sedimentary stratigraphy, and structure around the northern and western margins of the Hotailuh batholith, North-Central British Columbia; *in* Current Research, Part A, *Geological Survey of Canada*, Paper 80-1A, pages 37-40.

Anderson, R.G. (1983): Geology of the Hotailuh Batholith and Surrounding Volcanic and Sedimentary Rocks, North-Central British Columbia; unpublished Ph.D. thesis, *Carleton University*, 669 pages.

Anderson, R.G. (1984): Late Triassic and Jurassic Magmatism along the Stikine Arch and the Geology of the Stikine Batholith, North-Central British Columbia; *in* Current Research, Part A, *Geological Survey of Canada*, Paper 84-1A, pages 67-73.

Anderson, R.G. (1993): A Mesozoic stratigraphic and plutonic framework for northwestern Stikinia (Iskut River area), northwestern British Columbia, Canada; in Mesozoic Paleogeography of the western United States –II, (ed.) G. Dunne and K. McDougall; *Society of Economic Paleontologists and Mineralogists*, Volume 71, pages 477-494.

Anderson, R.G., and Bevier, M.L. (1990): A note on Mesozoic and Tertiary geochronometry of plutonic suites, Iskut River area, northwestern British Columbia; *in* Current Research, Part A, *Geological Survey of Canada*, Paper 90-1E, pages 141-147.

Ash, C.H. and Arksey, R.L. (1990): The Listwanite-Lode Gold Association in British Columbia; Geological Fieldwork 1989, *BC Ministry of Energy, Mines and Petroleum Resources*, Paper 1990-1, pages 359-364.

Ash, C.H., Macdonald, R.W.J., Stinson, P.K., Fraser, T.M., Nelson, K.J., Arden, K.M. and Lefebure, D.V. (1997): Geology and Mineral Occurrences of the Tatogga Lake Area; *BC Ministry of Energy, Mines and Petroleum Resources*, Open File 1997-3.

BC Geological Survey (2011): MINFILE BC mineral deposits database; *BC Ministry of Energy and Mines*, URL <http://minfile.ca> [November 2011].

Bamber, E.W. (2011): Report on 2 collections of upper Paleozoic invertebrate fossils from the Dease Lake area, northwestern British Columbia, submitted by D.P. Moynihan, BC Ministry of Energy and Mines, NTS 104-J-7, 104-J-8; *Geological Survey of Canada*, Paleontological Report 01-EWB-2011, 3 pages

Brown, D.A., Gunning, M.H. and Greig, C.J. (1996): The Stikine Project: Geology of Western Telegraph Creek Map Area, Northwestern British Columbia; *BC Ministry of Energy, Mines and Petroleum Resources*, Bulletin 95, 175 pages.

Brown, D.A., Logan, J.M., Gunning, M.H., Orchard, M.J., and Bamber, E.W. (1991): Stratigraphic Evolution of the Paleozoic Stikine Assemblage in the Stikine Iskut Rivers Area, Northwestern British Columbia (NTS 104G and 104B); in Contributions to the Geology and Geophysics of Northwestern British Columbia and Southeastern Alaska, Anderson, R.G., Editor, *Canadian Journal of Earth Sciences*, Volume 28, pages 958-972.

De Nys, F.J.G. (1980): Thundercloud Coal Project Technical Report; PetroCanada Exploration, *BC Ministry of Energy, Mines and Petroleum Resources*, Coal Assessment Report 243.

Dubé, B. and Gosselin, P. (2007): Greenstone-Hosted Quartz-Carbonate Vein Deposits; in Mineral Deposits of Canada: A Synthesis of Major Deposit Types, District Metallogeny, the Evolution of Geological Provinces & Exploration Methods, Edited by Wayne D. Goodfellow, *Geological Association of Canada*, Special Publication 5, pages 49-74.

Eisbacher, G.H. (1974): Sedimentary history and tectonic evolution of the Sustut and Sifton basins, North-central British Columbia; *Geological Survey of Canada*, Paper 73-31, 57 pages.

Evenchick, C. A. and Thorkelson, D.J. (2005): Geology of the Spatsizi River Map Area, North-Central British Columbia; *Geological Survey of Canada*, Bulletin 577, 276 pages.

Gabrielse, H., Monger, J.W.H., Leaming, S.F., Anderson, R.G., and Tipper, H.W. (1980): Geology of Dease Lake (104J) map-area, northwestern British Columbia; *Geological Survey of Canada*, Open File 707.

Gabrielse, H. (1998): Geology of Cry Lake and Dease Lake Map Areas, North-Central British Columbia; *Geological Survey of Canada*, Bulletin 504, 147 pages.

Geological Survey of Canada (1957): Operation Stikine; *Geological Survey of Canada*, Map 9-1957.

Gunning, M.H., Bamber, E.W., Brown, D.A., Rui, L., Mamet, B.L. and Orchard, M.J. (1994): The Permian Ambition Formation of Northwestern Stikinia, British Columbia; in Pangea: Global Environments and Resources, Embry, A.F., Beauchamp, B. and Glass, D.J., Editors, *Canadian Society of Petroleum Geologists*, Memoir 17, pages 589-619.

Hamilton, T. (1981): Late Cenozoic alkaline volcanic of the Level Mountain Range, northwestern British Columbia, geology, petrology and paleomagnetism; Ph.D. thesis, *The University of Alberta*, Edmonton, Alberta, 490 p.

Henderson, J.R., Kirkham, R.V., Henderson, M.N., Payne, J.G., Wright, T.O. and Wright, R.L. (1992): Stratigraphy and Structure of the Sulphurets Area, British Columbia; *in* Current Research, Part A, *Geological Survey of Canada*, Paper 92-1A, pages 323-332.

Iverson, O., Mahoney, B. and Logan, J.M. (2012): Dease Lake Geoscience Project, Part IV: Tsaybahe Group: Lithological and Geochemical Characterization of Middle Triassic Volcanism in the Stikine Arch, North-Central British Columbia; *BC Ministry of Energy and Mines*, Geological Fieldwork 2011, Report 2012-1.

Jackaman, W. (2012): QUEST-Northwest Project: new regional geochemical survey and sample reanalysis data (NTS 104F, G, H, I, J), northern British Columbia; *in* Geoscience BC Summary of Activities 2011, *Geoscience BC*, Report 2012-1.

Kasper, B.J., (1991): 1991 Geological and Geochemical report on the Huey and Duey claims; *BC Ministry of Energy, Mines and Petroleum Resources*, Assessment Report 21707.

Kerr, F.A. (1926): Dease Lake Area, Cassiar District British Columbia; *Geological Survey of Canada*, Map 2104.

Kerr, F.A. (1948): Lower Stikine and Iskut River Areas, British Columbia; *Geological Survey of Canada*, Memoir 246, 94 pages.

Logan, J.M. and Drobe, J.R. (1993): Geology and Mineral Occurrences of the Mess Lake Area, (104G/7W); in Geological Fieldwork 1992, Grant, B. and Newell, J.M.,

Editors, *BC Ministry of Energy, Mines and Petroleum Resources*, Paper 1993-1, pages 135-148.

Logan, J.M., Drobe, J.R. and McClelland, W.C. (2000): Geology of the Forrest Kerr-Mess Creek Area, Northwestern British Columbia (NTS 104B/10, 15 & 104G/2 & 7W); *BC Ministry of Energy, Mines and Petroleum Resources*, Bulletin 104, 163 pages.

Logan, J.M., Moynihan, D.P., and Diakow, L.J. (2012a): QUEST-Northwest Mapping: BC Geological Survey Dease Lake Geoscience Project (NTS 104J, 104I), Northern British Columbia; in Geoscience BC Summary of Activities 2011, *Geoscience BC*, Report 2012-1.

Logan, J.M., Moynihan, D.P., and Diakow, L.J. (2012b): Geology and Mineralization of the Dease Lake (104J/08) and East- Half of the Little Tuya River (104J/07E) Map Sheets, Northern British Columbia; *BC Ministry of Energy and Mines*, Open File 2012-?

Massey, N.W.D., MacIntyre, D.G., Desjardins, P.J. and Cooney, R.T. (2005): Digital Geology Map of British Columbia: Whole Province, *BC Ministry of Energy, Mines and Petroleum Resources*, Geofile 2005-1.

Monger, J.W.H. (1975): Upper Paleozoic rocks of the Atlin Terrane, northwestern British Columbia and south-central Yukon; *Geological Survey of Canada*, Paper 74-47, 63 pages.

Monger, J.W.H. (1980): Upper Triassic stratigraphy, Dease Lake and Tulsequah map areas, northwestern British Columbia; *Geological Survey of Canada*, Paper 80-1B, pages 1-9.

Moynihan, D.P. and Logan, J.M. (this volume): Dease Lake Geoscience Project, Part III: Age, Emplacement and Mineralization of the Snow Peak Pluton (NTS 104J/08); *BC Ministry of Energy and Mines*, Geological Fieldwork 2011, Report 2012-1.

Mihalynuk, M.G., Erdmer, P., Ghent, E.D., Cordey, F., Archibald, D.A., Friedman R.M. and Johannson, G.G. (2004): Coherent French Range blueschist: Subduction to exhumation in <2.5 Ma?, *Geological Society of America Bulletin*, Volume 116, pages 910-922.

Poulton, T.P. (2011): Report on 3 collections of Triassic and Jurassic samples collected in 2011 by Jim Logan, Larry Diakow, and David Moynihan (British Columbia Geological Survey) in Dease Lake map area, northern British Columbia (NTS 104J 08); *Geological Survey of Canada*, Paleontological Report TJ1-2011-TTP, 3 p.

Read, P.B. (1983): Geology, Classy Creek (10J/2E) and Stikine Canyon (104J/1W), British Columbia; *Geological Survey of Canada*, Open File 940.

Read, P.B. (1984): Geology Klastline River (104G/16E), Ealue Lake (104H/13W), Cake Hill (104I/4W), and Stikine Canyon (104J/1E), British Columbia; *Geological Survey of Canada*, Open File 1080.

Read, P.B., and Psutka, J.F., (1990): Geology of Ealue Lake East-Half (104H/13E) and Cullivan Creek (104H/14) Map Areas, British Columbia; *Geological Survey of Canada*, Open File 2241.

Read, P.B., Psutka, J.F., Brown, R.L. and Orchard, M.J. (1983): "Tahltanian" Orogeny and Younger Deformations, Grand Canyon of the Stikine British Columbia; *Geological Association of Canada*, Programs with Abstracts, May 11-13, Victoria, Volume 8, page A57.

Ryan, B., (1991): Geology and Potential Coal and Coalbed Methane Resource of the Tuya River Coal Basin (104J/2, 7); *BC Ministry of Energy, Mines and Petroleum Resources*, Paper 2001-1, pages 419–432.

Souther, J.G. (1971): Geology and Mineral Deposits of Tulsequah Map-area, British Columbia; *Geological Survey of Canada*, Memoir 362.

Souther, J.G. (1972): Telegraph Creek Map Area, British Columbia, *Geological Survey of Canada*, Paper 71-44, 38 pages.

Sellmer, H.W., G.M. Depaoli and D.G. Allen (1973): Tanzilla Property - Hu claims; *BC Ministry of Energy, Mines and Petroleum Resources*, Assessment Report 4399.

Simpson, K.A. (2012): QUEST-Northwest: Geoscience BC's new minerals project in northwest British Columbia (104G, 104J, parts of NTS 104A, B, F, H, I, K, 103O, P); *in* Geoscience BC Summary of Activities 2011, *Geoscience BC*, Report 2012-1.

Stevens, R.D., Delabio, R.N., and Lachance, G.R. (1982): Age determinations and geological studies, K-Ar isotopic ages, Report 15; *Geological Survey of Canada*, Paper 81-2, page 16.

Swenson, M. (2006): Geological Report on the Mac Property; *BC Ministry of Energy, Mines and Petroleum Resources*, Assessment Report 28309.

Tipper, H.W. (1978): Jurassic biostratigraphy, Cry Lake map area, British Columbia, *in* Current research, *Geological Survey of Canada*, Paper 78-1A, pages 25–27.

van Straaten, B.I., Logan, J.M. and Diakow, L.J. (this volume): Dease Lake Geoscience Project, Part II: Preliminary Report on the Mesozoic Magmatic History and Metallogeny of the Hotailuh Batholith and Surrounding Volcanic and Sedimentary Rocks; *BC Ministry of Energy and Mines*, Geological Fieldwork 2011, Paper 2012-1.

Vincent, B.D. (1979): Geological Mapping, Tuya River Property, British Columbia; Esso Minerals Canada; *BC Ministry of Energy, Mines and Petroleum Resources*, Coal Assessment Report 246.

Wanless R.K., Stevens, R.D., Lachance, G.R., and Delabio, R.N. (1972): Age determinations and geological studies; *Geological Survey of Canada*, Paper 71-2, pages 20–21.

Yorath, C.J. (1991): Upper Jurassic to Paleogene assemblages, Chapter 2; in Geology of the Cordilleran Orogen *in* Canada, Gabrielse, H. and Yorath, C.J., Editors, *Geological Survey of Canada*, Geology of Canada, no 4, pages 329-371.

Geology of the Hoodoo Mountain Area (NTS 104B/14W)

by M.G. Mihalynuk[1], A. Zagorevski[2] and F. Cordey[3]

KEYWORDS: Hoodoo Mountain, Sphaler Creek, Stikine assemblage, Stuhini Group, copper porphyry, Galore Creek, Dirk prospect, Telena prospect, volcanic-hosted massive sulphide, Rock and Roll, Andrei Icefield, Iskut River

INTRODUCTION

Hoodoo Mountain area is located between the enormous copper-gold resource defined at Galore Creek and the past-producing gold deposits of the Bronson Camp. Reserves at Galore Creek in proven and probable categories are 528 Mt grading 0.58% Cu, 0.32 g/t Au and 6.02 g/t Ag (Gill *et al.*, 2011). In the Bronson Camp, the Snip mine produced 32 million grams of gold, 12 million grams silver and nearly 250 000 kilograms copper from about 1.2 million tonnes between 1991 and 1999; Johnny Mountain produced for less than two years with produced, proven, probable and "possible" categories totalling 0.622 Mt at 19.54 g/t Au (MINFILE, 2011). Bronson Slope is underlain by a low-grade porphyry with a measured and indicated resource estimate stated to meet "CIMM resource standards and classifications" of 225 Mt grading 0.36 g/t Au, 2.22 g/t Ag, 0.13% Cu and 0.008% Mo plus 163 Mt grading 7.28% magnetite (Giroux and Gray, 2010). Despite the region's exceptional mineral endowment, large parts of the Hoodoo Mountain area lacked systematic mapping or were last mapped by Forrest Kerr in the 1920s during International Boundary Commission, which also generated the first topographical maps. To address this geoscience knowledge gap, a program of geological mapping and sampling was initiated in 2010, funded principally by the federal GEM program (Geoscience for Energy and Minerals Strategy) over the eastern half of the Hoodoo map area (NTS 104B/14E, Mihalynuk *et al.*, 2011a, b). Continuation of that mapping in 2011 focused on the western half of the Hoodoo Mountain area (NTS 104B/14W), and is the subject of this report. New or substantially revised information is included herein; see Mihalynuk *et al.* (2010, 2011a) for additional unit descriptions and previous work.

LOCATION AND ACCESS

Hoodoo Mountain area (NTS 104/14W) can be accessed either via the Bronson airstrip to the immediate south, or via the Espaw camp located at kilometre 91 on the incomplete Galore Creek access road, immediately north of the map area. At the time of our field program, both required air transport from Bob Quinn airstrip located on Highway 37, approximately 400 km by road from both Smithers and Terrace (Figure 1). Bob Quinn airstrip is 60 km from both Bronson airstrip and Espaw Camp.

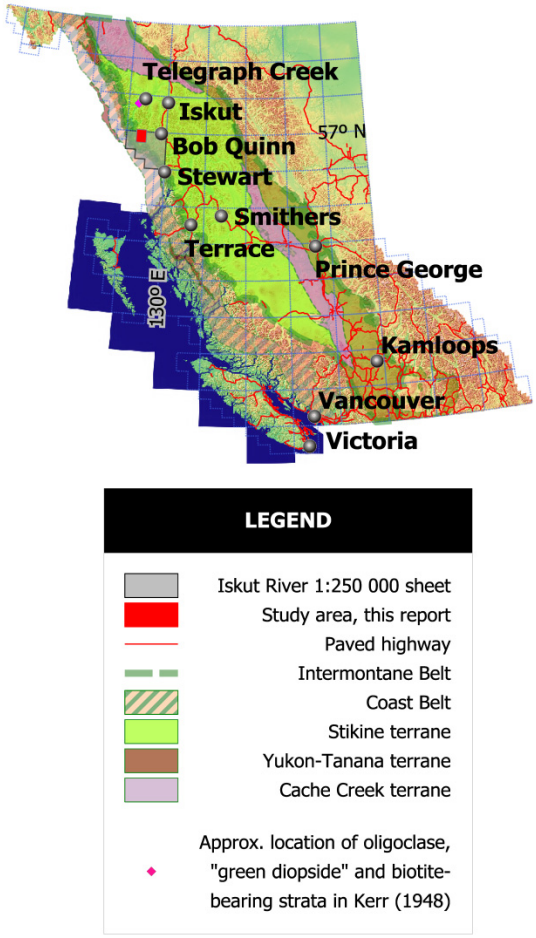

Figure 1. Location of the Iskut study area near the boundary of the Coast Belt and western Stikine terrane.

[1] *British Columbia Geological Survey, Victoria, BC*
[2] *Geological Survey of Canada, Natural Resources Canada, Ottawa, ON*
[3] *University of Lyon 1, France*

This publication is also available, free of charge, as colour digital files in Adobe Acrobat® PDF format from the BC Ministry of Energy and Mines website at http://www.empr.gov.bc.ca/Mining/Geoscience/PublicationsCatalogue/Fieldwork.

Our fieldwork focused on the mountain slopes between the Iskut River and Sphaler Creek. Work in this typically rainy coastal region is commonly curtailed by low cloud and inability to fly, the summer of 2011 was no exception. Our work was facilitated by the comfortable facilities at Espaw camp on Sphaler Creek, established by the Galore Creek Mining Company (GCMC) and operated by Romios Gold Corporation during our tenure. Helicopter services were supplied by Lakelse Air Ltd. Travel by foot out of the Espaw Camp is aided by the GCMC access road, which ends ~2 km west of the camp. In practicality, however, foot travel is limited to valleys south of the turbulent Sphaler Creek.

PREVIOUS WORK AND REGIONAL GEOLOGY

Much of the area within NTS 104B/14 had not been mapped as part of a systematic regional program prior to the start of our program in 2010. Between 1926 and 1929, Forrest Kerr covered the corridor along the Iskut River (Kerr, 1948; Figure 2), but Kerr designated the area between the Iskut River and Sphaler Creek as one "Large ice field with a few peaks rising above the ice level". However, deglaciation during the intervening 80+ years has exposed the terrain considerably. Many striking examples of kilometres of glacial retreat can be seen in the area (*e.g.* see retreat history of Twin Glacier, Figure 4 of Mihalynuk *et al.*, 2011a). Never-before-seen rock exposures are revealed by glacial retreat with each successive year.

Mihalynuk *et al.* (2010, 2011a) provide overviews of previous geological studies in the Iskut region, which are not repeated here. Not part of their overview, and specific to the Hoodoo west map sheet and adjacent area to the north, are exploration programs in the Hoodoo River area (Holbeck, 1983), on the south flank of Pheno Mountain (Doyle and Awmack, 1991), and the Trek property that spans Sphaler Creek (Caulfield, 1989; Awmack and Yamamura, 1988; Simmons, 2006) and extends east to "Quest Creek" (Kasper, 1989; informal names appear within quotation marks). Geological mapping conducted as part of these programs is compiled in Figure 3. Relying on such compilation as well as vantage point, airphoto, LandSAT5 and ASTER satellite imagery interpretation, we have extended our field observations to most parts of 104B/14W. One area that still lacks geological observations of any sort is around the Johnson Glacier (Figures 2, 3).

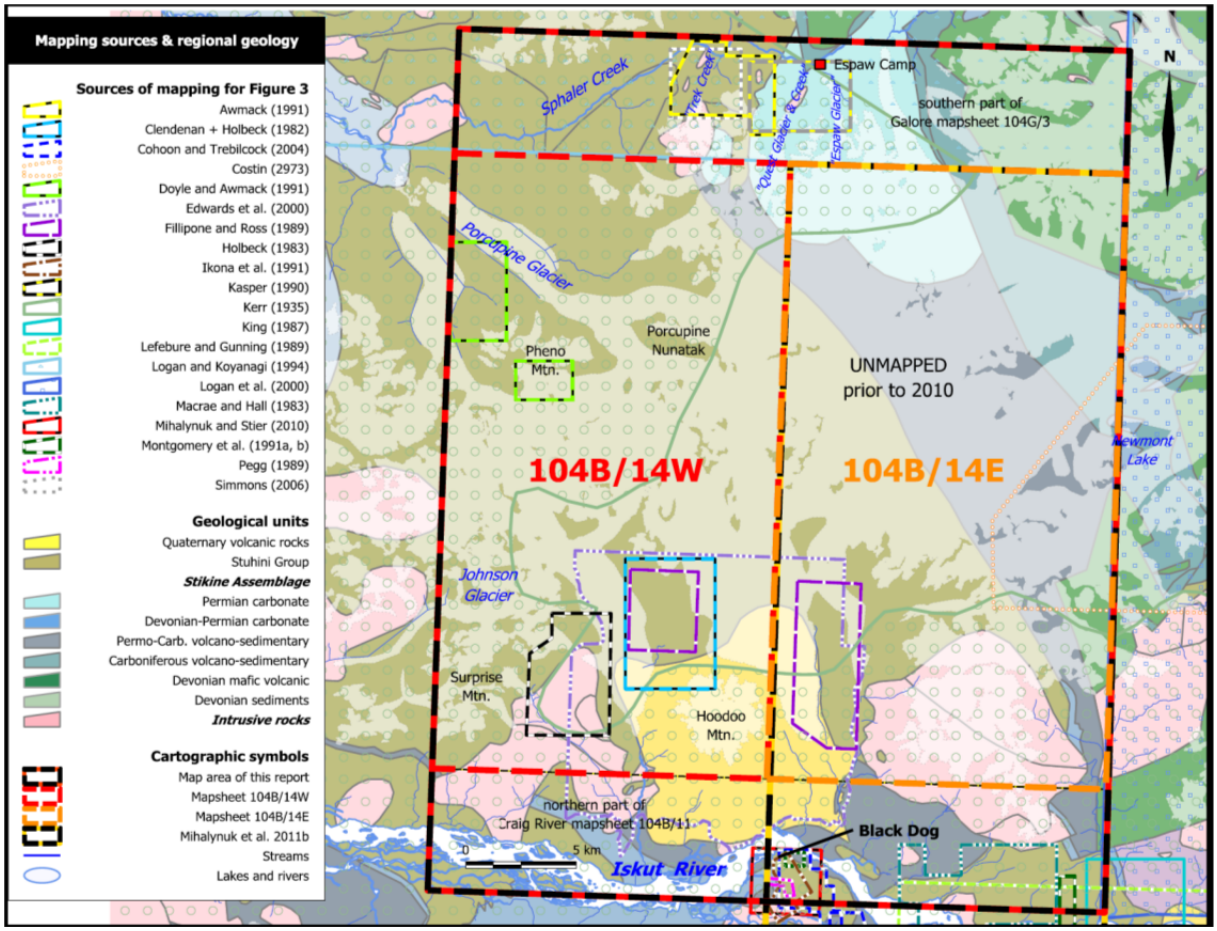

Figure 2. Sources of geological map information within the Hoodoo Mountain mapsheet (NTS 104B/14) and adjacent areas. Geological mapping and sampling in 2011 was focused in areas outlined by the western rectangle The regional geology portrayed within the study area (red rectangle) is largely after Kerr (1935) as compiled by (Massey *et al.*, 2005). Location of the Rock and Roll property (Black Dog surface showing) and important landmarks are also indicated.

Our work in 104B/14W continued to extend the geological relationships outlined by Mihalynuk *et al.* (2011b) and Logan *et al.* (2000) in the adjoining map sheets to the east and north respectively. Stratigraphic relationships between the rock packages indicate that Late Triassic Stuhini Group and Early Jurassic Hazelton Group arc and basinal strata unconformably overly a composite basement of deformed Late Paleozoic Stikine assemblage (Brown *et al.*, 1991). Structural deformation affecting Mesozoic Stuhini and Hazelton group strata include mainly east-northeast-directed thrust faults that interleave them with Paleozoic strata. High angle faults trend mainly north-northwest and northeast dissecting the interleaved strata. Eocene plutons cut the high angle faults with evidence of fault reactivation around the margins of the plutons.

STRATIGRAPHY

Hoodoo Mountain area is underlain by six volcano-stratigraphic packages that range in age from Carboniferous to Quaternary. Stratigraphic assignments in this report build upon those reported in Mihalynuk *et al.* (2011a) which rely extensively on Logan *et al.* (2000).

Paleozoic Stikine assemblage (Monger, 1977) rocks are restricted to: (a) chert, carbonate and volcanic strata in the far northeast of the Hoodoo (west) map sheet, (b) the adjacent "Quest Creek" (informal name on map in Kasper, 1989) valley farther north and (c) one <1 km^2 culmination in the upper Porcupine Glacier area (Figure 3):

1. Carboniferous mafic and felsic volcanic rocks and intercalated carbonate strata characterized by giant crinoid fossils have not yet been confirmed within the western Hoodoo map sheet; although they underlie about half of the northern and eastern margins of the eastern Hoodoo Mountain sheet (and they are mapped immediately north of 104B/14W). Permian carbonate-dominated strata characterized by large horn corals and giant fusulinids.

Three Mesozoic packages dominate the central and western map area:

2. Middle to Late Triassic strata overlying interbedded chert and limestone of presumed Permian age are composed of chert sharpstone conglomerate and turbiditic sandstone/argillite, bedded black chert, minor basalt and micritic carbonate containing *Halobiid* paper clams and ammonites.
3. Triassic arc strata characterized by coarse augite porphyritic basalt of the Stuhini Group (Souther, 1971) and extensive volcanic conglomerate and in eastern Hoodoo Mountain area. These strata are cut by alkaline intrusions that are associated with Cu-Au mineralization at the Dirk, Telena and Trek prospects (Chadwick and Close, 2009).
4. Jurassic strata mainly composed of turbiditic volcanic sandstone, argillite and conglomerate. Pebbles and cobbles are characterized by quartz and hornblende porphyritic volcanic and plutonic rocks.

Two Cenozoic magmatic rock packages span the map area:

5. A north-northwest trending belt of exhumed Eocene plutons cross the centre of the Hoodoo map sheet. These lie east of, and are geochemically distinct from,
6. Rocks of presumed Pliocene to Pleistocene age comprising volcanic strata of Hoodoo Mountain and flanking Pheno Mountains, two of the highest peaks in the Hoodoo area (Figure 3).

Paleozoic

Carboniferous volcanic rocks

Indistinctly pillowed, dark green mafic flows (Figure 4a) crop out in a belt that extends from near the mouth of Quest Creek" to the west side of upper "Quest Glacier" (Figure 3). They are strongly chlorite-epidote altered. Fine-grained felted feldspar may be observed in hand specimen with difficulty, otherwise, the unit is relatively featureless. Jasper outlines some pillows.

These pillow basalts are the presumed oldest rocks within the 2011 study area. Infolded with the mafic unit are layers of recrystallized limestone up to 5 m thick, also of presumed Carboniferous age, although giant crinoids typically contained in mid-Carboniferous carbonate are not present. Elsewhere the mafic flow unit is in contact with maroon tuff, and variable thicknesses of maroon tuff (<1 m to >5 m) occur between the mafic volcanic unit and recrystallized carbonate.

Maroon and green epiclastic and tuffaceous strata comprise a mappable unit extending ~1.5 km along Sphaler Creek upstream of "Quest Creek". Beds of dust to lapilli-sized fragments and epiclasts are centimetres to decimetres thick and may display grading (Figure 4b). In places protolith textures are well preserved, but only metres away texturally destructive foliation can be strongly developed and refolded to form a second, less intense fabric. These strata are intercalated with fine siliciclastic strata. Estimates of structural thickness based on our map data are not possible as the base of the volcanic units does not crop out in the mapped area. However, incorporating the mapping of Logan and Koyanagi (1994), a structural thickness of up to 400 m is indicated.

This unit may be correlative with lithologically similar units in eastern Hoodoo map area that occur together with rhyolite units from which a preliminary isotopic age of ~340 Ma was determined (Early Carboniferous (Viséan) age; N. Joyce, unpublished data).

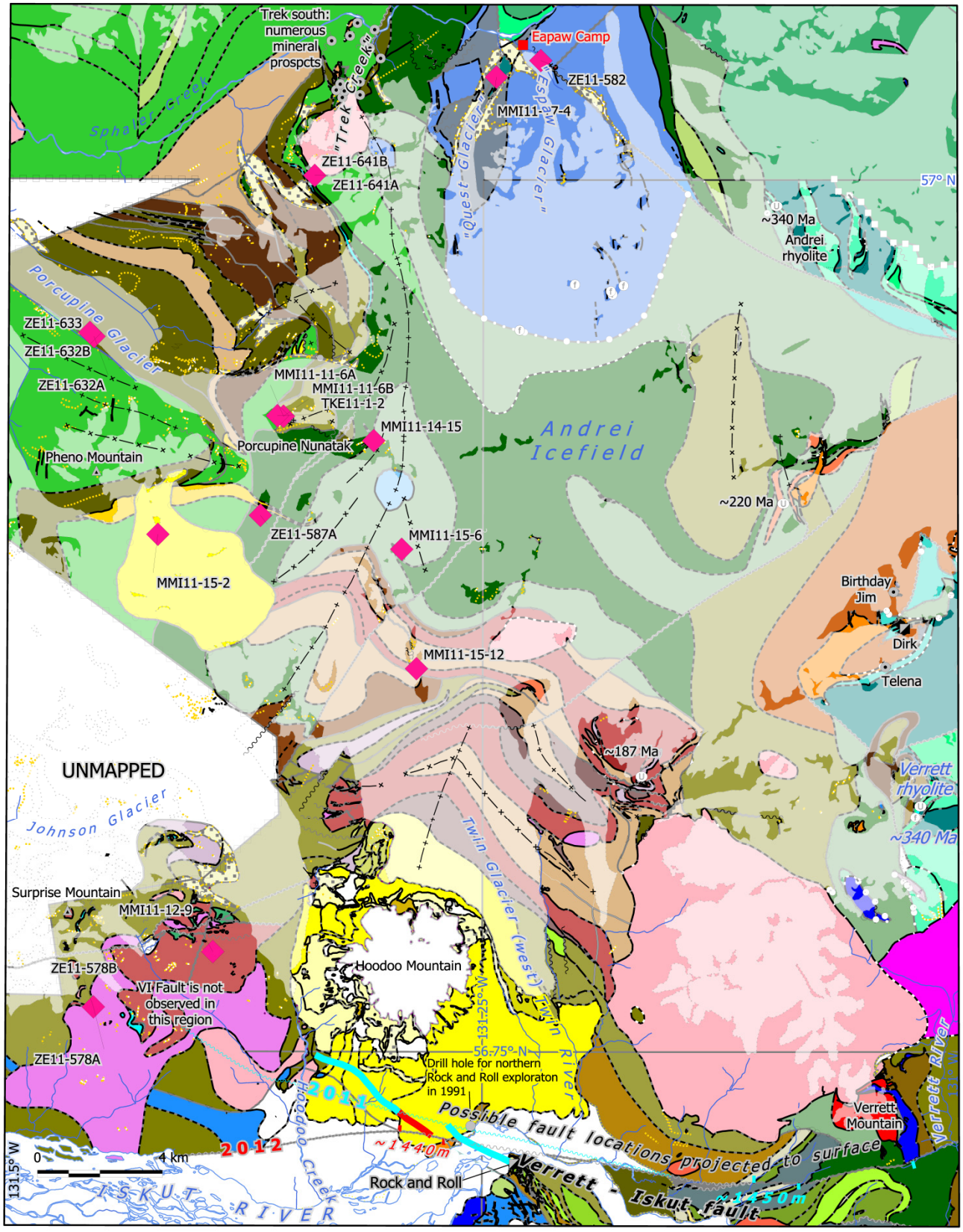

Figure 3. Geology of the Hoodoo Mountain – Iskut River area simplified after Mihalynuk *et al.* (2012). Refer to the detailed map of these authors for a full description of all units represented on Figure 3; not all minor units are included in the legend.

Layered Rocks

(Note colours muted beneath glaciers)

Pliocene to Holocene HPMVC

- porphyritic phonolite
- Pheno Mtn. "phonolitic rhyolite"
- Hoodoo-Pheno Mountain basalt
- Hoodoo Mtn. aphyric phonolite

Early Jurassic

- turbiditic calcareous wacke
- maroon ash tuff/tuffite, also in Late Triassic and Carboniferous
- dense breccia > lapilli-ash tuff
- hornblende-biotite ash flow ~187Ma
- argillaceous turbidite, fine wacke

Late Triassic (to Early Jurassic)

- orange wacke ± biotite/K-feldspar
- micritic carbonate
- well-bedded wacke ± chert clasts
- dacite ash flow ~220 Ma
- feldspar porphyry breccia, tuff, flow
- polymictic conglomerate
- feldspar pyroxene breccia ±pillowed

Middle-Late Triassic

- rusty graphitic argillite/siltstone

Paleozoic - Jurassic

(South of latitude of Hoodoo Peak)

- quartz sandstone
- siltstone ±volcanic / laminated
- chert (also Carboniferous-Permian)
- carbonaceous siltstone
- tuffaceousPhyllite/wacke
- andesite breccia and lesser ash
- mafic volcanic - tuff and minor flow
- sericite schist
- undivided sediment/volcanic
- felsic tuff and minor flows
- ash flow in Carboniferous
- argillite > volcanic sediment/tuff
- turbiditic, also Carboniferous

Early Permian

- limestone -massive to well-bedded

Carboniferous

- marble (± Permian, Devonian)
- fine siliciclastics, chert, limey
- tuffite with chert/exhalite
- volcanic wacke/conglomerate
- limestone, commonly crinoidal
- basalt -pillowed and breccia

Intrusive Rocks

Pliocene-Pleistocene

- Pheno Mtn. quartz monzonite

Eocene

- Early? Eocene granodiorite
- Jurassic-Eocene quartz diorite

Early to Middle Jurassic

- granodiorite, diorite, undivided

?Triassic - Jurassic

- coarse K-feldspar granodiorite
- diorite ±quartz diorite

Late Triassic

- K-feldspar - biotite syenite ~204 Ma

?Carboniferous

- Verrett graphic granite

Symbols

Contacts

- contact defined
- contact approximate
- contact inferred
- fault defined
- fault approximate
- fault inferred
- thrust defined
- thrust approximate
- thrust inferred
- unconformity defined
- unconformity approximate
- unconformity inferred

Other symbols

- form lines from imagery
- synform / syncline
- antiform / anticline
- limit of data
- moraine
- lakes
- glacier (transparent overlay)
- major streams
- U-Pb zircon age locality
- conodont fossil locality
- developed prospect
- mineral showing
- Geochemical sample site
- Former interpreted northern Verrett-Iskut fault trace

Figure 4. (a) Bright green and maroon epiclastic strata of presumed Carboniferous age are exposed along the banks of Sphaler Creek. (b) Maroon colouration is often incorrectly assumed to indicate subaerial deposition. At this locality, colour is an indicator of local oxidation fronts. Photo shows about 30 cm width of extensive creek exposures.

Fine siliciclastic strata and chert

Black, grey and rust, well bedded to boudinaged chert and siltstone-argillite in 3 to 15 cm thick beds occurs between the Carboniferous strata and mountainsides dominated by limestone (Figure 5). Where highly recrystallized, the chert is white or translucent. In places disrupted layers of sharpstone conglomerate comprises <3 cm diameter aphanitic olive, grey and black fragments in a foliated, calcareous matrix. In some sections volcanic ash appears within the margins of chert beds. Elsewhere, slippery light grey clay layers between chert beds are interpreted to as clay-altered ash tuff. This unit is correlated with a much less variable, bedded chert unit between Carboniferous and Permian carbonate units in east-central 104B/14E. Extensive deformation precludes estimation of stratigraphic thickness; unfaulted

Figure 5. Well-bedded chert and fine grained siliciclastic strata west of the mouth of "Quest Creek". Open to isoclinal folds plunge north (towards viewer and Sphaler Creek) and most thrust fault-fold relationships suggest a west-side-up vergence, but the opposite vergence is also indicated. Tim Davis for scale.

panels having a stratigraphic thickness of greater than 10 m thick are uncommon. Structural thickness of the unit is between 200 and 450 m, although it can be removed by faults.

A sample of chert was collected from this unit east of the top of "Quest Glacier" (northwest corner of 104B/14E; Figure 3). The unit contained a poor to moderately preserved radiolarian assemblage providing a Carboniferous age (Table 1).

Permian

Both well bedded and massive Permian carbonate units track northwards from extensive exposures underlying northern Andrei Icefield in 104B/14E to the toe of the "Espaw Glacier". Giant fusulinids are common within these units, indicative of a Permian age. For further descriptions of these units see Mihalynuk *et al.* (2011a).

An isolated exposure of interbedded light grey, fossil-poor limestone and irregular tan chert occurs on the north side of upper Porcupine Glacier (Figure 3). Carbonate layers range from 10 to 50 cm with 10 to 20 cm chert interbeds. These strata are interpreted to be Permian in age on the basis of correlation to Permian strata in the eastern Hoodoo Mountain map area. They are overlain by carbonate-rich matrix-supported chert sharpstone conglomerate (Figure 6). Although the contact is not exposed, it is interpreted to be an angular unconformity. Green felted feldspar dikes extensively crosscut and thermally alter the unit. The uncertainty over the degree of structural repetition renders thickness estimates difficult. Given that the base of the section is not observed, and the top may be bevelled by erosion, the

Table 1. Results of chert processing and radiolarian micropaleontology for sample ZE10-333.

SAMPLE No: ZE10-333
LOCALITY and COORDINATES: Nunatak at the top of Quest Glacier; 56.97971 -131.26344

GEOLOGICAL UNIT: Stikine Assemblage
LITHOLOGY: laminated chert, dark grey-black
OCCURRENCE OF RADIOLARIANS: confirmed
PRESERVATION: poor to moderate

RADIOLARIAN TAXA:
abundant spumellarians
- ?Arrectoalatus sp.
-Belowea sp.
- ?Ceratoikiscum sp.
-Entactinia multispinosa Won
-Entactinia sp.
-Entactinosphaera sp.
- ?Pylentonema sp.
OTHER: rare sponge spicules, silica fragments (matrix), pyrite, clays

AGE: CARBONIFEROUS (possibly late Mississippian-Pennsylvanian)
COMMENTS: the Carboniferous age is based on the entire assemblage. A "possible late Mississippian-Pennsylvanian" call is based on the range of Arrectoalatus sp. whose occurrence is not well established.

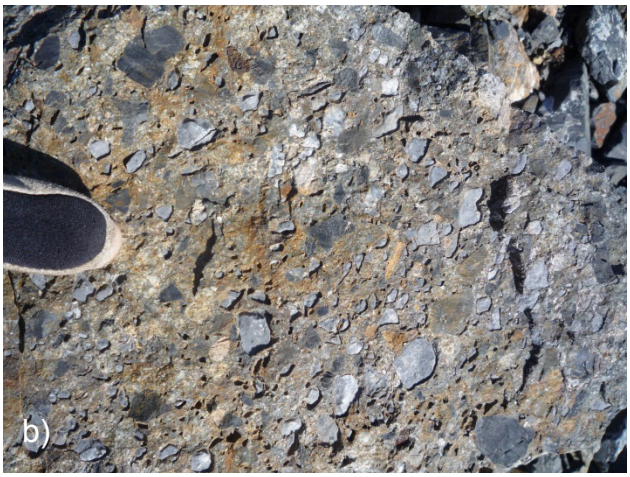

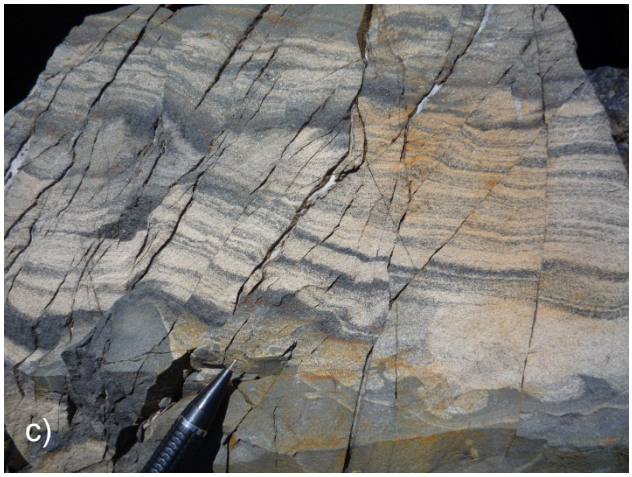

Figure 6. (a) Carbonate with irregular chert interbeds is overlain by (b) chert sharpstone conglomerate with a calcareous matrix. On the next outcropping ridge, chert sharpstone conglomerate is intercalated with feldspathic wacke (c) in which syn-depositional growth faults (some outlined by carbonate veinlets) and water-escape features are beautifully displayed.

layering-normal thickness is roughly estimated to be ~340 m.

Early to Middle Triassic?

Structurally overlying the sharpstone conglomerate–wacke unit is an irregularly bedded chert and fine siliciclastic unit with a structural thickness of no more than 100 m. Superficially like the Carboniferous chert-siliciclastic unit described above, decimetre thick chert beds in this unit range in colour from black and grey to dark green and may contain green volcanic dust and aphanitic angular fragments to coarse ash size. Siliciclastic rocks are interbedded graded sandstone-silty argillite turbidite beds 0.5-2 cm thick with scoured bases. A distinctive conglomerate layer within the unit contains

mainly rounded carbonate clasts as well as rounded black chert and rare altered porphyry clasts with equant green crystals, probably pyroxene, in a cream-coloured matrix.

This unit apparently underlies a distinctive micritic *Halobiid* carbonate packstone (*Halobiids* are ribbed, paper-thin bivalves of Carnian to middle Norian age) with sparse ammonites, and this relationship is repeated on both sides of a synform (although the carbonate unit is lost beneath cover). Similar stratigraphic relationships between fine siliciclastic rocks and micritic *Halobiid* packstone are described in Mihalynuk *et al.* (2011a) for an area in eastern 104B/14E (see that paper for further lithologic descriptions).

Late Triassic

Similar to the eastern Hoodoo map area, Late Triassic Stuhini Group strata are dominated by volcaniclastic units. In contrast to the predominance of polymictic boulder conglomerate with abundance of volcanic, carbonate, and intrusive clasts in the east Hoodoo Mountain area, western units predominantly contain volcanic clasts.

The hallmark unit of the Stuhini Group, coarse augite-phyric volcanic breccia, is present in relatively thin (~200-500 m thick) bands (although greater thicknesses could be hidden beneath glaciers). Bands of augite porphyry are overlain (and underlain in places) by more widespread epiclastic layers increasingly dominated by feldspar- rather than augite-phyric clasts. These epiclastic layers (Figure 7; see also "Feldspar-phyric breccia and epiclastic" in Mihalynuk *et al.*, 2011a) and lesser reworked maroon tuff layers ("Maroon tuff" in Mihalynuk *et al.*, 2011a) appear to interfinger with more distal sedimentary rocks (wacke and argillite) to the west (see Mihalynuk *et al.*, 2011a for descriptions).

Coarse biotite and K-feldspar-bearing conglomerate underlying tens of square kilometres in the east, are recognized only locally in the west, and the biotite and K-feldspar-porphyritic hypabyssal rocks from which they were derived have not yet been observed in the west. Interestingly, copper porphyry mineralization at the Trek property does lie along strike to the north of detrital biotite units exposed on the "Porcupine Nunatak" (see Economic Geology).

Late Triassic to Early Jurassic

Demarcation of the Triassic-Jurassic boundary within the volcanosedimentary succession in the western Hoodoo Mountain area has not been confirmed with isotopic or fossil age determinations. We suspect that it corresponds with the change from dark, carbonate-cemented conglomerate with abundant angular clasts of micritic and carbonaceous limestone (Figure 7b), feldspar-phyric and lesser pyroxene-phyric clasts, to deeper-water strata dominated by argillite to coarse wacke beds (Figure 8a). In southwest 104B/14W, fetid grey carbonate with a structural thickness of perhaps 100 m, is isolated within a

Figure 7. (a) Coarse reworked breccia fragments interbedded with coarse arkosic sandstone in northwest 104B/14W. About 1 km south of this locality the conglomerate overlies coarse augite porphyry breccia. (b) Poorly sorted carbonate-cemented conglomerate interpreted to approximately demark the Triassic-Jurassic boundary within the sedimentary-dominated succession in the western Hoodoo Mountain map sheet.

klippe atop well bedded, green tuffaceous wacke/tuffite. Although the base of the carbonate is strongly mylonitic, underlying wackes have an increasing lime interbed content towards the mylonite contact, suggesting that it is a décollement without significant stratigraphic throw. However, our preferred interpretation is that the underlying green tuffaceous wacke/tuffite unit is a distal correlative of a very well bedded green tuff/tuffite that envelopes an Early Jurassic (187.0 ±1.9 Ma, N. Joyce, personal communication, in Mihalynuk *et al.*, 2011b), dacite ash flow unit ~10 km northeast of Hoodoo Mountain (see Mihalynuk *et al.*, 2011a, "Hornblende-feldspar ash flow and breccia"), and that the mylonite represents a thrust fault between the tuffite and structurally overlying carbonate.

Strata of probable Jurassic age contain planar beds of conglomerate with well-rounded clasts (Figure 8b) having a high proportion of intraformational wacke, and quartz-phyric volcanic (Figure 9a) and hypabyssal clasts. Within this succession, tuffaceous rocks with flattened pumice

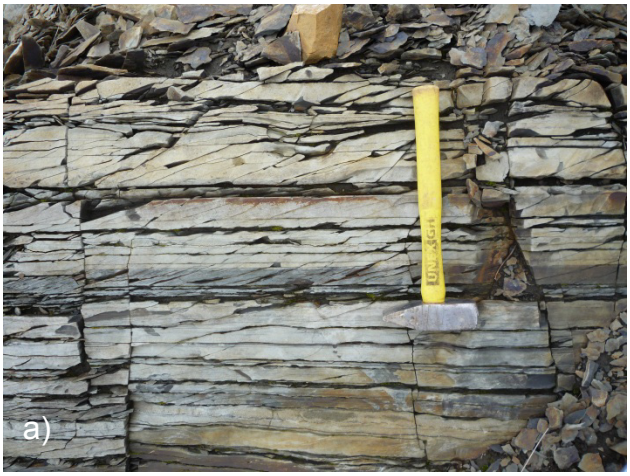

Figure 8. (a) Well-bedded turbiditic silt to sandstone beds with thin argillaceous interbeds. (b) Pebble to cobble conglomerate with medium to coarse-grained wacke interbeds.

Figure 9. (a) Matrix-supported conglomerate containing mainly quartz-phyric volcanic/hypabyssal clasts of presumed Early Jurassic age. (b) Ignimbritic feldspar porphyritic tuff is part of a volcanic/volcaniclastic section overlain (outside the photo to the north) by disrupted turbiditic strata.

blocks (Figure 9b) are broadly correlated with the Early Jurassic felsic volcanic units to the east Ammonites collected from these sections should help with age determination; results are pending.

Triassic-Jurassic stratigraphy records cessation of vigorous Triassic arc volcanism and deepening of the succeeding Triassic-Jurassic sedimentary basin. Abundance of quartz-phyric and intraformational clasts may indicate resumption of arc volcanism outside of the map area, but this volcanism is more evolved than mafic-dominated volcanism in the Triassic. Middle to Late Jurassic strata, typified by chert pebble conglomerate, have not been recognized in the Hoodoo Mountain map area.

Hoodoo - Pheno mountains volcanic complex

Majestic Hoodoo Mountain spans the southern boundary between the 2010 and 2011 map areas. It is an extinct, glacier-capped, Quaternary volcanic edifice (Figure 10a) that has been previously studied by Edwards (1997), Edwards and Russell (2002) and Edwards *et al.* (2000, 2002, and references therein). Unpublished isotopic age determinations indicate an early Quaternary to Recent history ranging from 2.8 to 0.009 Ma ($^{40}Ar/^{39}Ar$ with no error limits on personal communication from M. Villeneuve, 1998 in Edwards *et al.*, 2000; M. Villeneuve, unpublished in Edwards, 1997; and unpublished, but possibly disturbed, K-Ar whole rock age determinations of Souther and Armstrong in Breitsprecher and Mortensen, 2004). Volcanic textures support a history of interaction with glacial ice (Kerr, 1948; Edwards *et al.*, 2002 and references therein).

About 15 km north-northwest of Hoodoo Mountain is Pheno Mountain, one of the highest points in the map area. Its south flank is extensively underlain by volcanic and intrusive equivalents of the Hoodoo Mountain volcanic complex, herein we collectively term these volcanic relicts the Hoodoo-Pheno mountains volcanic complex (HPMVC). Elevations of the basal contacts of the volcanic unit at Pheno Mountain are not highly variable suggesting a Pliocene-Quaternary topography much gentler than today.

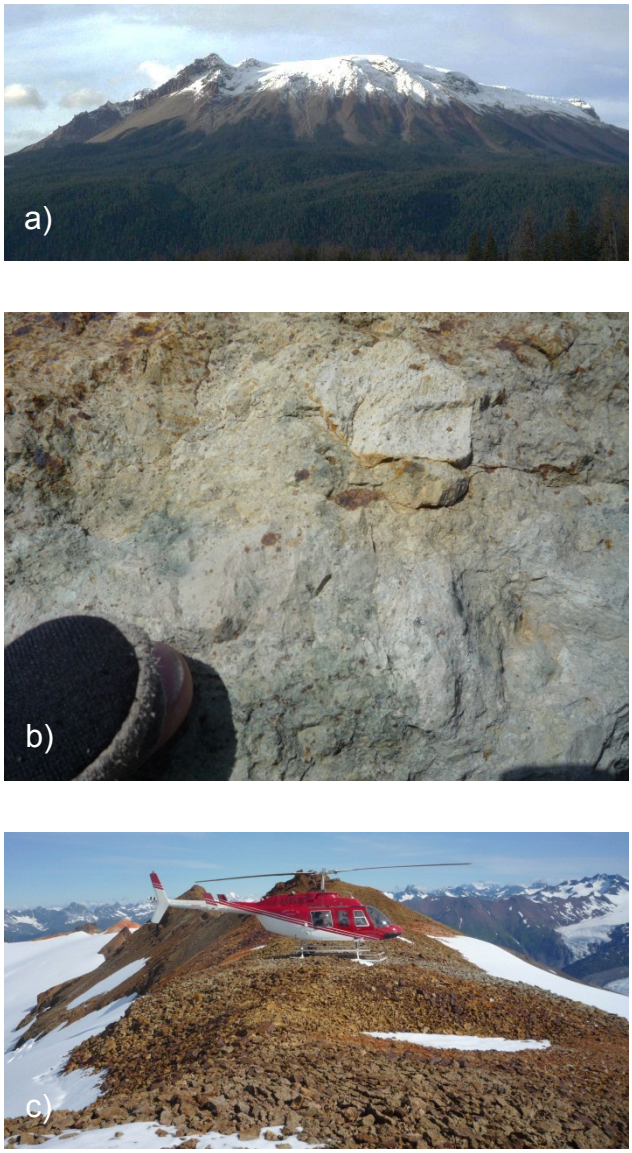

Figure 10. (a) Photo of Hoodoo Mountain looking northwest from the Iskut River. (b) Typical light-weathering lapilli tuff contains quartz-phyric fragments. (c) View to the north of weathering characteristic of Hoodoo peralkaline rhyolite. Note bright orange peak west of the helicopter tail is composed of altered Hoodoo volcanic rocks.

EXTRUSIVE COMPONENTS

Hoodoo Mountain is composed mainly of phonolitic flows and tuffaceous rocks, with lesser tephrite and trachyandesite volcanic and hypabyssal units (Edwards *et al.*, 2000). The south ridge of Pheno Mountain leads to a gentle snow peak with ribs of rock that are entirely comprised of light coloured, rusty-weathering peralkaline rhyolite (field term) lapilli tuff, lesser breccia and banded flows. Fresh surfaces are pale shades of grey, green and maroon. Medium-grained quartz eyes comprise 3-5% of the rock, together with 0.5 to 10% ghosted tabular to rounded, white to pink feldspar and 1-2% acicular chloritized crystals that were probably amphibole. Vesicles are irregularly developed, comprising up to several percent by volume of the rock. Vesicles up to 2 cm diameter are not filled, while 1-2 mm vesicles are filled with chlorite. Magnetic susceptibilities average ~0.15 x 10^{-3} SI. Rusty weathering is imparted by oxidation of pyrite (locally up to 5%) which is disseminated as cubes and irregular clots throughout all leucocratic units, both intrusive and extrusive. Parts of the unit appear strongly altered, but these parts were not collected for analysis.

HOODOO INTRUSIVE COMPONENTS

Glacier cirques dissect the southeast and southwest sides of Pheno Mountain exposing a west-striking tabular intrusive body about 800 m thick. It is composed of a white to rusty weathering alkali-feldspar porphyritic quartz monzonite to monzonite. Alkali feldspar is tabular up to 1 cm. North of the quartz monzonite, sub-parallel sills up to 3.5 m thick intrude deformed Jurassic tuffaceous country rocks.

Two types of HPMVC dikes are recognized: brown melanocratic white rhomb porphyry and leucocratic quartz-alkali feldspar porphyry. Melanocratic dikes are the most widespread and that apparently radiate from Hoodoo Mountain, especially within a northern corridor, extend at least 15 km. They are brown to black with rhombic alkali feldspar (Figure 11a) ranging from fine-grained in the chilled margin to coarse (up to 2 cm) within the dike interior where they comprise ~20% of the dike volume. Dikes attain thicknesses of 3 m, but most are 0.1 to 0.5 m thick and display sharp, parallel, chilled margins. Some dikes are banded, suggesting pulsed injection. Vesiculation is common, but vesicles rarely comprise more than 5% of the dike volume. Late brittle faults commonly offset the dikes (Figure 11a).

Leucocratic dikes are pale grey with pinkish or greenish casts, and commonly with rusty-weathering zones (Figures 11b). Their phenocryst contents are variable, but a typical dike will contain 25% alkali feldspar as single crystals or glomerocrysts up to 2 cm diameter. Quartz comprises 20% as fine to medium-grained eyes and may also mantle feldspars. A clear mineral that is softer than quartz occurs within the rock matrix. At high levels, chilled dike contacts are distinctive. Outside of the main dike body a frothy and siliceous zone 10-20 cm thick containing fragments of country rocks can envelope parts of the dike locally. Within the dike, chilled margins are flow banded and can be a deep blue colour (Figure 11c). If this colour is imparted by very fine-grained sodic amphibole (*e.g.* arfvedsonite), none have been recognized in hand specimen. Magnetic susceptibilities of both melanocratic and leucocratic dikes are typically higher than the extrusive peralkaline rhyolite, with averages ranging to 20 (x 10^{-3} SI).

HOODOO - PHENO COMPLEX GEOCHEMISTRY

Peralkaline rocks of Hoodoo Mountain are characterized by elevated concentrations of high field strength elements such as Nb, Ta, Hf, Th, U and Zr as

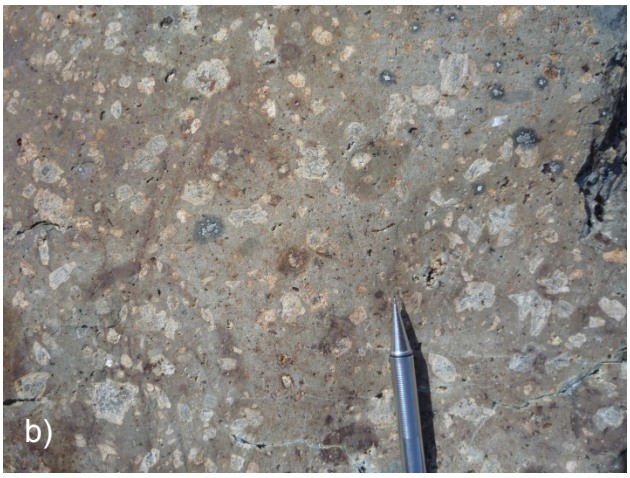

Figure 11. (a) Melanocratic, coarse alkali feldspar porphyritic dikes strike towards Hoodoo Mountain from a location about 18 km to the north. (b) Typical leucocratic quartz-alkali feldspar porphyry dike. (c) Leucocratic dike with commonly developed blue flow-banded margins.

well as most rare earth elements (Figure 12). Semiquantitative analyses of the Pheno Mountain volcanic and intrusive rocks were conducted in the field using a handheld XRF. These analyses demonstrate very strong Zr enrichment characteristic of peralkaline complexes. In addition, INAA analyses of these rocks acquired following the field season show elevated high field strength elements (HFSE) and rare earth elements (REE), (Table 2). Considering the serendipitous nature of this REE discovery, exploration for higher grade REE zones may be warranted (see Economic Geology).

Source of peralkaline magmas can vary from anatectic crustal melts to melting of metasomatized subcontinental mantle lithosphere (*e.g.* Schmitt *et al.*, 2000). Edwards *et al.* (2002) suggest that compositions of phonolitic volcanic rocks at Hoodoo Mountain may have been modified from primary, mantle-derived alkali-olivine basalt through a process of fractional crystallization and crustal assimilation. Petrogenesis of the Hoodoo-Pheno mountains volcanic complex (HPMVC) is beyond the scope of the current study; however, elevated U and Th within the Pheno Mountain suite of rocks analyzed show a U/Th ratio of 0.27, equivalent, within error, to average upper crustal values of 0.26 (Figure 13; Taylor and McLennan, 1985). REE abundances of rocks near Pheno Mountain as determined by Instrumental Neutron Activation Analysis (INAA) are compared with those from Hoodoo Mountain reported by Edwards (1997) as determined by Inductively Coupled Plasma Mass Spectroscopy (ICP-MS; Figure 12). Elemental abundances are comparable, except for europium, but it is not known if this discrepancy is due, at least in part, to comparison of results by two different geochemical techniques.

INTRUSIVE ROCKS

Western Hoodoo Mountain area is extensively cut by plutons, stocks and dikes that range in composition from gabbroic to granodioritic with minor intrusions as felsic as quartzolite. Most significant are a continuation of the Twin River granodiorite (Mihalynuk *et al.*, 2011b) belt across the northeast map area, as well as satellites of the Coast Plutonic Complex which are particularly prevalent in the southwest.

Eocene Twin River granodiorite belt

Twin River pluton (Mihalynuk *et al.*, 2011a, b) is a ~50 km^2, northwest-elongated pluton that underlies the eastern headwaters of the Twin River. Much smaller bodies crop out in a belt extending to the northwest, parallel with the dominant structural grain. A ~6 km^2 stock straddles the boundary between 104B/14E and W

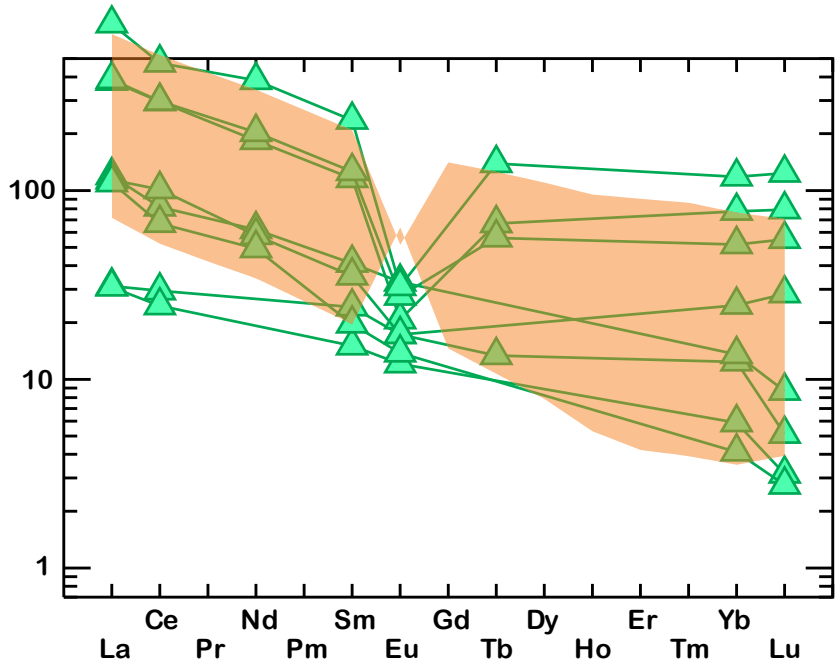

Figure 12. INAA geochemical analyses of HPMVC volcanic rocks from near Pheno Mountain. Rare Earth Elements are normalized with respect to chondrite using factors of Sun and Mcdonough (1989). The orange field are a comparison with ICP-MS sample analyses reported by Edwards *et al.* (2000).

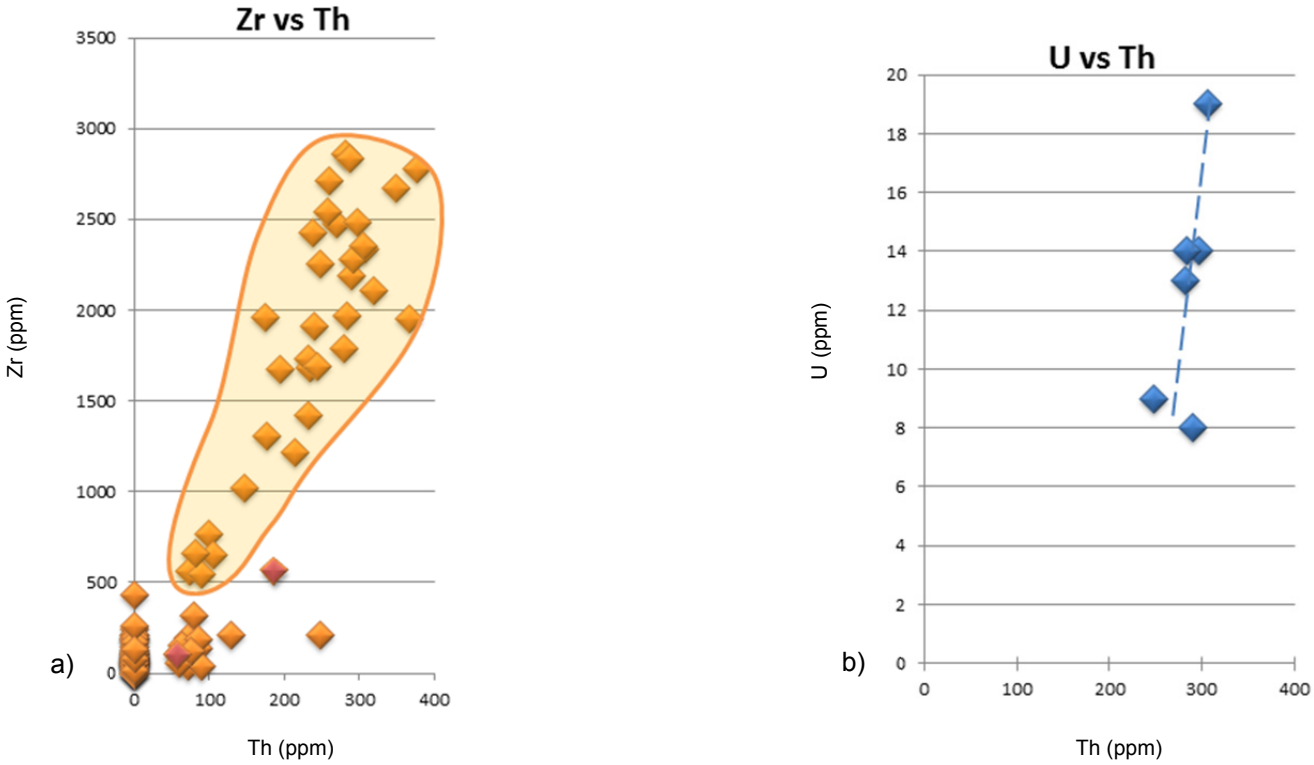

Figure 13. (a) Plot of Zr versus Th from 123 semiquantitative analyses of units within the Hoodoo west map area. All of the samples with Zr >500 ppm (N=31, shaded field) are part of the Hoodoo-Pheno mountains volcanic complex (HPMVC), and were collected mainly from volcanic and subvolcanic units in the Pheno Mountain area. One exception is a pyrite vein (red sample point) of unknown parentage. Detection limits for the handheld XRF vary on a per analysis basis, but averages for this dataset are Th=±40 ppm and Zr=±14 ppm. (b) Uranium versus thorium for HPMVC displays average crustal values of 0.27 (*cf.* 0.26 from Taylor and McLennan, 1985), suggesting derivation from a crustal source.

Table 2. Instrumental Neutron Activation Analysis (INAA) results from samples collected at sites shown on Figure 3. See Table 3 for grid coordinates.

		Analyte >	Au	Ag	As	Ba	Br	Ca	Co	Cr	Cs	Fe	Hf	Mo	Na	Rb	Sb	Sc	Se	Sn	Ta	Th	U	W	Zn	La	Ce	Nd	Sm	Eu	Tb	Yb	Lu	Mass
		Unit >	ppb	ppm	ppm	ppm	ppm	%	ppm	ppm	ppm	%	ppm	ppm	%	ppm	ppm	ppm	ppm	%	ppm	ppm	ppm	ppm	ppm	ppm	ppm	ppm	ppm	ppm	ppm	ppm	ppm	g
		MDL >	2	5	0.5	50	0.5	1	1	5	1	0.01	1	1	0.01	15	0.1	0.1	3	0.02	0.5	0.2	0.5	1	50	0.5	3	5	0.1	0.2	0.5	0.2	0.05	
Sample No.	**Lab No.**	**Type**																																
MMI11-11-6A	62286	Rock Pulp	9	< 5	4.1	240	< 0.5	< 1	< 1	132	< 1	2.78	31	< 1	3.65	41	1.8	1	< 3	< 0.02	9.4	22.4	9.4	< 1	< 50	81.3	158	73	18.3	1.2	3	15.2	2.35	29.4
MMI11-11-6B	62287	Rock Pulp	< 2	< 5	6	90	< 0.5	< 1	4	245	< 1	1.83	< 1	< 1	0.05	< 15	2	1.4	< 3	< 0.02	< 0.5	< 0.2	< 0.5	< 1	< 50	24.8	31	15	2.4	0.6	< 0.5	0.3	< 0.05	32.9
MMI11-12-9	62288	Rock Pulp	56	18	83.9	510	< 0.5	< 1	62	124	< 1	6.53	< 1	< 1	2.08	< 15	0.5	13.1	< 3	< 0.02	< 0.5	1.9	1.4	< 1	500	7.3	15	< 5	2.3	0.7	< 0.5	1	0.08	31.6
MMI11-14-15	62289	Rock Pulp	4	< 5	10.3	210	< 0.5	< 1	2	226	< 1	0.6	< 1	< 1	0.05	< 15	12.7	1	< 3	< 0.02	< 0.5	0.5	< 0.5	< 1	60	1.8	5	< 5	0.4	< 0.2	< 0.5	< 0.2	< 0.05	32.6
MMI11-15-2	62290	Rock Pulp	7	< 5	126	260	< 0.5	< 1	< 1	104	< 1	0.94	35	13	0.05	81	3.7	0.5	4	< 0.02	13.1	30.9	21.4	< 1	< 50	74.6	151	91	23.5	1.5	4.5	18.8	3	28.4
MMI11-15-6	62291	Rock Pulp	< 2	< 5	8.3	160	0.8	< 1	5	230	< 1	1.01	< 1	< 1	0.04	< 15	18.7	3	< 3	< 0.02	< 0.5	< 0.2	< 0.5	< 1	< 50	2.5	5	< 5	0.6	< 0.2	< 0.5	< 0.2	< 0.05	33.5
MMI11-15-12	62292	Rock Pulp	< 2	< 5	2.1	< 50	< 0.5	< 1	3	171	< 1	1.16	< 1	< 1	0.2	< 15	< 0.1	5.3	< 3	< 0.02	< 0.5	< 0.2	< 0.5	< 1	< 50	0.5	< 3	< 5	< 0.1	< 0.2	< 0.5	< 0.2	< 0.05	32.7
MMI11-17-4	62293	Rock Pulp	< 2	< 5	81.2	810	< 0.5	< 1	32	77	< 1	20.6	5	24	0.3	30	12.5	1.6	< 3	0.02	3.8	7.3	8.3	< 1	< 50	50.1	86	26	3.2	0.8	< 0.5	0.4	< 0.05	37.6
TKE11-1-2	62294	Rock Pulp	< 2	< 5	8.8	1350	< 0.5	2	11	74	3	3.64	< 1	< 1	2.98	57	2.9	14.6	< 3	< 0.02	< 0.5	3.3	1.8	< 1	< 50	9.7	20	9	1.9	0.4	< 0.5	0.9	0.15	29.8
ZE11-578A	62296	Rock Pulp	7	< 5	2.6	100	< 0.5	< 1	3	288	< 1	1.96	< 1	42	0.03	< 15	1.7	0.4	10	< 0.02	< 0.5	< 0.2	< 0.5	41	< 50	< 0.5	< 3	< 5	< 0.1	< 0.2	< 0.5	< 0.2	< 0.05	31.7
ZE11-578B	62297	Rock Pulp	< 2	< 5	1.5	< 50	< 0.5	< 1	< 1	309	< 1	0.88	< 1	7	0.02	< 15	0.7	< 0.1	< 3	< 0.02	< 0.5	< 0.2	< 0.5	252	< 50	< 0.5	< 3	< 5	< 0.1	< 0.2	< 0.5	< 0.2	< 0.05	33.4
ZE11-582	62298	Rock Pulp	4960	< 5	32600	< 50	< 0.5	< 1	31	130	< 1	18.1	< 1	< 1	0.08	< 15	489	0.8	22	< 0.02	< 0.5	< 0.2	3.6	154	< 50	< 0.5	< 3	< 5	< 0.1	< 0.2	< 0.5	< 0.2	< 0.05	44.2
ZE11-587A	62299	Rock Pulp	< 2	< 5	179	< 50	< 0.5	< 1	2	132	4	3.27	26	57	0.37	146	7.9	0.4	6	< 0.02	9.5	22.4	15.5	< 1	190	90	181	86	17.7	1.2	2.5	13.2	2.01	31.5
ZE11-632A	62300	Rock Pulp	18	< 5	144	1100	< 0.5	< 1	3	97	< 1	3.09	8	9	2.43	86	6.4	6.5	< 3	< 0.02	1.9	7.9	3.2	5	180	27	62	27	5.4	1	< 0.5	4.2	0.72	32.1
ZE11-632B	62301	Rock Pulp	4	< 5	20.4	< 50	< 0.5	< 1	< 1	43	2	3.39	16	19	0.18	244	2.4	1.2	< 3	0.05	6.9	13	3.7	3	200	91.8	182	95	19.3	1.6	2.1	8.8	1.4	30.2
ZE11-633	62302	Rock Pulp	< 2	< 5	546	< 50	< 0.5	< 1	< 1	114	< 1	3.33	35	7	2.53	77	8.8	0.4	< 3	< 0.02	11.3	26.4	5.9	< 1	410	181	290	179	36.1	1.8	5.2	20.1	3.14	34.3
ZE11-641A	62303	Rock Pulp	4	< 5	4.3	2210	< 0.5	3	6	109	3	2.07	3	24	2.9	114	1.9	4.5	< 3	< 0.02	< 0.5	11.6	4.5	18	70	26.1	41	23	3	0.8	< 0.5	0.7	0.07	29.9
ZE11-641B	62304	Rock Pulp	< 2	< 5	4.4	1750	< 0.5	< 1	8	157	3	4.11	3	27	2.38	67	0.9	3.7	< 3	0.05	< 0.5	8.8	4	< 1	< 50	17.6	31	15	2.5	0.6	< 0.5	0.7	0.06	33.7
Reference Materials																																		
MMI11-QUARTZ	62276	Rock Pulp	< 2	< 5	2.3	< 50	< 0.5	< 1	< 1	345	< 1	0.31	< 1	< 1	0.02	< 15	0.2	0.2	< 3	< 0.02	< 0.5	< 0.2	< 0.5	< 1	< 50	< 0.5	< 3	< 5	< 0.1	< 0.2	< 0.5	< 0.2	< 0.05	32.2
GSB-till	62295	Rock Pulp	47	< 5	75.7	1170	< 0.5	< 1	50	374	3	7.97	3	< 1	1.91	< 15	17.5	28	< 3	< 0.02	2.7	6.1	2.6	< 1	420	28.4	50	29	6.3	1.9	< 0.5	2.3	0.22	26.8
DMMAS 114 Measured			2250		1760	1710			40	91		3.34			1.98		9.7	6.8					17.2			16.9	27		2.4					
DMMAS 114 Certified value			2199		1624	1561			42	84		3.31			1.78		11.2	6.5					17.4			15.1	23.7		2.4					
Blank			< 2	< 5	< 0.5	< 50	< 0.5	< 1	< 1	< 5	< 1	< 0.01	< 1	< 1	< 0.01	< 15	< 0.1	< 0.1	< 3	< 0.02	< 0.5	< 0.2	< 0.5	< 1	< 50	< 0.5	< 3	< 5	< 0.1	< 0.2	< 0.5	< 0.2	< 0.05	

Analyses performed by Activation Laboratories Ltd., Ancaster

Method INAA 1D, 30g

and a stock of similar size extends less than a kilometre within 104B/14W, mainly contained by map sheet 104G/03 where it underlies the headwaters of "Trek Creek" (Figure 3). These bodies are composed mainly of hornblende-biotite granodiorite. They are blocky, and light grey to white-weathering. At "Trek Creek", medium-grained biotite>>hornblende granodiorite with ~10% chloritized mafic minerals comprises a pluton with a diameter ~3 km across its slightly elongated northeast axis. Border phases commonly contain mafic xenoliths. A strong thermo-metamorphic halo can affect country rocks more than 0.5 km from the surface contact. Proximal wacke is hornfelsed while distal intermediate breccia is epidote-chlorite altered.

Logan and Koyanagi (1994) report a K/Ar biotite age for the "Trek Creek" body of 47.3 ±1.7 Ma. Age determinations from the two bodies to the southeast within the belt are pending.

Quartzolite

Approximately 4 km east of Surprise Mountain, shallow to moderately dipping quartz veins coalesce downwards to form the continuous roof of a "flow-banded" felsic intrusion estimated to be comprised of >90% banded quartz with ~10% fine grained aplite bands. Only 200 m in its exposed, north-elongate dimension, this body is an oddity. It is orange and white weathering, and contains no visible sulphide mineralization. Age of the quartzolite body is unknown, but lack of any deformation suggest that it is Eocene or younger.

Blue-grey feldspar porphyry-gabbro complex

In the same area as the quartzolite body is a complex of blue-grey feldspar porphyry and gabbro. Intrusive contacts meander and it is not known if the intrusive phases comingle or are of entirely separate magmagenesis. Locally the gabbro does appear to cut the porphyry. In places the porphyry appears brecciated and may be volcanic in origin. Feldspar comprises ~10-15% of the porphyry, is medium grained and too turbid to permit identification of twin planes.

Gabbro is green to black weathering with medium to coarse equant crystals, probably uralitized pyroxene in an approximately equal volume of epidote-chlorite altered feldspathic matrix (Figure 14). Gabbro may be interlayered or contain screens to several metres thick of cherty argillite. Magnetic susceptibility of the gabbro is surprisingly low, averaging 0.75 (x10-3 SI). Age of these units is not known, but they are suspected to be Triassic or Jurassic. However, they may be younger, related to "Mesozoic to Tertiary" intrusions (below).

Mesozoic to Tertiary gabbro to granodiorite

Between Hoodoo and Surprise mountains is an irregular bimodal intrusion that cuts and thermally metamorphoses the well-bedded Triassic section. This

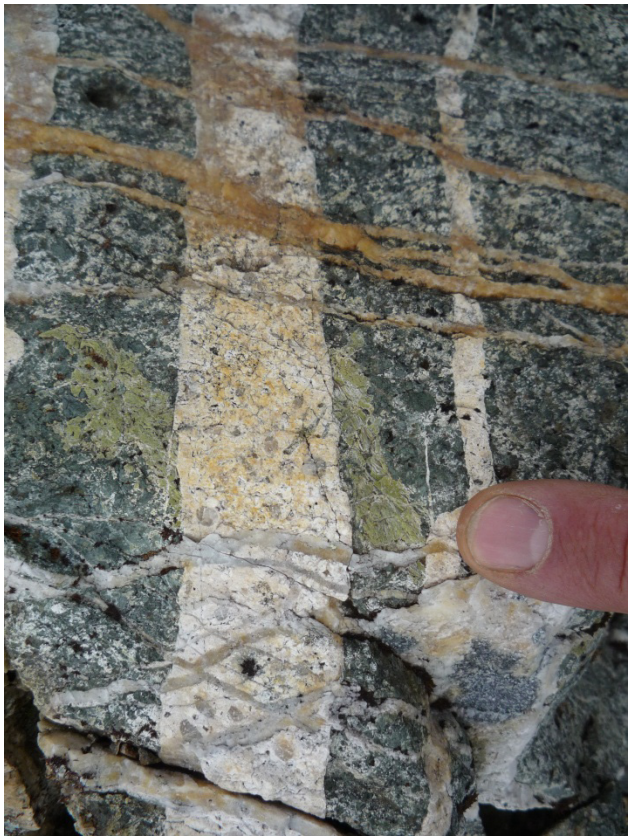

Figure 14. Epidote altered, dark green gabbro in Surprise Mountain area is cut by quartz-eye porphyritic granitoid, which is cut by white and rust sheeted quartz veins.

body may be equivalent to the "Mesozoic to Tertiary varitextured melano-granodiorite" of Mihalynuk *et al.* (2011a).

Away from the main intrusive mass, dikes and tongues of gabbro-quartz diorite are common within the overlying sedimentary rocks. At its eastern end the intrusion is variegated, but mainly composed of altered, medium to coarse grained pyroxene gabbro and quartz diorite. In this area, it weathers light grey-green and may display an orangish rind. Locally it is porphyritic with euhedral, green to black subidiomorphic pyroxene (probably largely replaced by amphibole) floating in a white feldspathic matrix in which turbid altered plagioclase (probably now albite) is locally replaced by epidote. Pyrite is finely disseminated (~0.25%) together with traces of chalcopyrite. More quartz dioritic compositions contain chloritized hornblende (25%) and platy biotite (<10%). Fresh biotite occurs locally within a ~1 m thick chilled contact. This has been sampled for $^{40}Ar/^{39}Ar$ age determination; results are pending. Intrusion of this body post-dates mylonitic fabrics in presumed Triassic limestone and foliated augite-phyric tuff. A Cretaceous or Eocene age is expected.

To the west, the body is dominated by chloritized, medium grained, acicular hornblende diorite. In places the western body is foliated. It is cut by quartz-eye feldspar porphyry dikes that may attain thicknesses of more than 3 m, and sheeted sets of rusty quartz veins containing

centimetre knots of pyrite as well as centimetre-long prismatic bismuthinite (see Economic Geology).

ECONOMIC GEOLOGY

Previous Exploration

A brief history of mineral exploration within the Hoodoo and adjacent areas dating to the 1900s is presented in Mihalynuk *et al.* (2011a) and is amply documented elsewhere (*e.g.* ARIS reports and MINFILE, 2011). Mineralization recognized in the eastern Hoodoo sheet includes volcanogenic massive sulphide-style mineralization of probable Late Triassic age (Bernales *et al.*, 2008) and Carboniferous age (Logan, 2004; Mihalynuk *et al.*, 2011a), and Late Triassic intrusion-related vein, skarn and disseminated mineralization (Chadwick and Close, 2009). We have recognized no VMS-style mineralization in the western Hoodoo sheet, however, we report on other new mineralization and pathfinders. In addition, 2011 was a busy year for exploration at the Trek copper porphyry property.

Trek Creek copper porphyry mineralization and regional potential

Trek

Currently, the most active mineral exploration project in the area is the Trek prospect. Mineralization was discovered at the Trek prospect in 1957 (Holtby, 1989). Successive exploration programs have led to discovery of numerous zones of mineralization including a swarm of breccia pipes with diameters between 3 and 15 m (Desautels, 2011). Drilling at the north Trek in 2011 returned a 22.1 metre intersection grading 1.25% Cu and 22.43 g/t Ag (Skimmer, 2011) as well as longer, lower grade intersections. We did not map or sample the mineralized zones on the Trek property, but they are reported to be related to a porphyry system of Late Triassic age (Skimmer, 2011; for up-to-date exploration results at the Trek and alkalic porphyry copper-gold targets at the Dirk-Telena in the eastern Hoodoo Mountain sheet, see Romios Gold Resources Inc. web site http://www.romios.com).

Regional alkalic porphyry potential

Mapping in the Porcupine nunatak area south of "Trek Creek" reveals detrital biotite-rich wacke in faulted sections. This same lithology forms an apron around the mineralizing eruptive centre at the Dirk prospect in east central 104B/14E (Mihalynuk *et al.*, 2011a), and close to the intrusive centre, coarse K-feldspar and chrome diopside are found. Near the Galore Creek deposit too, strata containing clasts of coarse K-feldspar crystals and biotite mark the time of mineralizing intrusions. Thus, these strata may be a vector for alkaline magmatism related to alkalic copper-gold porphyry mineralization, and therefore, a useful regional exploration tool.

A possible test of this exploration tool is the area southwest of Telegraph Creek (Figure 1) where Forest Kerr (1948) describes sediments overlying or nearly overlying the Triassic volcanic rocks: "…a unique coarse tuff is commonly found, andesitic in composition, with large crystals of acid oligoclase, unusually dark green diopside, and, rarely, a crystal of biotite. It is well displayed on Brewery Creek mountains and in Prichard Creek area" (page 29). It may be that these strata are related to an alkalic intrusive-extrusive centre. Exploration in the areas noted by Kerr is warranted to test this possibility.

Mineralization in 104B/14W

Mineralization encountered during our mapping within 104B/14W and adjacent to its northern boundary is located in three areas. From north to south these are: "Trek Creek"-"Espaw Glacier" area, south flank of Pheno Mountain, and the Hoodoo-Surprise mountains area.

Mineralized "Espaw Glacier" moraine

At the east side of the toe of "Espaw Glacier" a subrounded rusty, arsenopyrite-rich boulder was sampled (sample ZE11-582, Table 3: 29.9% Fe, >10% S and >1% As). Analysis of the boulder shows it to contain 6.1 g/t Au, 29 g/t Ag and 0.16% Cu. We are uncertain of the source of the boulder, but presume that it was carried by the glacier from some point up the east side of the "Espaw Glacier" valley.

Hoodoo Glacier – Surprise Mountain area mineralization and indicators

In the area between Hoodoo and Surprise mountains, persistently west dipping, volcanic tuff and derived sedimentary rocks and minor flows and sills are cut by diorite to granodiorite intrusions of Mesozoic or Eocene age. Near its western contact, the intrusion is cut by sheeted sets of rusty quartz veins (Figure 15a). A feldspar porphyritic unit within the sedimentary succession contains a series of quartz-chalcopyrite veins rarely up to 20 cm thick.

Rusty sheeted quartz veins

Thickness of the sheeted veins ranges from millimetres to a decimetre (Figure 15a). They are vuggy owing to removal by weathering of disseminations of cubes and knots of pyrite up to 1 cm diameter. Insoluble prisms and crystal clusters of bismuthinite, once intergrown with the pyrite, are more than 1 cm long (Figure 15b; confirmed by handheld XRF).

We analyzed two samples: one from the vein shown in Figure 15b and one from a nearby vein (sample ZE11-578A and B). Neither sample returned appreciable Au (5 ppb, Table 3, 7 ppb Table 2). However, elements known to be pathfinders for intrusive-related gold deposits (*cf.* Lefebure and Hart, 2005) are elevated beyond the limit of accurate measurement by the ICP-MS method (Table 3):

Table 3. Inductively Coupled Plasma Mass Spectrometry results for samples collected at sites shown on Figure 3. Grid coordinates are UTM zone 9, NAD83 (mean for CONUS).

		Analyte >	Mo	Cu	Pb	Zn	Ag	Ni	Co	Mn	Fe	As	Au	Th	Sr	Cd	Sb	Bi	V	Ca	P	La	Cr	Mg	Ba	Ti	B	Al	Na	K	W	Hg	Sc	Tl	S	Ga	Se	Te
		Unit >	ppm	ppm	ppm	ppm	ppm	ppm	ppm	ppm	%	ppm	PPB	ppm	ppm	ppm	ppm	ppm	ppm	%	%	ppm	ppm	%	ppm	%	ppm	%	%	%	ppm	ppm	ppm	ppm	%	ppm	ppm	ppm
		MDL >	0.1	0.1	0.1	1	0.1	0.1	0.1	1	0.01	0.5	0.5	0.1	1	0.1	0.1	0.1	2	0.01	0.001	1	1	0.01	1	0.001	20	0.01	0.001	0.01	0.1	0.01	0.1	0.1	0.05	1	0.5	0.2
Sample No.	**Lab No.**	**Type**																																				
MMI11-11-6A	62286	Rock Pulp	1.7	20.5	34.3	33	<0.1	2	0.8	62	3.07	2	1.8	6.5	3	<0.1	1	0.1	4	<0.01	0.009	35	77	0.01	12	0.006	<20	0.17	0.111	0.04	<0.1	<0.01	0.1	<0.1	0.61	3	1.3	<0.2
MMI11-11-6B	62287	Rock Pulp	0.2	67.6	2.8	18	<0.1	5.4	4.3	998	1.81	3.8	2.6	0.3	22	<0.1	0.2	<0.1	36	0.75	0.02	21	125	0.73	25	0.004	<20	0.66	0.003	0.01	<0.1	<0.01	1.4	<0.1	0.05	3	<0.5	<0.2
MMI11-12-9	62288	Rock Pulp	0.7	>10000.0	12.1	394	15.4	13.7	60.2	718	6.04	75.9	37.5	0.3	17	3.3	0.4	0.2	107	0.7	0.072	3	55	1.16	13	0.147	<20	1.87	0.046	0.03	0.1	0.05	4.8	<0.1	1.6	7	7.7	1
MMI11-14-15	62289	Rock Pulp	0.6	21.8	0.7	61	0.1	5.5	1.5	104	0.53	6.8	1	0.1	2	0.5	1.1	<0.1	8	0.03	0.013	<1	115	0.02	32	0.003	<20	0.13	0.002	0.04	<0.1	<0.01	0.5	<0.1	0.05	<1	0.6	<0.2
MMI11-15-2	62290	Rock Pulp	12.5	29.3	16.5	12	0.3	1.5	0.3	61	0.67	133.8	1.2	2.6	1	<0.1	0.6	0.1	<2	0.08	0.001	51	62	<0.01	4	0.005	<20	0.43	0.004	0.31	<0.1	<0.01	<0.1	0.1	0.18	7	<0.5	<0.2
MMI11-15-6	62291	Rock Pulp	0.2	1117.2	1.6	7	0.6	5.6	5	346	0.91	5.9	3.9	0.1	10	0.2	0.5	<0.1	11	0.94	0.02	2	126	0.14	30	0.001	<20	0.33	0.004	0.08	<0.1	<0.01	1	<0.1	0.07	<1	0.5	<0.2
MMI11-15-12	62292	Rock Pulp	<0.1	19.4	0.4	4	<0.1	3.5	1.6	142	0.36	0.6	0.9	<0.1	12	<0.1	<0.1	<0.1	6	0.36	0.001	<1	140	0.08	7	0.001	59	0.1	0.006	0.01	<0.1	<0.01	0.7	<0.1	<0.05	<1	<0.5	<0.2
MMI11-17-4	62293	Rock Pulp	26.2	13.9	35.1	48	0.3	116.2	39.2	152	25.97	99.7	0.6	0.4	45	0.5	1.4	<0.1	8	0.88	0.01	5	41	0.64	7	0.003	<20	1.32	0.04	0.13	<0.1	0.21	0.4	0.7	>10.00	7	<0.5	<0.2
TKE11-1-2	62294	Rock Pulp	0.1	77.5	9.7	45	<0.1	5.8	10.3	645	3.51	6	<0.5	1	84	<0.1	1.1	<0.1	80	1.84	0.076	6	33	0.95	211	0.041	<20	1.6	0.051	0.37	<0.1	<0.01	9.2	<0.1	0.41	5	<0.5	<0.2
ZE11-578A	62296	Rock Pulp	46.2	28.3	46	4	2.9	3.4	2	12	2.01	<0.5	5.5	0.1	1	<0.1	1.5	>2000.0	4	<0.01	0.002	<1	138	<0.01	15	0.002	<20	0.03	0.002	0.02	41.3	<0.01	0.1	<0.1	1.14	<1	10.1	3.9
ZE11-578B	62297	Rock Pulp	8	9.7	22.6	2	0.3	3.8	0.6	11	0.89	<0.5	0.6	<0.1	2	<0.1	0.5	766.6	<2	<0.01	<0.001	<1	145	<0.01	42	<0.001	<20	0.02	0.003	0.01	>100.0	<0.01	<0.1	<0.1	0.49	<1	4.6	1.5
ZE11-582	62298	Rock Pulp	2	1605.3	54.1	127	29.2	2.8	52.8	1657	29.94	>10000.0	6133	<0.1	70	3.1	551.6	32	6	1.86	0.003	<1	58	0.15	8	<0.001	<20	0.03	<0.001	<0.01	>100.0	<0.01	<0.1	<0.1	>10.00	<1	28.7	8.4
ZE11-587A	62299	Rock Pulp	46.6	10.6	24.5	218	0.1	1.5	0.7	190	2.91	177.6	<0.5	2.4	4	0.3	5.9	2.7	2	0.89	0.003	67	64	<0.01	10	0.056	<20	1.1	0.062	1.12	0.6	<0.01	<0.1	0.7	1.22	9	1.1	<0.2
ZE11-632A	62300	Rock Pulp	4.2	15.6	10.1	173	0.4	1.8	3	276	3.19	152.2	8.5	0.9	5	0.3	3	2	<2	0.18	0.03	15	57	0.02	58	0.003	<20	0.58	0.044	0.26	1	<0.01	1.2	<0.1	2	3	0.8	<0.2
ZE11-632B	62301	Rock Pulp	22.2	6	9.7	219	0.2	0.8	0.7	555	3.47	17.1	2.5	1.9	2	0.6	1.7	0.7	<2	0.33	0.008	86	26	0.02	2	0.005	<20	0.8	0.004	0.25	<0.1	<0.01	0.5	0.3	1.04	19	0.8	<0.2
ZE11-633	62302	Rock Pulp	2.9	13.4	32.8	428	0.3	1.7	0.7	746	3.53	550.4	3.9	3.7	1	0.8	7	1.3	<2	0.27	<0.001	182	63	0.01	1	0.005	<20	0.48	0.089	0.08	0.5	<0.01	<0.1	<0.1	2.2	6	<0.5	<0.2
ZE11-641A	62303	Rock Pulp	19.4	29	1.8	45	0.1	3.5	5.6	415	1.89	1.3	4.6	7.9	38	<0.1	0.1	1.6	30	1.26	0.053	13	55	0.46	396	0.07	<20	0.74	0.072	0.4	3.7	<0.01	2.9	0.1	0.83	4	0.6	<0.2
ZE11-641B	62304	Rock Pulp	25.1	59.1	2.7	44	0.3	3.4	9.7	329	4.02	1.6	10.4	7.1	20	<0.1	0.3	46.2	34	0.22	0.044	8	71	0.41	82	0.094	<20	0.77	0.085	0.41	0.5	<0.01	2.7	0.1	2.77	4	1.8	0.2
Pulp Duplicates																																						
MMI11-15-2	62290	Rock Pulp	12.5	29.3	16.5	12	0.3	1.5	0.3	61	0.67	133.8	1.2	2.6	1	<0.1	0.6	0.1	<2	0.08	0.001	51	62	<0.01	4	0.005	<20	0.43	0.004	0.31	<0.1	<0.01	<0.1	0.1	0.18	7	<0.5	<0.2
MMI11-15-2	62290	REP	13	29.7	17.5	13	0.3	1.7	0.3	65	0.68	135.7	1.6	2.9	1	<0.1	0.7	0.1	<2	0.09	0.001	52	65	<0.01	4	0.006	<20	0.44	0.004	0.32	<0.1	<0.01	<0.1	0.1	0.19	7	<0.5	<0.2
Reference Materials																																						
MMI11-QUARTZ	62276	Rock Pulp	0.3	4.8	<0.1	<1	<0.1	4.1	0.6	14	0.26	<0.5	1.2	<0.1	<1	<0.1	<0.1	<0.1	<2	<0.01	<0.001	<1	163	<0.01	2	<0.001	<20	<0.01	<0.001	<0.01	0.2	<0.01	<0.1	<0.1	<0.05	<1	<0.5	<0.2
GSB-till	62295	Rock Pulp	0.9	193.1	240	359	1.8	227.3	48.7	1685	7.25	67.9	20.5	3.9	19	0.9	8.4	0.4	107	0.35	0.114	15	235	2.94	298	0.083	<20	3.11	0.002	0.05	<0.1	0.33	15.8	<0.1	<0.05	9	0.7	0.3
	STD DS8		15.2	120.9	126.7	329	1.8	39.6	8.2	631	2.51	26.9	140.8	7.3	69	2.8	5	7.3	43	0.73	0.081	15	119	0.64	319	0.121	<20	0.99	0.101	0.44	2.6	0.18	2.4	5.4	0.21	5	5.5	5.1
	STD OREAS45CA		0.9	528.1	20.7	66	0.3	258.8	92.2	959	15.37	4.6	41.9	7.1	17	<0.1	<0.1	0.2	223	0.46	0.037	17	674	0.16	179	0.144	<20	3.7	0.004	0.07	<0.1	0.03	43	<0.1	0.07	20	0.9	<0.2
	BLANK		<0.1	<0.1	<0.1	<1	<0.1	<0.1	<0.1	<1	<0.01	<0.5	<0.5	<0.1	<1	<0.1	<0.1	<0.1	<2	<0.01	<0.001	<1	<1	<0.01	<1	<0.001	<20	<0.01	<0.001	<0.01	<0.1	<0.01	<0.1	<0.1	<0.05	<1	<0.5	<0.2

Analyses performed by ACME Analytical Laboratories Ltd., Vancouver
Method 1DX

Sample No.	Latitude	Longitude	Easting	Northing
MMI11-11-6A	56.93211	-131.35517	356684	6312298
MMI11-11-6B	56.93211	-131.35517	356684	6312298
MMI11-12-9	56.77849	-131.39136	353885	6295280
MMI11-14-15	56.92501	-131.30577	359663	6311405
MMI11-15-2	56.89816	-131.42105	352542	6308660
MMI11-15-6	56.89408	-131.29274	360341	6307937
MMI11-15-12	56.85986	-131.28482	360696	6304113
MMI11-17-4	57.02946	-131.24331	363846	6322902
TKE11-1-2	56.93225	-131.35835	356491	6312320
ZE11-578A	56.76251	-131.45384	350004	6293638
ZE11-578B	56.76251	-131.45384	350004	6293638

Sample No.	Latitude	Longitude	Easting	Northing
ZE11-582	57.03419	-131.21987	365285	6323382
ZE11-587A	56.90371	-131.36714	355847	6309162
ZE11-632A	56.95478	-131.45514	350693	6315034
ZE11-632B	56.95478	-131.45514	350693	6315034
ZE11-633	56.95589	-131.45731	350566	6315163
ZE11-641A	57.00116	-131.33908	357926	6319948
ZE11-641B	57.00116	-131.33908	357926	6319948
MMI11-15-2	56.89816	-131.42105	352542	6308660
MMI11-15-2	56.89816	-131.42105	352542	6308660

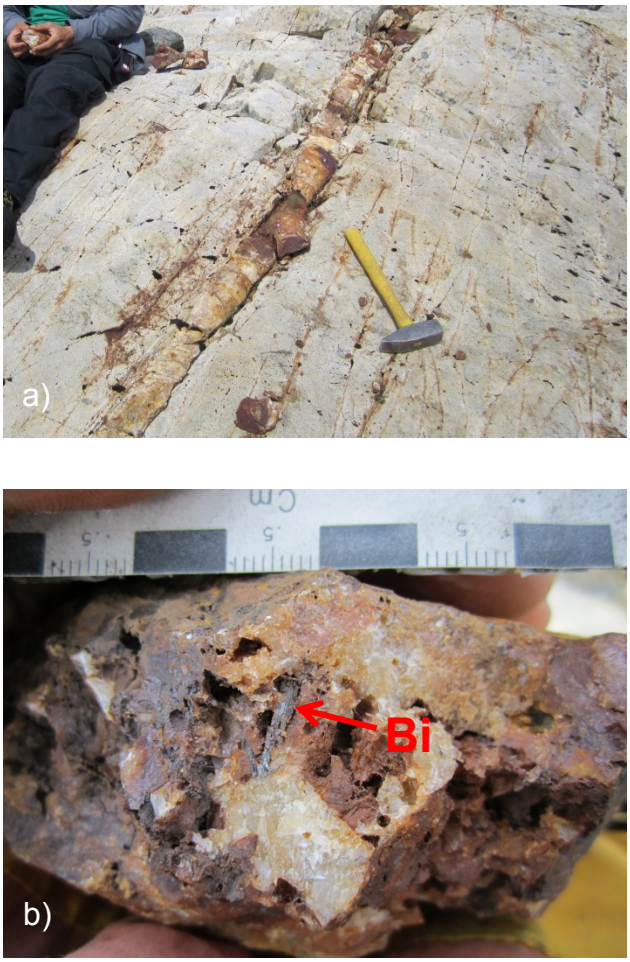

Figure 15. (a) Sheeted, rusty quartz veining in bleached granodiorite. Centimetre-thick veins are typical (beneath hammer). A close-up of the ~10 cm thick vein to the left of the hammer is shown in (b). (b) Vuggy, rusty quartz vein shows angular void outlines of pyrite cubes removed by weathering, and residual bismuthinite crystals (Bi).

Bi to >2000 ppm and W to >100 ppm. One of the samples contains 2.9 ppm Ag (ZE11-587A, Table 3).

In consideration of the small number of samples analyzed, the typical nugget effect in gold mineralization, the persistence of the sheeted veins, and the high concentration of pathfinder elements Bi and W as well as Ag, this area deserves further attention. It is, after all, within site of the Snip and Johnny Mountain gold mines, and considerable gold resources at the Bronson Slope (Figure 2).

Quartz-chalcopyrite veins

In one 5-10 m high cliff section, a ~6 m thickness of flow-banded, medium grained, crowded (30-50%) feldspar porphyry dips shallowly west with underlying strata conforming to its irregular lower surface (Figure 16a). A lithologically similar feldspar crystal tuff forms a 1-2 m thick unit a few metres up section from the porphyry. Intervening strata are tuffaceous siltstone and wacke (Figure 16b) and are locally strongly contorted with bedding ripped up by soft sediment deformation.

Within the feldspar porphyry are subparallel cockscomb quartz-carbonate-chalcopyrite veins. Some of the veins are conspicuous because of malachite staining (Figure 16c); others lack staining. One of the veins is 20 cm thick, but the most are <2 cm thick and are spaced 20 cm to 2 m along about 10 m of outcrop strike. We failed to find more of the vein material either further along or across strike. The mineralization appears mainly restricted to the porphyry; however, our search was far from exhaustive.

One aggregate sample was collected from all easily sampled veins and the adjacent porphyry hostrock. Analysis of this sample is shown in Table 3, sample MMI11-12-9. It yielded the following results: Cu >10 000 ppm, Zn 394 ppm, Ag 15.4 ppm, Au 37.5 ppb (56 ppb in Table 2). Given the cursory nature of our field observations and the interesting metal content of the veins, further work might be warranted.

Pheno Mountain REE – Zr content

Surprisingly strong enrichments in most trace elements within the volcanic and hypabyssal rocks at Pheno Mountain are shown in Table 2. Analyses for an incomplete suite of REE presented in Table 2 yields total REE (not REO) of between 0.035% and 0.072%. Comparisons can be made between the geochemistry of other peralkaline complexes such as Bokan Mountain ring dike complex, Alaska; Clay-Howells syeno-monzonite-carbonatite complex, northern Ontario; Dubbo trachyte intrusion, NSW, Australia; Kutessay, granophyre metasomatism, Kyrgyzstan; Kvanefjeld nepheline syenite, Greenland; and Thor Lake peralkaline intrusion, NWT, Canada (Table 4).

REE contents of peralkaline rhyolite tuff, dikes and monzonite and in the Pheno Mountain area are not comparable to world REE deposits. Yet for random samples collected over a ~20 km^2 area, with no expectation of elevated REEs, the analyses are encouraging and further sampling is warranted.

STRUCTURAL GEOLOGY

Structural styles observed in the western Hoodoo Mountain map area are like those described by Mihalynuk *et al.* (2011a) in the eastern map area. Folding, foliation, and faulting affect domains to varying degrees and penetrative fabrics are not regionally developed. For example, penetrative foliation developed within 15 km northeast and 5 km north of Hoodoo Mountain appears to die out farther afield. Beyond 5 km west of the peak, penetrative fabrics are no longer developed, but another few kilometers farther west, they are re-established. Pre-Neogene strata west of Pheno Mountain also display well-developed penetrative foliation. Such fabric development may be related to proximity of plutons and their extensions in the shallow crust. However, northeast of Hoodoo Mountain, the most likely candidate plutons, those of the Twin River pluton belt, apparently hornfels

Figure 16. (a) Dust and coarse ash tuff components of strata enveloping the porphyry unit. (b) Laminated sediment perfectly conform to the broken base of a porphyry layer. (c) Malachite staining on cliff face of feldspar porphyry adjacent to quartz-carbonate-chalcopyrite veins.

the fabrics and, therefore, must postdate them. Fabric development appears equally unrelated to a specific stratigraphic interval or structural level. For example, the Twin Glacier nunataks located about 6 km north-northeast and 9 km northeast of Hoodoo Mountain are underlain in part by Jurassic clastic rocks (as indicated by unpublished detrital zircon analyses–see above), which are penetratively deformed to the same extent as are those of probable Triassic age. On those nunataks, fabrics strike north-northwest, but within 6 km to the west, fabrics have been rotated to strike southwest (Figure 3). Fabric rotation appears related to major, north-trending fold with Hoodoo Mountain located in the hinge. This fold is important because if real, it would also fold a pre-existing Verrett-Iskut fault and impact the location of offset portions the Rock and Roll deposit stratigraphy (see below).

Table 4. Representative grades and tonnages of advanced projects or past-producing peralkaline REE complexes worldwide.

Name	Location	Tonnes / class	Total REO	Cut-off	Source*
Bokan Mountain	Southeast Alaska	6.7 Mt inferred	0.580%	0.20%	Robinson *et al.*, 2011
Clay-Howells	Northern Ontario	8.5 Mt inferred	0.73%	0.60%	Daigle, 2011
Kutessay (past producer)	Kyrgyzstan	16.8 Mt measured + indicated	0.22 – 0.27%	0.07%	State Reserve Committee (1996) ***
Kvanefjeld	Greenland	619 Mt indicated + inferred	1.06% + NaF + 0.22% Zn	defined by 0.015% U_3O_8	McIllree, 2010

*Where NI 43-101 compliance in resource calculation is stated as lacking, it is denoted by: ***

Folds and thrust belts

Fold and thrust-style deformation that is best displayed in the belt of Mesozoic strata extending northwest from Twin River pluton, flanks the west side of the Twin River pluton belt (Mihalynuk *et al.*, 2011a,b) at least as far north as Sphaler Creek where it is well exposed. Faults and folds mainly verge northeast, but vergence reversals are not uncommon, and regions of high fault and fold complexity arise (Figure 17).

Fold and thrust-style deformation also affects well-bedded, relatively incompetent chert and siliciclastic strata in the "Quest Creek" valley which are correlated with the "chert-claystone" unit of Mihalynuk *et al.* (2011a) of presumed late Carboniferous age. Faulting focused in this unit accommodates overthrusting of Permian atop Carboniferous strata north of Sphaler Creek (Logan and Koyanagi, 1994).

Late faults

Major steep discrete brittle-ductile faults crop out throughout the map area. Three regional-scale faults that juxtapose units of different character. Two are exposed in "Espaw Glacier" valley and "Quest Creek" valley. A third steep fault, the Verrett-Iskut (V-I) fault is well-exposed in the eastern Hoodoo Mountain area, but runs under cover and has not yet been observed within the western Hoodoo map area.

"Espaw Glacier" fault is very well exposed as a planar, steeply east-dipping fault surface (Figure 18) that projects south-southeastwards to link with the Andrei Glacier fault. Apparent offsets of >1 km on these Andrei Glacier fault segments (Mihalynuk *et al.*, 2011a) do not seem to affect stratigraphy in the Sphaler Creek valley north its confluence with "Espaw Creek".

"Quest Creek" fault is interpreted to extend along the axis of "Quest Creek" where it is exposed. Conglomerate and fault breccia fragments are strongly lineated in a subhorizontal direction within the fault (Figure 19). This fault may accommodate the competence contrast between well-bedded chert-siliciclastic (and argillite) unit and relatively massive greenstone.

Verrett-Iskut fault

Verrett-Iskut fault (V-I fault) is a discrete, high angle fault with 1450 to 1700 m of sinistral offset in the vicinity of Mount Verrett (Mihalynuk *et al.*, 2011a). Within map sheet 104B/14E Mihalynuk *et al.* (2011b) mapped the fault as trending west-southwest from Verrett Creek,

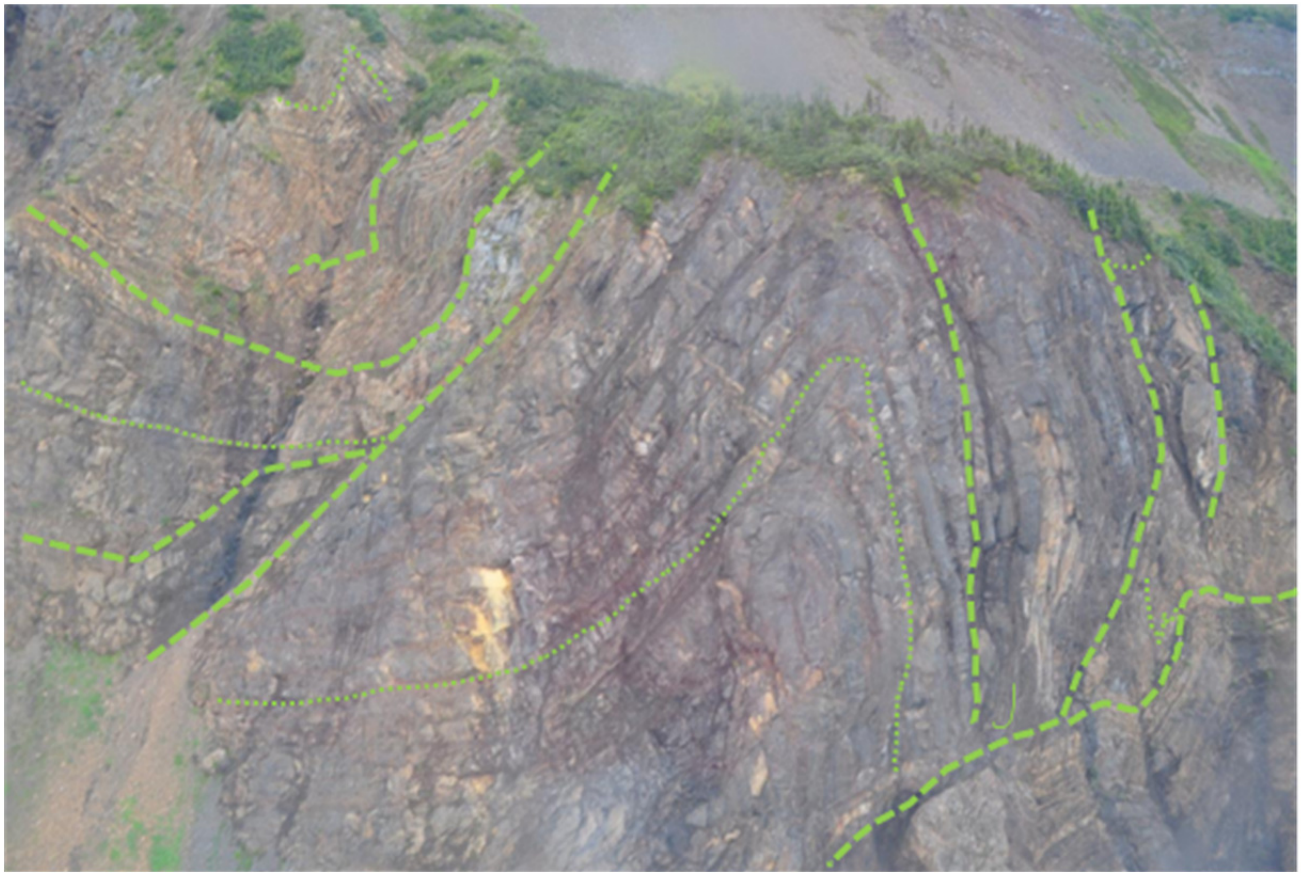

Figure 17. Zone of complex folding and thrust faults. View is of the Sphaler Creek south valley wall, looking towards the south. Most of these low angle faults ramp up section to the west and axial surfaces dip steeply east and west. Note low angle, coherent strata along the top edge of the photo above the talus slope (they persist outside of the photo to the east), presumably a significant décollement is hidden beneath the talus.

Figure 18. Trace of the "Espaw Glacier" fault here juxtaposes highly contorted graphitic and cherty argillite with massive carbonate. View is to the north-northwest. An along strike projection of the fault to the south-southeast links it with the Andrei Glacier fault (Figure 3).

Figure 19. Outcrop exposure of highly lineated fragments of broken country rock in the "Quest Creek" fault, along lower "Quest Creek". This fault accommodates ductility contrast between Upper Carboniferous chert-siliciclastic unit and Lower Carboniferous metabasite.

across the southeast flank of Mount Verrett, following a well defined, glacially scoured lineament until it is lost at elevations below 1200 m in the forest and below Iskut River gravels. Mihalynuk *et al.* (2011a) speculated on the trace of the fault and proposed two options for the location of its western continuation. Mapping in southwest 104B/14W shows that neither of these western options can be correct (especially the northern option, which is shown on Figure 3), and that the fault must track farther to the south. The new proposed fault trace (under cover) is shown on Figure 3. Accurate location of the fault and determination of offset is important because it bears on prediction of the location of offset portions of stratigraphy that may host continuation of the precious metal-rich Rock and Roll massive sulphide deposit. Location of the new fault trace takes into account revision of the mapping west of Hoodoo Mountain by Edwards *et al.* (2000), and a major north-trending fold with an axis located beneath Hoodoo Mountain. Such a fold would bend the V-I fault to the south, and offset by ~1500 m a belt of carbonate originally mapped by Kerr (1935). The resultant offset would place the potential continuation of Rock and Roll stratigraphy beneath the toes of phonolite lava flows low on the south flank of Hoodoo Mountain.

SUMMARY

More than eighty years after Forest Kerr conducted the first systematic geological mapping around the margins of the Hoodoo Mountain area, we attempted to complete mapping across the interior of the quadrangle. Despite conveniences unimagined by Kerr: helicopters, global positioning systems, satellite imagery, water repellent membranes, geographic information systems, isotopic age dating, and duct tape, we were faced with the same insurmountable obstacle, weather. Generally poor weather during the field season of 2011 ensured that part of the Hoodoo map area, the western edge between Surprise Mountain and upper Choquette Glacier, remained unmapped. Nevertheless, geoscientific knowledge of the area, much of it a clean slate before we arrived, has improved greatly. Fundamental geological information is particularly important in this part of the province given its very high mineral potential. It aids predictive metallogeny and the future design of mineral exploration programs in the area. Some key advancements are:

- Recognition of a westward fining of Late Triassic and Early Jurassic strata, with an arc axis that lay to the east in 104B/14E.
- Continuation of a thrust belt that shortened the sedimentary basin, generally, but not always placing western facies over more easterly facies.
- North trending regional folds that deform the thrust belt as well as metamorphic fabrics.
- North trending regional folds that may also affect Verrett-Iskut fault and location of potentially offset continuation of the hostrocks for the precious metal rich massive sulphide mineralization at the Rock and Roll deposit.
- Northern continuation of the Hoodoo Mountain phonolitic volcanic rocks at Pheno Mountain, together comprising the Hoodoo-Pheno mountains volcanic complex (HPMVC).
- Recognition extreme enrichment of Zr and many REEs within the HPMVC, with possibilities for REE exploration targets.

Laboratory components of our work on the Hoodoo Mountain area is on-going.

ACKNOWLEDGMENTS

This project would not have been possible without funding from the Geoscience for Energy and Minerals Strategy. GEMS program is administered by the Geological Survey of Canada, and its western component burdened the perennially-patient Steve Irwin of the GSC Vancouver office – to whom we are indebted. This project is also funded in part by an NSERC Discovery grant to Stephen T. Johnston of the University of Victoria. Modern camp accommodations were arranged through Romios Gold Resources Inc., thanks to the persistence of Scott Close and others. We also benefitted from Scott's local and regional geological expertise. Sephanie Wenker (University of Victoria) provided field base maps and geological support. Competent, cheerful and CHATTY field assistance was conveyed by Tim Davis and Tom Kelly, new graduates and volunteers from Cardiff University, UK.

REFERENCES

Awmack, H.J. (1991): 1990 Geological, geochemical and geophysical report on the Trek 1-6 Claims; *BC Ministry of Energy and Mines*, Assessment Report 20956, 30 pages.

Awmack, H.J. and Yamamura B.K. (1988): 1988 Summary Report on the Trek 1-6 Claims; *BC Ministry of Energy and Mines*, Assessment Report 18115.

Breitsprecher, K. and Mortensen, J.K. (2004): BC Age 2004A-1: a data base of isotopic age determinations for rock units from British Columbia; *BC Ministry of Energy, Mines and Petroleum Resources*, Open File 2004-03.

Bernales, S., Chadwick, P. and Guszowaty, E. (2008): 2008 exploration activities on the Romios Gold Resources, Inc. Newmont project, prepared for Romios Gold Resources; *BC Ministry of Energy, Mines and Petroleum Resources*, Assessment Report 30449, 59 pages plus 12 appendices.

Brown, D.A., Logan, J.M., Gunning, M.H., Orchard, M.I. and Bamber, W.E. (1991): Stratigraphic evolution of the Paleozoic Stikine Assemblage in the Stikine and Iskut Rivers area, northwestern British Columbia; *Canadian Journal of Earth Sciences*, Volume 28, pages 958-972.

Caulfield, D.A. (1989): 1989 Summary report on the Trek 1-6 Claims; *BC Ministry of Energy and Mines*, Assessment Report 19479.

Chadwick, P. and Close, S. (2009): Geological and geochemical report on the Dirk property, prepared for Romios Gold Resources; *BC Ministry of Energy, Mines and Petroleum Resources*, Assessment Report 31250, 31 pages plus appendices.

Cohoon, G.A. and Trebilcock, D.A. (2004a): Phiz Property geology and geochemistry surveys; *BC Ministry of Energy, Mines and Petroleum Resources*, Assessment Report 27555, 73 pages plus appendices and maps.

Cohoon, G.A. and Trebilcock, D.A. (2004b): Rock and Roll Project, Geology and Geochemical Surveys; *BC Ministry of Energy, Mines and Petroleum Resources*, Assessment Report 27582, 84 pages plus maps.

Cordey, F. (2011): Report on microfossils; unpublished report No. FC2011-GSC2, 2 pages.

Costin, C.P. (1973): Report of geological, geophysical, and physical work, Dirk claim group; *BC Ministry of Energy, Mines and Petroleum Resources*, Assessment Report 4150, 15 pages plus maps.

Daigle, P. (2011): Technical report on the Clay-Howells Fe-REE project, Ontario, Canada; *Rare Earth Metals Inc.*, On-line Document No. 1192410300-REP-R0001-01, 79 pages and appendices, [URL: http://www.rareearthmetals.ca/upload/documents/1192410300-rep-r0001-01-final.pdf].

Desautels, P. (2011): NI 43-101 Technical Report for the Trek Property; *Romios Gold Resources Inc.* company report, 122 pages, URL http://www.romios.com/i/pdf/2011-06-21_Trek_NI_43-101.pdf [November, 2011].

Edwards, B.R. (1997): Field, kinetic and thermodynamic studies of magmatic assimilation in the northern Cordilleran volcanic province, northwestern British Columbia; unpublished Ph.D. thesis, *The University of British Columbia*, 324 pages.

Edwards, B.R. and Russell, J.K. (2002): Glacial influences on morphology and eruptive products of Hoodoo Mountain volcano, Canada, in Volcano-Ice Interaction on Earth and Mars; in Smellie, J.L. and Chapman, M.G. (editors), *The Geological Society of London*, Special Publications, 202, pages 179-194.

Edwards, B.R., Russell, J.K. and Anderson, R.G. (2002): Subglacial, phonolitic volcanism at Hoodoo Mountain volcano, northern Canadian Cordillera; *Bulletin of Volcanology*, Volume 64, pages 254-272.

Edwards, B.R., Anderson, R.G., Russell, J.K., Hastings, N.L. and Guo, Y.T. (2000): The Quaternary Hoodoo Mountain Volcanic Complex and Paleozoic and Mesozoic basement rocks, parts of Hoodoo Mountain (NTS 104B/14) and Craig River (NTS 104B/11) map areas, northwestern British Columbia, *Geological Survey of Canada*, Open File 3721, scale 1:20 000.

Fillipone, J.A. and Ross, J.V. (1989): Stratigraphy and structure in the Twin Glacier-Hoodoo Mountain area, northwestern British Columbia (104B/ 14); in Geological fieldwork 1988, Smyth (Editor), *BC Ministry of Energy, Mines and Petroleum Resources*, 1989-1, pages 285-292.

Gill, R., Kulla, G., Wortman, G., Melnyk, J. and Rogers, D. (2011): Galore Creek Project, British Columbia, NI 43-101 Technical report on pre-feasibility study; *Novagold Resources Inc.* On-line Report, Project Number 166824, 380 pages, [URL: http://www.novagold.com/upload/technical_reports/Galore_Creek_NI_43-101_2011_Final.pdf].

Giroux, G.H. and Gray, J.H. (2010): Preliminary assessment update–Bronson Slope property for the Skyline Gold Corporation; *Skyline Gold Corporation*, On-line report, 266 pages, [URL: http://www.skylinegold.com/i/pdf/Skyline-Bronson_Slope_5Nov10_final_v2.pdf].

Holbeck, P. (1983): Report on the geology and geochemistry of the Hoodoo West claim group; *BC Ministry of Energy and Mines*, Assessment Report 12220, 13 pages plus maps.

Holtby, M. (1989): Rock chip sampling on Sphal 25, 27, 29, 31, and 33, Kim 38, 40, and 42 Claims; *BC Ministry of Energy, Mines and Petroleum Resources*, Assessment Report 19083, 10 pages plus 2 appendices and 2 maps.

Kasper, B. (1990): Geological and geochemical report on the Quest 1 and 2 claims; *BC Ministry of Energy and Mines*, Assessment Report 20021, 17 pages plus appendices and maps.

Kerr, F A. (1935): Stikine River Area, South Sheet, Cassiar District, British Columbia; *Geological Survey of Canada*, Map 311A, 1:126 720 scale.

Kerr, F.A. (1948): Lower Stikine and western Iskut River areas, British Columbia; *Geological Survey of Canada*, Memoir 246, 94 pages.

King, G.R. (1987): Geological and geochemical report on the Ian 1 to 4 claims, Iskut River area, Liard mining division, B.C.; *BC Ministry of Energy, Mines and Petroleum Resources*, Assessment Report 16953, 19 pages plus 6 appendices and 4 maps.

Lefebure, D.V. and Gunning, M.H. (1989): Geology of the Bronson Creek area, NTS 104B/10W, 11E [in part]; *BC Ministry of Energy, Mines and Petroleum Resources*, Open File 1989-28, 2 sheets, 1:25 000 scale.

Lefebure, D.V. and Hart, C. (2005): Plutonic-related Au quartz veins & veinlets; B.C. Mineral Deposit Profiles, *BC Ministry of Energy and Mines*, Profile L02, 8 pages, http://www.geology.gov.yk.ca/pdf/l02_plutonic_related_au_quartz_veins_and_veinlets.pdf.

Logan, J.M. (2004): Preliminary lithogeochemistry and polymetallic VHMS mineralization in Early Devonian and (?) Early Carboniferous volcanic rocks, Foremore property; in Geological fieldwork 2003, *BC Ministry of Energy, Mines and Petroleum Resources*, Paper 2004-1, pages 105-124.

Logan, J.M. and Koyanagi, V.M. (1994): Geology and mineral deposits of the Galore Creek area (104G/3, 4); *BC Ministry of Energy, Mines and Petroleum Resources*, Bulletin 92, 96 pages.

Logan, J.M., Drobe, J.R. and McClelland, W.C. (2000): Geology of the Forrest Kerr-Mess Creek Area, Northwestern British Columbia (NTS 104B/10, 15 & 104G/2 & 7W); *BC Ministry of Energy, Mines and Petroleum Resources*, Bulletin 104, 163 pages.

Massey, N.W.D., MacIntyre, D.G., Desjardins, P.J. and Cooney, R.T. (2005): Digital Geology Map of British Columbia: Whole Province, *BC Ministry of Energy, Mines and Petroleum Resources*, Geofile 2005-1.

Macrae, R., and Hall, B.V. (1983): Geological and geochemical report on the Hemlo west and Aurum claim group, Iskut River area, Liard Mining Division, *BC Ministry of Energy, Mines and Petroleum Resources*, Assessment Report 11320, 24 pages plus 4 appendices and 9 maps.

McIllree, R. (2010): Greenland Minerals Receives Permit for the Full Evaluation of the Kvanefjeld Multi-Element Project (REEs, U, Zn); Greenland Minerals and Energy Ltd., Company Announcement, On-line, 4 pages, [URL: Mihalynuk, M.G., Stier, T.J., Jones, M.I. and Johnston, S.T. (2010): Stratigraphic and structural setting of the Rock and Roll deposit, northwestern British Columbia; in Geological Fieldwork 2009, *BC Ministry of Energy, Mines and Petroleum Resources*, Paper 2010-1, pages 7-18.

Mihalynuk, M.G., Zagorevski, A., Logan, J.M., Kelly, T.P. and Davis, T.J. (2012): Preliminary geology of the Hoodoo Mountain area (104B/14 and adjacent parts of 104B/11 and 104G/3); *BC Ministry of Energy and Mines*, Open File 2012-3; *Geological Survey of Canada*, Open File 7051,1:50 000 scale map.

Mihalynuk, M.G., Logan, J.M., Zagorevski, A. and Joyce, N. (2011a): Geology and Mineralization of the Hoodoo Mountain Area (NTS 104B/14E): in Geological Fieldwork 2010, *BC Ministry of Energy and Mines*, Paper 2011-1, pages 37-64.

Mihalynuk, M.G., Logan, J.M. and Zagorevski, A. (2011b): East Hoodoo Mountain-Iskut River Geology (NTS 104B/14E, 11NE); *BC Ministry of Energy and Mines*, Open File 2011-4, 1:50 000 scale map.

MINFILE (2010): British Columbia mineral inventory database; *BC Ministry of Energy, Mines and Petroleum Resources*, online database, URL http://www.empr.gov.bc.ca/MINING/GEOSCIENCE/MINFILE/Pages/default.aspx [November, 2011].

Monger, J.W.H. (1977): Upper Paleozoic rocks of the western Canadian Cordillera and their bearing on Cordilleran evolution; *Canadian Journal of Earth Sciences*, Volume 14, pages 1832-1859.

Montgomery, A.T., Todoruk, S.L. and Ikona, C.K. (1991a): Assessment Report on the Rock and Roll Project; *BC Ministry of Energy, Mines and Petroleum Resources*, Assessment Report 20884, 18 pages plus figures, appendices and maps.

Montgomery, A.T., Todoruk, S.L. and Ikona, C.K. (1991b): 1990 Summary geological and geochemical report on the STU 8 & 9 mineral claims, Liard Mining Division; *BC Ministry of Energy, Mines and Petroleum Resources*, Assessment Report 21051, 15 pages plus figures, 8 appendices and 5 maps.

Pegg, R. (1989): Geological and Geochemical Report on the 1989 Exploration Program of the Rock and Roll property; *BC Ministry of Energy and Mines*, Assessment Report #19,566, 8 pages plus 8 appendices and 5 maps.http://www.ggg.gl/userfiles/file/ASX/GMEL-approved-to-evaluate-Kvanefjeld-inclusive-of-uranium.pdf].

Rayner, G.H. and Ney, C.S. (1964): Sphaler Creek Examination, Goat & Kim Claims; *BC Ministry of Energy and Mines*, Assessment Report 565, 6 pages and maps.

Robinson, R.J., Power, M.A. and Barker, J.C. (2011): Technical report on the exploration program and mineral resource estimate for the Bokan Mountain property Prince of Wales Island, Alaska; *Ucore Rare Metals Inc.*, On-line Report, 190 pages, [URL: http://ucore.com/Ucore_43-101.pdf].

Simmons, A. (2006): 2006 geological and geochemical report on the Trek Property, *BC Ministry of Energy and Mines*, Assessment Report 28624, 112 pages including appendices and maps.

Souther, J.G. (1971): Geology and mineral deposits of Tulsequah map-area, British Columbia; *Geological Survey of Canada*, Memoir, 362, 84 pages.

State Reserve Committee (1996): Historical reserves of REM approved by the Kyrgyz Republic TKZ at the Kutessay II deposit; in *Stans Energy Corp.*, On-line deposit overview, [URL: http://www.stansenergy.com/projects/kutessay-ii-ol/kutessay-ii-overview/].

Sun, S. and McDonough, W. F. (1989): Chemical and Isotopic Systematics of oceanic basalts: implications for mantle composition and processes; in A.D. Saunders and M.J. Norry (editors) Magmatism in the Ocean Basins,

Geological Society of London, Special Publication Volume Number 42, pages 313-345.

Taylor, S.R. and McLennan, S.M. (1985): The continental crust; its composition and evolution; *Blackwell, Oxford*, 312 pages.

Dease Lake Geoscience Project, Part III: Age, Emplacement and Mineralization of the Snow Peak Pluton (NTS 104J/08)

by D.P. Moynihan[1] and J.M. Logan[2]

KEYWORDS: QUEST-Northwest mapping, Geoscience BC, regional bedrock mapping, integrated multi-disciplinary studies, Paleocene plutonism, contact metamorphism, phase equilibria, molybdenite±gold mineralization

INTRODUCTION

The Snow Peak pluton is a small, steep sided, equidimensional body located in the northwestern part of the Dease Lake map sheet (NTS 104/J08). The intrusion is a relatively homogeneous, locally porphyritic quartz monzodiorite-granodiorite, which is hosted by Early Jurassic rocks of the Takwahoni Formation (Stikine terrane) immediately south of the terrane-bounding King Salmon fault (Figure 1). Mo±Au, W mineralization is developed along west-northwest trending fracture planes in the central part of the pluton.

This paper reviews the geology of the pluton and surrounding area and presents new geochronological and petrological data concerning its age and emplacement depth. Additional information on the regional geology is included in the accompanying paper by Logan *et al.*, 2012a.

COUNTRY ROCKS

The Takwahoni Formation in this area comprises a basal unit dominated by conglomerate and sandstone, and an overlying unit, which though variable, consists mostly of fine-medium sandstone and siltstone-mudstone (Figure 1). Lithologies in the contact aureole range from thickly to very thickly bedded massive sandstone and minor conglomerate with distinctive pink granitic clasts, to homogeneous sequences of laminated siltstone-mudstone with occasional sandstone beds.

Rocks in the area have been affected by two periods of deformation. The first lead to the development of east-west trending folds that are well exposed in the cirque north of Snow Peak (Figure 2) and the local development of a north dipping penetrative cleavage in fine-grained units. These structures are manifestations of a south-verging fold and thrust belt that developed in response to the amalgamation of the Stikine and Cache Creek terranes in the Middle Jurassic. Penetrative deformation of this age is widespread in rocks north of the King Salmon fault.

A later period of deformation produced north-trending upright folds. North-trending folds with km-scale wavelengths affect the map pattern (Logan *et al.,* 2012a), but associated smaller scale structures are only locally developed. Palaeocene-Eocene strata in the adjacent (NTS 104/J07) map sheet are folded by similar north-trending structures (Ryan, 1991), suggesting north-trending folds in the area may be early Tertiary or younger.

In the vicinity of Snow Peak, the Takwahoni Formation hosts a voluminous network of dikes and sills that typically range from tens of centimetres to metres thick (Figure 2c). Most of these dikes/sills are plagioclase porphyries, which commonly contain distinctive but sparsely distributed quartz "eyes", euhedral, oscillatory-zoned 2-10 mm plagioclase phenocrysts and slender hornblende crystals 1-3 mm long in a fine grained plagioclase-rich matrix (Figure 3a). Where present quartz phenocrysts commonly have rounded and embayed margins.

The network of dikes and sills end abruptly at the contact with the Snow Peak pluton; whereas they are abundant in the Takwahoni Formation, none was observed within the pluton. An older age for the dikes is also suggested by the presence of plagioclase porphyry xenoliths within the Snow Peak pluton (Figure 3b). These dikes are undeformed and crosscut east-west trending D1 folds (Figure 2d). Plagioclase porphyry dikes/sills have not been dated in the study area, but a U-Pb age of 155.2 ±1 Ma was obtained from a dike that is texturally and mineralogical similar, from a location further east in the NTS 104J/08 map sheet (Logan *et al.*, 2012b).

Many of the plagioclase porphyry dikes in the Snow Peak area are altered. In the field, their colour ranges from pale grey to brownish grey to yellow-brown with increasing degree of alteration. Carbonate alteration is most strongly developed, with minor sericite and chlorite. Adjacent to the Snow Peak pluton, hornblende in plagioclase porphyry dikes is replaced by biotite (Figure 3c).

[1] *Department of Geosciences, University of Calgary, Calgary, AB*
[2] *British Columbia Geological Survey, Victoria, BC*

This publication is also available, free of charge, as colour digital files in Adobe Acrobat® PDF format from the BC Ministry of Energy and Mines website at http://www.empr.gov.bc.ca/Mining/Geoscience/PublicationsCatalogue/Fieldwork.

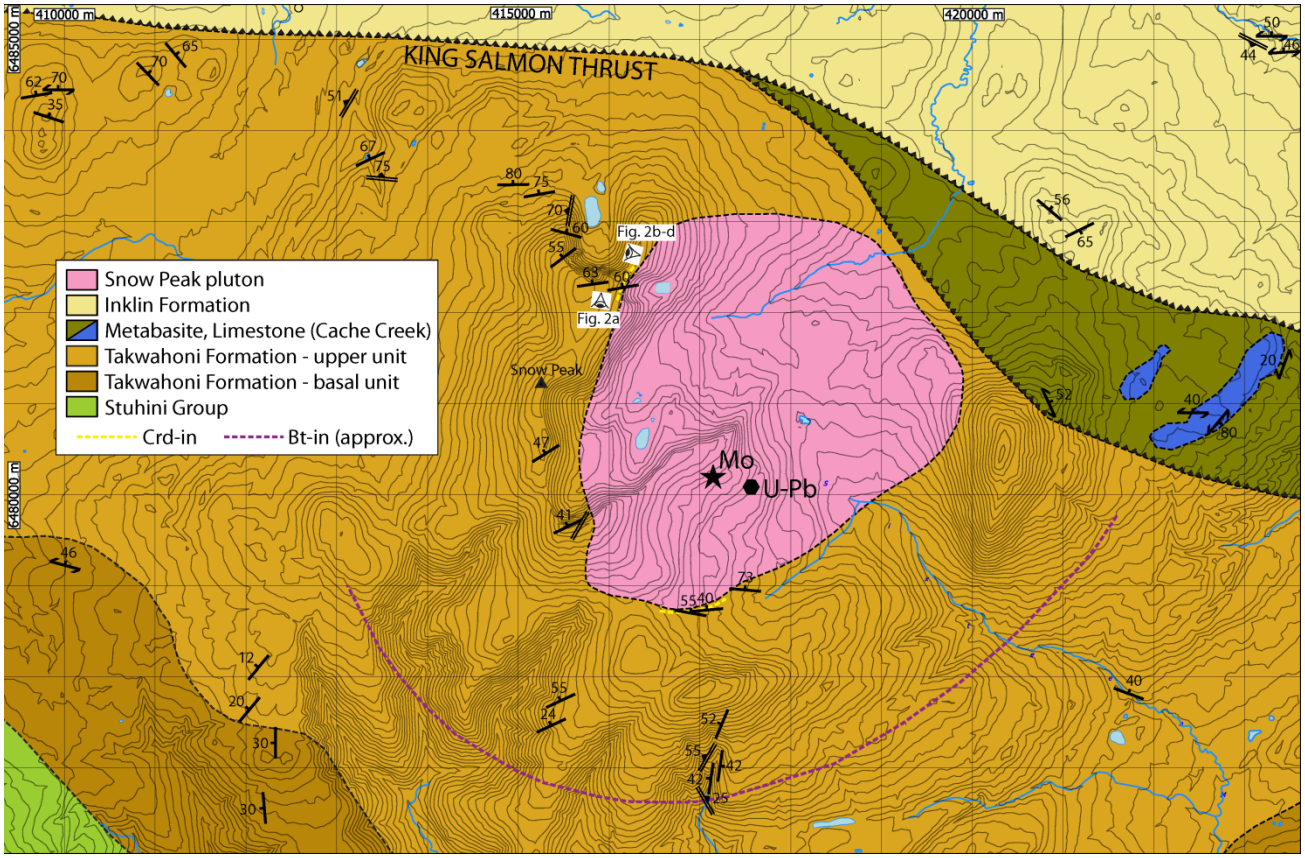

Figure 1. Map of the Snow Peak pluton and surrounding area. For location and regional geological setting, see Logan *et al.* (2012). The location of the U-Pb sample, the trench on the Mack prospect and approximate contact metamorphic isograds are shown. The eye symbols indicate the location and viewing direction of photographs shown in Figure 2.

Dikes of hornblende-plagioclase 'microdiorite' are also present in the area but are much less abundant than plagioclase porphyries. These rocks contain 1-2 mm long acicular hornblende crystals intergrown with plagioclase and are locally amygdaloidal. Non-porphyritic plagioclase-rich dikes are also present and a single outcrop of a distinctive dike (?) with primary flow banding was also encountered. This rock contains phenocrysts of plagioclase and quartz, in a matrix dominated by plagioclase and euhedral aligned biotite. Plagioclase phenocrysts are euhedral, whereas quartz ranges from euhedral to rounded and embayed.

SNOW PEAK PLUTON

The Snow Peak pluton occupies approximately 12 km^2, mostly underlying a subalpine bowl to the east of Snow Peak (Figure 1). The rock is a biotite-hornblende quartz monzodiorite to granodiorite that is locally weakly K-feldspar porphyritic (Figure 4a). CIPW normative compositions from a single sample (11JLO12-117) plot in the granodiorite field on QAP diagram (Streckeisen, 1976). Plagioclase forms oscillatory-zoned euhedral to subhedral laths that are typically 2-7 mm long. K-feldspar crystals are generally in the same size range but locally exceed 1 cm; they are anhedral-subhedral and often conform to the boundaries of plagioclase laths. The feldspars are intergrown with mafic phases and interstitial quartz. Quartz grains are generally <1 mm, but some larger 2-3 mm grains are present. Euhedral biotite and ragged acicular hornblende form crystals approximately 2 mm long and comprise approximately 5% of the rock. Euhedral titanite, magnetite and late pyrite form accessory phases. Magnetite is mostly clustered around mafic crystals, particularly hornblende, as is late replacement pyrite. There is minor alteration of mafic phases to chlorite and some sericitization of plagioclase.

Gabrielse (1998) reported a single K-Ar hornblende age of 73.5 Ma from the Snow Peak pluton, which is significantly younger than the age of other granitic intrusions in the area. New U-Pb data presented here (Figure 5) refine the age further, giving a crystallisation age of 64.4 ±0.5 Ma (earliest Palaeocene). The data were acquired by LA-ICPMS at the University of Washington, using procedures documented in the accompanying paper by Logan *et al.,* 2012b. The quoted age is a weighted mean of $^{206}Pb/^{238}U$ ages (n=44), excluding 6 outliers. This age provides an upper limit on the age of Mo ±Au, W mineralization; it also supports the conclusion reached from field relationships that the dike and sill swarm in the area is older and unrelated to the intrusion and its mineralization.

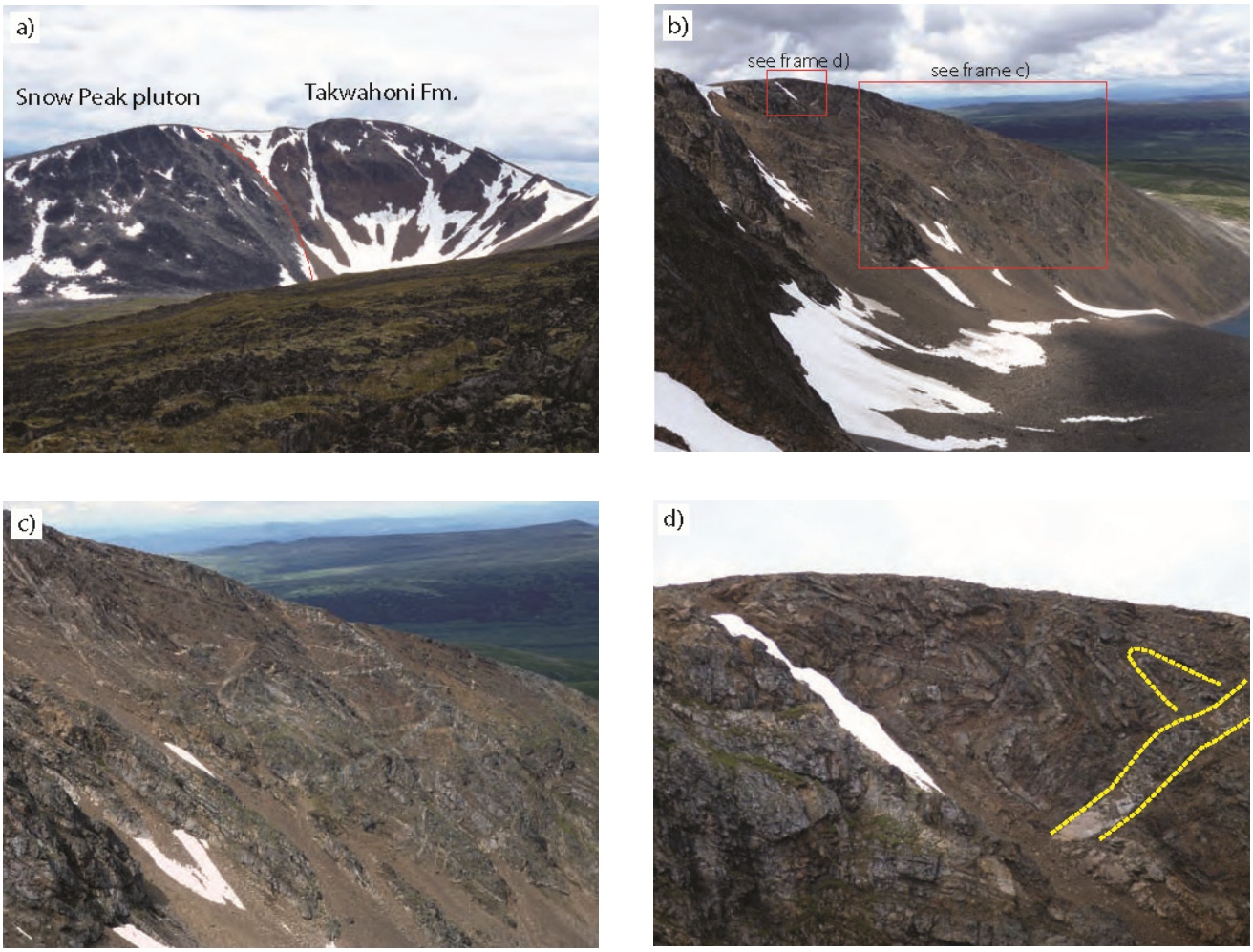

Figure 2. a) Steeply dipping contact between the Snow Peak pluton and rusty hornfelsed clastic rocks of the Takwahoni Formation. Looking south from above the north-facing cirque to the north of Snow Peak; relief is approximately 300 m. The position from which the photograph was taken is shown in Figure 1. b) Westerly view across the cirque north of Snow Peak, with insets showing the position of images in c) and d). The position from which the photographs were taken is shown in Figure 1. Relief is approximately 250 m. c) The Takwahoni Formation hosts a voluminous array of dikes and sills of plagioclase +/-quartz-eye porphyry. d) East-west trending (D1) folds with north dipping axial planes are visible in the cliff face. Undeformed dikes cut across fold axial planes and therefore postdate this deformation.

CONTACT METAMORPHISM

Intrusion of the Snow Peak pluton led to the formation of a contact metamorphic aureole in surrounding rocks of the Takwahoni Formation. The effects of contact metamorphism on rocks of the Cache Creek terrane to the northeast were not studied. In the Takwahoni Formation, the aureole is manifested in a broad region of rusty, indurated rock, which commonly has a mauve-coloured tint. The isotropic character and colour of the rock is related to the growth of fine grained metamorphic biotite, which grew with no preferred orientation. Throughout this biotite zone, much of the primary texture of the rocks is preserved, with detrital grains visible in thin section. In addition to biotite, pale green amphibole (tremolite-actinolite) crystallized in some calcareous layers.

Immediately adjacent to the intrusion (within tens of metres), fine-grained layers in the Takwahoni Formation are fully recrystallized into spotted cordierite-bearing hornfels (Figures 4b-d). Small cordierite spots generally <1 mm are abundant in pelitic layers and are concentrated in the finest grained parts of graded layers, locally producing a reversal in the direction of grain-size fining to one of coarsening. Spotted hornfels clasts are abundant in the felsenmeer that covers the area, but in situ samples were collected from only two areas - on the northwestern and southern flanks of the intrusion.

To determine P-T conditions during contact metamorphism, equilibrium assemblage diagrams were constructed for a number of samples using the software DOMINO (de Capitani and Petrakakis, 2010). These diagrams, which are specific to the rock composition for which they are constructed, depict the stable mineral assemblage as a function of temperature and pressure, assuming thermodynamic equilibrium. The phase

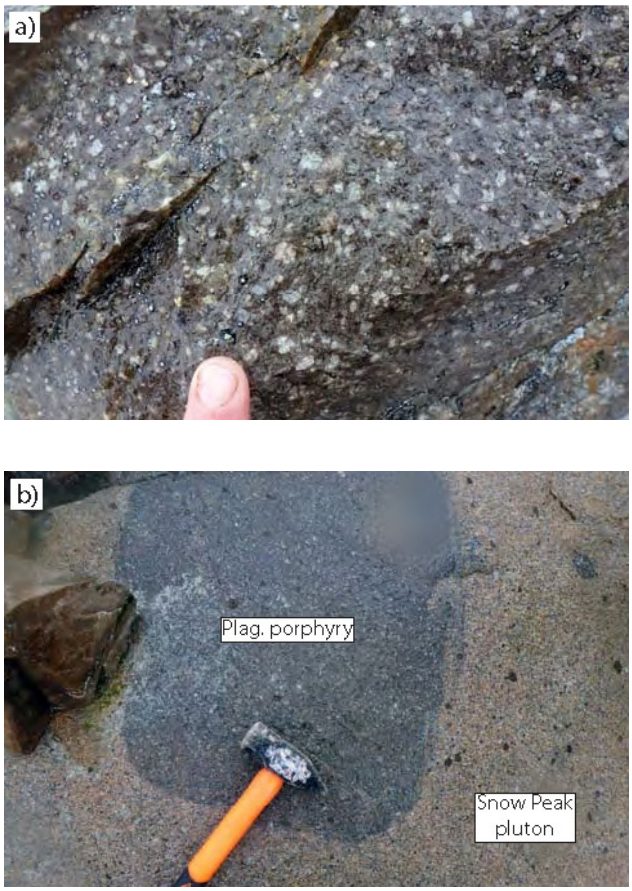

Figure 3. a) Typical plagioclase porphyry dike intruded into the Takwahoni Formation on Snow Peak showing characteristic texture of plagioclase and quartz phenocrysts within a fine grained, plagioclase-rich matrix. b) Rounded xenolith of plagioclase porphyry included in monzogranite of the Snow Peak pluton. c) Photomicrograph of plagioclase porphyry dike from west of the Snow Peak pluton showing plagioclase phenocryst and magmatic hornblende crystals replaced by secondary biotite. Field of view = 3 mm.

diagrams were constructed in the system MnO-Na2O-CaO-K2O-FeO-MgO-Al2O3-SiO2-H2O-TiO2 (MnNCKFMASHT) using version ds5.5 of the Holland and Powell (1998) thermodynamic database, and activity models listed by Coueslan *et al.,* 2011. Rock compositions were

Figure 4. a) Hornblende-biotite quartz monzodiorite of the Snow Peak pluton. Oscillatory-zoned plagioclase and K-feldspar crystals are intergrown with mafic phases and finer grained quartz. Minor titanite is also present. Field of view is 3 mm, x-nicols. b) Spotted cordierite hornfels derived from a fine-grained layer in the Takwahoni Formation. Cordierite crystals (dark spots) are concentrated in pelitic layers, particularly in finest grained parts of graded layers. c) Photomicrograph of 11DMO12-97 shows cordierite porphyroblast that has been replaced by biotite and plagioclase. Scale bars are 1 mm.

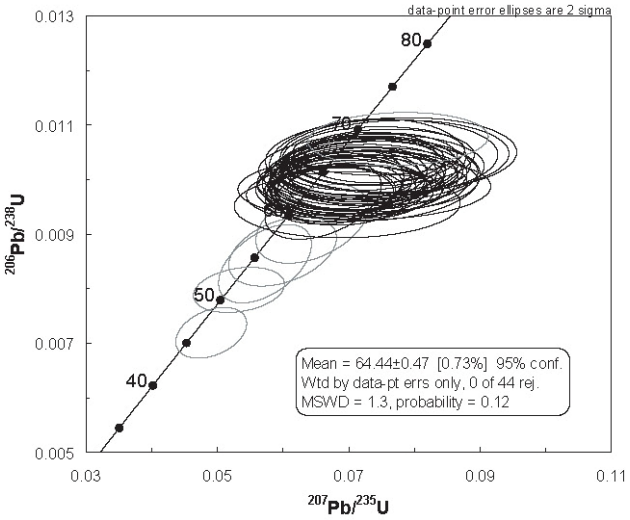

Figure 5. U-Pb Concordia plots for LA-ICPMS U-Pb data from the Snow Peak pluton. Excluding outliers, the weighted mean $^{206}Pb/^{238}U$ age is 64.4 +/-0.5 Ma. The sample was collected from (NAD 83) UTM 9V 417549 6480099, 1586 m (marked on Figure 1).

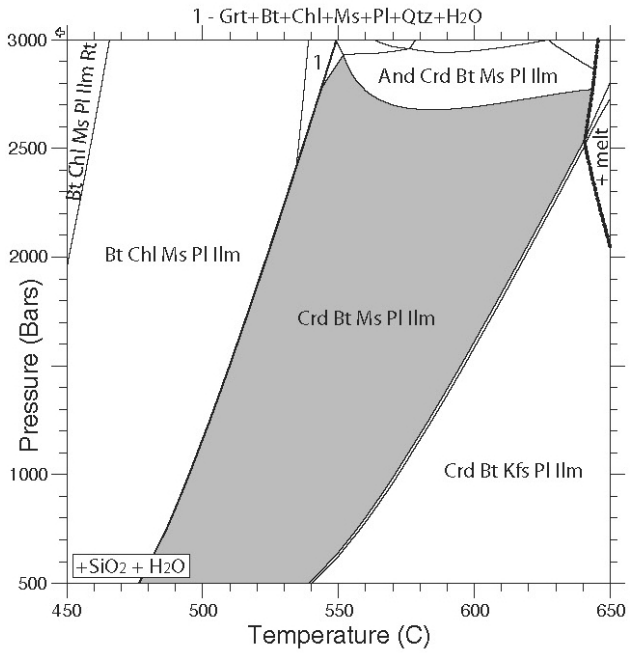

Figure 6. Equilibrium assemblage diagram for cordierite hornfels sample DMO11-39-346. The observed assemblage (shaded) implies emplacement of the pluton at P < ~2.75 kbar. The bulk composition of this sample, determined by XRF analysis, is presented in Table 1.

determined by x-ray fluorescence spectrometry (XRF) at Acme Analytical Laboratories Ltd in Vancouver.

A representative phase diagram for a cordierite-bearing hornfels (11DMO-39-346) from the southern flank of the pluton is presented in Figure 6. The observed assemblage of cordierite+biotite+muscovite+plagioclase+quartz+ilmenite (Crd+Bt+Ms+Pl+Qtz+Ilm) is stable below ~2.75 kbar over a temperature range of approximately 500-650ºC. Higher temperatures are ruled out as there is no K-feldspar and no evidence for melting of the rock here or elsewhere in the aureole. Assuming a crustal density of 2800 kg/m^3, the cordierite-bearing assemblage implies an emplacement depth of <10 km for the pluton. This relatively shallow depth explains the absence of minerals such as andalusite, staurolite and garnet, which are commonly found in contact metamorphosed metapelites, but are generally restricted to slightly higher pressures. Equilibrium assemblage diagrams predict growth of biotite at temperatures of 300-350ºC. This is lower than is typical for metapelites (Spear, 1993), and together with the low regional metamorphic grade, may help explain the large width of the aureole relative to the size of the intrusion.

Table 1. Whole rock x-ray fluorescence (XRF) major element analysis of 11DMO39-346: a metapelitic hornfels sample from the contact aureole of the Snow Peak pluton.

SiO_2	61.70%
TiO_2	0.58%
Al_2O_3	17.10%
Fe_2O_3	7.99%
MnO	0.12%
MgO	3.77%
CaO	0.80%
Na_2O	1.66%
K_2O	4.15%
P_2O_5	0.10%
Ba	0.21%
LOI	2.15%
Total	100.34%

MO (+AU, W) MINERALIZATION

The Snow Peak pluton hosts Mo±Au and W mineralization at the Mack prospect (MINFILE 104J 014), which is located in the southern part of the intrusion (Figure 1). Mineralization comprises coarse-grained (1-7 mm) molybdenite and pyrite crystals, which are disseminated along steeply dipping west-northwest trending fractures or narrow quartz veins (Figure 7). These discrete, rust-stained fractures are spaced at intervals of approximately 15-50 cm in a zone that extends for approximately 1 km. Sandler-Brown and Nevin (1976) reported quartz-filled mineralized fractures up to 7 mm wide, and observed finer grained disseminated molybdenite and pyrite in the hostrock within the mineralized zone. Trench sampling has returned typically low Au values (<0.06 g/t) but in several cases values of 1.5 to 1.6 g/t Au accompany elevated molybdenum values in the central part of the mineralized zone (Sandler-Brown and Nevin, 1976). Scheelite is also reported. Sandler-Brown and Nevin (1976) identified a geophysical anomaly that coincides with the mineralized

Figure 7. Molybdenite and pyrite crystals on fracture plane in the Snow Peak pluton at the Mack prospect.

zone, but no drilling has taken place to assess mineralization at depth. A sample of coarse-grained molybdenite from the Mack prospect was collected and is being prepared for dating using the Re-Os method at the University of Alberta, Edmonton.

CONCLUSIONS

The Snow Peak pluton records Early Paleocene magmatism and associated Mo±Au and W mineralization that is *ca.* 10 Ma. younger than lithologic and metallogenic similar plutons of the Late Cretaceous Surprise Lake Plutonic Suite of northern British Columbia and the Yukon (Woodsworth *et al.*, 1991). This younger magmatic epoch may be the plutonic equivalent of Carmacks Group volcanism exposed further north (Lowry *et al.*, 1986; Hart, 1995).

ACKNOWLEDGMENTS

Thanks to Megan Hogg, Olivia Iverson, Travis McCarron and Catie Young for assistance in the field. Jim and Sharon Reid of Pacific Western Helicopters Ltd. are thanked for safe, courteous flying and logistical support. Geoscience BC provided financial support for the field and analytical programs, and salary support for the first author and field assistants.

REFERENCES

Coueslan, C.G., Pattison, D.R.M. and Tinkham, D.K. (2011): Regional low-pressure amphibolite-facies metamorphism at the pipe II mine, Thompson nickel belt, Manitoba, and comparison of metamorphic isograds in metapelites and meta-iron formations; *The Canadian Mineralogist*, Volume 49, pages 721-747.

de Capitani, C. and Petrakakis, K. (2010): The computation of equilibrium assemblage diagrams with Theriak/Domino software; *American Mineralogist*, Volume 95, pages 1006-1016.

Hart, C.J.R. (1995): Magmatic and tectonic evolution of the eastern Coast and western Intermontane belts in southern Yukon Territory; M.Sc. thesis, *The University of British Columbia*, Vancouver, 198 pages.

Holland, T.J.B. and Powell, R. (1998): An internally consistent thermodynamic data set for phases of petrological interest; *Journal of Metamorphic Geology*, Volume 16, pages 309-343.

Gabrielse, H. (1998): Geology of Cry Lake and Dease Lake Map Areas, North-Central British Columbia; *Geological Survey of Canada*, Bulletin 504, 147 pages.

Logan, J.M., Moynihan, D.P., and Diakow, L.J. (2012a): Dease Lake Geoscience Project, Part I: Geology and Mineralization of the Dease Lake (104J/8) and East- Half of the Little Tuya River (104J/7E) Map Sheets, Northern British Columbia; this volume-Fieldwork 2011, *BC Ministry of Energy and Mines.*

Logan, J.M., van Straaten, B.I., Moynihan, D.P. and Diakow, L.J. (2012b): Geochronological results from the Dease Lake Geoscience Project, Northern British Columbia; *BC Ministry of Energy and Mines*, Geofile 2012-x.

Lowey, G.W., Sinclair, W.D. and Hills, L.V. (1986): Additional K-Ar isotopic dates for the Carmacks Group (Upper Cretaceous), west-central Yukon; *Canadian Journal of Earth Sciences*, Volume 23, pages 1857-1859.

Ryan, B., (1991): Geology and Potential Coal and Coalbed Methane Resource of the Tuya River Coal Basin (104J/2, 7); *BC Ministry of Energy, Mines and Petroleum Resources*, Paper 2001-1, pages 419-432.

Sadler-Brown, T.L. & Nevin, A.E. (1976): A report on a geological survey of the Mack 1 to 36 mineral claims and the Mack 1,2,7&8 fractional mineral claims, Snow Peak area, Liard mining district, B.C.; *BC Ministry of Energy, Mines and Petroleum Resources*, Assessment Report 6354.

Streckeisen, A. (1976): To each Plutonic Rock Its Proper Name; *Earth-Sciences Review*, Volume 12, pages 1-33.

Spear, F.S. (1993): Metamorphic Phase Equilibria and Pressure-Temperature-Time Paths; *Mineralogical Society of America*, Washington, D.C., 799 pages.

Woodsworth, G.J., Anderson, R.G., and Armstrong, R.L. (1991): Plutonic Regimes; Chapter 15 in Geology of the Cordilleran Orogen in Canada, Gabrielse, H. and Yorath, C.J., Editors, *Geological Survey of Canada*, Geology of Canada, No. 4, pages 491-531.

Geology of the Kutcho Assemblage between the Kehlechoa and Tucho Rivers, Northern British Columbia (NTS 104I/01, 02)

by P. Schiarizza[1]

KEYWORDS: Kutcho assemblage, Cache Creek complex, Sinwa Formation, Inklin Formation, Whitehorse trough, King Salmon fault, Nahlin fault, Kutcho Creek volcanogenic massive sulphide deposit

INTRODUCTION

The Kutcho project is a two-year bedrock mapping program initiated by the British Columbia Geological Survey Branch in 2010. The main goals of the project are to gain a better understanding of, and provide more detailed geological maps for, the Permo-Triassic Kutcho assemblage, which hosts the Kutcho Creek volcanogenic massive sulphide deposit. This study is a component of the Natural Resources Canada-led Edges (Multiple Metals-Northwest Canadian Cordillera (Yukon, British Columbia)) project, which is a contribution to the GEM (Geomapping for Energy and Minerals) program. The GEM program was initiated by the Federal Government in 2008 to enhance public geoscience knowledge in northern Canada, in order to stimulate economic activity in the energy and mineral sectors.

The 2010 mapping program covered about 200 square kilometres east of upper Kutcho Creek (Schiarizza, 2011a, b). Fieldwork in July and August 2011 covered an additional 200 square kilometres west of the creek, but also included some fill-in traverses within the 2010 map area. The 2011 field program was carried out by a single traverse team comprising the author and student assistant Matthew Newman (Simon Fraser University). Work was conducted from Kutcho Copper Corporation's exploration camp on Kutcho Creek. Operating funds were provided by the British Columbia Geological Survey Branch, a private-public partnership agreement with Kutcho Copper Corporation (a subsidiary of Capstone Mining Corporation) and the Geological Survey of Canada (Edges project).

The Kutcho project area is located in the southeast corner of NTS map sheet 104I (Cry Lake), and encompasses the transition between the Stikine Ranges of the Cassiar Mountains to the north and the Spatsizi Plateau to the south. The nearest community is Dease Lake, located on Highway 37, 100 km west-northwest of the Kutcho Creek deposit. A poor tote road connects the map area to Dease Lake, but the most efficient access is by air, facilitated by a gravel airstrip at the exploration camp on the west side of Kutcho Creek.

The geological interpretation presented here builds on studies carried out by the Geological Survey of Canada in the Cry Lake and Dease Lake map areas from 1956 to 1991 (summarized by Gabrielse, 1998), including regional studies of the Kutcho assemblage by Monger (1977), Monger and Thorstad (1978), Thorstad (1979, 1984) and Thorstad and Gabrielse (1986). It also incorporates work carried out in the vicinity of Kutcho Creek deposit by provincial government geologists from 1974 to 1977 (Panteleyev, 1975, 1978; Pearson and Panteleyev, 1976; Panteleyev and Pearson, 1977a, b), and detailed studies of the deposit and surrounding rocks by Bridge *et al.* (1986), Barrett *et al.* (1996) and Childe and Thompson (1997).

This report summarizes the geology of the entire project area, because the 2011 mapping program has prompted revisions to several aspects of the geology presented by Schiarizza (2011a) for the area east of Kutcho Creek. Those map units and structures for which the interpretation remains unchanged will be briefly summarized, with reference to the earlier report.

REGIONAL GEOLOGICAL SETTING

The geological setting of the Kutcho project area is shown on Figure 1. The map area is located at the east end of the King Salmon allochthon, a relatively narrow structural/stratigraphic belt that has been traced several hundred kilometres to the west-northwest, and separates the main exposures of the oceanic Cache Creek terrane to the north from those of the Stikine arc terrane to the south. The allochthon itself consists mainly of Early to Middle Jurassic clastic sedimentary rocks of the Inklin Formation, which forms the main exposure belt of the Whitehorse trough in northern British Columbia. The allochthon is bounded by the King Salmon and Nahlin faults, which are interpreted as northerly dipping thrust faults that were active in early Middle Jurassic time.

[1] *British Columbia Geological Survey, Victoria, BC*

This publication is also available, free of charge, as colour digital files in Adobe Acrobat® PDF format from the BC Ministry of Energy and Mines website at http://www.empr.gov.bc.ca/Mining/Geoscience/PublicationsCatalogue/Fieldwork.

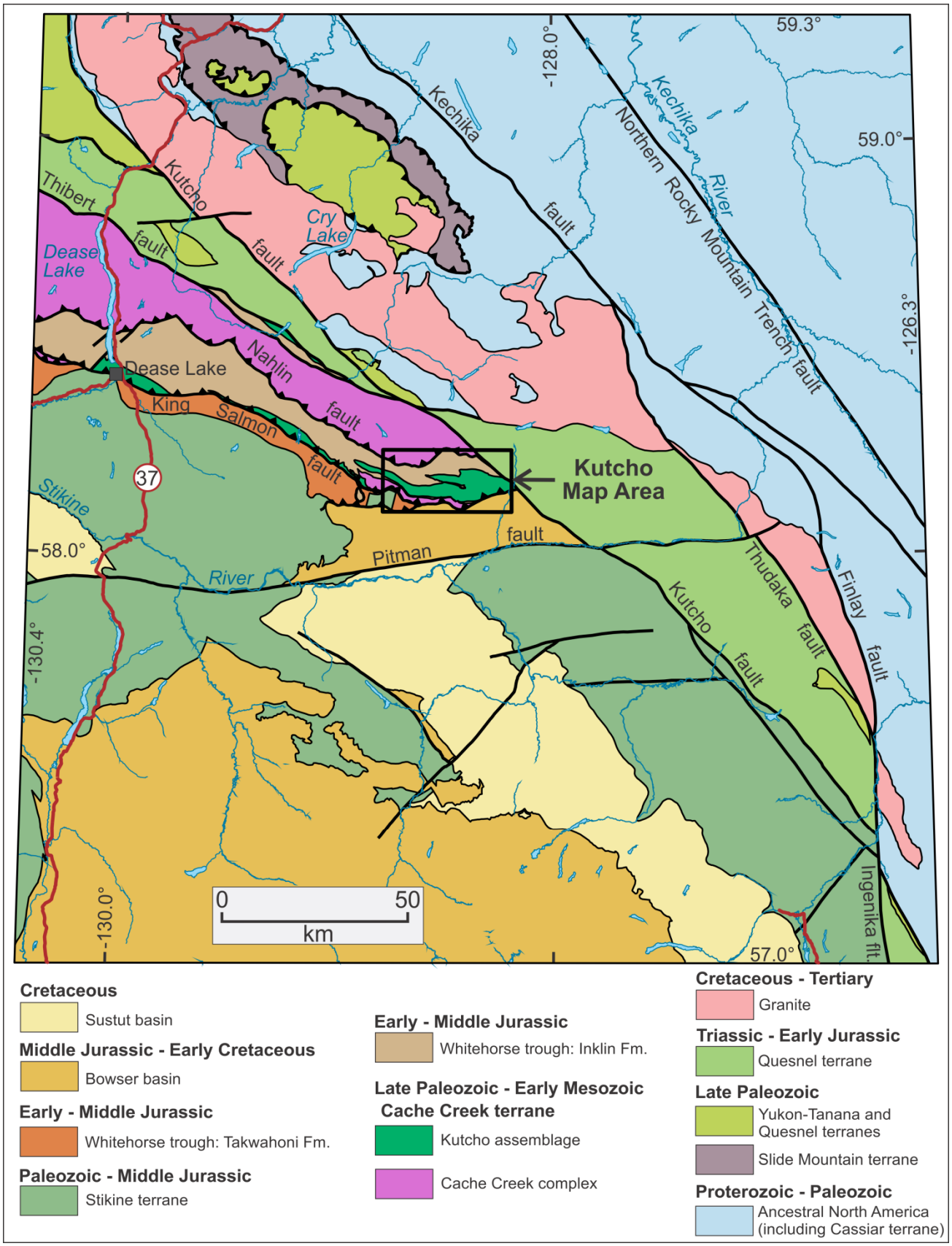

Figure 1. Regional geological setting of the Kutcho map area, after Massey *et al.* (2005).

The Cache Creek terrane is represented mainly by the Cache Creek complex, which includes structurally interleaved slices of chert, argillite, basalt, carbonate, wacke, gabbro and alpine ultramafic rocks, collectively ranging from Early Mississippian to Early Jurassic in age (Monger, 1975; Cordey *et al.*, 1991; Gabrielse, 1998; Mihalynuk *et al.*, 2004). Although the main belt of Cache Creek exposures is northeast of the Nahlin fault, slivers of the Cache Creek complex also occur within the eastern part of the King Salmon allochthon, where they are spatially associated with Permo-Triassic bimodal volcanic and volcaniclastic rocks of the Kutcho assemblage, which may represent a primitive oceanic arc sequence within Cache Creek terrane. The Kutcho assemblage and Cache Creek complex within the King Salmon allochthon are stratigraphically overlain by the Inklin Formation, indicating that they form part of the basement to the Whitehorse trough.

The Stikine terrane comprises a stacked succession of arc-derived volcanic, sedimentary and plutonic rocks that includes the Paleozoic Stikine assemblage, the Upper Triassic Stuhini Group and the Lower to Middle Jurassic Hazelton Group (Anderson, 1993). The Takwahoni Formation, exposed along the northeastern edge of Stikine terrane, comprises Lower to Middle Jurassic conglomerate and sandstone that are coeval with the finer grained clastic rocks of the Inklin Formation within the adjacent King Salmon allochthon. The two formations are interpreted as proximal and distal facies, respectively, of the Whitehorse trough, which may represent a forearc basin that formed along the margin of Stikine terrane (Johannson *et al.*, 1997; English *et al.*, 2005). A well-studied section of the Takwahoni Formation at Lisadele Lake in the Tulsequah map area records progressive unroofing of Stikine terrane in the Lower Jurassic section and a profound provenance shift marked by Cache Creek-derived chert pebble conglomerate in Middle Jurassic (Bajocian) rocks at the top of the section (Mihalynuk *et al.*, 2004; Shirmohammad *et al.*, 2007). The chert-rich Bajocian rocks may correlate with the basal part of the Middle Jurassic to Lower Cretaceous Bowser Basin, a successor basin that overlies large areas of Stikine terrane, but received a significant clastic input from Cache Creek terrane and other non-Stikine sources (Tipper and Richards, 1976; Evenchick *et al.*, 2007). Late Cretaceous clastic rocks of the Sustut Basin crop out mainly along the eastern margin of the Bowser Basin, where they were deposited during deformation of Bowser Basin strata in the Skeena fold belt (Evenchick, 1991; Evenchick *et al.*, 2007).

The King Salmon allochthon, together with adjacent Cache Creek and Stikine terranes, is truncated to the northeast by a system of northwest-striking faults that record significant dextral strike-slip displacement of Cretaceous and Tertiary age (Gabrielse, 1985, 1998; Gabrielse *et al.*, 2006). This fault system offsets the King Salmon allochthon from correlative rocks of the Sitlika assemblage, which crop out 300 km to the south in the Takla Lake area of central British Columbia (Monger *et al.*, 1978; Gabrielse, 1985; Schiarizza and Massey, 2010). The fault panels directly northeast of the Cache Creek – King Salmon – Stikine belts include mid-Paleozoic, late Paleozoic and Mesozoic arc sequences that are part of Yukon-Tanana and Quesnel terranes (Gabrielse, 1991; Nelson and Friedman, 2004). Farther northeast, these rocks are faulted against, and intruded by, a major belt of granitic rocks that includes the Cretaceous Cassiar Batholith. The rocks northeast of this granitic belt consist mainly of Proterozoic through Paleozoic sedimentary rocks of North American affinity, locally overlain by thrust slices of oceanic Slide Mountain terrane, Quesnel terrane and Yukon-Tanana terrane, which together comprise the Sylvester allochthon (Gabrielse, 1991; Nelson and Friedman, 2004).

GEOLOGICAL UNITS

The distribution of the main geological units within the Kutcho map area is shown on Figure 2. Figure 3 provides a more detailed map of the central part of the area, and shows subdivisions of the Kutcho assemblage and Whitehorse trough that are not indicated on Figure 2. Figure 4 presents schematic vertical cross-sections through the area, along lines that are indicated on figures 2 and 3.

The map area is underlain mainly by rocks within the King Salmon allochthon, including the Cache Creek complex, the Kutcho assemblage, and overlying Triassic-Jurassic metasedimentary rocks of the Whitehorse trough. All of these rocks, and a thick gabbroic sill that cuts the northern part of the Kutcho assemblage, are penetratively deformed and characterized by a cleavage or schistosity defined by greenschist facies mineral assemblages. South-verging folds and north dipping thrust faults that deform the main map units are broadly contemporaneous with the metamorphism and probably formed in early Middle Jurassic time. The allochthon is bounded to the south by the north dipping King Salmon thrust fault, and to the north by the Nahlin fault. Clastic sedimentary rocks of the Takwahoni Formation and Bowser Lake Group occur in the footwall of the King Salmon fault, and rocks of the Cache Creek complex crop out on the north side of the Nahlin fault. The northwest striking Kutcho fault truncates the King Salmon allochthon near the northeast edge of the map area, and juxtaposes it against undated plutonic rocks, mainly granodiorite and quartz diorite, which are part of the Quesnel terrane. The youngest rocks mapped in the area comprise small post-metamorphic plugs of diorite that cut the Kutcho assemblage. These plugs, and abundant sills and dikes of hornblende-pyroxene-plagioclase porphyry that are associated with them, are probably Eocene in age. Other post-metamorphic dikes, including lamprophyre and hornblende porphyry, are of unknown age.

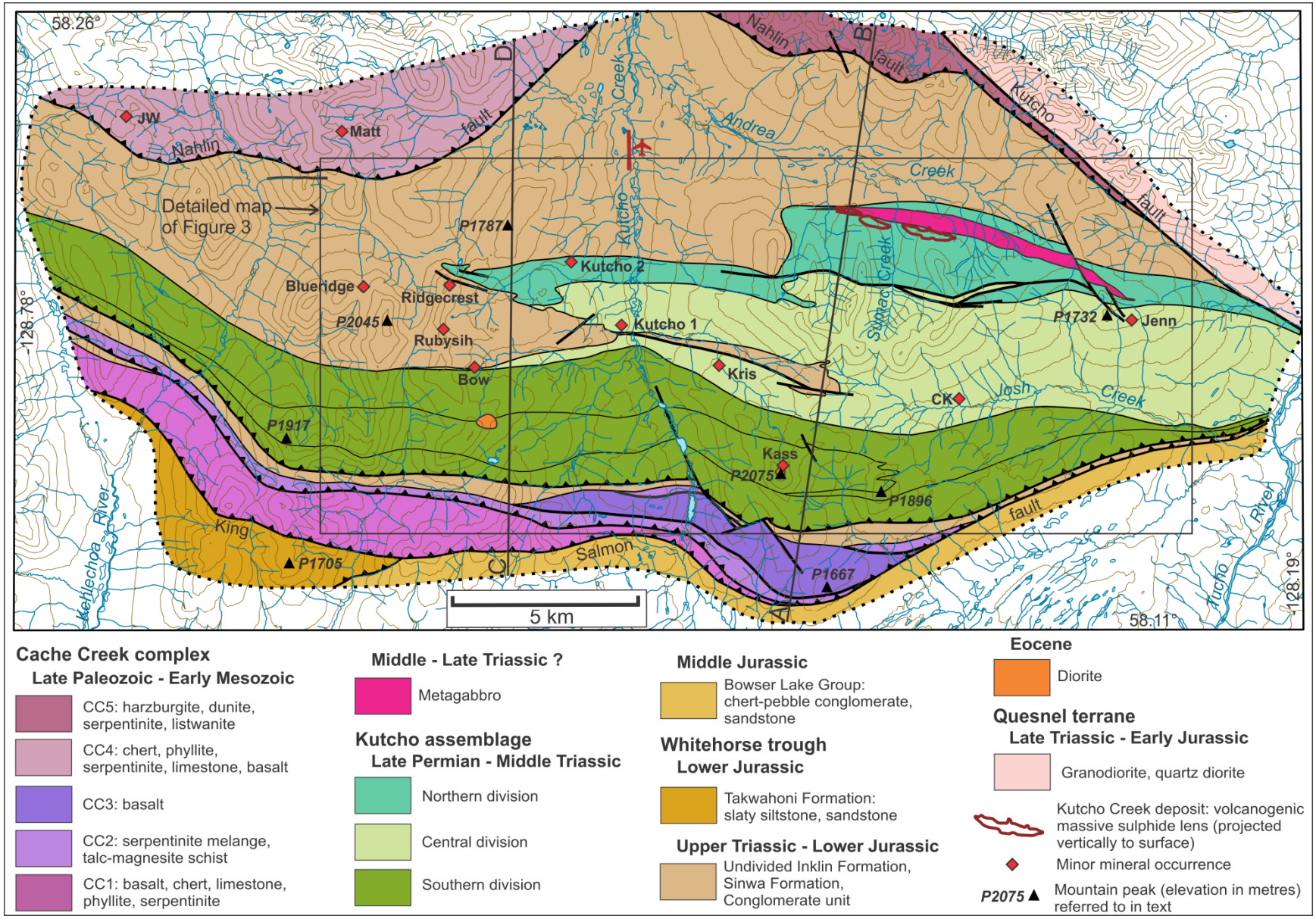

Figure 2. Generalized geology of the Kutcho map area, based mainly on 2010 and 2011 fieldwork.

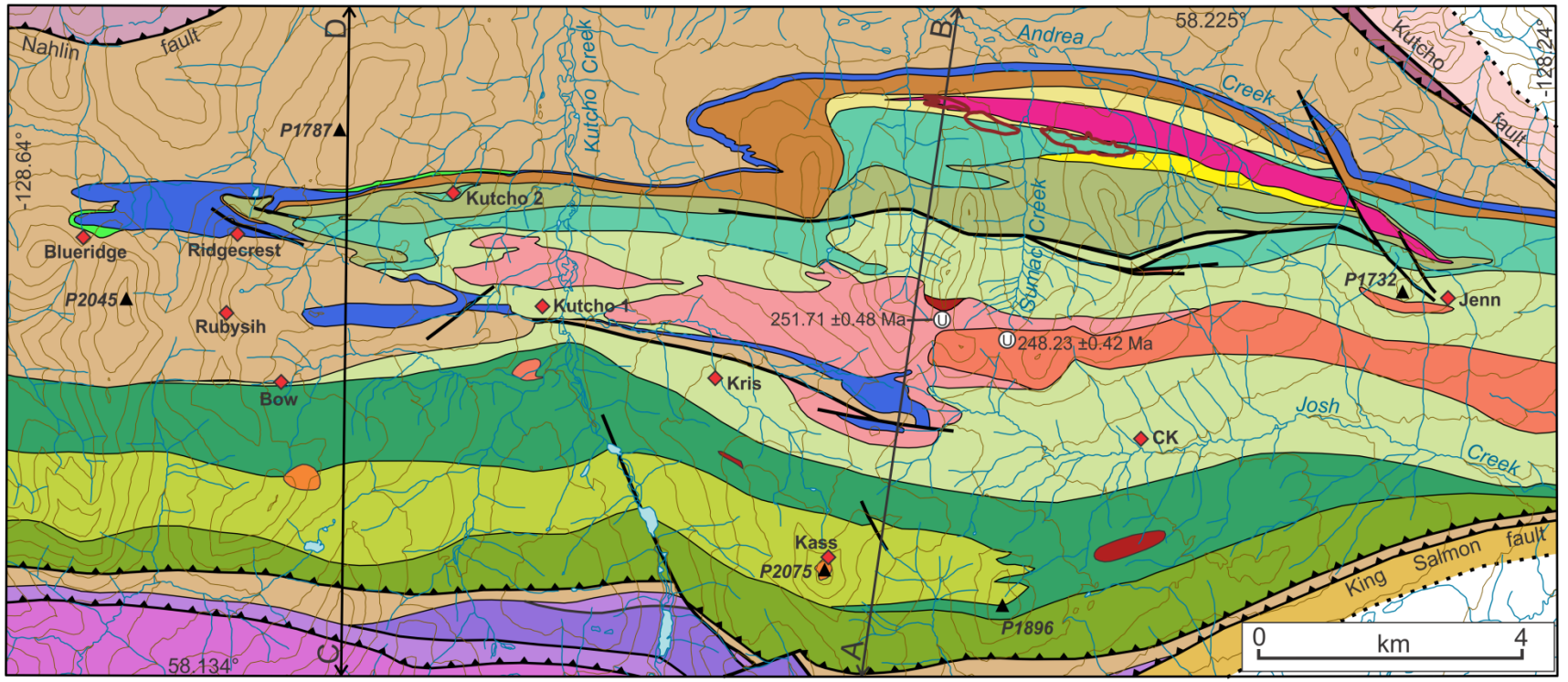

Kutcho assemblage
Southern division

- KS3: epidote-chlorite schist derived from mafic volcanic rocks
- KS2: felsic fragmental schist, metarhyolite, epidote-chlorite schist, sandstone, phyllite
- KS1: feldspathic schist; felsic fragmental schist

Kutcho assemblage
Intrusive rocks

- Tonalite
- Diorite

Central division

- Metarhyolite; epidote-chlorite schist; felsic fragmental schist; sandstone, phyllite, chert
- Metarhyolite

U/Pb zircon date (sample collected in 2010; dated by R. Friedman, UBC)

Kutcho assemblage
Northern division

- KNs: phyllite, siltstone, sandstone; gabbro
- KNa: pyritic quartz-sericite schist
- KNf: feldspathic sericite-chlorite schist; breccia, metarhyolite
- KNq: coarse quartz-eye chlorite-sericite schist; breccia

Whitehorse Trough
Early - Middle Jurassic

- Inklin Formation: slate, siltstone, sandstone, conglomerate, limestone
- Gritty feldspathic sandstone

Late Triassic

- Sinwa Formation: limestone, marble

Late Triassic ?

- Conglomerate; clasts derived from Kutcho assemblage

Figure 3. Geology of the central part of the Kutcho map area, showing detailed subdivisions of the Kutcho assemblage and Whitehorse trough.

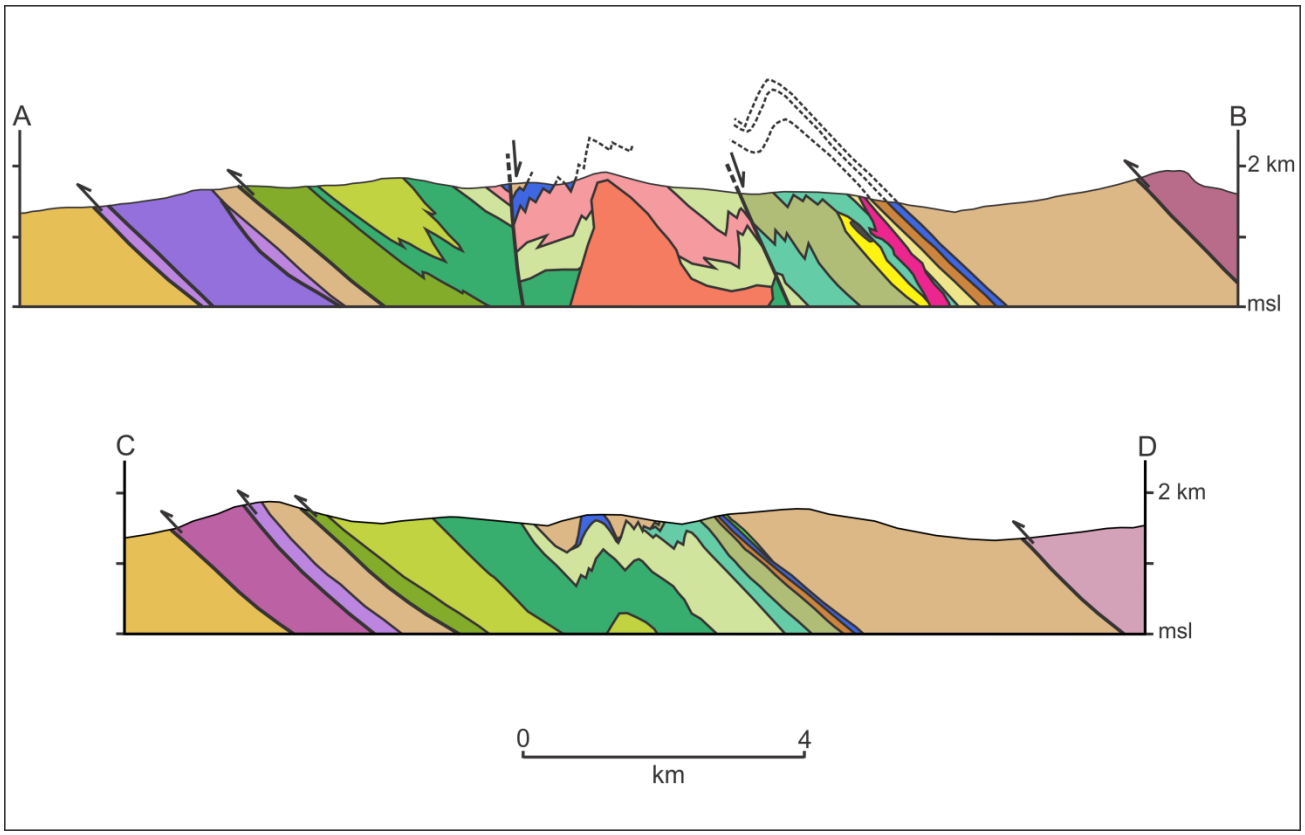

Figure 4. Schematic vertical cross-sections along lines A-B and C-D, shown in figures 2 and 3. See figures 2 and 3 for legend.

Cache Creek complex

The Cache Creek complex forms a narrow lens along the structural base of the King Salmon allochthon, in the central and western parts of the map area, where it is subdivided into 3 informal units, designated CC1, CC2 and CC3. The complex is also represented by two units that crop out north of the Nahlin fault; unit CC4 west of Kutcho Creek and unit CC5 east of the creek. There are no paleontologic or radiometric dates available for any of the Cache Creek rocks in the Kutcho map area.

UNIT CC1

Unit CC1 forms the structural base of the Cache Creek complex within the King Salmon allochthon. It is a heterogeneous unit dominated by three main components: chlorite schist and semischist derived from mafic volcanic rocks; siliceous phyllite and chert; and limestone. These components are structurally interleaved on a scale of metres to hundreds of metres. Individual units are lenticular and are typically separated from adjacent units by contacts that are parallel to the strong north-dipping schistosity.

Mafic volcanic rocks comprise light to dark green, typically rusty brown weathered chloritic schists and semischists that commonly contain abundant calcite and epidote as veins and/or disseminations. There is little indication of original mineralogy or texture at the outcrop scale, but a thin section shows a relict volcanic texture of intergrown plagioclase and clinopyroxene, partially overprinted by metamorphic chlorite, epidote and actinolite. Coarser grained epidote-chlorite-plagioclase schists occur locally, and were probably derived from diabasic or gabbroic intrusive phases. Narrow units of serpentinite were also noted within, or along the margins of, some of the mafic metavolcanic lenses.

Siliceous metasedimentary units consist mainly of light to dark grey or greenish grey platy quartz phyllites that comprise narrow lenses of very fine grained quartzose rock, typically less than 1 cm thick, separated by phyllitic partings containing sericite and chlorite. Grey or green chert is also common, and occurs as lenticular beds, 1 to 5 cm thick, separated by phyllitic partings. Narrow units of relatively homogeneous medium to dark grey phyllite or calcareous phyllite occur locally, but are not common.

Medium to dark grey, light grey weathered limestone occurs as units ranging from less than 1 m to more than 50 m thick. Some of the thick limestone units can be traced for several km. None of the limestone lenses are conspicuously fossiliferous, but samples collected during the 2011 field season are being processed for conodonts.

UNIT CC2

Unit CC2 is a serpentinite melange unit that comprises serpentinite and talc-magnesite schist which

enclose blocks and lenses of a variety of other Cache Creek lithologies. It forms a narrow unit that has been traced for about 20 kilometres within the King Salmon allochthon, where it structurally overlies unit CC1 or, near the western edge of the map area, an intervening lens of metasedimentary rocks assigned to the Inklin Formation. This belt of serpentinite melange forms the structurally highest unit of the Cache Creek complex in the west, but in the south-central part of the map area it is structurally overlain by a metabasalt unit that is assigned to unit CC3. Discontinuous lenses of serpentinite melange occur structurally above the metabasalt unit, and these are also assigned to unit CC2.

Irregularly-foliated green to black serpentinite is the dominant lithology within unit CC2. The mineralogy of the ultramafic protolith is generally not apparent, although a lens of harzburgite occurs within serpentinite at one locality near the west edge of the map area. Rusty weathered talc-magnesite schist is also common, and typically displays gradational, interfingering contacts with serpentinite. The largest knockers, ranging up to several hundred metres in size, comprise mafic intrusive complexes that are dominated by gabbro, but also include pyroxenite, feldspar pyroxenite, diabase and, rarely, diorite or quartz diorite. Mafic volcanic rocks, including chlorite schist, chloritic semischist and massive, silicified greenstone, are also very common, and occur as blocks ranging up to several tens of metres in size. Metasedimentary rocks are rare within the serpentinite melange, but metre-scale knockers of chert and cherty argillite occur locally.

UNIT CC3

Unit CC3 consists of metabasalt, with rare thin lenses of bedded chert and limestone, which forms a belt about 10 km long and up to 1.5 km wide near the east end of the Cache Creek exposures within the King Salmon allochthon. The medium to pale green, weakly to moderately schistose metabasalt forms monotonous greenish brown to rusty brown weathered exposures, as described by Schiarizza (2011a). Unit CC3 is structurally underlain by the main serpentinite melange belt assigned to unit CC2, but it is also overlain by apparently discontinuous lenses of similar serpentinite melange, also assigned to unit CC2. This arrangement, and the lithologic similarity between unit CC3 and basalt knockers that are common within unit CC2, suggests that unit CC3 is essentially a large lens within the serpentinite melange belt.

UNIT CC4

Cache Creek rocks north of the Nahlin fault in the northwestern part of the map area, which were examined only briefly during the 2011 field season, are assigned to unit CC4. Rocks in the central part of this belt, near the Matt showing, are dominated by a light to dark grey siliceous metasedimentary assemblage that includes thin-bedded chert, siliceous phyllite, cherty argillite and phyllite. Discontinuous layers of light grey weathered limestone, up to 10 m thick, are fairly common, and lenses of metabasalt and serpentinite occur locally. Similar rocks also occur in the flanking areas to the east and west, but here the assemblage includes a higher proportion of metabasalt, and also contains large amounts of serpentinite and talc-magnesite schist.

UNIT CC5

Unit CC5 consists of variably serpentinized ultramafic rocks, including harzburgite and dunite, which crop out on the north side of the Nahlin fault in the northeast part of the map area. These rocks are briefly described by Schiarizza (2011a). They are part of a widespread ophiolitic assemblage that forms a major part of the Cache Creek terrane of northern British Columbia (Monger, 1975; Terry, 1977; Ash, 2001; English *et al.*, 2010).

Kutcho assemblage

The Kutcho assemblage is a heterogeneous package of schists derived from felsic and mafic volcanic and volcaniclastic rocks and associated felsic and mafic intrusions. The widest belt of exposures, and the informal type area for the assemblage, is within the current map area (Thorstad and Gabrielse, 1986), but the Kutcho assemblage also occurs as several smaller lenses that have been mapped within the King Salmon allochthon as far west as Dease Lake (Gabrielse, 1998).

The history of nomenclature, age assignments and correlations for rocks now included in the Kutcho assemblage is summarized by Schiarizza (2011a). The assemblage is assigned a Permo-Triassic age based on U-Pb zircon dates presented by Childe and Thompson (1997), and new dates obtained during the current study. Childe and Thompson (1997) obtained primitive Nd isotopic signatures from Kutcho volcanic rocks and primitive Pb isotopic signatures from the syngenetic mineralization of the Kutcho Creek volcanogenic massive sulphide deposit. These data, together with geochemical data presented by Barrett *et al.* (1996), showing that mafic and felsic volcanic rocks from the northern part of the Kutcho assemblage have an arc tholeiite affinity, suggest that the Kutcho assemblage represents part of a primitive intra-oceanic arc.

Schiarizza (2011a) subdivided the Kutcho assemblage into three main divisions referred to as southern, central and northern. This same three-fold scheme is applied here, although nomenclature and definitions of some of the internal units within the northern and southern divisions have been modified. Although there are local fold repetitions, rocks within the assemblage generally dip and face to the north. Available dates, shown on Figure 5, indicate that the northern division is, at least in part, younger than the central division, consistent with a younger above older stratigraphic relationship. There are no dates yet available for the southern division; it appears to rest

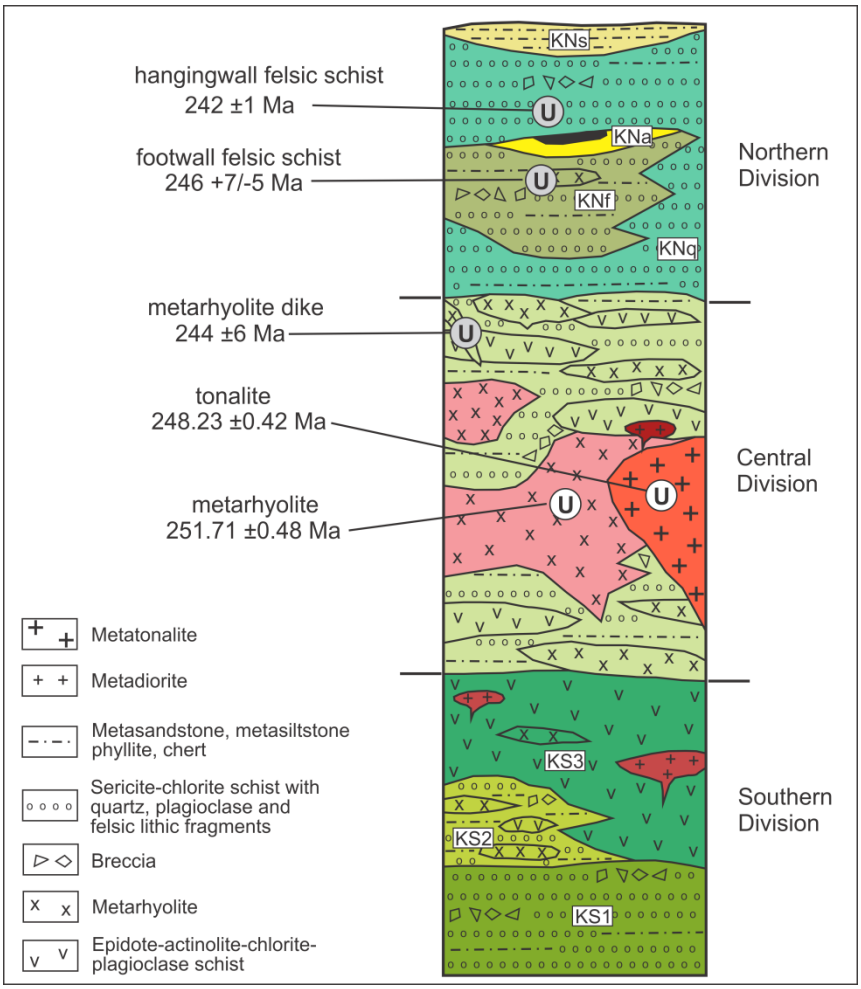

Figure 5. Schematic stratigraphic column through the Kutcho assemblage, showing main lithologic components and available age constraints. See Figure 3 for colour legend.

stratigraphically beneath the central division, but it might be a lateral equivalent, separated from the overlying rocks by a cryptic fault.

SOUTHERN DIVISION

Schiarizza (2011a) subdivided the southern division of the Kutcho assemblage into two units, a basal clastic and volcaniclastic unit referred to as KS1 and an overlying unit of mafic schists referred to as KS2. This scheme was modified by Schiarizza (2011b), who split the lower unit into two parts, KS1 and KS2, and assigned the upper mafic schists to unit KS3. This latter scheme is followed here, with an additional modification whereby clastic rocks that were included in the basal part of unit KS1 are taken out of the unit and assigned to the Inklin Formation. The basal contact of the Kutcho assemblage is an inferred north dipping thrust fault that places unit KS1 above these Inklin rocks.

Unit KS1

Unit KS1 comprises gritty and fragmental schists that were derived mainly from felsic epiclastic rocks. They are typically medium to dark green, and weather to a pale brownish green colour. Gritty varieties consist of plagioclase grains, 1-4 mm in size, within a well-foliated matrix that contains variable proportions of chlorite, sericite, quartz, plagioclase, calcite and epidote, and locally actinolite or stilpnomelane. The clastic plagioclase grains are commonly accompanied by smaller and less abundant quartz grains, and in some narrow intervals quartz predominates over plagioclase. Fragmental schists are similar, but include flattened, commonly epidote-altered lithic fragments (Figure 6). The lithic fragments are typically a few millimetres to a few centimetres in size, but coarser units, with lithic clasts up to 10 cm in longest dimension, occur locally. The fragments are dominated by aphanitic to very fine-grained felsite, locally with small feldspar and/or quartz phenocrysts. Fragments composed of fine grained, equigranular intergrowths of feldspar and quartz are also present, and one exposure, 1.5 km east of peak 1896, includes a substantial number of medium grained quartz monzonite clasts. The schists of unit KS1 locally display a crude stratification, and rarely occur as distinct thin to thick beds, some of which are graded (Schiarizza 2011a). The well-bedded intervals may include thin interbeds of fine to medium grained schisty quartz-feldspar metasandstone

Figure 6. Felsic fragmental schist, unit KS1, 4 km south-southeast of peak 2045.

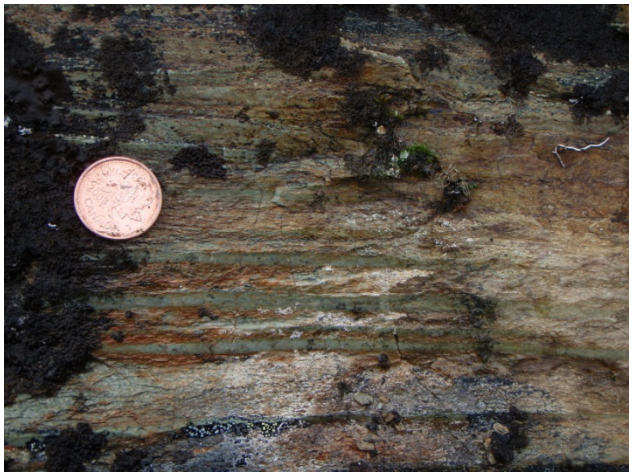

Figure 7. Thin-bedded metasandstone and metasiltstone, unit KS2, 4 km southwest of peak 2045.

and/or laminated phyllite and metasiltstone.

Unit KS2

Unit KS2 is a discontinuous map unit that extends from the slopes north of peak 1896, where it interfingers with unit KS3, westward to the area of peak 1917 (Figure 2). It apparently pinches out west of the latter area, as it was not recognized on traverses conducted between the two forks of the Kehlechoa River, along the western edge of the map area.

Unit KS2 includes gritty plagioclase-rich schists and felsic fragmental schists similar to those of unit KS1, but it also includes metarhyolite, chlorite schist derived from mafic volcanic rocks, and significant amounts of well-bedded metasedimentary rock. Metarhyolite forms light grey, weakly to strongly schistose units, from a few metres to a few tens of metres thick, which were probably derived from flows and/or sills. Relict plagioclase phenocrysts, generally less than 2 mm across, occur within a groundmass of very fine-grained quartz and feldspar, accompanied by flakes of chlorite and sericite, and, in some cases, minor amounts of epidote and biotite. Medium to dark green mafic volcanic units, up to several tens of metres thick, comprise thoroughly recrystallized calcite-epidote-actinolite-chlorite-plagioclase schists. Metasedimentary intervals range from a few metres to more than a hundred metres thick. Some are dominated by thin to thick beds of schistose metasandstone, containing detrital grains of mainly plagioclase and quartz, interbedded with green or grey, commonly laminated, phyllitic metasiltstone (Figure 7). Other intervals comprise vaguely laminated, fine grained epidote-chlorite-sericite-plagioclase-quartz schists, locally with relict silt to sand-size grains of quartz and plagioclase, which were probably derived from siltstones or fine tuffs. Conglomerate or breccia units occur locally, and form layers 10 to 20 m thick within metasandstone-dominated intervals. They consist of variably flattened fragments, up to 20 cm across, within a chlorite-sericite-plagioclase-quartz schist matrix. Fragments are mainly fine-grained felsite and sericite-quartz schist, but the clast population locally includes quartz-phyric metarhyolite, medium-grained tonalite, plagioclase porphyry, and minor amounts of dark grey phyllite and limestone.

Unit KS3

Unit KS3 consists mainly of chlorite schist derived from mafic volcanic rocks, but also includes narrow intervals of metarhyolite and felsic volcaniclastic rock. It forms the uppermost unit of the southern division and has been traced across the entire width of the Kutcho map area. It overlies unit KS1 in the eastern and far western parts of the map area, but interfingers with and overlies unit KS2 in the intervening area. Unit KS3 is overlain by the central division of the Kutcho assemblage through much of the map area, but is directly overlain by the Inklin Formation in the west, where the central division has apparently been removed beneath the unconformity at the base of the Whitehorse trough.

The predominant rock type of unit KS3 is medium to dark green, greenish brown weathered, variably calcareous actinolite-epidote-chlorite-plagioclase schist. The schist appears uniform and homogeneous in some exposures, but more commonly has an irregular mottled appearance resulting from patches and veins of pale green calcite-epidote cutting dark green schist. Elsewhere, the schist displays a thin, lenticular layering defined by the segregation of metamorphic minerals into alternating layers rich in chlorite±actinolite and calcite-epidote, respectively. Protolith textures are generally not evident on either the outcrop or thin section scale, although relict plagioclase phenocrysts occur in some thin sections, and small vesicles were observed in an exposure 500 m north of peak 1896. Fragmental schist, with epidote-altered fragments several centimetres in size, occurs locally, but it is not clear if the fragments were derived from autoclastic, pyroclastic or epiclastic processes.

Plagioclase-phyric metarhyolite, similar to metarhyolite bodies within unit KS2, is scattered throughout unit KS3, but is a relatively minor component

and typically forms narrow units less than 10 m wide. Felsic volcaniclastic rocks are also present, but are even less common. They comprise narrow units of sericite-plagioclase-quartz schist that contain quartz and plagioclase grains as well as small felsic lithic fragments.

CENTRAL DIVISION

The central division of the Kutcho assemblage is a heterogeneous succession of felsic and mafic volcanic, volcaniclastic and intrusive rocks that is exposed mainly east of Kutcho Creek, and is described by Schiarizza (2011a). This division is characterized by large amounts of coherent metarhyolite, but also includes a significant proportion of actinolite-epidote-chlorite-plagioclase schist derived from mafic volcanic rocks. The felsic and mafic metavolcanic units are intercalated with fragmental schists derived from felsic volcaniclastic rocks, bedded metasedimentary intervals that include metasandstone, metasiltstone, phyllite and chert, and local units of massive to vaguely laminated, commonly pyritic chert that may represent siliceous exhalites. This division also hosts substantial amounts of tonalite and diorite. Most components are intercalated on too fine a scale to be mapped separately, but a large rhyolite unit, and several intrusive units that crop out east of Kutcho Creek are shown on Figure 3.

Exposures of the central division west of Kutcho Creek comprise the same rocks types, in about the same proportions, that are present east of the creek. Metarhyolite predominates, and in part forms a large mappable body that straddles Kutcho Creek (Figure 3). Typical metarhyolites are light grey, weakly foliated rocks comprising distinct phenocrysts of quartz and plagioclase, 1-4 mm in size, within a very fine grained groundmass that includes quartz, plagioclase and scattered flakes of sericite (Figure 8). Calcareous actinolite-epidote-chlorite-plagioclase schist underlies a substantial area north and northeast of the Kutcho 1 mineral showing, and occurs as isolated exposures elsewhere (Figure 9). Light grey, massive to weakly foliated pyritic chert, probably derived from a siliceous exhalite, is intercalated with metarhyolite at the Kutcho 1 occurrence. Isolated exposures representing other components of the central division include chlorite-sericite schist with quartz, plagioclase and felsic lithic fragments, and feldspathic chlorite schist possibly derived from a feldspathic sandstone.

NORTHERN DIVISION

The northern division of the Kutcho assemblage is derived mainly from felsic volcaniclastic rocks, and consists of chlorite-sericite schists that contain variable proportions of quartz and feldspar crystals and felsic lithic fragments. Schiarizza (2011a), following previous workers (Bridge *et al.*, 1986; Barrett *et al.*, 1996; Childe and Thompson, 1997), subdivided this division into 4 units, KN1 through KN4, which comprise a north dipping and north-facing succession in the area of the Kutcho

Figure 8. Quartz-plagioclase-phyric metarhyolite, central division of the Kutcho assemblage, west of Kutcho Creek, 4 km south of the airstrip.

Figure 9. Epidote-chlorite schist, central division of the Kutcho assemblage, west of Kutcho Creek, 4 km south of the airstrip.

Creek VMS deposit. However, it was noted that coarse quartz-eye schists similar to those of unit KN3, which form the hangingwall of the deposit, also crop out along the southern margin of the northern division. The stratigraphic relationships of this southern belt of coarse quartz-eye schists was not established, but it was speculated that it might be a fault-bounded repetition of the hangingwall belt (Schiarizza, 2011a).

The 2011 mapping program demonstrates that the southern belt of coarse quartz-eye schists forms the stratigraphic base of the northern division, and overlies rocks of the central division on the slopes west and east of Kutcho Creek. These schists are here assigned to unit KNq, which is the most voluminous component of the northern division, and occurs at the base of the division, as well as at higher stratigraphic levels. Finer grained feldspathic schists that were formerly assigned to unit KN1 are here assigned to unit KNf, and appear to form a thick unit that is within unit KNq. Pyritic quartz-sericite schists (part of unit KN2 of Schiarizza, 2011a) that occur locally at the top of unit KNf, as part of the footwall alteration zone beneath the Kutcho Creek VMS deposit,

are assigned to unit KNa. Sedimentary rocks that form the uppermost unit of the Kutcho assemblage (unit KN4 of Schiarizza, 2011a) are now referred to as unit KNs.

Unit KNq

Unit KNq comprises schists, derived mainly from felsic volcaniclastic deposits, which characteristically contain very large quartz grains. These schists occur at the base of the northern division, and overlie rocks of the central division in apparently unfaulted sections on either side of Kutcho Creek, as well as to the northwest and northeast of peak 1732 in the eastern part of the map area. Unit KNq also occurs at higher stratigraphic levels within the northern division, where it overlies the Kutcho Creek massive sulphide lenses and is referred to as hangingwall quartz-feldspar crystal tuff (QFCT) by Bridge *et al.* (1986), and QFCT rhyolite by Barrett *et al.* (1996). The upper and lower belts of KNq schists apparently merge to form a single belt northeast of peak 1732, where intervening rocks, mainly unit KNf, have pinched out.

Unit KNq consists primarily of medium to pale green or silvery green, well foliated chlorite-sericite-plagioclase-quartz schists that contain abundant glassy quartz eyes, typically 2-10 mm in size, but locally to 1.5 cm (Figure 10). The quartz grains are highly strained and some have embayed margins. They are invariably accompanied by smaller plagioclase grains, typically 1-5 mm in size, which are variably altered to sericite and/or epidote, and commonly have subhedral or euhedral outlines. In many exposures the quartz and feldspar crystal grains are accompanied by scattered lithic fragments, typically less than 1 cm across but locally up to 3 cm in size. These lithic fragments include fine to medium-grained tonalite, very fine grained felsite, and quartz±plagioclase-phyric rhyolite. Most exposures of unit KNq are not apparently stratified, or display only vague hints of stratification, indicated by variations in the size, abundance and proportions of crystal grains. However, typical schists in the lower part of the unit on the ridges 4 km east of Kutcho Creek occur, in part, as distinct thin to thick beds intercalated with grey to green phyllitic siltstone. The lower part of unit KNq in this area also includes thin to medium beds of quartz-feldspar sandstone, and thin chert beds intercalated with siliceous phyllite. Thick graded beds also occur in the upper part of unit KNq, where they were intersected in diamond drill holes in the vicinity of the western sulphide lens (Esso lens) of the Kutcho Creek deposit (Bridge *et al.*, 1986).

A lens of coarse matrix-supported breccia, at least several tens of metres wide, is exposed within the upper part of unit KNq west of Sumac Creek. The matrix consists of coarse quartz-eye schist typical of the unit, and the vast majority of the clasts, which range up to 30 cm in size, are the same rock type. The clast population also includes a minor proportion of fine to medium grained equigranular quartzofeldspathic rock, and rare mafic clasts of calcareous epidote-chlorite schist. Parts of the breccia unit display hints of a crude stratification, and lenses of laminated coarse grained quartz-feldspar sandstone are intercalated with coarse breccia units locally (Barrett *et al.*, 1996)

Unit KNf

Unit KNf comprises feldspar and quartz-bearing schists derived from felsic volcaniclastic rocks, and also includes minor amounts of coherent metarhyolite. It forms a substantial unit that interfingers with, and is both underlain and overlain by, unit KNq. Unit KNf is mostly equivalent to unit KN1 of Schiarizza (2011a), but also includes some rocks that were assigned to unit KN2.

Typical schists of unit KNf are medium green on fresh surfaces and weather to a grey-green or brownish green colour. They are characterized by conspicuous grains of plagioclase, typically 1-4 mm in size, which are invariably accompanied by quartz grains of similar or smaller size, and commonly by felsic lithic fragments, mostly 2-10 mm in size but locally up to 3cm (Figure 11). The plagioclase typically forms whole or broken crystals

Figure 10. Coarse quartz-eye schist, unit KNq, 1800 m southeast of peak 1787.

Figure 11. Fragmental feldspathic schist, unit KNf, 1100 m southeast of peak 1787.

with subhedral shapes. The quartz crystals commonly display embayed margins, and locally include granophyric intergrowths of plagioclase. Lithic fragments are variably epidote altered and include aphanitic felsite, quartz-feldspar-phyric rhyolite, fine-grained diorite and tonalite. The relict mineral and lithic grains are enclosed in a fine grained, well-foliated matrix of chlorite, sericite, quartz and plagioclase, locally with significant amounts of epidote and carbonate. Typical feldspathic schist in one exposure west of Sumac Creek is intercalated with several narrow intervals of thin-bedded schist of similar composition but finer grain size. For the most part, however, the schists are not conspicuously bedded, although they commonly display hints of a crude stratification defined by variations in the size, abundance and proportions of crystal and lithic grains, as well as colour variations which reflect the sericite versus chlorite content of the foliated matrix. At one end of this spectrum are uncommon layers of coarse quartz-eye schist similar to those that characterize unit KNq, and at the other end are rare thin units of dark green chloritic schist without conspicuous mineral grains. Although the latter units are suspected to be uncommonly fine grained and mafic layers within the volcaniclastic succession, they might, alternatively, be derived from mafic flows or sills.

Coarse fragmental rocks occur within the upper part of unit KNf over a 1 km strike length southeast of peak 1787. Here, an interval about 20 m thick contains abundant moderately flattened lithic fragments, mainly <1-6 cm in size, but locally up to 15 cm in longest dimension. The fragments are of uniform composition, comprising fine to finely medium grained leucocratic diorite to quartz diorite. The fragmental rocks pass down-section into typical feldspathic schists that locally host sparsely scattered clasts, up to 40 cm across, of mainly aphanitic felsite and quartz porphyry.

Dark grey phyllite and laminated phyllitic siltstone occur as rare intercalations within the volcaniclastic schists of unit KNf, forming layers that rarely exceed a few metres in thickness. A distinctive unit that is exposed at the very top of the succession, directly beneath conglomerate of the Whitehorse trough, south of peak 1787, comprises green phyllite intercalated with thin beds and laminae of purplish brown-weathered silty phyllite, locally grading to a mottled green/purplish grey phyllite containing patches and veins of reddish calcite.

Narrow units of metarhyolite were noted within unit KNf at several localities, but are relatively rare. They typically comprise 10-25% quartz and plagioclase phenocrysts, 1-4 mm in size, within a very fine grained, weakly foliated groundmass of mainly quartz, plagioclase and sericite.

Unit KNa

Unit KNa is a narrow lens of rusty weathered schists that occur in the upper part of unit KNf, and comprise part of the hydrothermally altered footwall to the Kutcho Creek massive sulphide deposit (Figure 3). This unit consists mainly of pale grey to greenish grey, very fissile quartz-sericite schist that weathers rusty due to the presence of disseminated pyrite and flattened porphyroblasts of Fe-Mg carbonate. Small grains of quartz are common, as are flattened lithic fragments, up to a few centimetres long, of pale grey siliceous felsite, with or without small phenocrysts of quartz (Schiarizza, 2011a).

Unit KNs

Metasiltstone, metasandstone and phyllite that occur stratigraphically above coarse quartz-eye schists of unit KNq in the Andrea Creek area are assigned to unit KNs, which is the uppermost unit of the Kutcho assemblage within the map area. Unit KNs is cut by the large mappable metagabbro sill, as well as by thinner sills and dikes of similar metagabbro, and is stratigraphically overlain by the conglomerate unit of the Whitehorse trough. Unit KNs is described by Schiarizza (2011a) as unit KN4, and was not revisited in the 2011 field season.

INTRUSIVE ROCKS OF THE KUTCHO ASSEMBLAGE

Metatonalite forms three mappable bodies within unit KC east of Kutcho Creek, the largest of which is up to 1 km wide and more than 10 km long (Schiarizza, 2011a). Similar metatonalite forms a small plug within the upper part of unit KS3, about 500 m west of Kutcho Creek.

Small sill-like bodies of metadiorite, comprising relict plagioclase grains interspersed with a metamorphic assemblage of mainly epidote, actinolite, chlorite and calcite, are fairly common within units KS3 and KC, and were also noted within unit KS1. Only three of these bodies, two within unit KS3 and one within unit KC, are sufficiently large to be shown on Figure 3.

AGE OF THE KUTCHO ASSEMBLAGE

U-Pb zircon radiometric dates that constrain the age of the Kutcho assemblage are shown on Figure 5. Childe and Thompson (1997) present an Early to Middle Triassic date of 246 +7/-5 Ma for northern division rocks in the footwall of the Kutcho Creek VMS deposit, and a Middle Triassic date of 242 ±1 Ma for rocks directly above the deposit. They also provide a date of 244 ±6 Ma for a quartz-plagioclase porphyry dike to the south of the deposit, probably within the central division. Two additional ages from the central division are provided by samples collected during the 2010 field season, which were dated by Richard Friedman at the University of British Columbia. One sample was collected from the large rhyolite unit that is mapped within the division (Figure 3), and it provides a latest Permian date of 251.71 ±0.48 Ma. The other sample was collected from the large tonalite intrusion that cuts the rhyolite unit and other rocks of central division. It yields an Early Triassic date of 248.23 ±0.42 Ma.

Metarhyolite samples collected from the southern and

northern divisions of the Kutcho assemblage during the 2011 field program have been submitted for U-Pb zircon dating, but the results are not yet available.

Metagabbro cutting northern division of the Kutcho assemblage

Metagabbro, described by Schiarizza (2011a), forms a thick transgressive sill that has been traced for about 8 km within the northern division of the Kutcho assemblage, cutting up-section from east to west. Similar metagabbro is common as narrow dikes and sills within unit KNs, and has also been reported as dikes in felsic schists lower in the section (Childe and Thompson, 1997). The metagabbro cuts metasedimentary rocks of unit KNs, which overlie the youngest known volcanic rocks within the Kutcho assemblage, and it has a shoshonitic chemical signature that is distinct from the tholeiitic signature of mafic metavolcanic rocks of the Kutcho assemblage (Barrett *et al.*, 1996; Childe and Thompson, 1997). It may, therefore, be unrelated to the volcanic and plutonic rocks of the Kutcho assemblage. However, Childe and Thompson (1997) suggest that the gabbro is not significantly younger, because some gabbro units display peperitic textures where they contact metasedimentary rocks of unit KNs, and interaction zones where they contact underlying felsic metavolcanic rocks, suggesting that these units had not been completely lithified when they were intruded by the gabbro.

Whitehorse Trough

The Whitehorse trough within the Kutcho map area is represented by three units: a discontinuous conglomerate unit; an overlying limestone unit which is also discontinuous; and an extensive package of clastic metasedimentary rocks consisting mainly of metasandstone, metasiltstone and slate. The latter package is assigned to the Inklin Formation and forms the east end of a belt that has been traced westward through the Cry Lake and Dease Lake map areas (Gabrielse, 1998) into the type area of the Inklin Formation in the Tulsequah map area (Souther, 1971). The formation is not well dated anywhere along this belt (Gabrielse, 1998), but fossil data from contiguous strata farther to the northwest indicate a Lower to Middle Jurassic age (Pálfy and Hart, 1995; Johannson *et al.*, 1997; Mihalynuk, 1999).

The limestone unit within the Kutcho map area is correlated with the Upper Triassic Sinwa Formation. The Sinwa is also named for exposures in the Tulsequah map area, where it comprises late Upper Triassic (Norian) limestone that occurs in the hangingwall of the King Salmon thrust fault, and is stratigraphically overlain by the Inklin Formation (Souther, 1971). Exposures of Sinwa Formation are intermittent between the type area and the current map area (Gabrielse, 1998), but the correlation is reasonable, given the commonality of stratigraphic position directly beneath the Inklin Formation and structural setting within the King Salmon allochthon.

The conglomerate unit has been recognized by previous workers in the Kutcho area, but some have included it in the Kutcho assemblage (Bridge *et al.*, 1986; Thorstad and Gabrielse, 1986) and others have interpreted it as part of the stratigraphic succession that overlies the Kutcho assemblage (Panteleyev and Pearson, 1977b; Childe and Thompson, 1997). Here, it is included in the Whitehorse trough succession that overlies the Kutcho assemblage, probably across a significant unconformity. This interpretation is based on the abrupt lower contact of the conglomerate unit and the truncation of map units within the Kutcho assemblage against this basal contact (Figure 3), a provenance that is dominated by a variety of lithologic units within the underlying Kutcho assemblage, and a gradational contact with the overlying Sinwa Formation (Childe and Thompson, 1997; Schiarizza, 2011a).

A striking feature within the Kutcho map area is the southward truncation of the upper two divisions of the Kutcho assemblage across the basal contact of the Whitehorse trough. Farther south, at lower structural levels within the King Salmon allochthon, metasedimentary rocks of the Whitehorse trough rest, apparently stratigraphically, above the Cache Creek complex. These relationships attest to an unconformable relationship between the Whitehorse trough and underlying units, reflecting poorly understood pre-Jurassic deformation within the Cache Creek complex and Kutcho assemblage.

CONGLOMERATE UNIT

The conglomerate unit forms a single belt that has been traced for about 20 km, from the eastern part of the map area to the anticlinal fold closure southwest of peak 1787 (Figure 3). It occurs above the northern division of the Kutcho assemblage and below the Sinwa Formation along the entire length of this belt, but the basal contact truncates the upper units of the Kutcho northern division as it is traced from northeast to southwest. The conglomerate unit is commonly on the order of 100-200 m thick in the vicinity of the Kutcho Creek VMS deposit, but thins as it is traced westward from Kutcho Creek, and is only 10-20 m thick where it wraps around the fold closure southwest of peak 1787. It pinches out entirely a short distance southeast of the fold closure, and is generally absent south of that point, although conglomerate that might be correlative forms a narrow unit, less than 10 m thick, at the base of the Inklin Formation on the ridge west of the Bow mineral occurrence (Figure 3).

The conglomerate unit generally weathers to a light greenish grey to brownish grey colour, but locally is reddish brown. It consists of flattened pebbles and cobbles within a schistose matrix of sericite, chlorite and sand to silt-size grains of quartz and feldspar (Figure 12). The clast population is dominated by pale grey to greenish grey felsic rock types that include aphanitic felsite, quartz±plagioclase-phyric rhyolite, quartz-sericite

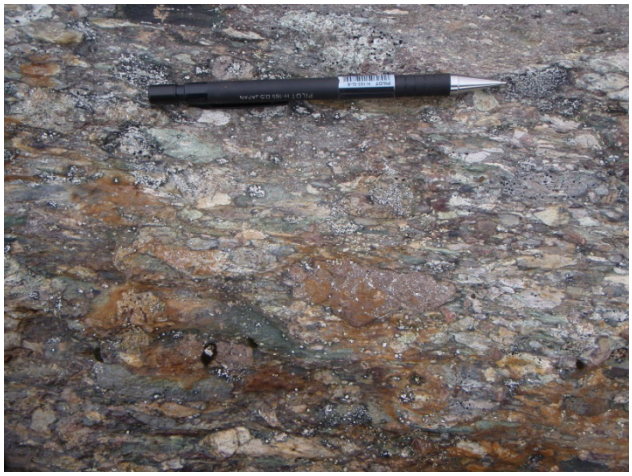

Figure 12. Conglomerate, base of the Whitehorse trough, 1300 m south-southwest of peak 1787.

schist and fine to coarse grained equigranular tonalite. Less common clast types include sericite-chlorite schist, chlorite schist, feldspathic chlorite schist and jasperoidal chert. All of these lithologic types are found within the underlying Kutcho assemblage. Foliation within the schistose clasts is parallel to, and continuous with, the matrix schistosity. The conglomerate is typically unstratified and poorly size-sorted, but a crude stratification is evident in some exposures, and locally the conglomerate is intercalated with thin to thick beds of schisty metasandstone, granule to small-pebble conglomerate, and sericite-quartz phyllite. Limestone is not common in the conglomerate unit west of Kutcho Creek, but in exposures east of the creek it occurs as occasional clasts, and as rare narrow lenses up to several tens of metres long. In a set of exposures northeast of the Kutcho Creek VMS deposit, conglomerate containing limestone clasts becomes common in the central part of the unit, and passes up section into conglomerate with a very limy matrix, which includes abundant clasts and rafts of limestone up to 1 m across (Schiarizza, 2011a).

SINWA FORMATION

The Sinwa Formation forms a continuous belt, between the conglomerate unit and the Inklin Formation, from the eastern part of the map area to the anticlinal fold closure southwest of peak 1787 (Figure 3). It is at least several tens of metres thick throughout most of the area east of Kutcho Creek, thins to only a few metres in some areas west of the creek, but forms a wide belt of exposures in the hinge zone of the anticline. The limestone pinches out on the south limb of the anticline, but forms a substantial belt of exposures 1 km farther south, in the core of another anticline, and is also exposed over a broad area in the hinge zone of a major syncline east of Kutcho Creek (Figure 3). In these latter areas, the conglomerate unit is absent, as is the northern division of the Kutcho assemblage, and the Sinwa Formation rests directly above rocks within the central division of the Kutcho assemblage. The coincidence of extensive limestone exposures with fold closures implies a significant component of structural thickening, but the exact mechanism by which this is achieved is not known.

The Sinwa Formation consists almost entirely of grey and white, weakly to moderately foliated, recrystallized limestone that typically forms monotonous exposures that weather to a uniform light grey to medium brownish grey colour. Medium to thick beds are displayed in a few exposures southwest of peak 1787 (Figure 13), and intervals of dark grey, fine-grained limestone and slaty limestone occur locally. The contact with the underlying conglomerate unit in the area east of Kutcho Creek is gradational (Schiarizza, 2011a), but the same contact west of the creek is sharp, as are basal contacts farther south, where the Sinwa Formation rests above the central division of the Kutcho assemblage.

Panteleyev and Pearson (1977b) and Monger (1977) report that fossils collected from the Sinwa Formation in the Kutcho map area include schleractinian corals, indicating a Middle Triassic or younger age. Macrofossils were not observed anywhere in the unit during the current study, and samples collected east of Kutcho Creek in 2010 did not yield conodonts. Additional samples, collected from Sinwa exposures west of the creek during the 2011 field season, are being processed for conodonts.

INKLIN FORMATION

The main exposures of the Inklin Formation form a wide belt that comprises the uppermost element of the King Salmon allochthon. These rocks are bounded to the north by the Nahlin fault, across which they are structurally overlain by rocks of the Cache Creek complex. This belt of Inklin rocks is folded through a series of west plunging, south-verging folds that are outlined by the basal contact of the formation, which rests above the Sinwa Formation in the northeast, but directly above the Kutcho assemblage to the southwest, where the Sinwa and conglomerate unit are missing. A narrow belt of Inklin rocks also occurs at lower structural levels within the King Salmon allochthon. These rocks rest

Figure 13. Bedded limestone, Sinwa Formation, 1500 m southwest of peak 1787.

stratigraphically (?) above the Cache Creek complex, and are structurally overlain by the basal part of the Kutcho assemblage across an inferred north dipping thrust fault. This belt of Inklin rocks forms the base of the King Salmon allochthon in the eastern part of the map area, where the Cache Creek complex has pinched out.

The Inklin Formation consists mainly of slate, metasiltstone and metasandstone. These rocks, together with minor amounts of limestone and conglomerate, are intercalated throughout the formation, but slate/metasiltstone intervals seem to be more common in the lower part, whereas metasandstone-dominated intervals become prevalent at higher stratigraphic levels and are, overall, the most abundant rock type present. Dark to medium grey slate typically contains small porphyroblasts of rusty Fe-Mg carbonate, and commonly displays laminations and thin interbeds of metasiltstone and slaty metasiltstone. Fine to coarse-grained metasandstone occurs as thin to thick, massive to graded beds intercalated with thinner interbeds of slate and metasiltstone (Figure 14). The metasandstones are typically schistose wackes containing plagioclase, quartz, and fine grained altered lithic clastic grains. One unusual sandstone unit, encountered in the southwestern part of the map area, in the upper part of the Inklin slice that overlies the Cache Creek complex, contains detrital grains of mainly plagioclase and hornblende.

Limestone is not common within the Inklin Formation, but occurs as narrow layers and lenses, typically only 1-2 m thick, that occur within both slate/siltstone and sandstone-dominated portions of the formation. Locally, limestone lenses occur within intervals of brown weathered calcareous sandstone. At one location, within the Inklin slice that overlies the Cache Creek complex, about 5 km west of Kutcho Creek, an interval of thin-bedded slate, siltstone and calcareous sandstone that includes thin limestone lenses also contains scattered calcareous concretions, up to 20 cm in diameter.

Conglomerate occurs locally within the main belt of Inklin rocks, but was not observed in the slice that overlies the Cache Creek complex. The conglomerate is mainly within metasandstone-dominated sections, but also occurs within slate/siltstone successions, and is commonly associated with units of limestone and/or calcareous metasandstone. It forms single or multiple thin to thick beds and may be the dominant rock type in sections up to several tens of metres thick. Conglomerate beds typically comprise a schistose metasandstone matrix that contains flattened pebbles of mainly felsic volcanic rock, accompanied by clasts of dark grey phyllite, laminated siltstone and limestone. At one locality, 1.5 km northeast of peak 2045, conglomerate occurs as a succession of several thick beds, each of which grades up into an interval of thin-bedded metasiltstone and metasandstone, capped by a layer, up to 40 cm thick, of laminated sandy limestone (Figure 15). The pebbles and cobbles in these conglomerate units consist of limestone and a variety of rounded felsic lithic clasts that include quartz-feldspar-phyric rhyolite, aphyric felsite, fine to medium-grained tonalite , sericite-quartz phyllite, and coarse quartz-eye volcaniclastic schist. These felsic clasts, and those in other conglomerate units, resemble rocks found in the underlying Kutcho assemblage.

The base of the Inklin Formation south and southeast of peak 1787, and on the opposite limb of the anticline north of peak 2045, comprises several tens of metres of grey-green gritty feldspathic sandstone and feldspathic sericite-chlorite schist that are very similar to the schists that characterize unit KNf of the Kutcho assemblage (Figure 3). These rocks have prompted some workers to infer that Kutcho-like volcanic activity continued, or was re-established, after deposition of the Sinwa Formation (Panteleyev, 1978; Troop, 1981; Alldrick and McLennan, 2010), and thus question the existence of a significant unconformity (Panteleyev, 1978) or the validity of the Sinwa correlation for the limestone unit (Alldrick and McLennan, 2010). The schists in question are clastic rocks that contain, in addition to abundant plagioclase, detrital quartz and fine grained altered lithic grains, not unlike other sandstone units within the Inklin Formation.

Figure 14. Thin to medium-bedded metasandstone, Inklin Formation, 1 km northwest of peak 2045.

Figure 15. Conglomerate unit within the Inklin Formation, 1.5 km northeast of peak 2045.

They are interbedded with narrow slate/siltstone intervals, and the unit south of peak 1787 passes along strike, to the west, into schistose conglomerate that contains pebbles of felsic volcanic rock and tonalite, as well as granules of quartz and feldspar. The feldspathic schists are here interpreted as clastic deposits derived from erosion of the older Kutcho assemblage, an interpretation that does not require a younger, post-Sinwa volcanic source.

Units south of the King Salmon fault

TAKWAHONI FORMATION

Rocks assigned to the Takwahoni Formation, following Gabrielse (1998), occur in the footwall of the King Salmon fault in the southwest corner of the Kutcho map area. The rocks in this area consist mainly of rusty weathered, dark to medium grey, moderately cleaved slaty siltstone. Medium grey to greenish grey, fine to coarse-grained sandstone occurs locally, and predominates in some sections up to several tens of metres thick. The sandstone commonly occurs as poorly defined medium to thick beds, but locally forms distinct thin to medium beds separated by thin interbeds of dark grey siltstone. Coarse-grained units locally contain scattered granules and small pebbles, 2-10 mm in size. The sandstones are mainly weakly foliated wackes, containing feldspar and volcanic-lithic grains that are heavily altered with sericite and calcite.

The Takwahoni Formation is not dated within the Kutcho map area, but according to Gabrielse (1998) these rocks are part of a greywacke-shale division that has yielded Lower Jurassic (Pliensbachian) fossils 20 km to the west (Tipper, 1978).

BOWSER LAKE GROUP

Clastic sedimentary rocks assigned to the Bowser Lake Group occur in the footwall of the King Salmon fault in the south-central and southeastern parts of the Kutcho map area. These rocks are separated from the Takwahoni Formation to the west by the inferred trace of a northerly dipping thrust fault, referred to as the Kehlechoa fault by Gabrielse (1998), that either merges with or is truncated by the King Salmon fault (Figure 1). East of Kutcho Creek, the Bowser Lake Group is represented mainly by chert-rich pebble conglomerate and chert-quartz sandstone, as described by Schiarizza (2011a). The few exposures examined west of the creek consist mainly of brown-weathered, bluish green, well-indurated coarse to medium-grained sandstone that contains plagioclase, clinopyroxene and volcanic-lithic grains. The sandstone commonly forms massive units, several metres to more than 10 m thick, that are interspersed with lesser amounts of medium to dark grey laminated siltstone that forms intervals up to 2 m thick. Locally, sandstone forms distinct thin to thick beds intercalated with laminated siltstone.

The Bowser Lake Group ranges from Middle Jurassic to Early Cretaceous in age (Evenchick *et al.*, 2007). The rocks are not dated within the current study area, but probably represent part of the lower, Middle Jurassic, portion of the group based on data outside the map area: The same panel of rocks has yielded Early Bajocian fossils about 25 km to the west, and is cut by a late Middle Jurassic pluton 15 km southeast of the map area (Gabrielse, 1998).

Quesnel terrane northeast of the Kutcho fault

Granitic rocks that crop out on the northeast side of the Kutcho fault are part of an unnamed and undated pluton, of suspected Early Jurassic age, within Quesnel terrane (Gabrielse, 1998). Those parts of the pluton examined by Schiarizza (2011a) include hornblende diorite to quartz diorite, hornblende-biotite tonalite and hornblende granodiorite.

Post-metamorphic intrusions

Small, intermediate to mafic, post-metamorphic intrusions are scattered sparsely through much of the map area, and are very common in the southern part of the King Salmon allochthon, for 6 to 8 km on either side of upper Kutcho Creek, where they cut rocks of the Kutcho assemblage, the Cache Creek complex and the Inklin Formation. The intrusions in this area are mainly porphyritic sills and dikes, ranging from a few metres to a few tens of metres wide, comprising phenocrysts of feldspar, hornblende and locally pyroxene, within a grey to brown, massive to platy, aphanitic to very fine grained feldspathic groundmass. Two small plugs that are mapped within this heavily diked area are probably part of the same suite. One comprises medium grained, equigranular diorite that cuts unit KS2 on peak 2075, 2.5 km east of the head of Kutcho Creek (Schiarizza, 2011a). The other plug consists of medium grained hornblende diorite, pyroxene hornblende porphyry and biotite hornblende porphyry, and cuts units KS2 and KS3 about 4.5 km west of upper Kutcho Creek (Figures 2 and 3). The post-metamorphic dikes, sills and stocks adjacent to upper Kutcho Creek are assigned an Eocene age, on the basis of a radiometric date obtained from a dike that crops out 1 km northeast of peak 2075. Stevens *et al.* (1982) report that a hornblende separate, containing about 10% biotite, from this dike yielded a K/Ar date of 55.4 ±3.0 Ma.

A dike of dark grey, brown-weathered, biotite-phyric lamprophyre cuts mafic schists of unit KS3 on a ridge crest about 2.7 km southeast of peak 2045. The dike is about 4 m wide and dips steeply to the north, roughly parallel with the schistosity of the enclosing schists. The lamprophyre contains scattered rounded xenoliths, <1-6 cm in size, of mainly diorite, gabbro and hornblendite.

A brownish grey hornblende porphyry dike, about 1 m wide, cuts feldspathic schists of unit KNf near the core of the major anticline, about 1.7 km southwest of peak 1787. The dike dips steeply to the southwest for part of its length, but when traced to the north displays an abrupt

change in orientation, attaining a steep easterly dip. It comprises a very fine-grained groundmass that contains acicular hornblende phenocrysts up to 8 mm long, small magnetite grains, and quartz-filled vesicles. It is suspected that this dike is younger than the Eocene dikes described previously, in part because the hornblende phenocrysts are distinctly less altered.

Dikes of fine grained, equigranular hornblende biotite diorite, typically less than 1 m wide, are fairly common within the Takwahoni Formation in the southwest corner of the map area, and may correlate with the Eocene dikes that are common in the King Salmon allochthon to the northeast. At one locality, the Takwahoni Formation also hosts a creamy white weathered felsic dike, comprising phenocrysts of hornblende, plagioclase and quartz, 1-3 mm in size, within a beige aphanitic groundmass.

STRUCTURE

Structure of the King Salmon allochthon

The King Salmon allochthon comprises predominantly north dipping map units that are deformed by south-verging folds and north dipping thrust faults. The folds formed at the same time as the penetrative schistosity or cleavage that is displayed by all units within the allochthon. This foliation is defined by the preferred orientation of greenschist facies metamorphic mineral assemblages and, in coarse-grained units, variably flattened primary crystal and lithic fragments. The bounding King Salmon and Nahlin thrust faults, as well as the inferred north dipping thrust faults within the allochthon, probably formed during the same deformational event, but in detail may be slightly younger. Constraints beyond the current map area suggest that this deformation occurred in early Middle Jurassic time (Tipper, 1978; Mihalynuk *et al.*, 1992, 2004).

The Kutcho assemblage and overlying sedimentary rocks of the Whitehorse trough underlie most of the allochthon, and comprise a predominantly north dipping and north-facing succession that is deformed by a series of west-plunging, south-verging folds that are well defined by the mapped contact between the two assemblages (Figures 3 and 4). The structural base of the Kutcho assemblage is not well exposed, but is inferred to be a north dipping thrust fault because north dipping and north-facing rocks of unit KS1 rest structurally above younger north dipping and north-facing rocks of the Inklin Formation. The narrow belt of Inklin rocks structurally beneath the Kutcho assemblage lies above units CC2 and CC3 of the Cache Creek complex through most of the area, but forms the immediate hangingwall to the King Salmon fault in the east, where Cache Creek rocks are absent. There is no indication of faulting in the few places where the Inklin/Cache Creek contact is well constrained, suggesting that the Inklin is in depositional contact with the Cache Creek. A post-Inklin fault is required at lower structural levels within the Cache Creek complex, where a thin sliver of Inklin rocks occurs between units CC1 and CC2 near the western edge of the map area. This structure in inferred to be a north dipping thrust fault, related to other Jurassic thrust faults of the King Salmon allochthon, at the structural base of unit CC2.

The penetrative schistosity that characterises the Jurassic and older rocks of the King Salmon allochthon dips steeply north and is axial planar to mesoscopic folds of bedding that are common within the Inklin Formation (Figure 16), and were observed locally within bedded units of the Kutcho assemblage. The axes of these mesoscopic folds, together with associated bedding/cleavage intersection lineations, plunge gently to the west-northwest or, less commonly, to the east-southeast. This folding (and the associated south-verging macroscopic folds) is reflected in a stereoplot of poles to bedding measured in the Kutcho assemblage and overlying Whitehorse trough sedimentary rocks (Figure 17), which define a great circle girdle, with a pole (280/06) that plots within the cluster of fold axes and intersection lineations. A younger generation of co-axial mesoscopic folds occurs rarely in the area east of Kutcho Creek (Schiarizza, 2011a), but these structures were not observed west of the creek. They comprise open folds of the main schistosity, with axes that plunge gently to the west-northwest, and an associated axial planar crenulation cleavage that dips 30 to 40 degrees to the north. The youngest mesoscopic structures observed in the map area

Figure 16. Synmetamorphic fold within the Inklin Formation, 1500 m east of peak 2045.

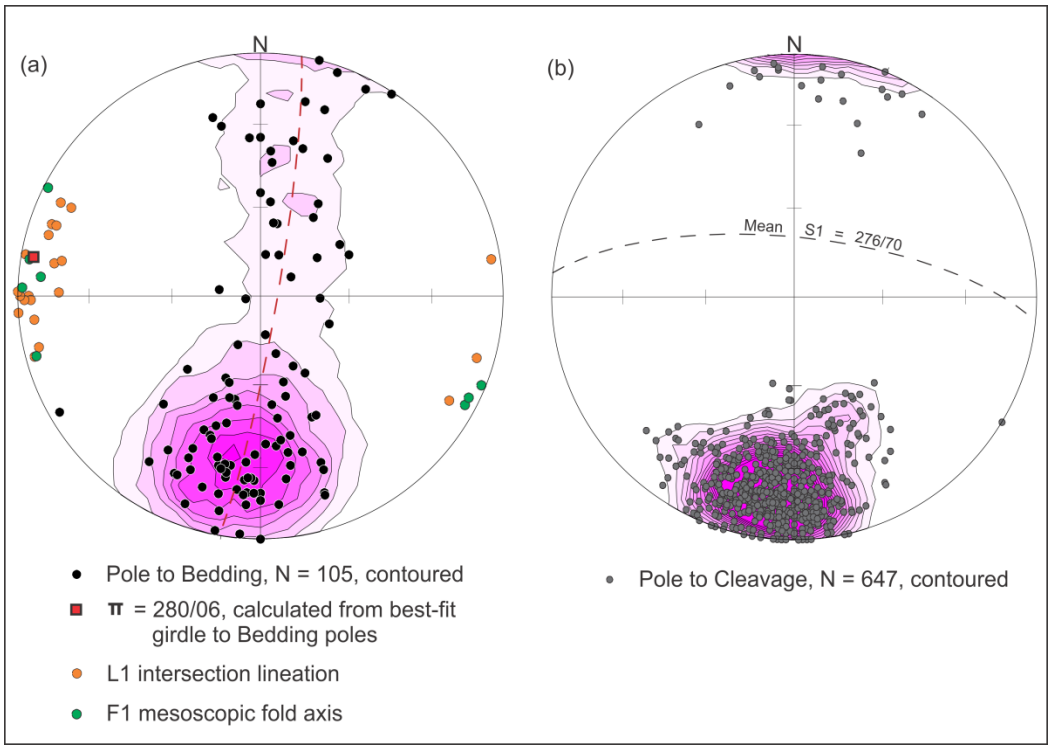

Figure 17. Lower hemisphere stereoplots of structural data from the Kutcho assemblage and overlying Whitehorse trough.

comprise post-metamorphic folds and kinks that warp the main schistosity across axes that plunge steeply to the northwest, north or northeast. Structures of this age have little apparent effect on the macroscopic geometry of the allochthon.

POST-METAMORPHIC FAULTS

Systems of west-trending faults occur along and near the contact between the central and northern divisions of the Kutcho assemblage south of the Kutcho Creek VMS deposit, and faults with a similar trend cut the south limb of the syncline north of peak 2075 (Figure 3). Stratigraphic separations across these faults suggests mainly north-side-down displacement. A small west-striking fault that is exposed in limestone cliffs northeast of peak 2045 has demonstrable north-side-down displacement where it drops a small lens of Inklin rocks into the Sinwa Formation (Figure 18)

Northwest-striking faults are inferred in several places within the Kutcho map area, where they mark offsets of the predominantly east trending lithologic contacts and structures that formed during synmetamorphic deformation. Northeast-striking faults are likewise inferred in a couple areas, but are less common. These late structures display both dextral and sinistral apparent offsets, but the actual sense of movement was not established.

Pre-Jurassic deformation

Hints of pre-Jurassic deformation within the Cache Creek complex and Kutcho assemblage are provided by

Figure 18. View to the west at a steep north-side-down fault that juxtaposes dark grey slates of the Inklin Formation against limestone of the Sinwa Formation.

relationships at the base of Whitehorse trough. The narrow belt of Inklin rocks in the southern part of the King Salmon allochthon overlies the Cache Creek complex across what is suspected, but not proven, to be a stratigraphic contact. This contact truncates the fault that juxtaposes units CC2 and CC3, suggesting that structures relating to development of the melange belt are older than the Inklin Formation. Structures that accommodate the marked lenticularity of lithologic units within unit CC1 are likewise suspected to have an older history, but have been overprinted by significant Jurassic strain. Pre-Inklin structures have not been identified within the Kutcho assemblage, but the systematic southward truncation of the northern and central divisions beneath the Whitehorse

trough suggests an older deformation that involved at least tilting of the succession.

Regional Faults

KING SALMON FAULT

The King Salmon fault is an important regional structure that forms the structural base of the King Salmon allochthon. It has been traced about 300 km west-northwest from the current map area, where it apparently merges with the long-lived, northwest trending Llewellyn fault zone (Mihalynuk, 1999). Where exposed, the King Salmon fault dips at low to moderate angles to the north, and displays deformation fabrics and map relationships consistent with south-directed thrust motion (Souther, 1971; Thorstad and Gabrielse, 1986; Gabrielse, 1998).

The King Salmon thrust fault crosses the southern part of the Kutcho map area, where it juxtaposes either the Cache Creek complex or the Inklin Formation above footwall rocks that include the Bowser Lake Group in the east and the Takwahoni Formation in the west. The trace of the fault is tightly constrained along Josh Creek, in the southeast corner of the map area, where it places Inklin Formation above the Bowser Lake Group. Here, south-directed thrusting is supported by mesoscopic structures near the contact, which include south-verging folds that deform the main synmetamorphic cleavage in hangingwall Inklin rocks, and north-dipping faults within footwall Bowser Lake Group (Schiarizza, 2011a). The trace of the King Salmon fault is also fairly well constrained in several places along the stretch that extends from peak 1667 to peak 1705 (Figure 2), but no structures or fabrics related to the fault were observed along this segment.

East of peak 1705, a northerly dipping thrust fault that places the Takwahoni Formation above the Bowser Lake Group is truncated by, or merges with, the King Salmon Fault (Figure 2). This structure, referred to as the Kehlechoa fault, has been traced about 30 km to the west (Figure 1; Gabrielse, 1998). The trace of the Kehlechoa fault is not well constrained in the current map area, but it marks a change in mesoscopic rock fabric, as rocks of the Takwahoni Formation are cleaved while those of the Bowser Lake Group are not (except in the immediate footwall of the King Salmon fault). Tipper (1978) noted a corresponding change in map-scale structural style in equivalent rocks to the west, where the Lower Jurassic rocks are involved in complex southwest-directed imbricate thrusting, whereas Middle Bajocian rocks display a less complex structural style involving mainly block faulting.

NAHLIN FAULT

The Nahlin fault has been traced from the current map area more than 350 km west-northwest to the Atlin Lake area (Souther, 1971; Mihalynuk *et al.*, 1992; Gabrielse, 1998). It forms the northeast boundary of the King Salmon allochthon, and juxtaposes the Inklin Formation, on the southwest side of the fault, with rocks of the Cache Creek complex to the northeast. The fault is generally interpreted as a northeast dipping thrust, although some segments dip steeply and may have a component of dextral strike-slip movement (Gabrielse, 1998).

The trace of the Nahlin fault is fairly well constrained on both the east and west sides of Kutcho Creek, but it was not studied in enough detail to establish its orientation or kinematic history. As noted by Schiarizza (2011a), the fault trace east of the creek is commonly marked by lenses of rock that may have been derived from the Sinwa Formation and Kutcho assemblage, consistent with the Nahlin fault being a thrust fault that ramped through these units into the overlying Inklin Formation.

KUTCHO FAULT

The Kutcho fault transects the northeast corner of the Kutcho map area, where it truncates the King Salmon allochthon and structurally overlying Cache Creek complex (unit CC5), and juxtaposes these map units against granitic rocks of Quesnel terrane. This structure is discussed by Schiarizza (2011a).

MINERAL OCCURRENCES

Mineral occurrences east of Kutcho Creek, including the important Kutcho Creek volcanogenic massive sulphide deposit, are described by Schiarizza (2011a). Occurrences west of the creek are described in this report. These include occurrences that are prospective for volcanogenic massive sulphide deposits, as well as younger vein deposits.

Kutcho 1

The Kutcho 1 occurrence is hosted by the central division of the Kutcho assemblage just to the west of Kutcho Creek, a little more than 4 km south of the airstrip. Mineralization comprises lenses of semimassive to massive sulphide within a pyritic cherty exhalite unit, which is intermittently exposed in an area measuring about 80 by 40 m (Belik, 1996).

Mineralization in the vicinity of the Kutcho 1 occurrence was encountered in a diamond drill hole cored by Noranda Exploration Company Limited in 1977. Chloritic schist intersected in hole NK-3 included a 3 m interval containing 2-5% pyrite with disseminated chalcopyrite, which contained 0.11% Cu (MacArthur, 1978). The area was re-staked and mapped by G. Belik in 1994, and optioned to Atna Resources Limited in 1996. Belik mapped the pyritic cherty exhalite unit in 1994, and during follow-up work for Atna Resources in 1996 excavated a pit where an angular float block of massive to semimassive pyrite-chalcopyrite was discovered within the unit. This pit exposed bedrock of highly siliceous rock with about 20% pyrite that locally displays primary

sulphide layering. A sample of this bedrock material yielded 3282 ppm Cu, 1110 ppm Pb, 1097 ppm Zn, 7.0 ppm Ag and 7 ppb Au (Belik, 1996). Several mineralized float boulders were encountered during excavation of the pit, including a 5 kg subangular block of well banded, siliceous, semimassive to massive sulphide, which contained 10 592 ppm Cu, 2234 ppm Pb, 1816 ppm Zn, 17.6 ppm Ag and 30 ppb Au (Belik, 1996). An exploration program by Atna Resources Limited in 1997 included 9 diamond drill holes, several of which were cored in the area of the Kutcho 1 showing (Holbek *et al.*, 1998). However, none of these holes were filed for assessment.

The pit excavated within the pyritic cherty exhalite unit was located during the 2011 mapping program, but it is partially caved and bedrock is no longer exposed. The cherty exhalite exposed near the pit is a light to medium grey, very siliceous rock with several per cent disseminated pyrite, and local lenses and patches of heavily disseminated to semimassive pyrite. Rocks to the east and northeast of the exhalite unit are mainly epidote-chlorite schists derived from mafic volcanic rocks. Rocks to the south and southeast include coherent units of quartz-plagioclase-phyric metarhyolite intercalated with pyritic siliceous exhalite similar to that near the pit, and two narrow units of mottled red/grey chert that are probably also exhalites (iron chert units of Belik, 1996). These iron chert units (Figure 19) commonly have 1-2% disseminated pyrite, and local narrow lenses of more heavily disseminated pyrite. A sample collected from one of the iron chert units, located 80 m southeast of the pit, contains 652.5 ppm Cu, 33.3 ppm Pb, 669 ppm Zn and 1.2 ppm Ag (Table 1, sample 11PSC-438).

Kutcho 2 (MINFILE 104I 072)

The Kutcho 2 showing occurs within the northern division of the Kutcho assemblage, 1800 m west of Kutcho Creek and about 3 km southwest of the airstrip. It comprises several narrow lenses of heavily disseminated to semimassive sulphides, mainly pyrite, pyrrhotite and chalcopyrite, which occur within zones of quartz-sericite-chlorite-altered rock that are more or less concordant with the schistosity in the surrounding coarse quartz-eye schists. These schists are part of a small lens assigned to unit KNq, which occurs within a belt of mainly finer grained plagioclase-rich schists assigned to unit KNf (Figure 3).

The mineralization at the Kutcho 2 occurrence was located by geologists working for Noranda Exploration Company Limited in the mid to late 1970s (Troop, 1981). It was later covered by claims staked by Atna Resources Limited and the mineralization, which is exposed in several small pits that were excavated by Noranda, was described and sampled by Belik (1996). A south-plunging diamond-drill hole, which was collared in conglomerate of the Whitehorse trough to the north of the showings, tested this mineralized interval at depth, but encountered only weakly altered felsic volcaniclastic rocks (Holbek *et al.*, 1998, drill hole KU97-01).

Mineralization exposed in one of the old pits at the Kutcho 2 occurrence comprises a lens, 6-11 cm wide that consists of limonite altered and silicified rock with heavily disseminated to massive sulphides (Figure 20). A grab sample of this material returned >10 000 ppm Cu, 103.1 ppm Pb, 253 ppm Zn, 45 ppm Ag and 4549.2 ppb Au (Table 1, sample 11PSC-480). A different pit, about 30 m to the west, exposes a couple metres of variably silicified rock with patches of chlorite±sericite and veins of Fe-Mg carbonate. Sulphides occur mainly in two zones, the largest about 30 cm wide and comprising intermittent heavy disseminations with patches of semimassive sulphides. A grab sample of this material returned >10 000 ppm Cu, 78.8 ppm Pb, 159 ppm Zn, 11.4 ppm Ag and 8228.2 ppb Au (Table 1, sample 11PSC-481).

Figure 19. Iron chert, central division of the Kutcho assemblage, Kutcho 1 showing.

Figure 20. Lens of massive to heavily disseminated sulphides, Kutcho 2 occurrence.

Table 1. Selected elements from analyses of mineralized and altered rock samples collected during the 2011 field season.

				Mo	Cu	Pb	Zn	Ag	As	Au	Sb	Ba	W	Hg
				PPM	PPM	PPM	PPM	PPM	PPM	PPB	PPM	PPM	PPM	PPM
				0.1	0.1	0.1	1	0.1	0.5	0.5	0.1	1	0.1	0.01
Sample	Easting	Northing	Rock Type											
11PSC-46	524864	6446260	py-ser-qtz schist, unit KS2	6.8	20.8	2.3	21	<0.1	19.7	1.5	0.2	21	<0.1	0.02
11PSC-53	525669	6446669	py in Eocene hb-bio porphyry	2.6	93.7	4.2	31	0.1	1.5	2.1	0.2	91	5.4	<0.01
11PSC-56	525504	6446638	py in Eocene hb porphyry	3.2	71.8	7	49	0.2	4	3.5	0.2	73	0.4	<0.01
11PSC-64	534771	6451708	pyritic chert, unit KNq	3	13.9	5.8	11	0.1	3.8	3.2	0.5	18	<0.1	0.01
11PSC-79	524663	6447795	py-ser-qtz schist, unit KS3	0.2	38.4	1.2	39	<0.1	6.7	1.6	<0.1	6	<0.1	<0.01
11PSC-81	524594	6448059	py-qtz alt'n, unit KS3	0.2	4.9	1.2	35	<0.1	<0.5	3.6	<0.1	2	<0.1	<0.01
11PSC-140	524657	6450389	Ridgecrest; qtz vn; py, ch, ga, mal, az	1.1	>10000.0	7652.8	1239	>100.0	829.4	96.3	>2000.0	11	<0.1	1.55
11PSC-161	526455	6451070	py in feldspathic sst; Inklin Fm	0.4	17.4	4.6	97	0.5	7.2	0.6	1.9	36	0.1	<0.01
11PSC-240	522260	6445979	diss py in qtz-ep alt'n; unit KS2	1.5	74.5	27	76	2.2	2.7	0.7	13.1	8	<0.1	0.01
11PSC-265	522719	6447069	qtz-ser-py alt'n; unit KS3	0.5	26.1	1.6	41	<0.1	17.1	<0.5	0.3	11	<0.1	0.01
11PSC-314	515514	6448828	listw anite; unit CC2	<0.1	10.4	1.7	12	0.2	1.5	0.7	1.7	5	<0.1	0.01
11PSC-386	531923	6448398	Kris; qtz-ser schist; py, cpy, mal	0.1	380.3	3	80	<0.1	38.6	1.4	0.8	12	<0.1	0.02
11PSC-410	521721	6454512	Matt; pitted siliceous phyllite; mal	33.3	4468.9	29.1	71	1.3	45	1.4	1.7	2335	<0.1	0.08
11PSC-431	529289	6449215	Kutcho 1; iron chert; py	2.6	14.3	1.9	5	0.3	1.8	15.6	0.3	36	0.2	0.21
11PSC-438	529344	6449274	Kutcho 1; iron chert; py	3.7	652.5	33.3	669	1.2	5.3	1.2	0.9	67	<0.1	0.46
11PSC-440	529307	6449337	Kutcho 1; siliceous exhalite; py	6	25	3.9	17	0.1	9.7	2.2	0.2	41	<0.1	<0.01
11PSC-450	526646	6447718	qtz-ser-py alt'n; unit KS3	0.2	41.1	1.9	100	0.1	7.5	0.8	0.4	26	<0.1	0.01
11PSC-467	522321	6450317	Blueridge; qtz vn; py, ch, ga, mal, az	0.4	6222.8	>10000.0	806	>100.0	612	128.7	>2000.0	23	<0.1	0.96
11PSC-480	527964	6451029	Kutcho 2; sulphide lens	1.8	>10000.0	103.1	253	45	3	4549.2	13.6	47	0.2	0.46
11PSC-481	527925	6451029	Kutcho 2; sulphide lens	0.4	>10000.0	78.8	159	11.4	5.6	8228.2	10.9	14	0.2	0.34

Samples analysed at ACME Analytical Laboratories Ltd. , Vancouver BC, by ICP-MS follow ing digestion of a 15 g sample split in hot Aqua Regia
Abbreviations: alt'n- alteration; az- azurite; bio- biotite; ch- chalcocite; cpy- chalcopyrite; ep- epidote; ga- galena; hb- hornblende; mal- malachite; py- pyrite; qtz- quartz; ser- sericite; vn- vein

Bow (MINFILE 104I 071)

The Bow occurrence, 4.5 km west of upper Kutcho Creek, refers to a mineralized quartz vein that was encountered in a diamond drill hole cored by Imperial Oil Ltd. in 1976. The hole, inclined 50º south, was collared in the Inklin Formation, but at 94 m entered a succession logged as quartz-sericite phyllite, quartzite and chlorite-calcite phyllite, which is probably part of the underlying Kutcho assemblage (unit KC). The mineralization is within this lower interval, and is described only as "minor bornite and chalcopyrite in one quartz vein" (Samoil, 1976).

Ridgecrest (MINFILE 104I 052)

The Ridgecrest showing comprises mineralized quartz veins that occur within the upper part of the Sinwa Formation, near the hinge of a major anticline, 5 km west of Kutcho Creek. The mineralized veins were mentioned by Gabrielse (1968), but there is no record indicating that there was any significant work performed on them. The Sinwa limestone in this area is host to numerous variably oriented quartz veins. Only a small percentage of the veins are mineralized, but small pods of mineralization are scattered over the entire 300 m strike length of good Sinwa exposures on the ridge top. Mineralization comprises small pockets of fine-grained sulphides, mainly pyrite, chalcocite and galena, accompanied by malachite and azurite. A grab sample from one of these mineralized pockets contains >10 000 ppm Cu, 7652.8 ppm Pb, 1239 ppm Zn, >100 ppm Ag, 96.3 ppb Au, 829.4 ppm As, >2000 ppm Sb and 1.55 ppm Hg (Table 1, sample 11PSC-140).

Blueridge

The Blueridge showing comprises small pockets of mineralization, identical to those at the Ridgecrest showing, scattered sparsely over several hundred metres on the ridge immediately to the west of the ridge containing the Ridgecrest mineralization. The intervening area probably hosts similar mineralization but bedrock is not exposed. Small pits and tunnels attest to past exploration of the Blueridge mineralization, but no work was ever filed for assessment purposes. Old claim posts in the vicinity of the workings are dated 1966. Although most of the mineralized veins are within the Sinwa Formation, as they are at the Ridgecrest occurrence, the largest pocket of mineralization observed is within quartz veins that are hosted by an isolated mass of coarse crystalline calcite that is apparently within the overlying Inklin Formation (indicated by the dot denoting the Blueridge showing on Figure 3). A grab sample of this mineralized material contains 6222.8 ppm Cu, >10 000 ppm Pb, 806 ppm Zn, >100 ppm Ag, 128.7 ppb Au, 612 ppm As, >2000 ppm Sb and 0.96 ppm Hg (Table 1, sample 11PSC-467).

Rubysih (MINFILE 104I 061)

The Rubysih showing is listed in MINFILE as quartz-siderite veins containing tetrahedrite and galena, hosted by the Inklin Formation about 1.5 km east of Peak 2045. This MINFILE listing is derived from a northern British Columbia mineral inventory assembled by Archer, Cathro and Associates. It states that the showing was examined in 1961 by the Cave Syndicate, and that a galena-rich sample yielded 30.3% Pb, 922 g/t Ag and

0.2 g/t Au, and another sample, containing abundant tetrahedrite, yielded 0.49% Cu, 0.7 g/t Ag and trace gold.

The Rubysih showing was not located during the present study, although veins of quartz and quartz-siderite are abundant in this area, and in many other parts of the Inklin Formation. However, none of those examined by the writer contain appreciable sulphide mineralization.

Matt

The Matt showing comprises a narrow mineralized layer that was encountered within Cache Creek metasedimentary rocks during the 2011 mapping program. It is located within unit CC4, 1 km north of the Nahlin fault and 7.8 km west of the Kutcho Creek airstrip (UTM grid coordinates 521721E, 6454512N). The mineralized unit is a layer of dark grey phyllite, 8 cm wide, which is stained with malachite and includes numerous small pits that may represent weathered-out sulphides. The host succession comprises siliceous phyllite, chert and cherty argillite, with local lenses of talc schist. A grab sample of malachite-stained rock from the pitted phyllite unit contains 4468.9 ppm Cu, 33.3 ppm Mo, 29.1 ppm Pb and 2335 ppm Ba (Table 1, sample 11PSC-410).

Eocene plug west of Kutcho Creek

The plug that cuts the KS2/KS3 contact 4.5 km west of upper Kutcho Creek commonly contains 1-3% pyrite, as disseminations, blebs and fracture coatings. A sample of pyritic rock from the central part of the plug yielded 93.7 ppm Cu, 2.6 ppm Mo and 5.4 ppm W (Table 1, sample 11PSC-53). A different sample, from near the west contact of the plug, contains 71.8 ppm Cu, 3.2 ppm Mo and 0.4 ppm W (Table 1, sample 11PSC-56).

JW (MINFILE 104I 066)

The Cache Creek complex in the hangingwall of the Nahlin fault, and particularly in the area between the Turnagain River and Kutcho Creek, hosts a large number of nephrite jade occurrences, including numerous producers and past-producers (Leaming, 1978; Simandl *et al.*, 2001). The JW occurrence, in the northwest corner of the Kutcho map area, is part of this domain. It comprises a number of nephrite occurrences, including boulders and in situ lenses, scattered over an area of several square kilometres within unit CC4, which here consists mainly of structurally interleaved serpentinite, metabasalt and limestone (Price, 1974). Twenty-five talus blocks from the JW occurrence were tested with a packsack drill in 1976, and found to comprise poor quality talcy nephrite (Price, 1976); no subsequent work has been recorded on the showing.

ACKNOWLEDGMENTS

I thank Matthew Newman for his capable assistance during fieldwork. I am grateful for the logistical and financial support provided by Kutcho Copper Corporation and the Geological Survey of Canada (Edges Project), which made the field program possible. I particularly thank Dani Alldrick for his efforts in arranging the partnership agreement with Kutcho Copper Corporation, and for sharing many ideas on the geology of the area; and Steve Irwin (Geological Survey of Canada) and JoAnne Nelson (British Columbia Geological Survey) who took care of many of the financial and logistical aspects of the Edges partnership.

REFERENCES

Alldrick, D. and McLennan, V.G. (2010): Geological assessment report on the Kutcho property, north central British Columbia; *BC Ministry of Energy, Mines and Petroleum Resources*, Assessment Report 31282, 45 pages.

Anderson, R.G. (1993): A Mesozoic stratigraphic and plutonic framework for northwestern Stikinia (Iskut River area), northwestern British Columbia, Canada; in Mesozoic Paleogeography of the Western United States-Part II, Dunne, G. and McDougall, K., Editors, *Society of Economic Paleontologists and Mineralogists*, Volume 71, pages 477-494.

Ash, C.H. (2001): Ophiolite related gold quartz veins in the North American Cordillera; *BC Ministry of Energy, Mines and Petroleum Resources*, Bulletin 108, 140 pages.

Barrett, T.J., Thompson, J.F.H. and Sherlock, R.L. (1996): Stratigraphic, lithogeochemical and tectonic setting of the Kutcho Creek massive sulphide deposit, northern British Columbia; *Exploration and Mining Geology*, Volume 5, pages 309-338.

Belik, G.D. (1996): Geological, geochemical and geophysical report on the Kutcho property (Kutcho 1-39 mineral claims), Liard Mining Division; *BC Ministry of Energy, Mines and Petroleum Resources*, Assessment Report 24866, 112 pages.

Bridge, D.A., Marr, J.M., Hashimoto, K., Obara, M. and Suzuki, R. (1986): Geology of the Kutcho Creek volcanogenic massive sulphide deposits, northern British Columbia; in Mineral Deposits of Northern Cordillera, Morin, J.A., Editor, *The Canadian Institute of Mining and Metallurgy*, Special Volume 37, pages 115-128.

Childe, F.C. and Thompson, J.F.H. (1997): Geological setting, U-Pb geochronology, and radiogenic isotopic characteristics of the Permo-Triassic Kutcho assemblage, north-central British Columbia; *Canadian Journal of Earth Sciences*, Volume 34, pages 1310-1324.

Cordey, F., Gordey, S.P. and Orchard, M.J. (1991): New biostratigraphic data for the northern Cache Creek terrane, Teslin map area, southern Yukon; in Current Research, Part E, *Geological Survey of Canada*, Paper 91-1E, pages 67-76.

English, J.M., Johannson, G.G., Johnston, S.T., Mihalynuk, M.G., Fowler, M. and Wight, K.L. (2005): Structure, stratigraphy and petroleum resource potential of the central Whitehorse Trough, northern Canadian Cordillera; *Bulletin of Canadian Petroleum Geology*, Volume 53, pages 130-153.

English, J.M., Mihalynuk, M.G. and Johnston, S.T. (2010): Geochemistry of the northern Cache Creek terrane and implications for accretionary processes in the Canadian

Cordillera; *Canadian Journal of Earth Sciences*, Volume 47, pages 13-34.

Evenchick, C.A. (1991): Geometry, evolution, and tectonic framework of the Skeena fold belt, north central British Columbia; *Tectonics*, Volume 10, pages 527-546.

Evenchick, C.A., McMechan, M.E., McNicoll, V.J. and Carr, S.D. (2007): A synthesis of the Jurassic-Cretaceous tectonic evolution of the central and southeastern Canadian Cordillera: Exploring links across the orogen; in Whence the mountains? Inquiries into the evolution of orogenic systems: A volume in honour of Raymond A. Price, Sears, J.W., Harms, T.A. and Evenchick, C.A., Editors, *The Geological Society of America*, Special Paper 433, pages 117-145.

Gabrielse, H. (1968): Operation Selwyn, 1967, Yukon Territory, District of Mackenzie, British Columbia; in Report of Activities, Part A, *Geological Survey of Canada*, Paper 68-1, Part A, pages 24-27.

Gabrielse, H. (1985): Major dextral transcurrent displacements along the northern Rocky Mountain Trench and related lineaments in north-central British Columbia; *Geological Society of America Bulletin*, Volume 96, pages 1-14.

Gabrielse, H. (1991): Late Paleozoic and Mesozoic terrane interactions in north-central British Columbia; *Canadian Journal of Earth Sciences*, Volume 28, pages 947-957.

Gabrielse, H. (1998): Geology of Cry Lake and Dease Lake map areas, north-central British Columbia; *Geological Survey of Canada*, Bulletin 504, 147 pages.

Gabrielse, H., Murphy, D.C. and Mortensen, J.K. (2006): Cretaceous and Cenozoic dextral orogen-parallel displacements, magmatism and paleogeography, north-central Canadian Cordillera; in Paleogeography of the North American Cordillera: evidence for and against large-scale displacements, Haggart, J.W., Enkin, R.J. and Monger, J.W.H., Editors, *Geological Association of Canada*, Special Paper 46, pages 255-276.

Holbek, P., Belik, G. and Wilson, R. (1998): Diamond drilling report on the Kutcho Creek project; *BC Ministry of Energy, Mines and Petroleum Resources*, Assessment Report 25465, 54 pages.

Johannson, G.G., Smith, P.L. and Gordey, S.P. (1997): Early Jurassic evolution of the northern Stikinian arc: evidence from the Laberge Group, northwestern British Columbia; *Canadian Journal of Earth Sciences*, Volume 234, pages 1030-1057.

Leaming, S.F. (1978): Jade in Canada; *Geological Survey of Canada*, Paper 78-19, 59 pages.

MacArthur, R. (1978): Report on diamond drilling, holes NK-1, NK-2, NK-3, Kutcho property, Liard Mining Division; *BC Ministry of Energy, Mines and Petroleum Resources*, Assessment Report 6686, Part 2, 14 pages.

Massey, N.W.D., MacIntyre, D.G., Desjardins, P.J. and Cooney, R.T. (2005): Digital geology map of British Columbia: whole province; *BC Ministry of Energy, Mines and Petroleum Resources*, GeoFile 2005-1.

Mihalynuk, M.G. (1999): Geology and mineral resources of the Tagish Lake area, northwestern British Columbia (NTS 104M/8, 9, 10E, 15; 104N/12W); *BC Ministry of Energy, Mines and Petroleum Resources*, Bulletin 105, 217 pages.

Mihalynuk, M.G., Smith, M.T., Gabites, J.E., Runkle, D. and Lefebure, D. (1992): Age of emplacement and basement character of the Cache Creek terrane as constrained by new isotopic and geochemical data; *Canadian Journal of Earth Sciences*, Volume 29, pages 2463-2477.

Mihalynuk, M.G., Erdmer, P., Ghent, E.D., Cordey, F., Archibald, D.A., Friedman, R.M. and Johannson, G.G. (2004): Coherent French Range blueschist: Subduction to exhumation in <2.5 Ma?; *Geological Society of America Bulletin*, Volume 116, pages 910-922.

Monger, J.W.H. (1975): Upper Paleozoic rocks of the Atlin Terrane, northwestern British Columbia and south-central Yukon; *Geological Survey of Canada*, Paper 74-47, 63 pages.

Monger, J.W.H. (1977): Upper Paleozoic rocks of northwestern British Columbia; in Report of Activities, Part A, *Geological Survey of Canada*, Paper 77-1A, pages 255-262.

Monger, J.W.H. and Thorstad, L. (1978): Lower Mesozoic stratigraphy, Cry Lake and Spatsizi map-areas, British Columbia; in Current Research, Part A, *Geological Survey of Canada*, Paper 78-1A, pages 21-24.

Monger, J.W.H., Richards, T.A. and Paterson, I.A. (1978): The hinterland belt of the Canadian Cordillera: new data from northern and central British Columbia; *Canadian Journal of Earth Sciences*, Volume 15, pages 823-830.

Nelson, J. and Friedman, R. (2004): Superimposed Quesnel (late Paleozoic-Jurassic) and Yukon-Tanana (Devonian-Mississippian) arc assemblages, Cassiar Mountains, northern British Columbia: field, U-Pb, and igneous petrochemical evidence; *Canadian Journal of Earth Sciences*, Volume 41, pages 1201-1235.

Pálfy, J. and Hart, C.J.R. (1995): Biostratigraphy of the Lower to Middle Jurassic Laberge Group, Whitehorse map area (105D), southern Yukon; in Yukon Exploration and Geology 1994, Exploration and Geological Services Division, Yukon; *Indian and Northern Affairs Canada*, pages 73-86.

Panteleyev, A. (1975): Jeff (104I-61): in Geology, Exploration and Mining in British Columbia 1974; *BC Ministry of Energy, Mines and Petroleum Resources*, pages 343-348.

Panteleyev, A. (1978): Kutcho Creek map-area (104I/1W); in Geological Fieldwork 1977, *BC Ministry of Energy, Mines and Petroleum Resources*, Paper 1978-1, page 43.

Panteleyev, A. and Pearson, D.E. (1977a): Kutcho Creek map-area (104I/1W); in Geology in British Columbia 1975; *BC Ministry of Energy, Mines and Petroleum Resources*, pages G87-G93.

Panteleyev, A. and Pearson, D.E. (1977b): Kutcho Creek map-area (104I/1W); in Geological Fieldwork 1976; *BC Ministry of Energy, Mines and Petroleum Resources*, Paper 1977-1, pages 74-76.

Pearson, D.E. and Panteleyev, A. (1976): Cupriferous iron sulphide deposits, Kutcho Creek map-area (104I/1W); in Geological Fieldwork 1975; *BC Ministry of Energy, Mines and Petroleum Resources*, Paper 1976-1, pages 86-92.

Price, B.J. (1974): Geological report on jade occurrences in the Provencher Lake area, Liard Mining District, British Columbia; *BC Ministry of Energy, Mines and Petroleum Resources*, Assessment Report 5100, 21 pages.

Price, B. (1976): Drilling report – JW claims, Liard Mining District; *BC Ministry of Energy, Mines and Petroleum Resources*, Assessment Report 6008, 7 pages.

Samoil, T.S. (1976): Drill report – Kutcho DDH #33, Bow 1-40 mineral claims, Liard Mining Division, 104I – 1W/2E;

BC Ministry of Energy, Mines and Petroleum Resources, Assessment Report 5911, 12 pages.

Schiarizza, P. (2011a): Geology of the Kutcho assemblage between Kutcho Creek and the Tucho River, northern British Columbia (NTS 104I/01); in Geological Fieldwork 2010, *BC Ministry of Energy, Mines and Petroleum Resources*, Paper 2011-1, pages 99-117.

Schiarizza, P. (2011b): Bedrock geology of the Andrea Creek area, part of NTS 104I/01; *BC Ministry of Energy and Mines*, Open File 2011-7, 1:25 000 scale.

Schiarizza, P. and Massey, N.W.D. (2010): Geochemistry of volcanic and plutonic rocks of the Sitlika assemblage, Takla Lake area, central British Columbia (NTS 093N/04, 05, 12, 13); in Geological Fieldwork 2009, *BC Ministry of Energy, Mines and Petroleum Resources*, Paper 2010-1, pages 55-67.

Shirmohammad, F., Smith, P.L., Anderson, R.G., Loxton, J. and McNicoll, V.J. (2007): Preliminary report on the Triassic and Jurassic stratigraphy and paleontology of the Sinwa and Takwahoni formations near Lisadele Lake, Tulsequah map area, northwestern British Columbia; *Geological Survey of Canada*, Current Research 2007-A9, 11 pages.

Simandl, G.J., Paradis, S. and Nelson, J.L. (2001): Jade and rhodonite deposits, British Columbia, Canada; in Proceedings of the 35th forum on the geology of industrial minerals-the Intermountain West Forum 1999, Bon, R.L., Riordan, R.F., Tripp, B.T. and Krukowski, S.T., Editors, *Utah Geological Survey*, Miscellaneous Publication 01-2, pages 163-171.

Souther, J.G. (1971): Geology and mineral deposits of Tulsequah map-area, British Columbia; *Geological Survey of Canada*, Memoir 362, 84 pages.

Stevens, R.D., Delabio, R.N. and Lachance, G.R. (1982): Age determinations and geological studies, K-Ar isotopic ages, report 15; *Geological Survey of Canada*, Paper 81-2, 56 pages.

Terry, J. (1977): Geology of the Nahlin ultramafic body, Atlin and Tulsequah map-areas, northwestern British Columbia; in Report of Activities, Part A, *Geological Survey of Canada*, Paper 77-1A, pages 263-266.

Thorstad, L.E. (1979): The lower Mesozoic King Salmon assemblage-Cry Lake map area, British Columbia; in Current Research, Part A, *Geological Survey of Canada*, Paper 79-1A, pages 21-24.

Thorstad, L.E. (1984): The Upper Triassic Kutcho Formation, Cassiar Mountains, north-central British Columbia; M.Sc. thesis, *The University of British Columbia*, 271 pages.

Thorstad, L.E. and Gabrielse, H. (1986): The Upper Triassic Kutcho Formation, Cassiar Mountains, north-central British Columbia; *Geological Survey of Canada*, Paper 86-16, 53 pages.

Tipper, H.W. (1978): Jurassic biostratigraphy, Cry Lake map-area, British Columbia; in Current Research, Part A, *Geological Survey of Canada*, Paper 78-1A, pages 25-27.

Tipper, H.W. and Richards, T.A. (1976): Jurassic stratigraphy and history of north-central British Columbia; *Geological Survey of Canada*, Bulletin 270, 73 pages.

Troop, D.G. (1981): Report on petrography and geology of the volcanic sequence, Kutcho 1-6 mineral claims, Kutcho property, Liard Mining Division; *BC Ministry of Energy, Mines and Petroleum Resources*, Assessment Report 9170, 18 pages.

Dease Lake Geoscience Project, Part II: Preliminary Report on the Mesozoic Magmatic History and Metallogeny of the Hotailuh Batholith and Surrounding Volcanic and Sedimentary Rocks

by B.I. van Straaten[1], J.M. Logan[1] and L.J. Diakow[1]

KEYWORDS: Geological mapping, Dease Lake, Stikine terrane, QUEST-Northwest, Hotailuh batholith, metallogeny, mineral occurrences

INTRODUCTION

This paper reports the preliminary results of a study on the magmatic history and metallogeny of the Hotailuh batholith, and is part of a larger British Columbia Geological Survey Dease Lake Geoscience Project (Logan *et al.*, 2012). The BCGS project is funded through Geoscience BCs QUEST-Northwest initiative, a program launched in early 2011 to stimulate mineral exploration in the northwestern part of the province along Highway 37. The Geoscience BC program includes two high resolution airborne magnetic surveys (Simpson, 2012), the collection of new regional stream sediment data and reanalysis of stream sediment samples (Jackaman, 2012), as well as new bedrock mapping described in this volume (Logan *et al.*; this paper; Moynihan and Logan; Iverson *et al.*). Collectively, these programs will provide detailed, high quality geoscience data that is intended to enhance metallic mineral exploration in an area of prospective geology adjacent to Highway 37, near Dease Lake, in northwestern British Columbia.

The study area is located within the Stikine terrane of the Canadian Cordillera, an aggregate of Late Paleozoic to Mesozoic magmatic arc successions accreted onto the North American margin during Middle Jurassic time (*e.g.* Gabrielse, 1991). The Stikine terrane comprises predominantly Triassic to Jurassic volcanic, sedimentary and plutonic rocks. This study focuses on the composite Hotailuh batholith (Figure 1), which has traditionally been subdivided into three plutonic suites of Late Triassic, Early Jurassic and Middle Jurassic age (Anderson, 1983; Gabrielse, 1998).

The main objectives of the Hotailuh project are to: 1) further refine the temporal magmatic and geochemical evolution of the batholith; 2) build a metallogenic framework that relates mineralization to magmatic events; and 3) identify prospective magmatic-hydrothermal systems in the area. Here, we present the field results, as well as results from assay analyses of mineralized samples. Results will be refined using techniques such as petrography (thin section study, feldspar staining), lithogeochemistry of least altered samples and geochronology. Furthermore, the results will be integrated with Geoscience BCs geophysical survey and updated regional stream sediment geochemistry databases as such information becomes available.

The composite Hotailuh batholith is exposed in a 2275 km^2 area southeast of Dease Lake. Nine weeks of 1:20 000-scale mapping by a two person team in summer 2011 included visits to 331 field stations and collection of 134 samples for laboratory study and analysis. The 2011 study focused on mapping within the Gnat Pass area and seven smaller areas to the east (Figure 1). The field areas were chosen for their mineral occurrences and suitability for understanding the internal geology and external contact relationships for various phases of the batholith. The study areas are covered by the 1:50 000 NTS map sheets 104I/04, 104I/03W, the southernmost part of 104I/05, and northernmost part of 104H/13. The Gnat Pass area is accessible by truck from Highway 37. Except for a section between Upper Gnat Lake and a point 7 km further south, the abandoned British Columbia railroad grade is driveable by truck up to the southern boundary of the study area. The remaining areas were mapped from fly camp locations accessed by helicopter chartered from Dease Lake.

The bedrock exposure is poor to moderate (5-10%) in the forested and brush-covered Gnat Pass area, except for exposures along road cuts, abandoned rail cuts and in old exploration trenches. The rock exposure improves dramatically above tree line, at approximately 1500 m. Exposure is best (10-30%) in the topographically higher areas of the Hotailuh batholith, with excellent exposure along alpine ridges, steep valley walls and cirques. However, glacial deposits and colluvium cover many alpine valleys, with only limited exposure in some creeks. Many of the exposures below, and especially above, treeline have an intense lichen cover. A notable exception is the lee side of alpine ridges where the thicker wind-accumulated winter snowpack appears to have inhibited lichen growth. These are prime locations for observing

[1] *British Columbia Geological Survey, Victoria, BC*

This publication is also available, free of charge, as colour digital files in Adobe Acrobat® PDF format from the BC Ministry of Energy and Mines website at http://www.empr.gov.bc.ca/Mining/Geoscience/PublicationsCatalogue/Fieldwork.

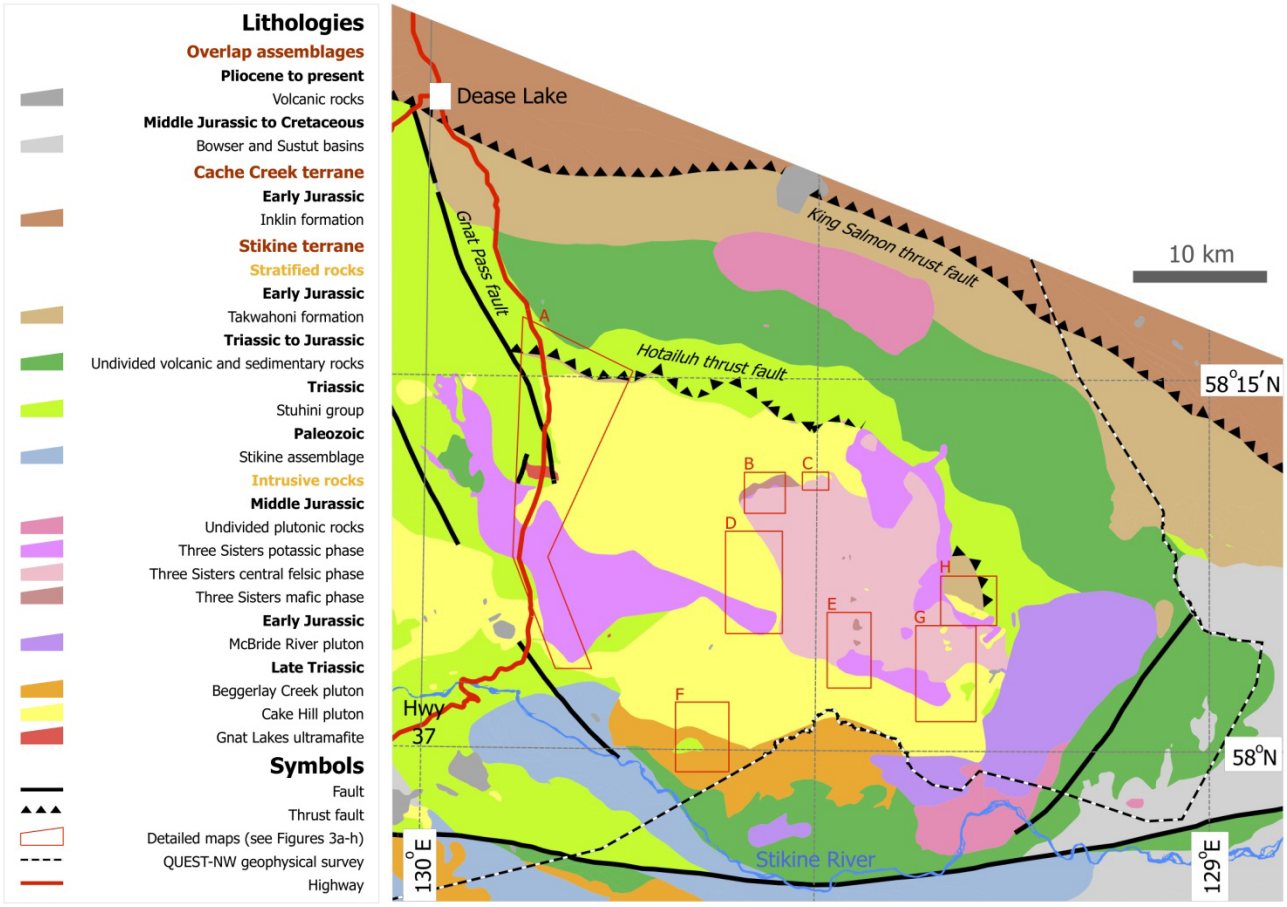

Figure 1. Regional geological setting of the Hotailuh batholith showing main lithologies and faults. Adapted from BC digital geological map compilation by Massey *et al.* (2005). The eight study areas are indicated, as well as the southern and eastern boundary of the QUEST-NW geophysical footprint.

complex crosscutting relationships among the intrusive phases of the batholith.

REGIONAL GEOLOGY

The study area is located near the north-northeastern margin of the Stikine terrane of the Canadian Cordillera (Figure 1), a volcanic island arc complex accreted onto the North American margin during Middle Jurassic time (Gabrielse, 1991; Nelson and Mihalynuk, 1993). The basement of the Stikine terrane is characterized by carbonate and volcanic rocks of the Devonian to Permian Stikine Assemblage, overlain by calcalkaline volcanic and associated sedimentary rocks of the Triassic Stuhini Group and Early to Middle Jurassic Hazelton Group (Marsden and Thorkelson, 1992; Currie and Parrish, 1997). The Stuhini Group volcanic rocks are predominantly mafic to intermediate in composition, whereas the Hazelton Group volcanic rocks are predominantly intermediate in composition with lesser felsic and mafic horizons (Marsden and Thorkelson, 1992).

Late Permian to Middle Triassic tholeiitic volcanism of the Kutcho assemblage formed a proto-arc on the inboard margin of the Stikine terrane, and was the subsequent locus for arc marginal clastic sedimentation in the Early Jurassic (English and Johnston, 2005; Schiarizza, 2011). Sedimentation within this forearc sedimentary basin (Whitehorse trough) comprises proximal conglomerates and more distal sandstones of the Takwahoni and Inklin formations, respectively. Closure of the Cache Creek ocean, subsequent collision with the Whitehorse trough and thrusting overtop the inboard margin of Stikinia occurred in the late Early to earliest Middle Jurassic (Ricketts *et al.*, 1992; Nelson and Mihalynuk, 1993). The rocks of the Cache Creek ocean and Whitehorse trough are currently exposed in a north-northwest striking belt north of Dease Lake (Figure 1), and are found in the hangingwall and footwall of the King Salmon thrust fault. The latter is generally interpreted as a major terrane bounding structure, separating autochthonous rocks of the Stikine terrane to the south from allochthonous rocks of the Cache Creek terrane to the north (*e.g.* Gabrielse, 1998). The Stikinia – Cache Creek accretionary event was complete by the Middle Jurassic (Bajocian), as indicated by sedimentation of Cache Creek derived chert clasts deposited in the molasse-type Bowser Basin to the south of the study area (Figure 1; Ricketts *et al.*, 1992).

Large granitoid plutons were emplaced during the Late Triassic to Middle Jurassic, and are exposed in an arcuate belt on the northern margin of the Bowser basin. This belt, commonly referred to as the Stikine arch, is centered on the Hotailuh batholith, and includes the Stikine pluton to the southeast and the Hickman batholith to the southwest (Anderson, 1983; Woodsworth *et al.*, 1991). Several smaller Late Jurassic to Cretaceous plutons are present within the Dease Lake area (Anderson and Bevier, 1992; Logan *et al.*, this volume).

Mineralization in the northern Stikine terrane comprises several Late Triassic to earliest Jurassic calcalkaline porphyry Cu-Mo±Au to alkaline porphyry Cu-Au deposits; notable examples include Galore Creek, Schaft Creek, KSM and GJ to the southwest, Red Chris to the south, and Kemess to the southeast (Ash *et al.*, 1997; Logan *et al.*, 2000; Duuring *et al.*, 2009; Norris *et al.*, 2011). These porphyry copper deposits are roughly located on the southwestern and southeastern apexes of the Stikine magmatic arch. Interestingly, despite the presence of similar rocks in the centre of the arch, no major porphyry copper deposits have been found in the immediate area of the Hotailuh batholith. Southwest of the study area, the Au-Ag-enriched Eskay Creek volcanogenic massive sulphide deposit is hosted in felsic volcanic rocks within the Early-Middle Jurassic Hazelton Group (Bartsch, 1993), and represents a relatively underexplored deposit type elsewhere in the Stikine terrane (Massey *et al.*, 1999).

GEOLOGICAL UNITS

Rock units encountered in the field are summarized in Table 1, and are described below from oldest to youngest. Magnetic susceptibility values for all rock units were measured in the field with a Terraplus KT-10 hand-held magnetic susceptibility meter. Magnetic susceptibility data is summarized in Figure 2, and shows clear distinctions between several major units.

All detailed geological maps presented here (Figures 3b-h) incorporate minor data from Anderson (1983) and Gabrielse (1998), as well as Read and Psutka (1990) and Evenchick and Thorkelson (2005) in the far south. The Gnat Pass compilation map in Figure 3a also incorporates data from Read (1984), Nixon *et al.* (1989; 1997) around the Gnat Lakes ultramafite, Dircks (1974) around the BCR property, Wetherill (1989; 1990) around the Dalvenie claims, Smith and Garagan (1990) around the Gnat Pass prospect, and preliminary detrital zircon results from near peak 2096 m (Iverson *et al.*, this volume). In addition, five preliminary U-Pb LA-ICP-MS zircon crystallization ages are reported as part of this study. Each age represents the mean of 16-50 analyses on individual zircon crystals, and is subject to further data processing and error propagation. Two standard deviation errors are ~2 Ma.

Rock classification schemes developed by the British Geological Survey (Gillespie and Styles, 1999;

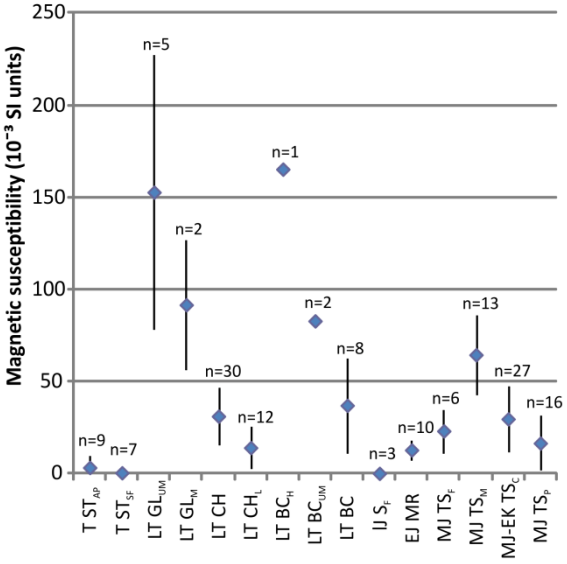

Figure 2. Graph showing the magnetic susceptibility values and one standard deviation for all major rock units. n = number of measurements, where each measurement represents the average of ten field measurements at one station point.

Hallsworth and Knox, 1999) are used throughout this paper. Notably, the reported crystal size in igneous rocks is the volumetrically dominant size; the mineral qualifying suffixes –bearing and –rich indicate that <5% and >20% of the rock comprises the mineral in question, respectively. In the field, a gabbro has been defined as a rock plotting in the diorite QAPF field, but containing ≥50% mafic minerals. Elevations for unnamed peaks ("peak ... m"; Figures 3a-h) are spot heights from British Columbia's TRIM database. All coordinates are in UTM NAD83 zone 9V.

Stratified rocks

TRIASSIC ROCKS

Rocks in the central and western part of the Gnat Pass valley predominantly comprise massive to foliated augite-phyric coherent rocks with lesser massive fine grained sedimentary rocks (Figure 3a; units T STAP and T STSF in Table 1 respectively), and have been assigned to the Triassic Stuhini Group (similar to assignments by Anderson, 1983 and Gabrielse, 1998). The coherent rocks represent extrusive rocks and/or sub-volcanic intrusions. The complex map pattern of the volcanic and sedimentary lithologies could be due to a number of factors such as faulting, folding, rapid lateral and vertical facies changes and/or irregular intrusion of augite porphyry into the sedimentary strata. The Stuhini augite-phyric rocks are cut by felsic dikes, likely genetically related to the Gnat Lakes ultramafite (unit LT GL$_F$, *ca.* 223 Ma), and appear to be intruded and partially assimilated by the Cake Hill pluton (unit LT CH, *ca.* 221-226 Ma). The Stuhini Group augite-phyric coherent rocks in the Gnat Pass valley north of Lower Gnat Lake are crosscut by the Gnat Pass intrusive (unit LT GP, *ca.* 217 Ma). These relationships, as well as their foliated nature (discussed below), suggest

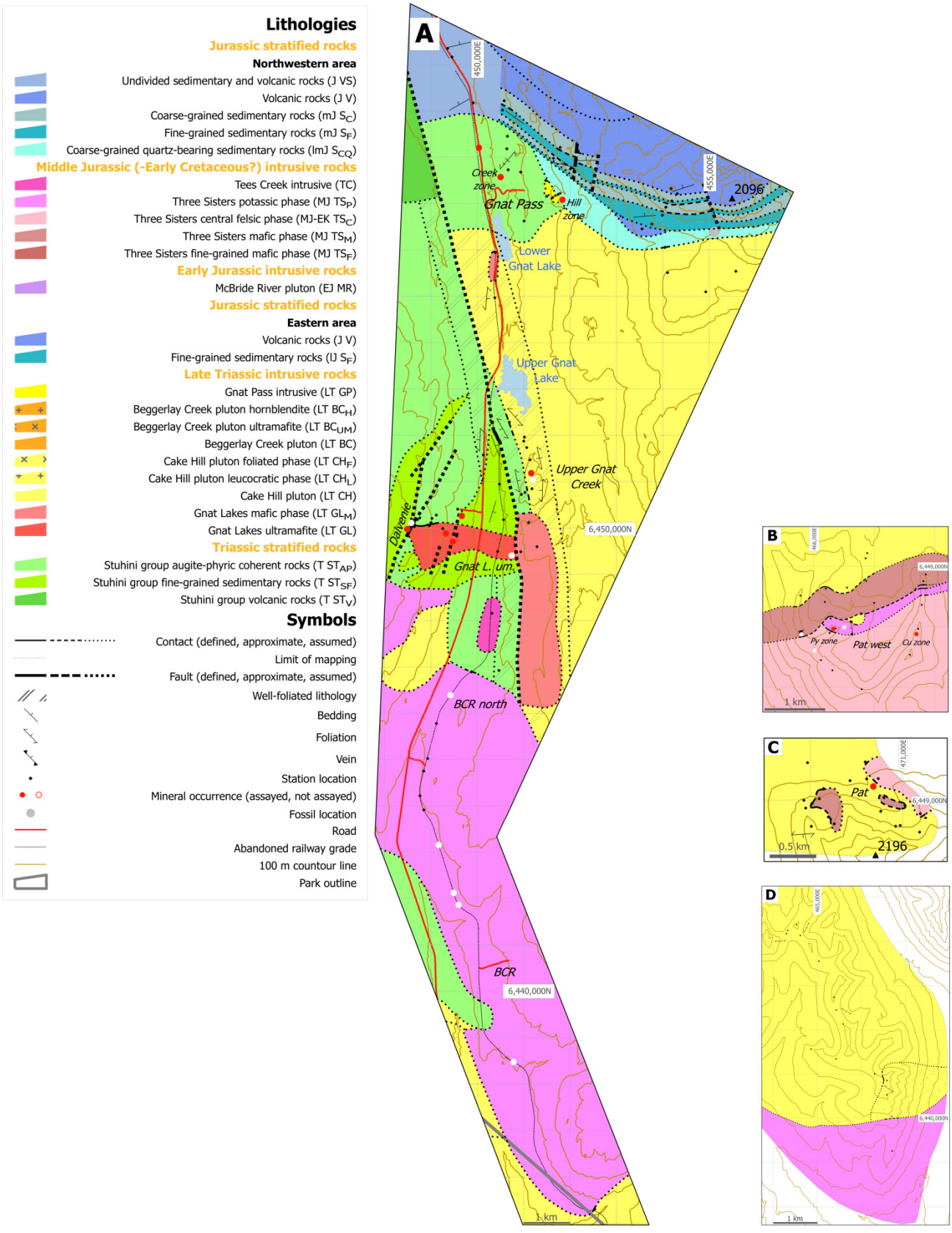

Figure 3. Detailed geological maps and legend of selected areas of the Hotailuh batholith. Location of each detailed map is indicated on Figure 1.

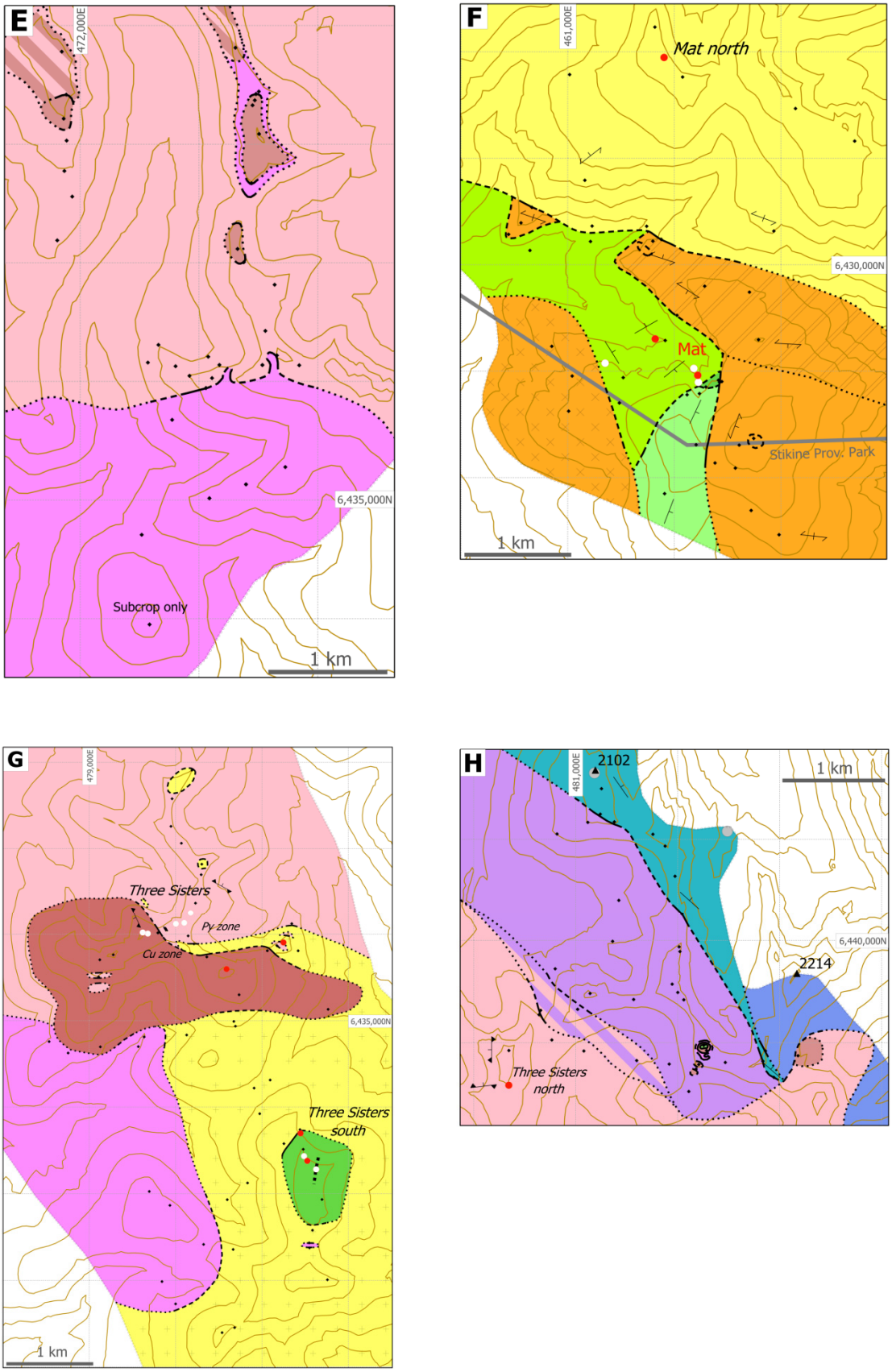

Figure 3. Continued.

Table 1: Summary of all geological units described in the field: a) Stratified rocks, b) Igneous rocks. Mineral abbreviations after Kretz (1983).

a) Stratified Rocks

Group	Area	Unit	Age	Code	Lithology
Jurassic sedimentary / volcanic (Hazelton?) group		Undivided	J	VS	Includes J V, mJ S_C, mJ S_F and lmJ S_{CQ}; see below.
	Northwestern area	Volcanic rocks	J	V	Granule, pebble and cobble-sized volcaniclastic conglomerate and pyroclastic breccia; contains Pl-Aug, Pl, Aug, Pl-Hbl-phyric, amygdaloidal clasts. Volcanic sediments commonly contain Aug crystals.
		Coarse-grained sedimentary rocks	mJ	S_C	Medium grey, medium bedded, medium and (very) coarse grained sandstone. Feldspathic ±lithic arenite. Minor interbedded siltstone; minor interbedded pebble conglomerate.
		Fine-grained sedimentary rocks	mJ	S_F	Dark grey to black, parallel laminated to (very) thinly bedded siltstone and fine-grained sandstone. Often recessive.
		Coarse-grained quartz-bearing sedimentary rocks	lmJ	S_{CQ}	Basal unit nonconformably(?) overlies Cake Hill pluton. Very coarse grained sandstone and pebble-sized conglomerate with granitoid clasts. Includes conglomerate, quartz-bearing feldspathic arenite, graphitic siltstone and micrite of Anderson (1983), Smith and Garagan (1990).
	Eastern area	Volcanic rocks	J	V	Pyroclastic breccia and volcaniclastic pebble-sized conglomerate; contains Hbl(?)-Pl-phyric clasts.
		Fine-grained sedimentary rocks	lJ	S_F	Alternating medium-dark grey (parallel) laminated siltstones, calcareous siltstones, fine to medium-grained sandstone and rare very thick bedded, likely Qtz-bearing, (very) coarse grained sandstone and granular conglomerate.
Triassic Stuhini Group	Entire area	Stuhini volcanic rocks	T	ST_V	Pyroclastic (?) breccia and volcaniclastic conglomerate; contains Pl-Aug-, Pl-phyric clasts. Laminated to (very) thinly bedded medium to very coarse grained volcaniclastic sandstone with some siltstone interbeds; Aug crystal bearing.
		Stuhini augite-phyric coherent rocks	T	ST_{AP}	Dark green, 1-5 mm euhedral, 20-40% Aug-phyric coherent rocks; rare Pl-Aug-phyric (ST_{PAP}). Can contain rare 1 m thick dark green fine grained sandstone intervals.
		Stuhini fine-grained sedimentary rocks	T	ST_{SF}	Medium to dark grey, laminated to very thinly bedded siltstone and fine to medium-grained sandstone. With minor concordant 0.5-1 m intervals of 2-5 mm 30-40% Aug-phyric coherent rocks.

Age abbreviations: l = lower, m = middle, u = upper, E = Early, M = Middle, L = Late, T = Triassic, J = Jurassic, K = Cretaceous.

b) Igneous Rocks

Suite	Pluton	Unit	Age	Code	Lithology
Middle Jurassic (-Early Cretaceous?) plutonic suite		Tees Creek intrusive	≤ MJ	TC	Altered Hbl-feldspar porphyry.
	Three Sisters pluton	Three Sisters potassic phase	MJ	TS_P	Bt (and Bt-bearing) granite, Qtz syenite and Qtz monzonite with Kfs>Pl. Equigranular 1 mm to 4 mm; often 5-20 mm Kfs porphyritic. Includes pink Bt porphyritic dikes.
		Three Sisters central felsic phase	MJ-EK?	TS_C	Bt and lesser Hbl-Bt (may include rare Bt-Hbl) Qtz monzonite and Qtz monzodiorite with Pl>Kfs. Equigranular, 2-3 mm; 4-5 mm Kfs porphyritic in places; dioritic xenoliths locally present.
		Three Sisters mafic phase	MJ	TS_M	Hbl-rich diorite (to Qtz diorite?). Acicular Hbl 0.5-4 mm to 2-7 mm; equant Hbl 1-2 mm to 4-10 mm.
		Three Sisters fine-grained mafic phase	MJ	TS_F	Hbl diorite (to Qtz diorite?). Equigranular, 1-1.5 mm, often 10 vol.% 1.5-3 mm Pl porphyritic.
Early Jurassic	McBride River	McBride River pluton	EJ	MR	Hbl monzogranite and granodiorite. Equigranular, 3 to 3-4 mm, with minor ubiquitous 4-7 mm Qtz blebs; tabular Hbl common.
Late Triassic plutonic suite		Gnat Pass intrusive	LT	GP	Hbl (and Hbl-bearing) diorite and granodiorite with lesser quartz diorite. Equigranular 2 mm euhedral-subhedral Pl, rarely 2-4 mm Qtz porphyritic.
	Beggerlay Creek pluton	Beggerlay Creek potassic dikes	LT	BC_P	Coarse pink Kfs (±Ep) dikes.
		Beggerlay Creek ultramafic body	LT	BC_{UM}	Highly altered (serpentinized?) plutonic ultramafic rock. Equigranular, 5 mm, massive.
		Beggerlay Creek pluton	LT	BC	Hbl-rich (and Bt-Hbl-rich) diorite to gabbro (BC) to rare Pl-bearing hornblendite (BC_H). Equigranular, 3-5 mm, massive to moderately foliated.
	Cake Hill pluton	Cake Hill foliated phase	LT	CH_F	Bt(?)-Hbl diorite and Qtz diorite. Foliated, equigranular, 1-3 mm.
		Cake Hill leucocratic phase	LT	CH_L	Light coloured and Ep altered Hbl Qtz diorite and tonalite(?). Equigranular, 1-2 to 2-3 mm, common tabular Hbl.
		Cake Hill pluton	LT	CH	Hbl to lesser Bt-Hbl Qtz monzodiorite and Qtz monzonite. Equigranular, 3-4 mm; tabular Hbl bearing, trace Ttn usually ubiquitous; trace Mag in places; massive to moderately foliated.
	Gnat Lakes ultramafite	Gnat Lakes felsic phase	LT	GL_F	Hbl granodiorite, monzodiorite and diorite. Equigranular 2 mm.
		Gnat Lakes mafic phase	LT	GL_M	Hbl-rich diorite and gabbro. Equigranular 1-5 mm Hbl.
		Gnat Lakes ultramafite	LT	GL_{UM}	Pl-bearing ultramafic rock (predominantly hornblendite) to rare pyroxene(?)-Hbl-rich gabbro. Equigranular 2-100 mm euhedral-subhedral Hbl, anhedral Pl.

a pre-*ca*. 226-217 Ma age for these rocks.

South of the Hotailuh batholith (Figure 3f), a succession of Stuhini Group rocks consists of predominantly sedimentary rocks grading into predominantly coherent rocks exposed at higher elevations (units T ST_{SF} and T ST_{AP} in Table 1, respectively). The approximate change from laminated and very thinly bedded siltstones and medium-grained sandstones with minor concordant intervals of massive augite-phyric coherent rocks to massive augite-phyric coherent rocks with rare fine grained sandstone intervals is well exposed in a steep gully. Here, laminated to very thinly bedded augite-bearing, medium grained volcaniclastic sandstones to granule-sized volcaniclastic conglomerates (unit T ST_V) occurs between these two rock units. Unfortunately, poor exposure and lichen-covered outcrops dominate the remainder of the area where it is often difficult to differentiate coarse grained, augite-bearing sediments from augite-phyric coherent rocks. This could explain the apparent lack of augite-bearing sediments at other locations near this contact. No way-up criteria were observed in the area, and although bedding in the southeastern half of the Stuhini succession has a uniform moderate southeasterly dip, structural disturbance appears to have occurred in the western half (Figure 3f). Based on the presence of augite-bearing volcaniclastic sediments, the augite-phyric coherent rocks most likely are extrusive in origin. The volcano-sedimentary rocks close to the Beggerlay Creek pluton contact are cut by coarse K-feldspar dikes that are presumed to be cogenetic with the latter pluton, implying a Late Triassic or older age for this Stuhini succession.

A limited number of Stuhini Group xenoliths occur within the Hotailuh batholith. A 0.5-1 km^2 raft or pendant of Stuhini is present within the Cake Hill leucocratic phase (Figure 3g) and comprises predominantly volcanic breccia and volcaniclastic conglomerate (unit T ST_V). To the east, a much smaller inclusion of augite-phyric coherent rocks (unit T ST_{AP}; Figure 3h) within the McBride River pluton is intruded and partly assimilated by the Three Sisters mafic phase. The augite-phyric rocks could be as young as Early Jurassic, but are included here based on their similarity to the Triassic Stuhini Group.

JURASSIC ROCKS

Sedimentary and volcanic rocks of Jurassic age were identified in the northwestern (Figure 3a) and eastern (Figure 3h) parts of the Hotailuh batholith.

Northwestern area

A succession of right-way-up Jurassic sedimentary rocks overlies the Cake Hill pluton (Figure 3a). It was mapped previously as a Lower Jurassic unit of the Takwahoni Formation overthrust by Lower to Upper Triassic Stuhini Group (Anderson, 1983; Gabrielse, 1998). However, preliminary U-Pb detrital zircon dates suggest the hangingwall rocks are also Jurassic in age (Iverson *et al.*, this volume).

The base of this succession comprises a coarse grained, quartz-rich sedimentary unit (lmJ S_{CQ} in Table 1), which was recognized in one outcrop. At this location it consists of a granitoid clast-bearing conglomerate and very coarse-grained sandstone (Figure 4). The lower contact lies within ten metres of intrusive rocks and may represent a nonconformable contact. Fossils from a sandy micrite associated with limey, quartz-bearing, feldspathic arenite located 4.5 km east of Lower Gnat Lake suggest an Early (to Middle?) Jurassic age (Henderson and Perry, 1981; Anderson, 1983, pages 209-214; Gabrielse, 1998, Appendix 2; Figure 3a). Conglomerate, quartz-bearing feldspathic arenite and graphitic siltstone intersected in drill core from a mineral prospect near Gnat Pass (Smith and Garagan, 1990; this study) appear similar to the rocks described above, and have been included in the basal unit.

The stratigraphically overlying package of rocks can be traced along most of the south-facing slopes of peak 2096 m, and consists of two coarsening-upward sequences of predominantly sedimentary rocks (Figure 3a; see also Figure 2, Iverson *et al.*, this volume). Preliminary results from three detrital zircon samples show distinct Middle Jurassic and Late Triassic populations (Iverson *et al.*, this volume). These results indicate that these rocks must be younger than the Triassic Stuhini Group. These sedimentary rock units (mJ S_F and mJ S_C in Table 1) dip moderately to the north, and are stratigraphically overlain by augite-phyric volcanic breccias (unit J V in Table 1). The coarse grained, quartz-bearing basal unit has traditionally been separated from these overlying, presumed Triassic Stuhini Group, rocks by the Hotailuh thrust (Anderson, 1983; Gabrielse, 1998). However, the new detrital zircon results eliminate the necessity for a thrust fault in this area

Figure 4. Very coarse grained sandstone to granule-sized conglomerate with several pebble-sized granitoid clasts (arrow). Altered Cake Hill pluton is exposed 10 m to the southeast and suggests a nonconformable contact. Hammer for scale.

(Figure 3a). A large outcrop of (hornblende)-plagioclase-phyric volcanic breccia is present southwest of peak 2096 m, between the basal quartz-bearing and the overlying fine grained sedimentary rock succession (Figure 3a). It does not appear to extend further east or west. The overlying fine-grained sediments contain two 10 m thick concordant columnar jointed augite-phyric coherent rock intervals, either representing fluidal flows or sills. The upper coarse-grained sediments in this unit comprise alternating medium-grained sandstones and concordant augite to plagioclase-augite phyric coherent rocks. The coherent intervals commonly contain a few percent disseminated pyrite, and either represent fluidal flows or sills. These exposures are correlated with similar plagioclase-augite phyric coherent rocks exposed in Gnat Creek. The fine to coarse grained stratified sedimentary rocks are overlain by volcanic breccias, and the entire sequence is cut by north trending subvertical faults.

The Jurassic rocks in this area are age equivalent with both the sedimentary Takwahoni Formation and the Hazelton Group. Marsden and Thorkelsen's (1992) definition for the Hazelton Group includes all Lower to Middle Jurassic volcanic and related sedimentary rocks on Stikinia, including the basinal sedimentary equivalents of the volcanic successions, and excludes distal strata whose origin is generally unrelated to Hazelton volcanism. Following this definition, the entire succession here is best assigned to the Hazelton Group.

Eastern area

A second succession of Jurassic sediments is present near peaks 2102 and 2214 m (Figure 3h). It was also mapped as Lower Jurassic Takwahoni Formation overthrust by Upper Triassic Stuhini Group (Anderson, 1983; Gabrielse, 1998).

The area around peak 2102 m at the eastern margin of the Hotailuh batholith comprises extensive exposures of reddish sedimentary rocks (Figures 3h, 5), previously assigned to the Takwahoni Formation (Gabrielse, 1998). The rocks comprise alternating medium to dark grey, parallel laminated siltstone, calcareous siltstone, fine to medium-grained sandstone and rare, very thickly bedded, likely quartz-bearing, coarse-grained sandstone to granule-sized conglomerate (unit lJ S_F in Table 1). The fine grained sedimentary rocks commonly contain a few percent disseminated and stratiform, very fine grained (0.05 mm) pyrite and are commonly iron oxide-stained. A sedimentary–intrusive rock contact is exposed in the south-facing headwall of peak 2102 m (Figures 3h, 5). Sedimentary rocks proximal to the margin of the *ca.* 190 Ma McBride River intrusion exhibit contact metamorphism. Fossils collected from this area suggest an Early to possibly Middle Jurassic (Toarcian and possibly Bajocian) age for these rocks (Gabrielse, 1998, Appendix 2). The Toarcian or younger (*i.e.* ≤183±1.5 Ma, International Commission on Stratigraphy, 2010) fossil constraint appears at odds with the pre-*ca.* 190 Ma

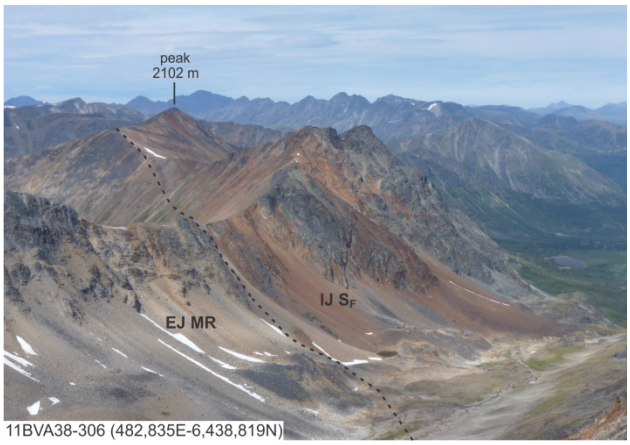

Figure 5. View northwest of peak 2102 m (on left) showing the contact between grey McBride River pluton on far left and rusty red, stratified sedimentary rocks (unit lJ S_F) on the right.

implied by the crosscutting relationship with the McBride pluton.

The exposures northeast of Lower Gnat Lake are part of a semicontinuous band of rocks previously assigned to the Triassic Stuhini Group on the north and northeastern margin of the Hotailuh batholith (Figure 1; Anderson, 1983; Gabrielse, 1998). The volcanic rocks in the eastern part of the batholith (Figure 3h) are presumed to be the easternmost extension of this belt. On the lower southwest ridge of peak 2214 m, black weathering, hornblende(?)-plagioclase phyric pyroclastic breccia and volcaniclastic pebble-sized conglomerate (unit J V in Table 1) stratigraphically overlie contact metamorphosed, well stratified fine grained sedimentary rocks similar to those exposed on peak 2102 m. No evidence for a thrust fault separating these two units could be found, and if the section is right-way-up, the volcanic rocks may be Early to Middle Jurassic in age, comparable to the succession northeast of Lower Gnat Lake.

Similar to interpretations for the Jurassic rocks in the northwestern area, the basal Lower Jurassic sedimentary rocks may represent deposition related to the Hazelton Group. Further work will need to address whether these rocks, and the entire band of volcanic and sedimentary rocks on the north and northeastern margin of the batholith, are part of the Hazelton Group.

Intrusive rocks

LATE TRIASSIC PLUTONIC SUITE

The Late Triassic plutons within the Cry Lake (104I) and Dease Lake (104J) 1:250 000 map sheets comprise the Stikine plutonic suite of Gabrielse (1998). Late Triassic plutonic rocks comprise about two-thirds of the Hotailuh batholith, and are exposed mainly in the west, northwest and southern part of the batholith (Figure 1). Here, we will only discuss the Late Triassic plutonic bodies within the main part of the Hotailuh batholith; namely the Cake Hill pluton, Beggerlay Creek pluton and Gnat Lakes ultramafite.

Gnat Lakes ultramafite

The Gnat Lakes ultramafite is a small 2.2 x 0.7 km body exposed both west and east of Highway 37, about three kilometres south of Upper Gnat Lake (Anderson, 1983; Nixon *et al.*, 1997; Figure 3a). The body comprises pyroxene(?)-hornblende gabbro and plagioclase-bearing ultramafite (likely predominantly hornblendite; unit LT GLUM). The body and its immediate surroundings has been mapped by Nixon *et al.* (1989, 1997), who describe it as an Alaskan-type ultramafic body based on the presence of hornblende clinopyroxenite, hornblendite and gabbro lithologies, minor zoning and distinctive whole rock and mineral chemistry data. The body has been dated by Zagorevski *et al.* (2011) as 223.2 ±2.0 Ma using the hornblende ^{40}Ar-^{39}Ar method. The ultramafic body is cut by irregular hornblende-bearing dikelets of granodiorite, monzonite and diorite composition, which form intrusive breccias (Figure 6). These leucocratic phases (unit LT GL_F in Table 1) have not been found outside of the Gnat Lake body, and are tentatively interpreted as cogenetic with the ultramafic body.

Anderson (1983) interpreted the Cake Hill pluton to predate the Gnat Lakes ultramafite, based on observations southwest of Lower Gnat Lake along the abandoned railroad grade. He reports (p. 85): "Irregular, dun weathering apophyses of hornblende pyroxenite engulf sphene-bearing, well foliated hornblende diorite and include rounded xenoliths of it." Upon revisiting these outcrops, we found intimately mixed ultramafic and mafic rock types, both cut by a felsic dike of Cake Hill composition (Figure 7). The mafic rocks exposed here are foliated, hornblende-rich diorites to gabbros, which both include and are included by plagioclase-bearing hornblendite. The mafic rocks are more hornblende-rich (40-60% hornblende) than typical Cake Hill. The felsic dike comprises foliated titanite-bearing hornblende diorite, and apart from the relatively low K-feldspar content (0-5% K-feldspar) appears similar to typical Cake Hill. Based on these observations we suggest that the Gnat Lakes body might predate the Cake Hill pluton. A similar mafic body is exposed immediately east of the main Gnat Lakes ultramafic body. The latter location also contains a decimetre-scale xenolith of ultramafic material similar to the Gnat Lakes ultramafic body. These relationships suggest a genetic link between the mafic phases and the Gnat Lakes ultramafite rather than to the Cake Hill pluton, which has made us reassign these rocks to a mafic subphase (LT GL_M, see Table 1, Figure 3a) of the Gnat Lakes body. These mafic exposures located immediately east of the Gnat Lakes ultramafite and other exposures located about 3 km south have been described as augite metagabbro by Read (1984) and Gabrielse (1998). To be consistent, these exposures have all been reassigned to the Gnat Lakes mafic subphase.

Cake Hill pluton

The Cake Hill pluton is the most areally extensive pluton of the Hotailuh batholith (Figure 1). The pluton is

Figure 6. Hornblende-bearing granodiorite (Gnat Lake felsic phase, GL_F) intruding and brecciating the Gnat Lake ultramafite (GL_{UM}). Hammer for scale.

Figure 7. Titanite-bearing hornblende diorite dike (CH) intruding hornblende-rich diorite to gabbro to plagioclase-bearing hornblendite (GL_M, GL_{UM}). Pencil for scale.

relatively homogeneous, xenolith free, comprises equigranular hornblende quartz monzodiorite to quartz monzonite, and contains trace amounts of titanite (LT CH in Table 1). Generally, the Cake Hill can be distinguished from the Three Sisters central felsic phase by the presence of abundant tabular hornblende rather than biotite, presence of trace titanite, rare presence of a moderately developed fabric, and possibly also a lack of fine grained dioritic xenoliths. A preliminary U-Pb zircon crystallisation age of *ca.* 226 Ma from the southern part of the Cake Hill pluton determined by this study

corroborates the 221±3 Ma age reported by Anderson and Bevier (1992). A light coloured, epidote altered, hornblende quartz diorite to tonalite (?) phase is present in the southeast corner of the batholith (Figure 3g). These rocks were mapped as the leucocratic phase of the Three Sisters by Anderson (1983, page 287), and were reinterpreted as Cake Hill by Gabrielse (1998). The rocks contain tabular, epidote-altered hornblende, appear K-feldspar-poor in the field (to be tested by staining and petrography), and resemble the main Cake Hill pluton. In addition, the unit contains several irregular metre-scale domains of hornblende quartz monzonite to quartz monzodiorite containing tabular hornblende and trace titanite, characteristic of the Cake Hill pluton. We adopt Gabrielse's interpretation, and have assigned the leucocratic unit to the Cake Hill pluton (unit LT CH_L in Table 1). The presence of a ~4 km wide west-northwest to east-southeast corridor of Cake Hill rocks connecting the southeasternmost exposures with the main pluton has not been confirmed during this study (*cf.* Figures 1, 3e), and remains to be tested. Several <1 km enclaves of hornblende quartz monzodiorite to quartz monzonite, presumed to represent Cake Hill, are hosted by the Three Sisters central felsic phase in the southeast (Figure 3g). However, gradational contacts complicate distinguishing these domains from surrounding biotite-hornblende to hornblende-biotite quartz monzodiorite and quartz monzonite of the Three Sisters central felsic phase. Similar relationships are found in the north-central part of the batholith, where differentiating Cake Hill from the Three Sisters central felsic phase is problematic (Figure 3c). In this area, rocks previously mapped as Three Sisters central felsic phase (Anderson, 1982; Gabrielse, 1998) are reinterpreted as Cake Hill based on the presence of tabular hornblende and trace titanite. Some of the ambiguity in distinguishing the Cake Hill from the Three Sisters central felsic phase is likely due to the (partial to complete) assimilation of Cake Hill by the Three Sisters central felsic phase pluton. A foliated, finer grained biotite(?)-hornblende diorite to quartz diorite is present in the southeast of Figure 3d, and has been assigned to the Late Triassic Cake Hill pluton due to the presence of hornblende and its foliated nature (LT CH_F in Table 1). The presence of Cake Hill rocks in the far southeast and eastern parts of the Hotailuh batholith suggests that this pluton occupied much of eastern half of the batholith before intrusion of the Three Sisters pluton.

Beggerlay Creek pluton

The Beggerlay Creek pluton is confined to the southern part of the Hotailuh batholith, and straddles the boundary between the NTS 104I and 104H map sheets north of the Stikine River. The pluton has been studied previously by Anderson (1983), Read and Psutka (1990), Gabrielse (1998) and Evenchick and Thorkelson (2005). We visited the pluton where it forms the southernmost part of the Hotailuh batholith (Figure 3f). All but the southwestern exposures in this area are comprised of hornblende-rich diorite to gabbro (unit LT BC) with minor plagioclase-bearing hornblendite domains (unit LT BC_H). Exposures in the southwest comprise highly altered (serpentinized?) plutonic ultramafic rocks (unit LT BC_{UM} in Table 1). The nature of the Beggerlay Creek – Cake Hill contact was reinterpreted, and now includes all hornblende-rich diorite and gabbro up to an abrupt change (over a 10 m covered interval) to titanite-bearing, hornblende quartz monzonite of the Cake Hill pluton (Figure 3f; *cf.* Anderson, 1983, pages 84-85, pages 139-140, Appendix 2.3c). Hornblende-rich diorite and gabbro closest to the contact, now assigned to the Beggerlay Creek pluton, are intensely foliated roughly parallel to the trace of the contact.

Minor coarse K-feldspar±epidote dikes (unit LT BC_P) crosscut the northwestern Beggerlay Creek pluton, and may be related to a 5 by 1 km biotite metasyenite phase of the Beggerlay Creek pluton mapped about 7 km to the east (Read and Psutka, 1990). Coarse K-feldspar dikes, similar to those within the Beggerlay Creek pluton, also crosscut the augite-phyric coherent rocks of the Stuhini Group near the contact with the mafic phases of the Beggerlay Creek intrusion. Intrusive relationships between the Beggerlay Creek and Cake Hill plutons were not observed, however Anderson (1983, pages 84-85, Appendix 2.3c) reports that in two locations a gabbro dike of suspected Beggerlay Creek affinity intrudes quartz monzodiorite of the Cake Hill.

EARLY JURASSIC MCBRIDE RIVER PLUTON

The McBride River pluton underlies an 8 x 20 km area at the easternmost margin of the Hotailuh batholith, dissected by the McBride River (Anderson, 1983; Gabrielse, 1998; Figure 1). The main body of the McBride River pluton was not visited during this study; however, we reassigned an intrusive body originally assigned to the Late Triassic Cake Hill pluton (Anderson, 1983; Gabrielse, 1998) to the McBride River pluton. It is composed of massive, equigranular (3-4 mm) hornblende monzogranite and granodiorite plutonic rocks that are significantly more quartz rich than typical Cake Hill, and, notably, contain minor but ubiquitous 4-7 mm quartz blebs, a feature common in the McBride River pluton (Anderson, 1983, p. 377). In addition, adjacent Toarcian to possibly Bajocian sedimentary strata (Gabrielse, 1998) are clearly contact metamorphosed by the pluton, providing a minimum Early Jurassic age that is untenable with the pluton being Late Triassic. We report a new preliminary U-Pb zircon crystallization age of *ca.* 190 Ma for this intrusive body, which is within error of the 184±8 Ma U-Pb zircon age for the main McBride River pluton established by Anderson and Bevier (1992).

MIDDLE JURASSIC (–EARLY CRETACEOUS?) THREE SISTERS PLUTON

The Three Sisters pluton comprises about one-third of the Hotailuh batholith. It is predominantly exposed in the eastern half of the batholith and also forms a significant exposure around and west of Highway 37

(Figure 1). The Three Sisters pluton is internally heterogeneous, and has been subdivided into four separate phases by Gabrielse (1998). The four phases studied include the fine grained mafic phase, mafic phase, central felsic phase and potassic phase (Table 1).

Fine grained mafic phase

The Three Sisters fine grained mafic phase is restricted to a 8 x 2 km body in the southeast of the Hotailuh batholith (Figure 3g); it also occurs as centimetre- to decimetre-sized xenoliths within parts of the Three Sisters central felsic phase. The fine grained mafic phase comprises massive, equigranular to sparsely plagioclase porphyritic, hornblende quartz (?) diorite with a 1-1.5 mm crystal size. Hornblende tonalite dikes intrude the fine grained mafic phase.

Mafic phase

The mafic phase is a volumetrically small unit of the Three Sisters pluton. Overall, it is fairly uniform compositionally, and comprises massive, equigranular, hornblende-rich diorite. Texturally, the rocks are varied, and comprise either acicular hornblende or equant blebby hornblende, with both textural types exhibiting wide variations in crystal size (1-20 mm). The mafic phase occurs as small to medium-sized (<1-2 km^2) bodies within the Three Sisters central felsic phase (Figure 3e). The central felsic phase intrudes into, as well as assimilates and includes fluidal fragments of the mafic phase. Furthermore, the fluidal domains of mafic phase within central felsic phase rocks often show a decrease in grain size towards the clast edge (Figure 8), interpreted as chilled margins. All evidence suggests that the two phases formed roughly at the same time. Similar mafic plutonic rocks crop out as several small (<0.5 km^2) bodies within the Cake Hill and McBride River plutons close to the contact with the main Three Sisters pluton (Figures 3c, h respectively). Where the mafic phase is present within these older plutonic rocks, the latter are observed intruding, and often including, the mafic phase rocks. Anderson (1983, p.86) reports similar observations at these locations, but also reports irregular mafic phase dikelets intruding Cake Hill, features interpreted to reflect remelting and remobilization of felsic rocks by intrusion of hot mafic melts. The remelting of felsic rocks by intrusion of mafic melts is a common feature in batholiths worldwide (*e.g.* Blundy and Sparks, 1992). In the southeast (Figure 3e), the mafic phase intrusions form subhorizontal tabular bodies confined to the highest ridge tops. In the north (Figure 3b), a body several square kilometres in size forms the margin of the Three Sisters pluton.

Central felsic phase

The areally most extensive phase occupies the central portion of the Three Sisters pluton. It consists of massive, equigranular (2-3 mm) biotite and lesser hornblende-biotite quartz monzonite and quartz monzodiorite, locally

Figure 8. Irregular xenolith of acicular hornblende diorite (TS_M) within hornblende-biotite quartz monzodiorite (TS_C). Note decrease in grain size within mafic xenolith from core to rim. Pencil for scale.

with K-feldspar phenocrysts. In addition to the internal variation in composition and texture, the central felsic phase encloses several other intrusive phases. For example, an estimated 15 to 50% of the north-south traverses along ridges in Figures 3e, g, h comprise either older (partly assimilated?) Cake Hill pluton, roughly coeval Three Sisters mafic phase, or crosscutting Three Sisters potassic phase. Notably, certain ridges that have been mapped by Anderson (1983) and Gabrielse (1998) as solely central felsic phase (north-south trending ridge in northwestern part of Figure 3e), comprise substantial proportions of other rock types.

The age of the central felsic phase is only constrained by K-Ar dates reported in the '70s and early '80s (see compilation in Anderson and Bevier, 1992). A preliminary U-Pb zircon crystallisation age from a biotite quartz monzonite exposed along the eastern margin of the Three Sisters pluton yielded a *ca.* 117 Ma age (this study). Ongoing research will address whether part or all of the Three Sisters central felsic phase may in fact be Early Cretaceous, rather than Middle Jurassic in age. This raises the possibility that some or all of the crosscutting potassic dikes, the roughly coeval mafic phase, as well as the fine grained mafic phase are significantly younger than previously recognized.

Potassic phase

The Three Sisters potassic phase comprises massive, equigranular (1-4 mm crystal size) to locally K-feldspar porphyritic (5-20 mm crystal size), biotite to rarely biotite-bearing, granite, quartz syenite and quartz monzonite. This phase occurs as a large body straddling Highway 37 that appears to be connected to the main part of the Three Sisters pluton through a relatively narrow (~1.5 km wide) corridor occupied by associated potassic phase rocks (Figure 1; Anderson, 1983; Gabrielse, 1998).

Elsewhere, several medium sized bodies of the potassic phase form the margin of the Three Sisters pluton in the eastern half of the batholith. Several smaller potassic phase bodies crosscut the central felsic phase pluton, and immediately adjacent plutons (Figure 3e, g, h).

A preliminary U-Pb zircon crystallisation age of *ca.* 165 Ma (this study) is only slightly younger than a 171±1 Ma date by Anderson and Bevier (1992) for these coarse grained intrusive rocks. Abundant fine grained, pink, biotite-phyric dikes, presumed to be related to the potassic phase, cut almost all adjacent plutonic and sedimentary rocks. The potassic and central felsic phases are distinguished by more quartz, less biotite and more K-feldspar than plagioclase in the potassic phase. In places, the potassic phase can be difficult to distinguish from the central felsic phase. Some areas mapped previously as the potassic phase corridor (Figure 1; Anderson, 1983; Gabrielse, 1998) consist of massive, relatively fine grained (1-2 mm crystal size), biotite quartz diorite (Figures 3d, e). Further investigations are needed to fully characterize distinctions between these phases.

OTHER INTRUSIVE ROCKS

In addition to the plutonic rocks described above, several small intrusive bodies and numerous dikes are present throughout the study area. A mineralized intrusive body is the "Gnat Pass intrusive" (unit LT GP in Table 1). Where unaltered, it comprises massive, equigranular (2 mm crystal size) to quartz porphyritic (2-4 mm crystal size), hornblende to hornblende-bearing diorite to quartz diorite and granodiorite. The intrusive occupies an area of ~0.1 km^2 in the "hill zone" (main zone) of the Gnat Pass mineral prospect (Smith and Garagan, 1990). A preliminary U-Pb zircon crystallisation age from the Gnat Pass intrusive at the hill zone yielded a *ca.* 217 Ma age (this study), only slightly younger than the Late Triassic plutons in the area. Similar intrusive bodies and dikes 1-10 m in width, generally also associated with minor sulphides, are found along Gnat Creek downstream of Lower Gnat Lake ("creek zone" of the Gnat Pass prospect) as well as along Highway 37 north of Lower Gnat Lake. In all areas, the intrusive cuts Triassic Stuhini Group augite-phyric coherent rocks. Interestingly, Asbury (1967) reports a 0.5 by 1 km-size granodiorite intrusion approximately 3.5 km northwest of Lower Gnat Lake. The body is described as "... a medium-grained, granular rock containing grey to pink plagioclase, an estimated 15% free quartz and 1% to 2% mafic minerals." This body is not shown on the regional geological map of Gabrielse (1998), and warrants additional study to determine its spatial extent and possible association with mineralization. In addition, possible cogenetic Fe-carbonate altered rhyodacite dikes that postdate all other units and are typically associated with sulphide mineralization are reported at the Dalvenie showing (Wetherill, 1990, page 13).

A small intrusion located further south of Gnat Pass is tentatively named the "Tees Creek intrusive". This altered hornblende-feldspar porphyry is exposed along the abandoned railroad about 1.5-3.5 km south of the Gnat Lakes ultramafite; it also occurs as irregular dikes intruding the coarse grained potassic phase of the Three Sisters pluton. The intrusive is associated with minor pyrite at the "BCR north" mineral occurrence.

STRUCTURAL GEOLOGY AND METAMORPHISM

Whereas the Hotailuh batholith appears to be mostly unaffected by post-intrusion contractional deformation, most surrounding sedimentary and volcanic rocks have been deformed. The area north of the Hotailuh batholith comprises predominantly moderately north-dipping strata, ascribed to result from south-directed thrusting along the King Salmon and Hotailuh faults (Gabrielse, 1998). The Gnat Pass area appears to be a major structural zone with evidence for a north to north-northwest striking ductile to brittle fault zone localized along part of the western margin of the Cake Hill pluton. Faulting and folding is common in Triassic sedimentary and volcanic rocks east of this fault zone (Read, 1984; Gabrielse, 1998). The structural style in the area south and east of the batholith is poorly understood. Two regional-scale faults inferred along the Stikine River include the Beggerlay Rapids and Pitman faults (Evenchick and Thorkelson, 2005).

Anderson (1983, pages 67-76) and Gabrielse (1998, page 64) described the Cake Hill pluton as pervasively or well foliated. However, we found the fabric within the Cake Hill pluton to be moderately developed to absent, except in a north-northwest striking zone in the Gnat Pass area where it is well developed. The fabric is defined by alignment of tabular hornblende crystals. Although moderately aligned hornblende is regularly observed in outcrop, it is commonly inconsistent over the metre scale. Where present, the orientation of the foliation measured herein is generally similar to the northwest-southeast striking, subvertical orientations reported by Anderson (1983). Except within the Gnat Pass zone (see below), the foliation is likely magmatic in origin.

Gnat Pass fault

The Gnat Pass fault strikes north-northwest, and is found on the western margin of the Hotailuh batholith. This subvertical brittle fault is exposed in a 2 m wide recessive zone in an exposure along the abandoned railroad. Augite-phyric coherent rocks on the east wall of the fault, as well as within at least 500 m on both sides of the fault, are intensely foliated, with foliation orientations parallel to the trend of the brittle fault. The foliation comprises newly formed green platy minerals (chlorite?) wrapped around relict augite phenocrysts, likely indicating greenschist facies metamorphic conditions. Sedimentary rocks on the west wall of the fault and further southwest lack a foliation, appear unmetamorphosed, and show bedding attitudes roughly parallel to the fault. In addition, granitoid rocks of the

Cake Hill pluton are well foliated up to a distance at least 750 m from the brittle fault. Foliation is defined by alignment of tabular hornblende, and the foliation is parallel to the brittle fault. Based on these observations, we infer the presence of a north-northwest striking, subvertical, ductile shear zone, roughly situated on the western margin of the Cake Hill pluton. Syn-intrusion shear would explain the relatively narrow band of foliated and metamorphosed country rocks, as well as the presence of a well-developed fabric formed by igneous hornblende in the pluton. The ductile shear zone became the locus of brittle deformation during subsequent cooling and/or exhumation.

The north-northwest striking belt of foliated rocks continues at least 3 km to the north and 5 km to the south where it appears to be cut by undeformed plutonic rocks of the Three Sisters potassic phase. Further north, the location of the Gnat Pass shear/fault zone is unconstrained, and it is inferred to truncate the Hotailuh thrust northwest of Lower Gnat Lake (Anderson, 1983; Gabrielse, 1998; Evenchick *et al.*, 2005). The northern terminus of this fault is inferred to intersect the King Salmon thrust fault, separating the Hotailuh allochthon from rocks further west (Figure 1; Gabrielse, 1998).

Hotailuh thrust fault

An exposure of the Hotailuh thrust could not be found during current mapping between Highway 37 and peak 2096 m (Figure 3a). Reported evidence for the fault is the presence of presumed Triassic Stuhini rocks overlying Early Jurassic fossil-bearing siliciclastic sedimentary rocks of the Takwahoni Formation (Anderson, 1983; Gabrielse, 1998). However, preliminary detrital zircon results (Iverson *et al.*, this volume) suggest a Middle Jurassic or younger age for the overlying package, leaving no requirement for the presence of a thrust fault in this particular location. On the eastern margin of the batholith (Figure 3h), the Hotailuh thrust has been inferred within steep and largely inaccessible topography surrounding peak 2214 m (Anderson, 1983; Gabrielse, 1998). Study of the lower southwest ridge of peak 2214 m found no evidence for a thrust fault, and if the section is right-way-up, the volcanic rocks previously assigned to the Triassic Stuhini Group may be Early to Middle Jurassic in age, comparable to the succession further west that yielded Jurassic detrital zircon populations.

Other structures and metamorphism

The succession of Middle Jurassic sedimentary and volcanic rocks around peak 2096 m is cut by several north-northeast to north-northwest trending, subvertical faults with stratigraphic offset suggesting a dextral strike slip and/or east-side-down dip slip motion. Another important structure is the Dalvenie fault, which hosts the Dalvenie copper-gold-silver prospect (Figure 3a). Several roughly parallel lineaments and/or possible faults are present in the immediate area (Figure 3a; Nixon *et al.*, 1989).

At the eastern margin of the Hotailuh batholith, sedimentary rocks with Early (to Middle?) Jurassic fossils are contact metamorphosed by the *ca.* 190 Ma hornblende monzogranite to granodiorite of the McBride River pluton (Figure 3h), providing an Early Jurassic or older age constraint for this sedimentary unit. Several skarn bodies comprising brown garnet, dark green pyroxene (?), light bright green vesuvianite (?) and/or white fibrous wollastonite (?) occur within about 50 m of the contact with the intrusive, and represent contact metamorphosed calcareous, fine grained sedimentary rocks. In addition, three apophyses of altered felsic intrusive rocks extend into the sedimentary rocks. Anderson (1983, p. 305) interpreted these intrusives as Late Triassic Cake Hill, and attributed the contact metamorphism to intrusion of the nearby Three Sisters pluton. Current mapping shows that the Three Sisters pluton is at least 1-1.5 km away from most of the calcic exoskarns, and given the very local skarn development near the monzogranite/granodiorite contact, it appears implausible that this contact metamorphism is caused by the intrusion of Three Sisters.

Mafic intrusive rocks of the Beggerlay Creek pluton are intensely foliated in a 500-750 m wide zone adjacent to the Cake Hill contact (Figure 3f). The steeply dipping, east to east-northeast striking foliation is defined by elongated (recrystallized?) hornblende and plagioclase, imparting an almost gneissic compositional banding in places.

MINERALIZATION

Five mineralized prospects and showings in the MINFILE database (see http://minfile.gov.bc.ca) have been visited within the Hotailuh study area. Most of these occur in the easily accessible Gnat Pass area where rock exposure is poor to moderate. An additional eight new mineral occurrences were identified, both within the Gnat Pass area, and on well-exposed ridges of the Hotailuh batholith.

A total of 20 mineralized (grab) samples were collected from 4 MINFILE locations, as well as 7 from the newly identified mineral occurrences. The samples were jaw crushed and pulverized in a Cr-steel mill at the Geological Survey sample preparation facilities in Victoria and analysed at Acme Labs in Vancouver. The samples were dissolved using a four-acid digestion followed by multi-element ICP-MS analysis. Gold was also analysed by lead-collection fire assay fusion followed by ICP-ES analysis. Values reported in Table 2 include analysis of one repeat on a jaw crushed reject sample, an external standard, and Acme's internal quality control duplicate samples and standard.

Table 2. Assay results and coordinates of mineralized rock samples collected during 2011 field work in the Hotailuh area.

Mineral occur.	Element				Au*	Ag	Cu	Mo	W	Sn	Bi	As	Sb	Ba	Pb	Zn	Rb	Sr	Cd	Ni	Co
	Units				ppb	ppm	ppm	ppm	ppm	ppm	ppm	ppm	ppm	ppm	ppm	ppm	ppm	ppm	ppm	ppm	ppm
	Detection limit				2	0.1	0.1	0.1	0.1	0.1	0.1	1	0.1	1	0.1	1	0.1	1	0.1	0.1	0.2
	Station no.	UTM E	UTM N	Unit																	
Gnat P.	BVA-5-30	450,034	6,458,207	LT GP	12	0.1	161	<0.1	1.0	0.3	0.9	30	4.2	463	4	5	79	211	<0.1	3	109
	BVA-9-48	450,502	6,457,572	LT GP	4	<0.1	34	0.4	0.5	0.6	0.1	7	2.4	598	2	23	66	182	<0.1	2	6
	JLO32-319	451,832	6,457,090	LT GP	41	0.6	7221	16.7	0.6	0.6	0.1	5	1.0	510	7	32	134	315	0.2	4	8
Dalv.	BVA-11-62a	448,489	6,449,977	T ST_{SF}	14	<0.1	87	<0.1	29.5	0.9	4.8	535	54.9	53	2	3	64	38	<0.1	230	31
	BVA-11-62b	448,489	6,449,977	T ST_{SF}	570	2	463	0.5	9.8	1.2	61.0	>10000	205	36	32	21	38	121	<0.1	53	93
Gnat Cr.	BVA-2-12	451,163	6,451,183	LT CH	1703	81.7	>10000	5.5	<0.1	0.1	483	<1	1.4	50	79	125	62	599	0.5	5	18
Gnat L. um.	BVA-11-57	449,665	6,450,261	T ST_{SF}	<2	<0.1	72	1.9	0.3	3.9	0.3	<1	0.3	341	11	33	64	21	<0.1	21	11
	BVA-11-58b	449,472	6,449,706	LT GL_F	<2	0.1	87	8.2	0.8	0.9	0.1	5	1.8	1005	8	78	19	689	<0.1	39	22
	BVA-11-59	449,321	6,449,882	LT GL_{UM}	5	0.2	402	3.7	0.2	1.3	0.1	2	1.9	245	4	93	5	424	0.2	30	96
	Acme Dup	,,	,,	,,	*4*																
Mat	BVA-26-184	462,220	6,428,961	T ST_{SF}	2	0.2	139	7.0	0.4	0.7	<0.1	4	<0.1	27	5	129	2	80	0.4	146	20
	BVA-26-187	461,821	6,429,303	T ST_{SF}	<2	0.1	133	0.9	0.2	0.6	<0.1	22	0.4	36	73	57	2	272	0.2	63	39
Mat N	BVA-25-172	461,904	6,431,947	LT CH	39	9.1	>10000	0.7	0.2	0.2	5.4	<1	0.4	3102	13	86	32	1120	0.1	25	22
Pat	BVA-13-74	470,681	6,449,148	LT CH?	32	1.1	2962	2.2	0.4	1.8	1.0	12	0.7	392	4	24	25	568	<0.1	10	20
Pat W	BVA-14-82	467,697	6,447,881	MJ-EK TSc	21	0.7	7079	0.1	2.4	1.1	0.6	19	1.3	1083	2	49	117	159	0.2	2	15
	BVA-15-90	466,323	6,447,968	MJ TSp	<2	<0.1	131	2.0	0.1	0.5	<0.1	4	<0.1	1179	4	7	84	461	<0.1	2	8
3 Sis. N	BVA-30-216	480,344	6,438,583	MJ-EK TSc	9	0.2	3645	6.4	>200	3.4	<0.1	3	0.4	130	3	92	19	195	0.2	5	51
3 Sis.	BVA-32-241	480,590	6,435,596	MJ TSf	80	<0.1	3520	0.8	6.1	0.7	0.2	<1	0.2	41	2	59	2	270	<0.1	3	15
	BVA-32-246	481,249	6,435,903	LT CH	<2	<0.1	144	3.8	3.2	2.7	<0.1	<1	<0.1	188	3	9	4	550	<0.1	2	15
3 Sis. S	BVA-33-253	481,447	6,433,699	T ST_V	<2	<0.1	55	6.8	1.1	0.8	0.1	5	0.2	40	1	3	2	1028	<0.1	10	124
	BVA-33-257	481,525	6,433,380	T ST_V	14	0.4	3367	314	33.3	3.1	2.4	11	2.7	51	2	58	9	521	<0.1	11	123
	Acme Dup	,,	,,	,,		*0.3*	*3452*	*332*	*39*	*3.2*	*2.3*	*9*	*2.6*	*51*	*2*	*59*	*9*	*537*	*<0.1*	*11*	*122*
	BVA-33-257Dup	,,	,,	,,	*14*	*0.3*	*2925*	*240*	*32*	*4.6*	*2.4*	*8*	*3.1*	*50*	*2*	*54*	*7*	*560*	*<0.1*	*12*	*105*
Standards	*RU-1*	-	-	*Standard*	*238*	*3.9*	*7546*	*10.9*	*8.5*	*9.9*	*18.9*	*67*	*0.9*	*31*	*380*	*>10000*	*9*	*88*	*60*	*32*	*104*
	*Expected***	-	-	,,	*300*	*7*	***8540***									***22370***			*70*	*70*	
	OREAS45C	-	-	*Standard*		*0.2*	*595*	*2.2*	*1.0*	*2.8*	*0.2*	*11*	*0.8*	*279*	*24*	*81*	*24*	*35*	*0.2*	*317*	*100*
	OREAS45C	-	-	,,		*0.1*	*591*	*2.6*	*1.2*	*3.0*	*0.2*	*10*	*0.8*	*272*	*25*	*79*	*24*	*39*	*0.1*	*302*	*98*
	*Expected***	-	-	,,		*0.28*	*620*	*2.26*	*1.06*	*2.9*	*0.21*	*10.1*	*0.79*	*270*	*24*	*83*	*24*	*36.4*	*0.15*	*333*	*104*

Significant values in yellow, anomalous values in orange, slightly elevated values in blue. Abbreviations used for mineral occurrences: Gnat P. = Gnat Pass, Gnat Cr. = Upper Gnat Creek, Dalv. = Dalvenie, Gnat L. um. = Gnat Lakes ultramafite, 3 Sis. = Three Sisters, W = west, N = north, S = south. For unit abbreviations, see Table 1.

* Analysed by lead-collection fire assay fusion followed by ICP-ES, all other elements analysed by four-acid digestion followed by ICP-MS.

** Recommended values for CANMET standard RU-1 in bold (Faye *et al.*, 1977). Expected values for Acme Labs internal standard.

Table 2. continued.

Element	Cr	V	Nb	Y	Zr	Sc	La	Hf	Ta	Ce	Th	U	Li	Be	Mn	Ti	Al	Fe	Mg	Ca	Na	K	P	S
Units	ppm	ppm	ppm	ppm	ppm	ppm	ppm	ppm	ppm	ppm	ppm	ppm	ppm	ppm	ppm	%	%	%	%	%	%	%	%	%
Detection limit	1	1	0.1	0.1	0.1	1	0.1	0.1	0.1	1	0.1	0.1	0.1	1	1	0.001	0.01	0.01	0.01	0.01	0.001	0.01	0.001	0.1
Station no.																								
BVA-5-30	63	24	2.0	2	22	1	2	0.9	<0.1	5	0.7	0.8	4	<1	23	0.08	7.7	2.5	0.1	0.1	4.09	1.82	0.01	1.6
BVA-9-48	30	39	3.3	3	40	3	5	1.3	0.2	12	1.6	1.0	7	2	103	0.15	7.9	1.5	0.1	0.2	4.53	2.39	0.05	0.2
JLO32-319	32	53	3.7	8	24	4	8	1.0	0.2	16	1.8	1.2	5	<1	221	0.20	7.1	1.3	0.2	0.5	2.10	5.76	0.08	0.5
BVA-11-62a	769	168	0.3	9	13	23	21	0.5	<0.1	41	0.2	0.4	16	<1	4597	0.22	3.9	3.9	0.7	5.0	0.03	1.75	0.10	0.1
BVA-11-62b	299	91	0.4	2	17	10	43	0.5	<0.1	60	0.5	1.3	22	<1	336	0.08	2.9	10.2	0.1	0.0	0.03	1.02	0.04	4.0
BVA-2-12	17	77	0.2	2	2	<1	6	<0.1	<0.1	6	0.2	7.1	10	<1	815	0.02	4.0	24.8	0.7	1.5	0.03	2.31	0.01	9.7
BVA-11-57	64	22	1.1	4	13	9	7	0.3	<0.1	22	1.0	0.3	17	<1	1088	0.11	3.9	1.3	1.0	0.1	0.10	1.76	0.02	0.4
BVA-11-58b	60	326	1.9	17	20	31	8	1.0	<0.1	19	0.7	0.4	4	<1	1249	0.65	7.6	6.5	3.6	5.8	3.57	0.84	0.30	0.1
BVA-11-59	88	511	1.9	17	31	64	4	1.3	<0.1	13	0.4	0.2	3	<1	1544	1.06	5.8	13.3	6.3	7.9	1.15	0.60	0.06	1.9
Acme Dup																								
BVA-26-184	105	333	6.0	21	24	22	14	0.8	0.4	27	2.9	1.4	2	<1	833	0.47	8.0	4.7	1.1	1.2	7.67	0.12	0.07	1.3
BVA-26-187	499	212	1.0	10	17	51	5	0.7	<0.1	12	1.1	0.5	11	<1	1741	0.31	4.8	5.9	6.4	10.4	1.88	0.09	0.18	1.0
BVA-25-172	27	107	4.2	6	4	<1	19	0.2	0.3	35	2.0	2.4	27	2	827	0.58	8.6	3.3	2.5	2.0	3.75	1.34	0.13	0.2
BVA-13-74	61	69	3.6	12	8	4	16	0.5	0.2	35	3.5	1.7	8	1	592	0.21	7.2	4.6	0.9	3.5	2.99	0.65	0.06	0.2
BVA-13-82	52	85	3.7	18	8	9	11	0.5	0.2	26	7.6	6.9	8	<1	811	0.22	6.8	3.3	0.8	0.5	2.23	3.05	0.09	<0.1
BVA-15-90	66	18	4.0	12	17	2	20	0.6	0.3	39	7.5	2.5	6	1	162	0.13	7.1	1.6	0.4	1.0	3.63	2.82	0.05	0.5
BVA-30-216	40	244	1.7	24	11	31	11	0.5	0.1	24	4.7	27.5	6	3	1683	0.18	5.1	22.0	2.0	3.2	1.11	0.70	0.07	<0.1
BVA-32-241	53	99	2.8	15	41	9	14	1.4	0.2	29	4.2	6.2	5	<1	627	0.26	6.6	5.4	1.9	1.6	3.53	0.09	0.07	<0.1
BVA-32-246	32	54	6.2	19	31	10	70	1.2	0.3	105	3.7	2.9	1	2	310	0.28	7.8	1.8	0.8	3.3	4.38	0.21	0.06	0.6
BVA-33-253	36	136	5.4	21	55	17	17	1.5	0.3	34	3.8	1.1	2	1	258	0.55	9.6	7.1	2.4	4.9	3.55	0.17	0.16	2.4
BVA-33-257	58	180	4.1	22	57	18	15	1.6	0.2	31	2.4	2.2	5	1	1906	0.43	5.7	16.3	3.5	3.3	0.68	0.20	0.10	1.8
Acme Dup	*59*	*182*	*4.2*	*22*	*61*	*17*	*15*	*1.5*	*0.2*	*32*	*2.5*	*2.3*	*5*	*1*	*1978*	*0.44*	*6.0*	*15.7*	*3.6*	*3.3*	*0.70*	*0.20*	*0.11*	*1.8*
BVA-33-257Dup	*67*	*182*	*3.8*	*23*	*56*	*19*	*17*	*1.6*	*0.2*	*34*	*2.5*	*2.5*	*5*	*1*	*1805*	*0.41*	*5.8*	*15.6*	*3.2*	*3.7*	*0.69*	*0.19*	*0.10*	*1.6*
Standard RU-1	*53*	*59*	*1.4*	*9*	*34*	*11*	*8*	*1.0*	*<0.1*	*17*	*1.2*	*0.8*	*5*	*<1*	*778*	*0.12*	*3.5*	*22.9*	*3.1*	*2.6*	*0.40*	*0.26*	*0.02*	*>10.0*
*Expected***															*1000*	*0.2*	*4.3*	***24.40***	*3.3*	*2.8*	*0.8*	*0.6*		***21.6***
OREAS45C	*934*	*252*	*23.1*	*13*	*160*	*59*	*26*	*4.1*	*1.4*	*49*	*10.1*	*2.2*	*15*	*<1*	*1111*	*1.05*	*6.9*	*17.5*	*0.2*	*0.5*	*0.10*	*0.34*	*0.05*	*<0.1*
OREAS45C	*925*	*239*	*22.9*	*12*	*173*	*58*	*25*	*4.2*	*1.5*	*52*	*10.7*	*2.3*	*15*	*<1*	*1113*	*1.11*	*7.2*	*18.5*	*0.3*	*0.5*	*0.10*	*0.34*	*0.05*	*<0.1*
*Expected***	*962*	*270*	*23.1*	*12.9*	*170*	*59.0*	*26.2*	*4.27*	*1.43*	*54*	*10.2*	*2.4*	*15.7*		*1160*	*1.131*	*7.59*	*18.33*	*0.25*	*0.48*	*0.097*	*0.36*	*0.051*	*0.02*

MINFILE prospects and showings

GNAT PASS (MINFILE 104I 001)

The Gnat Pass copper developed prospect is located immediately north to northeast of Lower Gnat Lake (Figure 3a), and comprises two different zones. The "hill zone" is about 1.1 km east of the lake outlet and was drilled in 1965 and 1989 (Smith and Garagan, 1990). Indicated reserves (non-NI 43-101 compliant) are 30.4 million tonnes grading 0.389 % copper, including 20 % dilution with wall rock grading 0.15 % copper (Lytton Minerals Ltd., 1972, reported in MINFILE 104I 001). The "creek zone" is exposed along the creek draining Lower Gnat Lake, about 750 m north of the lake outlet, and has not been drill tested.

Apart from minor outcrop at the hill zone and along Gnat Creek, very few exposures are present in the immediate area. Mapping conducted during this study indicates that the area is underlain by predominantly augite-phyric coherent rocks of the Triassic Stuhini Group. The augite-phyric rocks are cut at several locations by altered intrusive rocks. Where less altered, these intrusive rocks are plagioclase and sparsely quartz phyric, hornblende to hornblende-bearing diorites, quartz diorites and granodiorites, termed here the "Gnat Pass intrusive". These intrusive rocks are found both in the hill and creek zones, as well as one small outcrop along Highway 37. A preliminary U-Pb zircon crystallization age yields a date of *ca.* 217 Ma (this study). This age implies that these intrusive are part of the Late Triassic plutonic suite, and indicate a pre-217 Ma age for the augite-phyric coherent rocks. The Stuhini augite-phyric coherent rocks and associated intrusive rocks are overlain by a northeast dipping sequence of conglomerate, quartz-bearing feldspathic arenite and graphitic siltstone, as evident in the 1989 drill core (Smith and Garagan, 1990; this study). We have tentatively assigned these rocks to an Early (-Middle) Jurassic coarse grained quartz-rich sedimentary rock unit (lmJ S_{CQ}, Figure 3a). The contact between the Stuhini and siliciclastic rocks is generally brecciated (Smith and Garagan, 1990), however it is unclear whether this is caused by faulting, or a possible unconformable relationship exists. Assay results of 1989 drill core (Smith and Garagan, 1990) indicate that mineralization is mostly associated with the Stuhini Group and intrusive rocks; minor copper occurs in the brecciated contact zone, and only trace copper is present within the siliciclastic succession.

Silicification, tourmaline veining and Fe-carbonate cemented breccias are common in the hill zone. Here, chalcopyrite and pyrite range up to several percent, occur in disseminations or fracture fillings, and are also found within tourmaline veins and Fe-carbonate cement in brecciated zones. A grab sample from subcrop of quartz and plagioclase porphyritic granodiorite on the G-89-8 drill pad returned 0.7% Cu and slightly elevated Au and Mo (sample 11JLO32-319, Table 2). Several percent of pyrite associated with possible K-feldspar alteration is found just north of the creek zone, and pyrite associated with Fe-carbonate alteration is found in the small intrusion along Highway 37. Assay samples of altered intrusive rocks from both locations (11BVA09-48, 11BVA05-30) returned no significant mineralization.

DALVENIE (MINFILE 104I 003)

The Dalvenie gold-copper-silver prospect is located immediately west of the Gnat Lakes ultramafite (Figure 3a). The prospect was mapped, trenched and drilled in the 1960's. Results from the program indicated a 1146 m long mineralized shear zone (Dalvenie shear) with short intercepts of up to 1.5 m containing 4.8 g/tonne gold and 3.73% copper (Wetherill, 1990). The report describes a 10-15 m wide, steeply west dipping shear zone that separates the Gnat Lakes ultramafic body on the east from sedimentary and volcanic rocks on the west side of the fault zone. The shear zone contains abundant, weathered grey quartz; 5 cm wide zones of massive pyrite, chalcopyrite and arsenopyrite; disseminated pyrite and chalcopyrite; and is locally silicified (Wetherill, 1990). Bornite, hematite, siderite, barite, magnetite, pyrrhotite and sphalerite have also been reported (MINFILE 104I 003). A polymictic breccia zone was identified along the trace of the Dalvenie shear, and associated mineralization was sampled (Table 2). Two assay samples were taken about 2 m apart and show the highly variable metal content of the prospect. A sulphide rich sample (11BVA11-62b) returned values of 0.57 g/t Au, > 1% As, anomalous Sb and Bi and slightly elevated Cu and Ag. A intensely silicified and sericitized sample (11BVA11-62a) contained 535 ppm As as well as slightly elevated Sb, Bi and W.

BCR (MINFILE 104I 068)

The BCR copper-zinc-lead-molybdenum showing is located along the abandoned British Columbia railway grade, about 12.5 km south of Upper Gnat Lake (Figure 3a). It is hosted within biotite granites and quartz syenites belonging to the potassic phase of the Middle Jurassic Three Sisters pluton. The rocks contain chalcopyrite with minor sphalerite, galena and molybdenite in north trending sets of fractures, locally with argillic and quartz-sericite alteration envelopes (MINFILE 104I 068). Fifteen percussion holes with a total length of 437 m were drilled along the British Columbia railway grade and drill roads marked 'BCR' on Figure 3a. Samples from drill core returned low copper (<112 ppm) and zinc (<81 ppm; Dircks, 1974). The few outcrops along the British Columbia railroad grade within 1 to 2.5 km north and 1 km south of the drilled area are intensely iron oxide stained and contain several percent disseminated and fracture-hosted pyrite (this study; marked on Figure 3a). Salmon pink K-feldspar alteration developed along epidote-filled fractures is common within the plutonic rocks of the Gnat Pass area, and locally increases in intensity south of the BCR showing. Despite discouraging

drill results, the large alteration footprint of this showing warrants additional investigation.

PAT (MINFILE 104I 043)

The Pat copper-molybdenum showing is centred around a drift covered valley north of peak 2196 m (Figure 3c). In addition to copper ± molybdenum soil anomalies, several small mineralized outcrops have been described to the south and southeast of the valley (Sadlier-Brown and Chisholm, 1971; Sadlier-Brown and Nevin, 1977). The mineralization reported by these authors comprises disseminations and siliceous veins carrying chalcopyrite and/or molybdenite. In one outcrop, mineralization is characterized by 1-10 mm pyrite±copper sulphide veins with silicified haloes. An assay sample from this location returned 0.3% Cu and slightly elevated Au and Ag (11BVA13-74 in Table 2). The veins are hosted by biotite-hornblende quartz monzonite and quartz monzodiorite, most likely related to the Cake Hill pluton. Biotite quartz monzonite and quartz monzodiorite, interpreted as the central felsic phase of the Three Sisters pluton, is exposed 100 m to the northeast of this mineral occurrence (Figure 3c).

MAT (MINFILE 104I 034)

The Mat copper-lead-zinc showings are located in a deeply incised forested valley system on the southern margin of the Cake Hill pluton, several kilometres north of the Stikine River (Figures 1, 3f). The area south and southwest of the showing is part of the Stikine River Provincial Park. Poorly exposed fine grained, stratified sedimentary rocks are found in the valleys and are overlain by more competent augite-phyric coherent rocks exposed at topographically higher levels (Figure 3f). Both the sedimentary and volcanic rocks, as well as surrounding foliated hornblende diorites and gabbros, ultramafic rocks and hornblende quartz monzonites, have been reported to host copper, lead and/or zinc sulphide occurrences (McAusland, 1971). In addition, a soil survey (McAusland, 1971) indicated moderately elevated values of nickel (>300 ppm) over part of the survey area, likely related to occurrences of ultramafic rocks. We identified several sulphide occurrences in the fine grained sedimentary rocks, and one within the Cake Hill pluton (see "Mat north" new mineral occurrence). The mineralization within the sedimentary rocks occurs in laminated to very thinly bedded siltstones to medium-grained sandstones, and forms stratiform and more irregular-shaped bodies up to 20 m wide. The sulphides occur as fine to very fine grained disseminations, stratiform horizons and/or within veinlets. Silicification and/or quartz-pyrite veins occur locally. No copper oxides, copper sulphides, galena or sphalerite were observed, possibly due to their very fine grain size. Two assay samples returned no significant metal values (11BVA26-184, 187 in Table 2).

New mineral occurrences

Eight new mineralized and/or alteration zones were discovered within the Hotailuh batholith. Mineralized samples were collected and submitted for base and precious metal assay analysis. Pending further petrographic work, the locations have been described as 'mineral occurrences' rather than 'showings'.

TRIASSIC OCCURRENCES

Four of the new zones are hosted in probable Late Triassic rocks, and include the "Upper Gnat Creek", "Mat north", "Gnat Lakes ultramafite" and "Three Sisters south" mineral occurrences.

The "Upper Gnat Creek" occurrence is located 1.5 km south of Upper Gnat Lake, on a brush and forest-covered ridge about 750 m east of the British Columbia railroad grade. The occurrence comprises a 1-10 cm wide vein of massive sulphides (locally widening to a 20 by 20 cm pod) with associated copper oxide staining, within well-foliated Cake Hill plutonic rocks. The wider mineralized zone is associated with brecciated wallrocks (Figure 9). An assay sample of the massive sulphide breccia returned significant results of 1.7 g/t Au, 82 g/t Ag, >1 % Cu and 483 ppm Bi (11BVA02-12a in Table 2). An outcrop containing copper sulphide-bearing veinlets was found in the same hostrock about 140 m further southeast along the ridge.

The "Mat north" mineral occurrence is found on the east face of an alpine ridge, a couple of kilometres north of the Mat showing. It is hosted by the Late Triassic Cake Hill pluton, and comprises decimetre-size pods containing about 5% disseminated sulphides (pyrite, possible bornite; chrysocolla and malachite staining common). One assay sample returned >1% Cu and slightly elevated Ag, Au and Bi (11BVA25-172 in Table 2). Abundant coarse grained euhedral biotite immediately surrounds the mineralized pods, but is absent further away in the plutonic rocks. The occurrence might be similar to one described by McAusland (1971) where bornite is found in epidote stringers within the Cake Hill pluton.

The "Gnat Lakes ultramafite" occurrences occur within, or immediately surrounding, the Gnat Lakes ultramafite. They are spatially associated with significant topographic lineaments, interpreted as faults, and might be genetically linked to the Dalvenie prospect. Subcrop of intensely silicified and sericite (?) altered, fine grained Stuhini sedimentary rocks contains several percent disseminated pyrite and occurs along strike of a topographic lineament (sample 11BVA11-57 in Table 2). Several ultramafic outcrops contain disseminated pyrite, either directly within ultramafic rocks or associated with later crosscutting felsic dikes (samples 11BVA11-59 and 58b, respectively). Only one of three samples assayed (11BVA11-59 in Table 2) returned slightly elevated copper values. In addition, the easternmost exposures of the ultramafic body contain several percent sulphides and are associated with another north trending topographic

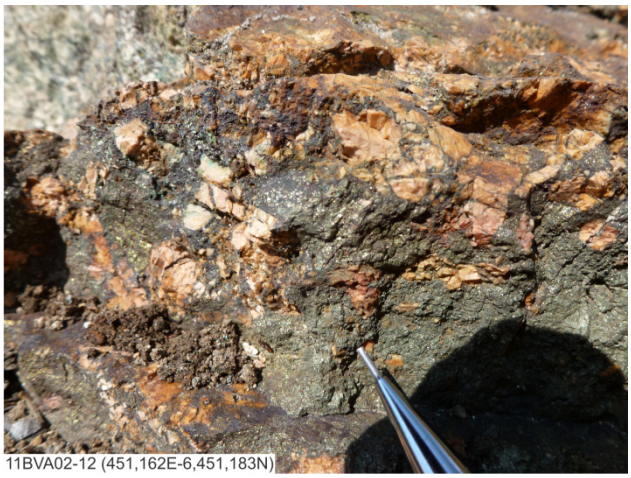

Figure 9. Mineralization at "Upper Gnat Creek". Intensely pink-orange altered and brecciated plutonic rock clasts within massive sulphide matrix. Pencil for scale.

lineament, believed to be the southern extension of the Gnat Pass fault.

The "Three Sisters south" mineral occurrence is hosted in a kilometre size Stuhini inclusion within the leucocratic Cake Hill pluton (LT CHL in Table 1, Figure 3g). Mineralization consists of several zones with 1-5% pyrite disseminated and in veinlets, locally associated with green actinolite. The linear and recessive nature of the gullies suggests that the ≤20 m-wide pyritic zones represent north-northwest to northeast striking subvertical faults cutting the Stuhini succession. One of two assay samples (11BVA33-257 in Table 2) returned 0.3% Cu, 0.03% Mo and slightly elevated W.

THREE SISTERS OCCURRENCES

The remaining four new zones, the "Pat west", "Three Sisters", "Three Sisters north", and "BCR north" mineral occurrences, are hosted in Middle Jurassic (and/or Early Cretaceous?) intrusive rocks of the Three Sisters pluton.

The "Pat west" occurrences are subvertical, roughly east to northeast-trending zones hosted in the Three Sisters pluton, and are spread over the entire local map area (Figure 3b). A one metre wide zone exposed on the easternmost ridge contains quartz+pyrite±copper sulphide veins hosted in biotite quartz monzonite and quartz monzodiorite of the central felsic phase, and returned assay values of 0.7% Cu (11BVA14-82). The mineralized central and western gossanous exposures are larger in aerial extent (30-50 m wide, ≥200-300 m long), contain disseminated pyrite and/or quartz + pyrite veins, and lack copper sulphides. An assay from the latter location (11BVA15-90) did not return any anomalous values.

The "Three Sisters" occurrences are named after the group of peaks on which the fine grained mafic phase of the Three Sisters pluton is exposed (Figure 3g). They are found within the northern margin of the fine grained mafic phase, and within the adjacent central felsic phase and leucocratic Cake Hill pluton. A brown-orange weathering zone, up to 200 m wide and 2 km long, is exposed within the Three Sisters central felsic phase close to contact with the fine grained mafic phase (Figure 10). The zone contains abundant west-northwest striking and steeply north dipping goethite-coated fractures after pyrite, and pyrite is also disseminated throughout the hostrock. Three small exposures with quartz+pyrite±chalcopyrite±epidote veins, locally associated with in situ brecciation, are found several hundred metres to the south and southwest of this zone and are hosted in the fine grained mafic phase. One assay sample from the latter location (11BVA32-241) returned 0.35% Cu and slightly elevated Au. An assay sample from the gossanous pyrite zone (11BVA32-246) returned no anomalous values.

The "Three Sisters north" occurrence is hosted within the Three Sisters central felsic phase. The rocks are intensely veined (roughly 5% veins by volume in a several metre wide interval), with one 10 cm wide east-southeast oriented, steeply north dipping, epidote+actinolite+sulphide vein. The assay results for this vein indicate 0.36% Cu, >200 ppm W and slightly elevated U (11BVA30-216 in Table 2).

The "BCR north" occurrence is situated on the British Columbia railroad grade 7 km south of Upper Gnat Lake. It is associated with irregular bodies of (potassic?) altered hornblende-feldspar porphyry (Tees Creek intrusive, see Table 1) intruding the Three Sisters potassic phase. Minor pyrite is evident in this location, disseminated in both the fringes of the Tees Creek and adjacent potassic phase intrusive.

DISCUSSION AND CONCLUSIONS

Geological units

The Hotailuh batholith comprises a number of different plutons and plutonic phases. It can be subdivided into three plutonic suites, the Late Triassic (*ca.* 222-226 Ma), Early Jurassic (*ca.* 184-190 Ma) and a Middle Jurassic–Early Cretaceous suite (*ca.* 165-171 Ma and *ca.* 117 Ma, respectively).

The Late Triassic plutonic suite comprises, in decreasing age, the Gnat Lake ultramafic to mafic bodies, Cake Hill felsic pluton and Beggerlay Creek ultramafic to mafic pluton. Similar mineralogy, texture, compositional variation and magnetic susceptibility may indicate a genetic link between the Gnat Lake and Beggerlay Creek plutons. Limited evidence of crosscutting relationships suggest that the Gnat Lake ultramafite is older than the Cake Hill pluton, and earlier studies by Anderson (1983) suggest that the Beggerlay Creek pluton is younger than the Cake Hill pluton. However, demonstrable crosscutting relationships are rare, and perhaps all Late Triassic mafic–ultramafic plutonic rocks are roughly age equivalent. The Late Triassic plutonic suite is spatially associated with, and in places intrudes, poorly exposed and poorly dated, intermediate-mafic volcanic and

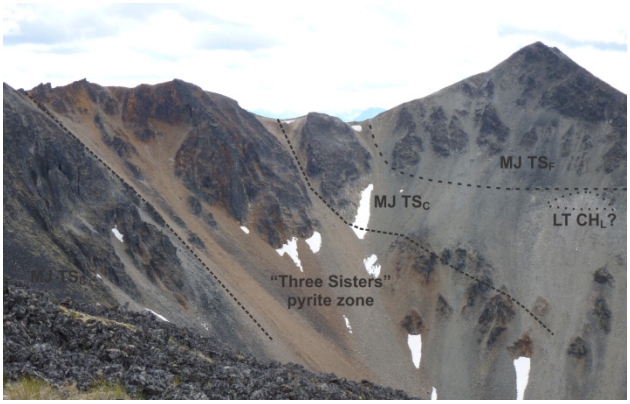

Figure 10. View south towards westernmost peak hosting the Three Sisters fine grained mafic phase, showing orange-brown altered zone of the "Three Sisters" mineral occurrence. Zone is intensely goethite-stained, contains abundant disseminated pyrite and pyrite in steeply dipping, west-northwest striking fractures. The Three Sisters central felsic phase (TS_C) is exposed along the ridge in the foreground; the Three Sisters fine grained mafic phase (TS_F) is exposed on the right-hand peak. Light-coloured scree below this peak may be an inclusion of the Cake Hill leucocratic phase (CH_L).

sedimentary rocks of the Triassic Stuhini Group.

The Early Jurassic plutonic suite comprises the McBride River felsic pluton exposed on the easternmost edge of the batholith. An area within the eastern part of the batholith has been reinterpreted as a large apophysis of the McBride River pluton. The pluton has contact metamorphosed Lower Jurassic, fine grained, stratified sedimentary rocks.

The Three Sisters pluton comprises at least four phases, namely the early fine grained mafic phase, a subsequent mafic phase, central felsic phase, and a crosscutting potassic phase. Preliminary U-Pb zircon crystallization ages confirm the Middle Jurassic age for the coarse grained Three Sisters potassic phase. However, an Early Cretaceous age for the Three Sisters central felsic phase raises the possibility that part or all of this pluton is much younger than previously recognized.

Northwest of Lower Gnat Lake, a granitoid clast-bearing conglomerate nonconformably overlies the Cake Hill pluton, and is correlated with Lower(-Middle) Jurassic, quartz-bearing, coarse grained sedimentary rocks reported within the immediate area. The latter are overlain by rocks previously assigned to the Triassic Stuhini Group (Anderson, 1983; Gabrielse, 1998) that in light of new U-Pb detrital zircon data are reinterpreted here as Middle Jurassic sedimentary and volcanic rocks (Iverson *et al.*, this volume). Evidence for the presence of the Hotailuh thrust in the present study areas appears to be lacking. The Lower to Middle Jurassic sedimentary and volcanic successions studied herein (Figures 3a, h) are part of a belt of rocks exposed on the north and northeastern margin of the batholith. The Lower Jurassic rocks have previously been assigned to the Takwahoni Formation, a formation predominantly composed of greywacke, siltstone, shale, conglomerate and minor limestone exposed in the footwall of the King Salmon thrust fault (Gabrielse, 1998). However, another important Lower to Middle Jurassic unit in Stikinia is the Hazelton Group, a succession of volcanic and sedimentary rocks. Following definitions by Marsden and Thorkelson (1992), and in light of the new U-Pb detrital zircon dates (Iverson *et al.*, this volume), the entire succession of volcanic and sedimentary rocks around peak 2096 m (Figure 3a) is reassigned to the Hazelton Group. In addition, the entire belt of rocks along the north and northeastern margin of the batholith may be part of the Hazelton Group.

Mineralization

The Gnat Pass area appears especially well endowed with mineral occurrences. In addition to the mineral occurrences described here, many other showings are present just outside of the map area shown in Figure 3a (*e.g.* Louise (MINFILE 104I 054), Bell (MINFILE 104I 033), Moss (MINFILE 104I 029), Kay 19, 49 (MINFILE 104I 037, 026), and Crown (MINFILE 104I 046). The latter three comprise the Pliny project that is currently under exploration by West Cirque Resources (2011). The area is cut by the north-northwest trending Gnat Pass ductile shear zone/brittle fault. The shear zone likely formed during emplacement of the Cake Hill pluton in the Late Triassic, was the locus of subsequent brittle faulting (this study), and may have been reactivated during south-verging thrusting in the Middle Jurassic (*e.g.* Gabrielse, 1998). These structures likely played an important role in the introduction of magmas, fluids and associated mineralization in the Gnat Pass corridor.

Mineralization hosted in Late Triassic rocks varies widely in hostrock, metal tenor and mineralization style and comprises:

- Cu only at the Gnat Pass porphyry-style prospect;
- Au+As±Sb (Cu, Ag reported) hosted in a shear/fault zone at the Dalvenie prospect;
- Au+Cu+Ag massive sulphide vein in felsic plutonic rocks at the newly discovered "Upper Gnat Creek" mineral occurrence;
- Cu±Mo pyritic fault zones in Stuhini volcanics at "Three Sisters south";
- Cu with trace Ag as small bodies within the Cake Hill pluton at "Mat north";
- Cu+Pb+Zn (reported) within stratiform to irregular bodies at the Mat showing; and
- Cu (and Mo reported) at the vein-hosted Pat showing, found within the Late Triassic Cake Hill pluton, but closely associated with the Three Sisters pluton.

Mineralization hosted in the Three Sisters pluton appears less variable, and comprises:

- Cu only at the "Pat west" and "Three Sisters" mineral occurrences;

- Cu±W at the "Three Sisters north" mineral occurrence; and
- Cu+Zn+Pb+Mo reported at the BCR showing.

Possible metal zonation is present in both the "Pat west" and "Three Sisters" occurrences, with relatively large, gossanous, pyrite-dominated zones trending towards smaller quartz vein-hosted, pyrite+copper sulphide occurrences. Assay samples indicate 0.3-0.7% Cu in the copper sulphide-bearing zones, and Cu±W in the possibly related "Three Sisters north" occurrence.

The presence of mineralization in both the Late Triassic rocks and the Three Sisters Middle Jurassic (-Early Cretaceous?) pluton is suggestive of at least two mineralizing events within the Hotailuh batholith. Known intrusion-related mineral deposits in the northern Stikine tectonic terrane are predominantly of Late Triassic to Early Jurassic age (*e.g.* Red Chris, Galore, Shaft, GJ, KSM), and little to no Middle Jurassic to Early Cretaceous deposits have been recognized. Importantly, the presence of mineral showings and occurrences hosted in the Three Sisters pluton suggests that these younger intrusions might deserve more attention than previously received.

FUTURE WORK

The subsequent stage of the QUEST-Northwest Hotailuh project will focus on the petrology and geochemistry of intrusive phases within the batholith using feldspar staining techniques, thin section study and lithogeochemistry data of least altered samples. Additional study of mineralized and/or altered samples will include transmission and reflective light studies of thin sections. Five rock samples have been submitted for ^{40}Ar-^{39}Ar hornblende and biotite geochronology; results are pending. The digital geological dataset will be integrated with the QUEST-Northwest airborne geophysical survey and regional geochemical stream sediment survey. The combined results will allow for the development of a metallogenic framework relating mineralization and magmatism, and be used to indicate anomalous areas of potential interest for mineral exploration.

ACKNOWLEDGMENTS

We would like to acknowledge financial support from Geoscience BC that covered field, analytical and salary costs associated with the Hotailuh project. Travis McCarron, Catie Young, Meagan Hogg and Olivia Iverson are thanked for their capable assistance during the field season. A warm thanks to Patricia McIntosh for opening her home for our use during the summer mapping project, to Jan Anderson and Dempsey Callison for the cooking, logistical support and help in setting up camp, and to Pacific Western Helicopters for safe flying and efficient communication. Thanks also to Bob Anderson for sharing his knowledge of the Hotailuh batholith during discussions and Graham Nixon for a thorough review of this paper.

REFERENCES

Anderson, R.G. (1983): Geology of the Hotailuh batholith and surrounding volcanic and sedimentary rocks, north-central British Columbia; *Carleton University*, Ottawa, Canada, unpublished Ph.D. dissertation, 669 pages.

Anderson, R.G. and Bevier, M.L. (1992): New Late Triassic and Early Jurassic U-Pb zircon ages from the Hotailuh batholith, Cry Lake map area, north-central British Columbia; in Radiogenic Age and Isotope Studies (Report 6); *Geological Survey of Canada*, Paper 92-2, pages 145-152.

Asbury, D.W. (1967): Report of geological, magnetometer and geochemical soil surveys on Moss claims 53 to 71, Gnat Lake, B.C.; *BC Ministry of Energy, Mines and Petroleum Resources*, Assessment Report 1106, 10 pages.

Ash, C.H., Macdonald, R.W.J. and Friedman, R.M. (1997): Stratigraphy of the Tatogga Lake area, northwestern British Columbia (104H/12&13, 104G/9&16); *BC Ministry of Energy, Mines and Petroleum Resources*, Geological Fieldwork 1996, Paper 1997-1, pages 283-290.

Bartsch, R.D. (1993): Volcanic stratigraphy and lithochemistry of the Lower Jurassic Hazelton Group, host to the Eskay Creek precious and base metal volcanogenic deposit; *The University of British Columbia*, Vancouver, Canada, unpublished M.Sc. thesis, 124 pages.

Blundy, J.D. and Sparks, R.S.J. (1992): Petrogenesis of mafic inclusions in granitoids of the Adamello Massif, Italy; *Journal of Petrology*, Volume 33 (5), pages 1039-1104.

Currie, L.D. and Parrish, R.R. (1997): Paleozoic and Mesozoic rocks of Stikinia exposed in northwestern British Columbia: Implications for correlations in the northern Cordillera; *Geological Society of America Bulletin*, Volume 107 (11), pages 1402-1420.

Dircks, N.J. (1974): Percussion drilling report for Railway property 104I/4W; *BC Ministry of Energy, Mines and Petroleum Resources*, Assessment Report 5298, 24 pages.

Duuring, P., Rowins, S.M., McKinley, B.S.M., Dickinson, J.M., Diakow, L.J., Kim, Y.-S. and Creaser, R.A. (2009): Magmatic and structural controls on porphyry-style Cu-Au-Mo mineralization at Kemess South, Toodoggone District of British Columbia, Canada; *Mineralium Deposita*, Volume 44, pages 435-462.

English, J.M. and Johnston, S.T. (2005): Collisional orogenesis in the northern Canadian Cordillera: Implications for Cordilleran crustal structure, ophiolite emplacement, continental growth, and the terrane hypothesis; *Earth and Planetary Science Letters*, Volume 232, pages 333-344.

Evenchick, C.A. and Thorkelson, D.J. (2005): Geology of the Spatsizi River map area, north-central British Columbia; *Geological Survey of Canada*, Bulletin 577, 189 pages.

Evenchick, C.A., Gabrielse, H. and Snyder, D. (2005): Crustal structure and lithology of the northern Canadian Cordillera: alternative interpretations of SNORCLE seismic reflection lines 21 and 2b; *Canadian Journal of Earth Sciences*, Volume 42, pages 1149-1161.

Faye, G.H., Bowman, W.S. and Sutarno, R. (1977): Zinc-copper ore RU-1: Its characterization and preparation for use as a

certified reference material; *Ministry of Energy, Mines and Resources Canada*, Canada Centre for Mineral and Energy Technology Report 77-7, 18 pages.

Gabrielse, H. (1991): Late Paleozoic and Mesozoic terrane interactions in north-central British Columbia; Canadian *Journal of Earth Sciences*, Volume 28, pages 947-957.

Gabrielse, H. (1998): Geology of Cry Lake and Dease Lake map areas, north-central British Columbia; *Geological Survey of Canada*, Bulletin 504, 118 pages.

Gillespie, M.R. and Styles, M.T. (1999): Classification of igneous rocks; *British Geological Survey*, BGS Rock Classification Scheme, Volume 1, Research Report RR 99-06, 52 pages.

Hallsworth, C.R. and Knox, R.W.O'B. (1999): Classification of sediments and sedimentary rocks; *British Geological Survey*, BGS Rock Classification Scheme, Volume 3, Research Report RR 99-03, 44 pages.

Henderson, C.M. and Perry, D.G. (1981): A Lower Jurassic heteroporid bryozoan and associated biota, Turnagain Lake, British Columbia; *Canadian Journal of Earth Sciences*, Volume 18, pages 457-468.

International Commission on Stratigraphy (2010): International stratigraphic chart; Available online at http://www.stratigraphy.org/ics%20chart/09_2010/StratChart2010.pdf

Iverson, O., Mahoney, J.B. and Logan, J.M. (this volume): Dease Lake Geoscience Project, Part IV: Tsaybahe Group: lithological and geochemical characterization of Middle Triassic volcanism in the Stikine Arch, North-central British Columbia; *BC Ministry of Energy and Mines*, Geological Fieldwork 2011, Paper 2012-1.

Jackaman, W. (2012): QUEST-Northwest Project: new regional geochemical survey and sample reanalysis data (NTS 104F,G,H,I,J), northern British Columbia; *Geoscience BC*, Summary of Activities 2011, Report 2012-1.

Kretz, R. (1983): Symbols for rock-forming minerals; *American Mineralogist*, Volume 68, pages 277-279.

Logan, J.M., Drobe, J.R. and McClelland, W.C. (2000): Geology of the Forrest Kerr-Mess Creek area, northwestern British Columbia (NTS 104B/10, 15 & 104G/2 & 7W); *BC Ministry of Energy and Mines*, Bulletin 104, 132 pages.

Logan, J.M., Diakow, L.J., van Straaten, B.I., Moynihan, D.P. and Iverson, O. (2012): QUEST-Northwest Mapping, BC Geological Survey Dease Lake Geoscience Project, northern British Columbia; *Geoscience BC*, Summary of Activities 2011, Report 2012-1.

Logan, J.M., Moynihan, D.P. and Diakow, L.J. (this volume): Dease Lake Geoscience Project, Part I: Geology and mineralization of the Dease Lake (104J/8) and east-half of the Little Tuya River (104J/7E) map sheets, northern British Columbia; *BC Ministry of Energy and Mines*, Geological Fieldwork 2011, Report 2012-1.

Marsden, H. and Thorkelson, D.J. (1992): Geology of the Hazelton volcanic belt in British Columbia: Implications for the Early to Middle Jurassic evolution of Stikinia; *Tectonics*, Volume 11 (6), pages 1266-1287.

Massey, N.W.D., Alldrick, D.J. and Lefebure, D.V. (1999): Potential for subaqueous hot-spring (Eskay Creek) deposits in British Columbia; *BC Ministry of Energy and Mines*, Open File Report 1999-14, 54 pages.

Massey, N.W.D., Macintyre, D.G., Desjardins, P.J. and Cooney, R.T. (2005): Digital geology map of British Columbia: Whole Province; *BC Ministry of Energy, Mines and Petroleum Resources*, Geofile 2005-1.

McAusland, J.H. (1971): Combined geochemical, geophysical, and geological report on mineral claims Mat 1 to Mat 26 inclusive; *BC Ministry of Energy, Mines and Petroleum Resources*, Assessment Report 3028, 9 pages.

Moynihan, D.P. and Logan, J.M. (this volume): Dease Lake Geoscience Project, Part III: Age, emplacement and mineralization of the Cretaceous Snow peak pluton; *BC Ministry of Energy and Mines*, Geological Fieldwork 2011, Report 2012-1.

Nelson, J. and Mihalynuk, M. (1993): Cache Creek ocean: Closure or enclosure?; *Geology*, Volume 21, pages 173-176.

Nixon, G.T., Ash, C.H., Connelly, J.N. and Case, G. (1989): Alaskan-type mafic-ultramafic rocks in British Columbia: The Gnat Lakes, Hickman, and Menard Creek complexes; *BC Ministry of Energy, Mines and Petroleum Resources*, Geological Fieldwork 1988, Paper 1989-1, pages 429-442.

Nixon, G.T., Hammack, J.L, Ash, C.H., Cabri, L.J., Case, G., Connelly, J.N., Heaman, L.M., Laflamme, J.H.G., Nuttall, C., Paterson, W.P.E. and Wong, R.H. (1997): Geology and platinum-group-element mineralization of Alaskan-type ultramafic-mafic complexes in British Columbia; *BC Ministry of Energy and Mines*, Bulletin 93, 132 pages.

Norris, J.R., Hart, C.J.R., Tosdal, R.M. and Rees, C. (2011): Magmatic evolution, mineralization and alteration of the Red Chris copper-gold porphyry deposit, northwestern British Columbia (NTS 104H/12W); *Geoscience BC*, Summary of Activities 2010, Report 2011-1, pages 33-44.

Read, P.B. (1983): Geology, Classy Creek (104J/2E) and Stikine Canyon (104J/1W), British Columbia; *Geological Survey of Canada*, Open File Map 940.

Read, P.B. (1984): Geology, Klastine River (104G/16E), Ealue Lake (104H/13W), Cake Hill (104I/4W) and Stikine Canyon (104J/1E), British Columbia; *Geological Survey of Canada*, Open File Map 1080.

Read, P.B. and Psutka, J.F. (1990): Geology, Ealue Lake east-half (104H/13E) and Cullivan Creek (104H/14) map areas, British Columbia; *Geological Survey of Canada*, Open File Map 2241.

Ricketts, B.D., Evenchick, C.A., Anderson, R.G. and Murphy, D.C. (1992): Bowser basin, northern British Columbia: Constraints on the timing of initial subsidence and Stikina-North America terrane interactions; *Geology*, Volume 20, pages 1119-1122.

Sadlier-Brown, T.L. and Chisholm, E.O. (1971): A geochemical report on the Pat claims (1 to 24); *BC Ministry of Energy, Mines and Petroleum Resources*, Assessment Report 3963, 6 pages.

Sadlier-Brown, T.L. and Nevin, A.E. (1977): A report on geochemical and geophysical surveys of the Mac group; *BC Ministry of Energy, Mines and Petroleum Resources*, Assessment Report 6323, 33 pages.

Schiarizza, P. (2011): Geology of the Kutcho assemblage between Kutcho Creek and the Tucho River, northern British Columbia (NTS 104I/01); *BC Ministry of Energy and Mines*, Geological Fieldwork 2010, Paper 2011-1, pages 99-118.

Simpson, K.A. (2012): QUEST-Northwest: Geoscience BC's new minerals project in northwest British Columbia (104G, 104J, parts of NTS 104A,B,F,H,I,K, 103O,P); *Geoscience BC*, Summary of Activities 2011, Report 2012-1.

Smith, G. and Garagan, T. (1990): Summary report on the 1989 exploration program on the Gnat Pass property; *BC Ministry of Energy, Mines and Petroleum Resources*, Assessment Report 20408, 156 pages.

West Cirque Resources Ltd. (2011); West Cirque discovers new copper-gold zone; stakes Pliny property; *West Cirque Resources*, Press Release, Aug. 11, 2011.

Wetherill, J.F. (1989): Geological report on the Pass 40 claim; *BC Ministry of Energy, Mines and Petroleum Resources*, Assessment Report 19177, 23 pages.

Wetherill, J.F. (1990): Geological, geochemical and geophysical report on the Gnat Pass property; Equity Silver Mines Limited, *BC Ministry of Energy, Mines and Petroleum Resources*, Assessment Report 19885, 176 pages

Woodsworth, G.J., Anderson, R.G. and Armstrong, R.L. (1991): Plutonic regimes; in Geology of the Cordilleran Orogen in Canada, Gabrielse, H. and Yorath, C.J. (eds.); *Geological Survey of Canada*, Geology of Canada, no. 4, pages 491-531.

Zagorevski, A., Joyce, N., Mihalynuk, M. and Logan, J. (2011): Regional U/Pb zircon and Ar/Ar geochronology of Carboniferous to Early Jurassic Stikinia; *AME BC Mineral Exploration Roundup*, January 2011, poster presentation.

Geochemical Characteristics of Mississippian to Pliensbachian Volcanic and Hypabyssal Rocks in the Hoodoo Mountain Area (NTS 104B/14E)

by A. Zagorevski[1], M.G. Mihalynuk[2] and J.M. Logan[2]

KEYWORDS: Hoodoo Mountain, Andrei Icefield, Andrei Glacier, Stikine assemblage, Stuhini Group, Hazelton Group, Iskut River, Twin Glacier River, whole-rock geochemistry

INTRODUCTION

Carboniferous to Jurassic rocks of the northwestern Stikinia commonly comprise thick successions of petrographically similar sedimentary, volcaniclastic and consanguineous hypabyssal rocks. The similarity of these sequences leads to ambiguity in correlations of units, hampering the establishment of a consistent stratigraphic framework in the predominantly ice and snow-covered Hoodoo Mountain area (NTS 104B/14; Figure 1). In addition, this part of Stikinia contains economically important, diverse and epoch specific metallotects that include; Carboniferous Kuroko type VHMS, Triassic Besshi type VMS, Triassic and Jurassic calcalkaline and alkaline Cu-Au-Ag±Mo porphyry, skarn and vein deposits and Jurassic submarine exhalative Au-Ag-rich VMS mineralization. The majority of these deposits are either stratabound or directly related to short-lived magmatic events making stratigraphic position a critical factor in understanding which deposit types are likely to be present. The purpose of this contribution is to test the utility of whole rock geochemistry to discriminate and calibrate the Mississippian to Pliensbachian stratigraphy proposed by Mihalynuk *et al.* (2011a; 2011b), thereby providing a means of directing cost effective and successful mineral exploration throughout the varied stratigraphy of the area.

REGIONAL STRATIGRAPHY

The Hoodoo Mountain area (NTS 104/14E; Figure 1) is underlain by rocks characteristic of northwestern Stikinia (Stikine terrane). In the adjacent areas, Stikinia comprises well-stratified, middle Paleozoic to early Mesozoic sedimentary, volcanic and plutonic rocks. The Early Devonian to Permian Paleozoic Stikine assemblage

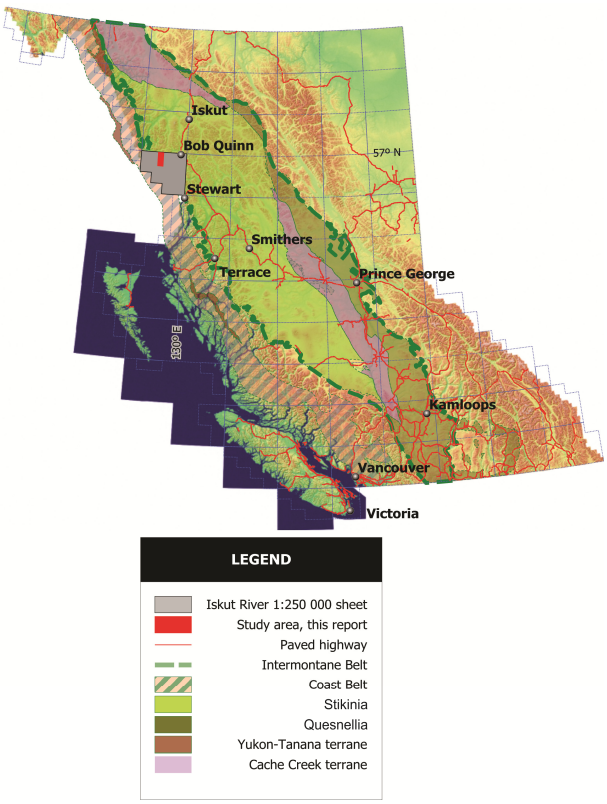

Figure 1. Location of the Iskut study area (red) shown within NTS 104B map sheet (grey), near the boundary of the Coast Belt and western Stikine terrane.

and Late Triassic Stuhini Group are overlain by the Early Jurassic Hazelton Group (Monger, 1977; Anderson, 1993; Logan *et al.*, 2000). In the Forrest Kerr area, the Stikine assemblage contains Lower to Middle Devonian strata (Read *et al.*, 1989), whereas equivalent rocks are unknown in the Hoodoo Mountain area. Both Carboniferous and Permian portions of the Stikine assemblage are characterized in part by carbonate units. The Carboniferous bimodal, volcano-sedimentary rocks are typically separated by a mid-Carboniferous carbonate that is characterized by locally abundant large crinoid columnals (Logan *et al.*, 2000). Up section, the Permian Stikine assemblage in the Hoodoo Mountain area is characterized by predominantly massive to bedded carbonate and chert layers, containing large and abundant rugosan horn corals and, locally, packstone with giant foraminifera. This contrasts with adjacent areas, where

[1] *Geological Survey of Canada, Ottawa, ON*
[2] *British Columbia Geological Survey, Victoria, BC*

This publication is also available, free of charge, as colour digital files in Adobe Acrobat® PDF format from the BC Ministry of Energy and Mines website at http://www.empr.gov.bc.ca/Mining/Geoscience/PublicationsCatalogue/Fieldwork.

volcaniclastic rocks are observed within the Permian section (Brown *et al.*, 1996; Logan *et al.*, 2000).

The Late Triassic Stuhini Group unconformably overlies the Stikine assemblage (Logan *et al.*, 2000), although this contact has not been directly observed in the eastern Hoodoo Mountain area. Stuhini Group strata can be broadly divided into two packages. The lower Stuhini Group strata are characterized by basinal shale, limestone and epiclastic volcanic rocks that grade into and are overlain by volcanic and conglomeratic rocks of the upper Stuhini Group. The upper Stuhini Group characteristically contains augite and feldspar porphyritic volcanic rocks, and polymictic conglomerate containing volcanic and plutonic derived clasts. A distinctive brown and orange-weathering, coarse biotite and K-feldspar-phyric tuff and volcanogenic conglomerate is also believed to be Late Triassic (Norian) on the basis of dated subvolcanic intrusions (Newmount Lake property: Romios Gold Resources Inc., 2008) and correlation with similar rocks in the Galore Creek area (Logan and Koyanagi, 1994).

The Early to Middle Jurassic Hazelton Group overlies Stuhini Group strata above an angular unconformity (Henderson *et al.*, 1992; Brown *et al.*, 1996). McDonald *et al.* (1996) simplified the stratigraphy of the Hazelton Group in the Iskut area into lower (Early Jurassic) and upper (Early to Middle Jurassic) sequences. The lower sequence of the Hazelton Group includes a basal coarse clastic unit, overlain by andesitic to rhyolitic volcanic rocks that in turn are overlain by turbiditic siliclastic rocks. The age of the lower sequence is constrained by Hettangian to Upper Aalenian fossil collections and *ca.* 194-186 Ma U/Pb zircon ages (Macdonald *et al.*, 1996). The upper sequence is dominated by *ca.* 181-173 Ma (Childe *et al.*, 1994) bimodal volcanic rocks that occupy the Eskay rift of Alldrick *et al.* (2005) and Aalenian to Bajocian (?) fossil collections (Nadaraju, 1993). The age overlap between lower and the upper sequences reflects the regional continuity of the medial sedimentary unit and the discontinuous and diachronous nature of the upper rift volcanic sequence.

ANALYTICAL METHODS

Forty-four representative volcanic, epiclastic and intrusive samples were collected across the study area (Figure 2). Very few suitable lithologies were identified in the Jurassic section and as such, the Hazelton Group is underrepresented. Whole rock geochemistry samples of altered and non-altered rocks were screened to ensure internal homogeneity. The samples were trimmed with a diamond saw to remove veins and to minimize weathering. Major and trace elements were analyzed at Acme Laboratories using ICP-ES and ICP-MS following lithium metaborate/tetraborate fusion and nitric acid digestion (analytical code 4A4B). A summary of results is presented in Table 1. Full analytical dataset and background information is presented in Zagorevski *et al.* (2011a).

GEOCHEMICAL SUITE DESCRIPTION AND RESULTS

Mississippian Stikine assemblage

Felsic volcanic rocks

The rhyolitic rocks comprise several volcanic types including massive flows, columnar jointed flows, tuff breccia and lapilli tuff. Lapilli tuff commonly contains altered tube pumice (Figure 3a) and flow-banded clasts. The rhyolite samples are quartz and feldspar glomeroporphyritic and contain abundant glass. U-Pb dating of two samples of rhyolite yielded *ca.* 340 Ma crystallization ages (Zagorevski *et al.*, 2012). Rhyolite is locally associated with jasperite and barite exhalite horizons that host finely laminated chalcopyrite mineralization (Mihalynuk *et al.*, 2011b).

Felsic volcanic rocks plot in the rhyolite and dacite fields on rock type discrimination plot (Figures 4a, b). They are characterized by light rare earth (LREE) and Th enrichment, and depletion of Nb on normal mid-ocean ridge basalt (N-MORB) normalized extended trace element plots (Figure 5a). They plot in volcanic arc field on tectonic discrimination plot (Figure 4c). The trace element profiles closely resemble other Early to Middle Carboniferous strata in adjacent areas (Gunning, 1997; Logan, 2004).

Mafic volcanic rocks

Mississippian pillowed mafic flows are sparsely to strongly vesicular. They are sparsely porphyritic and contain trachytic feldspar and, locally, pyroxene pseudomorphs. Ground mass is typically dominated by feldspar microlites (Figure 3b). Basalts are interlayered with bedded, graded and locally-sourced mafic pebble conglomerate. Contacts between the rhyolite and basalt units are conformable and interfingering.

Three samples of pillow basalt plot in the basalt field on the Nb/Y-Zr/Ti plot and in the andesite field on the Zr/TiO_2-SiO_2 plot, suggesting pervasive silicification (Figures 4a, b). Each sample has a distinct normalized extended trace element profile, suggesting that they form parts of several distinct mafic suites; however, all samples are characterized by LREE, Th enrichment and high-field strength element (HFSE) depletion characteristic of arc settings (Figure 5b). All samples plot in the volcanic arc tholeiite field on tectonic discrimination plot (Figure 4d). The normalized extended trace element profiles in part overlap other Early to Middle Carboniferous strata in adjacent areas (Figure 5b; Gunning, 1997; Logan, 2004).

Granite

An extensive granitoid that was interpreted to be Late Devonian to early Mississippian age (Verrett pluton: Logan *et al.*, 2000) extends into the Hoodoo Mountain

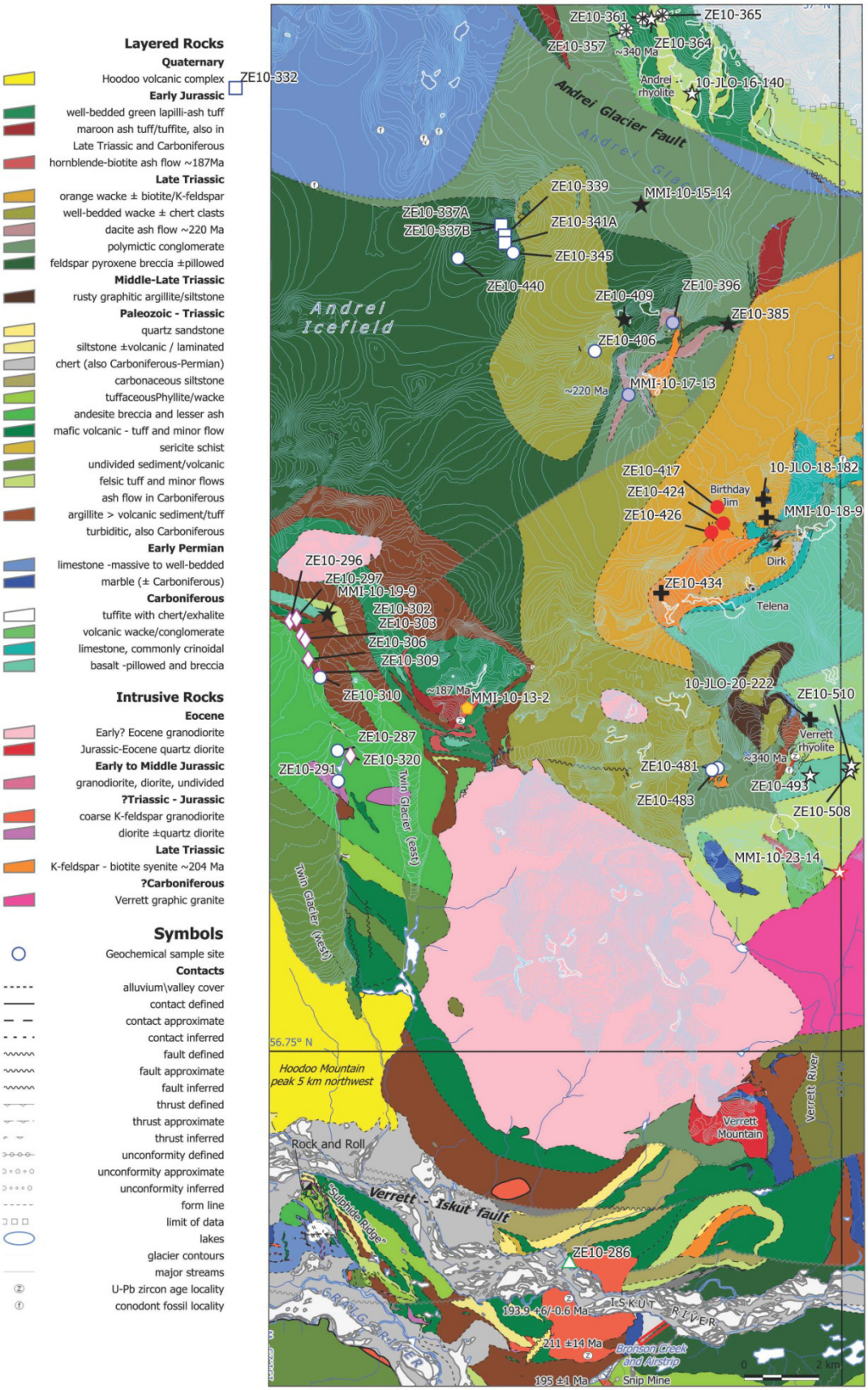

Figure 2. Geology of the Hoodoo Mountain area (from Mihalynuk *et al.*, 2011a). Whole-rock geochemistry sample locations utilize the same symbols as in Figure 4.

Table 1. Summary of geochemical data from NTS 104B/14E.

	Carboniferous					lTr											ITr or younger		eJr	
	Verette granite	basalt/andesite		rhyolite		basalt		Fs-porphyry		Cpx-porphyry		dacite		alkali tuff		alkali intusive		hbl-dykes		dacite	kfs granite
		μ (3)	*S.D.*	*μ (5)*	*S.D.*	*μ (6)*	*S.D.*	*μ (8)*	*S.D.*	*μ (5)*	*S.D.*	*μ (2)*	*S.D.*	*μ (3)*	*S.D.*	*μ (4)*	*S.D.*	*μ (5)*	*S.D.*		
SiO2	76.76	56.68	5.19	74.16	3.71	54.38	5.21	49.54	2.67	49.80	1.34	65.64	1.17	46.18	7.61	47.67	2.59	50.43	1.66	61.86	60.09
Al2O3	11.81	15.35	2.58	12.17	0.81	16.57	0.98	16.89	1.89	13.85	1.62	16.23	0.20	13.66	2.25	12.83	0.62	16.13	0.34	15.51	18.57
Fe2O3	1.03	8.12	2.66	3.31	1.90	7.00	2.56	9.45	1.85	10.66	1.62	3.16	0.41	8.80	0.97	8.01	0.92	9.29	1.16	6.52	1.91
MgO	0.21	2.75	1.34	1.24	0.59	4.67	3.44	5.47	1.68	7.83	1.35	1.52	0.06	3.33	2.54	4.17	2.60	4.91	0.69	1.47	0.45
CaO	1.87	4.90	0.45	1.04	0.72	6.55	2.29	6.89	3.85	8.27	2.10	1.76	0.42	8.16	3.44	8.78	1.47	6.50	1.05	3.89	3.19
Na2O	3.91	4.82	0.17	3.56	1.82	3.60	0.70	3.78	1.40	2.68	0.83	5.93	0.21	0.60	0.65	1.19	0.69	3.77	0.37	3.84	3.71
K2O	1.64	1.28	1.07	2.17	2.73	2.06	2.08	2.25	1.34	2.18	0.35	2.61	0.05	8.72	1.82	7.39	2.23	3.68	1.43	3.03	6.99
TiO2	0.16	1.15	0.22	0.30	0.19	0.93	0.28	0.94	0.10	0.82	0.08	0.36	0.03	0.61	0.20	0.70	0.14	1.56	0.47	0.64	0.39
P2O5	0.03	0.71	0.52	0.07	0.05	0.34	0.10	0.33	0.09	0.34	0.06	0.15	0.03	0.44	0.05	0.64	0.06	0.33	0.09	0.19	0.14
MnO	0.04	0.13	0.04	0.04	0.02	0.14	0.03	0.17	0.02	0.17	0.02	0.06	0.01	0.15	0.07	0.15	0.02	0.14	0.01	0.10	0.06
Cr2O3	0.00	0.00	0.00	0.00	0.00	0.01	0.01	0.01	0.01	0.04	0.02	0.00	0.00	0.01	0.01	0.02	0.02	0.02	0.01	0.00	0.00
Total	99.93	99.85	0.05	99.92	0.04	99.72	0.07	99.69	0.06	99.69	0.03	99.72	0.01	99.57	0.10	99.44	0.13	99.64	0.03	99.73	99.42
LOI	2.50	3.97	1.78	1.86	1.02	3.48	1.62	3.96	1.71	3.02	0.73	2.30	0.14	8.93	6.91	7.90	1.63	2.88	0.52	2.70	3.90
Ba	494	280	29	423	330	799	585	888	412	563	101	1369	60	2004	387	2930	860	1253	303	1502	4106
Cs	3.20	0.33	0.06	0.46	0.53	5.17	10.57	3.59	2.89	0.56	0.27	0.85	0.49	3.30	1.56	2.78	2.67	0.28	0.16	0.90	2.00
Hf	3.80	1.97	1.14	3.34	0.74	2.83	0.88	2.36	0.91	1.64	0.15	2.95	0.35	1.97	0.32	2.00	0.14	2.70	0.49	2.40	2.60
Nb	3.40	1.83	1.25	2.68	0.47	6.60	2.27	5.64	3.68	2.86	0.52	3.55	0.07	9.93	4.71	10.88	0.85	7.14	1.00	4.40	6.30
Pb	5.20	1.97	0.85	1.32	0.68	2.70	4.22	4.78	6.05	1.40	0.54	5.75	4.45	4.63	2.82	9.30	5.39	3.76	2.55	2.30	3.00
Rb	28.9	11.7	8.1	20.0	20.7	44.3	55.7	49.6	30.3	34.9	16.5	43.3	11.6	180.0	60.5	126.5	49.8	48.6	18.5	88.6	157.2
Sr	58	239	122	142	117	584	214	517	232	462	33	801	72	753	424	883	329	668	77	508	863
Th	3.90	1.13	0.85	3.24	1.90	3.72	1.78	2.91	2.47	1.30	0.35	2.55	0.21	2.90	0.90	3.45	0.37	5.44	4.10	5.30	5.10
U	2.00	0.70	0.46	1.38	0.48	1.53	0.63	1.29	1.00	0.70	0.16	1.50	0.14	1.43	0.15	1.58	0.13	1.88	1.52	2.50	6.00
Y	38.50	44.53	23.06	31.24	9.61	21.97	2.69	19.90	3.31	17.18	1.49	9.15	0.49	13.87	1.97	14.88	2.38	18.62	1.71	14.50	12.90
Zr	120	55	30	105	27	105	38	90	44	59	7	95	17	79	10	68	10	94	22	94	83
La	6.80	13.13	9.72	10.26	5.54	19.32	5.19	14.16	6.35	7.78	1.50	12.15	0.21	13.13	5.20	15.83	1.14	18.42	4.54	14.80	25.30
Ce	17.40	26.87	16.10	23.14	11.61	39.00	9.74	30.03	11.76	18.24	3.40	24.45	0.07	27.17	11.00	31.20	2.06	38.84	7.70	29.80	39.30
Pr	2.46	4.34	2.72	3.08	1.43	4.88	1.07	3.75	1.13	2.47	0.40	3.11	0.24	3.11	1.23	3.60	0.30	5.07	0.76	3.29	4.33
Nd	12.00	21.73	12.33	13.68	6.39	20.62	3.72	16.08	3.73	11.84	1.52	13.30	1.13	13.00	4.59	15.43	1.09	22.62	3.61	13.20	16.80
Sm	3.48	5.89	3.41	3.58	1.59	4.09	0.37	3.68	0.58	2.91	0.28	2.57	0.13	2.70	0.86	3.14	0.31	4.64	0.39	2.79	3.24
Eu	0.65	1.88	0.71	0.84	0.45	1.38	0.07	1.14	0.29	0.95	0.08	0.77	0.02	0.85	0.23	0.96	0.09	1.42	0.10	0.82	1.06
Gd	4.67	7.51	4.32	4.24	1.81	4.07	0.45	3.67	0.41	3.21	0.22	2.12	0.04	2.65	0.57	3.05	0.30	4.30	0.45	2.75	2.83
Tb	0.93	1.29	0.75	0.78	0.31	0.67	0.08	0.61	0.08	0.53	0.03	0.31	0.01	0.42	0.08	0.47	0.07	0.65	0.05	0.43	0.43
Dy	5.85	7.88	4.57	4.88	1.75	3.75	0.52	3.38	0.45	2.98	0.14	1.54	0.08	2.38	0.47	2.57	0.42	3.36	0.25	2.49	2.29
Ho	1.36	1.67	0.97	1.09	0.35	0.76	0.11	0.71	0.10	0.63	0.05	0.29	0.01	0.51	0.05	0.52	0.09	0.67	0.09	0.50	0.47
Er	4.12	4.89	2.94	3.40	1.01	2.24	0.29	2.07	0.33	1.75	0.12	0.83	0.01	1.55	0.25	1.47	0.26	1.84	0.26	1.47	1.35
Tm	0.64	0.75	0.46	0.55	0.16	0.34	0.04	0.31	0.05	0.27	0.02	0.13	0.00	0.23	0.02	0.23	0.04	0.27	0.04	0.23	0.22
Yb	4.24	4.62	2.92	3.69	1.00	2.12	0.23	2.02	0.35	1.69	0.18	0.85	0.03	1.50	0.21	1.50	0.25	1.76	0.26	1.55	1.51
Lu	0.67	0.69	0.42	0.57	0.15	0.32	0.04	0.31	0.06	0.26	0.03	0.13	0.00	0.23	0.03	0.23	0.03	0.26	0.04	0.25	0.25

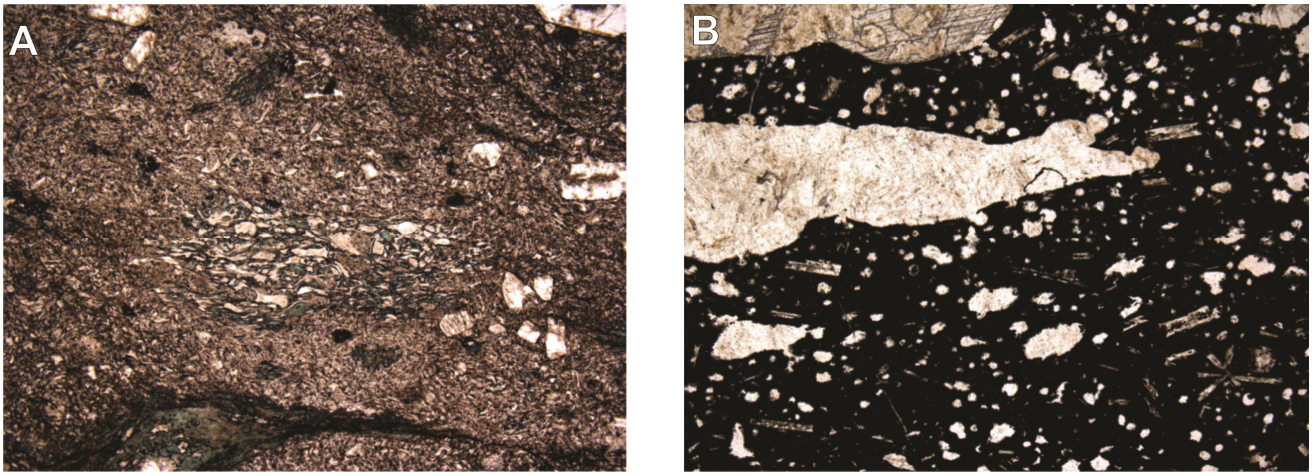

Figure 3. Representative photomicrographs of Mississippian units. A) Rhyolite lapilli tuff with altered (tube) pumice clast (FOV 7 mm). B) Trachytic basalt with large carbonate-filled pipe vesicles (FOV 3.5 mm).

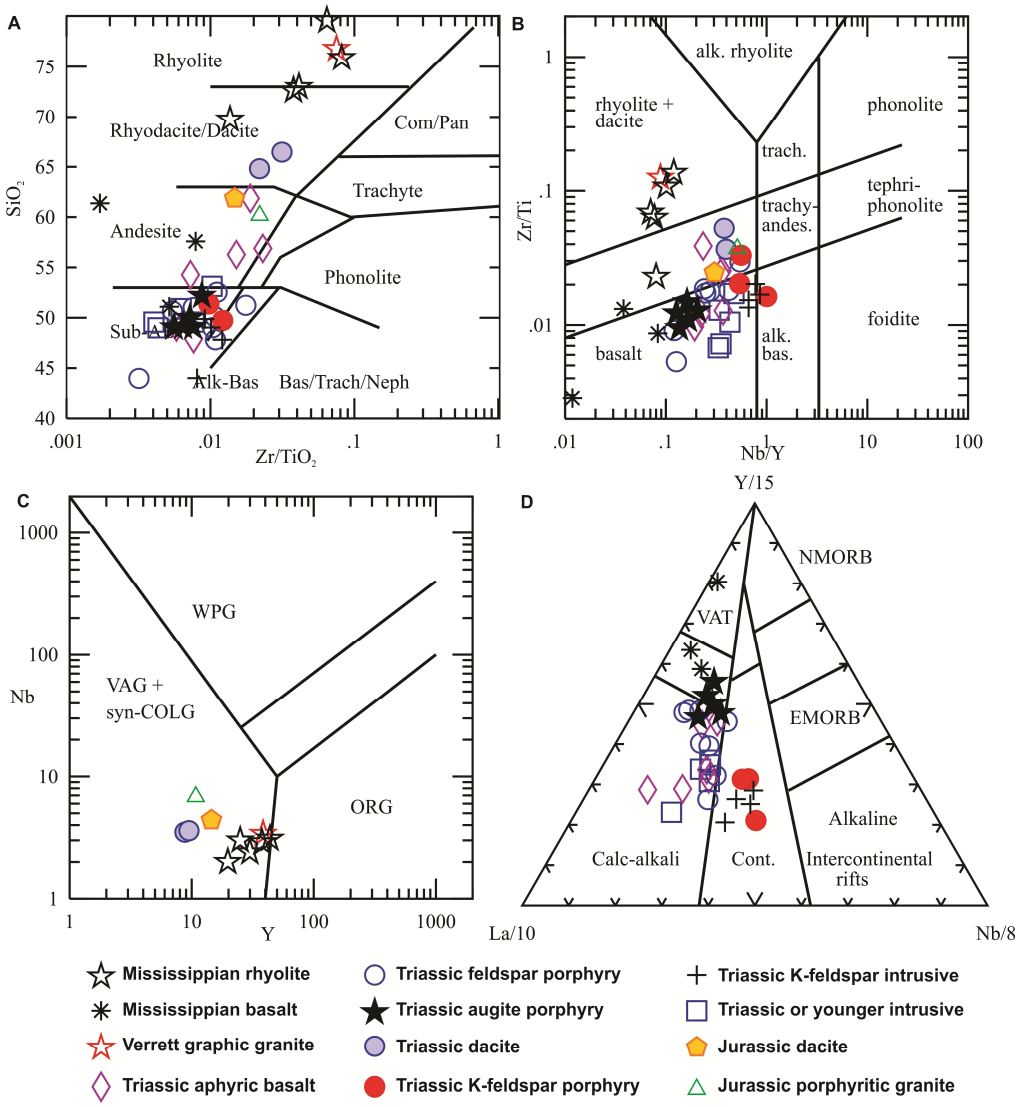

Figure 4. Rock type and tectonic discrimination plots of major units in the Hoodoo Mountain area (Winchester and Floyd, 1977; Pearce *et al.*, 1984; Cabanis and Lecolle, 1989; Pearce, 1996).

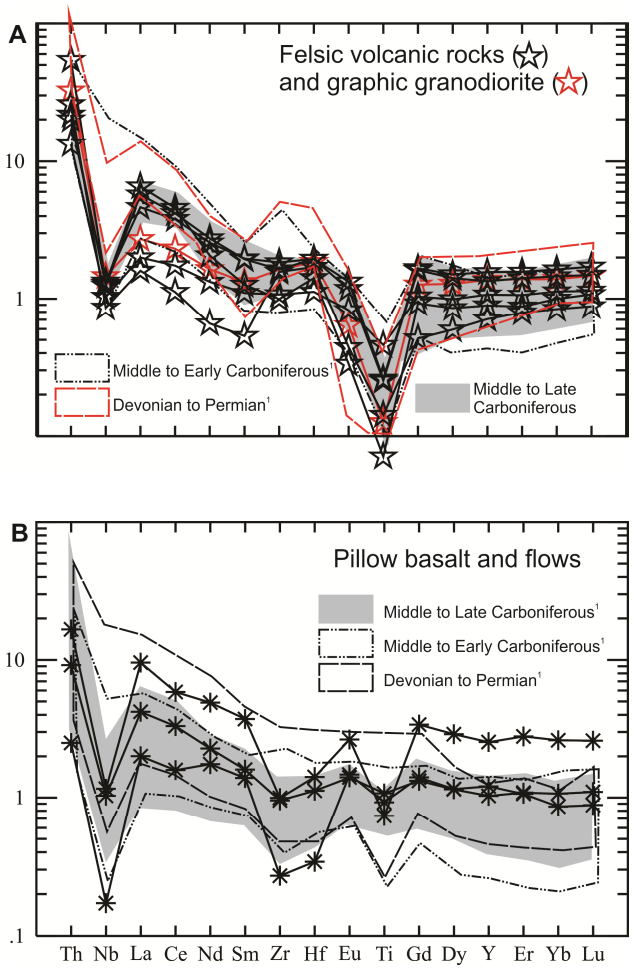

Figure 5. Trace element profiles of Mississippian rocks (N-MORB normalization from Sun and McDonough, 1989; [1]Gunning, 1997).

area (Figure 2), where it comprises predominantly cream to orange-coloured, medium to coarse grained, graphic leucogranite (see Figure 19 in Mihalynuk *et al.*, 2011b). An attempt to date the granite failed to yield any zircon (R. Friedman, personal communication, 2011). Since it appears to intrude dated Carboniferous strata in the study area, it has been reinterpreted to be Carboniferous or younger (Mihalynuk *et al.*, 2011b).

Geochemistry of the granite sample shows LREE, Th enrichment and Nb depletion on N-MORB normalized extended trace element plots (Figure 5a). It plots in the volcanic arc field on tectonic discrimination plots (Figure 4c). The trace element profile closely resembles Early to Middle Carboniferous volcanic rocks in the Hoodoo Mountain and adjacent areas.

Triassic Stuhini Group

The Triassic Stuhini Group is the most spatially extensive Mesozoic unit in the eastern Hoodoo Mountain area. The Stuhini Group is divided into five petrographically distinct volcanic units: aphyric basalt, feldspar porphyry, augite porphyry, dacite, and K-feldspar porphyry (Figures 6, 7). In general, each petrographic type is spatially restricted; suggesting that they belong to different magmatic centres or were erupted at different times. The dacite unit has a U-Pb crystallization age of *ca.* 223 Ma (Zagorevski *et al.*, 2012). Ar/Ar geochronology and fossil identification to constrain the stratigraphic order for the remaining units is ongoing.

Aphyric basalt

A nunatak to the north of Twin Glaciers preserves a thick sequence of basaltic volcanic, hypabyssal, and epiclastic rocks. The volcanic rocks include aphyric to very sparsely feldspar porphyritic, variably amygdaloidal massive flows, lapilli tuff and tuff breccia (Figure 6a). The hypocrystalline groundmass is dominated by felty to trachytic plagioclase microlites. Amygdales range from finely disseminated throughout the groundmass to large elongate pipe vesicles. Interlayered epiclastic rocks comprise locally-derived sandy to conglomeratic mafic turbidite. They are locally associated with calcareous wacke, fossiliferous shale, fossiliferous sandstone and chert.

Three samples of tuff breccia, two samples of massive flows and one sample of diabase plot in basalt and andesite fields on rock type discrimination diagrams (Figures 4a, b). All samples are characterized by LREE, Th enrichment and Nb, Ti depletion characteristic of arc settings (Figure 8a). In contrast to the Carboniferous mafic rocks (Figure 5), Nb is enriched relative to HREE, suggesting an enriched source. All samples plot in the calcalkaline field on tectonic discrimination plot (Figure 4d). The normalized extended trace element profiles overlap Late Triassic basalts in adjacent areas (Figure 8a; Brown *et al.*, 1996; Gunning, 1997).

Feldspar-porphyry

The feldspar porphyritic rocks include lapilli tuff and tuff breccia that are dominated by feldspar phenocrysts with lesser clinopyroxene and minor amphibole. Trachytic textures are common. Amphibole is observed in some samples where it is xenocrystic and clearly derived from cognate or accidental (Wright *et al.*, 1980) hornblende-diorite fragments (Figure 6b). Some blocks display trachytic feldspars with hornblende phenocrysts set in a glassy matrix (Figure 6b), indicating that some hornblende-porphyritic magma cooled rapidly. Ar/Ar analysis of a sample of hornblende from this unit is pending.

Eight samples of feldspar-porphyritic tuff and hypabyssal intrusive rocks were selected for analysis. Samples with visible xenoliths and xenocrysts were not analyzed to minimize the risk of contamination. Single volcanic fragments were collected where possible from breccias to minimize the effect of contamination and mixing of multiple lithologies. All eight samples plot in the basalt field on the rock type discrimination diagrams (Figures 4a, b). Similar to the aphyric basalt, all samples are characterized by LREE, Th enrichment and Nb, Ti depletion characteristic of arc settings (Figure 8b). All

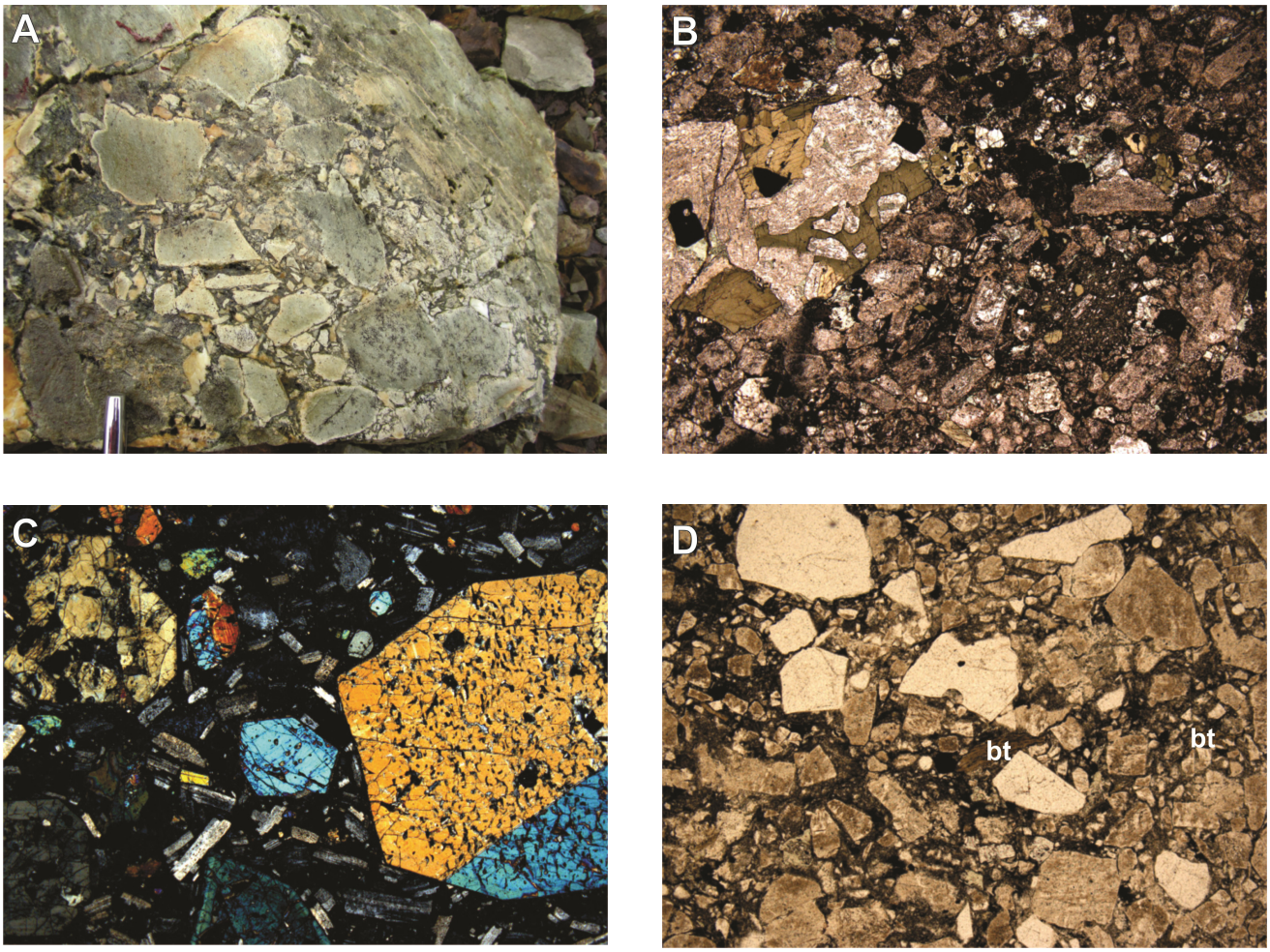

Figure 6. Representative photos and photomicrographs of Triassic calcalkaline units. A) Aphyric basalt tuff breccia (8 mm pen tip for scale). B) Feldspar porphyritic tuff with accidental gabbro clasts and hornblende xenocrysts and trachytic hornblende–feldspar lapilli (FOV 7 mm). C) Augite porphyry with sieve textured pyroxene crystals (FOV 7 mm). D) Dacite tuff with altered biotite (FOV 3.5 mm).

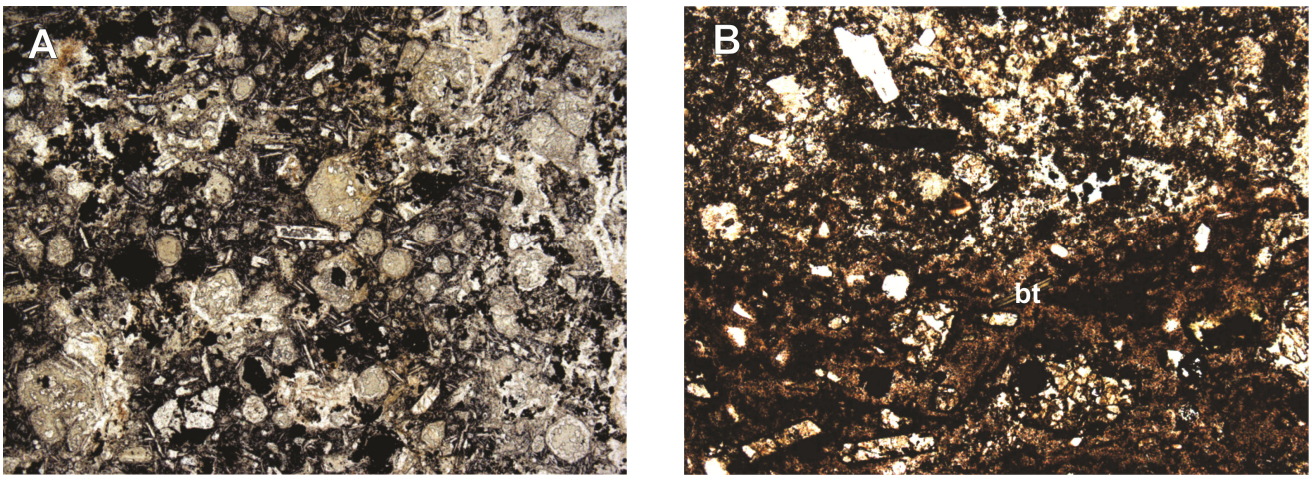

Figure 7. Representative photomicrographs of Triassic alkaline units. A) Spherical pseudomorphs suggest presence of altered leucite (FOV 3.5 mm). B) Lapilli tuff with characteristic biotite porphyritic lapilli (FOV 3.5 mm).

samples plot in the calcalkaline field on tectonic discrimination plot (Figure 4d). The normalized extended trace element profiles overlap Late Triassic feldspar-porphyritic andesites in adjacent areas (Figure 8b; Brown *et al.*, 1996; Gunning, 1997).

Augite porphyry

Augite porphyritic rock samples include lapilli tuff, tuff breccia, flows and sills. They are dominated by coarse clinopyroxene phenocrysts and subordinate to equally abundant amounts of feldspar phenocrysts. Coarse clinopyroxene crystals are commonly sieve-textured and contain thin, inclusion-free, coherent rims (Figure 6c). Medium to fine grained augite crystals also contain evidence of resorption followed by attainment of equilibrium with the melt.

Five samples of augite porphyry plot in the basalt field on the rock type discrimination plots (Figures 4a, b). Similar to the aphyric and feldspar-phyric basalts, all samples are characterized by LREE, Th enrichment and Nb, Ti depletion characteristic of arc settings (Figure 8c). All samples plot in the transitional area between volcanic arc tholeiite and calcalkaline basalt fields on tectonic discrimination plot (Figure 4d). The normalized extended trace element profiles overlap Late Triassic augite-porphyritic basalt in adjacent areas (Figure 8c; Brown *et al.*, 1996; Gunning, 1997).

Dacite

Triassic dacitic rocks comprise hypabyssal and extrusive quartz-feldspar porphyry and related crystal-rich tuffaceous rocks that occupy a thick package of cobble to boulder polymictic volcanic conglomerate. Crystal tuffs commonly contain minor biotite and accessory titanite. One sample yielded *ca.* 223 Ma U/Pb zircon age (Zagorevski *et al.*, 2012).

Two samples of dacite tuff were analyzed and they display LREE, Th enrichment and Nb depletion on N-MORB normalized extended trace element plots (Figure 8d). They plot in the volcanic arc field on tectonic discrimination plot (Figure 4c). Their trace element profile is distinctly more depleted in HREE as compared to the Early to Middle Carboniferous felsic volcanic rocks and Triassic dacite in adjacent areas (Figure 8d, Gunning, 1997).

K-feldspar porphyritic rocks

The K-feldspar porphyritic rocks appear to be restricted to isolated volcanic centres and comprise volcanic breccias/diatremes that are intercalated with rusty-weathering siliciclastic sediments and consanguineous K-feldspar porphyritic syenitic intrusive rocks. Potassium feldspar megacrystic intrusive rocks that mark these centres are locally affected by intense calcsilicate alteration and locally the volcanic, volcaniclastic and hypabyssal rocks host precious and base metal mineralization (Chadwick and Close, 2009). Some units contain distinctive, 0.5 to 3 cm round pseudomorphs after leucite (Figure 7a). Others contain primary biotite, pyroxene and/or amphibole that are typically strongly altered or completely pseudomorphed (Figure 7b). Most of the samples are feldspathoid (leucite±nepheline) normative.

Three samples of fragments from a tuff breccia were analyzed. They plot near the boundary between sub-alkaline and alkaline basalt (Figures 4a, b). All samples are characterized by LREE, Th enrichment; however, in contrast to other Late Triassic basalts, Nb is only slightly depleted relative to La (Figure 8e). All plot in the continental rift field on tectonic discrimination plot (Figure 4d). The normalized extended trace element profiles overlap Late Triassic (Norian) feldspar-porphyritic basalt in adjacent areas (Gunning, 1997). Four samples of intrusive rocks overlap the volcanic rocks on tectonic discrimination and extended trace element plots (Figures 4d, 8e). All samples geochemically overlap the alkaline Zippa Mt. pluton melanosyenite and syenite (Figure 8e).

Late Triassic or younger

Triassic or younger hornblende-bearing mafic dikes are concentrated in a dike complex in the central part of the field area (Figure 2). The variegated dikes have a sheeted appearance (*i.e.*, dike-in-dike) and range from hornblende-pyroxene phyric hypocrystalline to hornblende-plagioclase pegmatites (see Figure 21 in Mihalynuk *et al.*, 2011b). All varieties contain brown hornblende needles and prisms. Locally, fine-grained dikes are hornblende and pyroxene porphyritic (Figure 9a). Ar-Ar hornblende age results are pending for several samples of this unit.

Five dikes were sampled at different localities. Analyses of all the dikes display LREE and Th enrichment and Nb, Ti depletion characteristic of arc settings (Figure 8f). All samples plot in the calcalkaline field on tectonic discrimination plot (Figure 4d). The normalized extended trace element profiles overlap Late Triassic volcanic rocks in the study and adjacent areas.

Jurassic Hazelton Group

Hornblende and plagioclase porphyritic volcaniclastic rocks are locally common and characterize the Jurassic strata in the study area. A *ca.* 187 Ma U-Pb zircon crystallization age (Zagorevski *et al.*, 2012) from oxyhornblende-phyric, sparse quartz-eye dacite ash flow tuff constrains these rocks to the top of the lower sequence of the Hazelton Group (Macdonald *et al.* 1996). This tuff is interlayered with quartz-bearing, turbiditic volcanic sandstone, conglomerate, massive to bedded maroon to bright green tuff and lapilli tuff (Figure 9b).

A sample of Jurassic dacite tuff is characterized by LREE and Th enrichment, and Nb depletion on a N-MORB normalized extended trace element plot Figure 10a). It plots in the volcanic arc field on tectonic

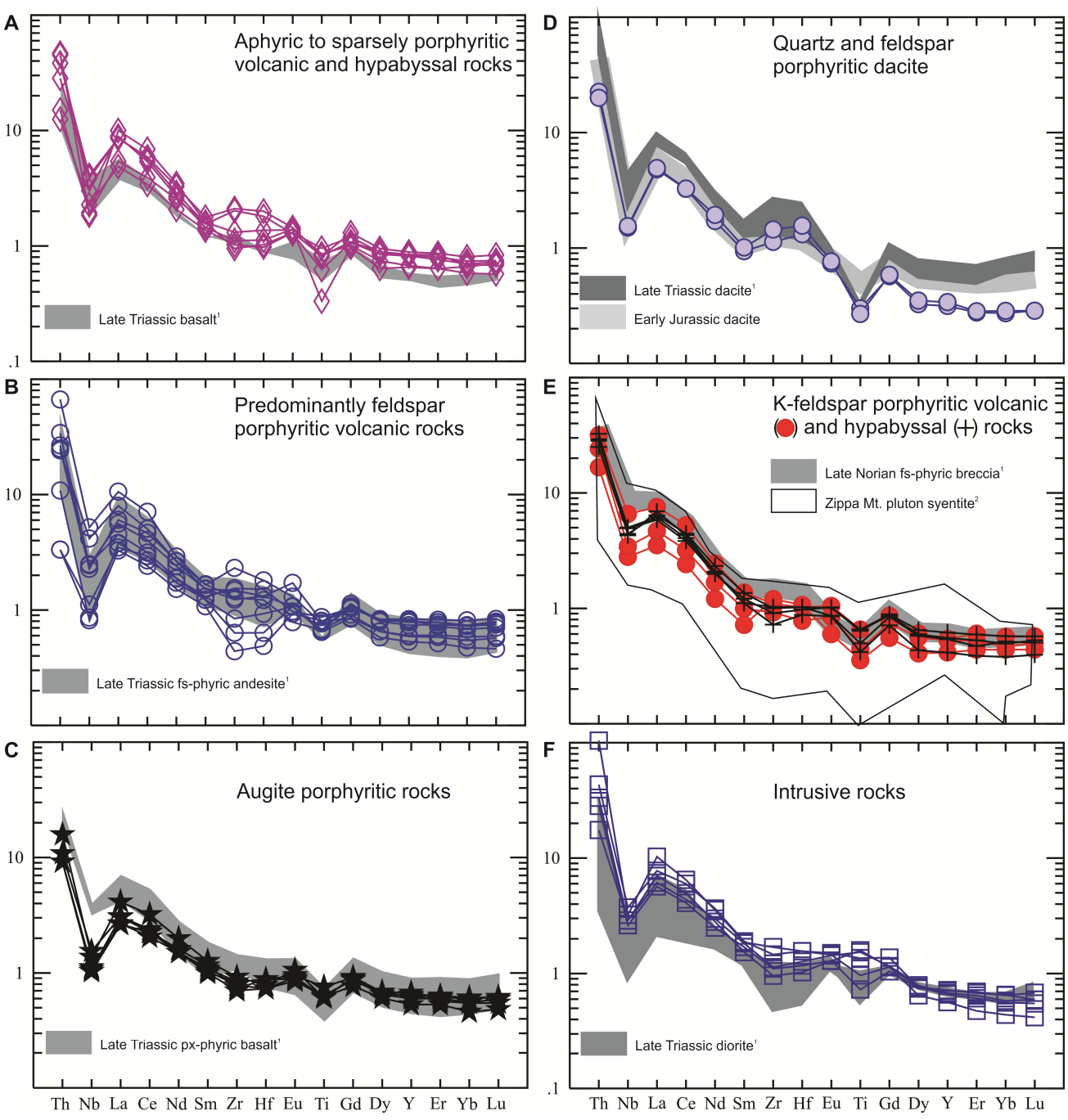

Figure 8. Trace element profiles of Triassic rocks (N-MORB normalization from Sun and McDonough, 1989; [1]Gunning, 1997; [2]Coulson *et al.*, 1999).

discrimination plot (Figure 4c). The trace element profile is distinctly more depleted in HREE compared to the Early Carboniferous and Middle Jurassic volcanic rocks in the Hoodoo Mountain and adjacent areas (Figures 5a, 10a). From a geochemical perspective, the Jurassic dacite tuff is chemically similar to the Late Triassic dacite in the study and adjacent areas (Figure 10a).

Early Jurassic K-feldspar porphyry

A small, coarsely K-feldspar porphyritic to megacrystic monzogranite pluton occurs along the Iskut River Valley (Figure 2; Iskut Mass of Kerr, 1948). The pluton previously yielded discordant and uncertain U/Pb zircon crystallization ages of between 225 and 197 Ma (Macdonald *et al.*, 1992), but a concordant *ca.* 196 Ma age has been recently obtained (Zagorevski *et al.*, 2012).

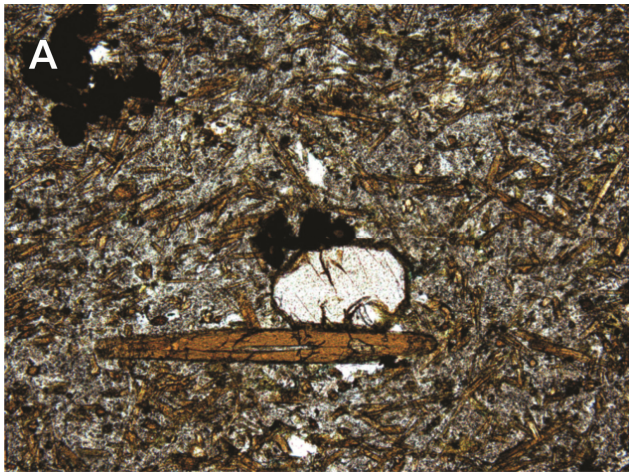

Figure 9. A. Photomicrograph of Triassic or younger hornblende porphyritic dike (FOV 1.75 mm). B) Jurassic dacitic tuff.

The K-feldspar porphyry contains quartz, distinguishing it from the Norian K-feldspar porphyritic rocks. One sample displays LREE and Th enrichment and Nb depletion on a N-MORB normalized extended trace element plot (Figure 10b). It plots in the volcanic arc field on tectonic discrimination plot (Figure 4c).

DISCUSSION

The Paleozoic to Mesozoic volcano-sedimentary and consanguineous plutonic rocks of the Hoodoo Mountain area are assigned to the Early Carboniferous to Permian Paleozoic Stikine assemblage, Late Triassic Stuhini Group and the Early Jurassic Hazelton Group on the basis of lithology and limited age dating. Whereas some lithologic characteristics of these units are unique (see previous also Logan *et al.*, 2000; Mihalynuk *et al.*, 2011b), they commonly contain indistinct lithologies complicating stratigraphic correlations in poorly exposed or constrained area. Whereas isotopic age dating can provide unique solutions, it is expensive. Here we utilize whole rock geochemical analyses from rocks in the Hoodoo Mountain area to test the utility of geochemistry in stratigraphic correlation and to identify the geochemical fingerprints of mineralized sequences.

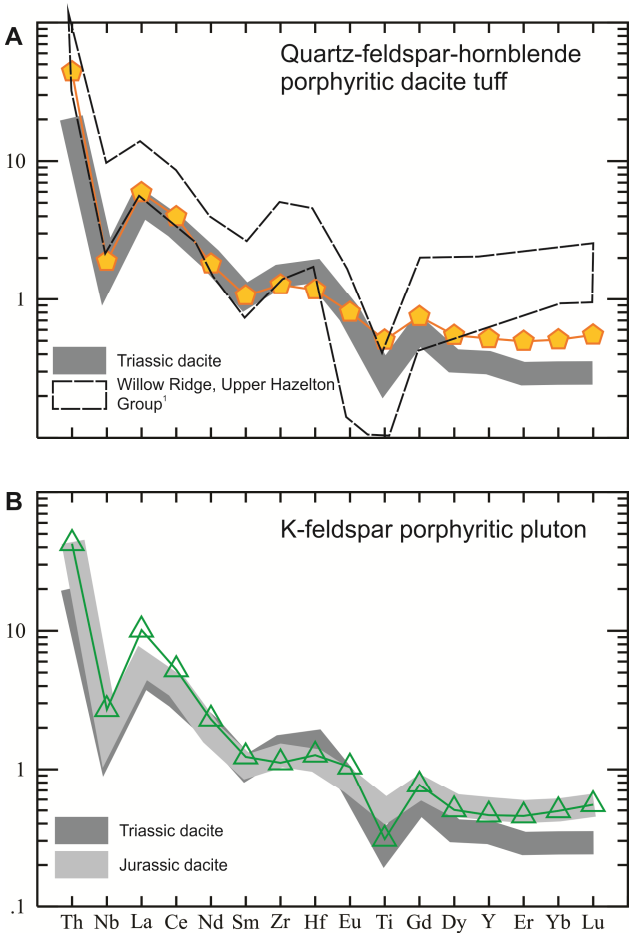

Figure 10. Trace element profile of Jurassic dacite and Jurassic monzodiorite (N-MORB normalization from Sun and McDonough, 1989; [1]Barresi and Dostal, 2005).

Mississippian Stikine assemblage

Volcanic rocks of the Mississippian Stikine assemblage (Monger, 1977) include rhyolite and pillow basalt that host VMS-style mineralization (Logan *et al.*, 2000; Logan, 2004; Mihalynuk *et al.*, 2011b). The geochemical characteristics of both felsic and mafic rocks indicate a volcanic arc setting as previously proposed by many authors (*e.g.* Logan *et al.*, 2000; Logan, 2004). Rhyolitic rocks have low La/Yb(n) ratios characteristic of VMS-prospective tholeiitic FIII rhyolites (Lesher *et al.*, 1986). The Verrett graphic granite in the east part of the mapped area (Figure 2) has indistinguishable geochemical characteristics and is interpreted to form a subvolcanic pluton to the Mississippian arc. Regionally, the Mississippian Stikine assemblage is geochemically distinct from the Late Triassic and Early Jurassic rocks (see following); however, felsic rocks are geochemically similar to the VMS-prospective Middle Jurassic strata of the Eskay rift (Alldrick *et al.*, 2005; Barresi and Dostal, 2005), indicating occurrence of similar supra-subduction zone environments (*i.e.* nascent arc, back arc, arc rift) of different ages.

Triassic Stuhini Group

Late Triassic Stuhini Group can be subdivided into five petrographically distinct volcanic and hypabyssal units. Overall, the petrographic characteristics may be a useful stratigraphic marker pending further age investigations. Generally, the aphyric basalt, feldspar porphyry and augite porphyry have similar trace element chemistry. All of the calcalkaline rocks have similar LREE, Th enrichments, Nb depletion characteristic of arc environments. The similar geochemistry suggests that the mafic rocks were derived from a similar source and that the dacitic rocks could have been produced by either partial melting or differentiation of the same mafic calcalkaline source. The geochemical coverage is still inadequate to calibrate the Late Triassic calcalkaline stratigraphy of the Hoodoo Mountain area.

The K-feldspar porphyritic, silica undersaturated, volcanic and syenitic rocks form a petrographically and geochemically distinct unit that is associated with skarn and base metal vein mineralization at the Dirk and Telena properties and surrounding area (Chadwick and Close, 2009; Mihalynuk *et al.*, 2011b). These rocks are characterized by Th and LREE enrichment without any appreciable Nb depletion, suggesting that they were derived from an enriched source distinct from the other Late Triassic sources. To the north of the study area, similar rocks have been constrained to be Late Norian (Brown *et al.*, 1996; Logan *et al.*, 2000) and are associated with alkali porphyry mineralization at Galore Creek (*ca.* 210 to 205 Ma: Logan and Koyanagi, 1994; Mortensen *et al.*, 1995). To the east similar aged intrusive rocks underlie the Newmount Lake property (*ca.* 203–214 Ma; Romios Gold Resources Inc., 2008). To the south, similar rocks form part of the latest Triassic alkalic Zippa Mountain pluton (Coulson *et al.*, 1999). Alkalic rocks tend to occur in tectonic settings where undepleted mantle melt can transit the crust relatively unimpeded, such as in rift and post-collisional settings (Richards, 2009). As such, Late Norian to Rhaetian alkalic magmatism in NW Stikinia represents a significant change in the tectonic setting and magma sources from the preceding Late Triassic calcalkalic arc magmatism.

Early Jurassic rocks

The presence of hornblende and plagioclase porphyritic volcaniclastic rocks generally distinguishes the Early Jurassic Hazelton Group from the Late Triassic Stuhini Group volcano-sedimentary rocks in the study area. Trace element geochemistry of the Jurassic tuff and K-feldspar porphyritic rocks indicate that they were formed in a similar arc source to the Triassic volcanic rocks. Hence, the petrography of the Jurassic rocks is the most reliable discriminant from the Triassic strata. In contrast, the petrographically similar Mississippian strata (*e.g.* similar phenocryst assemblages) are geochemically distinct from the Early Jurassic rocks in the Hoodoo Mountain area (Figures 8, 10).

SUMMARY

Mississippian to Pliensbachian volcanic and hypabyssal rocks were analyzed to test the utility of geochemistry to discriminate petrographically similar sequences and to geochemically calibrate the stratigraphy in the Hoodoo Mountain area (NTS 104B/14E). The cross-calibration of stratigraphy and geochemistry also constrains the tectonic and metallogenic evolution of Stikinia and its Jurassic overlap sequences. Our study confirms the utility of geochemistry in stratigraphic calibration and predictive metallogeny. For example, the Mississippian bimodal tholeiitic volcanic sequence is distinct from Late Triassic and Early Jurassic calcalkaline volcanic rocks. Trace element characteristics of these rocks are indicative of VMS-prospective environments consistent with the known VMS-style mineralization in the Iskut (Logan *et al.*, 2000; Logan, 2004; Mihalynuk *et al.*, 2011b) and adjacent areas (Macdonald *et al.*, 1996). The Late Triassic to Early Jurassic calcalkaline sequences display distinct petrographic characteristics (see Logan *et al.*, 2000; Mihalynuk *et al.*, 2011b) that can be utilized in stratigraphic correlations; however, geochemistry appears to have limited use in the discrimination. The alkali volcanic rocks of presumed Norian age are an exception to this caveat. The presence of rhomb porphyries, biotite and chrome diopside geochemical characteristics make these Norian alkali rocks petrographically and geochemically distinct within the predominantly calcalkaline volcanic sequences of the Late Triassic (Logan and Koyanagi, 1994; Mihalynuk *et al.*, 2011b). The frequent association of alkali rocks and Cu-Au mineralization (Logan and Koyanagi, 1994; Romios Gold Resources Inc., 2008; Chadwick and Close, 2009) makes them an important target for mineral exploration in northwestern British Columbia. Ongoing studies in 2012 will follow-up results of the 2011 fieldwork (Mihalynuk *et al.*, 2012) and continue to test the prospectivity of the Hoodoo Mountain area.

ACKNOWLEDGMENTS

This study has been funded through the Geological Survey of Canada GEM initiative (Geological Survey of Canada contribution #20110289), Pacific Northwest Capital and University of Victoria (British Columbia Ministry of Energy, Mines and Resources Partnership Fund). Renaud Soucy la Roche is thanked for his tireless assistance during 2010 field work. Neil Rogers is thanked for detailed and constructive review.

REFERENCES

Alldrick, D.J., Nelson, J.L. and Barresi, T. (2005): Tracking the Eskay Rift through northern British Columbia: geology and mineral occurrences of the upper Iskut River area; Geological Fieldwork 2004, *BC Ministry of Energy, Mines and Petroleum Resources*, Paper 2005-1, pages 1-30.

Anderson, R.G. (1993): A Mesozoic stratigraphic and plutonic framework for northwestern Stikinia (Iskut River area), northwestern British Columbia, Canada; in G.C. Dunne and K.A. McDougall (Editors), Mesozoic paleogeography of the western United States, II; *Society of Economic Paleontologists and Mineralogists*, Pacific Section, Los Angeles, CA, pages 477-494.

Barresi, T. and Dostal, J. (2005): Geochemistry and Petrography of Upper Hazelton Group Volcanics: VHMS-Favourable Stratigraphy in the Iskut River and Telegraph Creek Map Areas, Northwestern British Columbia; Geological Fieldwork 2004, *BC Ministry of Energy, Mines and Petroleum Resources*, Paper 2005-1, pages 39-48.

Brown, D.A., Gunning, M.H. and Greig, C.J. (1996): The Stikine project: geology of western Telegraph Creek map area, northwestern British Columbia (NTS104G/5, 6, 11W 12 and 13); *BC Ministry of Energy, Mines and Petroleum Resources*, Bulletin 95; 183 pages.

Cabanis, B. and Lecolle, M. (1989): Le diagramme La/10-Y/15-Nb/8; un outil pour la discrimination des series volcaniques et la mise en evidence des processus de melange et/ou de contamination crustale. The La/10-Y/15-Nb/8 diagram; a tool for distinguishing volcanic series and discovering crustal mixing and/or contamination; Comptes Rendus de l'Academie des Sciences, Serie 2, Mecanique, Physique, Chimie, Sciences de l'Univers, *Sciences de la Terre*, 309(20), pages 2023-2029.

Chadwick, P. and Close, S. (2009): Geological and geochemical report on the Dirk property, prepared for Romios Gold Resources; *BC Ministry of Energy, Mines and Petroleum Resources*, Assessment Report 31250, 31 pages plus appendices.

Childe, F., Barrett, T.J. and McGuigan, P.J. (1994): The Granduc VMS deposit, northwestern British Columbia, U-Pb ages and Pb isotope relations; Abstracts with Programs; *Geological Society of America*, 26(7), 381 pages.

Coulson, I.M., Russell, J.K. and Dipple, G.M. (1999): Origins of the Zippa Mountain Pluton, a Late Triassic, arc-derived, ultrapotassic magma from the Canadian Cordillera; *Canadian Journal of Earth Sciences*, 36(9), pages 1415-1434.

Gunning, M.H. (1997): Definition and interpretation of Paleozoic volcanic domains, northwestern Stikinia, Iskut River area, British Columbia; *University of Western Ontario*, Canada, 531 pages.

Henderson, J.R., Kirkham, R.V., Henderson, M.N., Payne, J.G., Wright, T.O. and Wright, R.L. (1992): Stratigraphy and Structure of the Sulphurets Area, British Columbia; in Current Research, Part A, *Geological Survey of Canada*, Paper 92-1A, pages 323-332.

Kerr, F.A. (1948): Lower Stikine and western Iskut River areas, British Columbia; *Geological Survey of Canada*, Memoir 246, 94 pages.

Lesher, C.M., Goodwin, A.M., Campbell, I.H. and Gorton, M.P. (1986): Trace-element geochemistry of ore-associated and barren, felsic metavolcanic rocks in the Superior Province, Canada; *Canadian Journal of Earth Sciences*, 23(2), pages 222-237.

Logan, J. (2004): Preliminary Lithogeochemistry and Polymetallic VHMS Mineralization in Early Devonian and(?) Early Carboniferous Volcanic Rocks, Foremore Property; Geological Fieldwork 2003, *BC Ministry of Energy, Mines and Petroleum Resources*, Paper 2004-1, pages 105-124.

Logan, J.M., Drobe, J.R. and McClelland, W.C. (2000): Geology of the Forrest Kerr-Mess Creek area, northwestern British Columbia (NTS 104B/10, 15 & 104G/2 & 7W); *BC Ministry of Energy and Mines*, Energy and Minerals Division, Geological Survey Branch, Bulletin 104, 163 pages.

Logan, J.M. and Koyanagi, V.M. (1994): Geology and mineral deposits of the Galore Creek area (104G/3, 4); *BC Ministry of Energy, Mines and Petroleum Resources*, Bulletin 92, 95 pages.

Macdonald, A.J., Lewis, P.D., Thompson, J.F.H., Nadaraju, G., Bartsch, R., Bridge, D.J., Rhys, D.A., Roth, T., Kaip, A., Godwin, C.I. and Sinclair, A.J. (1996): Metallogeny of an Early to Middle Jurassic arc, Iskut River area, northwestern British Columbia; *Economic Geology*, 91(6), pages 1098-1147.

Macdonald, A.J., van der Hayden, P., Lefebure, D.V. and Alldrick, D.J. (1992): Geochronometry of the Iskut River Area - An update (104A and B); in Geological Fieldwork 1991, *BC Ministry of Energy, Mines and Petroleum Resources*, Paper 1992-1, pages 495-501.

Mihalynuk, M., Logan, J. and Zagorevski, A. (2011a): East Hoodoo Mountain-Iskut River Geology (NTS 104B/14E, 11NE); *Geological Survey of Canada*, Open File 6739, scale 1:50 000; doi:10.4095/288739.

Mihalynuk, M., Logan, J., Zagorevski, A. and Joyce, N. (2011b): Geology and mineralization in the Hoodoo Mountain area (NTS 104B/14E); Geological Fieldwork 2010, *BC Ministry of Forests, Mines and Lands*, Paper 2011-1, pages 37-63.

Mihalynuk, M., Zagorevski, A. and Cordey, F. (2012): Geology of the Hoodoo Mountain area (NTS 104B/14); Geological Fieldwork 2011, *BC Ministry of Forests, Mines and Lands*, Paper 2012-1, this volume.

Monger, J.W.H. (1977): Upper Paleozoic rocks of the western Canadian Cordillera and their bearing on Cordilleran evolution; *Canadian Journal of Earth Sciences*, 14(8), pages 1832-1859.

Mortensen, J.K., Ghosh, D.K. and Ferri, F. (1995): U/Pb geochronology of intrusive rocks associated with Cu-Au deposits in the Canadian Cordillera; in T.G. Schroeter (Editor), Porphyry deposits of the Northwestern Cordillera of North America, *Canadian Institute of Mining, Metallurgy and Petroleum*; Special Volume 46, pages 142-158.

Nadaraju, G. (1993): Triassic-Jurassic Biochronology of the eastern Iskut River map area, northwestern British Columbia; unpublished M.Sc. thesis, *The University of British Columbia*, 268 pages.

Pearce, J.A. (1996): A user's guide to basalt discrimination diagrams; in D.A. Wyman (Editor), Trace element geochemistry of volcanic rocks: Applications for massive sulphide exploration; *Geological Association of Canada*, Short Course, pages 79-113.

Pearce, J.A., Harris, N.B.W. and Tindle, A.G. (1984): Trace element discrimination diagrams for the tectonic interpretation of granitic rocks; *Journal of Petrology*, 25(4), pages 956-983.

Read, P.B., Brown, R.L., Psutka, J.F., Moore, J.M., Journeay, M., Lane, L.S. and Orchard, M.J. (1989): Geology of

Parts of Snippaker Creek (104B/10), Forrest Kerr Creek (104B/15), Bob Quinn Lake (104B/16), Iskut River (104G/1), and More Creek (104G/2); *Geological Survey of Canada*, Open File 2094.

Richards, J.P. (2009): Postsubduction porphyry Cu-Au and epithermal Au deposits; products of remelting of subduction-modified lithosphere; *Geology*, 37(3), pages 247-250.

Romios Gold Resources Inc. (2008): Petrographic and age determinations for intrusives at Romios Gold's Newmont Lake property suggest intrusives are close in age to Galore Creek deposit; Press Release, June 23, 2008; [URL: http://www.romios.com/s/NewsReleases.asp?ReportID=308698&_Type=Press- Release&_Title=Petrographic-and-Age-Determinations-for-Intrusives-at-Romios-Golds-Newmont-...].

Sun, S.S. and McDonough, W.F. (1989): Chemical and isotopic systematics of oceanic basalts, implications for mantle composition and processes; *Geological Society*, Special Publications 42, pages 313-345.

Winchester, J.A. and Floyd, P.A. (1977): Geochemical discrimination of different magma series and their differentiation products using immobile elements; *Chemical Geology*, 20(4), pages 325-343.

Wright, J.V., Smith, A.L. and Self, S. (1980): A working terminology of pyroclastic deposits; *Journal of Volcanology and Geothermal Research*, 8(2-4), 22 pages.

Zagorevski, A., Mihalynuk, M. and Logan, J. (2011): Tabulated geochemical data of the Hoodoo Mountain area (104B/14E); *Geological Survey of Canada*, Open File 7040, 1 CD-ROM.

Zagorevski, A., Mihalynuk, M.G., Logan, J.M., Joyce, N. and Friedman, R. (2012): Geochemistry and geochronology of Mississippian to Pliensbachian volcanic and hypabyssal rocks in the Hoodoo Mountain area (NTS 104B/14E); *Mineral Exploration Roundup 2012*, Technical session abstracts.

Structural Geology of the Alexander Terrane in the vicinity of Porcher Island, Northwestern British Columbia

by J.J. Angen[1], C. van Staal[1,2] and S. Lin[1]

KEYWORDS: Alexander terrane, Coast Plutonic Complex, Cretaceous, Porcher Island, structural, shear zones, shear bands, transpression, conjugate

INTRODUCTION

This report summarizes the preliminary results of a two year study, mainly using detailed structural analysis combined with U-Pb geochronology, to elucidate the structural history of Porcher Island and the surrounding area in northwestern British Columbia (Figure 1). This work is a contribution to the North Coast subproject of the Edges Multiple Metals – NW Canadian Cordillera (British Columbia and Yukon) Project, the overall scope and results of which are elaborated upon by Nelson *et al*. (2012, this volume).

The study area is situated near the eastern margin of the southern Alexander terrane (Figure 1). The tectonic and paleogeographic history of the Alexander terrane is complex, and differs significantly from that of terranes which developed closer to the paleo-Pacific margin of North America (Gehrels and Saleeby, 1987; Colpron and Nelson, 2009). Excellent coastal exposures and a polyphase structural history make this area a strategic location to study the various tectonic events recorded by the southern Alexander terrane. New U-Pb geochronology combined with structural observations within the Ogden Channel complex (Nelson *et al*., 2010a) has led to the identification of a Late Silurian to Early Devonian tectonomagmatic event. Original interaction of the Alexander terrane with the paleo-Pacific margin of North America is interpreted as pre-Middle Jurassic (Gehrels *et al*., 1992; van der Heyden, 1992; McClelland and Mattinson, 2000; Saleeby, 2000; Gehrels, 2001). The boundary has since undergone significant contraction and extension-related deformation, with both sinistral and dextral transcurrent components. New evidence indicates that sinistral and dextral shear zones were in part coeval, forming a conjugate set.

[1] *University of Waterloo, Waterloo, ON*
[2] *Geological Survey of Canada, Vancouver, BC*

This publication is also available, free of charge, as colour digital files in Adobe Acrobat® PDF format from the BC Ministry of Energy and Mines website at http://www.empr.gov.bc.ca/Mining/Geoscience/PublicationsCatalogue/Fieldwork.

PREVIOUS WORK AND GEOLOGICAL SETTING

The original 1:250 000-scale mapping of the study area was conducted by Roddick (1970) and Hutchison (1982). More recent 1:50 000-scale mapping has been conducted by Nelson *et al*. (2010a, 2010b, 2012). The open file map based on these studies is the basis for Figure 2. Most of the field area is underlain by rocks assigned to the Alexander terrane, with minor constituents assigned to the Yukon-Tanana terrane and Gravina belt. Stratigraphic units of the Alexander terrane include the arc-like volcanic rocks and associated sedimentary rocks of the Ordovician Descon Formation, siliciclastic equivalents of the Devonian Karheen Formation in southeast Alaska (Eberlein and Churkin, 1970), as well as the newly identified Kumealon unit (Nelson *et al*., 2012). The local equivalent of the Karheen Formation is rusty, arkosic sedimentary rocks and marble of the Mathieson Channel Formation defined by Nelson *et al*. (2011a, b) and extended into the present area (Nelson *et al*., 2012). Gehrels *et al*. (1983) proposed that the Karheen Formation represents a clastic wedge associated with the hypothesized Silurian-Devonian Klakas orogeny, during which the primitive Alexander terrane was amalgamated with a pericratonic fragment to the southwest. Plutonic rocks of the Alexander terrane range from Ordovician to Permian with the Ogden Channel complex and Porcher Creek pluton comprising a Late Silurian to Early Devonian intermediate plutonic suite (Nelson *et al*., 2012). The Billy Bay complex is spatially and genetically associated with the Ogden Channel complex, but has a larger supracrustal component (Nelson *et al*., 2012). The Kumealon unit comprises felsic to mafic volcanic rocks, pelitic schists, and minor, interbedded marble. It also includes two infolds of thick marble containing tuffaceous partings (Nelson *et al*., 2012). Consistent Permian U-Pb ages (J.B. Mahoney, unpublished data, 2011) suggest a correlation with the Station Creek Formation of Wrangellia (Gardner *et al*., 1988). A sequence of thin bedded psammitic schists along Telegraph Passage (Figure 2) is assigned to the Middle Jurassic to Lower Cretaceous Gravina belt as defined by Berg *et al*. (1972). One locality within Kumealon inlet (Figure 2) produced a detrital zircon population characteristic of the Yukon Tanana terrane (J.B. Mahoney, unpublished data, 2010).

Deformation within and directly south of the study area has been attributed previously to mid-Cretaceous

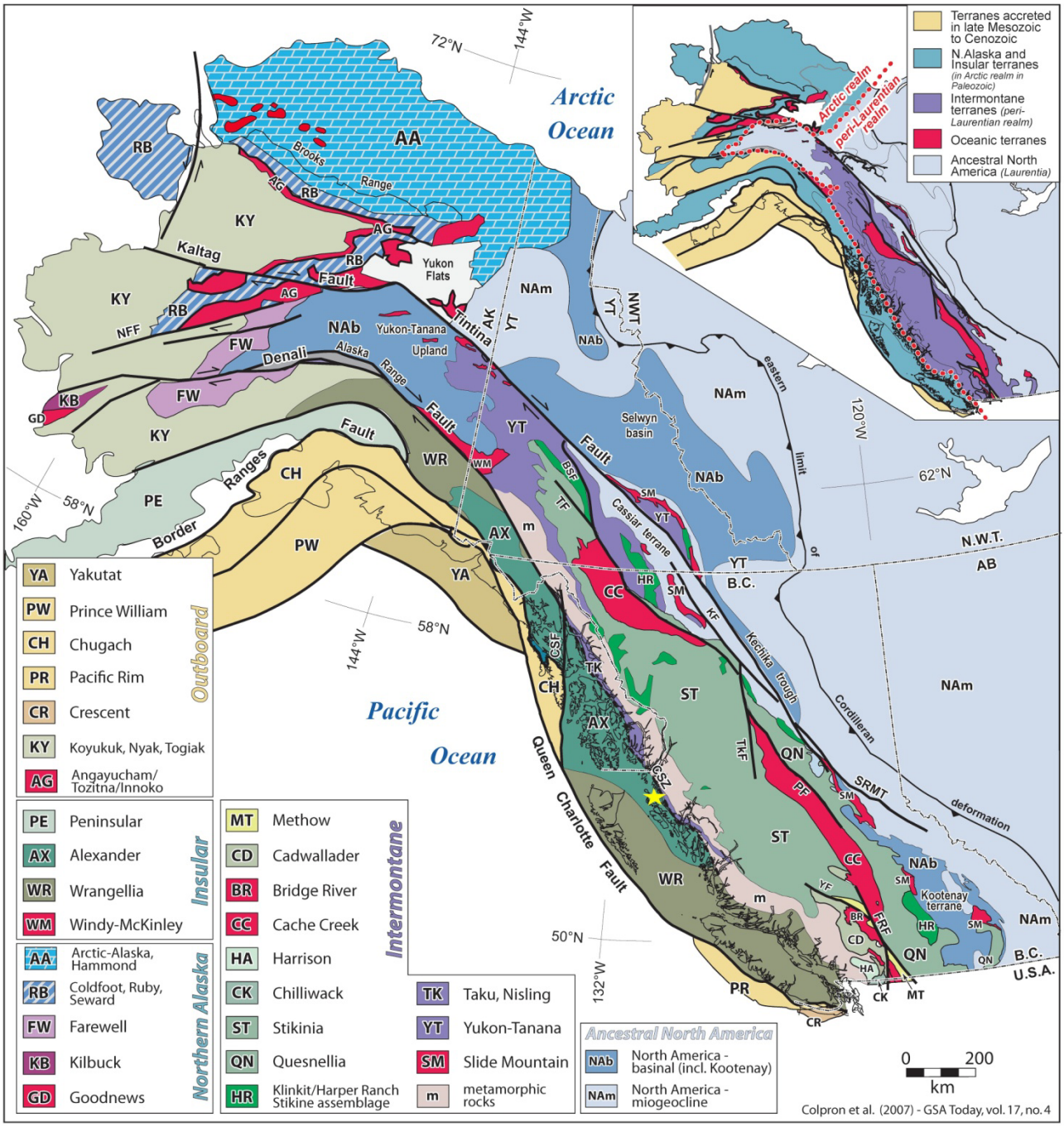

Figure 1. Location of the study area within the context of terranes of the northern Cordillera. The yellow star indicates the location of the current study (modified after Colpron *et al*., 2007).

sinistral transpression (Chardon *et al*., 1999; Chardon, 2003). On the basis of shear sense indicators, trajectories of compiled foliation measurements, and U-Pb crystallization and Ar-Ar cooling ages, Chardon *et al*. (1999) defined three northwest striking sinistral shear zones, which were active between approximately 110 and 87 Ma. From northeast to southwest these are the Grenville Channel, Kitkatla, and Principe-Laredo shear zones. These shear zones form part of a much more extensive zone of mid-Cretaceous sinistral shearing along the western margin of the Canadian Cordillera (Hurlow, 1993; Schiarizza *et al*., 1997; Israel, 2001; Evenchick, 2001; Israel *et al*., 2006).

On the other hand, researchers working farther to the north near Prince Rupert and in southeast Alaska have emphasized the importance of orogen-normal shortening during the mid-Cretaceous in the form of west to southwest-vergent thrusting (Crawford *et al*., 1987; Rubin *et al*., 1990; Rubin and Saleeby, 1992; Haeussler, 1992; McClelland *et al*., 1992; Crawford *et al*., 2000; McClelland and Mattinson, 2000). This thrusting was

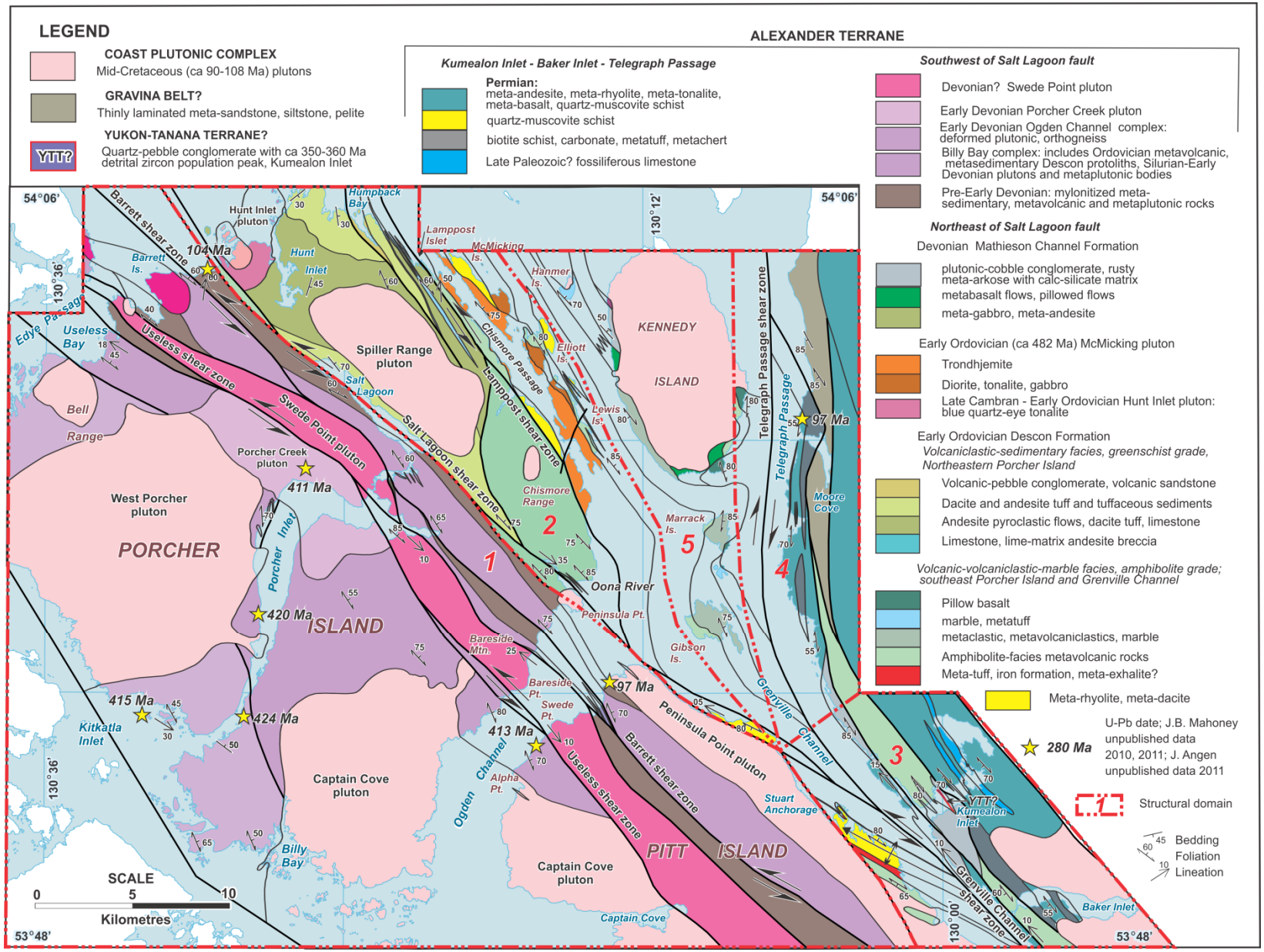

Figure 2. Geology and structural domains of Porcher Island and Grenville Channel area (modified after Nelson *et al.*, 2010b, 2012).

identified both by shear sense indicators and by inverted metamorphic gradients. Rubin and Saleeby (1992) report lineations and kinematic observations consistent with sinistral reverse motion on steeply northeast dipping shear zones in southeast Alaska. This deformation is reported as synkinematic to the *ca.* 101 Ma Moth Bay pluton (Rubin and Saleeby, 1987; no errors given). An earlier phase of thrusting associated with moderately northeast dipping foliations is constrained as post 113 Ma by the youngest affected strata. Wide angle seismic reflection data of the Portland Canal ACCRETE transect in southeast Alaska indicated that these thrusts are crustal-scale features, which can be traced to mid-crustal depths where they are truncated by the younger Coast shear zone (Morozov *et al*., 1998). McClelland *et al*. (1992) reported synkinematic ages along the Sumdum-Fanshaw fault system, which indicate that the steep southwest-vergent thrusts were active at 92.9 ±3 Ma and truncate earlier, shallower fabrics.

The Ecstall pluton has been interpreted to have been emplaced synkinematically with respect to thrusting (Crawford *et al*., 1987; 2000), and/or sinistral shearing (van der Heyden, 1989; Chardon *et al*., 1999). U-Pb zircon dating of the pluton has yielded ages of 90.5 ±1.0 Ma and 91.5 ±1.0 Ma (Butler *et al*., 2002). Subsequently, Chardon (2003) proposed that the Ecstall pluton intruded during sinistral transpression, with the deformation being partitioned into reverse and transcurrent shear zones. Intrusion of the Ecstall pluton had a major impact on the local strain field and was interpreted to have caused dextral shearing along a portion of the Prince Rupert thrust within an overall sinistral system. Detailed Lu-Hf dating of garnets, however, suggests that regional metamorphism occurred between 108 and 102 Ma, with a 10 Ma gap between the main phase of transpression and emplacement of the Ecstall pluton (Wolf *et al*., 2010).

STRUCTURES

The tectonometamorphic history of the area is complex and generally has transformed the rocks into metamorphic tectonites, with the grade of metamorphism varying from upper greenschist to upper amphibolite facies. The main structure is a penetrative composite transposition foliation, which is generally steeply dipping and nearly everywhere accompanied by mineral and/or stretching lineations with varying plunges. The stretching lineation is defined by elongated clasts, mineral aggregates and boudinage. Where both mineral and stretching lineations are present, they are generally parallel. The foliation locally contains at least two generations (F_1 and F_2) of intrafolial tight to isoclinal folds (Figure 3a), emphasizing its composite origin.

The deformation of the area was heterogeneous and characterised by laterally continuous zones of high strain ranging from 10 to 200 metres in width, represented by mylonite and a highly planar fabric best described as straight gneiss (Figure 3b; Hanmer and Passchier, 1991). They are separated from the surrounding lower strained rocks by marked strain gradients. The presence of asymmetric shear sense indicators, such as S-C fabrics, in the high strain tectonites indicates they represent shear zones formed by non-coaxial strain. The shear zones have various trends and their shear sense indicators suggest that in part they record different kinematic evolutions.

The map area has been divided into five domains based on their dominant structural features, metamorphism, and kinematic evolution of their structures (Figure 2). Domain 1 is a northwest-striking domain, which includes the Useless and Barrett shear zones and Paleozoic structures that are not evident in the other domains (see below). Domain 2 is also a northwest-striking domain, at a lower metamorphic grade than domain 1. It comprises two major shear zones: the Salt Lagoon and Lamppost shear zones. Domain 3 is also northwest striking and includes the Grenville Channel shear zone. Domain 4 is north striking and characterized by the Telegraph Passage shear zone and adjacent wallrocks. Domain 5 is northwest striking, similar to domains 2 and 3, but contains no significant shear zones.

Domain 1

Domain 1 comprises the southwestern portion of Porcher Island and western Pitt Island (Figure 2). It is characterized by northwest to west-northwest striking, moderately to steeply northeast dipping foliations and highly variable lineations. It includes the Useless and Barrett shear zones. Inconsistent shear sense indicators suggest these shear zones accommodated protracted deformation histories characterised by varying kinematics. Unpublished U-Pb zircon ages from the synkinematic Ogden Channel complex and Porcher Creek pluton indicate a significant Late Silurian to Early Devonian deformation event (Figures 2, 3c). Associated kinematic indicators suggest sinistral reverse sense of motion (Figure 3a; Nelson *et al*., 2012). It is not yet clear how much of the structural development of domain 1 can be attributed to this mid-Paleozoic event, and how much to superimposed Cretaceous sinistral kinematics. An increase in metamorphic grade (epidote amphibolite to amphibolite facies) is observed from southwest to northeast up to the moderately to steeply northeast dipping Salt Lagoon fault, which forms the northeastern boundary of domain 1.

USELESS SHEAR ZONE

The Useless shear zone is characterised by mylonite and is spatially associated with the tabular, elongated Swede Point pluton (Figure 2). The pluton has been overprinted, at least in part, by the shear zone, as it locally contains S-C fabrics (Figure 3d). However, inferred consanguineous dikes locally cut the mylonite (Figure 3e), suggesting the pluton was emplaced late synkinematically. Shallowly southeast plunging ridge-and-groove lineations within Swede Point pluton, as defined by Lin *et al.* (2007), suggest the sinistral shear

after pluton emplacement had a minor reverse component. Dating of the Swede Point pluton using ID-TIMS yielded an age of *ca.* 382 ±14 Ma. However, the analysed zircons have complicated U-Pb systematics, making their age suspect (van der Heyden, 1989). Additional dating of the Swede Point pluton, and associated dikes, using LA-ICPMS indicated the existence of both mid-Cretaceous and older zircon growth, but failed to produce a reliable crystallization age for the pluton (J.J. Angen; J.B. Mahoney, unpublished data, 2011). The existing 382 Ma age may be a composite of an Early Devonian crystallization age as is typical of the members of the associated synkinematic Ogden Channel complex, and mid-Cretaceous metamorphic overgrowths; alternatively, the data may reflect a mid-Cretaceous crystallization age with abundant inherited xenocrystic cores. Both of these interpretations indicate that the Early Devonian shear zones were subsequently reactivated during a mid-Cretaceous tectonometamorphic or tectonomagmatic event.

The mylonite contains rare long limbed isoclinal folds (Figure 3b) and accommodated sinistral reverse motion. Shear sense indicators in the adjacent lower strain zones suggest the kinematic history was probably complex because both sinistral normal and sinistral reverse sense of shear have been observed, as well as two phases of folding (Figures 3a, f).

BARRETT SHEAR ZONE

The Barrett shear zone is located immediately north of the Useless shear zone, localised in a discontinuous belt of metasedimentary screens enclosed by the orthogneiss of the Ogden Channel complex (Figure 2). The best exposures of the Barrett shear zone are along the northwestern shore of Porcher Island (Figure 2). The orthogneiss contains straight gneiss with isoclinal F_1 folds that are refolded by asymmetrical sinistral F_2 folds (Figure 4a). F_2 fold hinge lines along the northwestern Porcher Island exposure are generally parallel to the stretching lineations, plunging moderately to the north as previously documented by Nelson *et al*., 2010a (Figure 4b). Locally sheath folds have been observed (Figure 4c), but elsewhere folds appear cylindrical without formation of sheath-like geometries (*cf*. Jiang and Williams, 1998).

A swarm of mylonitized pegmatite dikes are observed both crosscutting the F_2 folds parallel to the axial planes and incorporated in folding (Figure 4d). Lineations within the mylonitized dikes vary from shallowly northwest to steeply north plunging, and δ-porphyroclasts associated with these lineations indicate sinistral oblique normal motion. One of these dikes yielded a U-Pb zircon LA-ICPMS age of 104.5 ±0.9 Ma (J.B. Mahoney, unpublished data), indicating that at least some of the shearing was mid-Cretaceous.

Domain 2

Domain 2 includes the northeastern part of Porcher Island, as well as McMicking, Elliot, and Lewis islands (Figure 2). It includes the Salt Lagoon and Lamppost shear zones, the former bounding its southwestern margin. This domain is characterized by moderately to steeply northeast dipping foliations and variable lineations, similar to domain 1. It is distinguished on the basis of lithological and metamorphic contrasts, being comprised mainly of greenschist grade metavolcanic and metasedimentary rocks of the Ordovician Descon Formation. Structurally, it lacks evidence for the Early Devonian deformation event observed in domain 1.

SALT LAGOON SHEAR ZONE

The Salt Lagoon shear zone is topographically defined by a steep valley bisecting Porcher Island (Figure 2). This shear zone is interpreted as a major structure because it separates the Ogden Channel orthogneiss to the southwest from the Descon Formation to the northeast. It is characterised by a mylonite zone, which has a width of 100 metres or less and dips moderately to steeply to the northeast. Shear sense indicators comprise folded and/or boudinaged veins and dikes, porphyroclasts, and drag folds. They indicate dominantly sinistral shear with minor superimposed dextral shear. Stretching lineations plunge moderately to the southeast and to the northwest, suggesting a complicated movement history.

Granodioritic dikes in the wallrocks of the Salt Lagoon shear zone show evidence for stretching and folding consistent with a small amount of sinistral shear (Figure 5). They are therefore interpreted to have intruded late synkinematically with respect to sinistral shearing. The dikes yielded a U-Pb zircon age of 96.8 ±4.8 Ma (ID-TIMS unpublished data).

LAMPPOST SHEAR ZONE

The Lamppost shear zone is a 50-100 metre wide, heterogeneous deformation zone, comprising numerous smaller scale, anastomosing greenschist grade shear zones. This structure occurs along the northeastern shore of Porcher Island (Figure 2). It is localised in rocks of the Descon Formation and separates the *ca.* 482 ±15 Ma McMicking trondhjemite (Gehrels and Boghossian, 2000) from metavolcanic rocks and interlayered marble to the south. Shear sense indicators such as S-C fabrics and boudinaged veins record sinistral-normal shear, consistent with a component of the motion observed in the Salt Lagoon shear zone.

Domain 3

Domain 3 comprises highly strained rocks on both margins of Grenville Channel (Figure 2). It is cored by the Grenville Channel fault itself, which lies under the strong topographic linear of the shipping channel. The notable structures in this domain are the nearly upright, shallowly northwest plunging, open to isoclinal F_2 folds and an accompanying S_2 axial planar foliation. Strain increases and the folds become tighter upon approaching the Grenville Channel shear zone from the northeast, through Kumealon Inlet (Figure 2). A cobble

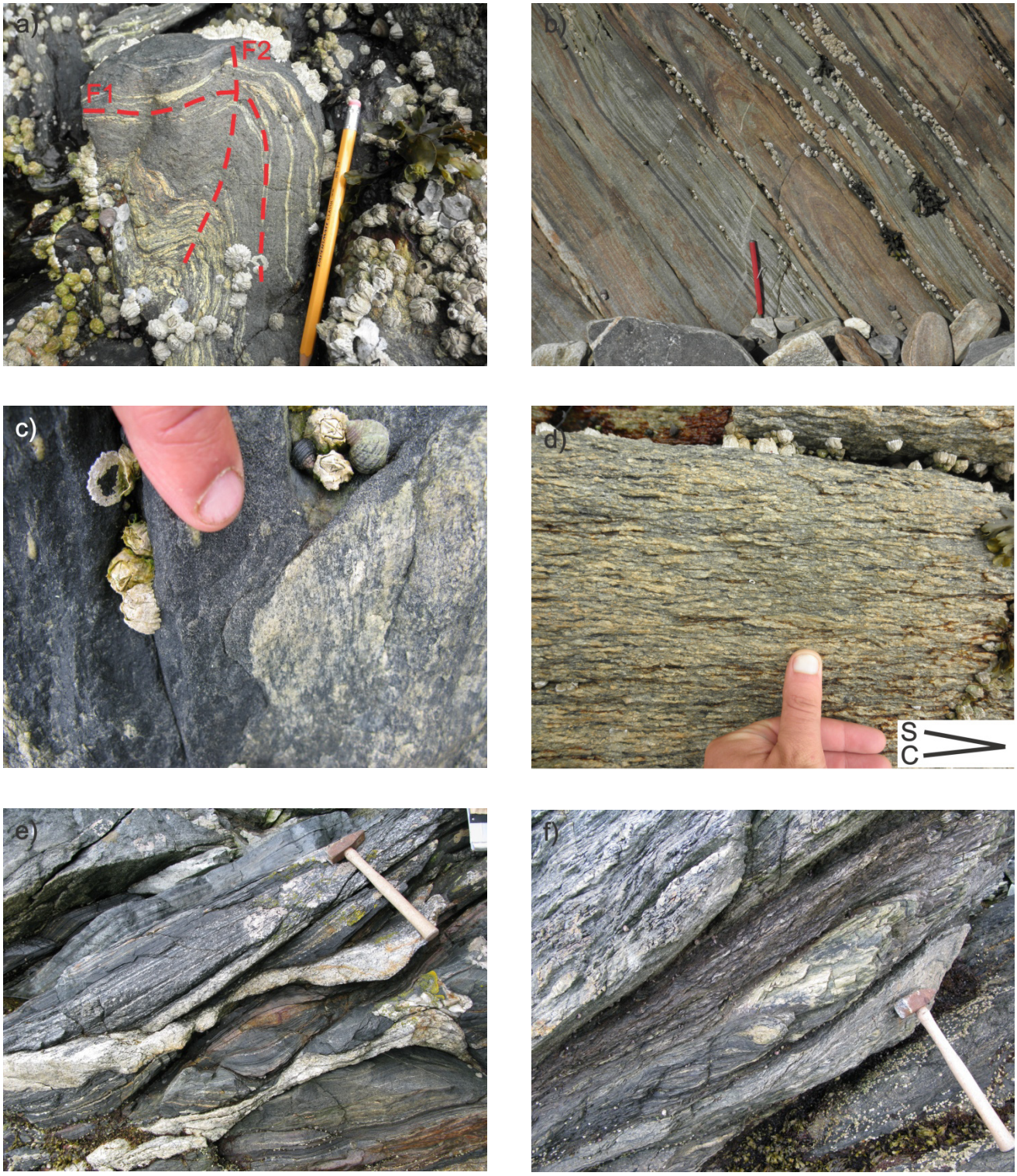

Figure 3. Structural observations within Domain 1. a) Ogden Channel orthogneiss with F_1 isoclinal folds refolded around F_2 folds. Dotted lines represent axial traces, photograph was taken looking down toward the northwest. Both phases of folding are consistent with sinistral reverse sense of shear, Useless shear zone south of Bareside Point on southeastern Porcher Island; b) Straight gneiss of the Ogden Channel complex including a long limbed isoclinal fold, Useless shear zone north of Bareside Point on southeastern Porcher Island; c) foliated dike which crosscuts stronger foliation in adjacent dike, both *ca.* 412-413 Ma, Ogden Channel complex, northwestern Pitt Island; d) S-C fabric within the Swede Point pluton indicating sinistral shear, Bareside point on southeastern Porcher Island; e) Weakly deformed leucotonalite dikes crosscutting amphibolite grade straight gneiss of the Ogden Channel complex, Useless Bay on northwestern Porcher Island; f) Evidence for sinistral normal motion including a sigma porphyroclast and shear bands, Useless Bay on northwestern Porcher Island.

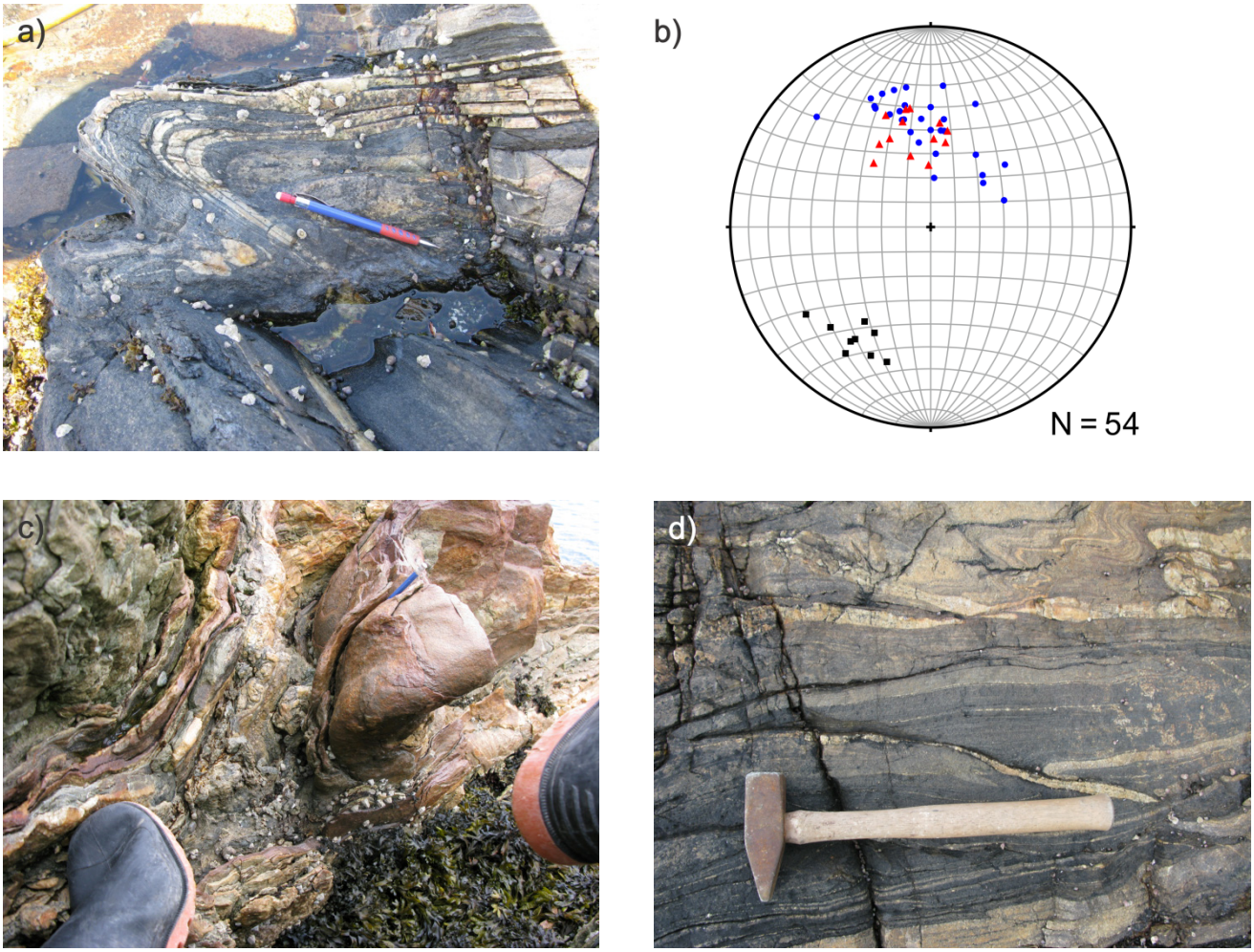

Figure 4. Structures associated with the Barrett shear zone, from both northwestern and southeastern Porcher Island. a) F_1 isoclinal folds refolded around F_2 folds, northwestern Porcher Island; b) Lower hemisphere, equal area stereonet plot of lineations and foliations from the Barrett shear zone along northwestern Porcher Island. Fold hinge lines and crenulation lineations are plotted as blue circles, and stretching lineations are plotted as red triangles. Poles to transposition foliation are plotted as black squares; c) Highly curvilinear hinge of a sheath fold along the Barrett shear zone, southeastern Porcher Island; d) Mylonitized pegmatite dikes both cutting F_2 folds parallel to their axial planes, and being incorporated in folding, northwestern Porcher Island.

conglomerate approximately 500 metres from the mouth of Kumealon Inlet records aspect ratios of 6:1 whereas pillow basalt at the mouth of the inlet records aspect ratios of 20:1 (Figures 6a, b). This strain gradient culminates with formation of a composite $S_{1\text{-}2}$ transposition foliation and is accompanied by an increase in sinistral shear sense indicators (Figure 6c). Boudinage and intense rodding (L>S tectonites) record a dominant horizontal stretching in the shear zone (Figure 6d).

Domain 3 includes the apparent structural boundary between rocks assigned to the Alexander terrane and those assigned to the Yukon Tanana terrane. The proposed boundary zone between the two terranes is exposed in the northeastern portion of Kumealon Inlet. The inferred structural contact is outlined by a thin, isoclinally F_2 folded layer (~20 cm thick) of virtually monomineralic, coarse-grained garnet parallel to S_1. It occurs along the contacts of a quartz pebble conglomerate which produced a Mississippian detrital zircon spectra characteristic of the Yukon Tanana terrane (J.B. Mahoney, unpublished data; Nelson *et al*., 2012). This 'garnetite' layer is interpreted as the metamorphic product of a hydrothermally altered fault zone. The F_2 folds here generally have a northeast vergence with a shallowly southwest dipping enveloping surface. A strong crenulation lineation is parallel to the F_2 fold axes and stretching lineations. Rare kyanite blades locally occur along this lineation as well. Wolf *et al*. (2010) published a 102.6 ±3.7 Ma Lu-Hf age of garnet porphyroblasts within Kumealon Inlet, suggesting that peak metamorphism and associated deformation took place during the mid-Cretaceous.

Domain 4

Domain 4 is a narrow zone along the shores of Telegraph Passage (Figure 2). It comprises the

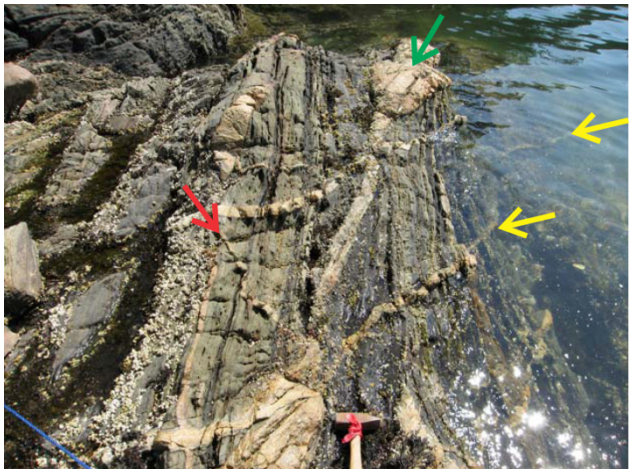

Figure 5. Granodioritic dikes late synkinematic to sinistral shear near the Salt Lagoon shear zone, northwestern Pitt Island. The red arrow indicates a dike in the shortening quadrant, exhibiting folds; the green arrow indicates a dike in the extensional quadrant, exhibiting pinch and swell structures; and the two yellow arrows indicate a single dike which has rotated from the shortening quadrant into the extensional quadrant and thus contains folds as well as pinch and swell structures.

anomalously north striking Telegraph Passage shear zone and its wallrocks. The wallrocks preserve a strain gradient and display steepening and a slight clockwise deflection of the S_1 foliation on approaching the shear zone. The Telegraph Passage shear zone itself is poorly exposed, because it is largely under water. Lineations along the eastern shore of Telegraph passage plunge moderately to the south. Asymmetric folds, obliquely boudinaged veins and the sense of deflection and/or refraction of the foliations indicate dextral motion with a west side up component (Figures 7a, b). The large degree of separation of boudins in pulled-apart veins and pegmatite dikes suggest the main stretching was subhorizontal. All structures are consistent with a predominantly dextral horizontal component of shear. The Telegraph Passage shear zone lies on strike with the Prince Rupert shear zone to the north, which in part also records dextral sense of shear (Chardon, 2003).

A quartz diorite dike was collected which crosscuts well developed foliation, contains a weakly developed foliation, and records stretching consistent with dextral

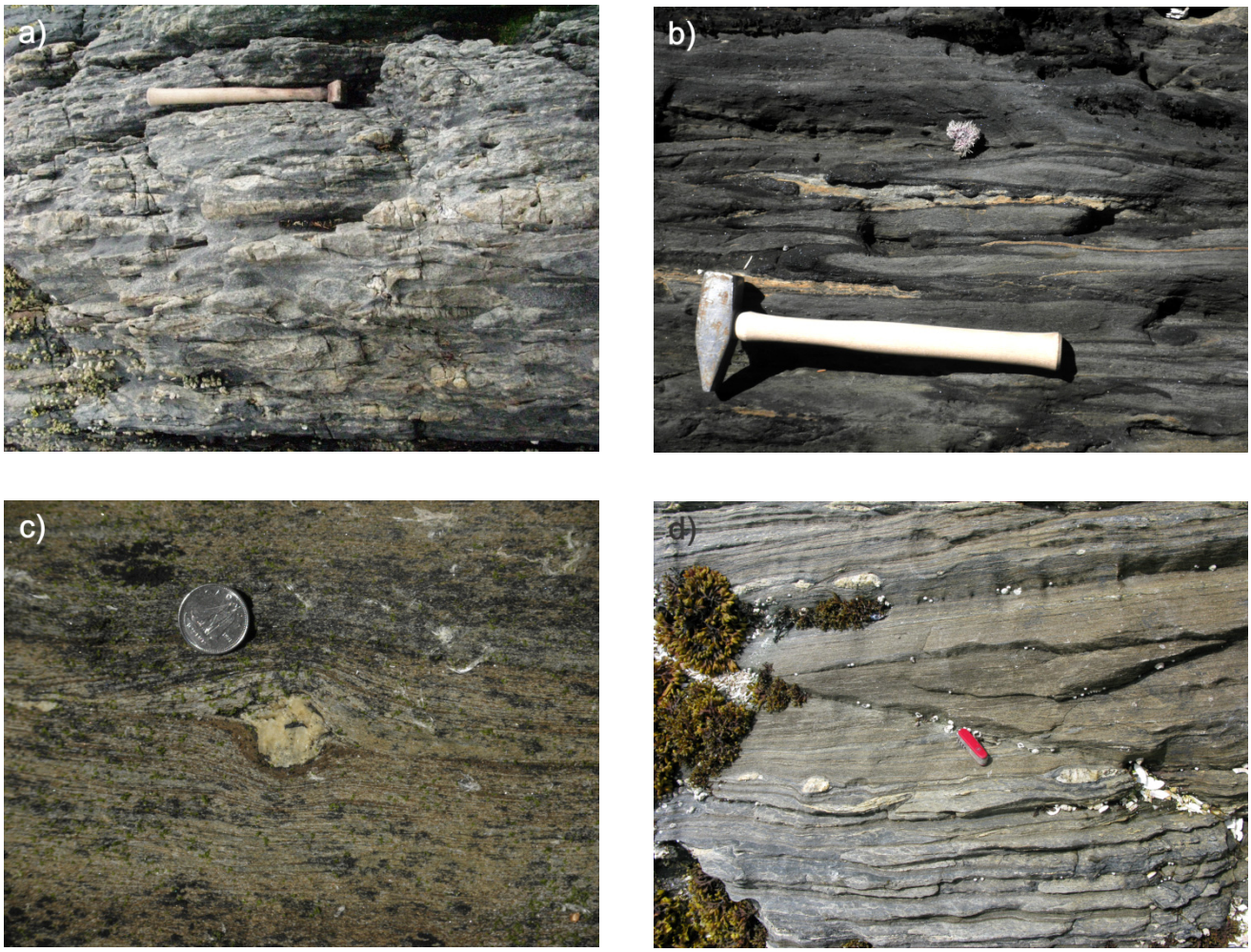

Figure 6. Structural features of domain 3. a) Cobble conglomerate of the Mathieson Channel Formation with 6:1 aspect ratios; b) Pillow basalt of the Descon Formation with 20:1 aspect ratios; c) Sigma porphyroclast indicating sinistral shear; d) Boudinage of a vein indicating significant horizontal stretching associated with sinistral shear.

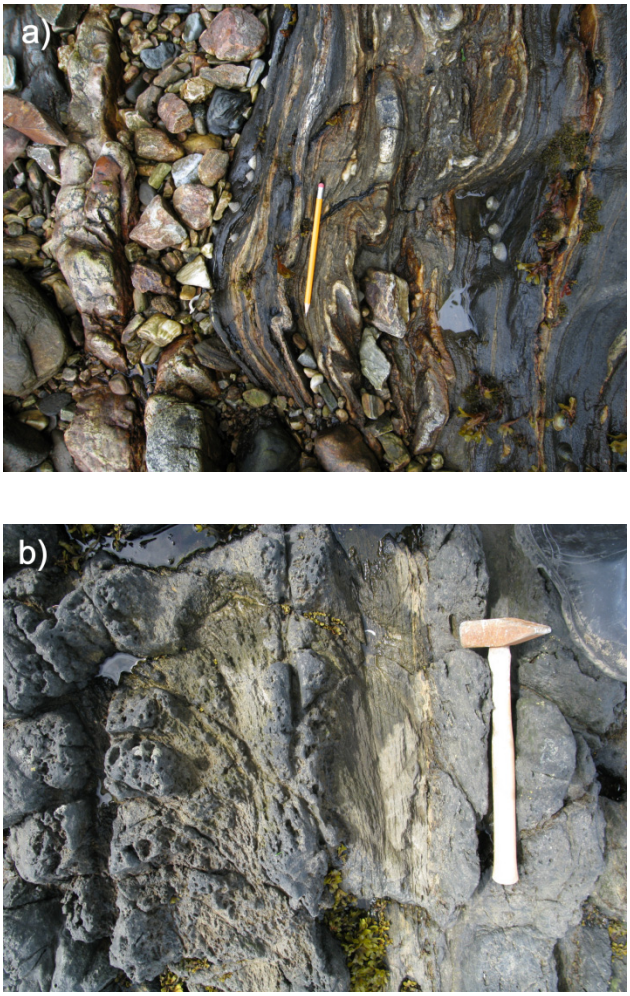

Figure 7. Kinematic indicators associated with Telegraph Passage shear zone along the eastern shore of Telegraph Passage. a) Strongly asymmetric folds indicating dextral shear; b) Dextral deflection of foliation into a local high strain zone.

shear. This dike yielded a U-Pb zircon age of 97.2 ±2.1 Ma (ID-TIMS unpublished data), suggesting that the dextral Telegraph Passage shear zone was roughly coeval with shear in the sinistral Grenville Channel and Salt Lagoon shear zones. Nevertheless, the north-striking foliation associated with the Telegraph Passage shear zone was deflected sinistrally by the northwest striking Grenville Channel shear zone to the south, indicating that sinistral shearing outlasted dextral shearing, at least locally.

Another north striking dextral shear zone has been documented south of Grenville Channel, approximately 100 km to the southeast (Chardon *et al*., 1999). Nelson *et al*. (2012) estimate that mid-Cretaceous offset along the Grenville Channel shear zone was approximately 5 kilometres; therefore, this is unlikely to represent the continuation of the Telegraph Passage shear zone. It may, however, represent another conjugate to the northwest striking Grenville Channel shear zone.

Domain 5

This is a complex zone occupying the apex situated between the northwest striking Lamppost shear zone of domain 2 and the north striking Telegraph Passage shear zone of domain 4. The dominant foliation dips moderately to steeply to the northeast. As in domain 3, open to isoclinal upright folds are common; however, here the plunges of the hinge lines display much more variation, between northwest and southeast. A significant feature of this domain is the presence of a conjugate set of small scale sinistral and dextral shear bands, which are parallel to the large scale shear zones (Figures 8a-c). The conjugate angle of the shear bands is 117°, well within the range of observed and predicted values for ductile conjugate faults (Zheng *et al*., 2004, 2011).

DISCUSSION

Age and nature of the various phases of deformation

The structural observations summarized herein contribute to the understanding of the complex tectonic history of the Alexander terrane. They have been divided into one Paleozoic and two Mesozoic events on the basis of existing timing constraints.

D_{1P}

The Alexander terrane preserves strong evidence, within domain 1, for formation of a northeast dipping transposition foliation, isoclinal folding and sinistral oblique reverse shearing coeval with Late Silurian to Early Devonian intrusion of the Ogden Channel plutonic complex (Nelson *et al*., 2012). These Paleozoic structures are referred to herein as D_{1p} (Paleozoic). The very weakly deformed *ca.* 411 Ma Porcher Creek pluton suggests that $D1_p$ ended in the Early Devonian. So far, no evidence of Paleozoic transposition fabrics has been found north of the Salt Lagoon shear zone. On northeastern Porcher Island (domain 2), volcanic rocks of the Descon Formation typically display well preserved primary textures, and transposition fabrics are restricted to the vicinity of discrete shear zones.

D_{1M}

Observed D_1 structures in domains 2 to 5 are solely represented by S_1, which is continuous across the inferred Alexander-Yukon-Tanana terrane boundary in domain 3. This implies S_1 in these domains formed during or after the initial latest Triassic-Middle Jurassic docking of these two terranes (Gehrels *et al*., 1992; van der Heyden, 1992; McClelland and Mattinson, 2000; Saleeby, 2000; Gehrels, 2001). The responsible deformation is therefore referred to herein as D_{1m} (Mesozoic), to highlight its difference from D_{1p} in domain 1.

The age of D_{1m} is poorly constrained between the late Triassic and the mid-Cretaceous age of D_2 (see below) and attainment of peak metamorphism. S_1 is parallel to

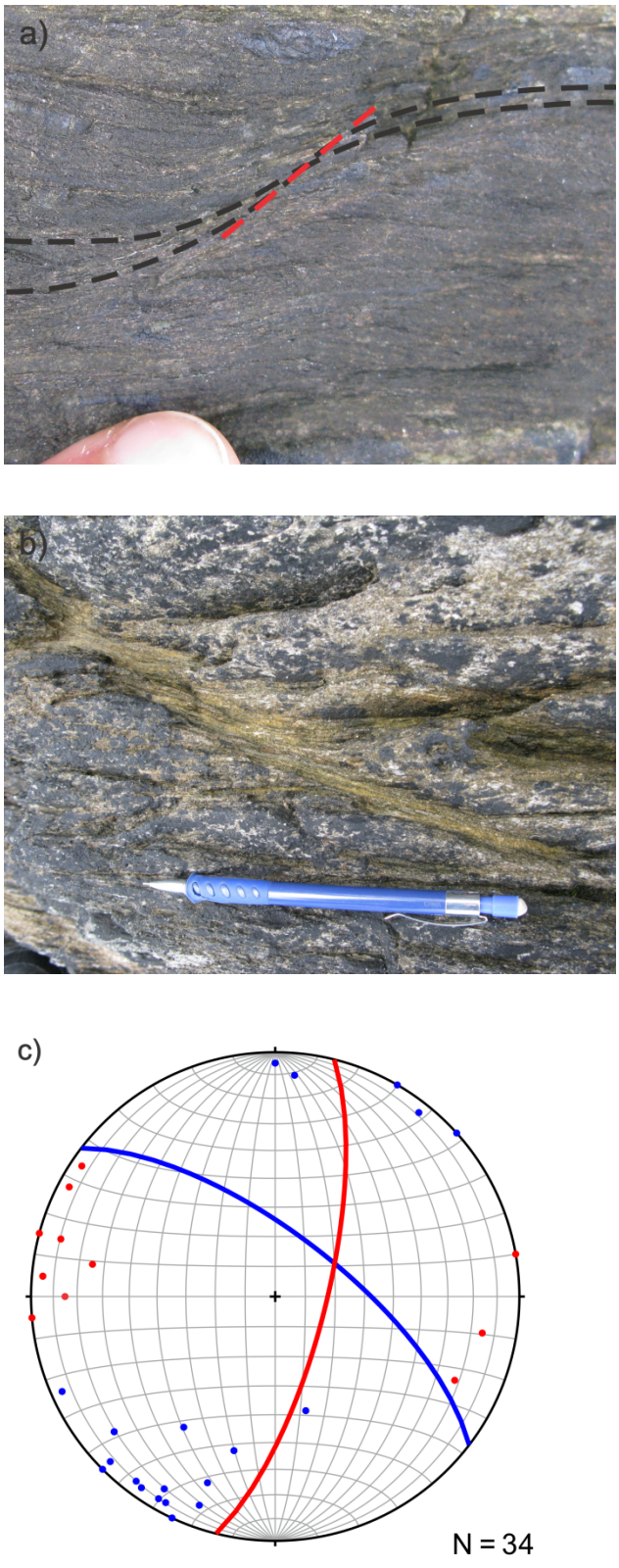

Figure 8. Shear bands in domain 5. a) Sinistral shear band, foliation traces (black dashed lines) curve into shear band (red dashed line) indicating sinistral shear; b) Dextral shear band; c) Lower hemisphere, equal area stereonet plot showing poles to sinistral shear bands in blue and poles to dextral shear bands in red, average values are plotted as the corresponding planes.

the contacts between the major lithological units, including the 'garnetite' layer interpreted as the cryptic terrane-bounding fault. This fault formed prior to peak metamorphism, and was subsequently annealed to its current representation.

D_2

D_2 encompasses F_2 upright folding of the pre-existing transposition foliation, formation of the S_2 axial planar foliation, and formation of a conjugate set of shears, both on outcrop scale (shear band) and map scale (shear zone). Although there are minor differences in the nature of the D_2 structures from one domain to another, there is a strong consistency in their overall structural style and kinematics, suggesting they formed during the same deformation event. Existing geochronological constraints indicate that D_2-related sinistral and dextral shearing was mid-Cretaceous (104-97 Ma), which is coeval with peak metamorphism (Wolf *et al*., 2010).

Significance and tectonic setting of D_{1p}

D_{1p} structures have been recognised solely in domain 1. Here F_2 folds refold earlier F_1 isoclines, which in turn fold an older foliation in amphibolite facies tectonite. These F_1 isoclines and the older foliation have only been observed in domain 1 and formed synkinematic with respect to the emplacement of intrusions in the Late Silurian to Early Devonian Ogden Channel complex. Domain 1 thus appears to contain an earlier phase of structures compared to those recorded elsewhere. In addition, plutonic correlatives of the Ogden Channel complex are absent in the other domains. We tentatively attribute this difference in deformation and plutonic history to domain 1 having been situated in a different tectonic setting within the Alexander terrane than the other domains during the Early Devonian. The Ogden Channel complex of domain 1 represents the previously undocumented lower crustal roots of a Late Silurian to Early Devonian magmatic arc, Nelson *et al*. (2012) suggested that it formed during amalgamation of primitive arc and pericratonic fragments within the Alexander terrane, assigning it to the Klakas orogeny of Gehrels *et al*. (1983). The orientation and sense of shear of D_{1p} structures indicates sinistral transpression and southwest vergence, similar to southwest vergent thrusts ascribed to the Klakas orogeny by Gehrels *et al*. (1996).

Significance and tectonic setting of D_{1m}

The distribution of the Alexander and proposed Yukon Tanana terrane rocks in Kumealon Inlet (see above) suggests that the cryptic D_{1m} fault was folded, together with S_1, into upright, shallowly northwest plunging F_2 folds in domain 3. At present, the quartz-pebble conglomerate and its surrounding pelite and garnetite occupy the core of a tight F_2 fold, surrounded by Alexander terrane units. The F_2 folds are slightly asymmetric and verge to the northeast. The F_2 enveloping surface has a shallow dip to the west. Since an enveloping

surface connects the crests or troughs of a given layer, S_1 probably had a shallow dip prior to F_2 in this domain. The upright nature of F_2 folds throughout the area described herein, suggest that S_1 in general was a shallowly-dipping structure prior to F_2, although its paleodip is unknown at present. Given the probable shallow dip of S_1 prior to F_2, its parallelism to lithological contacts, and development prior to peak metamorphism, we suggest that D_{1m} formed during thrusting and concomitant thickening. If correct, D_{1m} may be related to the initial latest Triassic – Middle Jurassic interaction of these terranes (Gehrels *et al*., 1992; van der Heyden, 1992; McClelland and Mattinson, 2000; Saleeby, 2000; Gehrels, 2001). Alternatively, D_{1m} and D_2 could represent a continuous deformation event whereby D_{1m} thrusting progressed to folding and formation of steeply dipping shear zones.

Significance and tectonic setting of D_2

The outstanding structures in the area are northwest striking, steeply northeast dipping shear zones on outcrop and map scales, which overall have accommodated an important component of sinistral transcurrent shear. Some of these shear zones also accommodated a significant dip slip component; both reverse and normal sense of movements have been observed. However, the relative timing of these dip slip components is poorly known at present, although both the normal and reverse motions accompanied the sinistral shear. The area also contains a subordinate, north striking, steeply west dipping shear zone, the Telegraph Passage shear zone, which mainly has accommodated dextral transcurrent movements with a minor reverse component (west-side-up). Based on relationships observed in outcrop, we have interpreted that both sets of transcurrent shear zones originally formed as a conjugate pair. Evidence from domain 4 suggests that sinistral shear in the Grenville Channel shear zone outlasted dextral shear in the Telegraph Passage shear zone. Dominance of one shear zone over the other in such a way is a common feature of conjugate shear zones (Ramsay and Huber, 1987). This interpretation implies that the bulk shortening direction during initial shear zone development was oriented northeast-southwest, which is perpendicular to the axial planes of the more upright F_2 folds in domains 3 and 5. This observation supports our interpretation that shearing and F_2 folding form part of the same progressive deformation event (D_2). Following earlier workers (Monger *et al*., 1994; Chardon *et al*; 1999; Israel *et al*., 2006; Gehrels *et al*., 2009) we relate D_2 to an overall sinistral transpressive deformation regime associated with southward motion of the Alexander terrane relative to the paleo-Pacific margin of Laurentia during the mid-Cretaceous.

ACKNOWLEDGMENTS

This paper forms part of J.J. Angen's M.Sc. thesis at the University of Waterloo. We thank JoAnne Nelson and Brian Mahoney for fruitful discussions and ongoing communication. The skiff used to carry out this project was generously supplied by Don Willson. We thank Todd Lau and Jean-Luc Pilote for their excellent assistance in the field. Thanks to all the residents of Oona River, who made us feel so welcome. Thanks to Bart Proctor and Bob Letts for countless boat trips and even more advice. A special thanks goes out to Jan Lemon for always finding a way to accommodate our logistical problems with a smile. This research was funded by NRCan through the GEM project. The manuscript was greatly improved as a result of a detailed review by JoAnne Nelson. This is Earth Sciences Sector (ESS) contribution #20110288.

REFERENCES

Berg, H.C., Jones, D.L. and Richter, D.H. (1972): Gravina-Nutzotin belt: tectonic significance of an upper Mesozoic sedimentary and volcanic sequence in southern and southeastern Alaska; *U.S. Geological Survey,* Professional Paper 800-D, pages D1-D24.

Butler, R.F., Gehrels, G.E., Baldwin, S.L. and Davidson, C. (2002): Paleomagnetism and geochronology of the Ecstall pluton in the Coast Mountains of British Columbia; Evidence for local deformation rather than large-scale transport; *Journal of Geophysical Research,* Volume 107, pages 3-13.

Chardon, D. (2003): Strain partitioning and batholith emplacement at the root of a transpressive magmatic arc; *Journal of Structural Geology,* Volume 25, pages 91-97.

Chardon, D., Andronicos, C.L. and Hollister, L.S. (1999): Large-scale transpressive shear zone patterns and displacements within magmatic arcs: the Coast Plutonic Complex, British Columbia; *Tectonics*, Volume 16, pages 278-292.

Colpron, M. and Nelson, J. (2009): A Palaeozoic Northwest Passage: incursion of Caledonian, Baltican and Siberian terranes into eastern Panthalassa, and the early evolution of the North American Cordillera; *in* Cawood, P.A. and Kroner, A. eds., Earth Accretionary Systems in Space and Time; *The Geological Society of London,* Special Publications, Volume 318, pages 273-307.

Colpron, M., Nelson, J. and Murphy, D. (2007): Northern Cordilleran terranes and their interactions through time; *GSA Today*, Volume 17, pages 4-10.

Crawford, M.L., Hollister, L.S. and Woodsworth, G.J. (1987): Crustal deformation and regional metamorphism across a terrane boundary, Coast Plutonic Complex, British Columbia; *Tectonics,* Volume 6, pages 343-361.

Crawford, M.L., Crawford, W.A. and Gehrels, G.E. (2000): Terrane assembly and structural relationships in the eastern Prince Rupert quadrangle, British Columbia; *in* Stowell, H.H., McClelland, W.C., eds., Tectonics of the Coast Mountains, Southeastern Alaska and British Columbia; *Geological Society of America*, Special Paper 343, pages 1-21.

Eberlein, G.D. and Churkin, M.J. (1970): Paleozoic stratigraphy in the northwest coastal area of Prince of Wales Island, southeastern Alaska; *U.S. Geological Survey*, Bulletin 1284, 67 pages.

Evenchick, C.A. (2001): Northeast-trending folds in the western Skeena fold belt, northern Canadian Cordillera: a record of early Cretaceous sinistral plate convergence; *Journal of Structural Geology,* Volume 23, pages 1123-1140.

Gardner, M.C., Bergman, S.C., Cushing, G.W., MacKevett, E.M. Jr., Plafker, G., Campbell, R.B., Dodds, C.J., McClelland, W.C. and Mueller, P.A. (1988): Pennsylvanian pluton stitching of Wrangellia and the Alexander terrane, Wrangell Mountains, Alaska; *Geology*, Volume 16, pages 967-971.

Gehrels, G.E. (2001): Geology of the Chatham Sound region, southeast Alaska and coastal British Columbia; *Canadian Journal of Earth Sciences*, Volume 38, pages 1579-1599.

Gehrels, G.E. and Boghossian, N.D. (2000): Reconnaissance geology and U-Pb geochronology of the west flank of the Coast Mountains between Bella Coola and Prince Rupert, coastal British Columbia; *in* Stowell, H.H. and McClelland, W.C., eds., Tectonics of the Coast Mountains, Southeastern Alaska and British Columbia; *Geological Society of America,* Special Paper 343, pages 61-76.

Gehrels, G.E. and Saleeby, J.B. (1987): Geologic framework, tectonic evolution, and displacement history of the Alexander terrane; *Tectonics*, Volume 6, pages 151-173.

Gehrels, G.E., Saleeby, J.B. and Berg, H.C. (1983): Preliminary description of the Klakas orogeny in the southern Alexander terrane, southeastern Alaska; *in* Stephens, C.H., ed., Pre-Jurassic Rocks in Western North American Suspect Terranes; *Pacific Section, Society of Economic Paleontologists and Mineralogists*, pages 131-141.

Gehrels, G.E., McClelland, W.C., Samson, S.D., Patchett, J.P. and Orchard, M.J. (1992): Geology of the western flank of the Coast Mountains between Cape Fanshaw and Taku Inlet, southeastern Alaska; *Tectonics*, Volume 11, pages 567-585.

Gehrels, G. E., Butler, R. F. and Bazard, D. R. (1996): Detrital zircon geochronology of the Alexander terrane, southeastern Alaska; *Geological Society of America Bulletin*, Volume 108, pages 722-734.

Gehrels, G., Rusmore, M., Woodsworth, G., Crawford, M., Andronicos, C., Hollister, L., Patchett, J., Ducea, M., Butler, R., Klepeis, K., Davidson, C., Friedman, R., Haggart, J., Mahoney, B., Crawford, W., Pearson, D. and Girardi, J. (2009): U-Th-Pb geochronology of the Coast Mountains batholith in north-coastal British Columbia: constraints on age and tectonic evolution; *Geological Society of America Bulletin*, Volume 121, pages 1341-1361.

Haeussler, P.J. (1992): Structural evolution of an arc-basin: The Gravina Belt in central southeastern Alaska; *Tectonics*, Volume 11, pages 1245-1265.

Hanmer, S. and Passchier, C.W. (1991): Shear sense indicators, a review; *Geological Survey of Canada*, Paper 90, pages 1-71.

Hurlow, H.A. (1993): Mid-Cretaceous strike-slip and contractional fault zones in the western Intermontane terrane, and their relation to the North Cascades-southeastern Coast Belt orogen; *Tectonics*, Volume 12, pages 1240-1257.

Hutchison, W.W. (1982): Geology of the Prince Rupert – Skeena map area, British Columbia; *Geological Survey of Canada* Memoir 394, 115 pages, with 1:250 000 scale geological map, GSC Map 1427A.

Israel, S. (2001): Structural and stratigraphic relationships within the Tchaikazan River area, southwestern British Columbia: Implications for the tectonic evolution of the southern Coast belt; M.Sc. Thesis; *University of British Columbia*, 129 pages.

Israel, S., Schiarizza, P., Kennedy, L.A., Friedman, R.M. and Villeneuve, M. (2006): Evidence for Early to Late Cretaceous sinistral deformation in the Tchaikazan River area, southwestern British Columbia: Implications for the tectonic evolution of the southern Coast belt; *in* Haggart, J.W., Enkin, R.J., and Monger, J.W.H., eds., Paleogeography of the North American Cordillera: Evidence For and Against Large-Scale Displacements; *Geological Association of Canada*, Special Paper 46, pages 331-350.

Jiang, D. and Williams, P.F. (1999): When do dragfolds not develop into sheath folds in shear zones?; *Journal of Structural Geology,* Volume 21, pages 577-583.

Lin, S., Jiang, D. and Williams, P.F. (2007): Importance of differentiating ductile slickenside striations from stretching lineations and variation of shear direction across a high-strain zone; *Journal of Structural Geology*, Volume 29, pages 850-862.

McClelland and Mattinson, J.M. (2000): Cretaceous-Tertiary evolution of the western Coast Mountains, central southeastern Alaska; *in* Stowell, H.H., McClelland, W.C., eds., Tectonics of the Coast Mountains, Southeastern Alaska and British Columbia; *Geological Society of America,* Special Paper 343, pages 159-182.

McClelland, W.C., Gehrels, G.E., Samson, S.D. and Patchett, P.J. (1992): Structural and geochronologic relations along the western flank of the Coast Mountains Batholith: Stikine River to Cape Fanshaw, central southeastern Alaska; *Journal of Structural Geology*, Volume 14, pages 475-489.

Monger, J.W.H., van der Heyden, P., Journeay, J.M., Evenchick, C.A. and Mahoney, J.B. (1994): Jurassic-Cretaceous basins along the Canadian Coast belt: Their bearing on pre-mid-Cretaceous sinistral displacements; *Geology*, Volume 22, pages 175-178.

Morozov, I.B., Smithson, S.B., Hollister, L.S. and Diebold, J.B. (1998): Wide-angle seismic imaging across accreted terranes, southeastern Alaska and western British Columbia; *Tectonophysics*, Volume 299, pages 281-296.

Nelson, J.L., Mahoney, J.B., Gehrels, G.E., van Staal, C. and Potter, J.J. (2010a): Geology and mineral potential of Porcher Island, northern Grenville Channel and vicinity, northwestern British Columbia; *BC Ministry of Energy, Mines and Petroleum Resources*, Geological Fieldwork 2009, pages 19-42.

Nelson, J.L., Mahoney, J.B., Gehrels, G.E. (2010b): Geology and mineral potential of the Porcher Island–Grenville Channel area, northwestern British Columbia (parts of 103G/15,16, H/13, J/1 and 2); *BC Ministry of Energy and Mines*, Open File 2010-03; *Geological Survey of Canada*, Open File 6654, scale 1:50 000.

Nelson, J.L., Diakow, L.J., Karl, S., Mahoney, J.B., Gehrels, G.E., Pecha, M. and van Staal, C. (2011): Geology and Mineral Potential of the Southern Alexander terrane and western Coast Plutonic Complex near Klemtu, northwestern British Columbia; *BC Ministry of Energy and Mines*, Geological Fieldwork 2010, pages 73-97.

Nelson, J.L., Diakow, J.B., Mahoney, J.B., van Staal, C., Pecha, M., Angen, J., Gehrels, G. and Lau, T. (2012, this volume): North Coast project: Tectonics and metallogeny of the Alexander terrane, and Cretaceous sinistral

shearing of the western Coast belt; *BC Ministry of Energy and Mines*; Geological Fieldwork 2011, in press.

Ramsay, J.G. and Huber, M.I. (1987): The techniques of modern structural geology: Volume 2 Folds and Faults; *Academic Press;* San Diego, California. 391 pages.

Roddick, J.A. (1970): Douglas Channel-Hecate Straight map-area, British Columbia; *Geological Survey of Canada*, Paper 70-41, 70 pages.

Rubin, C.M. and Saleeby, J.B. (1987): The inner boundary zone of the Alexander terrane in southern Southeastern Alaska, a newly discovered thrust belt; *Geological Society of America Abstracts with Programs*, Volume 19, pages 455.

Rubin, C.M. and Saleeby, J.B. (1992): Tectonic history of the eastern edge of the Alexander terrane, southeast Alaska; *Tectonics*, Volume 11, pages 586-602.

Rubin, C.M., Saleeby, J.B, Cowan, D.S., Brandon, M.T. and McGroder, M.F. (1990): Regionally extensive mid-Cretaceous west-vergent thrust system in the northwestern Cordillera: Implications for continental margin tectonism; *Geology,* Volume 18, pages 276-280.

Saleeby, J.B. (2000): Geochronologic investigations along the Alexander-Taku terrane boundary, southern Revillagigedo Island to Cape Fox areas, southeast Alaska; *in* Stowell, H.H., McClelland, W.C., eds., Tectonics of the Coast Mountains, Southeastern Alaska and British Columbia; *Geological Society of America,* Special Paper 343, pages 107-143.

Schiarizza, P., Gaba, R.G., Glover, J.K., Garver, J.I. and Umhoefer, P.J. (1997): Geology and mineral occurrences of the Taseko – Bridge River area: *BC Ministry of Employment and Investment*, Bulletin 100, 291 pages.

van der Heyden, P. (1989): U–Pb and K–Ar geochronometry of the Coast Plutonic Complex, 53°–54° N, and implication for the Insular–Intermontane superterrane boundary, British Columbia; unpublished Ph.D. Thesis; *University of British Columbia*, 392 pages.

van der Heyden, P. (1992): A Middle Jurassic to Early Tertiary Andean-Sierran arc model for the Coast Belt of British Columbia; *Tectonics*, Volume 11, pages 82-97.

Wolf, D.E., Andronicos, C.L., Vervoort, J.D., Mansfield, M.R. and Chardon, D. (2010): Application of Lu-Hf garnet dating to unravel the relationships between deformation, metamorphism and plutonism: An example from the Prince Rupert area, British Columbia; *Tectonophysics,* Volume 485, pages 62-77.

Zheng, Y.D., Wang, T., Ma, M. and Davis, G.A. (2004): Maximum effective moment criterion and the origin of low-angle normal faults; *Journal of Structural Geology*, Volume 26, pages 271-285.

Zheng, Y., Zhang, J. and Wang, T. (2011): Puzzles and the maximum-effective-moment (MEM) criterion in structural geology; *Journal of Structural Geology*, Volume 33, pages 1394-1405.

U-Pb Isotopic Ages from Volcanic Rocks near Ootsa Lake and Francois Lake, West-Central British Columbia

by T. Ferbey[1] and L.J. Diakow[1]

KEYWORDS: U-Pb zircon isotopic age, Ootsa Lake, Francois Lake, Ootsa Lake Group, Kasalka Group, Late Cretaceous magmatism

INTRODUCTION

Uranium-lead isotopic dates have been determined for porphyritic dacites previously assigned to the Eocene Ootsa Lake Group by Massey *et al.* (2005). Two rock samples were collected for U-Pb geochronology from isolated exposures in central Stikine terrane between Ootsa Lake and Francois Lake during a Quaternary geology and till geochemistry program conducted in Nadina River map area (NTS 093E/15) in 2009 (Ferbey, 2010; Figure 1). The new dates indicate that they are Late Cretaceous and are provisionally included as late volcanic components of the Kasalka Group, a continental margin, magmatic-arc sequence that extends across central Stikine terrane. Regionally, Late Cretaceous magmatic-arc rocks in central Stikine terrane are an important source for porphyry style Cu-Mo mineralization, and currently the focus of exploration for volcanic-hosted, bulk tonnage gold-silver-base metal mineralization.

GENERAL GEOLOGY

The Nadina River map area is centrally located within the Stikine terrane, on the southern flank of the Skeena Arch. The Stikine terrane comprises subduction-related island-arc magmatic rocks that were emplaced from Carboniferous through Early Jurassic time. The Jurassic arc components belong to the Hazelton Group and include volcanic and sedimentary rocks associated with a few widely spaced, coeval plutons that together define the Skeena Arch. The Skeena Arch in Late Jurassic time was a broad highland region underlain by Hazelton Group and older arc strata that effectively formed much of the south and southeast margin for Late Jurassic to Early Cretaceous marine deltaic and slope clastic facies deposited in the Bowser Basin. In contrast to these clastic deposits from the Bowser Lake Group north of the arch, Early Cretaceous marine clastic and rare volcanic deposits of the Skeena Group succeeded by Late Cretaceous and Eocene continental volcanic arc sequences of the Kasalka, Ootsa and Endako groups overlap the southern flank of the Skeena Arch.

The bedrock geology of Nadina Lake area was first mapped by Hedley (1935) and subsequently during regional mapping surveys of the Whitesail Lake map sheet (NTS 093E) by Duffell (1959) and Woodsworth (1980). The oldest rocks, the Hazelton Group, composed of feldspathic sandstone containing Middle Jurassic macrofossils, underlie the area adjacent to Tahtsa Reach and west of Shelford Hills (Woodsworth, 1980; Diakow and Mihalynuk, 1987; Figure 1). According to Woodsworth (1980), rhyolite and andesite flows and fragmental deposits assigned to the Late Cretaceous Kasalka Group underlie the central portion of Nadina Lake map area, at Shelford Hills. In subdued topography east and southeast of Shelford Hills between Francois and Ootsa lakes, Woodsworth (1980) recognized isolated occurrences of felsic volcanic rocks which he designated as latest Cretaceous to Eocene (unit uKEv) comprising part of either the Kasalka Group or Ootsa Lake Group. In this area, bedrock is generally scarce and limited to small, isolated outcrops surrounded by near-continuous cover composed of till and glaciofluvial sediments deposited during the Late Wisconsinan Fraser glaciation (Ferbey, 2010).

ANALYTICAL TECHNIQUE

Samples collected for U-Pb zircon isotopic age determinations were prepared and analyzed by Apatite to Zircon Inc. (Viola, Idaho). Analytical results determined by laser ablation inductively-coupled-plasma mass spectrometry (LA-ICP-MS) are presented in Tables 1 and 2 for samples 10TFE060 and 10TFE061, respectively.

Laser Ablation Inductively-Coupled-Plasma Mass Spectrometry

Zircons were extracted using standard mineral-separation techniques at the laboratories of Apatite to Zircon Inc. Zircons (both standards and unknowns) were then mounted in 1 cm^2 epoxy wafers, and ground down to expose internal grain surfaces prior to final polishing. Wafers were etched in 5.5M HNO_3 for 20 seconds at 21°C to thoroughly clean the surface of the grains prior to

[1] *British Columbia Geological Survey, Victoria, BC*

This publication is also available, free of charge, as colour digital files in Adobe Acrobat® PDF format from the BC Ministry of Energy and Mines website at http://www.empr.gov.bc.ca/Mining/Geoscience/PublicationsCatalogue/Fieldwork.

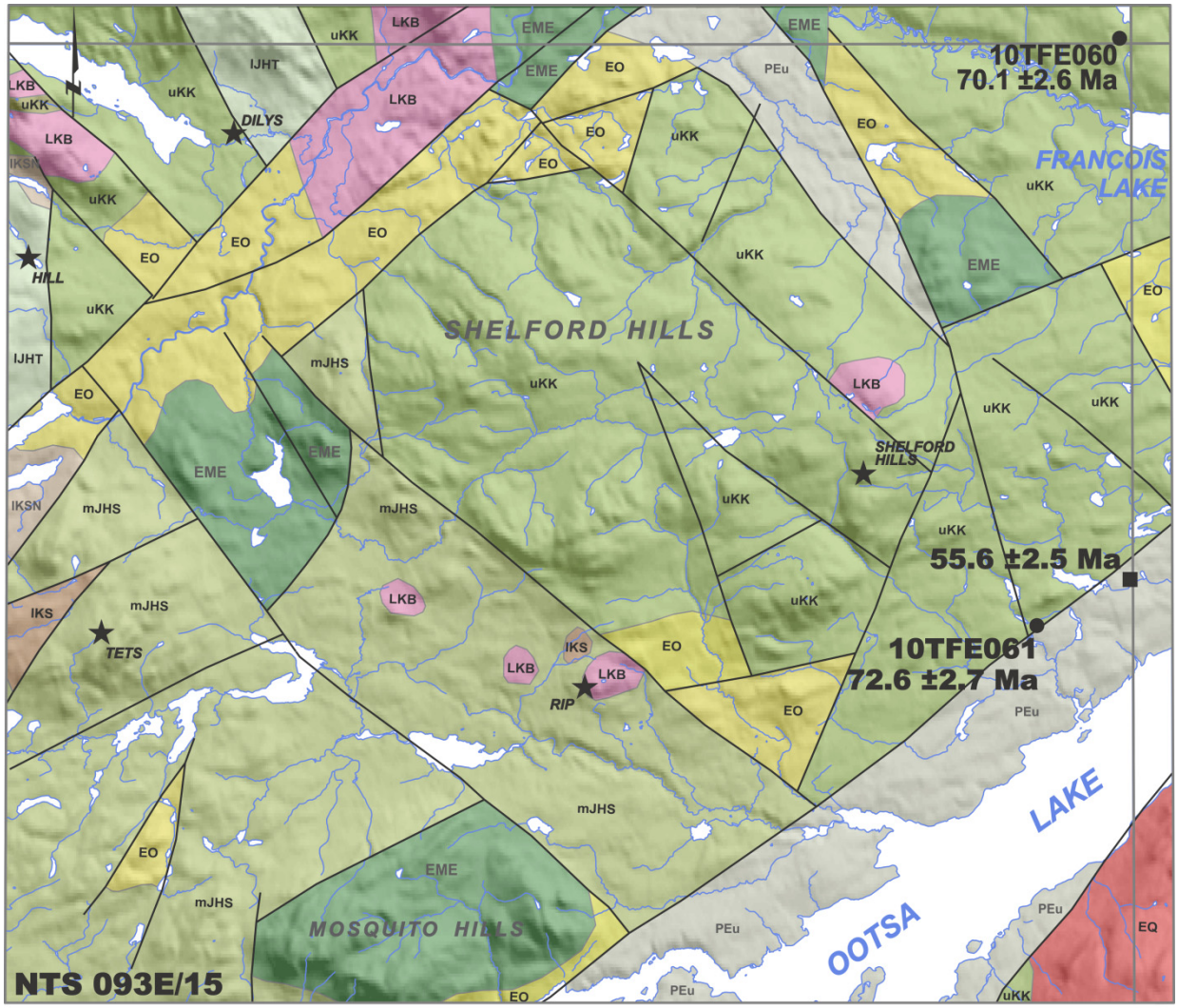

★ *metallic mineral occurrence (showing)*

● *U-Pb zircon isotopic age date (this study)*

■ *K-Ar isotopic age date (Stevens et al., 1982)*

0 5 10 15
kilometres

Eocene to Lower Miocene

EME *Endako Group* — *basaltic volcanic rocks*

Eocene

EO *Ootsa Lake Group* — *rhyolite, felsic volcanic rocks*

Paleocene to Eocene

PEu *undivided sedimentary rocks*

Lower and Upper Cretaceous

uKK *Kasalka Group* — *andesitic volcanic rocks*

IKS *Skeena Group* — *undivided sedimentary rocks*

IKSN *Mt. Ney Volcanics* — *undivided volcanic rocks*

Lower and Middle Jurassic Hazelton Group

mJHS *Smithers Formation* — *undivided sedimentary rocks*

IJHT *Telkwa Formation* — *calc-alkaline volcanic rocks*

Intrusions

EQ *Eocene Quanchus plutonic suite* — *feldspar porphyritic intrusive rocks*

LKB *Late Cretaceous Bulkley plutonic suite* — *granodioritic intrusive rocks*

Figure 1. Bedrock geology of NTS 093E/15 (Nadina River) and adjacent areas to the north and east (modified from Massey *et al.*, 2005). Shown in black dots are sample locations for U-Pb zircon isotopic age determinations.

Table 1. Laser ablation inductively-coupled-plasma mass spectrometry U-Pb data for sample 10TFE060.

	Isotopic Ratios				Age (Ma)	
analysis	$^{207}Pb/^{235}U$	±2σ error	$^{206}Pb/^{238}U$	±2σ error	$^{206}Pb/^{238}U$	±2σ error
115706_002	0.0738	0.0025	0.0108	0.0005	69.08	3.10
115706_004	0.0758	0.0025	0.0105	0.0005	67.16	3.04
115706_006	0.0810	0.0025	0.0109	0.0005	70.01	3.16
115706_009	0.0794	0.0025	0.0112	0.0005	71.77	3.25
115706_010	0.0739	0.0025	0.0112	0.0005	71.55	3.19
115706_011	0.0720	0.0025	0.0104	0.0005	66.51	3.09
115706_012	0.0774	0.0025	0.0107	0.0005	68.76	3.09
115706_017	0.0737	0.0025	0.0108	0.0005	69.17	3.12
115706_019	0.0728	0.0025	0.0106	0.0005	68.07	3.04
115706_020	0.0754	0.0025	0.0106	0.0005	67.94	3.05
115706_025	0.0789	0.0025	0.0116	0.0005	74.22	3.34
115706_027	0.0734	0.0025	0.0107	0.0005	68.87	3.08
115706_029	0.0752	0.0025	0.0112	0.0005	71.58	3.23
115706_032	0.0735	0.0025	0.0108	0.0005	69.31	3.13
115706_034	0.0716	0.0025	0.0104	0.0005	66.40	2.97
115706_035	0.0730	0.0025	0.0106	0.0005	68.11	3.06
115706_036	0.0741	0.0025	0.0107	0.0005	68.71	3.07
115706_037	0.2553	0.0025	0.0140	0.0039	89.44	25.08
115706_039	0.1281	0.0025	0.0085	0.0024	54.42	15.31
115706_041	0.0725	0.0025	0.0107	0.0005	68.70	3.16
115706_043	0.0739	0.0025	0.0108	0.0005	69.20	3.11
115706_045	0.0751	0.0025	0.0109	0.0005	70.02	3.15
115706_046	0.0750	0.0025	0.0109	0.0005	69.71	3.22
115706_047	0.0859	0.0025	0.0111	0.0005	71.20	3.41
115706_048	0.0743	0.0025	0.0108	0.0005	69.07	3.13
115706_050	0.0774	0.0025	0.0110	0.0005	70.62	3.17
115706_051	0.0752	0.0025	0.0111	0.0005	71.07	3.17
115706_054	0.0749	0.0025	0.0107	0.0005	68.92	3.09
115706_058	0.0765	0.0025	0.0107	0.0005	68.66	3.08
115706_062	0.0736	0.0025	0.0109	0.0005	69.59	3.11
115706_064	0.0737	0.0025	0.0109	0.0005	69.57	3.14
115706_065	0.1077	0.0025	0.0118	0.0005	75.81	3.53
115706_066	0.0778	0.0025	0.0107	0.0005	68.92	3.10
115706_067	0.0823	0.0025	0.0113	0.0005	72.72	3.28
115706_069	0.0768	0.0025	0.0115	0.0005	73.65	3.30
115706_073	0.0721	0.0025	0.0108	0.0005	69.23	3.11
115706_075	0.0716	0.0025	0.0104	0.0005	66.75	2.99
115706_078	0.0796	0.0025	0.0111	0.0005	71.00	3.22
115706_082	0.0811	0.0025	0.0117	0.0006	75.25	3.59
115706_084	0.0756	0.0025	0.0113	0.0005	72.24	3.23
115706_086	0.1306	0.0025	0.0119	0.0006	76.06	3.78
115706_087	0.0799	0.0025	0.0111	0.0005	71.22	3.21
115706_088	0.0747	0.0025	0.0109	0.0005	70.07	3.15
115706_090	0.0728	0.0025	0.0109	0.0005	70.11	3.13
115706_091	0.0764	0.0025	0.0115	0.0005	73.86	3.32
115706_094	0.0731	0.0025	0.0111	0.0005	71.16	3.19
115706_095	0.0728	0.0025	0.0111	0.0005	71.02	3.25
115706_096	0.0724	0.0025	0.0108	0.0005	69.09	3.10
115706_098	0.0770	0.0025	0.0114	0.0005	72.77	3.52
115706_099	0.0750	0.0025	0.0107	0.0005	68.41	3.06
115706_100	0.0732	0.0025	0.0109	0.0005	70.19	3.14
115706_103	0.0761	0.0025	0.0110	0.0005	70.58	3.17
115706_105	0.0770	0.0025	0.0110	0.0005	70.82	3.16
115706_110	0.0843	0.0025	0.0114	0.0005	72.98	3.25

Table 2. Laser ablation inductively-coupled-plasma mass spectrometry U-Pb data for sample 10TFE061.

	Isotopic Ratios				Age (Ma)	
analysis	$^{207}Pb/^{235}U$	±2σ error	$^{206}Pb/^{238}U$	±2σ error	$^{206}Pb/^{238}U$	±2σ error
115707_001	0.0851	0.0031	0.0121	0.0005	77.46	3.52
115707_002	0.0753	0.0025	0.0112	0.0005	71.73	3.23
115707_003	0.0769	0.0026	0.0110	0.0005	70.82	3.20
115707_005	0.0777	0.0025	0.0113	0.0005	72.57	3.26
115707_006	0.0806	0.0026	0.0116	0.0005	74.20	3.36
115707_008	0.0755	0.0024	0.0112	0.0005	71.99	3.26
115707_009	0.0774	0.0026	0.0114	0.0005	73.01	3.32
115707_010	0.0799	0.0030	0.0113	0.0005	72.15	3.32
115707_017	0.0766	0.0025	0.0115	0.0005	73.80	3.32
115707_021	0.0761	0.0027	0.0108	0.0005	69.36	3.12
115707_022	0.0791	0.0026	0.0115	0.0005	73.79	3.33
115707_024	0.0788	0.0027	0.0116	0.0005	74.35	3.35
115707_025	0.0819	0.0031	0.0119	0.0005	76.31	3.53
115707_028	0.0742	0.0028	0.0110	0.0005	70.54	3.22
115707_029	0.0763	0.0026	0.0111	0.0005	71.32	3.18
115707_032	0.0799	0.0025	0.0117	0.0005	75.09	3.36
115707_033	0.0761	0.0025	0.0112	0.0005	71.83	3.23
115707_034	0.0769	0.0025	0.0111	0.0005	71.21	3.18
115707_035	0.0764	0.0025	0.0114	0.0005	73.04	3.29
115707_037	0.0739	0.0023	0.0110	0.0005	70.21	3.14
115707_038	0.0757	0.0026	0.0110	0.0005	70.81	3.18
115707_042	0.0771	0.0025	0.0111	0.0005	70.87	3.18
115707_043	0.1493	0.0568	0.0117	0.0007	75.25	4.57
115707_045	0.0762	0.0025	0.0110	0.0005	70.67	3.16
115707_050	0.0762	0.0024	0.0112	0.0005	71.92	3.21
115707_052	0.0750	0.0023	0.0112	0.0005	71.48	3.18
115707_054	0.0747	0.0024	0.0110	0.0005	70.53	3.15
115707_055	0.0779	0.0024	0.0117	0.0005	74.73	3.35
115707_058	0.0785	0.0027	0.0114	0.0005	73.02	3.35
115707_059	0.0758	0.0024	0.0112	0.0005	72.00	3.22
115707_061	0.1334	0.0197	0.0117	0.0007	75.16	4.61
115707_063	0.0813	0.0059	0.0111	0.0006	71.39	3.91
115707_066	0.0834	0.0109	0.0114	0.0005	73.22	3.35
115707_067	0.0785	0.0027	0.0115	0.0005	73.78	3.31
115707_069	0.0765	0.0024	0.0114	0.0005	73.01	3.26
115707_070	0.0753	0.0023	0.0112	0.0005	71.78	3.22
115707_074	0.0797	0.0027	0.0113	0.0005	72.14	3.24
115707_082	0.0760	0.0025	0.0112	0.0005	71.79	3.21
115707_083	0.0906	0.0057	0.0120	0.0006	76.88	3.79
115707_084	0.0788	0.0025	0.0117	0.0005	74.94	3.34
115707_085	0.0743	0.0025	0.0110	0.0005	70.67	3.21
115707_091	0.0759	0.0026	0.0112	0.0005	72.03	3.26
115707_094	0.0761	0.0024	0.0113	0.0005	72.48	3.24
115707_095	0.0829	0.0037	0.0120	0.0006	77.01	3.56
115707_098	0.0806	0.0025	0.0118	0.0005	75.81	3.42
115707_099	0.0756	0.0056	0.0107	0.0005	68.66	3.27
115707_100	0.0775	0.0025	0.0113	0.0005	72.47	3.24
115707_101	0.0875	0.0037	0.0121	0.0005	77.51	3.52
115707_105	0.0737	0.0025	0.0110	0.0005	70.49	3.17
115707_106	0.0748	0.0036	0.0108	0.0005	69.51	3.20
115707_107	0.0778	0.0026	0.0113	0.0005	72.43	3.24
115707_108	0.0751	0.0024	0.0112	0.0005	71.88	3.22
115707_109	0.0781	0.0025	0.0112	0.0005	72.09	3.21
115707_110	0.0791	0.0030	0.0118	0.0005	75.38	3.52

analysis. Grains, and the locations for laser spots on these grains, were selected using transmitted light with an optical microscope at a magnification of 2000x. This approach is preferred over the use of cathodoluminescence (CF) 2-D imaging as it allows for the recognition and characterization of features below the surface of individual grains, including the presence of inclusions and the orientation of fractures which may result in spurious isotopic counts.

Isotopic analyses were performed with a New Wave UP-213 laser ablation system, in conjunction with a ThermoFinnigan Element2 single collector, double-focusing magnetic-sector LA-ICP-MS, in the GeoAnalytical Lab at Washington State University (Pullman, Washington). For all analyses (both standard and unknown), laser-beam diameter was set at 20 μm and the laser frequency was set at 5 Hz yielding ablation pits ~10-15 μm deep. Helium and Ar gas were used to deliver the ablated material into the plasma source of the mass spectrometer. Each analysis of 250 cycles took approximately 30 seconds to complete, and consisted of a 6 second integration on peaks with the laser turned off (for background measurements), followed by a 25 second integration with the laser firing. A delay of up to 30 seconds occurred between analyses in order to purge the previous analysis and prepare for the next.

For each spot, fractionation factor-corrected isotopic ratios and ages were then calculated using data collected during scans 70-250 for each analysis. Errors for the isotopic ratios and ages are based on the fitting errors of the respective isotopes. Up to 181 individual scans, each yielding isotopic ratios and ages, are available for ultimate preferred age calculation. Plotting of analytical results was completed in Isoplot3 v. 3.71 (Ludwig, 2008).

VOLCANIC ROCK SAMPLES AND GEOCHRONOLOGY RESULTS

Two widely spaced bedrock exposures sampled between Francois Lake and Ootsa Lake for U-Pb geochronology during the Quaternary geology program consist of a relatively unaltered lava flow (10TFE060) and an altered lava flow (10TFE061). These samples were analyzed for 37 elements by inductively coupled plasma mass spectrometry (ICP-MS), following an aqua regia digestion. Determinations for copper, molybdenum, lead, zinc, silver, and gold, and pathfinder elements such as arsenic, antimony, and mercury are low in both samples.

Sample 10TFE060, located about 2 km north on the Parrot Lakes Road from the west end of Francois Lake (Figure 1), is a subdued outcrop 20 metres wide. It is composed of massive, maroon-weathered lava flow containing up to 25 volume percent white plagioclase phenocrysts, 1 to 4 millimetres in diameter, and a trace of biotite within an oxidized groundmass dusted with fine hematite (Figure 2). Major oxide analyses indicate this sample is dacitic in composition (71.04 wt.% SiO_2). Based on a weighted average of 54 $^{206}Pb/^{238}U$ dates, the crystallization age for this dacite is determined to be 72.6 ±2.7 Ma (Figure 3).

Sample 10TFE061, is from an abandoned roadside quarry 75 m wide located just off the Wisteria Main logging road, west of Wisteria on Ootsa Lake (Figure 1). It consists of massive, porphyritic and locally flow-laminated and brecciated lava flows in which primary volcanic textures are intact but replaced by microscopic quartz, clay minerals and finely disseminated and wisps of pyrite (Figure 4). They exhibit pervasive alteration and have weathered to a yellowish off white with a chalky appearance. Major element analyses reflect the secondary mineralogy, evident from a high SiO_2 composition (77.52 wt.% SiO_2) suggestive of rhyolite. Based on a weighted average of 54 $^{206}Pb/^{238}U$ dates, the crystallization age for this volcanic flow is determined to be 70.1 ±2.6 Ma (Figure 5). These dates are considered to be equivalent.

DISCUSSION

The U-Pb ages confirm inclusion of these rocks within a Late Cretaceous volcanic unit originally mapped by Woodsworth (1980). This volcanic unit is exposed locally through thin glacial cover between Francois and Ootsa lakes. Near the southern sample site at Ootsa Lake (sample 10TFE061), it apparently is succeeded by felsic volcanic rocks resembling the Ootsa Lake Group, dated by the K-Ar method on biotite at 55.6 ±2.5 Ma (Stevens *et al.*, 1982).

Volcanic deposits of Late Cretaceous (*ca*. 67.5-75.3 Ma, Campanian to Maastrichtian) age are uncommon, but have been mapped in isolated localities spanning the breadth of Stikine terrane in central British Columbia (Figure 6). They typically occur as relatively thin tuffs, breccias and flows of andesitic to rhyolitic composition and form rare plutonic bodies (Diakow and Levson, 1997; Diakow, 2006). Because of their spatial association with plutons from the Bulkley Intrusive Suite (*ca.* 88-70 Ma) and/or co-magmatic volcanic rocks of the Kasalka Group, they presumably represent a waning stage of continental-margin arc-magmatism manifest as relatively small-volume felsic eruptive centres with areally restricted distribution.

A well-established genetic association exists between biotite-hornblende granodiorite and quartz diorite of the Late Cretaceous Bulkley suite and Cu±Mo±Au porphyry, polymetallic vein and other styles of mineralization across the Skeena Arch (Carter, 1981; MacIntyre 1985, 2006, 2007). Polymetallic Au-Ag-Zn-Pb-Cu vein mineralization at the past-producing Silver Queen mine, located 25 km northwest of the study area, is associated with porphyritic andesites and hypabyssal intrusions that yield *ca.* 77-75 Ma K-Ar dates (Church and Barakso, 1990), suggesting a correlation with the Kasalka Group (Leitch *et al.*, 1990, 1992; Figure 6).

In the Fawnie Range, located 110 km southeast of the study area, a quartz monzonite stock, garnet-sulphide bearing felsic dikes, and volcanic rocks of andesite to

Figure 2. Sample 10TFE060, a maroon-weathered, plagioclase-phyric dacite.

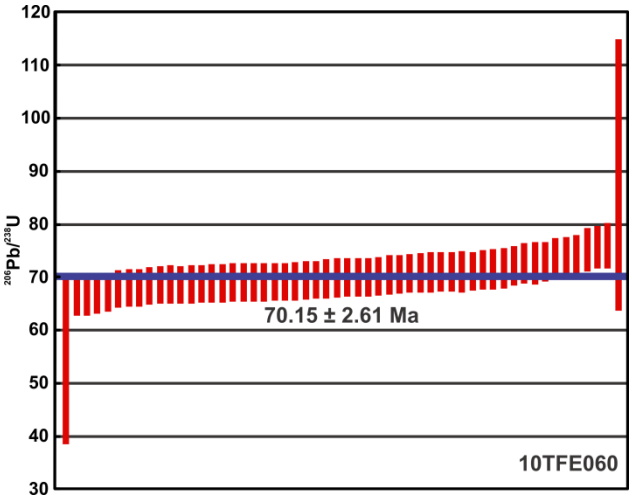

Figure 3. Crystallization age for sample 10TFE060 based on a weighted average of 54 $^{206}Pb/^{238}U$ dates from laser ablation data collected from zircon cores.

Figure 4. Sample 10TFE061, a massive, quartz and clay altered, porphyritic volcanic flow.

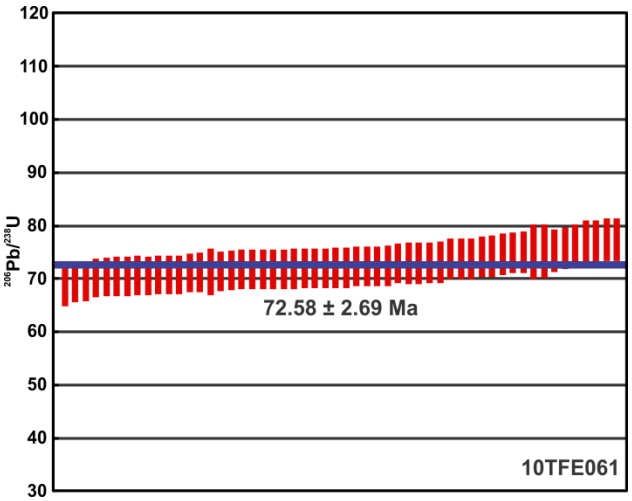

Figure 5. Crystallization age for sample 10TFE061 based on a weighted average of 54 $^{206}Pb/^{238}U$ dates from laser ablation data collected from zircon cores.

rhyolite composition mark the known southeastern extent of Late Cretaceous magmatic rocks, all of which are temporally equivalent to those in the study area (Diakow *et al.*, 1996; Diakow and Levson, 1997; Figure 6). Low grade, disseminated Ag±Zn±Pb±Au mineralization at the Capoose deposit is associated with rhyolite dikes and sills (D. Pawliuk, Silver Quest Resources Ltd., personal communication, 2011). These rocks outside the mineralized zone yield *ca.* 71Ma U-Pb dates (Friedman *et al.*, 2001). The Blackwater-Davidson deposit, 23 km southeast of Capoose, is a low grade disseminated gold deposit with mineralogic features resembling Capoose (*i.e.* garnet-sulphide-felsic rock association). However, this deposit exhibits alteration characteristics associated with low-sulphidation epithermal Au but lacks quartz veining. A recent resource estimate of the Blackwater Davidson deposit, at a cutoff grade of 0.4 g/t Au, indicates 53 million tonnes grading 1.06 g/t Au and 5.6 g/t Ag (Simpson, 2011).

The co-genetic relationship between Late Cretaceous magmatic rocks and precious-metal mineralization at the Capoose and Blackwater-Davidson deposits emphasizes the importance of U-Pb geochronology to discriminate favourable rock successions of similar age for greenfield exploration. New geochronology presented in this paper expands the known distribution of the youngest deposits of the Late Cretaceous Kasalka Group. However, the distribution of this potentially mineralized magmatic tract beyond the Fawnie Range southward, in the Interior Plateau region, remains unknown.

ACKNOWLEDGMENTS

L. Howarth is thanked for her assistance in the field. P.B. O'Sullivan (Apatite to Zircon Inc.) is thanked for the timely preparation and analysis of samples for U-Pb dates. A.S. Hickin is gratefully acknowledged for his generous support of this project. G.T. Nixon is thanked for his review of this manuscript.

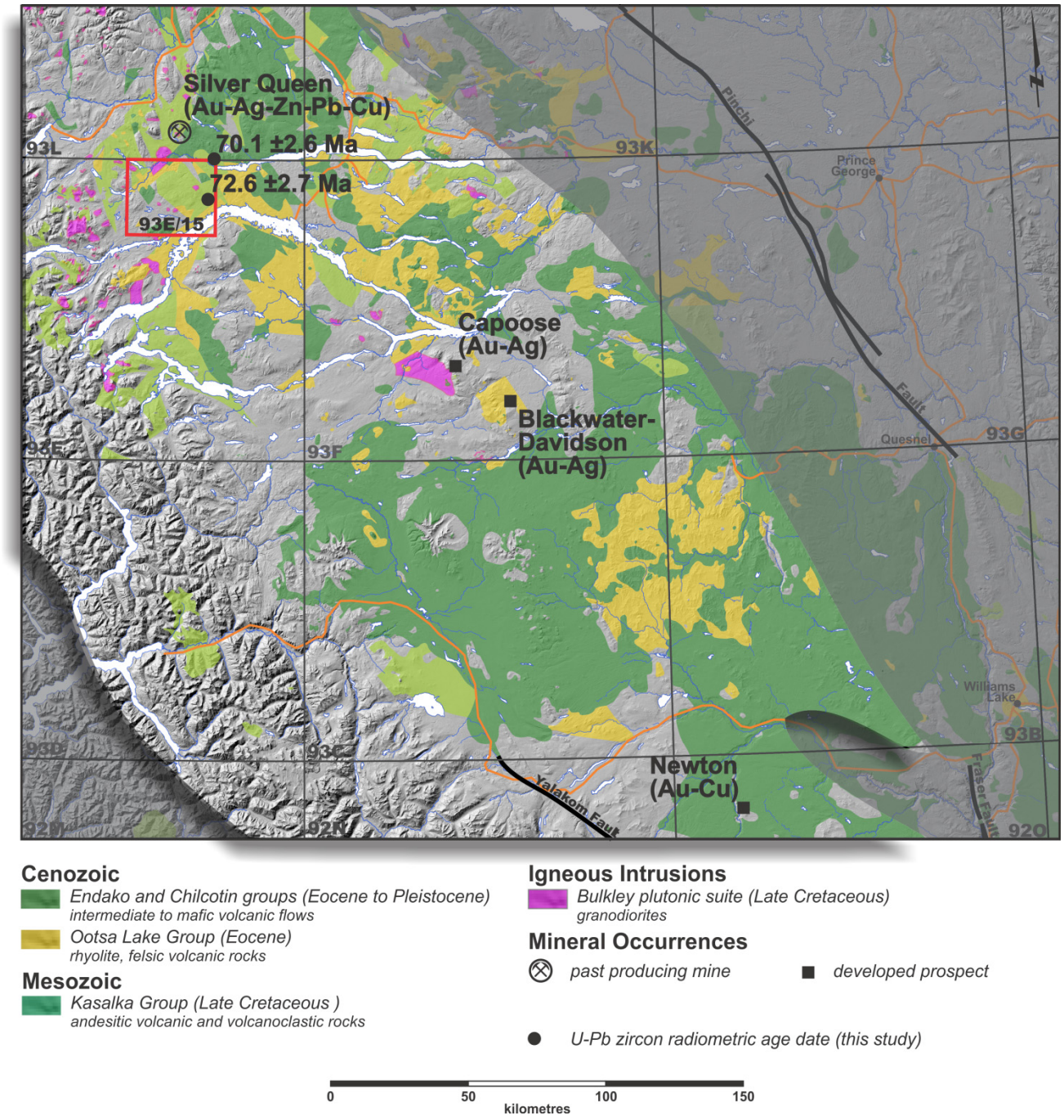

Figure 6. Spatial distribution of Late Cretaceous volcanic rocks within Stikine terrane (highlighted; modified from Massey *et al.*, 2005), showing locations of U-Pb zircon isotopic dates presented in this paper.

REFERENCES

Carter, N.C. (1981): Porphyry copper and molybdenum deposits, west-central British Columbia; *BC Ministry of Energy, Mines and Petroleum Resources*, Bulletin 64, 150 pages.

Church, B.N. and Barakso, J.J. (1990): Geology, lithogeochemistry and mineralization in the Buck Creek area, British Columbia; *BC Ministry of Energy, Mines and Petroleum Resources*, Paper 1990-2, 95 pages.

Diakow, L.J. (2006) Geology of the Tahtsa Ranges between Eutsuk Lake and Morice Lake, Whitesail Lake map area, west-central British Columbia; *BC Ministry of Energy and Mines*, Geoscience Map 2006-5, 1:150 000 scale.

Diakow, L.J. and Mihalynuk, M. (1987): Geology of Whitesail Reach and Troitsa Lake Areas (93E/10W, 11E); *BC Ministry of Energy, Mines and Petroleum Resources,* Open File 1987-4.

Diakow, L.J. and Levson, V.M. (1997): Bedrock and surficial geology of the southern Nechako Plateau, central British Columbia; *BC Ministry of Employment and Investment*, Geoscience Map 1997-2, 1:100 000 scale.

Diakow, L.J., Webster, I.C.L., Richards, T.A. and Tipper, H.W. (1996): Geology of the Fawnie and Nechako ranges, southern Nechako Plateau, central British Columbia; *in* Interior Plateau geoscience project: Summary of geological, geochemical and geophysical studies (NTS 092N; 092O, 093B; 093C; 093F; 093G; 093K); L.J Diakow, P. Metcalfe and J. Newell, editors, *BC Ministry of Employment and Investment*, Paper 1997-2 and *Geological Survey of Canada*, Open File 3448.

Duffell, S. (1959): Whitesail Lake map-area, British Columbia; *Geological Survey of Canada*, Memoir 299, 199 pages.

Ferbey, T. (2010): Quaternary geology and till geochemistry of the Nadina River map area (NTS 093E/15), west-central British Columbia; *BC Ministry of Energy, Mines and Petroleum Resources*, Paper 2010, pages 43-53.

Friedman, R.M.; Diakow, L.J.; Lane, R.A. and Mortensen, J.K. (2001): New U-Pb age constraints on latest Cretaceous magmatism and associated mineralization in the Fawnie Range, Nechako Plateau, central British Columbia; *Canadian Journal of Earth Sciences*, Volume 38, pages 619-637.

Hedley, M.S. (1935): Tahtsa-Morice area; *Geological Survey of Canada*, Map 367A, scale 1 inch to 4 miles.

Leitch, C.H.B., Hood, C.T., Cheng, X. and Sinclair, A.J. (1990): Geology of the Silver Queen mine area, Owen Lake, central British Columbia; *BC Ministry of Energy, Mines and Petroleum Resources*, Paper 1990-1, pages 287-295.

Leitch, C.H.B., Hood, C.T., Cheng, X. and Sinclair, A.J. (1992): Tip Top Hill volcanics: Late Cretaceous Kasalka Group rocks hosting Eocene epithermal base- and precious-metal veins at Owen Lake, west-central British Columbia; *Canadian Journal of Earth Sciences*, Volume 29, pages 854-864.

Ludwig, K.R. (2008): Isoplot3.6, a geochronological toolkit for Microsoft Excel; *University of California at Berkeley*, Berkeley Geochronology Center, Special Publication No. 4, 78 pages.

MacIntyre, D.G. (1985): Geology and mineral deposits of the Tahtsa Lake district west central British Columbia, *BC Ministry of Energy, Mines and Petroleum Resources*, Bulletin 75, 82 pages

MacIntyre, D.G. (2006): Geology and mineral deposits of the Skeena Arch, west-central British Columbia: A geosciences BC digital data compilation project; Geological Fieldwork 2005, *BC Ministry of Energy, Mines and Petroleum Resources,* Paper 2006-1, pages 301-312.

MacIntyre, D.G. (2007): Skeena Arch metallogenic data and Map (093E,L,M; south half of 094D, east half of 103I and southeast corner of 103P); *Geoscience BC* Report 2007-5 and *BC Ministry of Energy, Mines and Petroleum Resources*, Geofile 2007-3.

Massey, N.W.D., MacIntyre, D.G., Desjardins, P.J. and Cooney, R.T. (2005): Digital geology map of British Columbia: whole province; *BC Ministry of Energy, Mines and Petroleum Resources*, GeoFile 2005-1, 1:250 000 scale, URL <http://www.empr.gov.bc.ca/ Mining/Geoscience/ PublicationsCatalogue/Geofiles/Pages/2005-1.aspx>

Simpson, R.G. (2011): Technical report Blackwater gold project; unpublished company report, *Silver Quest Resources Ltd.*, 73 pages.

Stevens, R.D., Delabio, R.N. and Lachance, G.R. (1982): Age determinations and geological studies K-Ar isotopic ages, Report 15; *Geological Survey of Canada*, Paper 81-2, pages 8-9.

Woodsworth, G.J. (1980): Geology of Whitesail Lake (93E) map-area; *Geological Survey of Canada*, Open File 708.

North Coast Project: Tectonics and Metallogeny of the Alexander Terrane, and Cretaceous Sinistral Shearing of the Western Coast Belt

by J.L. Nelson[1], L.J. Diakow[1], J.B. Mahoney[2], C. van Staal[3], M. Pecha[4], J.J. Angen[5], G. Gehrels[4] and T. Lau[2]

KEYWORDS: Alexander terrane, Grenville Channel fault, Coast Mountains, Coast Plutonic Complex

INTRODUCTION AND PROJECT HIGHLIGHTS

This article presents the results of the final field season of a three year collaborative geological investigation of north coastal British Columbia (Figures 1, 2) between the British Columbia Geological Survey, Geological Survey of Canada, and university partners University of Wisconsin at Eau Claire and University of Arizona. The North Coast bedrock mapping and mineral deposit study is part of a cooperative, Natural Resources Canada (NRCan)-led endeavor, the Edges Multiple Metals – NW Canadian Cordillera (B.C. and Yukon) Project. The first two years involved detailed mapping on and near Porcher Island in 2009 and near Klemtu in 2010, and production of open file maps (Nelson *et al.*, 2010a, 2011a). In this final field season the focus was 1) to complete regional-scale geological coverage of the intervening area from Grenville Channel to northern Princess Royal Island in order to update the provincial geological map for all of north coastal British Columbia, a very preliminary draft of which appears as Figure 3 in this paper; and 2) to address problems and questions arising from mapping and U-Pb isotopic results obtained earlier in the program.

Highlights from the 2011 field season include:

- Discovered new VMS showings on southern Kennedy Island, hosted by Ordovician rhyolite.
- Visited the Pitt showings on Pitt Island, the only previously documented VMS occurrence in the southern Alexander terrane of British Columbia, and collected sulphide samples for lead isotopic signatures, for comparison with Neoproterozoic and Ordovician deposits in southeast Alaska.
- Collected and analysed a suite of samples of meta-igneous rocks east of northern Grenville and Telegraph channels; Permian ages throughout this belt document a previously-unknown, late Paleozoic volcanic-sedimentary unit with related dikes in intrusive contact with the Alexander terrane.
- Investigated a large tract of Late Silurian to Early Devonian (*ca.* 424-411 Ma) orthogneiss-plutonic complex on Porcher Island, intruded during a Caledonian-age deformational event that probably marked the amalgamation of pericratonic and primitive arc elements within the composite Alexander terrane.
- Traced out Grenville Channel fault for 300 kilometres along strike, collecting key plutonic phases that precisely constrain stages of sinistral motion in Early to mid-Cretaceous time.

REGIONAL GEOLOGICAL AND TECTONIC FRAMEWORK

The northern coastal area of British Columbia is underlain in part by rocks of the southern Alexander terrane, a large composite crustal fragment that underlies most of southeastern Alaska and extends farther north into part of the St. Elias Range on the Yukon-Alaskan border, (Figure 1; Wheeler *et al.*, 1991). The Alexander terrane as a whole has attracted considerable exploration interest because of the volcanogenic massive sulphide deposits that it hosts, including Niblack and others on southern Prince of Wales Island, just north of the British Columbia-Alaska border, as well as a trend of Triassic deposits, notably Windy Craggy and the Greens Creek mine (Figure 1). In the northern coastal region of British Columbia, the Alexander terrane is flanked by variably metamorphosed and deformed metasedimentary-metavolcanic rock units that comprise the Banks Island assemblage to the west, and the Gravina belt and the Yukon-Tanana terrane to the east (Figure 2). The Banks

[1] *British Columbia Geological Survey, Victoria, BC*
[2] *University of Wisconsin at Eau Claire, WI, United States*
[3] *Geological Survey of Canada, Vancouver, BC*
[4] *University of Arizona, Tucson, AZ, United States*
[5] *University of Waterloo, Waterloo, ON*

This publication is also available, free of charge, as colour digital files in Adobe Acrobat® PDF format from the BC Ministry of Energy and Mines website at http://www.empr.gov.bc.ca/Mining/Geoscience/PublicationsCatalogue/Fieldwork.

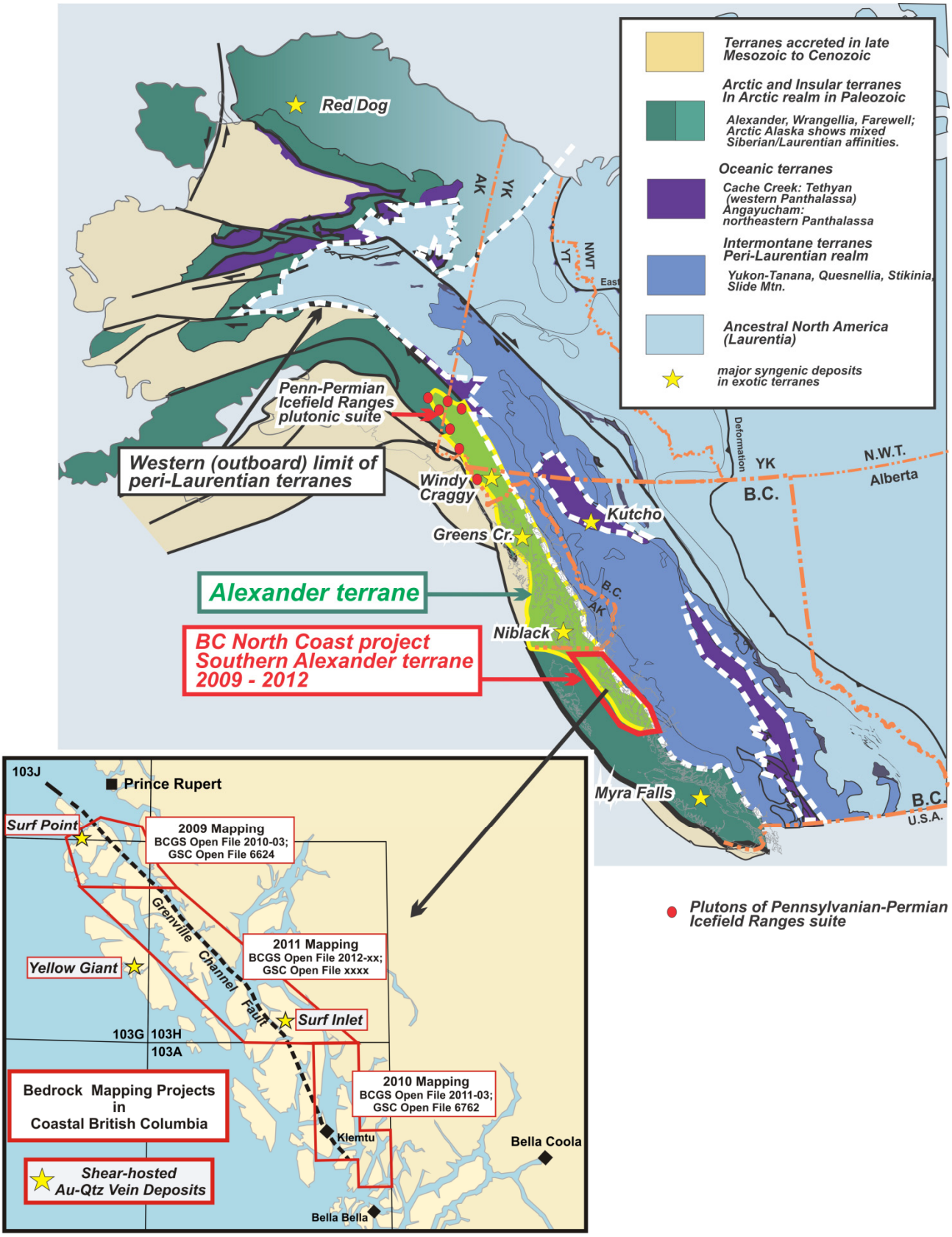

Figure 1. Location of the North Coast project in the context of northern Cordilleran terranes and in terms of local geography. Inset shows 2009, 2010 and 2011 field map footprints. Also shown on inset: trace of Grenville Channel fault, and location of major gold deposits.

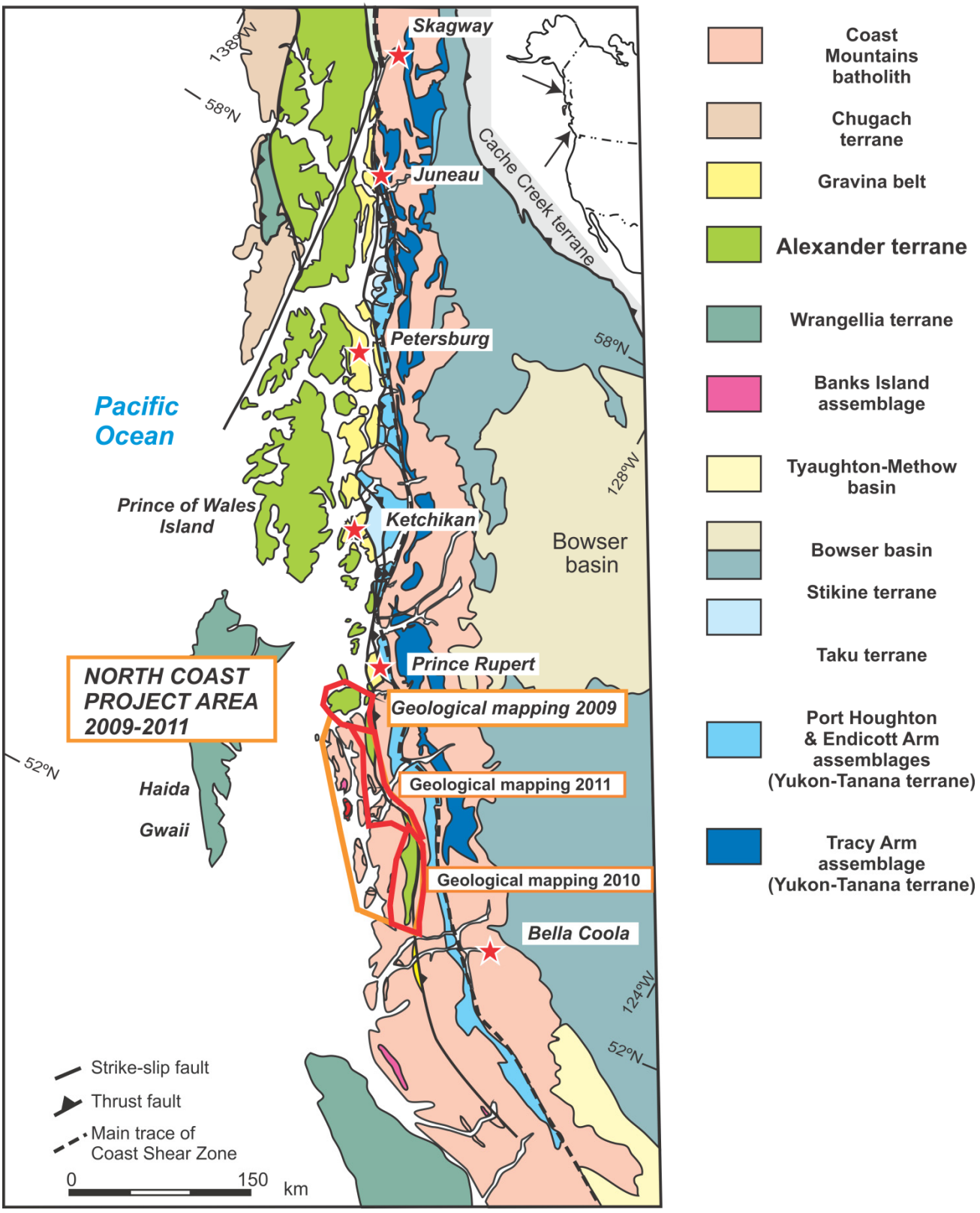

Figure 2. Regional geology and terrane map of northern coastal British Columbia and southeastern Alaska; G.E. Gehrels, 2009.

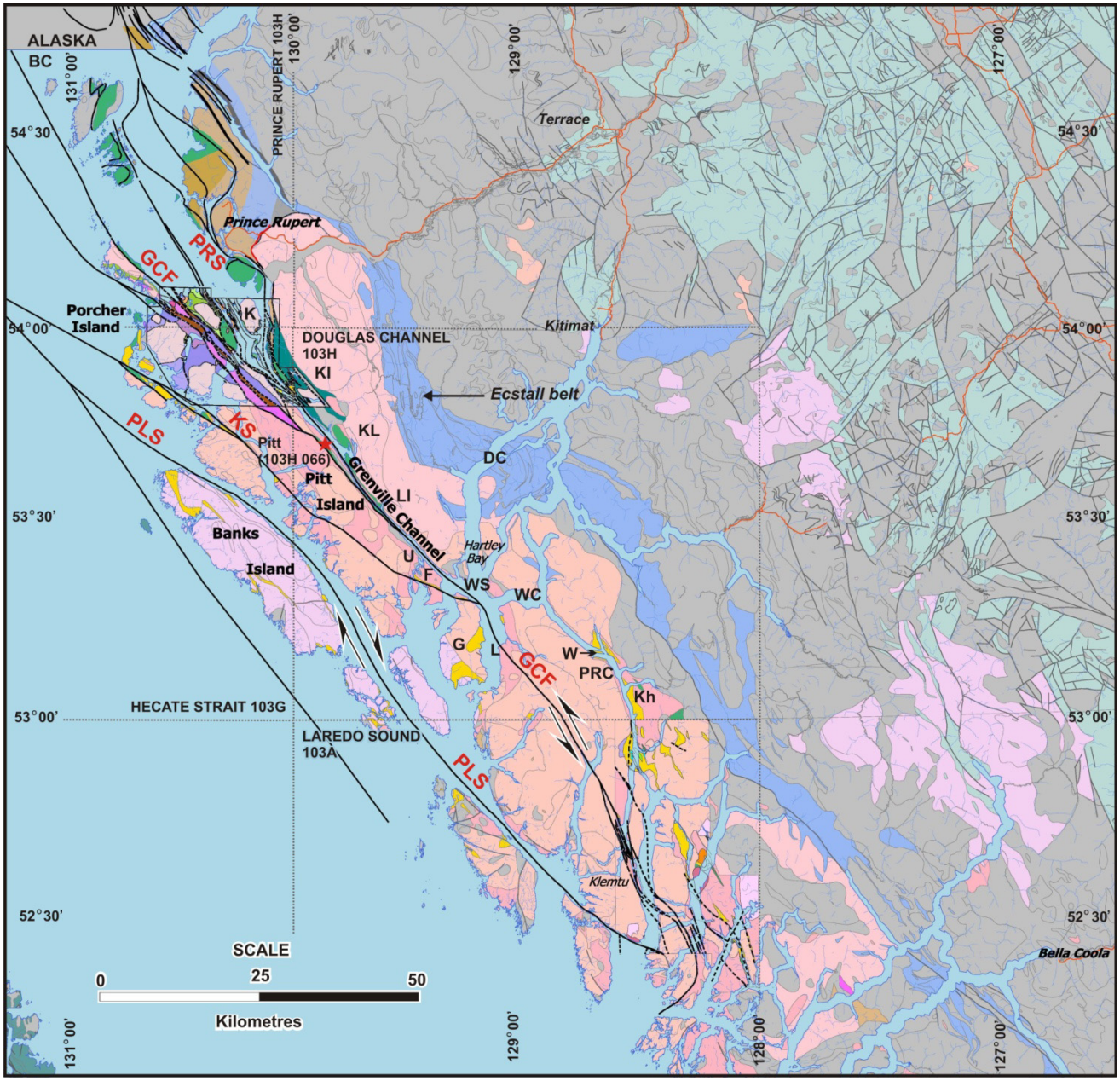

Figure 3. Preliminary revision of British Columbia north and central coast map tile. Geology from BC Geology Map; Nelson *et al.* (2010a, 2011a; this paper); Gehrels, 2001, Gehrels and Boghossian (2000); pluton ages from data in Gehrels *et al.* (2009). Geographic abbreviations: DC–Douglas Channel; F–Farrant Island; G–Gil Island; K–Kennedy Island; Kh–Khutze Inlet; KI–Kumealon Inlet; KL–Klewnuggit Inlet; L–Leading Point; LI–Lowe Inlet; PRC–Princess Royal Channel; U–Union Passage; W–Work Island; WC–Whale Channel; WS–Wright Sound. Faults: GCF–Grenville Channel fault; KS–Kitkatla shear PLS–Principe-Laredo shear; PRS–Prince Rupert shear zone.

Island assemblage is a poorly understood siliciclastic unit of pericratonic affinity that has only been recognized along the outer coast of northern British Columbia (Gehrels and Boghossian, 2000).

All of the supracrustal units are extensively intruded by Late Jurassic to Late Cretaceous plutonic bodies of the Coast Plutonic Complex. In much of the western Coast belt, plutonic exposures are so extensive that older supracrustal rocks are confined to narrow pendants within them.

Alexander terrane

The Alexander terrane in southeastern Alaska and northern coastal British Columbia consists of a broad range of volcanic, sedimentary, and plutonic rocks and their metamorphic equivalents that are primarily of Late Proterozoic to early Paleozoic age, overlain in places by thin younger sequences (Figure 4a). Most of the terrane in southeastern Alaska was assigned to the Craig subterrane by Berg *et al.* (1978; definition refined by Gehrels and Berg, 1994). In southeastern Alaska, these rocks have

LEGEND

Figure 3. continued; Legend for map.

undergone limited post-Paleozoic metamorphism, deformation, and plutonism. Farther to the southeast, in northern coastal British Columbia, Cretaceous plutons become more widespread and the degree of Mesozoic metamorphism and deformation increases. In spite of these younger overprinting events, it has been possible to correlate geologic units of southeastern Alaska with those of northern coastal British Columbia. The following unit descriptions are taken from the well-preserved portion of the Alexander terrane in southern southeastern Alaska as described in Eberlein *et al.* (1983), Gehrels and Saleeby (1987) and Gehrels *et al.* (1996).

The oldest rocks recognized in the Alexander terrane in southeastern Alaska consist of Late Proterozoic to Cambrian metavolcanic and metasedimentary assemblages of the Wales Group (Figure 4; Gehrels and Saleeby, 1987). Metavolcanic components range from mafic to felsic in composition - pillowed flows and flow breccias, and pyroclastic deposits of tuffaceous breccia and tuff. Metasedimentary components consist of volcanic-derived metagreywacke, pelitic phyllite or schist, and marble. These supracrustal rocks are intruded by bodies of complexly interlayered gabbro, diorite, tonalite, and granodiorite. Our U-Pb results so far from northern coastal British Columbia have not shown any igneous protoliths older than latest Cambrian; therefore the Wales Group is not recognized here.

In southeastern Alaska, rocks of the Wales Group are overlain by a less deformed, Early Ordovician to Late Silurian suite of volcanic and sedimentary rocks referred to as the Descon Formation (Eberlein *et al.*, 1983; Gehrels and Saleeby, 1987). Dioritic to granitic plutons that are coeval (and probably cogenetic) with volcanic rocks of the Descon Formation are widespread. Mapping and U-Pb dating on and near Porcher Island has established the widespread presence of Descon-equivalent metavolcanic sequences (Nelson *et al.*, 2010a, b).

Lower Paleozoic strata of the Alexander terrane in southeastern Alaska are overlain unconformably by a variety of Devonian strata that commonly include a basal clastic sequence (conglomerates and sandstones, including red beds) of the Karheen Formation, mafic volcanic rocks of the Coronados Volcanics and St. Joseph Islands Volcanics, and limestones of the Wadleigh Formation (Eberlein and Churkin, 1970). The basal conglomerate is interpreted to represent a major phase of uplift and erosion, the Klakas orogeny, as it overlies and contains clasts of a wide variety of older rocks including a preponderance of Silurian plutonic clasts (Gehrels *et al.*, 1983a; Gehrels and Saleeby, 1987). Devonian and younger volcanic units are mafic or bimodal mafic-felsic, and of limited extent. They probably are the products of local rift-related extrusive events.

Devonian clastic-carbonate sequences are abundant in the Alexander terrane in north coastal British Columbia (Figure 3). Throughout this region we have assigned them to the Mathieson Channel Formation, because of their broad extent, physical separation from the main Karheen Formation, and somewhat different nature from it, notably the prominence of carbonate strata (Nelson *et al.*, 2011b and this paper). The variability of siliciclastic and carbonate facies and the presence of locally derived, plutonic-sourced conglomerates and bimodal volcanic sequences in these formations suggest that they were deposited in a series sub-basins formed by rifting.

Younger strata in the Alexander terrane of southeast Alaska include fine to medium grained clastic rocks, carbonate, minor basalt of Carboniferous and Permian age, and local Triassic basal conglomerates overlain by bimodal mafic-felsic volcanic rocks, carbonate, and volcaniclastic strata. The Late Jurassic to Early Cretaceous Gravina belt, described separately below, unconformably overlies the Alexander terrane (Figure 4).

Other terranes and assemblages

BANKS ISLAND ASSEMBLAGE

The Banks Island assemblage (Figures 2, 3) has been recognized as a distinct unit of possible continental margin affinity, based on the predominance of interlayered quartzites (meta-quartz arenites) and marbles, which are rare in the generally more primitive Paleozoic arc-related assemblages of the Alexander terrane; and on the presence of significant populations of Precambrian detrital zircons (Gehrels and Boghossian, 2000; G. Gehrels, unpublished data, 2011). These rocks are exposed on the outer coast of Banks Island, on northwestern Porcher Island, and on the outer islands as far south as Klemtu. The dominant lithic components are strongly deformed and regionally metamorphosed metaclastic quartzites. They commonly occur in centimetre-scale bands interlayered with marble in thicknesses of several centimetres to several tens of metres, and pelitic phyllite/schist. Everywhere, these rocks have a well-developed foliation and display outcrop-scale isoclinal folds. Pelitic components have been metamorphosed to biotite phyllite or schist, and garnet is present in some regions.

The age of the Banks Island assemblage is constrained by the following relationships: (1) detrital zircons recovered from two quartzites are as young as ~415 Ma (Silurian-Devonian boundary; G. Gehrels, unpublished data) (2) an orthogneiss on Aristazabal Island that has undergone the regional deformation and amphibolite-facies metamorphism along with the adjacent marble and metabasite has yielded a U-Pb age of 357 Ma (Early Mississippian), and (3) plutons of Late Jurassic age intrude these rocks (Gehrels *et al.*, 2009), across the regional foliation and folds. These constraints suggest that the Banks Island assemblage accumulated during mid-Paleozoic time.

Mapping in 2011 of pendants on Gil, Farrant and Pitt islands, previously assigned by Gehrels and Boghossian (2000) to the Banks Island assemblage, shows that these

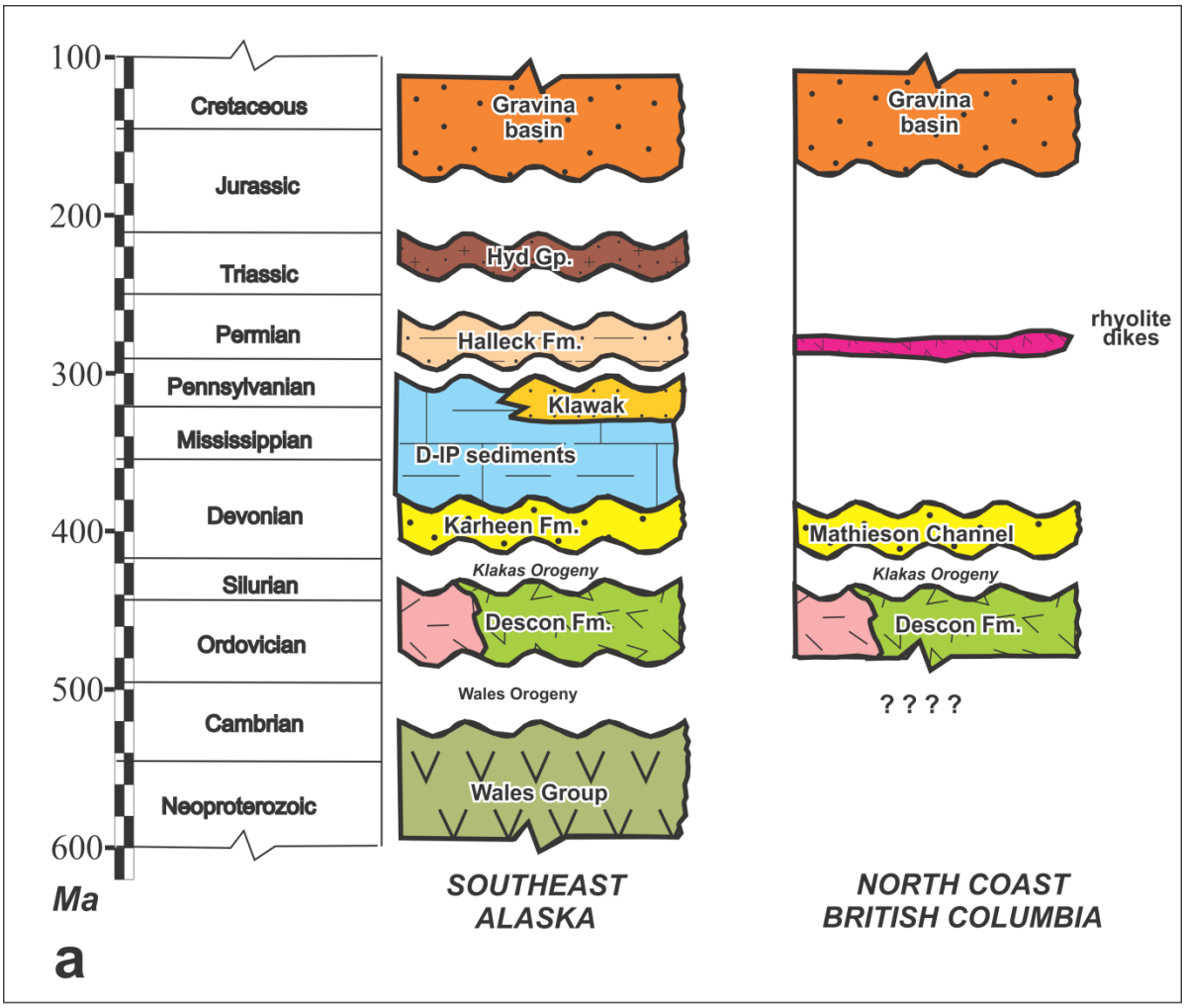

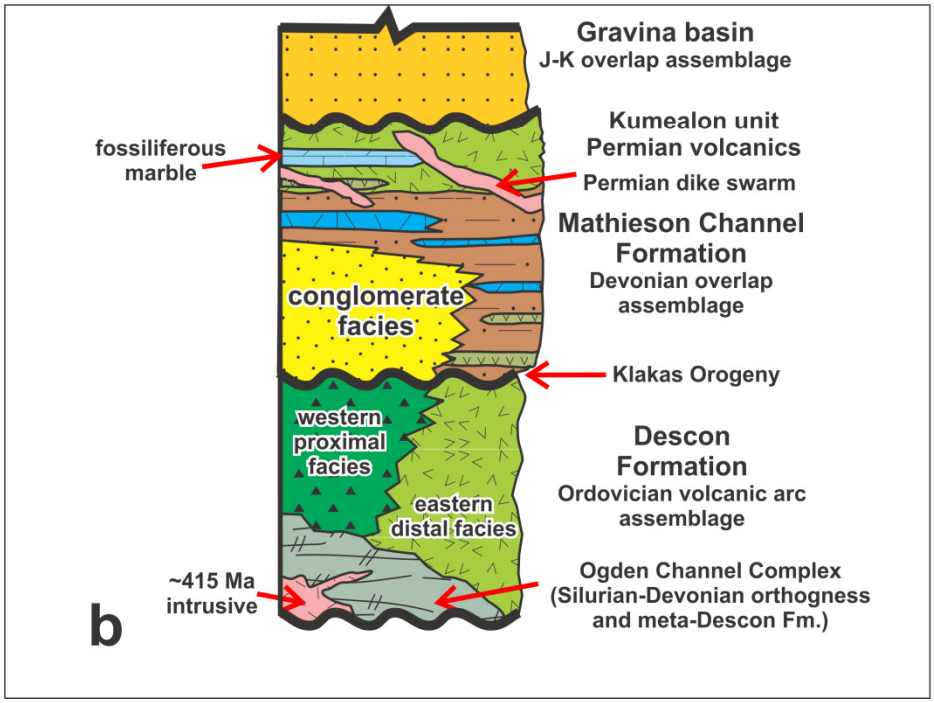

Figure 4. a) Stratigraphic columns for Alexander terrane of southeastern Alaska and coastal northwestern British Columbia; b) Schematic stratigraphic column for coastal northwestern British Columbia.

strata strongly resemble the Mathieson Channel Formation as described in the region farther south between Return Channel and Graham Reach (Nelson *et al.,* 2011a, b). Preliminary results of detrital zircon analysis shows significant Precambrian populations from samples in this area, a feature characteristic of Banks Island detrital signatures (M. Pecha, unpublished data, 2011). The two units may have passed transitionally into each other, with a change of provenance from partly pericontinental on Banks Island to purely Ordovician-Silurian-Devonian igneous sources to the south and east captured within the Mathieson Channel formation (Mahoney *et al.*, 2011). It would thus represent a clastic overlap between a pre-Devonian primitive arc fragment (Craig subterrane of Alexander terrane) and a pericratonic one ("Banks Islandia"), which accreted to each other during the Klakas orogeny.

YUKON-TANANA TERRANE

East of the Alexander terrane, metavolcanic and metasedimentary rocks of the Yukon-Tanana terrane underlie the western Coast Mountains, along the length of southeastern Alaska and northern coastal British Columbia (Figures 1, 2, 3). In general, these rocks form a panel that dips eastward and youngs westward, suggesting an overall inverted stratigraphy. Using the nomenclature defined in southeastern Alaska (Gehrels *et al.*, 1992), the Yukon-Tanana terrane includes the following units :

- Tracy Arm assemblage: This package contains marbles, quartzites, pelitic schists, and orthogneisses, which are commonly high in metamorphic grade and migmatitic. The age of this unit is constrained as Devonian or older based on ages from the overlying Endicott Arm assemblage.
- Endicott Arm assemblage: This unit has a distinctive basal conglomerate containing clasts derived from the Tracy Arm assemblage. Overlying strata include greenschist- to amphibolite facies felsic to mafic metavolcanic rocks, pelitic schists, and minor marble. Available faunal and U-Pb geochronologic constraints suggest that most strata are Devonian-Mississippian in age.
- Port Houghton assemblage: These strata gradationally overlie the Endicott Arm assemblage and consist of greenschist to amphibolite-facies metaturbidites, pelitic schist, and metabasalt. Available faunal constraints suggest that most strata are late Paleozoic in age.

Near Douglas Channel in northwestern British Columbia, the Ecstall belt (Figure 3; Alldrick, 2001; Alldrick *et al.*, 2001; see also Gareau and Woodsworth, 2000), with its enclosed Devonian volcanogenic deposits, is also assigned to the Yukon-Tanana terrane. The host units are equivalent to the middle, Endicott Arm assemblage of southeastern Alaska.

GRAVINA BELT, AND ALEXANDER-YUKON-TANANA TERRANE RELATIONSHIPS

Rocks of the Alexander terrane are overlain by Upper Jurassic to Upper Cretaceous (Oxfordian to Cenomanian) turbidites and subordinate mafic volcanic rocks of the Gravina belt. These rocks can be traced, generally along the inboard margin of the Alexander terrane, for the length of southeastern Alaska (Berg *et al.*, 1972) and into northern coastal British Columbia (Figures 1, 2). In the Chatham Strait area, Gehrels (2001) has identified a unit of mid-Jurassic basalt and rhyolite, the Moffatt volcanics, at the depositional base of the Gravina belt. It unconformably overlies Alexander terrane on Dundas Island; on Tongass Island in southeastern Alaska and on the mainland east of Port Simpson (Lax Kw'alaams). The same basalts and rhyolites overlie a sequence of metavolcanic and metasedimentary rocks that have been assigned to the Yukon-Tanana terrane. Thus in this area, the mid-Jurassic Moffatt volcanics and younger Gravina belt form an overlap on both terranes.

The initial age of accretion of Alexander to Yukon-Tanana terrane has been a long-standing topic of debate among coastal researchers. Crawford *et al.* (1987, 2001) have assigned it to the Early to early Late Cretaceous, based on analysis of the broad belt of high-grade metamorphism, plutonism and southwest-vergent thick-skinned deformation centred around the terrane boundary near Prince Rupert. However, van der Heyden (1992) described pre-Late Jurassic ductile deformation in the eastern Coast Mountains north of Bella Coola, positing that it was a response to initial Insular-Intermontane terrane accretion, largely masked to the west by subsequent tectonism and extensive emplacement of plutons. The pre-Gravina Duncan Canal shear zone in the eastern Alexander terrane of southeastern Alaska may have formed during its accretion (McClelland and Gehrels, 1990). Rubin and Saleeby (1992) and McClelland *et al.* (1992) described the Gravina belt as an overlap sequence on both Alexander and Intermontane terranes. Support for pre-Gravina accretion is also provided by detrital zircons derived from both Alexander (490-410 Ma) and Yukon-Tanana terrane (390-340 Ma) in Gravina clastic strata (Kapp and Gehrels, 1998; G. Gehrels, unpublished data, 2010).

Plutons of the western Coast Plutonic Complex

Plutons of the Coast Plutonic Complex occur as isolated bodies in northern and western portions of northern coastal British Columbia, and increase in size and number southeastward to form huge continuous masses of plutonic rock (Gehrels *et al.*, 2009; Figure 3). Compositionally, most are tonalite and granodiorite, with subordinate diorite and minor gabbro and leucogranodiorite. A large majority of plutons have hornblende >biotite, plagioclase>>orthoclase, and are rich in titanite. Some plutonic suites contain euhedral epidote that is interpreted to be magmatic in origin.

According to a recent comprehensive geochronological summary (Gehrels *et al.*, 2009), plutonic U-Pb ages record a history of eastward migration of emplacement across the Coast belt. The westernmost plutons are 160-140 Ma (Late Jurassic) tonalites and granodiorites on the outer islands (Figure 3). An extensive suite of compositionally similar Early Cretaceous (120-100 Ma) bodies lies east of the Late Jurassic belt. A nearly continuous band of 100-85 Ma plutons (*e.g.*, Ecstall pluton of Hutchison, 1982) underlies the western reaches of the Coast Mountains proper, succeeded eastward by mainly tonalitic sills of ~70-60 Ma (Latest Cretaceous-earliest Tertiary age). The central and eastern portions of the Coast Mountains are underlain by voluminous 60-50 Ma (Eocene) granodiorite bodies. The emplacement depth of plutons also increases from west to east into the Coast Mountains, as shown by hornblende barometric studies conducted by Butler *et al.* (2001). This work suggests that westernmost Late Jurassic bodies were emplaced at depths of ~15 km, whereas Early Cretaceous plutons to the east were slightly deeper, ~20 km. Even farther east, mid-Cretaceous plutons of the Ecstall belt were emplaced at significantly greater depths, perhaps 25-30 km. This increase in depth of emplacement correlates well with the eastward increase in metamorphic grade.

The Grenville Channel fault and Early to mid-Cretaceous sinistral tectonics within the Coast Plutonic Complex

A mid-Cretaceous sinistral transcurrent fault regime was first documented by Chardon *et al.* (1999). Work on this project in the area around Porcher Island in 2009 established the importance of Cretaceous sinistral faulting there, with many fault strands crossing the island and converging southward into the Grenville Channel fault through Grenville Channel (Figure 5; Nelson *et al.*, 2010a, b). Thesis work by Joel Angen in 2010-2011 has provided additional detail about the shear systems in Porcher Island area and also has constrained their age to mid-Cretaceous (*ca.* 105-96 Ma; Angen *et al.* this volume). In the course of regional mapping in 2010, the southern extension of the Grenville Channel fault and its splays in the Laredo Sound map-area near Klemtu were recognized similarly as a locus of mid-Cretaceous sinistral shearing. Also in this area, a somewhat older Early Cretaceous event of distributed shear occurred during amphibolite facies metamorphism (Nelson *et al.*, 2011b). Magmatic ages constrain the timing of the distributed sinistral shear event between 123 and 105 Ma, the age of the syn-kinematic versus post-kinematic plutons. These observations provide an important dimension to the mid-Cretaceous sinistral shear history of the northern Grenville Channel fault and its splays. Intense region-specific fabric development in the *ca.* 123 Ma plutonic suite indicates that this deformation is entirely Early Cretaceous, rather than a continuation of the mid-Jurassic accretion kinematics of Alexander and Yukon-Tanana terranes (Nelson *et al.*, 2011b).

NORTH COAST GEOLOGICAL STUDIES IN 2011

Update on VMS occurrences and VMS potential in the southern Alexander terrane

Ordovician basalt-andesite-dacite-rhyolite volcanic successions and probably cogenetic plutons underlie much of northeastern Porcher and Pitt islands and their vicinity (Figure 5; Nelson *et al.*, 2010a; J.B. Mahoney, unpublished U-Pb zircon data). They are equivalent to the Descon Formation and informally-named Moira unit in southeastern Alaska, which host known VMS mineralization (Gehrels *et al.*, 1983b; Slack *et al.*, 2005). Dacites and rhyolites probably originated as domes or cryptodomes at small volcanic centres. Felsic tuffs form discrete beds in the metre to decimetre range, as well as sets of laminae in dominantly andesite volcaniclastic sequences. These rocks overall are favourable hosts for Kuroko-style volcanogenic massive sulphide (VMS) occurrences.

More specific geologic indicators of Ordovician VMS environments include:

- Stratabound, stratiform magnetite along the northeastern side of Porcher Island immediately northeast of the Lamppost fault, and on the eastern side of Pitt Island near Stuart Anchorage (MINFILE 103G 016, Royal and 103J 031, Star; others shown on Nelson *et al.*, 2010a).
- Schists containing manganoan zoisite and axinite occur in association with the iron formation in Stuart Anchorage, and also within the Oona River unit on the northeastern shoulder of Pitt Island, which because of their unusual compositions and association with felsic metatuffs and iron formation are interpreted as metamorphosed exhalites.
- VMS showings on southern Kennedy Island discovered in 2011, hosted by rhyolite dated as Ordovician by U-Pb methods on zircon (J.B. Mahoney, unpublished data, 2011).

VMS PROSPECT ON PITT ISLAND

The best known local example of syngenetic stratiform sulphide mineralization on Pitt Island is the Pitt prospect or Pitt/Trinity claim group (MINFILE 103H 066), located 7.5 km northwest of the entrance to Klewnuggit Inlet on Grenville Channel (Figure 3). In 1980, attracted by a rusty gossan in Pyrite Creek, the discovery of massive sulphides led to exploration and property mapping to determine the geological setting of this polymetallic mineralization (Bradley, 1987). Subsequent exploration in 1992 adopted previously defined lithostratigraphic units, and conducted ground and airborne geophysical surveys that led to the discovery of additional showings (Bohme, 1993; Lo, 1992).

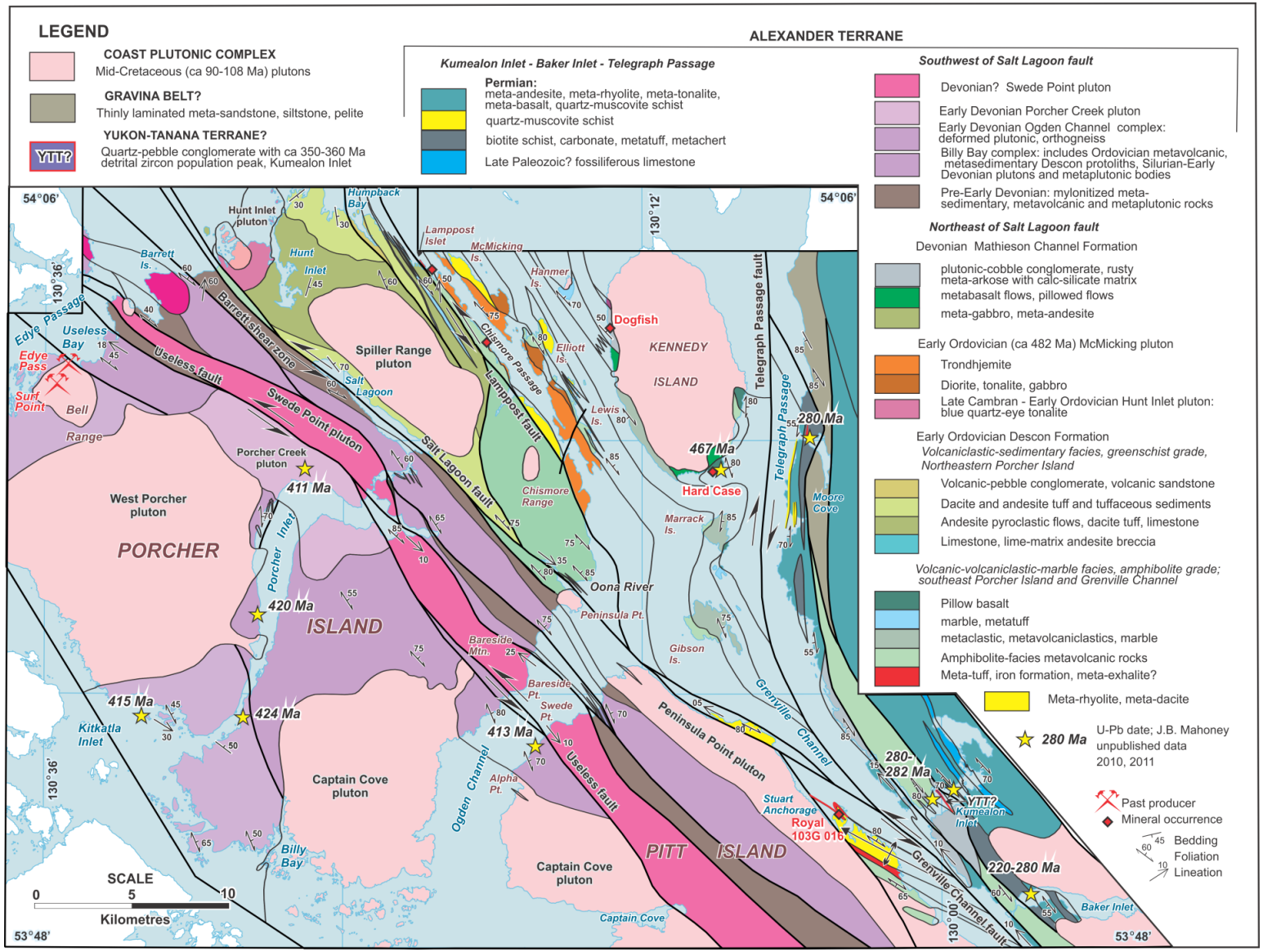

Figure 5. Geology of Porcher Island and vicinity; 2009 mapping with 2011 updates and additions.

The Pitt/Trinity claim group consists of three separate mineralized zones in two separate inliers of metasedimentary-metavolcanic rocks within foliated Cretaceous plutons that parallel the regional northwest structure (Bohme, 1993). The Pyrite Creek and Pitt zones contain most of the known mineralized showings. Located 3.5 kilometres apart along strike, they correspond with a prominent northwesterly topographic lineament, marked by incised drainages and rusty oxidized gossans, along which evidence for a major fault is reported (Bohme, 1993). In both zones, pyrite-rich, semimassive and massive sulphides occur in quartz-muscovite schist interlayered with meta-arenite (quartzite), ±garnet-quartz-biotite schist and carbonaceous argillite (Figure 6). The true thickness of sulphides varies between 0.2 and 1.6 metres. Principal sulphide minerals consist of pyrite, chalcopyrite, sphalerite, pyrrhotite, galena, covellite and possibly bornite. Based on values of 1.0-5.5% Ba in assays, barite is suspected. Drill intersections of the Pyrite Creek zone returned between 0.94 and 2.2% Cu, 0.41 to 1.2% Pb and 1.5 to 4.9% Zn over 2 metre widths. Reported values of precious metals are low (Bohme, 1993). The B Creek zone is in a separate metasedimentary-metavolcanic inlier 2.5 kilometres northeast of Pyrite Creek.

In 2011, a brief property visit to examine and sample host rocks containing stratiform sulphide mineralization focussed on the Pyrite Creek zone. The topographically higher part of this zone, where numerous sulphide showings occur in an incised north-flowing creek (Bohme, 1993), consists of meta-arenite forming massive thick layers, alternating with thinner garnet-biotite schist. Felsic schist comprises a thin, one-half metre thick friable weathered layer exposed at creek level. It is composed mainly of muscovite and quartz with disseminated and semimassive millimetre-thick bands of pyrite-chalcopyrite±sphalerite±galena. Unfortunately, a sample of this felsic tuff layer failed to yield zircons for U-Pb geochronology. Another sample currently being processed for detrital zircon geochronology is a clean, well-sorted meta-arenite. Its detrital zircon population will determine affiliation of syngenetic sulphide host rocks with either Ordovician Descon Formation (or Moira unit) or Devonian Mathieson Channel Formation. Two sulphide samples will be submitted for Pb-isotopic analysis, for comparison with data from volcanogenic occurrences in southeastern Alaska (Slack *et al.*, 2005).

The strong structural control of the Pitt trend, thin width of the sulphide-rich zone and predominance of epigenetic, discontinuous vein-style mineralization suggest that it was possibly a feeder zone, controlled by a penecontemporaneous, basin-bounding fault. The Pitt trend structure has now been remobilized to form the southwestern boundary of the Grenville Channel shear zone on Pitt Island. Remobilization of original normal faults into later compressional and/or transcurrent structures is a common feature of syngenetic mineralized systems (Nelson, 1998).

NEW SHOWINGS NEAR PORCHER ISLAND

The Hard Case showing of VMS-style mineralization was discovered during field studies in 2011, on the southeastern shore of Kennedy Island (Figure 5) . It mainly comprises massive pyrite-pyrrhotite with accessory chalcopyrite and sphalerite and stockwork-like mineralization hosted by a felsic pyroclastic rock, components of which have been replaced by sulphide (Figure 7a). This unit overlies metabasalt interpreted as part of the Ordovician-Silurian Descon Formation, and below conglomerate and cross-bedded sandstone of the Mathieson Channel Formation (Nelson *et al.*, 2010b, 2011b). The host rhyolite breccia has yielded an Ordovician, *ca.* 467 Ma U-Pb age (J.B. Mahoney, unpublished data, 2011). The Dogfish showing is a second VMS-style occurrence identified in 2011 situated in the same stratigraphic setting on southwestern Kennedy Island as the Hard Case showing. Mineralization occurs in intensely quartz-sericite-altered volcanic protoliths, as disseminated pyrite and pyrrhotite, massive pyrrhotite, local pyrite, sphalerite and minor chalcopyrite, and brecciated, sulphide-bearing quartz-sericite schist veined by pyrrhotite and sphalerite (Figure 7b). Because Kennedy Island is protected as part of the Kennedy Island Conservancy Area, these two new occurrences are not potential exploration targets in themselves. However, they do highlight the fertility for additional discoveries of VMS-style deposits in this region. In sulphide textures and lithic associations they resemble an occurrence of massive marcasite-pyrite in Ordovician felsic breccia (Figures 7c, d), located on the western side of Digby Island, near the Prince Rupert airport. This site yielded a U-Pb zircon age of *ca.* 472 Ma (Gehrels and Boghossian, 2000).

The Mathieson Channel Formation: a regional Devonian clastic overlap sequence in southern Alexander terrane

The Mathieson Channel Formation is a widely distributed unit in the southern Alexander terrane in north coastal British Columbia, as of this year mapped semi-continuously over a 235 kilometre strike length from Laredo Sound map sheet (NTS 103A), northwest to Prince Rupert map sheet (NTS 103J; see Figure 3).

Originally recognized and defined in Laredo Sound map sheet (NTS 103A), it was subdivided into five provisional stratified members composed of varying proportions of sedimentary and volcanic protoliths that have undergone polyphase deformation and amphibolite facies metamorphism (Nelson *et al.*, 2011b). Based on detrital zircon populations, the Mathieson Channel Formation correlates temporally with the Early Devonian Karheen Formation in Alexander terrane of southeast Alaska. Lithological contrasts between the two formations indicate differences in environments of deposition. In particular, the Mathieson Channel Formation is dominated by interlayered siliciclastic and carbonate, as opposed to the purely clastic Karheen Formation.

Figure 6. View of rusty quartz-sericite schist along the Pitt zone linear.

Mapping in 2011 has shown continuity of character between outcrops in the type area in Laredo Sound, northward to exposures of sandstone on Kennedy Island that Nelson *et al.* (2010a, b) originally assigned to the Karheen Formation. Because of their local consistency and geographic isolation from type exposures of the Karheen Formation in southeast Alaska, we recommend that all related rocks in northwestern British Columbia be assigned to the Mathieson Channel Formation (Figure 4b).

Rock units of the Mathieson Channel Formation in northern Laredo Sound area extend northwest into Douglas Channel map sheet (NTS 103H), traced throughout the Princess Royal Channel-Whale Channel-Grenville Channel corridor in 2011 (Figure 3). In this area, the formation occupies comparatively narrow bands within broader Cretaceous plutonic bodies, paralleling much of Grenville and Princess Royal channels. These bands reflect strong tranposition of original bedded units, parallel to regionally persistent northwest trending strike-slip faults and a pervasive subvertical foliation. In contrast, broader panels of Mathieson Channel strata are found southwest of the Grenville Channel fault on eastern and southern Gil Island and farther northwest in Union Passage. These panels, oriented obliquely to the regional northwest structural fabric, exhibit characteristic tightly appressed folds that perhaps account for stratigraphic repetition and greater structural thicknesses. Preliminary detrital zircon results from these packages show significant Precambrian populations (M. Pecha, unpublished data, 2011), which are absent in Mathieson Channel samples northeast of the Grenville Channel fault. Nevertheless, the rock units are not readily distinguishable: they both consist of interlayered arenite and carbonate, with possibly more detrital quartz in pendants southwest of the Grenville Channel fault. The siliciclastic-carbonate rocks on Gil Island and along Union Passage were considered part of the Banks Island assemblage by Gehrels and Boghossian (2000). We note that this corresponds to a provenance difference (partly pericratonic versus solely mid-Paleozoic) within a single mappable unit. The present Grenville Channel fault appears to mark the boundary between the two sources.

The lower contact of the Mathieson Channel Formation is exposed on Kennedy Island (Figure 5), where it overlies well preserved pillow basalts that are believed to be continuous with metavolcanic rocks of the underlying Descon Formation. Other metabasalt units that

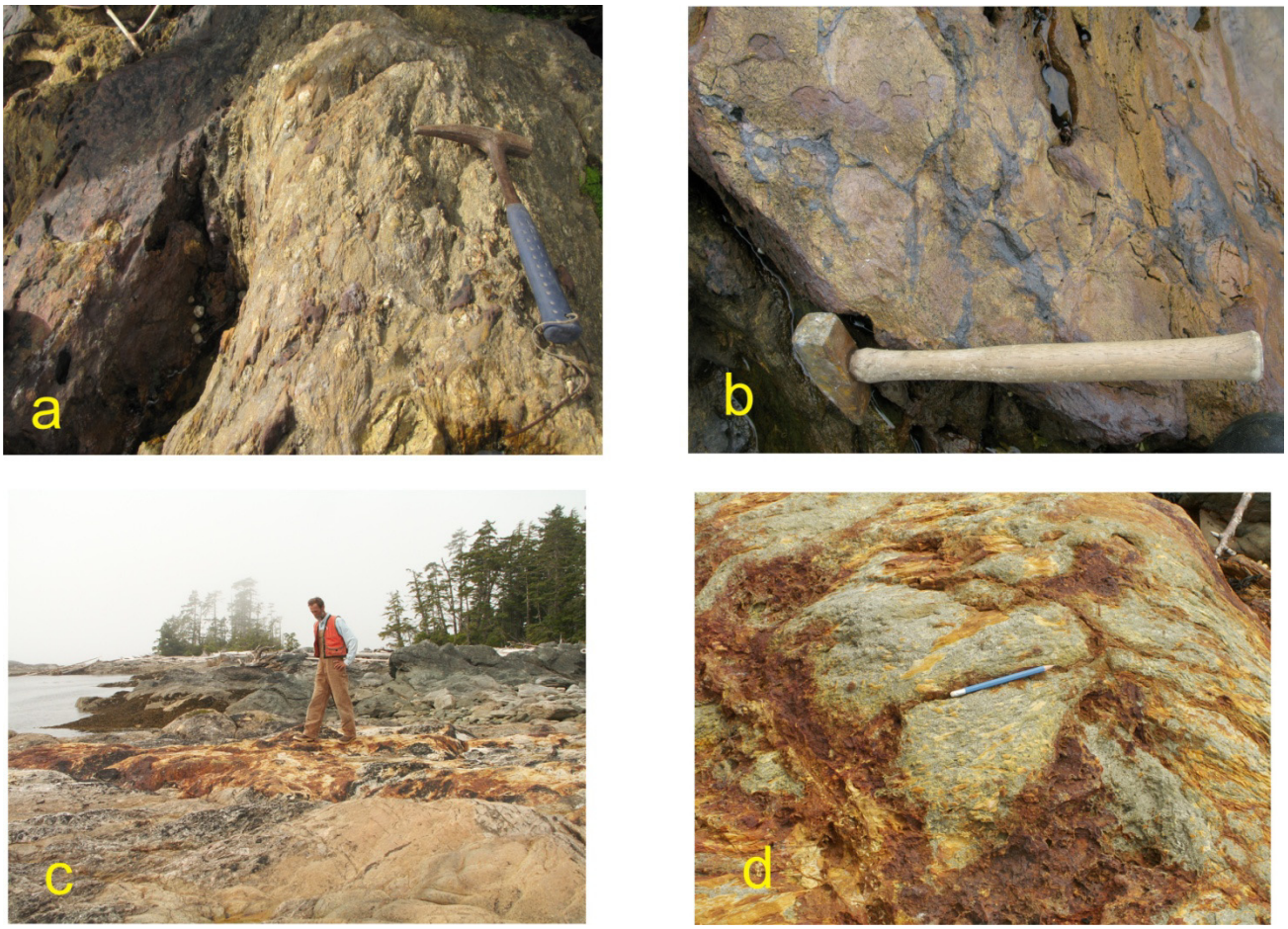

Figure 7. a) Hard Case showing, with massive sulphides replacing matrix of felsic breccia; b) Dogfish showing, displaying brecciated sulphide-bearing quartz-sericite schist surrounded by pyrrhotite and sphalerite; c) Massive marcasite-pyrite in Ordovician metarhyolite, Digby Island; George Gehrels examining the site of *ca.* 472 Ma U-Pb zircon sample reported in Gehrels and Boghossian (2000); d) Detail of Digby Island metarhyolite breccia with irregular replacement and fracture-filling sulphides.

underlie the clastic part of the formation in Laredo Sound map area (Nelson *et al.*, 2011a,b) and also in Kumealon Inlet (Figure 5) may belong either to the Ordovician Descon Formation, or be part of the Mathieson Channel Formation itself. No U-Pb ages are available to resolve this issue. Although not in direct contact, possibly overlying rocks are found locally along Princess Royal Channel south of Khutze Inlet. They consist of garnet-biotite grade metasandstone, which is tentatively assigned to the Upper Jurassic to mid-Cretaceous Gravina belt.

Most stratigraphic members recognized as part of the Mathieson Channel Formation in Laredo Sound area (Nelson *et al.*, 2011b) extend into the current study area. However, maintaining existing subdivisions is difficult, due to the gradational nature of contacts separating metasedimentary rocks that overall appear less extensive and thinner towards the northwest in Douglas Channel area. Consequently, in this area the Mathieson Channel Formation is considered an unsubdivided map unit, composed of variable proportions of meta-arenite and metagreywacke, with lesser marble and calcsilicate and pelitic schist and locally abundant conglomerate, that in places alternate with intervals of metavolcanic rocks of intermediate to mafic compositions. A multitude of mafic and pegmatitic felsic dikes and attenuated apophyses of larger, simple and composite plutons intrude, and locally comprise a significant volume within the interlayered metasedimentary assemblage. Felsic rocks occur in rare, isolated narrow bands in the Mathieson Channel Formation (Nelson *et al.*, 2011a, b). Another possible occurrence, west of Grenville Channel on Pitt Island, consists of sulphide-rich quartz-sericite schist, derived presumably from a felsic volcanic protolith. This felsic unit was the focus of past mining exploration for volcanogenic massive sulphide mineralization at the Pitt showing. Metaconglomerate, locally present in Laredo Sound area, is notably absent from the Mathieson Channel Formation in Douglas Channel area; it however recurs farther north at Kennedy Island and Kumealon Inlet (Figures 3, 5; Nelson, *et al.*, 2010a, b).

METASILICICLASTIC-MARBLE-VOLCANIC UNIT

This unit typifies the varied lithological character of the Mathieson Channel formation in the Douglas Channel area, comprising an aggregate of the "clastic-carbonate, marble, and volcanic member" subdivisions established for the formation in Laredo Sound area (Nelson *et al.*, 2011a, b).

The metasiliciclastic lithologies form parallel, thin to medium-thick, subvertical pale grey to dark grey-green layers, weathering to rusty brownish orange hues (Figure 8). This weathered coloration reflects ubiquitous iron-bearing phases, probably metamorphic pyrite and/or pyrrhotite derived from authigenic hematite (see Nelson *et al.*, 2011b). The siliciclastic components, composed of fine to medium grained, well-sorted quartz and plagioclase, with or without orthoclase, form resistant layers exhibiting internal parallel laminations. The laminations are defined by slight variations in texture and color and aligned minerals, particularly biotite. Psammitic schist interlayers attest to a greater argillaceous content in the matrix of some quartzofeldspathic rocks, distinguished by their relatively recessive, biotite-rich, and crumbly weathering. Pelite, composed of biotite-garnet schist, occupies centimetre-thick layers separating marble-siliclastic layers throughout the unit exposed along the eastern shore of Grenville Channel between Klewnuggit and Lowe inlets.

Marble in siliciclastic sections is clean, off-white and medium crystalline. It weathers yellowish tan in recessive, relatively sparse, spaced layers typically less than several tens of centimetres thick (Figure 8). An unusually thick interval dominated by marble with subordinate siliciclastic layers crops out semi-continuously for about 2 kilometres in western Union Passage, north of Hinton Island. Marble layers have preferential tendency to deform plastically relative to adjacent siliciclastic layers. This strain partioning yields contorted marble layers that display varying scales of tight folds. Any thinner siliclastic and orthoamphibolite layers that commonly interlayer thicker marbles also record strain in the form of folds, boudins or become segmented with the broken fragments aligned in trains. Calcsilicate layers, identified by their pale green weathering and metamorphic mineralogy, including diopside, garnet and epidote, indicate original siliclastic intervals containing a high proportion of carbonate cement.

Figure 8. Interlayered siliciclastic and marble, southern Gil Island.

Metavolcanic rocks comprise a significant component of the Mathieson Channel Formation in parts of Laredo Sound map area, where they are commonly interlayered with marble (Nelson *et al.*, 2011b). However, similar rocks in Douglas Channel map area are far less voluminous, found mainly at several mappable sections along the eastern shoreline of Princess Royal Channel, directly east of Work Island, and in Grenville Channel, several kilometres south of the entrance to Klewnuggit Inlet. At these localities, intervals of massive flows of basaltic composition, up to tens of metres wide, alternate across abrupt contacts with layered siliciclastic rocks containing sparse, thin layers of marble. The flows are dark green, massive varieties of aphryic metabasite and rare sparsely plagioclase-phyric metabasalts. Alteration of basalt by epidote is widespread, as diffuse rounded clots and crosscutting veins.

AGE OF THE MATHIESON CHANNEL FORMATION

An attempt to obtain a U-Pb zircon date on rare felsic volcanic rocks from the Mathieson Channel Formation was unsuccessful because the sample was devoid of zircon. The sampled rocks was from a laminated rhyolite flow in Return Channel, Laredo Sound area (see Nelson *et al.*, 2011b).

Detrital zircon geochronology on metamorphosed siliciclastic assemblages in north coastal British Columbia is utilized to unravel the depositional history of southern Alexander terrane and correlate with its less metamorphosed counterparts in southeast Alaska (Gehrels and Boghossian, 2000; Mahoney *et al.*, 2011). Recent detrital zircon data for the Mathieson Channel Formation, determined by J.B. Mahoney, have been obtained from meta-arenaceous and conglomeratic samples collected from opposite ends of the mapped extent of these rocks, including samples from Laredo Sound map sheet in the south, and Prince Rupert and Douglas Channel map areas in the north (Mahoney *et al.*, 2011). Meta-arenite/meta-arkose samples collected in 2011 from the intervening Douglas Channel map sheet are currently in analysis, with pending results intended for future publication.

Detrital zircon samples (N=13) for the Mathieson Channel Formation show a consistent zircon population range between 400 Ma and 460 Ma, with a peak at 426 Ma (Mahoney *et al.*, 2011). These data also confirm the

initial detrital zircon age for the Mathieson Channel Formation from conglomeratic rocks on Pooley Island in Laredo Sound map area, which shows a unimodal signature centred at about 420 Ma (Gehrels and Boghossian, 2000). Collectively, the detrital zircon data suggest that deposition of the Mathieson Channel Formation initiated in Early Devonian time. The quartz-feldspar-rich arenaceous rocks that characterise the formation suggest a source region probably composed of chemically evolved granitoid rocks of Middle Ordovician to Early Devonian age.

The Ogden Channel complex: a Late Silurian-Early Devonian syntectonic intrusive complex within the Alexander terrane

LITHOLOGIES AND FIELD CHARACTERISTICS

The Ogden Channel complex is located on southwestern Porcher Island, bounded to the northeast by the Salt Lagoon fault (Figure 5). It is a felsic to mafic plutonic suite, with intermediate rocks such as tonalite and quartz diorite being most common. The bodies of this suite intruded syn-tectonically during regional deformation and amphibolite facies metamorphism that produced a foliation of varying intensity on outcrop and map scale. Where deformation is intense, the plutonic rocks have been transformed into orthogneisses and amphibolite (Figure 9a). Mutual crosscutting relationships between the various plutonic members and the foliation, and relationships such as deformed xenoliths of one igneous member in another, less deformed host (Figure 9b) attest to their syntectonic nature. The Ogden Channel complex strongly resembles the middle to lower crustal segments of other syntectonic magmatic arc complexes, such as the Notre Dame arc in western Newfoundland (van Staal *et al.*, 2007) and the Westcoast Crystalline and Wark-Colquitz gneiss complexes of Vancouver Island, deformed Early Jurassic intrusive-metamorphic complexes thought to be a deep level of the Bonanza arc (DeBari *et al.*, 1999).

Included now as subunits of the Ogden Channel complex are the Billy Bay complex and Porcher Creek pluton, in contrast to earlier interpretations of these units (see Nelson *et al.*, 2010b). The Billy Bay complex contains more identifiable volcanic protoliths compared to the Ogden Channel complex, intermixed with strongly deformed plutonic phases. U-Pb results so far include an Ordovician detrital zircon population in a meta-arkose, an Early Devonian igneous age from a felsic lapilli tuff, and a latest Silurian igneous age from granitoid similar to one dated in the Ogden Channel complex nearby (Figure 5; J.B. Mahoney, unpublished data, 2010, 2011). Originally, this complex was interpreted as the deep roots of the Descon arc (Nelson *et al.*, 2010b). However, it contains an abundance of deformed plutons of similar mid-Paleozoic age and character to those in the main Ogden Channel complex. This suggests that it is a variant of the complex that includes more supracrustal material , both older Descon strata and penecontemporaneous mid-Paleozoic volcanic units (Figure 4b). The epidote amphibolite facies metamorphism within it is a further point of similarity.

The Porcher Creek pluton is a weakly to undeformed mainly tonalite-diorite body that was originally considered Early Cretaceous based on its resemblance to plutons of that suite (Nelson *et al.*, 2010a, b). However, it returned a U-Pb zircon age of *ca.* 411 Ma (J.B. Mahoney, unpublished data, 2010). It crosscuts deformed metaplutonic rocks of the Ogden Channel complex, and is itself late to post tectonic (Figure 9c).

STRUCTURE

Deformation of the Ogden Channel complex is typically heterogeneous, characterised by steeply northeast dipping, anastomosing mylonitic shear zones of varying width and associated folding (Figure 10a). Lineations vary in plunge and range between downdip and horizontal. Combined with abundant shear-sense indicators (*e.g.* S-C shear bands, porphyroclasts) they suggest sinistral oblique reverse motion (Figure 10b) directed to the southwest, which is consistent with the vergence of the folds. Involvement of melt phases in shear zones, and crosscutting dikes, show that many of these structures were synmagmatic (Figure 10a).

AGE AND TECTONIC AFFINITY

The Ogden Channel complex was originally interpreted as an intrusive equivalent to the arc volcanic rocks of the Ediacaran to Early Cambrian Wales Group (Gehrels and Saleeby, 1987), based on their arc-like composition, variable degree of deformation and amphibolite facies metamorphism (Nelson *et al.*, 2010b). New U-Pb zircon geochronology suggests that this suite intruded in a relatively short period during the late Silurian to Early Devonian, based on ages of 424-413 and 411 Ma for highly deformed metadiorite and metagranodiorite within the Ogden Channel complex; and much more weakly deformed diorite and tonalite of the Porcher Creek pluton, respectively (J.B. Mahoney, J. Angen; unpublished data; 2010, 2011). The Ogden Channel complex is thus unrelated to the Wales arc. It post-dates igneous activity associated with the Descon arc, based upon both U-Pb data from extrusive units in the immediate area (no younger than 469 Ma), and on regional stratigraphic relationships. Descon volcanics in southeastern Alaska are overlain by late Early to Late Silurian carbonates of the Heceta Limestone (Eberlein and Churkin, 1970; Ovenshine and Webster, 1970) and Early to Late Silurian clastics of the Bay of Pillars Formation (Brew *et al.*, 1984). The event that the Ogden Channel complex does correspond to is the Klakas orogeny of Gehrels *et al.* (1983a, 1996). The sinistral-transpressive, southwest-vergent structures in it are consistent with the southwesterly tectonic transport direction documented by Gehrels *et al.* (1996) in the

Figure 9. a) Amphibolitic orthogneiss in Ogden Channel complex; b) Foliated dike cutting orthogneissic dike; the older dike has yielded a *ca.* 412 Ma U-Pb age (J.B. Mahoney, unpublished data, 2011); c) Porcher Creek pluton: unfoliated tonalite with foliated inclusions (*ca.* 411 Ma, unpublished U-Pb data, J.B. Mahoney, 2010).

southwestern Alaskan panhandle. The main age of plutonism in the Ogden Channel complex is coeval with the cumulative early Paleozoic detrital zircon peak (*ca.*

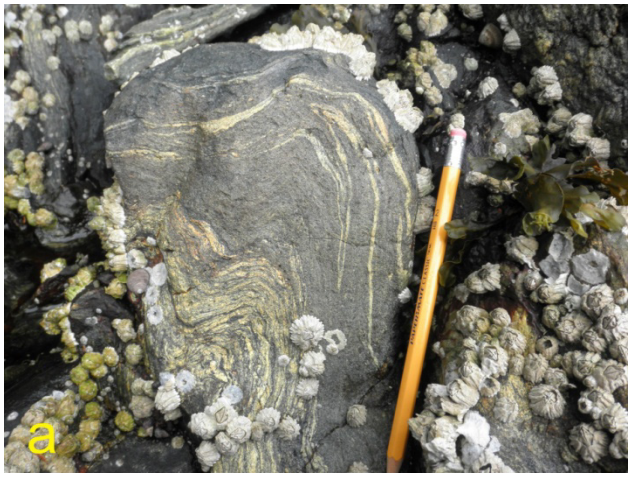

Figure 10. a) Synplutonic mylonitic shear zone in Ogden Channel complex; b) Sinistral shear bands, Ogden Channel complex.

410-420 Ma) in the Banks Island clastic rocks, and slightly younger than the *ca.* 426 Ma cumulative detrital zircon peak from the Mathieson Channel Formation (Mahoney *et al.*, 2011).

Gehrels *et al.* (1996) interpreted the Karheen Formation as a clastic overlap related to collision of the primitive arc of the Alexander terrane of southeastern Alaska (Craig subterrane) with an unknown pericratonic fragment to the west. They hypothesized an event named the Klakas orogeny, based on the sudden appearance of coarse conglomerate and presence of Precambrian detrital grains in the Karheen Formation. The pericratonic Banks Island belt is located west (outboard) of the Ogden Channel complex, although there is a belt of intervening exposures of Ordovician volcaniclastics along Kitkatla Channel. We hypothesise that the Ogden Channel complex was part of a short-lived magmatic arc that developed near a collisional subterrane boundary sutured during the Klakas orogeny, between the Craig subterrane of Alexander, and a pericratonic fragment that underlay and sourced the Banks Island assemblage. The Mathieson Channel Formation, like the Karheen Formation farther north, represents the associated clastic overlap sequence.

Kumealon unit: A new late Paleozoic intrusive/supracrustal suite east of northern Grenville Channel and Telegraph Passage

In 2009, mapping and U-Pb geochronology on the mainland shores near Kumealon and Baker inlets identified several units that do not occur elsewhere within the Alexander terrane. These were assigned to the Yukon-Tanana terrane (Nelson *et al.*, 2010a). Re-examination and detailed re-sampling of these exposures became an important component of the 2011 field program.

The Alexander terrane in western Kumealon Inlet consists of two isoclinally interfolded and locally strongly sheared units: dark green amphibolite-facies metabasalt and minor marble of the Descon Formation, which is overlain by plutonic-cobble conglomerate and rusty meta-arkose of the Mathieson Channel Formation (Figure 11a). At one locality, a pyrite-bearing felsic fragmental pyroclastic rock marks the contact, similar to what is observed on Kennedy Island to the west. A typical Mathieson Channel detrital age spectra has been obtained from one of the conglomerates (G. Gehrels, unpublished data, 2007). Both of these units are extensively intruded by voluminous, thick, pale green, pre-kinematic felsic dikes that contain anhedral metamorphic garnets, particularly near their margins. Relict chilled margins were observed in 2011 (Figure 11b), establishing that these are indeed transposed dikes, and not metasedimentary layers as was originally thought (Nelson *et al.*, 2011a, b). One of the dikes yielded a Permian U-Pb age of *ca.* 280 Ma (J.B. Mahoney, unpublished data, 2011), in accord with an earlier analysis (J.B. Mahoney, unpublished data, 2010).

Near the eastern limit of the combined Mathieson Channel–metabasalt section, a narrow lens of quartz-pebble conglomerate lies within the amphibolite (Figure 11c). It shows a typical, Early Mississippian Yukon Tanana detrital zircon signature (Figure 5; J.B. Mahoney, unpublished data, 2010). The contact between the quartz-pebble conglomerate and the metabasalt on both sides of it is a layer of nearly pure garnet approximately 20 cm thick (Figure 11d), which has been interpreted tentatively as a metamorphosed and altered clay-rich fault gouge. If correct, the Alexander terrane structurally underlies a tightly synformal klippe of Yukon-Tanana terrane, which was thrust above it before a phase of regional folding characterized by nearly upright folds.

Seventy-five metres east of the quartz-pebble conglomerate, across a sharp contact, the dominant unit becomes mainly meta-andesite with lesser metabasalt, metadacite, muscovitic orthogneiss and quartz-muscovite-cordierite-sillimanite schist. These rocks were assigned to the Yukon-Tanana terrane by Nelson *et al.* (2010a, b); however, the transposed section contains felsic dikes identical to those within the Alexander unit to the west. Permian U-Pb ages have been obtained from two bodies of kyanite-bearing muscovitic orthogneiss at this locality, and the metavolcanic unit continues south into Baker Inlet, where a polymictic felsic breccia (Figure 11e) has also yielded a Permian age (J.B. Mahoney, unpublished data, 2011). The metavolcanic unit is in gradational contact with two units of marble containing tuffaceous partings and impure marble, probably the same body repeated by isoclinal folding (Figure 5). Sparse macrofauna including brachiopods and solitary corals were observed (Figure 11f), but not sufficient for constraining the age of the marble beyond probably middle to late Paleozoic. Small bodies of quartz-sericite schist, pyritic quartz-sericite schist and metamorphosed silicified rhyolite near Moore Cove east of Telegraph Passage were originally assigned to the Alexander terrane, and considered to be Ordovician metarhyolites (Nelson *et al.*, 2010a, b). A metarhyolite sample collected in 2011 has returned a Permian age (J.B. Mahoney, unpublished data, 2011). On the basis of this and the set of U-Pb dates from Kumealon and Baker inlets, a new late Paleozoic, mainly Early Permian intrusive/supracrustal unit, the Kumealon unit, has been identified along the length of the mainland coast between northern Grenville Channel and Telegraph Passage. It includes a varied suite of probably arc-related volcanic rocks, basalt, andesite, and rhyolite. Permian muscovitic granites intrude the westernmost volcanics north of Kumealon Inlet, along strike with a zone of pre- metamorphic quartz-muscovite alteration south of the inlet (now as coarse grained quartz-muscovite-garnet-kyanite-sillimanite+cordierite schist). Coeval, Permian fine grained felsic dikes intrude both the volcanic pile and the underlying strata of the Alexander terrane. They establish that the mid-Paleozoic and older Alexander terrane was the basement to the late Paleozoic volcanogenic Kumealon unit (Figure 4b).

The Kumealon unit has no correlatives in the Alexander terrane of southeastern Alaska, where the only late Paleozoic volcanic units are minor basalts interlayered with platform carbonates. Its closest parallel is the Icefield Ranges plutonic suite (Figure 1) and cogenetic Station Creek Formation in the St. Elias Mountains of southwestern Yukon and adjacent eastern Alaska. Plutons of the Icefield Ranges suite have been dated by K-Ar and U-Pb methods as *ca.* 270-310 Ma (Dodds and Campbell, 1988; Gardner *et al.*, 1988; L. Beranek, unpublished data, 2011). The Pennsylvanian (*ca.* 309 Ma, U-Pb zircon) Barnard Glacier pluton cuts both coeval volcanic rocks of the Station Creek Formation and the lower Paleozoic Kaskawulsh Group of the Alexander terrane (Gardner *et al.*, 1988). This relationship is highly significant in Cordilleran tectonics, because the Pennsylvanian-Lower Permian Station Creek Formation in turn is in stratigraphic continuity with the Triassic Nikolai basalts, hallmark of the terrane Wrangellia. The intervening Early Permian Hasen Creek Formation contains fossiliferous limestones (Israel and Cobbett, 2008), a possible equivalent of the marble in Kumealon Inlet.

Correlation of the Permian Kumealon unit with the Station Creek Formation and Icefield Ranges plutonic

Figure 11. Units in Kumealon and Baker inlets. a) Mathieson Channel plutonic-clast conglomerate; b) Metamorphosed felsic dikes, *ca.* 280 Ma; c) Quartz-pebble conglomerate with *ca.* 350-360 Ma detrital peak signature; d) Garnetite in pelite near contact of quartz-pebble conglomerate and amphibolite; e) Felsic heterolithic breccia, *ca.* 280 Ma, Baker Inlet; f) Solitary corals in limestone, Kumealon Inlet.

suite would lead to two important tectonic implications. The correlation would provide a second instance of late Paleozoic "Wrangellian" arc terrane being built on a pre-existing Alexander basement; additional confirmation that Wrangellia probably developed as in intra-oceanic arc attached at one end to the Alexander crustal fragment, in a similar setting to the relationship between the modern Aleutian arc and the Kamchatka Peninsula. Further, the absence of comparable Pennsylvanian-Permian igneous suites elsewhere in the Alexander terrane could suggest that the Kumealon unit and its underlying rocks might restore to a location west of the St. Elias Mountains, perhaps near the southern cut-off of the Icefield suite near Windy Craggy (Figure 1). This would require approximately 800 km of post-Paleozoic sinistral strike-slip motion.

New Investigations of the Grenville Channel fault between northern Grenville Channel and Princess Royal Island

Mapping in 2009 and 2010 covered the northern and southern extents of the Grenville Channel fault and demonstrated significant, albeit not quantified, sinistral motion along it in Early to mid-Cretaceous time. In the course of field work in 2011, these two sections were linked, via tracing of the fault along Grenville Channel, past the northern tip of Gil Island, to its shoreline exposure on western Princess Royal Island (Figure 3).

Work of this project in 2009 showed that the structural framework of Porcher Island and its vicinity is dominated by a series of northwesterly sinistral fault strands (Figure 2; Nelson *et al.*, 2010a, b; Angen *et al.*, this volume). These strands converge southward into the Grenville Channel fault. Field work in 2011 traced the Grenville Channel fault along Grenville Channel southwards into Wright Sound, where it deflects around northeastern Gil Island, thence following a more southerly trajectory, entering Princess Royal Island at Leading Point (Figure 3). Although undocumented by current regional mapping, the fault crosses Princess Royal Island, its trace corresponding with a topographic linear of aligned drainages, lakes and inlets (Figure 3; Nelson *et al.*, 2011b, Figure 17). The Grenville Channel fault exits Princess Royal Island in the southeast via a broad zone of splay faults near Cougar Bay on Tolmie Channel, mapped in 2010 (Nelson *et al.*, 2011a), and continues southeast across the islands between Finlayson and Mathieson channels as spaced high-strain zones with sinistral kinematic indicators (Nelson, *et al.*, 2011b). The southerly extent and nature of the Grenville Channel fault beyond Mathieson Channel is unknown and a potential topic for future study.

The segment of the Grenville Channel fault along Grenville Channel is a narrow zone of extremely high strain affecting juxtaposed orthogneiss, several similar protomylonitic tonalite intrusions, and subvertically layered Mathieson Channel Formation. Rocks forming the eastern shore of the channel consist in part of the Mathieson Channel Formation, in which schistose fabric is prevalent in mainly thin pelitic layers containing biotite and garnet porphyroblasts. Skarn bands consisting of garnet-diopside-epidote form contorted and boudinaged bands in contact with, and as enclaves in, tonalite. The tonalite here is sheared, evident from augen-shaped porphyroclasts with trails of finer grained feldspar in asymmetric pressure shadows, which impart a streaky protomylonitic foliation.

Two tonalite bodies, located along opposite side of Grenville channel near Lowe Inlet, have identical mineralogy and protomylonitic fabrics. However, uranium-lead-zircon geochronology on these two tonalitic intrusions indicates that, despite their similarities, they are separate plutons; the older west of the channel, 108.2 ±1.4 Ma, and the younger sampled at James Point at the entrance to Lowe Inlet, 95.2 ±1.5 Ma (M. Pecha, unpublished data, 2011). The younger date gives a maximum constraint for late ductile deformation on the Grenville Channel segment of the fault. The older tonalite, which is associated with banded dioritic orthogneiss, continues down the west side of the channel to Farrant Island. Both tonalite and banded orthogneiss include highly strained bands and enclaves of metasedimentary rocks of the Mathieson Channel Formation. Throughout Grenville Channel all rocks display a persistent northwest trending, subvertical penetrative foliation and mineral lineation that plunges consistently between 30 and 40 degrees towards the southeast, and kinematic indicators suggest sinistral reverse motion.

The Grenville Channel fault under Grenville Channel is part of broader zone of very strong foliation developed for several kilometres on both sides of the channel. It is expressed as a pattern of northwesterly topographic linears, and development of extreme foliation and lineation in plutonic phases as young as 95 Ma. The western side of Ecstall pluton is well-foliated and shows weakly developed sinistral indicators at the mouth of Lowe Inlet; however, the interior of the pluton at this latitude is not deformed.

On northern Gil Island, pre mid-Cretaceous banded orthogneiss is cut off by an weakly foliated garnet-bearing tonalite pluton dated as *ca.* 100 Ma (age data from Gehrels *et al.,* 2009). The expression of the Grenville Channel fault here is similar to that in Grenville Channel, partly obliterated by this later intrusive phase (Figures 12a, b). Where the fault passes onto Princess Royal Island, a narrow zone of protomylonite lies between identical mid-Cretaceous (*ca.* 104-106 Ma), enclave-bearing, weakly magmatically foliated but otherwise undeformed tonalites, which are probably parts of same body. Displacement of the margin of this large tonalite pluton across the Grenville Channel fault suggests sinistral offset in the order of 5 kilometres (Figure 3). As is the case in the area around Klemtu, the younger (*ca.* 95-106 Ma) large tonalite bodies are cut by discrete strands of the Grenville Channel fault, but are not penetratively foliated in their interiors.

Diorite of presumed pre-mid-Cretaceous age continues southwest of the Grenville Channel fault along the shores of Farrant Island. From orthogneiss in the shear zone on the northern shore, fabric development declines markedly. More than a few hundred metres from the fault, it is not foliated. On southern Gil Island, a Late Jurassic *ca.* 148 Ma tonalitic pluton (G. Gehrels, unpublished data, 2010) is also undeformed (Figure 13). Relationships here are similar to those observed on Banks Island, where Late Jurassic plutons crosscut structures in transposed metasedimentary rocks.

Figure 12. a) Banded orthogneiss of probable Early Cretaceous age, northern Farrant Island; b) Undeformed tonalite, northernmost Gil Island, with inclusions of banded orthogneiss, *ca.* 100 Ma.

Figure 13. Undeformed tonalite, southern Gil Island; dated at *ca.* 148 Ma (G. Gehrels, unpublished data, 2010).

SIGNIFICANCE AND ROLE OF THE GRENVILLE CHANNEL FAULT IN CRETACEOUS TECTONICS OF THE COAST BELT

The Grenville Channel fault is of regional extent, over 300 kilometres in strike length. Throughout its length it manifests as a continuous, strong but fairly narrow zone of intense ductile shearing. At its widest near Grenville Channel, the zone is several kilometres in width. On northern Princess Royal Island, the fault zone comprises less than a hundred metres of mylonite between exposures of unfoliated tonalite. To the north, on Porcher Island, it consists of a set of splays, each a discrete but fairly narrow ductile shear zone. A similar pattern is seen in Laredo Sound map area near Klemtu. The latest movement on the Grenville Channel fault is *ca.* 105-96 Ma, based on offsets of and fabric development within dated plutonic bodies (Nelson *et al.*, 2010b, 2011b; Angen *et al.*, 2012, this volume). Earlier motion is probable, corresponding to regional-scale fabric development in the *ca.* 123-116 Ma Early Cretaceous plutonic suite northeast of the fault in Laredo Sound area, which is crosscut by *ca.* 106-95 Ma plutons (Nelson *et al.*, 2011b). This zone of deformation extends eastward until it is caught up in younger high strain zones such as the Coast shear zone (*ca.* 50-70 Ma).

There is a strong contrast between the degree of Early Cretaceous regional deformation across the Grenville Channel fault. To the northeast, penetrative fabrics showing sinistral asymmetry are widely developed. To the southwest, however, Early Cretaceous and older units were apparently not affected by this event. Farrant Island is underlain by undeformed pre-100 Ma diorite. Late Jurassic plutons on Gil as well as on Banks Island are similarly post-kinematic. Furthermore, most of the deformation in Ogden Channel complex now appears to have been Early Devonian, except along discrete splays of the Grenville Channel fault such as the Useless fault (Angen *et al.*, 2012, this volume). All of these observations suggest an absence of Cretaceous regional penetrative ductile deformation in most of the block that lies between the Grenville Channel fault and Kitkatla shear. The Grenville Channel fault seems to mark a strain boundary between a broad zone of Early Cretaceous sinistral ductile deformation to the northeast, and an outboard rigid block. The fault itself localized the last, mid-Cretaceous, focused sinistral motion. Displacement of the tonalite on northern Princess Royal Island suggests a fairly modest magnitude, about 5 kilometres for this final phase of motion (Figure 3). The Grenville Channel as a strong, persistent topographic linear marks the northeastern edge of the rigid block.

Regional considerations point to hundreds of kilometres of sinistral motion across the Coast belt in Early to mid Cretaceous time. Primary evidence is the closure of the Bridge River–Tyaughton basin, which Monger *et al.* (1994) consider to be the result of southward displacement of the western Coast belt by approximately 400 km. Also, the northern edge of west-northwest trending belt of mid to Late Jurassic arc-related volcanism and plutonism lies at about 54 degrees, near Kitimat, east of Coast Mountains. To the west, the mid to Late Jurassic magmatic province is best developed on northern Vancouver Island and the adjacent mainland. If

its northern limit is assumed to lie at about the latitude of northern Vancouver Island, 51 degrees, then the apparent sinistral offset across the Coast belt is about 400 km, equivalent to displacement necessary to close the Tyaughton basin. However, the northern limit of the mid to Late Jurassic plutonic belt in the west is still not well understood. There is a paucity of available ages for the entire Coast Plutonic Complex between Bella Bella and Bute Inlet. Gehrels *et al.* (2009) presented an extensive U-Pb database for the Coast Mountains north of Bella Bella, and the southern Coast Mountains have been extensively studied (*cf.* Monger and McNicoll 1993; Monger and Journeay, 1994). The region in between represents a large gap in current knowledge.

The Late Jurassic intrusive body on Gil Island is part of a more extensive suite that outcrops extensively on Banks Island, probably dextrally offset approximately 80 kilometres to the northwest on the Cenozoic Principe-Laredo fault (Figure 3). The body on southern Gil Island may be an isolated outlier. However, if it represents the true northern extent of the mid to Late Jurassic plutonic belt, then it only lies 100 kilometres south of the northern limit of age-equivalent magmatism east of the Coast Mountains near Kitimat; as a pinning point this would reduce the required Early to mid-Cretaceous sinistral offset to less than a hundred kilometres. Resolution of this puzzle will require systematic dating of plutons in the region in between.

In any event, assuming that there was Cretaceous sinistral motion across the Coast Mountains of 100 to 400, or even 800 (Monger and Struik, 2006), kilometres in total, our results show that only a small fraction of that motion occurred along the Grenville Channel fault after about 108 Ma. Instead, it probably occurred as distributed shear, mainly in Early Cretaceous time, in the broad region between the Grenville Channel fault and the Pootlass shear near Bella Coola (Mahoney *et al.*, 2009).

FUTURE WORK ON THE NORTH COAST PROJECT

The 2011 season concluded the collection of field data and samples related to this project. So far we have produced, but not published, about 20 U-Pb dates; with 15 more samples in processing. A suite of over 50 metavolcanic samples have been analysed for major and trace elements in order to characterize the mainly Ordovician magmatism. Once these important data sets are edited and complete, a series of papers are planned to cover the various themes that have emerged during the project: the history and tectonic significance of Ordovician magmatism in the Alexander terrane, along with its implications for VMS potential; the ultimate crustal origins of the Alexander terrane and the Devonian accretionary events within it. The thesis work of Joel Angen continues, with its focus on the history of sinistral Cretaceous faulting and deformation within the Coast belt of northern British Columbia. This detailed work will complement more regional results. An open file map will be released in 2012-13 that will incorporate new mapping and analytical results of this project. An ultimate aim of the project is an extensive update of the existing digital coverage of the northern Coast belt on the provincial government's online BC Geology Map, based on the new mapping and U-Pb dating results.

ACKNOWLEDGMENTS

Support from Captain Don Willson, Silverking Ventures, was essential in all aspects of our work. Literally we would have been dead in the water without his skills. Forward motion was also enabled by backing from the GEM (Geology for Energy and Minerals) Program, Cordilleran Multiple Metals, which provided both financial resources and a community of researchers dedicated to unravelling the mysteries of the Canadian Cordillera. M. Metzler was of great help to the project; and we thank the community of Oona River, particularly Jan Lemon, for generous support and friendship.

REFERENCES

Alldrick, D.J. (2001): Geology and mineral deposits of the Ecstall belt, northwest B.C.: Geological Fieldwork 2000, *BC Ministry of Energy and Mines*, Paper 2001-1, pages 279-306.

Alldrick, D.J., Friedman, R.M. and Childe, F.C. (2001): Age and geologic history of the Ecstall greenstone belt, northwest B.C; Geological Fieldwork 2000, *BC Ministry of Energy and Mines*, Paper 2001-1, pages 269-278.

Angen, J.J., van Staal, C. and Lin, S. (2012, this volume): Structural geology of the Alexander terrane in the vicinity of Porcher Island, northwestern British Columbia; Geological Fieldwork 2011, *BC Ministry of Energy and Mines*.

Berg, H.C., Jones, D.L. and Richter, D.H. (1972): Gravina-Nutzotin belt–tectonic significance of an upper Mesozoic sedimentary and volcanic sequence in southern and southeastern Alaska; *U.S. Geological Survey*, Professional Paper 800-D, pages D1-D24.

Berg, H.C., Jones, D.L. and Coney, P.J. (1978): Map showing pre-Cenozoic tectonostratigraphic terranes of southeastern Alaska and adjacent areas; *U.S. Geological Survey*, Open-File Report 78-1085, 1:1 000 000 scale.

Bohme, D.M. (1993): Geological, geochemical and geophysical report on the Pitt/Trinity claim group; *BC Ministry of Energy, Mines and Petroleum Resources*, Assessment Report 22912, 34 pages.

Bradley, W. (1987): Report of exploration on the Trinity Property, BP Resources Canada; *BC Ministry of Energy Mines and Petroleum Resources*, Assessment Report 15674, 57 pages.

Brew, D.A., Ovenshine, A.T., Karl, S.M. and Hunt, S.J. (1984): Preliminary reconnaissance geologic map of the Petersburg and parts of the Port Alexander and Sumdum 1:250 000 quadrangles, southeastern Alaska; *U.S. Geological Survey*, Open-File Report 84-405, 43 pages.

Butler, R.F., Gehrels, G.E., Hart, W., Davidson, C. and Crawford, M.L. (2006): Paleomagnetism of Late Jurassic to mid-Cretaceous plutons near Prince Rupert, British

Columbia, in Haggart, J.W., Enkin, R.J., and Monger, J.W.H., eds., Paleogeography of the North American Cordillera: Evidence for and against large-scale displacements; *Geological Association of Canada*, Special Paper 46, pages 171-200.

Chardon, D., Andronicos, C.L. and Hollister, L.S. (1999): Large-scale transpressive shear zone patterns and displacements within magmatic arcs: The Coast Plutonic Complex, British Columbia; *Tectonics*, Volume 18, pages 278-292.

Crawford, M.L., Hollister, L.S. and Woodworth, G.J. (1987): Crustal deformation and regional metamorphism across a terrane boundary, Coast Plutonic Complex, British Columbia; *Tectonics*, Volume 6, pages 343-361.

Crawford, M.L., Crawford, W.A. and Gehrels, G. (2001): Terrane assembly and structural relationships in the eastern Prince Rupert quadrangle, British Columbia; in Stowell, H.H. and McClelland, W.C., editors, Tectonics of the Coast Mountains, Southeastern Alaska and British Columbia, *Geological Society of America*, Special Paper 343, pages 1-22.

DeBari, S.M., Anderson, R.G. and Mortensen, J.K. (1999): Correlation among lower to upper crustal components in an island arc: the Jurassic Bonanza arc, Vancouver Island, Canada; *Canadian Journal of Earth Sciences*, Volume 36, pages 1371-1413.

Dodds, C.J. and Campbell, R.B. (1988): Potassium-argon ages of mainly intrusive rocks in the Saint Elias Mountains, Yukon and British Columbia; *Geological Survey of Canada*, Paper 87-16, 43 pages.

Eberlein, G.D. and Churkin, M.J. (1970): Paleozoic stratigraphy in the northwest coastal area of Prince of Wales Island, southeastern Alaska; *U.S. Geological Survey*, Bulletin 1284, 67 pages.

Eberlein, G.D., Churkin, M. Jr., Carter, C., Berg, H.C. and Ovenshine, A.T. (1983): Geology of the Craig quadrangle, Alaska; *U.S. Geological Survey*, Open File Report 83-91, 28 pages.

Gardner, M.C., Bergman, S.C., Cushing, G.W., MacKevett, E.M. Jr., Plafker, G., Campbell, R.B., Dodds, C.J., McClelland, W.C. and Mueller, P.A. (1988): Pennsylvanian pluton stitching of Wrangellia and the Alexander terrane, Wrangell Mountains, Alaska; *Geology*, Volume 16, pages 967-971.

Gareau, S.A. and Woodsworth, G.J. (2000): Yukon-Tanana terrane in the Scotia-Quaal belt, Coast Plutonic Complex, central-western British Columbia; in Stowell, H.H. and McClelland, W.C., editors, Tectonics of the Coast Mountains, Southeastern Alaska and British Columbia, *Geological Society of America*, Special Paper 343, pages 23-44.

Gehrels, G.E. (2001): Geology of the Chatham Sound region, southeast Alaska and coastal British Columbia; *Canadian Journal of Earth Sciences*, Volume 38, pages 1579-1599.

Gehrels, G.E. and Berg, H.C. (1994): Geology of southeastern Alaska; in The Geology of Alaska; Volume G-1, The Geology of North America, *The Geological Society of America*, pages 451-467.

Gehrels, G.E. and Boghossian, N.D. (2000): Reconnaissance geology and U-Pb geochronology of the west flank of the Coast Mountains between Bella Coola and Prince Rupert, coastal British Columbia; in Stowell, H.H. and McClelland, W.C., editors, Tectonics of the Coast Mountains, Southeastern Alaska and British Columbia, *Geological Society of America*, Special Paper 343, pages 61-76.

Gehrels, G.E. and Saleeby, J.B. (1987): Geology of southern Prince of Wales Island, southeastern Alaska; *Geological Society of America*, Bulletin, Volume 98, pages 123-137.

Gehrels, G.E., Berg, H.C. and Saleeby, J.B. (1983b): Ordovician Silurian volcanogenic massive sulfide deposits on southern Prince of Wales Island and the Barrier Islands, southeastern Alaska; *U.S. Geological Survey*, Open File Report 83318, 11 pages.

Gehrels, G.E., Saleeby, J.B., and Berg, H.C.(1983a): Preliminary description of the Late Silurian-Early Devonian Klakas orogeny in the southern Alexander terrane, in Pre-Jurassic rocks in western North American suspect terranes, edited by C.H. Stevens, pages 131-141, Pacific Section, *Society of Economic Paleontologists and Mineralogists*, Los Angeles.

Gehrels, G., McClelland, W.C., Samson, S.D. and Patchett, P.J. (1992): Geology of the western flank of the Coast Mountains between Cape Fanshaw and Taku Inlet, southeastern Alaska; *Tectonics*, Volume 11, pages 567-585.

Gehrels, G.E., Butler, R.F. and Bazard, D.R. (1996): Detrital zircon geochronology of the Alexander terrane, southeastern Alaska; *Geological Society of America*, Bulletin, Volume 108, pages 722–734.

Gehrels, G., Rusmore, M., Woodsworth, G., Crawford, M., Andronicos, C., Hollister, L., Patchett, J., Ducea, M., Butler, R., Klepeis, K., Davidson, C., Friedman, R., Haggart, J., Mahoney, B., Crawford, W., Pearson D. and Girardi, J. (2009): U-Th-Pb geochronology of the Coast Mountains batholith in north-coastal British Columbia: Constraints on age and tectonic evolution; *Geological Society of America*, Bulletin, Volume 121, pages 1341-1361.

Hutchison, W.W. (1982): Geology of the Prince Rupert – Skeena map area, British Columbia; *Geological Survey of Canada*, Memoir 394, 115 pages, with 1:250 000 scale geological map GSC Map 1427A.

Israel, S. and Cobbett, R. (2008): Kluane Ranges bedrock geology, White River area (parts of NTS 115F/9, 15 and 16; 115G/12 and 115K/1,2); *Yukon Energy, Mines and Resources*, Yukon Geological Survey, Yukon Exploration and Geology 2007, pages 153-167.

Kapp, P.A. and Gehrels, G. (1998): Detrital zircon constraints on the tectonic evolution of the Gravina belt, southeastern Alaska; *Canadian Journal of Earth Sciences*, Volume 35, pages 253-268.

Lo, B.B.H. (1992): Geophysical report on a helicopter-borne electromagnetic and magnetometer survey at the Pitt/Trinity property, British Columbia, NTS 103H/12; *BC Ministry of Energy and Mines and Petroleum Resources*, Assessment Report 22475, 45 pages.

Mahoney, J.B., Gordee, S.M., Haggart, J.W., Friedman, R.M., Diakow, L.J. and Woodsworth, G.J. (2009): Magmatic evolution of the eastern Coast Plutonic Complex, Bella Coola region, west-central British Columbia; *Geological Society of America*, Bulletin, Volume 121, pages 1362-1380.

Mahoney, J.B., Nelson, J., Gehrels, G., Karl, S., Diakow, L. and Angen, J. (2011): Paleozoic evolution of the southern Alexander terrane, northwest British Columbia; *2011*

Geological Society of America Annual Meeting, Minneapolis, Minnesota, Abstract with Programs, Volume43, page 440.

McClelland, W.C. and Gehrels, G.E. (1990): Geology of the Duncan Canal shear zone: Evidence for Early to mid-Jurassic deformation of the Alexander terrane, southeastern Alaska; *Geological Society of America*, Bulletin, Volume 102, pages 1378-1392.

McClelland, W.C., Gehrels, G.E. and Saleeby, J.B. (1992): Upper Jurassic-Lower Cretaceous basinal strata along the Cordilleran margin: Implications for the accretionary history of the Alexander-Wrangellia-Peninsular terrane; *Tectonics*, Volume 11, pages 823-835.

Monger, J.W.H. and Journeay, J.M. (1994): Guide to the geology and tectonic evolution of the southern Coast Mountains; *Geological Survey of Canada*, Open File 2490, 77 pages, 1:500 000 scale map.

Monger, J.W.H. and McNicoll, V.J. (1993): New U-Pb dates from southwestern Coast Belt, British Columbia; in Radiogenic Ages and Isotopic Studies: Report 7; *Geological Survey of Canada*, Paper 93-2, pages 119-126.

Monger, J.W.F. and Struik, L.C. (2006): Chilliwack terrane: a slice of Stikinia? A tale of terrane transfer; in Haggart, J.W., Enkin, R.J. and Monger, J.W.H., editors, Paleogeography of the North American Cordillera: evidence for and against large-scale displacements; *Geological Association of Canada*, Special Paper 46, pages 351-368.

Monger, J.W.H., van der Heyden, P., Journeay, J.M., Evenchick, C.A. and Mahoney, J.B. (1994): Jurassic-Cretaceous basins along the Canadian Coast belt: their bearing on pre-mid-Cretaceous sinistral displacements; *Geology*, Volume 22, pages 175-178.

Nelson, J. (1998): The quiet counter-revolution: Structural control of syngenetic deposits; *Geoscience Canada*, Volume 24, No. 2, pages 91-98.

Nelson, J.L., Mahoney, J.B. and Gehrels, G.E. (2010a): Geology of Porcher Island and northern Grenville Channel, northwestern British Columbia (parts of 103G/15,16, H/13, J/1 and 2); *BC Ministry of Energy and Mines*, Open File 2010-03, Geological Survey of Canada, Open File 6654, 1:50 000 scale.

Nelson, J.L., Mahoney, J.B., Gehrels, G.E., van Staal, C. and Potter, J.J. (2010b): Geology and mineral potential of Porcher Island, northern Grenville Channel and vicinity, northwestern British Columbia; *BC Ministry of Energy and Mines*, Geological Fieldwork 2009, pages 19-42.

Nelson, J.L., Diakow, L.J., Karl, S., Mahoney, J.B., Gehrels G.E., Pecha, M. and van Staal, C. (2011a): Geology of the mid-coast region of British Columbia near Klemtu, parts of Laredo Sound map area, NTS 103A/08, 09, 15 and 16; *BC Ministry of Energy and Mines*, Open File 2011-03, Geological Survey of Canada Open File 6762, 1:50 000 scale.

Nelson, J.L., Diakow, L.J., Karl, S., Mahoney, J.B., Gehrels G.E., Pecha, M. and van Staal, C. (2011b): Geology and mineral potential of the southern Alexander terrane and western Coast Plutonic Complex near Klemtu, northwestern British Columbia; *BC Ministry of Energy and Mines*, Geological Fieldwork 2010, pages 73-98.

Ovenshine, A.T. and Webster, G.D. (1970): Age and stratigraphy of the Heceta Limestone in northern Sea Otter Sound, southeastern Alaska; *U.S. Geological Survey*, Professional Paper 700-C, pages 170-174.

Rubin, C.M. and Saleeby, J.B. (1992): Tectonic history of the eastern edge of the Alexander terrane, southeast Alaska; *Tectonics*, Volume 11, pages 586-602.

Slack, J.F., Shanks, W.C., Karl, S.M., Gemery, P.A., Bitterbender, P.E. and Ridley, W.I. (2005): Geochemical and sulphur-isotopic signatures of volcanogenic massive sulphide deposits on Prince of Wales Island and vicinity, southeastern Alaska; in Studies by the U.S. Geological Survey in Alaska 2005, *U.S. Geological Survey*, Professional Paper 1732-C, 37 pages.

van der Heyden, P. (1992): A Middle Jurassic to Early Tertiary Andean-Sierran arc model for the Coast Belt of British Columbia; *Tectonics*, Volume 11, pages 82-97.

van Staal, C.R., Whalen J.B., McNicoll, V.J., Pehrsson, S., Lissenberg, C.J., Zagorevski, A., van Breemen, O. and Jenner, G.A. (2007): The Notre Dame arc and the Taconic Orogeny in Newfoundland; in Hatcher, R.D. Jr., Carlson, M.P., McBride, J.H. and Martínez Catalán, J.R., editors, 4-D framework of continental crust; *Geological Society of America*, Memoir 200, pages 511–552.

Wheeler, J.O., Brookfield, A.J., Gabrielse, H., Monger, J.W.H., Tipper, H.W. and Woodsworth, G.J. (1991): Terrane map of the Canadian Cordillera; *Geological Survey of Canada*, Map 1713A, 1:2 000 000 scale.

Compositional Features and Rare Metal Mineralization of the Hellroaring Creek Stock, Southeastern British Columbia (NTS 082F/09)

by S.G. Soloviev[1]

KEYWORDS: East Kootenay, rare metal granite, pegmatite, greisen, beryl, columbite-tantalite

INTRODUCTION

For a long time, the Hellroaring Creek stock has attracted significant interest due to its association with a large body of granitic pegmatites and substantial beryllium and other rare metal (Nb, Ta, Sn) mineralization. Most efforts, however, were spent on studying the large-crystalline pegmatite outcropping within the Hellroaring Creek stock (MINFILE 082FNE110), and the term "Hellroaring Creek pegmatite" is often equalized to the term "Hellroaring Creek stock". Meantime, this large-crystalline pegmatite composes just a minor fraction of the stock that incorporates much larger volumes of various granitic rocks bearing signatures of the "specialty granites" (Pollard, 1995; Pollard, 1989a, b). This is consistent with many characteristic features of the granites including their distinct rare metal metallogeny and a broad occurrence of the rare metal mineralization in the granites in addition to the much more localized pegmatitic bodies. Other, more evolved pegmatite bodies are located distal to the Hellroaring Creek stock.

Field observations on the pegmatites, granites and their relationships combined with the compositional data allow revealing evolutional trends of the Hellroaring Creek stock granites and pegmatites similar to general trend documented by London (2008). In total, the data on the textural and compositional features of the granites make it possible to compare these with similar "specialty rare metal granites" worldwide (Simandl, 2002). If the "specialty granites" are recognized in British Columbia as a distinct rare metal deposit type, this can further contribute to a better understanding of the rare metal metallogeny of this region.

EXPLORATION HISTORY

According to Smith and Brown (1998), the pegmatite occurrence associated with the Hellroaring Creek stock was originally located by Rice (1941), during a regional study, and a more detailed map was published by Leech (1957). It was regarded as an intrusion of possible economic interest for beryllium and industrial minerals. Then, it was staked as a beryllium prospect and explored by various operators (*i.e.*, Richfield Oil Corp. *etc.*) by stripping, blasting, sampling and mapping; as a result, it was estimated that the northern end of the stock contains no NI 43-101 compliant resource of 500 000 tonnes of the mineralized material grading 0.1% BeO (Wasylyshyn, 1984; MINFILE, 2011). Limited studies by the Geological Survey of Canada have identified the presence of Nb-Ta minerals (Mulligan, 1968). In 1984-85, Lumberton Mines Ltd. further investigated the beryllium potential by drilling seven drillholes totalling 500 m; the beryllium content in the drill core was determined by the beryllium scincillator tool, with just control assaying, and returned low grade values (Wasylyshyn, 1984).

In 1985-87, Lumberton Mines Ltd. performed further exploration of the Hellroaring Creek stock pegmatite, this time focused on the ceramic feldspar. Twenty-one drillholes were drilled totalling 2012.4 m; it was determined, after the subsequent small-scale metallurgical bench testing, that the pegmatite contains a considerable amount of glass and ceramic grade feldspar (Pudifin, 1986).

In 1999-2001, another significant exploration program for beryllium including prospecting and diamond drilling was carried out by Chapleau Resources Ltd. (Anderson, 2001; Soloviev, 2001). The work expanded the area with identified beryllium mineralization; however, the drilling, although it encountered a number of significant intercepts, failed to prove the consistency and continuity of the mineralized sectors that would be sufficient for further development of beryllium resources. Some efforts were spent on investigating the tantalum potential of the Hellroaring Creek stock and the nearby Lightning Creek pegmatite as well as other pegmatite occurrences known in the area. Although no economic concentrations of tantalum were outlined, the work indicated locally elevated to high grade tantalum and niobium as well as tin mineralization associated with the pegmatites and "pegmatoid" (stockscheider) varieties of the granites (Soloviev, 2001). In 2002-05, the Hellroaring Creek pegmatite and other pegmatite bodies known in the area were investigated for their gemstone potential (Brown, 2003; Legun, 2004, 2005).

[1] *International GeoSol Consulting Inc., Calgary, AB*

This publication is also available, free of charge, as colour digital files in Adobe Acrobat® PDF format from the BC Ministry of Energy and Mines website at http://www.empr.gov.bc.ca/Mining/Geoscience/PublicationsCatalogue/Fieldwork.

DISTRICT GEOLOGY AND METALLOGENY

The Hellroaring Creek stock is situated in southeastern British Columbia, some 20 km southwest of Kimberley and 31 km west-northwest of Cranbrook (Figure 1). The area lies west of the Rocky Mountain Trench within the Purcell Anticlinorium of the Omineca orogenic belt, a Proterozoic pericratonic terrane subjected to tectonic and magmatic activation (of distal subduction-related and/or anorogenic type) occurred mainly in the Mesozoic (Hoy, 1993; Hoy and Van der Heyden, 1988). The area also comprises an older (Precambrian) metasedimentary package and younger (Mesozoic) igneous suites.

The Cranbrook area (Figure 2) is underlain by Mesoproterozoic terrigenous clastic, carbonate, and minor volcanic rocks of the Purcell Supergroup that is believed to have formed in an intracontinental rift system (Hoy, 1993; Hoy *et al.*, 1995; Lydon, 2007). They include the basal Aldridge Formation composed of siliciclastic turbidites 4000 m thick and informally divided into the Lower, Middle, and Upper units. The Lower Aldridge, the base of which is not exposed, comprises about 1500 m of thin to medium-bedded argillite, wacke and quartzitic wacke generally interpreted as distal turbidites. The Sullivan SEDEX orebody occurs at the top of this division (Lydon, 2007). The Middle Aldridge is about 2500 m of grey to rusty, dominantly medium to thick bedded quartzitic wacke turbidites with minor thin-bedded argillites, some of which form finely laminated marker beds (time stratigraphic units correlated over great distances within the Purcell Basin). The Upper Aldridge includes about 300 m of dark argillite and grey siltite. The Aldridge Formation is tectonically (?) overlain by the Creston Formation, consisting of quartzites and grey, green and maroon wackes up to 1800 m thick (Hoy, 1993). In turn, the Creston Formation is overlain by the Kitchener Formation that includes oolitic limestone and dolomitic siltstone (Hoy, 1993). The Purcell Supergroup has been intruded by sills, somewhat discordant sheets and dikes of the 1443 ±10 Ma Moyie Sill suite, most prominent in the lower portions of the Aldridge Formation.

The Hellroaring Creek stock is believed to have been emplaced after the earliest Moyie intrusions (gabbroic sills) and after the first deformation of the Aldridge Formation and, thus, have an age of approximately 1300 Ma (Ryan and Blenkinsop, 1971). However, this age was questioned by Ethier *et al.* (1976) who noted an ambiguous relationship of the stocks to the gabbroic sills as well as general uncertainties of the age correlation between the Moyie intrusions and the Aldridge Formation.

The Purcell Supergroup is intruded also by a number of dikes, stocks and larger plutons of mostly granodiorite, monzonite, and possibly syenite composition that are assigned to the Mesozoic (Hoy and Van der Heyden,

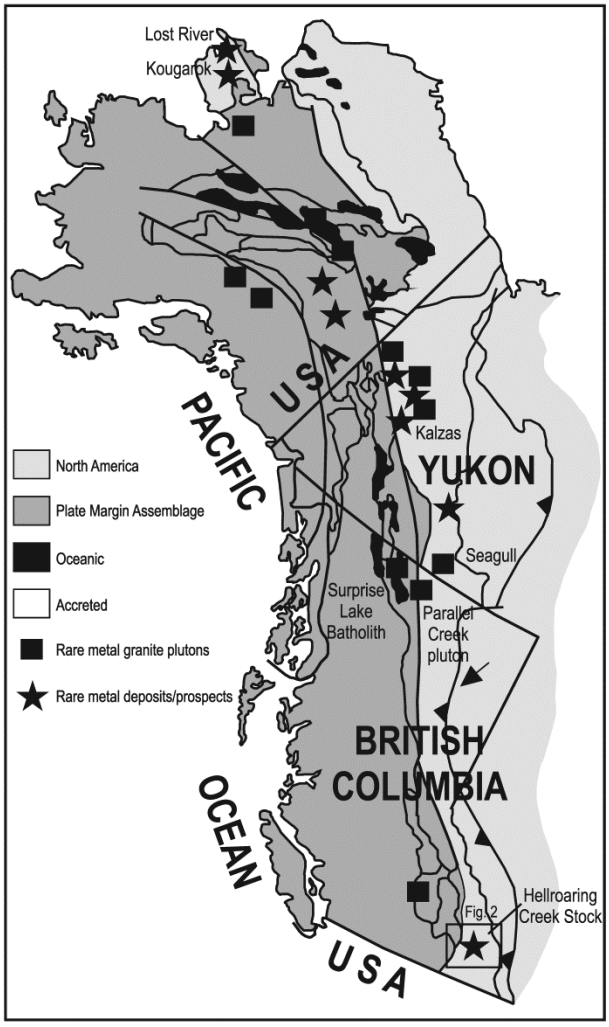

Figure 1. Regional position of the Hellroaring Creek stock and other possible rare metal-bearing granites and pegmatites in the Cordilleran structures. Tectonic assemblage map after Wheeler and McFeely (1991) shows the distribution of North American, plate margin, oceanic and accreted rocks of the Canadian and Alaskan Cordillera, the location of rare metal granite plutons and selected deposits and occurrences.

1988). The larger intrusions, composed essentially of granodiorite, likely correspond to the mid-Cretaceous Bayonne plutonic suite. As defined by Logan (2002), this suite comprises monzogranite, granodiorite, biotite granite, and biotite-muscovite granite. The hornblende-biotite granite is metaluminous to weakly peraluminous; the biotite-muscovite granites, aplites and pegmatites are strongly peraluminous. In the Cranbrook area, the Bayonne suite is represented by the large Reade Lake stock, smaller Kiakho, Grassy Mountain and other stocks as well as by the Angus Creek stock situated south of the Hellroaring Creek stock (Hoy and van der Heyden, 1988). It should be noted that distinguishing the biotite-muscovite rocks of the Bayonne suite from similar in composition granites of the Hellroaring Creek stock and similar (Precambrian?) smaller intrusions nearby is not always fully evident, especially where tourmaline is absent. Abundance of tourmaline as well as common stockscheider textures of marginal varieties, together with

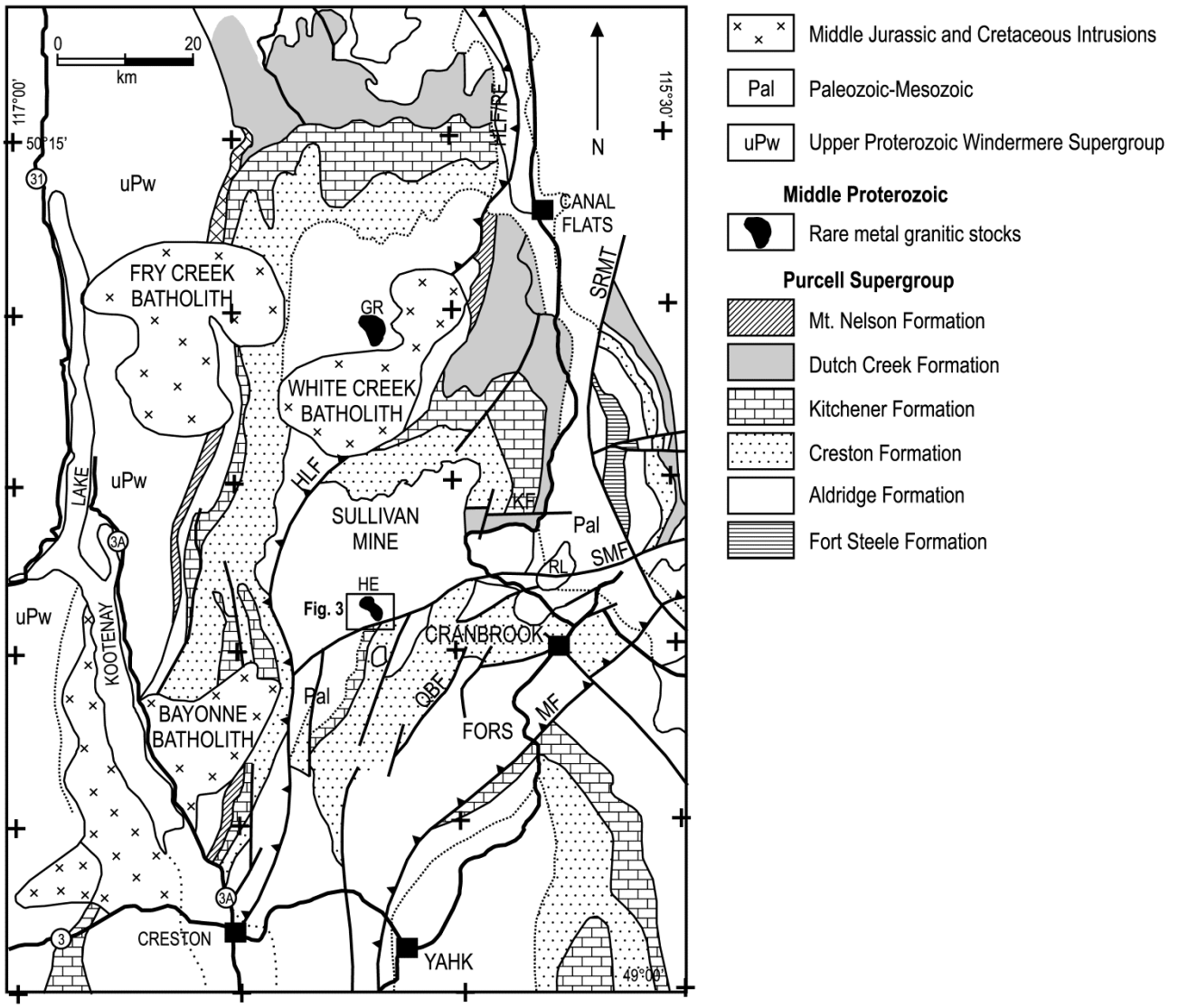

Figure 2. Simplified geology map of southeastern British Columbia (Purcell Anticlinorium) showing location of the Hellroaring Creek stock (modified after Smith and Brown, 1998; Hoy *et al.*, 1995). HE – Hellroaring Creek stock, HLF – Hall Lake fault, KF – Kimberley fault, GR – Greenland Creek stock, MF – Moyie fault, OBF – Old Baldy fault, PF – Purcell fault, SMF – St. Mary fault, SRMT – Southern Rocky Mountain Trench.

enrichment in muscovite, certain geochemical affinity (Li, F, Sn *etc.*) and specific set of accessory minerals, may be helpful in the case of the most evolved varieties.

The Precambrian metallogeny of the area is essentially determined by the lead-zinc deposits and occurrences including the giant Sullivan SEDEX-style deposit and a number of much smaller Pb-Zn occurrences that are hypothesized to correspond with this age and style of mineralization (Hoy *et al.*, 1995). The Precambrian age is currently assigned to the pegmatites including the Hellroaring Creek pegmatite (Ryan and Blenkinsop, 1971) and smaller micaceous, ceramic feldspar and beryllium pegmatites of the Matthew Creek (MINFILE 082FNE088), Greenland Creek (MINFILE 082FNE112) and other occurrences (McFarlane and Pattison, 2000; Brown, 2003), although some other occurrences of similar (beryl *etc.*) mineralization are considered to be Cretaceous, such as those associated with the White Creek batholith and Shaw Creek stock. (Smith and Brown, 1998; Brown, 2003). In general, however, the Mesozoic metallogeny is dominated by intrusive-related gold and associated occurrences (Logan, 2002; Soloviev, 2010).

HELLROARING CREEK STOCK

The Hellroaring Creek stock is a slightly elongated (about 3 by 1 km across) pluton of granitic rocks intruding the Precambrian metaterrigenous rocks and gabbroic "Moyie sills" (Figure 3). The pluton has complex internal structure. Various interpretations of this structure can be suggested. In particular, the structure may be interpreted as a series of bedding-subparallel granitic

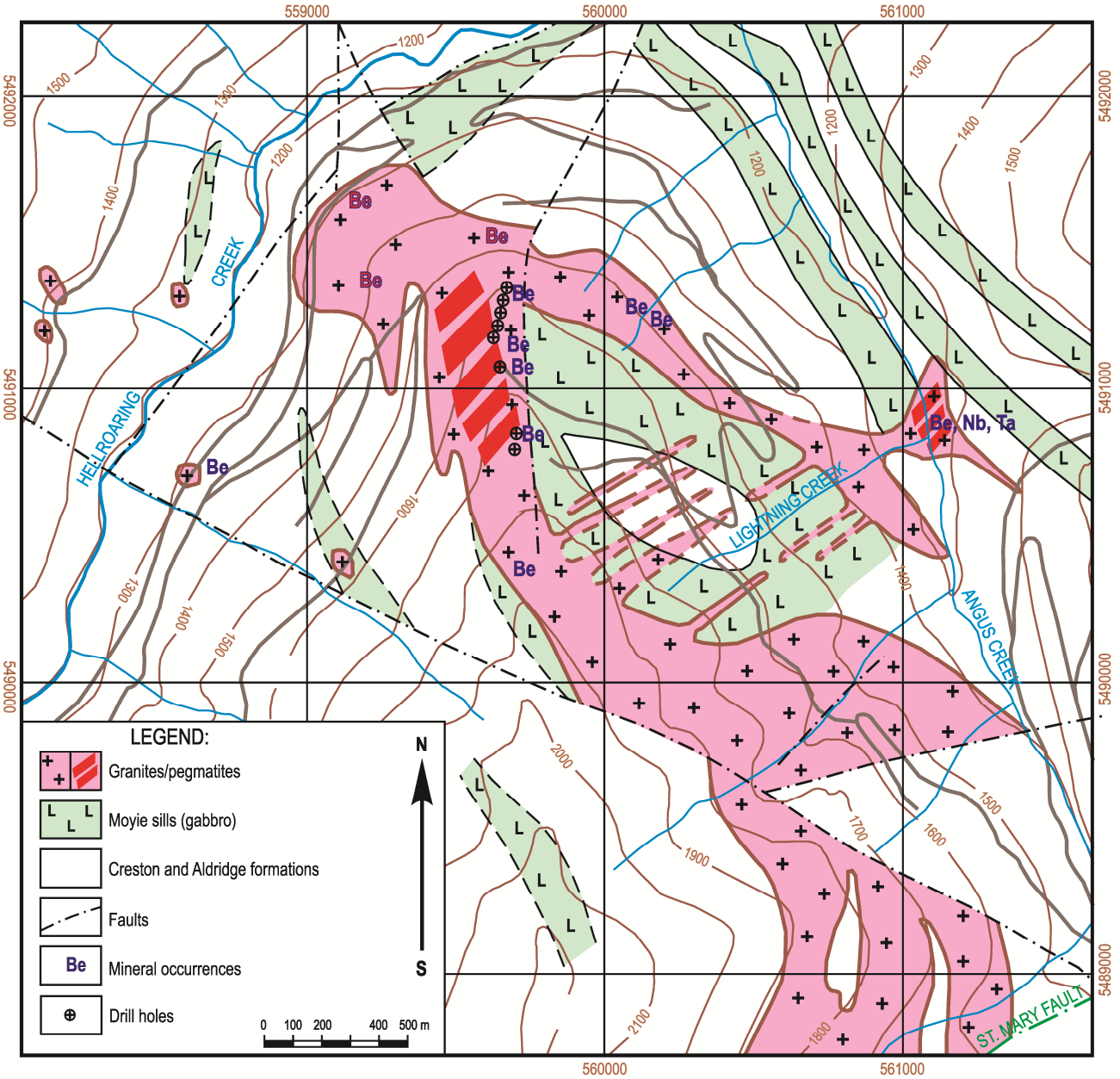

Figure 3. Simplified geological map of the Hellroaring Creek stock showing locations of the pegmatites and identified occurrences of rare metal mineralization (compiled data by David Pighin, personal communication; White, 1987; MacLean and White, 1991; Smith and Brown, 1998; Brown, 2003).

bodies (granitic sills) intruded like "saddle veins" into folded metasedimentary rocks. More plausibly, the stock may be interpreted as a sort of asymmetric ring or semi-ring structure fully or partially surrounding a large block of metasedimentary rocks intruded by the "Moyie sills". Finally, the stock may represent a dome-like intrusive body complicated by roof pendants, and the large block of metasedimentary rocks intruded by the "Moyie sills" may represent one of such roof pendants. Also, several smaller separated intrusive bodies possibly representing various intrusive phases can be suggested within the stock.

In addition, the Hellroaring Creek stock is accompanied by a number of smaller similar intrusions found at some distance (hundreds of metres to a few kilometres) and representing, probably, satellite stocks or cupolas. Pegmatite bodies are also found at a distance from the main pluton contacts, together with relatively small stocks (large dikes?) of aplitic granites.

The contact aureole consists of various altered lithologies including thin bedded lenses of altered pyroxene-garnet skarns with molybdoscheelite and molybdenite, vein-like bodies of quartz-micaceous greisens (?) with beryl, and quartz-sulphide veins with sphalerite, galena, *etc*.

The irregularity of the internal structure of the stock is emphasized by the distribution of various intrusive rocks. In particular, the pegmatites and stockscheider-like varieties of the granites occur mostly in the northern part of the stock; in contrast, more regularly grained to equigranular varieties predominate in its southern part. There are a number of the rock varieties that differ in their abundance, textural appearance, mineral and chemical composition.

INTRUSIVE ROCK TYPES

As noted above, the Hellroaring Creek granite+pegmatite stock incorporates a large number of rock varieties that differ largely in textures and, to a lesser extent, in mineral and chemical composition (Figure 4). Their apparent evolutional sequence may generally be presented as follows:

1. Fine to medium grained equigranular rock typically distinguished as biotite to biotite-muscovite granodiorite. The rock is grey to darker grey, medium grained, seems to be almost equigranular, and is composed of K-feldspar (30-35 vol.%), quartz (20-25 vol.%), plagioclase (30-35 vol.%), and usually strongly altered biotite (5-10 vol.%) replaced by finer grained muscovite. Feldspars are also partially replaced by muscovite and chlorite. This rock is locally observed in variously sized xenoliths found in the other intrusive rocks distinguished in the stock so that it may represent the early intrusion phase.
2. Medium to coarse grained equigranular rock typically distinguished as muscovite to muscovite-tourmaline granite. This rock contains xenoliths of the biotite to biotite-muscovite granodiorite and thus is considered to be a younger phase. The rock is light grey to light pinkish grey and is composed of K-feldspar (25-30 vol.%), quartz (~30 vol.%), plagioclase (25-30 vol.%), with muscovite occupying 5-20 vol.% and black tourmaline occupying 0-20 vol.%. Muscovite and tourmaline typically occur in expense of one another but locally both can be absent.
3. Medium to coarse grained irregularly-textured muscovite-tourmaline to tourmaline-muscovite granite. This granite often contains irregularly-shaped vugs filled with coarse-grained segregations of quartz (±feldspars, ±tourmaline) indicating that the pluton reached fluid saturation and is able to produce pegmatitic and aplitic dikes (*cf.* London, 2008).
4. Coarse grained to large crystalline, equigranular to irregularly-grained "pegmatoid", or stockscheider-style granitic rock represents further development of this process, *i.e.*, further saturation in water and volatiles, with spreading of the "water-saturated" textures over a greater volume of the granite. The irregularly grained varieties are porphyritic (porphyrocrysts of K-feldspar, black tourmaline and quartz), "pegmatoid" to giant crystalline pegmatitic, banded, and patchy, with short vein-like, small lens-like, *etc.* aggregations of coarser to very coarse grained and even giant crystalline K-feldspar, or K-feldspar+quartz (±tourmaline) patches surrounded by medium grained granitic groundmass. These sectors of textural irregularities vary in size from a few centimetres (observed in hand specimens) to several metres and even tens of metres totally forming a domain-like textural appearance of the rock. These small and large textural domains have both gradual and sharp contacts to more regularly grained medium grained variety of the granite. The relative volume of the "pegmatoid" rocks definitely increases upward, toward the roof of the pluton: at deeper levels, they can be found in small lenses and domains whereas at the higher levels they compose almost whole volume of the pluton. A characteristic feature of the rocks occurred in finer grained and more equigranular variety is the dark gray, smoky and even almost black, morion-like color of quartz. Locally, such quartz occurs in the pegmatoid variety.
5. Coarse and irregularly grained granitic rock containing large potassic feldspar segregations (locally gigantic phenocrysts); these phenocrysts, however, compose a subordinated fraction of the rock and are surrounded by more equigranular tourmaline-muscovite or muscovite-tourmaline granite. This rock gradually evolves into similar rock, in which large potassic feldspar segregations and phenocrysts exhibit internal graphic (with small quartz intergrowths) texture.
6. Coarse crystalline pegmatites occurred within the principal granitic body but likely on its periphery, such as the major well studied ceramic pegmatite occurrence known as the Hellroaring Creek pegmatite. It should be emphasized that even this large pegmatite occurrence, in fact, incorporates a number of smaller pegmatite bodies, or their assemblage, with common mutual boundaries evolving into one another rather than a single large pegmatite body. These pegmatites are composed of predominating potassic feldspar and quartz forming typical blocky, graphic and skeletal textures, with usually subordinated amounts of muscovite and tourmaline.

The pegmatite is closely associated with banded variety of the granite occurred locally that contains thin (few centimetres thick) bands ("layers") of strongly

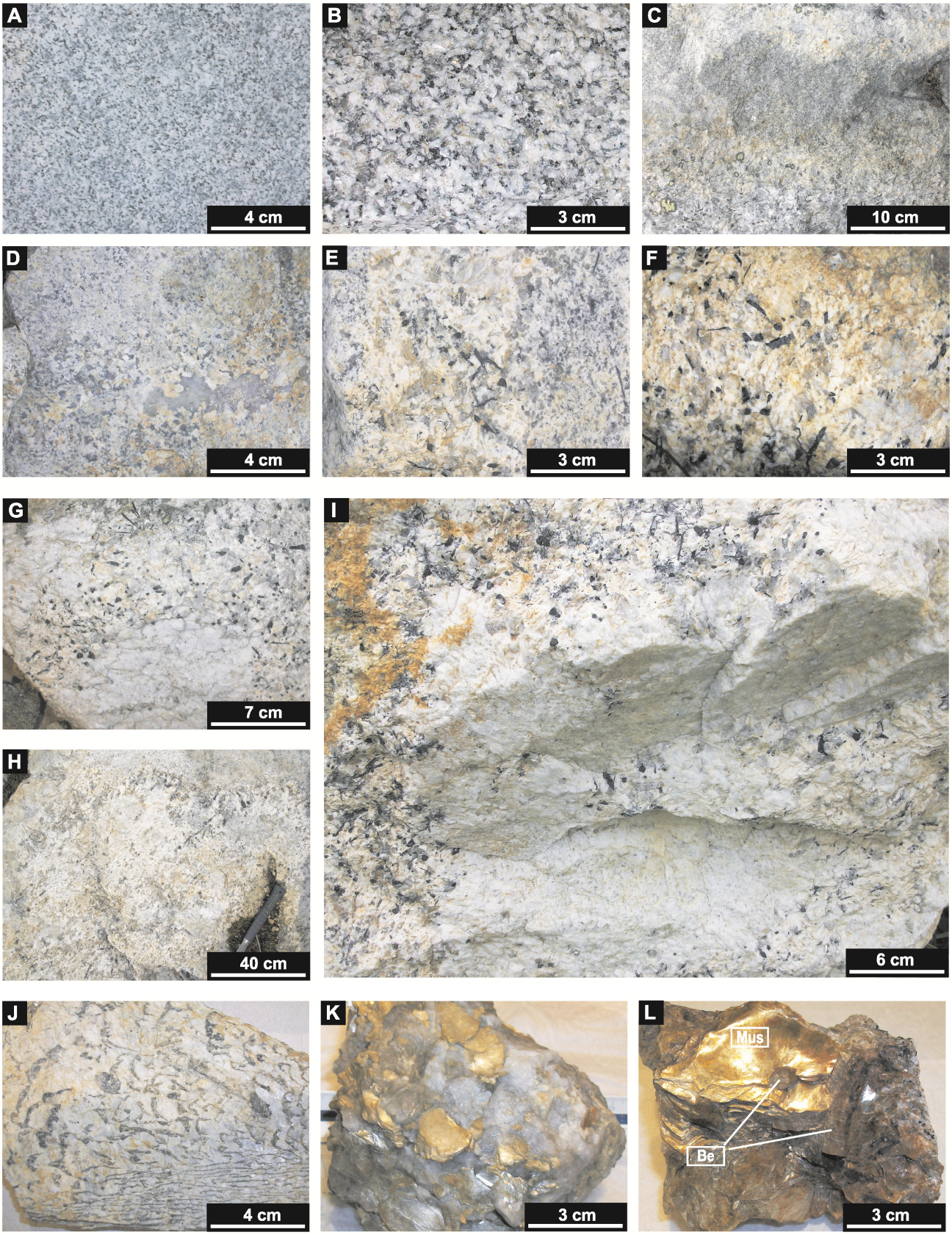
A
4 cm
B
3 cm
C
10 cm
D
4 cm
E
3 cm
F
3 cm
G
7 cm
H
40 cm
I
6 cm
J
4 cm
K
3 cm
L
Mus
Be
3 cm

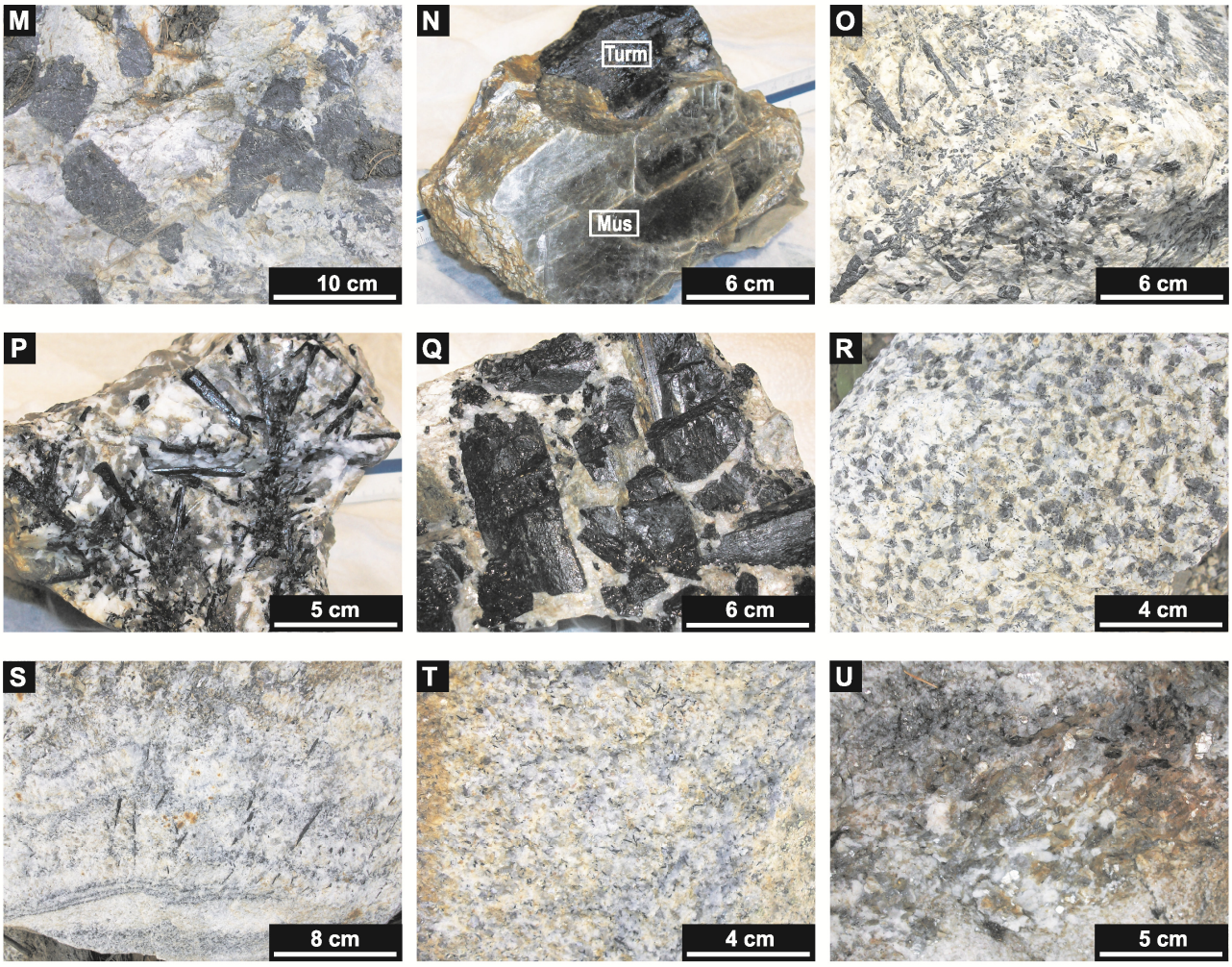

Figure 4. Major types of granites and pegmatites of the Hellroaring Creek stock. A-J – gradual evolution from early granite to granitic pegmatites (granite-pegmatite transition): A – fine-grained biotite (±muscovite) granite of apparently early phase; B – coarse grained equigranular muscovite-tourmaline granite of the later phase (?); C – xenolith of the fine-grained biotite (±muscovite) granite in the coarse grained equigranular muscovite-tourmaline granite evolving into irregularly grained ("pegmatoid", or stockscheider-style) muscovite-tourmaline granite; D – equigranular to irregularly grained muscovite-tourmaline granite with vugs filled in with coarse grained quartz-feldspar aggregate indicative for high degree of magma saturation in water and volatiles; E – further evolution of the granite, with patchy distribution of the pegmatoid (stockscheider-style) domains in more equigranular granitic variety (almost equally abundant); F - pegmatoid (stockscheider-style) granite; G – "pegmatoid" (stockscheider-style) granite incorporating large but still insulated blocky crystals and crystal aggregates of potassic feldspar; H – "spreading" of the stockscheider-style granite with blocky crystals of potassic feldspar over the equigranular muscovite-tourmaline granite, with tourmaline prisms radiating across the contact; the stockscheider-style granite can be called also as "undifferentiated pegmatite" but occurs within the equigranular granite and is not fracture controlled suggesting rather subsolidus state of the host granite at the time of the "pegmatite" crystallization; I – larger domain-like block of potassic feldspar found in the stockscheider-style granite; the potassic feldspar exhibits "initialization" of the internal graphic texture formation; J – fully-developed graphic texture in large granite-hosted pegmatite aggregates (ceramic pegmatites); K-N – some varieties of the pegmatites: K – coarse crystalline quartz-muscovite pegmatite; L – large crystalline essentially muscovite pegmatite with prismatic beryl crystals; M – large (blocky) crystals of black tourmaline; N – large crystalline muscovite-tourmaline pegmatite (Lightning Creek); O-T – minor types of granites and pegmatites: O – tourmaline-albite granite; P – radiating tourmaline aggregates with quartz and feldspars (part of the tourmaline-albite granite); Q – partially brecciated tourmaline crystals ("tourmaline breccia") in fine grained quartz-feldspar matrix; R – tourmaline granite with rounded quartz crystals; S – albite layering in pegmatite, with outward radiating tourmaline crystals; T - fine to medium grained equigranular tourmaline-muscovite granite (the latest phase ?); U – greisen-like patchy and veined muscovite aggregates replacing (?) over granite. Abbreviations on Figures. 4L and 4N: Mus – muscovite, Be – beryl, Tur – tourmaline.

tourmaline-enriched (about 30 vol.%, locally up to 60% and more black tourmaline, both fine, medium and coarse grained) rock alternating with tourmaline-free, usually coarse grained essentially K-feldspar+quartz bands and coarse-grained quartz+white mica bands. There is some regular distribution of various bands: tourmaline-rich and typically finer grained bands occur on a greater distance from the pegmatite, whereas tourmaline-depleted and gradually more and more coarser grained K-feldspar+quartz and further quartz+white mica bands are most proximal to the pegmatite.

7. Finally, coarse crystalline pegmatites occurred outside the principal granitic pluton such as that distinguished as the Lightning Creek pegmatite. The latter is characterized by intense development of fine-grained ("sugary") albite occurred on the periphery of the innermost quartz zone and apparently in the footwall of the pegmatite body as a whole. The pegmatite body is also characterized by the presence of apatite and garnet closely associated with albite, together with beryllium (beryl), tin (cassiterite) and niobium-tantalum (columbite) mineralization. Locally, apatite is quite an abundant accessory mineral and forms thick prismatic crystals and their aggregations; garnet is second in importance forming small (up to 3 by 10 cm) lens-like aggregations.

In addition to the granite and pegmatite varieties described above and representing their major types, the pluton incorporates a number of definitely minor rock varieties likely occurred just in localized sectors ("pockets") with or with no spatial relationships to pegmatites. These minor rock varieties include, in particular, various tourmaline-rich rocks such as tourmaline breccias, with variably sized fragments of tourmaline crystals cemented by fine grained quartz-feldspar matrix, and coarse to medium grained tourmaline granites, with variably oriented long (up to 1 by 10 cm) tourmaline crystals enriching the granites (up to 20-30 vol.%) and locally forming star-like aggregates. Other minor varieties include granites with smoky to morion quartz phenocrysts, fine to medium grained tourmaline-albite granites, leucocratic granites and granite-porphyry, aplites, *etc.*

In particular, the fine to medium grained tourmaline-albite to tourmaline-albite-muscovite granites are relatively more abundant and were observed in drill core, in numerous outcrops, rubblecrops, and float boulders. The rock is light grey due to constant presence of fine grained (thin needles) black tourmaline (5-10 vol.%), is fine to medium grained and usually enough equigranular or with small porphyrocrysts of K-feldspar. Controversial relationships were observed between the tourmaline-albite to tourmaline-albite-muscovite granites and the muscovite-tourmaline granites described above. In particular, these tourmaline-albite to tourmaline-albite-muscovite granites form thin (10-50 cm) apophyses cutting through much coarser grained and pegmatoid varieties of the muscovite-tourmaline granite. Locally, large crystals of tourmaline oriented across the contact form "a crown" around these apophyses emphasizing their later emplacement as a comparison to that of the muscovite-tourmaline granite. However, in other cases, a gradual transition from the coarser grained muscovite-tourmaline granite to the finer grained tourmaline-albite to tourmaline-albite-muscovite granites was observed.

Some of these relationships can be explained, if to assume that the coarser grained muscovite-tourmaline granite represents an apical, fluid-enriched and early crystallized facies, whereas the finer grained tourmaline-albite to tourmaline-albite-muscovite granites represent relatively deeper facies exhibiting gradual transition to the coarser-grained tourmaline-muscovite granite upward but cutting through the already crystallized crust along minor fractures. Also, perhaps, there are several varieties (even intrusion phases?) of the tourmaline-albite to tourmaline-albite-muscovite granites.

Leucocratic granite observed in large outcrops is white, leucocratic, usually tourmaline-free (macroscopically), medium to fine-grained rock composed in equal proportions of quartz, albite, and K-feldspar; there are some, probably, very local sectors of micropegmatoid and slightly coarser grained pegmatoid texture. Accessory pyrite and, probably, other sulphides are very common. Leucocratic granite porphyry observed in float boulders and in the outcrops is pink-coloured rock with numerous rounded quartz porphyrocrysts (about 5 mm across) (totally, up to 25-30 vol.%) surrounded by very fine grained feldspar-quartz groundmass. Accessory pyrite and, perhaps, other sulphides are also very common.

Aplite was observed in numerous but small veinlets cutting the leucocratic granite and, also, in numerous and often large boulders found in float including those occurred nearby the Lightning Creek pegmatite. In addition, gradual transitions of large-crystalline pegmatites to fine grained aplitic rocks are locally observed. This is fine grained, sugary in appearance, equigranular rock composed of albite, quartz, and minor K-feldspar. Similarly to other late leucocratic granitic phases, this rock is enriched in pyrite and, perhaps, other sulphides.

In total, the granitic and pegmatitic rocks found in the Hellroaring Creek stock form a distinct assemblage of compositionally similar and likely genetically related rocks. Their general evolutional pathways can be illustrated on the basis of the recently obtained data on the contents and distribution of the major and trace elements in the rocks.

GEOCHEMICAL FEATURES OF THE GRANITES AND PEGMATITES

The results of chemical assaying of the granitic and pegmatitic rocks are presented in Table 1. These assay results represent the major types of the rocks including medium to coarse grained equigranular muscovite to muscovite-tourmaline granites; coarse grained to pegmatoid granites (stockscheider); pegmatites; albite-tourmaline granites; and albitic (leucocratic and aplitic) granites. The assay results include the contents of the petrogenic and most notable trace elements (including rare metals) as well as boron and fluorine contents.

It can be seen that the stockscheider-style granites are characterized by somewhat elevated, as compared to the equigranular muscovite-tourmaline granites, sodium

contents in expense of potassium contents. This is attributed to the elevated contents of sodic (essentially albitic) plagioclase substituting potassic feldspar and is typical for the roof zones of the "specialty granite" plutons evolving toward albite-enriched granites (London, 2008). This evolution is accompanied by some increase in the contents of P, F, B and some trace elements such as Be and Li; however, this trend appears to occur quite sporadically and is better expressed in some more evolved and/or albite-enriched varieties. The granites are characterized by strong europium minimum and nearly symmetric distribution of LREE and HREE that is typical for the rare metal-bearing granites (*cf.* Cuney *et al.*, 1992).

Much greater enrichment in P and F as well as Li, Cs, Be, Nb, Ta and Sn is observed in the pegmatites representing a higher degree of magmatic melt evolution. The pegmatites assayed represent different compositional zones of the respective pegmatite bodies; this explains variations in the Na/K ratios, SiO_2, Al_2O_3, boron and phosphorus contents. The higher P contents are associated with higher K, Ca and Mn values, in expense of Na; the higher Ca values can also be attributed to the high apatite content, whereas the high potassic contents are associated with elevated content of micas (muscovite and likely its Li and Rb varieties). The later is consistent with also elevated values of F, Li, Rb and Cs, although some Rb may be contained also in potassic feldspar. The elevated Mn values are attributed to the abundance of Mn-rich garnet that is observed petrographically. The most apatite-enriched pegmatite contains elevated abundances of REE (especially LREE).

Plotting the assay data on the K/Rb *vs.* Cs diagram suggested by London (2008) for estimation of the evolution degree of rare metal granites and pegmatites shows a common evolutional trend toward less potassic, more cesium-enriched varieties from the Hellroaring Creek granites to micaceous ceramic pegmatites forming the largest pegmatite occurrence found within the Hellroaring Creek stock itself, and then to the pegmatites found at the Lightning Creek occurrence (Figure 5). The latter are characterized by quite a high degree of the evolution that, however, is below the evolutional level of spodumene and lepidolite-bearing pegmatites; this is consistent with the absence of these minerals and generally low Li content in the studied pegmatites. Nevertheless, the trend is indicative of the possible formation of more evolved pegmatites under favored conditions, perhaps at a greater distance from the pluton.

PEGMATITES

The major pegmatite occurrence of the Hellroaring Creek stock was described in a number of publications (Ryan and Blenkinsop, 1971; Smith and Brown, 1998; Brown, 2003; Legun, 2004, 2005) and reports (Wasylyshyn, 1984; Pudifin, 1986; Anderson, 2001; Soloviev, 2001). The pegmatite occurs within the Hellroaring Creek granitic stock and occupies an area of some 500 by 200 m (Figure 1), where the coarse grained to large-crystalline pegmatites are outcropped on the surface. The vertical extent of the pegmatite was not confidently determined by drilling; however, it appears that the pegmatite (*i.e.* the large-crystalline rock) does not extend for more than few tens of metres and then evolves into coarse-grained granite; however, other (smaller and subconcordant?) pegmatite bodies are likely present to a depth of at least some 100 m from the surface. Smaller pegmatite bodies likely occur in other parts of the stock.

Typical zonation of the pegmatites occurs as follows: outer coarse grained to large crystalline tourmaline+potassic feldspar+muscovite+quartz zone – intermediate potassic feldspar+quartz zone (±muscovite) – inner monomineralic quartz zone (±muscovite), or "core". Muscovite forms coarse books that are most common and locally abundant along the boundary of the intermediate and the inner zones locally forming a distinct muscovite zone, locally with vein-like apophyses; however, in some pegmatites muscovite is almost totally absent. Some monomineralic blocks of potassic feldspar are 1-2 m across and 2-3 m in length, and so are the largest quartz lenses representing the innermost pegmatite zones. The pegmatite is locally strongly enriched in black tourmaline that can compose up to 60-80 vol.% of the rock. In such sectors, very large (up to 10 by 20-30 cm) tourmaline crystals are common and are surrounded by much finer grained K-feldspar (±quartz, muscovite) groundmass, which in other sectors can be large crystalline. Beryl is locally present in the pegmatites, typically in the outer to intermediate zones or in the muscovite-rich zones (Figure 6). Ethier and Campbell (1977) determined the tourmaline composition as shorl with characteristically high iron and low calcium content. However, some tourmaline crystals show a distinct color zoning from black to dark olive-green, thus, indicating more evolved (toward shorl-dravite and dravite (?) compositions.

In contrast, the pegmatitic body found in the Lightning (Angus) Creek sector is represented by very coarse grained to large-crystalline (single crystals up to 20-30 cm in size) rock outcropped for several metres of its thickness (?); however, floated fragments of the same rock were observed on the creek walls for the distance of, at least, 100 m above *(i.e.*, these are not the fragments just transported from the outcrop) the creek floor. As a result, a length of the pegmatite body of some 100 m can be easily accepted.

The major minerals composing the pegmatite are K-feldspar, quartz, and very large crystals and books of silver-white to greenish muscovite. Black tourmaline is a common constituent; it also forms large (up to 10 by 30 cm) crystals. Typically, the pegmatite contains about 40 vol.% of K-feldspar, 30% quartz, 20% tourmaline, and 10% muscovite, but locally tourmaline can be absent and muscovite or quartz can predominate over K-feldspar; in

Table 1. Representative analyses of granites and pegmatites from the Hellroaring Creek stock (wt.%, ppm).

	1	2	3	4	5	6	7	8	9	10	11	12	13	14
	Medium to coarse grained equigranular muscovite and muscovite-tourmaline granites							Coarse grained to pegmatoid stockscheider-style granites						
Sample field #	015	017	026	031	033	012	013	016	022	023	025	027	028	032
Northing	559680	559695	559795	560708	560695	560148	560151	559685	559615	559655	559612	559602	559635	560704
Easting	5491234	5491310	5490811	5490012	5490023	5490743	5490739	5491286	5490643	5490699	5490722	5490725	5490712	5490018
SiO_2	75.91	76.67	74.66	75.26	74.44	74.03	76.10	74.88	75.86	72.43	74.59	74.91	75.19	76.20
TiO_2	0.02	0.01	0.01	0.07	0.04	0.02	0.07	0.02	0.02	0.02	0.05	0.01	0.02	0.06
Al_2O_3	14.17	14.07	14.54	14.91	14.64	14.85	13.67	14.81	13.50	15.23	14.79	14.43	14.28	14.27
Fe_2O_3	0.76	1.79	1.05	0.87	0.68	1.27	1.30	0.50	1.61	2.06	3.53	1.21	1.34	2.79
MnO	0.01	0.24	0.02	0.01	0.02	0.01	0.01	0.02	0.09	0.48	0.08	0.03	0.05	0.04
MgO	0.10	0.08	0.10	0.18	0.12	0.19	0.29	0.05	0.10	0.08	0.25	0.08	0.08	0.58
CaO	0.30	0.55	0.66	0.70	0.55	0.61	0.57	0.31	0.50	0.62	0.30	0.51	0.54	0.25
Na_2O	4.36	4.93	4.26	4.23	3.67	5.74	3.63	7.03	5.57	6.96	4.14	5.95	5.96	3.88
K_2O	3.32	1.16	3.30	2.09	5.34	1.19	1.75	1.57	0.50	0.41	0.45	1.42	1.03	0.89
P_2O_5	0.11	0.10	0.14	0.04	0.08	0.06	0.11	0.07	0.09	0.06	0.05	0.07	0.11	0.04
CO_2	0.07	0.10	<0.05	<0.05	<0.05	<0.05	<0.05	<0.05	0.07	<0.05	<0.05	<0.05	<0.05	<0.05
S tot.	<0.01	<0.01	<0.01	<0.01	<0.01	<0.01	<0.01	<0.01	0.02	<0.01	<0.01	<0.01	<0.01	<0.01
LOI	0.90	0.40	0.40	1.40	0.50	1.00	1.60	0.60	0.80	0.60	0.80	0.50	0.60	0.90
Total	99.96	99.96	99.12	99.73	100.09	98.93	98.96	99.84	98.61	98.92	99.02	99.10	99.20	99.87
B	33	682	345	61	239	620	342	66	651	384	1673	467	587	1264
F	100	190	230	310	90	100	240	100	210	170	540	150	170	370
Ba	81	7	<5	18	94	6	102	19	<5	<5	<5	8	7	36
Sr	58	9	6	48	33	24	88	29	10	5.4	5	13	11	22
Co	1.3	<0.5	<0.5	<0.5	<0.5	<0.5	<0.5	0.6	<0.5	<0.5	<0.5	<0.5	<0.5	1.0
Ni	5	5	5	5	5	2	6	4	6	2	2	1	6	2
Li	4	10	10	10	4	5	10	4	9	12	29	7	8	7
Rb	118	96	268	119	201	63	95	91	36	20	41	125	84	46
Cs	3	7	7	5	7	2	3	3	2	2	5	9	4	1
Be	3	14	5	5	5	14	3	4	12	10	18	6	12	9
Zr	22	32	45	105	23	57	71	41	32	164	29	19	29	54
Hf	1.1	1.6	2.4	3.8	0.9	2.6	2.4	2.1	1.8	10.7	1.9	1.0	1.8	2.7
Nb	4.5	6.7	4.8	12.6	0.8	4.3	9.4	2.4	2.5	6.1	2.4	2.5	2.6	1.4
Ta	1.3	1.4	1.8	1.6	0.2	0.9	2.3	0.5	0.7	5.1	1.3	1.0	1.3	0.6
Sc	1	1	1	12	1	1	3	1	2	2	1	1	1	3
Sn	6	17	11	14	5	7	7	7	10	5	8	5	5	5
Mo	4	4	3	4	3	4	4	3	4	3	4	3	4	3
W	4	3	2	9	2	10	7	2	3	8	11	8	2	9
Y	5.6	6.9	13.0	55.2	7.3	12.8	15.2	6.2	13.2	17.7	2.7	5.3	5.0	11.7
La	2.0	2.0	4.1	16.9	2.0	6.3	8.6	2.7	5.2	2.2	9.5	2.0	2.1	1.9
Ce	4.4	4.6	9.6	34.8	4.0	15.1	21.0	6.4	11.7	5.4	23.3	4.3	4.9	4.4
Nd	2.0	2.0	4.0	14.7	1.7	6.1	8.9	2.1	4.6	2.3	9.5	1.8	2.0	1.8
Sm	0.7	0.8	1.8	4.8	0.7	2.3	3.0	0.8	1.9	1.0	4.0	0.8	0.8	0.9
Eu	0.11	<0.05	<0.05	0.34	0.17	0.08	0.44	<0.05	<0.05	<0.05	<0.05	<0.05	<0.05	0.12
Gd	0.62	0.64	1.41	5.92	0.83	1.74	2.31	0.70	1.28	0.95	2.24	0.66	0.64	1.07
Tb	0.16	0.19	0.38	1.35	0.20	0.39	0.51	0.16	0.33	0.36	0.30	0.15	0.14	0.28
Yb	0.87	1.17	1.95	6.11	0.92	1.96	1.74	1.29	2.87	3.32	0.25	0.85	0.87	2.21
Lu	0.14	0.17	0.34	0.92	0.14	0.30	0.26	0.21	0.41	0.47	0.03	0.13	0.13	0.34

Table 1. continued.

	15	16	17	18	19	20	21	22	23	24	25	26	27	28	29	30
					Pegmatites					Fine to coarse grained albite-tourmaline granites				Leucogranites and aplites		
Sample field #	014	018	036	037	038	039	042	043	044	020	021	024	029	009	010	030
Northing	560154	559620	561121	561118	561120	561117	561110	561111	561112	559820	559840	559765	559630	560456	560450	560890
Easting	5490755	5491205	5490920	5490915	5490918	5490922	5490920	5490921	5490922	5490403	5490455	5490615	5490719	5490355	5490359	5489878
SiO_2	75.63	65.18	59.04	74.03	61.69	72.60	73.13	52.20	69.64	75.36	76.80	72.82	76.23	74.70	73.73	76.06
TiO_2	0.06	0.07	0.02	0.03	0.02	0.03	0.05	0.02	0.01	0.01	0.02	0.01	0.04	0.01	<0.01	0.02
Al_2O_3	14.56	20.30	20.49	15.16	18.56	11.48	15.06	9.60	15.72	14.48	14.64	15.76	14.99	14.80	14.19	14.36
Fe_2O_3	1.36	3.00	1.10	1.14	1.78	2.42	1.98	1.19	1.55	1.22	1.25	2.02	2.99	0.53	0.53	0.44
MnO	0.05	0.10	0.39	0.03	0.24	2.17	0.07	1.18	1.09	0.03	0.07	0.06	0.03	0.01	0.01	0.01
MgO	0.19	0.24	0.05	0.05	0.14	0.10	0.12	0.03	0.02	0.12	0.09	0.11	0.44	0.05	0.05	0.07
CaO	0.25	1.52	4.89	0.47	4.18	3.55	0.87	17.90	1.85	0.72	0.68	0.47	0.55	0.25	0.57	0.20
Na_2O	2.31	7.73	4.09	7.46	2.53	0.77	3.74	0.33	5.30	4.72	5.67	6.64	4.13	6.32	6.59	7.60
K_2O	3.12	0.63	4.02	0.40	4.36	2.57	1.94	1.96	1.69	2.86	1.72	0.38	0.84	2.51	1.67	0.49
P_2O_5	0.15	0.87	3.68	0.25	3.10	2.61	0.56	13.02	1.28	0.11	0.08	0.20	0.04	0.12	0.10	0.04
CO_2	<0.05	<0.05	<0.05	0.15	0.08	0.12	0.08	0.19	<0.05	<0.05	<0.05	<0.05	<0.05	<0.05	<0.05	0.08
S tot.	0.08	<0.01	<0.01	<0.01	<0.01	0.01	<0.01	0.01	0.01	<0.01	<0.01	<0.01	0.02	0.02	<0.01	<0.01
LOI	1.90	0.70	2.00	0.50	2.40	1.70	0.90	1.10	1.00	0.20	0.40	1.00	0.60	0.60	0.70	0.70
Total	99.59	100.34	99.77	99.51	99.00	99.99	98.32	98.52	99.16	99.82	99.40	99.45	100.48	99.86	98.13	99.87
B	38	2283	91	429	89	63	766	59	44	475	451	680	1344	6	6	9
F	220	1050	4450	550	3950	3050	1450	18950	1750	140	180	310	340	70	<10	<10
Ba	76	22	13	12	140	61	15	19	50	<5	<5	8	7	27	18	13
Sr	51	17	12	12	24	16	14	54	19	8	8	19	11	33	29	34
Co	1.3	1.3	<0.5	<0.5	0.6	<0.5	<0.5	<0.5	<0.5	<0.5	<0.5	<0.5	0.6	0.6	1.0	0.6
Ni	2	2	1	5	6	2	2	5	2	1	5	6	2	4	1	1
Li	5	28	71	19	40	36	39	92	58	7	9	9	10	4	5	3
Rb	187	65	1023	62	834	400	442	551	396	213	132	34	55	107	66	21
Cs	6	27	93	8	144	130	38	246	218	8	10	2	3	3	3	1
Be	9	12	494	78	15	1055	9	4980	2113	8	15	8	4	1	4	3
Zr	17	12	5	5	3	6	8	3	7	45	34	60	39	6	26	8
Hf	1.1	1.2	<0.5	<0.5	<0.5	<0.5	0.6	<0.5	<0.5	2.0	1.5	3.5	1.7	<0.5	1.2	<0.5
Nb	40.9	5.9	1484.0	14.7	70.0	20.8	38.5	63.9	31.2	8.5	3.3	0.6	2.6	5.6	2.6	2.3
Ta	10.0	10.3	344.0	6.3	44.6	7.8	12.1	30.2	14.1	3.8	1.8	0.3	2.0	1.6	1.1	0.7
Sc	3	1	1	<1	1	1	<1	1	1	2	1	1	6	1	1	<1
Sn	21	25	265	20	225	106	120	144	110	7	7	7	6	6	4	4
Mo	4	3	2	3	2	4	4	3	3	3	3	4	4	3	3	2
W	18	9	26	3	9	6	12	5	9	7	2	2	14	4	8	5
Y	5.8	8.7	11.2	2.7	10.7	13.6	1.9	36.6	5.6	13.3	11.3	5.2	8.3	6.2	12.2	2.2
La	5.3	5.4	14.4	1.4	12.5	10.5	1.8	44.0	6.3	4.6	3.9	3.5	3.2	2.2	3.6	0.7
Ce	10.8	14.6	31.8	3.4	27.2	25.3	4.3	106.6	14.0	10.5	8.4	9.0	7.7	4.0	7.9	1.4
Nd	4.5	7.1	13.6	1.7	10.4	10.2	1.8	47.0	5.7	4.3	3.4	4.0	3.5	1.5	3.4	0.6
Sm	1.6	4.8	7.6	1.1	5.4	5.5	1.1	26.3	3.0	1.6	1.2	1.4	1.3	0.7	1.3	0.3
Eu	0.19	<0.05	0.12	<0.05	0.19	0.22	0.07	0.46	0.06	<0.05	<0.05	<0.05	<0.05	0.12	0.09	0.09
Gd	1.22	4.33	6.33	1.29	3.85	4.44	0.88	19.93	2.12	1.35	1.02	0.97	1.13	0.68	1.16	0.31
Tb	0.23	1.00	1.12	0.23	0.69	0.80	0.15	3.30	0.37	0.34	0.28	0.19	0.24	0.17	0.33	0.07
Yb	0.39	0.30	0.44	0.10	0.85	1.47	0.08	1.88	0.45	2.22	2.16	0.81	1.36	0.72	1.70	0.29
Lu	0.07	0.03	0.06	0.02	0.12	0.22	<0.01	0.24	0.06	0.36	0.34	0.12	0.22	0.11	0.26	0.04

Notes: The assaying was performed in ACME Analytical Laboratories Ltd. by ICP/ES analysis (Mo, Ni, Li, B, F) and by whole rock ICP/MS analysis (major oxides, Ba, Sc, REE and other trace elements). Iron content is presented as sum of Fe_2O_3 and FeO expressed as Fe_2O_3. Samples 009-033 – Hellroaring Creek stock (granites and pegmatites), samples 036-044 – Lightning Creek pegmatite. Samples from pegmatites: 014 – small (1 m thick) zoned body of essentially muscovite (from outer coarse muscovite and muscovite-quartz to inner fine grained muscovite-quartz-feldspar) pegmatite found in metasedimentary rocks near the Hellroaring Creek stock; 018 – giant-crystalline K-feldspar-quartz-tourmaline pegmatite with minor muscovite (2 vol.%); 036 - coarse to giant-crystalline K-feldspar-quartz-muscovite pegmatite from the Hellroaring Creek stock; 037 – fine-grained essentially aplitic pegmatite showing, with rare coarse crystals of potassic feldspar, showing gradual transition to coarse-grained quartz-K-feldspar-muscovite pegmatite; 038 - coarse to fine grained K-feldspar-muscovite-quartz pegmatite (outer zone); 039 - similar to 038 but locally enriched in garnet; 042 - giant-crystalline K-feldspar-quartz-muscovite-black tourmaline pegmatite; 043 - similar to 036 but with large crystals of greenish apatite; 044 - similar to 039 but more muscovite (locally up to 40 vol.%).

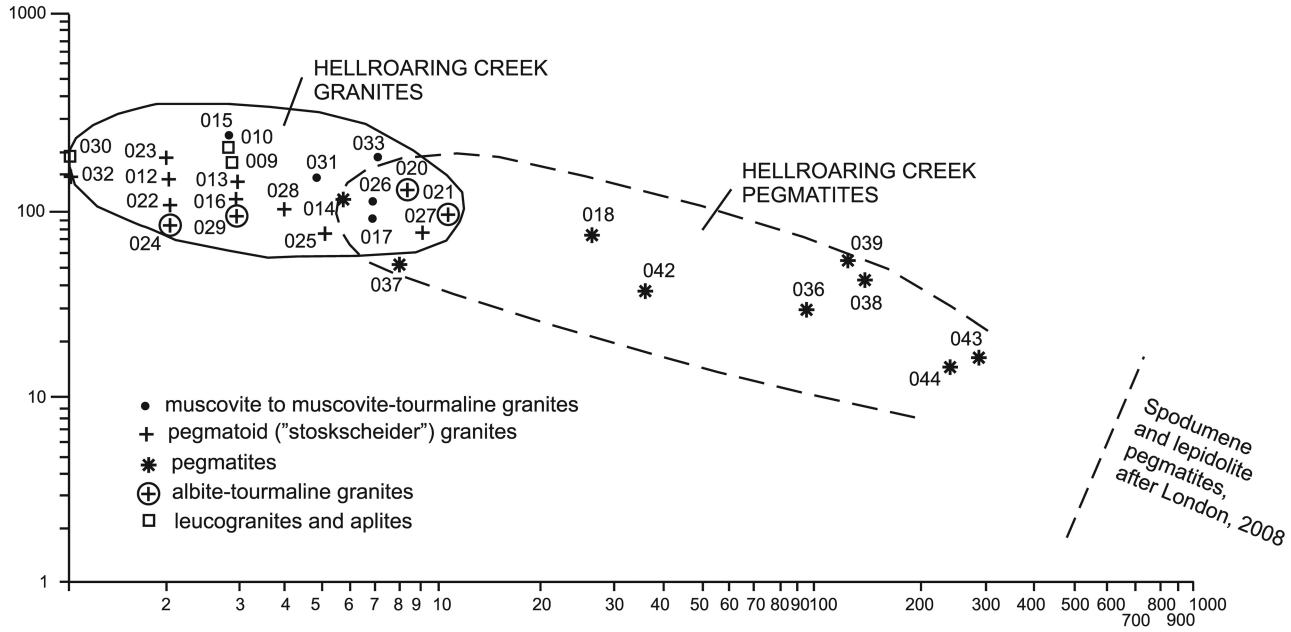

Figure 5. Data on the Hellroaring Creek granites and pegmatites plotted on the K/Rb *vs.* Cs diagram showing gradual evolution of the granites and pegmatites toward more evolved compositions (London, 2008). The sample numbers are sample field numbers listed in Table 1.

Figure 6. Giant beryl crystal from the Hellroaring Creek pegmatite (collection of David Pighin).

other sectors, quartz and tourmaline are the main constituents. Locally, large (several centimetres across) crystals of greenish beryl are present.

Marginal zones of the pegmatite are much finer grained and are composed of medium to fine grained white muscovite, fine grained greenish to light green muscovite, medium-grained quartz and K-feldspar, medium to fine grained black tourmaline found in variable proportions. These zones are locally enriched in fine-grained albite, and contain segregations of small well-shaped apatite and garnet crystals. The same zones contain also prismatic crystals of yellowish green beryl up to 3 by 0.5 cm in size. The pegmatites contain also elevated tin grades (Table 1) that may reflect the presence of fine disseminated cassiterite and/or other Sn-bearing minerals (nigerite, *etc.*).

On the other hand, a gradual transition of the coarse grained quartz-K-feldspar-muscovite pegmatite to fine grained (sugary) essentially albitic aplite (fine grained albite-quartz-K-feldspar groundmass, with scattered small porphyrocrysts of K-feldspar), locally enriched in tourmaline, was observed.

The assay results (Table 1) indicate local enrichment of the pegmatite in tantalum and niobium, with niobium predominating over tantalum and suggesting the possible presence of columbite. Beryl is locally abundant but there is apparently no any correlation between Ta+Nb and Be grades; thus, columbite and beryl may belong to different mineral assemblages of the pegmatite. Low lithium concentrations (Table 1) suggest that lithium resides in muscovite crystal structure rather than spodumene, petalite or lepidolite. High fluorine content could be possibly accounted for fluorine substitution in muscovite and fluorapatite; other minerals containing elevated fluorine (such as triplite, triphylite, *etc.*) can also be present in the pegmatite. All this data shows that the pegmatite belongs to the beryl-columbite-phosphate subtype (*cf.* Cerny, 1993; London, 2008).

Other smaller, metric-scale, pegmatite bodies were observed in the metasedimentary rocks near the periphery of the Hellroaring Creek stock. Some of these bodies include coarse-grained muscovite (muscovite+quartz) outer zone and fine grained muscovite+quartz(+K-feldspar?) inner zone, whereas other bodies are composed of large crystalline (locally in excess of 5-7 cm across) K-feldspar (up to 60 vol.%), quartz (about 25%), black tourmaline (15%), with only minor muscovite (<2%).

ALBITE AND MICA-ENRICHED GRANITES

There are several styles of albite aggregations observed in the granites and pegmatites of the Hellroaring Creek stock and the nearby Lightning Creek pegmatite. They can be arranged as follows:

1. Coarse grained albite crystals and their intergrowths irregularly (spots, segregations, *etc.*) distributed in the granitic rock. Usually, colourless or milky quartz (often in contrast to smoky quartz of the granite) and fine grained, light (silverish, greenish, brownish, yellowish, *etc.*) micas are associated with albite. Tourmaline is also common and is represented often by large long idiomorphic crystals.
2. Medium to fine grained intergranular dissemination of albite partially overprinting K-feldspar and other minerals of granite; this causes an occurrence of irregularities in the texture of granite (occurrence of finer grained "spots" within coarse-grained texture, *etc.*).
3. Fine grained (sugary) albite aggregations forming large "spots" and almost wholly substituting the rock (granite); fine-grained quartz and coarser grained light greenish mica are associated with albite. Fine crystalline tourmaline and fine grained pink garnet are also common.
4. Fine grained (sugary) albite aggregations exhibiting banded, layered distribution, or even alternating albite and quartz bands.

It appears to be reasonable to assume that, although a part of albite (especially larger crystals) are with no doubt primary magmatic in origin forming from magmatic melt in the course of its crystallization, some part of albite may be associated with later possibly metasomatic process ("albitization"), thus replacing the early albite and other primary magmatic minerals of the granites and pegmatites (*cf.* Schwartz, 1992). The albite-rich rocks locally bear elevated content of beryl and possibly Ta-Nb and Sn minerals that is, in some locations, detected by assaying (Table 1).

There are several types of muscovite-bearing granites; the mica occurs both in the form of large books and scales saturating the granites to various degrees and distributed more or less evenly, and in the form of short vein-like aggregations, short stringers and veinlets, or just muscovite-rich patches, in which muscovite occurs together with quartz, tourmaline and locally albite. Similarly to albite, a part of this muscovite can be assigned to the magmatic crystallization, whereas the other part resembles metasomatic formations like quartz-muscovite, quartz-tourmaline-muscovite and other greisens. This is especially suggestive in local sectors, where the granites are anomalously enriched in muscovite (from 10 vol.% to 20-40 vol.%) and quartz, with gradual transition to almost muscovite-free granite, and in exocontact zones, where muscovite to muscovite-quartz formations overprint the host metasedimentary rocks and gabbroic dikes. Correspondingly, the essentially quartz-muscovite greisens contain some black tourmaline (usually <5 vol.%) and albite (about 10-20 vol.%) irregularly distributed in the rock. Less common essentially quartz-tourmaline to quartz-tourmaline-muscovite greisens are composed of quartz (60-80 vol.%) and coarse grained black tourmaline (20-30 vol.%), with minor importance of muscovite (0-20 vol.%). Such muscovite-rich aggregates locally contain fine disseminated to larger-crystalline beryl.

RARE METAL MINERALIZATION

The surface grab samples of the Hellroaring Creek stock granites listed in Table 1 encountered just occasional slightly elevated values of tantalum and niobium (Table 1). A random surface sampling of the Hellroaring Creek stock granites performed in 2000-2001 has identified some number of appreciable rare metal (Be, Ta, *etc.*) values (Table 2). Beryllium mineralization appears to be more widespread in the pegmatites and nearby granites of the Hellroaring Creek stock exposed on the surface, where large beryl crystals attaining 5.5 kg in weight and over 30 cm in length were noted (Figure 6). As noted above, the previous work on the property conducted by Richfield Oil Corporation has indicated the north (actually northwestern) end of the Hellroaring Creek stock contains no NI 43-101 compliant resource of 500 000 tonnes of the mineralized material averaging 0.1% BeO (Wasylyshyn, 1984; Pudifin, 1986).

More often, than in surface grab samples, Ta-Nb mineralization is encountered by systematic sampling of drill core (*i.e.*, on deeper levels of the stock than those exposed on the surface?). In particular, the drilling performed in 2000-2001 by Chapleau Resources Ltd. encountered the areas of preferential concentration of beryllium mineralization in the uppermost part of the granitic stock, in relation with the stockscheider-style granites (Soloviev, 2001). These areas appear to be shaped as discontinuous thin flat-lying lenses extending for few tens of metres along strike and in width. The best intercepts included those in the range of some 450-700 ppm Be over 8-12 m; they are parts of thicker intervals attaining some 270 ppm Be over 23 m. In part, these areas of beryllium concentration are coincident with smaller zones of enrichment in tantalum averaging some 40-50 ppm Ta over 5-8 m (including narrower zones of stronger enrichment up to 120-140 ppm Ta over 1 m). In general, it was demonstrated that these intervals of enrichment and Be and Ta occur preferably in the uppermost 20-30 m (not deeper than 55 m) from the surface, *i.e.*, in the topmost part of the granitic stock.

Assaying of the core from the historical drillholes drilled in 1985-86 by Lumberton Mines Ltd. in the northwestern sector of the Hellroaring Creek stock indicated the presence of elevated tantalum contents at

Table 2. Contents of the rare metals in some surface grab samples of the Hellroaring Creek stock granites (data of Chapleau Resources Ltd.).

NN	Sample Description	Ta, ppm	Nb, ppm	Rb, ppm	Cs, ppm	Sn, ppm	Be, ppm
1463	Medium to coarse grained pegmatoid granite, moderately albitized, quartz+K-feldspar+albite-90%, muscovite-10%, black tourmaline <1%	278.5	715.4	121.3	68.1	32	3329
1467	Same	497.2	1478.5	60.4	26.7	15	920

Table 3. Contents of the rare metals in historical drill core (data of Chapleau Resources Ltd.).

Sample Number	Drillhole Number and Interval	Sample Description	Ta, ppm	Nb, ppm	Rb, ppm	Cs, ppm	Sn, ppm	Be, ppm
1201	86-7, 85.0-86.6 m	Coarse grained, irregularly-grained to stockscheider-style tourmaline-muscovite granite	30.0	35.6	517.7	30.4	31	473
1225	86-7, 108.6-109.6 m	"	39.4	61.7	394.5	33.3	72	53
1226	86-7, 109.6-110.6 m	"	41.7	92.1	459.2	44.3	100	222
1227	86-7, 110.6-111.6 m	"	22.5	59.4	327.0	26.0	66	161
1228	86-7, 111.6-112.6 m	"	31.7	46.0	297.8	25.4	62	70
1231	86-7, 114.6-115.6 m	"	23.3	57.9	439.8	49.6	92	76
1233	86-7, 116.6-117.6 m	"	27.8	104.8	880.1	86.5	171	81
1240	86-7, 123.6-124.6 m	"	20.3	52.4	341.1	15.5	32	179
1241	86-7, 124.6-125.6 m	"	38.3	43.1	579.7	58.2	92	24
4421	86-7, 10.5-11.0 m	"	64.3	74.3	549.3	47.4	81	38
4422	86-7, 11.0-12.0 m	"	219.4	197.9	462.7	45.7	38	734
8803	86-3, 106.0-107.0 m	"	40.6	48.5	93.5	2.9	8	63
8742	86-3, 45.5-46.5 m	"	39.6	141.8	676.0	42.7	60	41
8654	86-1, 83.5-84.5 m	"	22.7	69.3	655.5	42.2	28	522
8605	86-1, 35.8-36.8 m	"	28.9	44.8	826.4	50.1	46	63
1278	86-1, 8.0-9.0 m	"	98.5	284.4	565.0	26.3	32	80
8677	86-2, 14.2-15.2 m	"	20.6	49.0	216.9	15.8	17	138

deeper levels of the stock (Table 3). However, the intervals encountered at the higher (shallower) level of the pluton still bear greater Ta values. The high variability in the Ta/Nb ratios suggests the presence of (besides of columbite-tantalite) other Ta-Nb minerals and/or the presence of various generations of columbite-tantalite with respectively variable Ta-Nb contents. Also, the assay results locally suggest the presence of cassiterite. In general, taking into account the greatly predominating volume of the granites over that of the pegmatites related to the Hellroaring Creek stock, it can be suggested that the predominating amount of the rare metals is associated with the granites rather than with the pegmatites.

The Lightning Creek pegmatite is definitely more evolved (it has higher concentrations of F, Li, Rb, Cs, and Ta) (Table 1) than the pegmatites occurred within the Hellroaring Creek stock and/or closer to its boundaries. This is consistent with the general Cerny (1993), London (2008) model. The Lightning Creek pegmatite contains also beryl and more significant Ta mineralization; according to Mulligan (1968), "..... the pegmatite is a part of a large mass that extends across the ridge from Hellroaring Creek to Angus Creek [Lightning Creek showing – S.S.]. Beryl is also found in Angus Creek [Lightning Creek showing – S.S.] ....most of the beryl was intimately associated with muscovite near the boundaries of quartz segregations. Columbite-tantalite occurs in crystals more than an inch across....minor amounts of tin were reported in composite samples of pegmatite....."

DISCUSSION AND CONCLUSIONS SUMMARY

The data presented suggest that the geological model of the Hellroaring Creek stock should incorporate the features typical for both "specialty rare metal granite" and granitic pegmatite deposits. In particular, the predominating granite bears petrologic and geochemical features of the "specialty rare metal bearing granites" indicating a high degree of evolution (fractionation, *etc.*) of the intrusive rocks, high degree of the magma saturation in volatile components (fluids) and their especial concentration at the topmost levels of the pluton, with the occurrence of the "pegmatoid" (stockscheider-style) "crust" marginal varieties in the endocontact and especially at the upper levels of the pluton. The granite is enriched in albite, especially in marginal varieties, and is characterized by broad although scattered occurrence of

disseminated Be, Ta, Nb, Sn mineralization. These features resemble those occurred in granite intrusions representing the respective rare metal granite deposits (*e.g.*, Phuket in Thailand, Beauvoir in France, Abu Dabbab in Egypt, Orlovka and Etyka in Transbaikalia, Russia, Yuichun in China, *etc.*) that typically contain significant tonnages of low-grade rare metal (Ta-Nb, Be, Sn) mineralization (Pollard *et al.*, 1995; Simandl, 2002). At these deposits, the most of Ta-Nb mineralization (tantalite-columbite, Ta-cassiterite, struverite, microlite) is found in the uppermost sectors of the rare metal granite intrusions. Tantalum grades vary from 120 to 300 ppm Ta_2O_5, occasionally higher, and these grades correspond to the ores typically involved in mining. Background grades are as low as 50-80 ppm Ta_2O_5. Vertical extent of tantalum enrichment zones is usually up to 50 m although rarely is as much as 100-150 m and even 200 m (at flat-dipping contacts). Tantalum minerals form very fine dissemination (usually the grains are of 0.1-0.5 mm and up to 1 mm in size). Beryllium mineralization, if present, occurs slightly above the Ta-Nb-enriched zones, in association with micaceous assemblages, part of which may correspond to greisens. Thus the broad occurrence of scattered zones of enrichment of the Hellroaring Creek granites in Be, Ta, Nb, Sn may be suggestive for more voluminous (and perhaps higher-grade) concentrations of the rare metals that may be revealed in the course of further exploration.

Pegmatites are generally uncommon for the rare metal granite deposits but, if occurred, these are located in some (0.5-3 km) distance from the main pluton and change their mineral composition in dependence on the distance from the pluton. Correspondingly, for the pegmatites associated with the Hellroaring Creek stock, a spatial model suggested by Cerny (1993) and London (2008) can be applied. This model would include the muscovite-ceramic pegmatites occurred in the most proximity to the parental ("fertile") pluton (actually, within the plutonic endocontact), and then beryl pegmatite, Li pegmatites and albite-lepidolite and elbaite pegmatites occurred with increasing distance from the granites. The Ta-Nb mineralization occurs in the all types of the pegmatites starting with the beryl pegmatites but attains its maximum in the Li and albite-lepidolite pegmatites; the Ta/Nb ratio in columbite-tantalite increases from the beryl through lithium to albite-lepidolite pegmatites.

A common issue of the preferential occurrence of either rare metal granites or pegmatites is usually resolved by considering their different depth of formation. Specifically, the granite plutons responsible for the formation of rare metal-bearing pegmatites as well as these pegmatites themselves are formed at moderate depths (under the pressure of 2-4 kbar); these plutons have no indications of late- and postmagmatic alteration or mineralization of the granites, thus, indicating a fluid (+metals) concentration in pegmatite-forming residual melt+fluid removed from the granite via relatively large and well-developed fractures only (Cerny, 1993). In contrast, the rare metal granite intrusion, which are intensely late and postmagmatically altered and often accompanied by greisens and related vein systems, in virtually total absence of pegmatites, were formed at relatively shallow levels (under the pressure of 1-2 kbar) that was, probably, the reason for another style of the fluid behavior and release. Correspondingly, the "open" and "closed" magmatic-fluidal systems are distinguished (Pollard *et al.*, 1987; Pollard, 1989 a, b; Suwimonprecha *et al.*, 1995; London, 2008).

Consequently, the Hellroaring Creek stock granite and related pegmatites may represent a genetic link between the typical pegmatite deposits (and associated "fertile" granites) formed at greater depth, and the typical rare metal granite deposits formed at shallower depth. In this regard, the Phuket and other deposits in Thailand show a distinct similarity to the Hellroaring Creek stock granites and pegmatites, as they also incorporate both Sn-Ta-bearing rare metal granites and significant pegmatites (Suwimonprecha *et al.*, 1995). This deposit is also similar to Hellroaring Creek stock by its enrichment in boron, whereas many other rare metal granites are preferentially enriched in fluorine (*cf.* Pollard *et al.*, 1987).

Finally, referring the Hellroaring Creek stock granites to as the "specialty rare metal granites" highlights the potential of recognizing this style of rare metal deposits in the Cordilleran orogenic belt. A brief review of apparently similar granite plutons accompanied by the rare metal (Ta-Nb, Sn, Be, *etc.*) mineralization reveals a distinct belt of deposits and occurrences traceable in the region that may be allocated to this style (Figure 1); this belt may be, at least in part, coincident with the Cordilleran belt of muscovite granites (Miller and Bradfish, 1980). Pell and Hora (1990) were, probably, the first who pointed out the possible presence of the regional-scale belt of the "specialty granites" in North America, and provided Surprise Lake batholith and Parallel Creek intrusion as examples of these in British Columbia. Most notable of the "specialty rare metal granites" and associated deposits/occurrences include Kougarok Sn-Ta and Lost River Sn-Be deposits in Alaska (Puchner, 1986; Hudson and Arth, 1983), Kalzas W-Sn (+Ta?) deposit in Yukon, Seagull, Surprise Lake and Parallel Creek plutons and associated Sn occurrences in Yukon and Northern British Columbia (Liverton, 1999) and a number of smaller and/or less studied occurrences. An apparent feature of these occurrences is the intrusion of relatively small stocks of the rare metal (Ta-Nb, Be) granites after the emplacement of much larger plutons of less evolved stanniferous granites; thus, the larger plutons of Sn-bearing granites may be considered to be initial exploration targets for revealing more localized rare metal mineralization related to supplementary and more evolved rare metal granites. However, most of these occurrences are Mesozoic, whereas the Hellroaring Creek stock is currently assigned to the Proterozoic. This may call for additional radiologic dating of the Hellroaring Creek

stock granites and pegmatites; alternatively, this may indicate a broad time span of the rare metal granites and related mineralization, thus, suggesting the potential for their discovery in various Cordilleran terranes.

ACKNOWLEDGMENTS

The author thanks Jim Stypula, CEO of Chapleau Resources Ltd., for support and permission to publish the data on the Hellroaring Creek prospect. The field visits performed together were very productive for obtaining new data on the rock relationships leading to fruitful discussions. Significant support to the author was provided also by Eric Wiltzen, Alan Rella, and Robin Sudo. Some data on the prospect geology and mineralization was generously sheared by David Pighin. Earlier prospect visits were conducted in a company of David Pighin, Doug Anderson, Rick Walker and Lee Groat; the relevant discussions highlighted many of the topics considered in the present paper. The paper benefited from editorial review by George Simandl of the British Columbia Geological Survey.

REFERENCES

Anderson, D. (2001): Diamond Drilling Assessment Report on the Horn/Beryl Claims; *BC Ministry of Energy, Mines and Petroleum Resources*, Assessment Report 26501, 50 pages.

Brown J.A. (2003): Mineralogy and geochemistry of beryl and rare-metal bearing granitic pegmatites in the Kootenay region of southeastern British Columbia. *BC Ministry of Energy, Mines and Petroleum Resources,* Geological Fieldwork 2002, Paper 2003-1, pages 167-183.

Cerny, P. (1993): Rare-element granitic pegmatites. Part 2: Regional to global environments and petrogenesis; *Ore Deposit Models*, Volume l.2 (Geoscience Canada reprint series; Volume 6), pages 49-62.

Cuney, M., Marignac, C. and Weisbrod, A. (1992): The Beauvoir topaz-lepidolite-albite granite (Massif Central, France): The disseminated magmatic Sn-Li-Ta-Nb-Be mineralization; *Economic Geology*, Volume 87, pages.1766-1794.

Ethier, V.G. and Campbell, F.A. (1977): Tourmaline concentrations in Proterozoic sediments of the southern Cordillera of Canada and their economic significance; *Canadian Journal of Earth Sciences*, Volume.14, pages 2348-2363.

Ethier, V. G., Campbell, F.A., Both, R.A. and Krouse, H. R. (1976): Geological setting of the Sullivan orebody and estimates of temperatures and pressure of metamorphism: *Economic Geology*, Volume 71, pages 1570-1588.

Höy, T. (1993): Geology of the Purcell Supergroup in the Fernie west-half map area, SE British Columbia; *BC Ministry of Energy, Mines and Petroleum Resources*, Bulletin 84, 157 pages.

Höy, T. and van der Heyden, P. (1988): Geochemistry, geochronology, and tectonic implications of two quartz monzonite intrusions, Purcell Mountains, southeastern British Columbia; *Canadian Journal of Earth Sciences*, Volume 25, pages 106-115.

Höy, T., Price, R.A, Legun, A., Grant, B. and Brown, D. (1995): Purcell Supergroup, geological compilation map; *BC Ministry of Energy, Mines and Petroleum Resources*, Geoscience Map 1995-1, scale 1:250 000.

Hudson, T. and Arth, J.G. (1983): Tin granites of Seward Peninsula, Alaska; *Bulletin of the Geological Society of America*, Volume.94, pages 768-790.

Leech, G.B. (1957): St. Mary Lake, British Columbia; *Geological. Survey of Canada;* Preliminary Map series, 15-1957.

Legun, A.S. (2004): The potential for emeralds in B.C. – a preliminary overview; *BC Ministry of Energy, Mines and Petroleum Resources,* Geological Fieldwork 2003, Paper 2004-1, pages 219-230.

Legun, A.S. (2005): Potential for gem beryl and schist hosted emeralds in British Columbia; *BC Ministry of Energy, Mines and Petroleum Resources*, GeoFile 2005-16, 20 pages.

Liverton, T. (1999): Highly evolved tin granites: a Canadian example; *Revista Brasileira de Geociências*, Volume 29(1), pages 9-16.

Logan, J. (2002): Intrusion-related gold mineral occurrences of the Bayonne magmatic belt; *BC Ministry of Energy and Mines*, Geological Fieldwork 2001, Paper 2002-1, pages 237-246.

London, D. (2008): Pegmatites. *The Canadian Mineralogist Special Publ. 10,* 347 pages.

Lydon, J.W. (2007): Geology and metallogeny of the Belt-Purcell Basin; in Mineral Deposits of Canada: A Synthesis of Major Deposit Types. District Metallogeny, the Evolution of Geological Provinces, and Exploration Methods, Goodfellow, W.D., ed., *Geological Association of Canada,* Mineral Deposit Division*,* Special Publication 5, pages 581-607.

MacLean, M.E. and White, G.V. (1991): Feldspathic mineral occurrences in British Columbia; *BC Ministry of Energy and Mines*, Open File 1991-10, 96 pages.

McFarlane, C.R.M. and Pattison, D.R.M. (2000): Geology of the Matthew Creek metamorphic zone, southeast British Columbia: a window into Middle Proterozoic metamorphism in the Purcell Basin; *Canadian Journal of Earth Sciences*, Volume. 37, pages 1073-1092.

Miller, C.F. and Bradfish, L.J. (1980): An inner Cordilleran belt of muscovite-bearing plutons; *Geology*, v.8, pp. 412-416.

MINFILE (2011): British Columbia mineral deposits database; *BC Ministry of Energy, Mines and Petroleum Resources*, URL <http://minfile.ca> [November 2011].

Mulligan, R. (1968): Geology of Canadian beryllium deposits; *Geological Survey of Canada,* Economic geology report, no. 23. pages 61-62.

Pell, J. and Hora, Z.D. (1990): High-tech metals in British Columbia; *BC Ministry of Energy, Mines and Petroleum Resources*, Information Circular 1990-19, 26 pages.

Pollard, P.J. (1995): Geology of rare metal deposits: An introduction and overview; *Economic Geology*, v. 90, pages 489-494.

Pollard, P.J. (1989a): Geochemistry of granites associated with tantalum and niobium mineralization; in Möller, P., Cerný, P. and Saupé, F. (eds.): Lanthanides, tantalum and niobium, Berlin, *Springer-Verlag*, pages 142-165.

Pollard, P.J. (1989b): Geologic characteristics and genetic problems associated with the development of granite-

hosted deposits of tantalum and niobium. In Möller, P., Cerný, P. and Saupé, F. (eds.): Lanthanides, tantalum and niobium, Berlin, *Springer-Verlag*, pages 240-256.

Pollard, P.J., Nakapadungrat, S. and Taylor, R.G. (1995): The Phuket Supersuite, Southwest Thailand: Fractionated I-type granites associated with tin-tantalum mineralization. *Economic Geology*, v.90, pages 586-602.

Pollard, P.J., Pichavant, M. and Charoy, B. (1987): Contrasting evolution of fluorine- and boron-rich tin systems; *Mineralium Deposita*, Volume.22, pages 315-321.

Puchner, C.C. (1986): Geology, alteration, and mineralization of the Kougarok Sn deposit, Seward Peninsula, Alaska; *Economic Geology*, Volume.81, pages 1775-1794.

Pudifin, S.M. (1986): Hellroaring Group industrial mineral project, British Columbia, Fort Steele Mining Division; *BC Ministry of Energy, Mines and Petroleum Resources*, Assessment Report 15760, 244 pages.

Rice, H.M.A. (1941): Nelson map area, east half, British Columbia. *Geological Survey of Canada*, Memoir 228.

Ryan, B.D. and Blenkinsop, J. (1971) Geology and geochronology of the Hellroaring Creek stock, British Columbia. *Canadian Journal of Earth Sciences*, Volume.8, pages 85-95.

Schwartz, M.O. (1992): Geochemical criteria for distinguishing magmatic and metasomatic albite-enrichment in granitoids - examples from the Ta-Li granite Yuichun (China) and the Sn-W deposit Tikus (Indonesia); *Mineralium Deposita*, Volume.27, pages 101-108.

Simandl, G.J. (2002): Tantalum market and resources: an overview; *BC Ministry of Energy, Mines and Petroleum Resources,* Geological Fieldwork 2001, Paper 2002-1, pages 313-318.

Smith, M. and Brown, D.A. (1998): Preliminary report on a Proterozoic (?) stock in the Purcell Supergroup and comparison to the Cretaceous White Creek Batholith, southeastern British Columbia. *BC Ministry of Energy, Mines and Petroleum Resources,* Geological Fieldwork 1997, Paper 1998-1, pages 11-1 to 11-7.

Soloviev, S.G. (2001): Assessment report on diamond drilling, Horn/PAKK property; *BC Ministry of Energy, Mines and Petroleum Resources*, Assessment Report 26693, 149 pages.

Soloviev, S.G. (2010): Evaluation of 'reduced' intrusive-related gold mineralization in the area west of Cranbrook, southeastern British Columbia (NTS 082F/49, 082F/50, 082F/59, 082F/60, 082G/41, 082G/51); *BC Ministry of Energy and Mines*, Geological Fieldwork 2009, Paper 2010-1, pages 97-111.

Suwimonprecha, P., Cerny, P., and Friedrich, G. (1995): Rare metal mineralization related to granites and pegmatites, Phuket, Thailand; *Economic Geology*, v.90, pages 603-615.

Wasylyshyn, R. (1984): Assessment report, Hellroaring Group, Fort Steele Mining Division: *BC Ministry of Energy, Mines and Petroleum Resources*, Assessment Report 13415, 100 pages.

White, G. (1987): Hellroaring Creek Pegmatite; *BC Ministry of Energy and Mines*, Exploration in B.C. 1987, pages B109-B116.

Evaluation of Rare Earth Element-enriched Sedimentary Phosphate Deposits Using Portable X-ray Fluorescence (XRF) Instruments

by R. Fajber[1] and G.J. Simandl[1,2]

KEYWORDS: Portable XRF, rare earth elements, phosphate, exploration

EXECUTIVE SUMMARY

Sedimentary phosphate deposits (Mineral deposit profile F07; Simandl *et al.,* 2012), consist mainly of the apatite group mineral [$(Ca_5(PO_4)_3(OH,F,Cl)$] commonly referred to as francolite. Such deposits supply most of the phosphate rock used by the ammonia phosphate fertilizer industry. The 2010 world phosphate rock production is estimated at 176 million tonnes (Cordier, 2011). In recent years sedimentary phosphate deposits have also been considered as a potential fluorine resource (Simandl, 2009) and it is possible that rare earth elements (REE) may also be recovered from some sedimentary deposits as by-products (Simandl *et al.*, 2011a, b). Portable XRF technology is relatively new. To the authors' knowledge there are no publicly available documents describing its use in the exploration and development of sedimentary phosphate deposits containing elevated concentrations of lanthanides and Y as by-products. Thirty-two samples of phosphate rock (pulps) from the Fernie Formation (southeastern British Columbia) were analysed using a hand-held XRF analyser as well as by a lithium metaborate fusion–inductively coupled plasma (LMB-ICPMS) method. The results from both methods were compared; correction factors for the portable XRF analyser were established and their effectiveness was tested. Portable hand-held XRF analysers that are currently on the market have their technical limitations. If correction factors are established, hand-held instruments can be used in exploration for phosphate deposits by analyzing samples directly for phosphorus (P), identifying zones of phosphate rocks rich in rare earth elements (REE), and delineating zones with unacceptable levels of deleterious elements such as uranium (U).

[1] *British Columbia Geological Survey, Victoria, BC*
[2] *School of Earth and Ocean Sciences, University of Victoria, Victoria, BC*

This publication is also available, free of charge, as colour digital files in Adobe Acrobat® PDF format from the BC Ministry of Energy and Mines website at http://www.empr.gov.bc.ca/Mining/Geoscience/PublicationsCatalogue/Fieldwork.

INTRODUCTION

British Columbia is known to host at least 62 known occurrences of sedimentary type phosphate. Several of these occurrences were previously investigated and documented as potential sources of phosphates (Butrenchuk, 1987, 1988, 1996; Norman and Renning, 2009a, b), Y (Pell, 1991) and REE (Simandl *et al.,* 2011a, b); however, none of them are currently in production. In recent years, prices of REE have risen sharply due to an imbalance between supply and demand (Simandl 2010, 2011a, b). The REE and Y content of many phosphate rocks could now justify more detailed investigations of their recovery during fertilizer production from phosphate rocks.

Portable XRF technology was derived from the traditional XRF during the late 1960s and further technological evolution led to the development of hand-held XRF analysers. Laboratory XRF instruments commonly rely on careful sample preparation in the form of pressed powder pellets and fused beads or glass disks to maximize precision and accuracy of the readings. Portable hand-held XRF analysers are subject to the same analytical constrains as their large laboratory equivalents as well as additional limitations due to limited voltage and power at the x-ray source. When used in the field, hand-held XRF analysers do not benefit from sample homogenization and sample preparation of their larger stationary laboratory counterparts. For these reasons initial orientation studies are required prior to any large scale use of hand-held portable XRF equipment. The first stage of any orientation study relies on finely ground and homogenized samples (pulps) in order to minimize errors due to natural textural variations of rocks. In case of sedimentary phosphate deposits the textural variations can be: bedding, laminations, graded bedding, as well as clasts and post-depositional fracture fillings, veinlets, the presence of non-pervasive alteration and weathering (in sedimentary rocks). The effects of uneven broken rock surfaces on hand samples or drill cores are also eliminated using finely ground samples. Additional limitations are described in the "Operator of Portable X-ray Fluorescence Analysers Certification Information and Examination Preparation Booklet" (Murphy *et al,*. 2010). The use of these instruments is well established in a variety of industrial applications including recycling, scrap metal testing, and consumer safety controls.

The main objectives of this study were; to determine the practical limitations of hand-held XRF technology in phosphate exploration, to determine whether or not calibration is needed for portable XRF technology to be effective at analyzing both major and trace elements within a phosphatic matrix, and to determine the effectiveness of the calibration factors on pulps.

Thirty-two samples from the Fernie Formation were selected with concentrations of P ranging from 0.15 to 27.5% and concentrations of REE ranging from 99.1 to 1498.98 ppm. These samples were originally collected and analysed by Butrenchuk (1987) but have recently been re-analysed using modern analytical methods (Simandl *et al.*, 2011b). The results of portable XRF data were compared with the results of modern analytical methods.

INSTRUMENTATION

The hand-held portable XRF used for this study was a Thermo Scientific Niton XL3t (serial number 67749, manufactured in the U.S.A., 2011), supplied by Elemental Controls Limited (Toronto). The instrument (Figure 1) uses a Ag x-ray tube (no radioactive source), with a maximum current of 0.2 mA, a maximum voltage of 50 kV, and a maximum power of 2 watts. The instrument was used in "Mining Cu/Zn mode" for all analyses. The instrument operates on four different filters in order to obtain accurate measurements of a wide range of elements (Table 1). An optional calibration allowing for La, Ce, Pr, and Nd analysis on the "High" filter was done by Elemental Controls Limited (Toronto). This instrument is one of the first able to be able to analyse Pr and Nd without the use of a radioactive source. Other instruments with radioactive sources have already been used for mapping and grade control, and have even been applied to heavy REE. For example, Avalon uses a Thermo-Scientific Niton XLP-522K hand-held analyser for mapping and grade control of fine grained REE minerals present in their drill core (Bakker *et al.*, 2011).

Figure 1. The hand-held portable XRF used for this study was a Thermo Scientific Niton XL3t.

METHODOLOGY - DATA ACQUISITION

All samples were collected by Butrenchuk prior to 1988. Samples were crushed, milled, homogenized, and then analysed using a bench top Philips 1440 wavelength dispersive x-ray fluorescence spectrometer and volumetric techniques by British Columbia Geological Survey Analytical Sciences Laboratory. The results of that analytical work were reported by Butrenchuk (1996). The samples pulps were re-analysed in 2009 (Simandl *et al.,* 2011b) using lithium-borate fusion followed by ICP-MS (LMB-ICPMS) at ALS Laboratories in Vancouver. The re-analysis was required since the results reported by Butrenchuk (1996) do not include most of the REEs.

Before hand-held XRF analysis began, the analyser was allowed to warm up for 150 seconds and a system check was conducted. Three standards were tested first before a phosphate rock pulp was analysed. These standards consisted of a certified 99.995% SiO_2 blank, Standard Reference Material 2780 (May and Rumble 2004), and Certified Reference Material "TRLK" Rare Earth Ore "CGL 124" (Registration Number: USZ 42-2006; Mongolia Central Geological Laboratory). All standards were contained in sample cups covered by a 4.0µ thick polypropylene film. Standards were placed into a portable field test stand and then analysed using the instrument in "Mining Cu/Zn" mode with all 4 beam times set to 45 seconds for a total of 3 minutes.

The same sample cups and 4.0µ thick polypropylene film (Figure 2) were used to hold phosphate pulps because our preliminary investigations concluded that analyzing through the Kraft® paper bags in which the pulps were stored resulted in unacceptable levels of x-ray attenuation, especially when determining concentrations of light elements such as P (Figures 3 and 4). The improvement in quality of the data achieved through the use of polypropylene is also readily apparent by comparing the coefficient of determination, R^2, from measurements made through the Kraft® paper bags and through polypropylene (Figures 3 and 4). Sample cups were filled to the three quarter mark (~19 mm) with pulp, then filled with gauze and capped (Figure 2). After use, the samples were immediately placed into individual plastic bags to avoid contamination on the film and to preserve them for follow-up research. Both standards and pulp samples were analysed using the instrument in "Mining Cu/Zn" mode. The instrument's 4 beam times were set to 45 seconds for a total of 3 minutes per reading. Five measurements were taken on each pulp sample. After every five phosphate pulp samples (or 25 measurements), the same three standards (as described above) were re-analysed. Systematic re-analysis of the standards showed negligible instrument drift throughout the experiment. A survey meter was used at all times to alert the operator an unexpected release of radiation.

Table 1. Filters used, time of analysis and elements analysed by the portable XRF. Cr, V and Ti were analysed using the "Main" filters and then these were re-analysed using the "Low" filter for higher accuracy at low concentrations. Similarly, Sb, Sn, Cd and Ag were re-analysed using the "High" filter for higher accuracy at low concentrations. Bal* stands for balance. It represents x-ray energy levels that the analyser does not attribute to a particular element.

Filter	Analytical time interval (seconds)	Elements Analysed
Main	45	Sb, Sn, Cd, Ag, Mo, Nb, Th, Zr, Bal*, Y, Sr, U, Rb, Bi, Au, Se, As, Pb, W, Zn, Cu, Ni, Co, Fe, Mn, Cr, V, Ti
Low	45	Cr, V, Ti, Ca, K
High	45	Nd, Pr, Ce, La, Ba, Sb, Sn, Cd, Ag
Light	45	Al, P, Si, Cl, S, Mg

Figure 2. Typical sample cups covered by 4.0µ thick polypropylene film.

Both authors are certified by Natural Resources Canada to operate portable XRF instruments in compliance with the Health Canada Safety Code 34/ISO 20807 and followed all required safety procedures specified by Murphy *et al.* (2010).

METHODOLOGY - DATA PROCESSING AND INTERPRETATION

The practical usefulness of portable XRF and its limitations in mineral exploration can be visually assessed using X-Y scatter diagrams, with the Y-axis representing the portable XRF data (XRF) and the X-axis representing the results of the ICP-MS analysis after a lithium borate fusion (Figures 5 and 6). Each point on these graphs represent one of the 5 XRF measurements versus a corresponding LMB-ICPMS analysis.

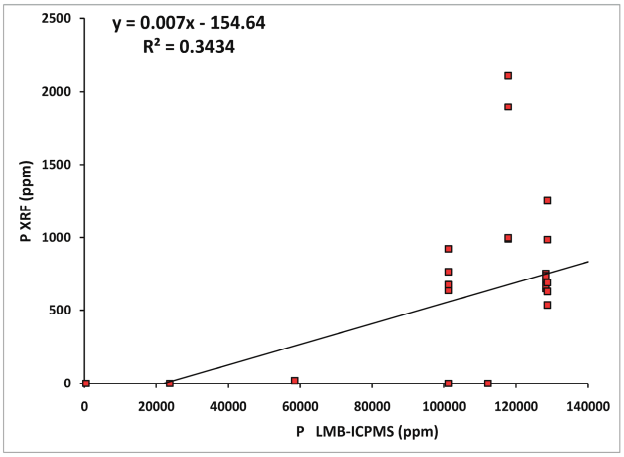

Figure 3. Qualitative comparison of hand-held portable XRF readings obtained by analysing pulps for phosphorus through standard Kraft® paper bags relative to LMB-ICPMS results.

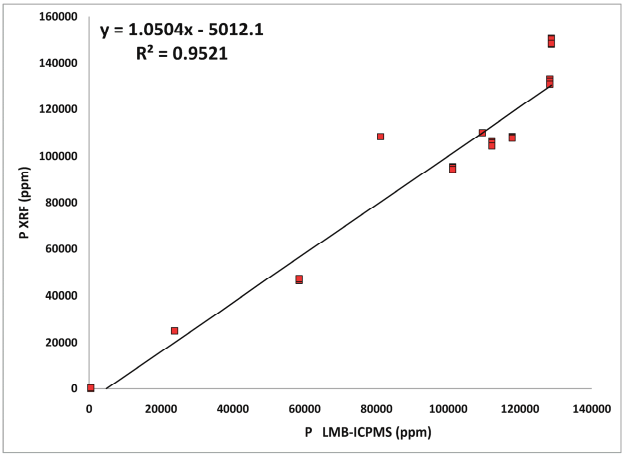

Figure 4. Qualitative comparison of hand-held portable XRF readings obtained by analysing pulps for phosphorus through 4 micron thick polypropylene relative to LMB-ICPMS results.

Based on the total of 160 measurements taken on 32 pulps of phosphate rock samples, the hand-held portable XRF analyser was able to provide an effective quantitative measurement with excellent correlation (R^2>0.85) to the LMB-ICPMS data (Table 2) for 13 elements (Ba, Mo, Y, Sr, U, Rb, Zn, Fe, Ca, P, Si, S and Mg). A reasonable quantitative or semi-quantitative estimates with good correlation (0.5<R^2<0.85) between the hand-held XRF and LMB-ICPMS data sets were achieved for 6 elements (Nd, Ce, La, Zr, W, and Al).

Table 2. Comparison of the correlation between the portable XRF readings and LMB-ICPMS data using the coefficient of determination R^2. The range of analyses (minimum and maximum value) for each element is provided in ppm.

Filter	Element	R^2	ICP-MS	
			Min*	Max*
High	Nd	0.5417	13.4	347.0
	Pr	0.3677	4.3	79.1
	Ce	0.6258	45.0	247.0
	La	0.8303	29.3	388.0
	Ba	0.98520	295.0	7660.0
High/Main	Sn	-	<1	2.0
	Ag	-	<1	<1
Main	Mo	0.97450	<2	67.0
	Nb	0.29250	1.8	20.4
	Th	0.0406	2.1	15.5
	Zr	0.69810	104.0	350.0
	Y	0.9955	5.9	871.0
	Sr	0.9941	118.0	1365.0
	U	0.9611	2.4	53.6
	Rb	0.98780	10.2	68.8
	Pb	0.00006	<5	11.0
	W	0.75940	9.0	229.0
	Zn	0.96070	24.0	572.0
	Cu	0.43150	8.0	58.0
	Ni	0.0757	12.0	174.0
	Co	-	2.7	24.3
	Fe	0.99360	4686.3	31754.9
	Mn	-	77.4	309.8
Low/Main	Cr	-	50.0	250.0
	V	-	30.0	146.0
	Ti	-	659.4	3237.4
Low	Ca	0.97380	4431.0	316604.0
	K	0.90080	2905.5	18429.0
Light	Al	0.83480	9261.7	80179.0
	P	0.9411	436.4	128741.0
	Si	0.9598	58664.0	362268.0
	S	0.98280	900.0	37500.0
	Mg	-	1327.0	21471.0

Legend
Excellent Correlation
Good Correlation
Correlation Observed
No Correlation

R^2 is the coefficient of determination. It ranges from 0 to +1.0. Zero indicates complete absence of a systematic relationship, while 1 indicates a perfect relationship.

Using the same approach, only limited interpretation ($0.25<R^2<0.5$) can be achieved for 3 elements (Pr, Nb, Cu). There was no practically significant correlation ($0.25<R^2$) between portable XRF analyser and the LMB-ICPMS data sets for three elements (Th, Pb and Ni). Eleven elements (Bi, Au, Co, Mn, Cr, V, Ti, Sb, Sn, Cd and Ag) were not detected by the analyser in any of the samples. The REE with atomic numbers greater than 60 (heavier than neodymium) were not able to be analysed using this instrument.

The hand-held portable XRF analyser was also programmed to detect Se, As, Au, Bi, Cd, Sb and Cl. However, these elements were not analysed by the LMB-ICPMS method used, so a comparison between these data sets was not possible. These elements are excluded from the following discussion. For the purpose of this study, the data on the X axis (LMB-ICPMS) can be considered as nearly error-free relative to the data on the Y axis (hand-held portable XRF).

If there was a near perfect match between the LMB-ICPMS and hand-held portable XRF data, there would be minimal scatter of points over an element concentration range. Ideally, the resulting regression line would have a slope of unity (m=1), and would pass through the origin (b=0). The coefficient of determination (R^2) would be equal to one. If the hand-held portable XRF systematically under-estimated or overestimated the "true" (ICP-MS) value, then the slope of the regression line will not be one. Mathematical processing and testing of relationships between corresponding hand-held XRF and LMB-ICPMS data for selected elements allows us to create correction factors based on this premise. The use of such factors does to some extent, correct the bias, revealed in plots so that the corrected XRF values are closer a hypothetical (perfect) relationship.

The general equation of the regression line is

$y = mx + b$

where "m" is the slope of the line and "b" is the y-intercept. The slope can be determined using the formula

$$m = \frac{y_2 - y_1}{x_2 - x_1}$$

Where x_1, y_1 is one pair of LMB-ICPMS (x) and hand-held XRF (y) analytical values corresponding to the first sample and x_2, y_2 is a pair of analytical results corresponding to the second sample (plotting directly on the line). In the case of our regression lines shown in Figures 5 and 6 the expression can be written as:

$$[Hand\text{-}held\ XRF\ reading] = m[LMB\text{-}ICPMS\ result] + b$$

Since we are assuming that the results of LMB-CPMS analyses are almost error-free (compared to the XRF values), then the correction equation will be in the form

$$[Corrected\ XRF\ reading] = \frac{1}{m}\ ([Hand\ held\ XRF\ reading] - b)$$

or

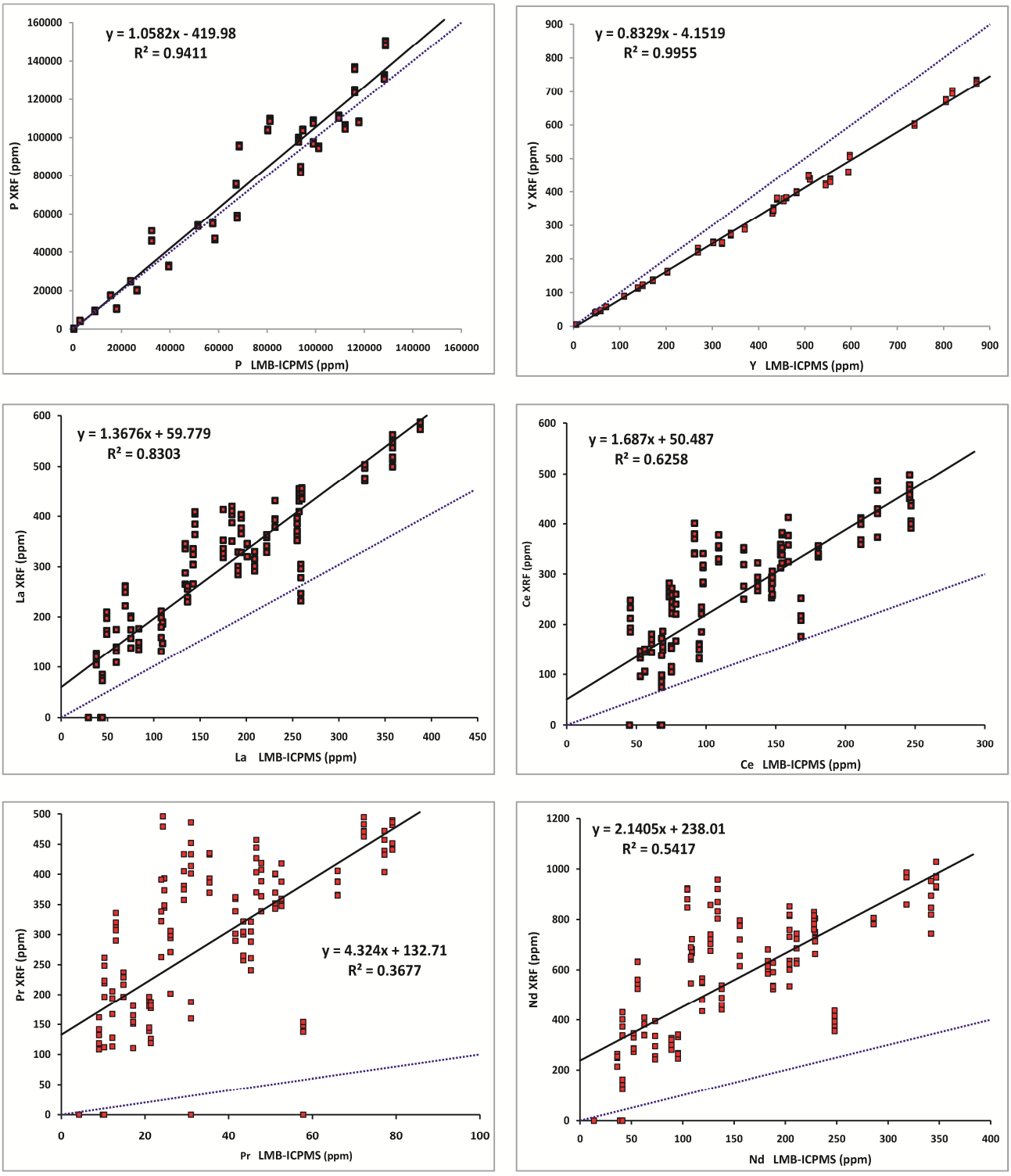

Figure 5. Scatter diagrams, with the Y-axis representing the portable XRF data (XRF) and the X-axis representing the results of the LMB-ICPMS for P, Y, La, Ce, Pr and Nd. In each case, blue dotted line represents perfect theoretical regression line with a slope of unity (m=1). Black line represents actual regression line. Bias revealed in a comparison between the two lines is explained in the text.

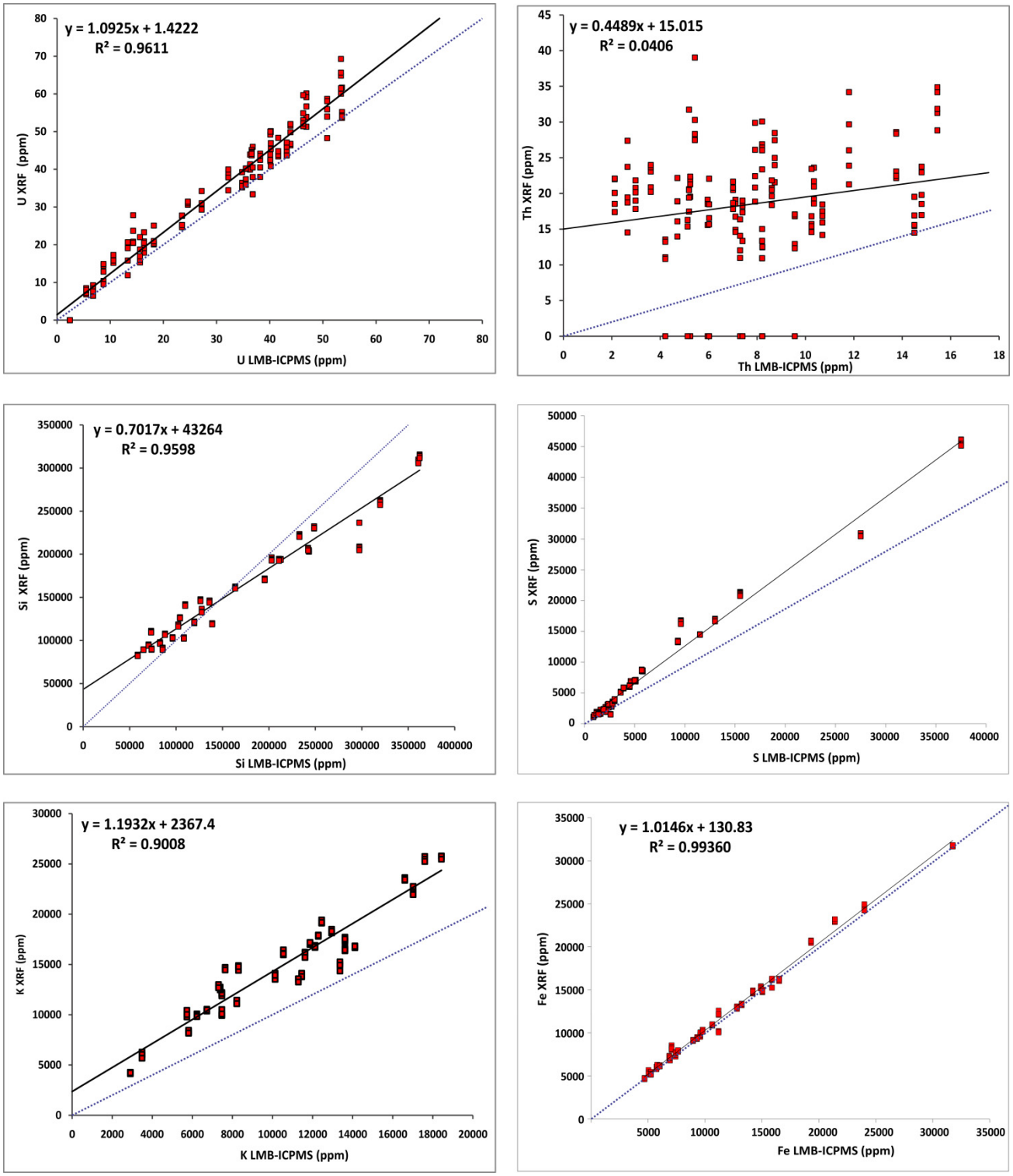

Figure 6. Scatter diagrams, with the Y-axis representing the portable XRF data (XRF) and the X-axis representing the results of the LMB-ICPMS for U, Th, Si, S, K and Fe. In each case, blue dotted line represents perfect theoretical regression line with a slope of unity (m=1). Black line represents actual regression line. Bias revealed in a comparison between the two lines is explained in the text.

[Corrected XRF reading]=n[XRF reading]+c

where $n = \frac{1}{m}$ and $c = \frac{-b}{m}$

A value of "m" greater than 1 represents overestimation by hand-held XRF relative to the LMB-ICPMS value; a value of "m" less than 1 represents an underestimation. If "n" is greater than 1, then the use of correction factor will reduce the bias (improve the accuracy); however, it will increase the spread of the portable XRF data. If the value of "n" is less than 1 then the correction factor will reduce the bias (improve the accuracy) and decrease the spread of the values (improve precision). If the value of b is greater than 0, then b represents the lowest theoretical value of that element that will be given even if that element is not present in a sample. If the value of b is less than 0, then it can be used to calculate the x intercept of the regression line. This intercept represents the smallest concentration of a given element that the XRF can be expected to read.

A simple test was used to compare the relative error between the hand-held XRF analytical results without calibration and the corrected results (after calibration). The absolute value of the difference of data for each portable XRF measurement and the corresponding lab (LMB-ICPMS) measurement was then divided by the lab (LMB-ICPMS) measurement. The average of this value was taken over all measurements. This quantity is called the mean absolute percentage error (Nau, 2005). It can be expressed as:

$$[Mean\ Absolute\ Percentage\ Error] = \frac{1}{n}\sum \frac{|[XRF]_i - [Lab]_i|}{[Lab]i}$$

where n is the number of measurements. Similarly, the mean absolute percentage error was calculated using corrected hand-held XRF values. The mean absolute percentage error estimates (Table 3) were used to provide numerical indication of the improvements achieved through the use of correction factors. The mean absolute percentage error estimate may not be statistically the best approach (Swanson *et al.,* 2011); however, it is the simplest way to convey the information to geologists and prospectors.

Phosphorus, REE and Y

Correlation between P values measured by the portable XRF and LMB-ICPMS data is excellent. The values obtained using the hand-held portable XRF analyser are very similar to the laboratory data (Figure 5). Correlation between the corresponding LMB-ICPMS and portable XRF for Y is also excellent across a wide range of concentrations; however, the portable XRF does significantly underestimate the Y content relative to the LMB-ICPMS (Figure 5). Good correlation exists between the portable XRF data and the LMB-ICPMS data for La (Figure 5), although the portable XRF overestimates the La content. Ce and Nd also display good correlation (Figure 5), but the overestimation of portable XRF values compared with LMB-ICPMS values is even more significant. In the case of Nd, overall, the portable XRF overestimates lab values by more than 100%.

The data from the portable XRF for Pr displays a wide range of scatter, and only a weak correlation with the LMB-ICPMS (Figure 5). This weak correlation is at least in part due to low concentrations of Pr (<100 ppm) in phosphate rocks. Only a qualitative trend can be inferred from the data. The analyser also overestimates Pr concentrations by more than 300% relative to LMB-ICPMS laboratory results.

Other Elements of interest

Uranium and thorium (Th) concentrations are carefully monitored by fertilizer manufacturers. High concentrations of these elements in ammonia phosphate fertilizers are not desirable as they can potentially accumulate in agricultural soil due to repetitive application of fertilizer, and eventually be incorporate into food crops in unacceptable concentrations. If these elements are not incorporated into phosphate fertilizer products or recovered during fertilizer production, they move into effluents associated with phosphogypsum stockpiles and could pose a danger to public health. Reasonable agreement exists between the U data acquired using the hand-held portable XRF unit and corresponding LMB-ICPMS data (Figure 6). The use of hand-held XRF to monitor U concentrations in the phosphate rock is therefore justified as a viable field-based method. Similar relation exists between hand-held XRF unit and corresponding LMB-ICPMS analyses for Mo and Rb.

Thorium content of phosphate rocks used in this study is very low (<20 ppm) and in some cases below the detection limit of the LMB-ICPMS. As expected at low concentrations, there is a much higher degree of scatter between the hand-held portable XRF data and results (Figure 5), and no meaningful correlation can be obtained. Other elements that are present in low concentrations and display similar patterns to Th are Nb, Pb and Ni. Silicon (Si) concentrations determined using hand-held XRF display good precision and excellent correlation when compared to the LMB-ICPMS (Figure 6) but the concentrations obtained using hand-held XRF tend to be significantly underestimated. Similar tendencies are apparent for Ca, Al, Sr and Ba. Sulphur displays slight increase in scatter for samples containing concentrations above 10 000 ppm (Figure 6).

Potassium and Fe illustrate two distinct trends (Figure 5). In the case of K, the hand-held XRF analyser overestimates K concentrations relative to the LMB-ICPMS with an intercept larger than 2000 ppm (0.2%). This indicates that the hand-held XRF analysed could display over 0.2% on a sample where the LMB-ICPMS would not detect any K. It is possible that the high intercept of K is due to spectral overlap with other elements In the case of Fe, there is a very good match between hand-held XRF and LMB-ICPMS methods; however, unlike in the case of K, the Fe regression line has only a small intercept (130.83 ppm, compared with

Table 3. Comparison of accuracy of the portable XRF results before and after correction using the Mean Absolute Percentage Error approach. See the text for formulae used and definitions of m, b, n and c. Mean % E (w/o cor) stands for the "Mean Absolute Percentage Error" prior to correction. Mean % E (w cor) stands for the "Mean Absolute Percentage Error" after correction.

Element	R^2	Mean % E (w/o cor)	m	b	n	c	Mean % E (w cor)
Nd	0.5417	356.00%	2.1405	238.01	0.4671806	-111.19365	63.48%
Pr	0.3677	993.17%	4.324	132.71	0.2312673	-30.691489	64.64%
Ce	0.6258	53.63%	1.687	50.487	0.5927682	-29.92709	41.48%
La	0.8303	96.49%	1.3676	59.779	0.731208	-43.71088	23.94%
Ba	0.98520	15.31%	0.8268	50.595	1.2094823	-61.193759	15.06%
Mo	0.97450	22.51%	0.7467	0.5137	1.3392259	-0.6879604	9.95%
Zr	0.69810	28.05%	0.6102	21.537	1.6388069	-35.294985	11.65%
Y	0.9955	17.65%	0.8329	-4.1519	1.2006243	4.9848721	6.72%
Sr	0.9941	33.52%	0.6622	0.2542	1.5101178	-0.3838719	2.53%
U	0.9611	19.52%	1.0925	1.422	0.9153318	-1.3016018	9.84%
Rb	0.98780	47.45%	0.492	0.8044	2.0325203	-1.6349593	4.83%
Zn	0.96070	17.46%	0.9388	-3.6733	1.0651896	3.912761	17.01%
Fe	0.99360	3.93%	1.0146	130.83	0.9856101	-128.94737	3.01%
Ca	0.97380	11.84%	0.8758	1694.5	1.1418132	-1934.8025	7.08%
K	0.90080	45.95%	1.1932	2367.4	0.8380825	-1984.0764	12.02%
Al	0.83480	22.26%	0.454	11005	2.2026432	-24240.088	24.73%
P	0.9239	18.63%	1.0512	-324.7	0.9512938	308.88508	16.64%
Si	0.9598	16.25%	0.7017	43264	1.4251104	-61655.978	9.40%
S	0.98280	32.14%	1.2089	529.03	0.8271983	-437.61271	18.68%

Legend
Excellent Correlation
Good Correllation
Correlation Observed
Total of 32 samples

R^2 is the coefficient of determination. It ranges from 0 to +1.0. Zero indicates complete absence of a systematic relationship, while 1 indicates a perfect relationship.

a lowest reported LMB-ICPMS value of more than 5000 ppm). The slope of the Fe regression line is nearly matching unity and there is little scatter (similar to phosphorus).

DISCUSSION

Linear regression equations for 20 elements that have good correlation between analytical methods or are economically significant (Table 2) were used to create correction equations for the hand-held XRF relative to the LMB-ICPMS, Significant deviation from the theoretical 1:1 regression line for hand-held XRF versus corresponding LMB-IPMS data exists for most of these elements. In these cases, if there is also a significant correlation indicated by a large positive coefficient of determination (R^2) the instrument calibration or equivalent mathematical treatment of the raw hand-held XRF generated data can greatly improve the quality of hand-held portable XRF analyses.

In the case of P (Figure 7, Table 3) the mean percentage error decreases only slightly; while in the case of Y (Figure 8, Table 3), the mean percentage error decreases from 17.65 to 6.75%. This is due to the fact that most of the error in the P calibration curve is random and not systematic, in this case the correction curve can only have a small effect on the overall accuracy of the method. For elements with a high degree of systematic error such as Pr, the correction factors may significantly increase the accuracy (Figure 9, Table 3); however, the resulting values may still be considered as qualitative estimates at best. In the case of La, the correction values improve the accuracy significantly, although several outliers still exist (Figure 10), and these outliers are not improved significantly. For elements at low concentrations such as U (Figure 11), the accuracy improves significantly with the correction factors. Higher concentrations of U need to be tested in order to determine if the correction factors can be used outside of this fairly limited concentration interval. From a practical point of view, the correction

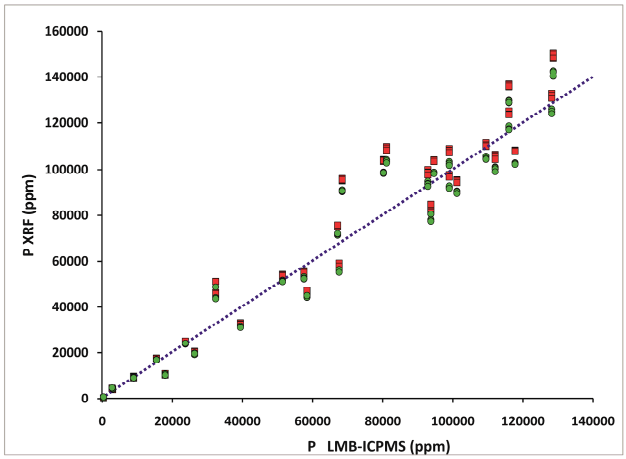

Figure 7. Comparison of uncorrected and corrected hand-held portable XRF data for phosphorus (P). Red squares and green circles represent uncorrected and corrected data, respectively. The dotted blue line coincides with a perfect (theoretical) correlation between the portable XRF and LMB-ICPMS data.

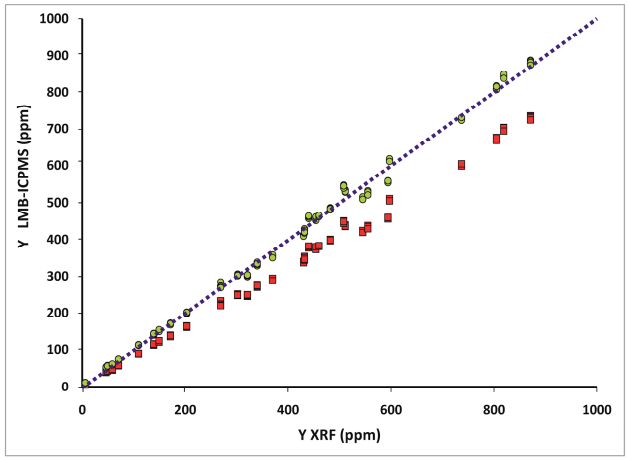

Figure 8. Comparison of uncorrected and corrected hand-held portable XRF data for yttrium (Y). Red squares and green circles represent uncorrected and corrected data, respectively. The dotted blue line coincides with a perfect (theoretical) correlation between the portable XRF and LMB-ICPMS data.

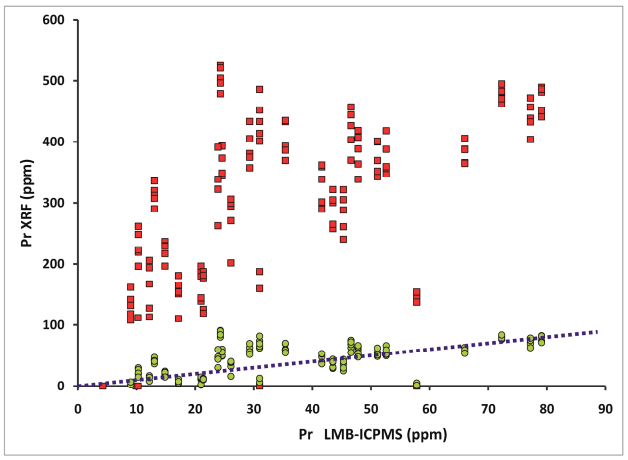

Figure 9. Comparison of uncorrected and corrected hand-held portable XRF data for praseodymium (Pr). Red squares and green circles represent uncorrected and corrected data respectively. The dotted blue line coincides with a perfect (theoretical) correlation between the portable XRF and LMB-ICPMS data.

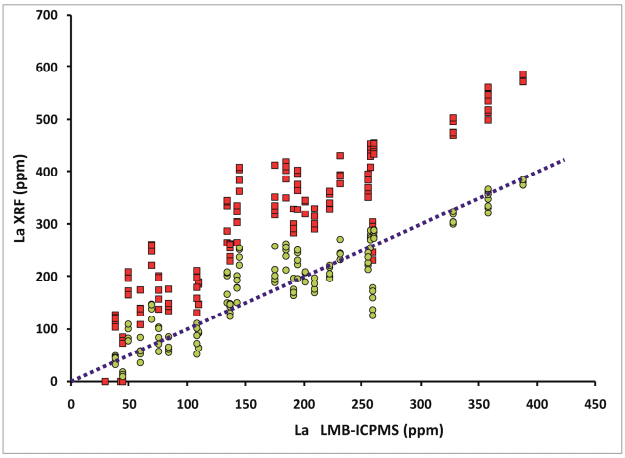

Figure 10. Comparison of uncorrected and corrected hand-held portable XRF data for lanthanum (La). Red squares and green circles represent uncorrected and corrected data, respectively. The dotted blue line coincides with a perfect (theoretical) correlation between the portable XRF and LMB-ICPMS data.

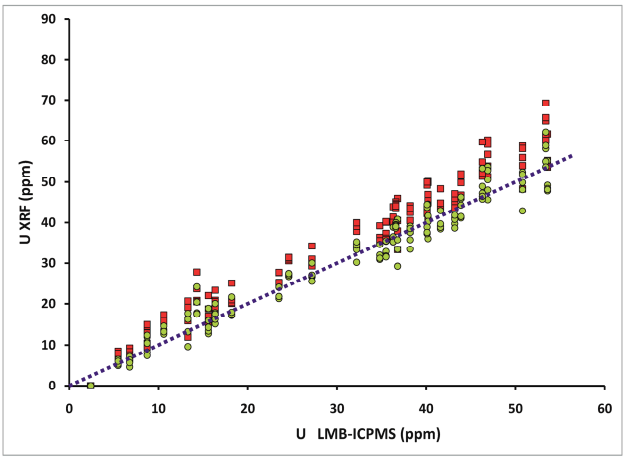

Figure 11. Comparison of uncorrected and corrected hand-held portable XRF data for uranium (U). Red squares and green circles represent uncorrected and corrected data, respectively. The dotted blue line coincides with a perfect (theoretical) correlation between the portable XRF and LMB-ICPMS data.

factors suggest that any sample measuring less than 100 ppm U with this method will almost certainly have a concentration of U below the limit (500 ppm U) requiring special precautions for exploration established in the Health, Safety and Reclamation Code for Mines in British Columbia (British Columbia Mines Act).

The increase in accuracy through the use of correction factors is apparent if we compare distribution of corrected and uncorrected hand-held portable XRF readings relative to the results of LMB-ICPMS analyses (Figures 7 to 11, Table 3).

CONCLUSION

Portable, hand-held XRF technology can be used to determine quantitative, semi-quantitative or qualitative concentrations of major, minor and trace elements present in a phosphate matrix, as shown in the phosphate ±REE occurrences of the Fernie Formation, British Columbia. From the field geologist's point of view, P and Fe

concentrations can be detected in all of the samples and can be measured accurately enough within the tested range of concentrations. The few random discrepancies between LMB-ICPMS analyses and hand-held portable XRF data are probably due to sample inhomogeneity of the pulp. For preliminary assessment of P and Fe content there is no need for use of correction factors.

Acceptable quantitative and semi-quantitative determinations of Nd, Pr, Ce, La, Ba, Mo, Zr, Y, Sr, U, Rb, Zn, Ca, K, Al, P, Si and S could be obtained using the hand-held XRF instrument. However, to achieve these results the readings acquired using the hand-held portable XRF instrument have to be corrected to a known laboratory method using samples of similar concentrations. The portable XRF determinations of Y and REE are of special interest to exploration geologists and geochemists. Light REE (La, Ce, Pr, Nd) and Y results acquired using the hand-held XRF are subject to systematic overestimation relative to laboratory results. Systematic over or under-estimations by XRF instruments are commonly caused by chemical matrix effects (such as absorption and enhancement of the intensity of XRF lines, *etc.*). Heavy REE (HREE) are present in low concentrations; furthermore, portable hand-held XRF instruments without a radioactive source are not able to analyse for them. Other instruments such as the Thermo Scientific Niton XLP-522K, which allows the detection of HREEs (including Sm, Eu, Gd, Tb and Dy), may be more useful in these applications.

In summary, hand-held portable XRF instruments, such as Thermo Scientific Niton XL3t, can be effectively used in exploration for phosphate (±yttrium and REE-bearing) rocks; however, an orientation study is recommended before the use of the hand-held XRF instrument is applied on a large scale. The first stage of the orientation test should be similar to this study. If satisfactory, the second stage should involve analyses of hand specimens corresponding to the pulps to alert the operator of scattered values attributable to effects of textural variations and uneven rock surfaces.

ACKNOWLEDGMENTS

This project was supported financially by the Targeted Geoscience Initiative No.4 (TGI-4) and it would not have been possible without collaboration from Keith Gratton and Jeff Mabbutt (Elemental Controls Limited) who provided the instrument for this study. The authors also wish to thank Suzanne Paradis (Geological Survey of Canada, Sidney, British Columbia), Ray Lett (British Columbia Geological Survey) and to Manzur (Mac) Chaudhry for their constructive comments and suggestions.

REFERENCES

Bakker, F., Delaney, B., Mercer, B. and Qi, D. (2011): Technical Report on the Nechalacho Deposit, Thor Lake Project, Northwest Territories, Canada, NI 43-101 Report, *Avalon Rare Metals Inc.*, Toronto, Ontario, 289 pages.

Butrenchuk, S.B. (1987): Phosphate in southeastern British Columbia; *BC Ministry of Energy Mines and Petroleum Resources*; Open File 1987-16, 103 pages.

Butrenchuk, S.B. (1988): Phosphate inventory northeastern British Columbia; in Geological Fieldwork 1987, *BC Ministry of Energy and Mines and Petroleum Resources*, Paper 1988-1, pages 397-410.

Butrenchuk, S. (1996): Phosphate Deposits in British Columbia; BC Ministry of Employment and Investment, *BC Geological Survey*, BCGS-Bulletin 98, 126 pages.

Cordier, D.J. (2011): Phosphates, in: Mineral Commodity Summaries, January 2011, *U.S. Geological Survey*, pages 128-129.

May, W.E. and Rumble, J. Jr. (2003): Certificate of Analysis–Standard Reference Material 2780; *National Institute of Standards and Technology*, Gaithersburg, Maryland, U.S.A.

Murphy, R.V., Maharaj, H., Lachapelle, J. and Yuen, P. K. (2010): Operator of Portable X-ray Fluorescence Analysers Certification Information and Examination Preparation Booklet Version 3–December 2010; *Natural Resources Canada (NRCan)*, Government of Canada, 64 pages.

Nau, R. (2005): What's the bottom line? How to compare models; in Decision 411 Forecasting, class notes, *Duke University*, Durham, North Carolina, U.S.A. Updated, May 16th 2005, accessed Sept.11th, 2011; http://www.duke.edu/~rnau/411home.htm

Norman, G. and Renning, M. (2009a): 2008 Reconnaissance Exploration and Hand Trenching Assessment report on the Wapiti phosphate project Wapiti & W2-W15 Claims, submitted by Pacific Ridge Exploration Ltd. and Lateegra Gold Corp.; *BC Ministry of Energy, Mines and Petroleum Resources*, Assessment Report 30717, 26 pages plus maps and appendices.

Norman, G. and Renning, M. (2009b): 2008 Reconnaissance Exploration and Hand Trenching Assessment report on the Tumbler Ridge phosphate project PH1-PH-122 claims; submitted by Pacific Ridge Exploration Ltd., *BC Ministry of Energy, Mines and Petroleum Resources*, Assessment Report 30719, 40 pages plus maps and appendices.

Pell, J. (1991): Yttrium Enriched Phosphorites in the Fernie Basin, Southeastern British Columbia; in Hora, Z.D., Hamilton, W.N., Grant, K. and Kelly, P.D., eds., Industrial Minerals of Alberta and British Columbia, Canada, Proceedings of the 27th Forum on the Geology of Industrial Minerals, *BC Ministry of Energy Mines and Petroleum Resources*, Open File 1991-23, pages 117-124.

Simandl, G.J. (2009): Fluorspar Market Review and Selected Fluorite Deposits in British Columbia, Canada; *BC Ministry of Energy, Mines and Petroleum Resources*, Geofile 2009-3, poster.

Simandl, G.J. (2010): Geological Constraints on Rare Earth Element Resources and their Availability–A Canadian Perspective; in *Proceedings of the Twenty-First Canadian Conference on Markets for Industrial Minerals, Vancouver, BC*, October 19-20, 2010, Blendon Information Services, 12 pages.

Simandl, G. J., Fajber, R. and Ferri, F. (2011a): Rare Earth Element Concentrations in Phosphate Deposits, Sulphur

Mountain Formation, Northeastern British Columbia, Canada; *BC Ministry of Energy and Mines*; Geofile 2011-09.

Simandl, G.J., Fajber, R. and Grieve, D. (2011b): Rare Earth Element Concentrations in Phosphate Deposits, Fernie Formation, Southeastern British Columbia, Canada; *BC Ministry of Energy and Mines*; Geofile 2011-08.

Simandl, G.J, Paradis, S. and Fajber, R. (2012): Deposit Profile F07: Upwelling-type Phosphate; in Geological Fieldwork 2011, *BC Ministry of Energy and Mines*, in press.

Swanson, D.A., Tayman, J. and Bryan, M.T. (2011): MAPE-R: A rescaled measure of accuracy for cross-sectional forecasts; http://cssd.ucr.edu/Papers/PDFs/MAPE- R%20EMPIRICAL%20V24%20Swanson%20Tayman%20Bryan.pdf; accessed November 2011.

Carbonate-hosted, Nonsulphide Zn (hypogene) Mineral Deposit Profile E18

by S. Paradis[1] and G.J. Simandl[2]

IDENTIFICATION

SYNONYMS

Zinc-oxides, willemite-dominant deposits

COMMODITIES (*BYPRODUCTS*)

Zn, Pb (*Mn, Fe, Cu, V, Cd, Ag*)

EXAMPLES

(British Columbia - *Canada*/*International*): *Structurally-controlled replacement deposits: Abenab West (Namibia), Berg Aukas (Namibia), Kabwe (Zambia), Star Zinc (Zambia),Vazante (Brazil), Ariense (Brazil), Beltana (Australia), Aroona (Australia), Reliance (Australia). Stratiform deposits: Abu Samar (Sudan), Desert View (US), Franklin/Sterling Hill (US).*

GEOLOGICAL CHARACTERISTICS

CAPSULE DESCRIPTION

Zinc oxide minerals, such as willemite, franklinite or zincite, occur as massive to disseminated zones hosted primarily by carbonate rocks. The two subtypes of hypogene carbonate-hosted nonsulphide Zn-Pb deposits are:

1) structurally-controlled replacement deposits in the form of podiform bodies, veins, and irregular pipes consisting mainly of willemite (±sphalerite, ±hematite, ±franklinite and ±zincite) and spatially associated with fractures and fault zones; and
2) stratiform deposits forming lenses of franklinite-willemite-zincite (±gahnite) located in highly metamorphosed terrains.

TECTONIC SETTING(S)

The structurally-controlled replacement deposits are located in intracratonic or continental margin environments in fault-controlled sedimentary basins within orogenic belts.

The stratiform deposits are located in sedimentary or volcano-sedimentary basins within orogenic belts.

DEPOSITIONAL ENVIRONMENT / GEOLOGICAL SETTING

Hostrocks to the structurally-controlled hypogene nonsulphide Zn-Pb deposits are carbonates deposited in platform successions. Shallowing-upward basins or proximity to major unconformities separating a reduced, carbonate-rich succession (below) from an oxidized sequence of terrestrial sedimentary rocks (above) are frequent settings (*e.g.*, Beltana and Vazante deposits; Groves *et al.*, 2003; Monteiro *et al.*, 2006).

In case of stratiform deposits, metamorphic overprint obliterated all textural/structural indicators of depositional environment.

AGE OF MINERALIZATION

Ages of hypogene nonsulphide Zn deposits are poorly constrained between the Proterozoic to Paleozoic time.

HOST / ASSOCIATED ROCK TYPES

Structurally-controlled deposits are commonly hosted by dolostone, limestone, dolomitized limestone, argillaceous carbonate, marble and slate.

Stratiform deposits are typically hosted by metasedimentary rocks, such as calcitic and dolomitic marble, interlayered with metavolcanic and igneous intrusive rocks (Hague *et al.*, 1956; Hitzman *et al.*, 2003).

DEPOSIT FORM

Structurally-controlled deposits are highly irregular, consisting of podiform bodies, veins within fault and shear zones, joint and fissure-fills, and open-space fills in breccia pipe-like karst structures. Individual podiform ore bodies range from a few tens to a few hundreds of metres in the two dimensions parallel with bedding. Perpendicular to bedding, dimensions are usually a few tens of metres.

Stratiform nonsulphide deposits consist of a series of stratabound discontinuous tabular lenses that considerably

[1] *Geological Survey of Canada, Sidney, BC*
[2] *British Columbia Geological Survey, Victoria, BC*

This publication is also available, free of charge, as colour digital files in Adobe Acrobat® PDF format from the BC Ministry of Energy and Mines website at http://www.empr.gov.bc.ca/Mining/Geoscience/PublicationsCatalogue/Fieldwork.

varied in thickness and length from few tens of metres to few hundreds of metres.

TEXTURE / STRUCTURE

Mineralization in the structurally-controlled deposits is heterogeneous, resulting from various depositional mechanisms such as massive replacement of various hematitic and/or zincian dolomite wallrock facies, dissemination, internal sedimentation, fracture and vein fill, and brecciation. The massive ore is commonly granular and fine grained, and appears as finely porous to compact cryptocrystalline masses. The internal sediments consist of fine laminations of zinc oxide minerals in open cavities. Colloform or crustiform bands, rosettes and spherulites of willemite are deposited as vein and vug fill and in the matrix of breccias (Figures 1, 2).

Mineralization in the stratiform tabular lenses consists of massive to disseminated equigranular, subrounded aggregates of Zn-rich minerals (Figures 3, 4, 5). The ores may have gneissic or disseminated textures, and minerals are generally coarse grained (>2-3 mm) and euhedral to subhedral (Hitzman *et al.*, 2003).

ORE MINERALOGY (Principal and *subordinate*)

Structurally-controlled replacement deposits: Willemite, *cerussite, coronadite, covellite, descloizite, franklinite, gahnite, galena, genthelvite, hedyphane, hemimorphite, hetaerolite, hydrozincite, mimetite, native silver, sauconite, scholzite, smithsonite, sphalerite, tarbuttite, vanadinite and zincite.*

Stratiform deposits: Franklinite, willemite, zincite, *adamite, anglesite, arsenopyrite, aurichalcite, azurite, chalcophanite, chalcopyrite, cuprite, gahnite, galena, hemimorphite, hetaerolite, hydrozincite, magnetite, malachite, melangerite, sauconite, smithsonite, sphalerite, tephroite and zincian fayalite (roepperite).*

GANGUE MINERALOGY (Principal and *subordinate*)

Structurally-controlled replacement deposits: Calcite, manganoan calcite, dolomite, ferroan dolomite, *apatite, barite, hematite, magnetite, quartz, siderite, Zn-rich chlorite.* Stratiform deposits: Calcite, manganoan calcite, dolomite, ferroan dolomite, *alleghanyite, apatite, aragonite, barite, fluorite, garnet, goethite, graphite, hematite, leucophoenicite, jacobsite, löllingite, phlogopite, quartz, siderite, sonolite and rhodonite.*

Figure 1. Early dark red willemite covered by white willemite filling open spaces; Beltana mine, Australia. Pencil for scale. Photo used with permission of Data Metallogenica (www.datametallogenica.com).

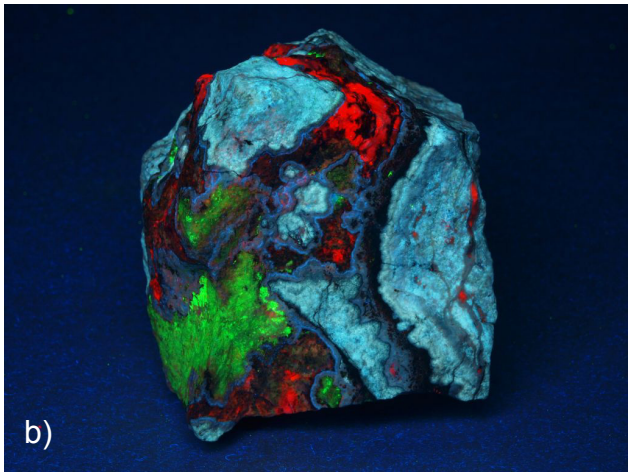

Figure 2. Zn-rich blocky ore from Beltana (Puttapa) consisting mostly of willemite. a) Under daylight conditions. b) Same photo under short wave ultraviolet light. Willemite fluoresces pale blue and shows green phosphorescence. Calcite fluoresces red. Specimen measures 9 by 8 by 8 cm. Photo used with permission of Dr. Earl R. Verbeek, Resident Geologist, Sterling Hill Mining Museum, Ogdensburg, New Jersey, U.S.A.

ALTERATION MINERALOGY

The structurally-controlled replacement deposits display pre to syn-mineralization alteration of the host carbonate rocks that is largely fracture-controlled and extends for about 50 m to 20 km from the major structures. Alteration consists of silicification and formation of a broad halo of net-veined breccia filled by dolomite, ankerite, siderite, hematite, jasper, and chlorite. Post-mineralization alteration locally consists of hematite, Zn-chlorite, and dolomite assemblage, and/or calcite replacing earlier dolomite and zinc minerals. No alteration mineralogy is reported for stratiform deposits.

Figure 3. Typical granular willemite-franklinite-calcite ore from Sterling Hill (U.S.A.). Specimen measures 13 by 9.5 by 6.5 cm. Willemite is brownish red, franklinite and calcite are black and white, respectively. Photo used with permission of Dr. Earl R. Verbeek, Resident Geologist, Sterling Hill Mining Museum, Ogdensburg, New Jersey, U.S.A.

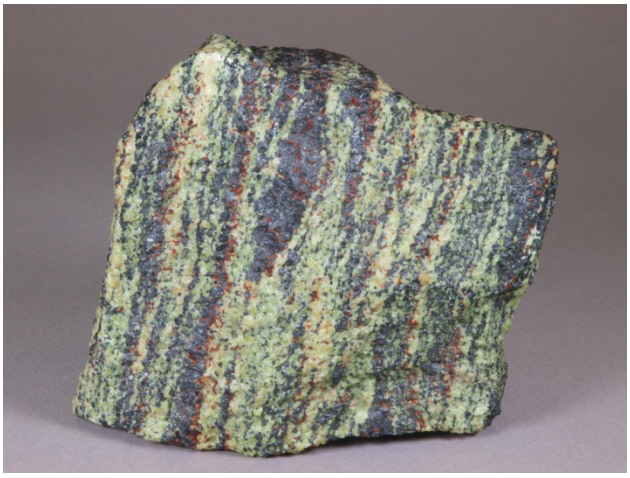

Figure 4. "Classic" granular ore from Franklin deposit (U.S.A.) showing pronounced gneissic foliation with green willemite, black franklinite, and minor red zincite. The colour of much willemite at Franklin is some shade of green; at Sterling Hill, it is usually brown, tan or brownish red. Specimen measures 10 by 10 by 7 cm. Photo used with permission of Dr. Earl R. Verbeek, Resident Geologist, Sterling Hill Mining Museum, Ogdensburg, New Jersey, U.S.A.

In the case of stratiform deposits, any original pre-metamorphic alteration mineralogy was probably destroyed by metamorphic overprint. The exception may be Desert View deposit (United States), which could have a preserved manganese halo (Leavens and Patton, 2008). Sphalerite present in some structurally-controlled replacement and stratiform deposits is replaced by willemite under hydrothermal conditions (*i.e.*, at temperatures higher than 100˚C; Brugger *et al.*, 2003).

WEATHERING

Nonsulphides in both deposit types can be altered by supergene processes to minerals observed in supergene nonsulphide zinc deposits. Supergene mineral assemblages form a near-surface direct-replacement cap

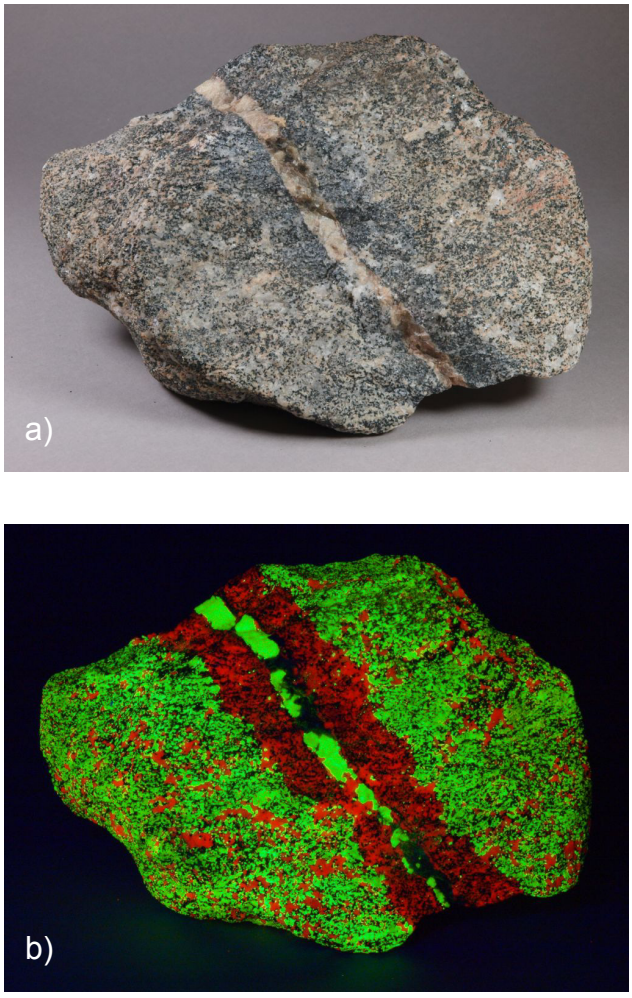

Figure 5. Sterling Hill franklinite-willemite-calcite ore. a) Daylight photograph of granular franklinite-willemite-calcite ore cut by a vein of willemite. The vein is enveloped by diffuse alteration zone. b) Same photograph under short wave ultraviolet light (colour-adjusted). Willemite fluoresces yellowish green and calcite fluoresces red. Specimen measures 17 cm in longest dimension. Photo used with permission of Dr. Earl R. Verbeek, Resident Geologist, Sterling Hill Mining Museum, Ogdensburg, New Jersey, U.S.A.

above many structurally-controlled replacement deposits. For example, an assemblage of hemimorphite, hydrozincite, and minrecordite form a cap above the willemite bodies of the Vazante deposit (Brazil). On the periphery of the Beltana deposit (Australia), hemimorphite and smithsonite formed by weathering of willemite. An assemblage of hemimorphite, cerussite, smithsonite, quartz, descloizite, pyromorphite, goethite, hematite, and iron-aluminum-manganese oxides replaces sulphides and willemite-bearing assemblages within the Kabwe (Zambia) and Berg Aukas (Namibia) deposits (Schneider *et al.*, 2008).

In the case of stratiform deposits, at least some goethite and hematite form by surface alteration of franklinite. Ferric oxide and hydroxide minerals are abundant within the Franklin and Sterling Hill deposits. Furthermore, under these conditions, hemimorphite, cerussite and hydrozincite commonly replace zincite.

ORE CONTROLS

For structurally-controlled deposits, the main controls are favourable sedimentary successions with proper redox states and potential structural zones for fluid ore mixing, *i.e.*, regional basement structural features, such as growth faults, normal and reverse faults, and shear zones.

Favorable sedimentary hosts are important for the localization of stratiform zinc oxides deposits. Faults may also have played a role in the localization of stratiform deposits but metamorphism and deformation have obliterated all evidences.

GENETIC MODEL

Structurally-controlled deposits formed where reduced, moderate to high temperature (100–330°C), Zn-rich, sulphur-poor fluid encountered a cooler, less saline, oxidized, sulphur-poor fluid of seawater, groundwater, or basinal origin (Hitzman *et al.*, 2003). The fundamental difference between the two deposit subtypes may be the site of fluid mixing (Hitzman *et al.*, 2003). The structurally-controlled deposits formed where fluids from a reduced sedimentary succession moved upwards along structures and encountered fluids that originated in oxidizing environment.

There is no consensus regarding the origin of the stratiform nonsulphide zinc deposits (*e.g.*, Franklin and Sterling Hill metamorphosed orebodies) because the nature of the primary mineralization is difficult to decipher. The stratiform deposits may have formed where Zn-rich hydrothermal fluids discharged into an oxidized, sulphur-poor body of water *(i.e.*, exhalative Zn carbonate-silicate oxide accumulations). Such mixing and accumulations of manganiferous sulphides and iron oxides may occur at the sediment/water interface or within sediments immediately beneath such body of water. There is also a possibility that the current ore assemblages may be the post-metamorphic equivalent of hemimorphite and hydrous Mn and Fe-oxides derived from the oxidation of preexisting sulphides. In general, high fO_2/fS_2, oxidizing and alkaline conditions at neutral to basic pH, and elevated temperatures favor stability of willemite relative to sphalerite (Brugger *et al.*, 2003).

ASSOCIATED DEPOSIT TYPES

Carbonate-hosted, nonsulphide Zn-Pb (supergene, B09), Mississippi Valley-type (MVT, E12), and Irish-type (E13) are the most commonly associated deposits. Other potentially associated deposits are stratiform Zn sulphide and Fe (oxide or sulphide), Broken Hill-type (S01), magnetite *(i.e.*, iron oxide deposits), sedimentary manganese (F01), and carbonate-hosted Cu±Pb±Zn (E02) deposits.

COMMENTS

These deposits are unusual in that they produce zinc, occasionally lead, and little else. The chemistry of the fluids responsible for the hypogene structurally-controlled nonsulphide deposits is similar to solutions produced in many continental sedimentary basins. Therefore these deposits could be found in the same districts as MVT, Irish-type and potentially sedimentary exhalative (SEDEX) deposits. British Columbia has prospective strata for these deposits in the miogeoclinal carbonate platform rocks of the Ancestral North America continental margin and in the pericratonic rocks of the Kootenay terrane.

EXPLORATION GUIDES

GEOCHEMICAL SIGNATURE

Colorimetric field test for secondary zinc minerals ("Zinc Zap") and hand-held x-ray fluorescence spectrometry are useful in exploration for nonsulphide Pb-Zn deposits in general (Paradis and Simandl, 2011; Simandl *et al.*, 2011). Positive Zn anomalies in residual soils and stream sediments and elevated concentrations of Pb, Mn, Fe, Cu, V, U, La, Cd, and As are also expected. Analysis of heavy mineral concentrates (identification of Zn-Pb nonsulphides) in stream and overburden may be effective in areas lacking deep weathering. Short wave ultraviolet light may help to detect an increase in the Mn content of calcite in proximity to deposit with these manganoan calcite fluorescing orange-red to red; however, calcite may also appear white, cream, yellow-orange, green or pink. If fluorescence of calcite is due to divalent Mn the colour of fluorescence will be orange-red to red. The other colours mentioned are due to different activators (quite diverse in calcite). Willemite may fluoresce green, yellow-orange or yellow under short wave ultraviolet light. Under long wave ultraviolet radiation, zincite may fluoresce yellow. Primary metamorphic zincite at Franklin and Sterling Hill does not fluoresce. Secondary zincite in veins or disseminated hydrothermal grains fluoresces in some specimens, but such zincite is uncommon and volumetrically insignificant. Willemite, ferroan dolomite, and supergene minerals such as hydrozincite and smithsonite, give distinct spectral responses in the short-wave near infrared portion of the spectrum (Hitzman *et al.*, 2003; McConachy *et al.*, 2009). Hyperspectral imaging holds promise as a useful tool for accurate mapping of structures, lithologies, and alteration.

GEOPHYSICAL SIGNATURE

Deposits may produce a gravity signature. Electrical methods will not be successful due to the absence or small amounts of sulphides. Deposits that contain magnetite and franklinite can produce a magnetic response; a larger response should be observed with stratiform nonsulphide deposits.

OTHER EXPLORATION GUIDES

Knowledge of the basin sedimentary succession with proper redox states and identification of potential zones for fluid mixing within major structures permits to focus

exploration efforts. Discovery of outcropping hypogene Zn-Pb nonsulphide deposits depends on recognition and knowledge of the physical properties of common nonsulphide zinc minerals. The selection of grassroot exploration areas should target sedimentary rock sequences that have known nonsulphide (supergene and hypogene) zinc prospects, stratiform manganese deposits, Mississippi Valley-type deposits or Broken Hill-type deposits.

ECONOMIC FACTORS

TYPICAL GRADE AND TONNAGE

Most of the known deposits (except Vazante with 28.5 Mt at 18.3% Zn, and Franklin with 21.8 Mt at 19.5% Zn) fall in the range of <1 to 10 Mt and grade 5 to 38% Zn and 0 to 11% Pb. They may contain low concentrations of Mn, Fe, Cu, V, Cd, Ag, and Ba.

ECONOMIC LIMITATIONS

Some deposits (*e.g.*, Beltana and Aroona) are amenable to open pit mining operations; however, most hypogene nonsulphide deposits are exploited by underground mining.

IMPORTANCE

Nonsulphide deposits were the main source of zinc prior to the 1930s. Following the development of differential flotation and breakthroughs in smelting technology, the mining industry turned its attention almost entirely to sulphide ores. Today, most zinc is derived from sulphide ore. The nonsulphide deposits provided roughly 7% of the world's zinc production in 2009. Hypogene nonsulphide deposits are relatively rare compared to supergene nonsulphide deposits, and they currently represent less than 2% of the zinc production.

ACKNOWLEDGMENTS

This manuscript benefited from reviews by Maria Boni (Università di Napoli, Italy), Donald Sangster (Geological Consultant, Ottawa) and David Lefebure (currently with Lefebure GeoLogic Ltd., Salt Spring Island, BC, Canada; former chief geologist of the British Columbia Geological Survey, Victoria, Canada). The project started under the umbrella of the Cordilleran Targeted Geoscience Initiative-3 Program of the Geological Survey of Canada, and was done in collaboration with the British Columbia Geological Survey.

SELECTED BIBLIOGRAPHY

Boni, M., Terracciano, R., Balassone, G., Gleeson, S. and Matthews, A. (2011): The carbonate-hosted willemite prospects of the Zambezi metamorphic belt (Zambia); *Mineralium Deposita*, Volume 46, pages 707-729; http://www.springerlink.com/content/c1817l13765j7365/fulltext.pdf.

Brugger, J., McPhail, D.C., Waters, J., Wallace, M. and Lees, T. (2003): Formation of willemite in hydrothermal environments; *Economic Geology*, Volume 98, pages 819-835.

Groves, I., Carman, C.E. and Dunlap, W.J. (2003): Geology of the Beltana willemite deposit, Flinders Ranges, South Australia; *Economic Geology*, Volume 98, pages 797-818.

Hague, J.M., Baum, J.L., Herrmann, L.A. and Pickering, R.J. (1956): Geology and structure of the Franklin-Sterling area, New Jersey; *Bulletin of the Geological Society of America*, Volume 67, pages 436-474.

Heyl, A.V. and Bozion, C.N. (1962): Oxidized zinc deposits of the United States, Part 1, General geology; *United States Geological Survey*, Bulletin 1135-A, 52 pages.

Hitzman, M.W., Reynolds, N.A., Sangster, D.F., Cameron, R.A. and Carman, C.E. (2003): Classification, genesis, and exploration guides for nonsulphide zinc deposits; *Economic Geology*, Volume 98, Number 4, pages 685-714.

Johnson, C.A. (2001): Geochemical constraints on the origin of the Sterling Hill and Franklin zinc deposits, and the Furnace magnetite bed, northwestern New Jersey; *Society of Economic Geologists Guidebook Series*, Volume 35, pages 89-97.

Johnson, C.A. and Skinner, B.J. (2003): Geochemistry of the Furnace magnetite bed, Franklin, New Jersey, and the relationship between stratiform iron oxide ores and stratiform zinc oxide-silicate ores in the New Jersey Highlands; *Economic Geology*, Volume 98, pages 837-854.

Leavens, P.B. and Patton, J.D. (2008): The Desert View Mine. San Bernardino Mountains, California: a possible intermediate between Långban, Sweden and Franklin, New Jersey; *Axis*, Volume 4, Number 1, pages 1-13.

McConachy, T.F., Yang, K., Boni, M. and Evans, N.J. (2009): Spectral reflectance: preliminary data on a new technique with potential for non-sulphide base metal exploration; *Geochemistry: Exploration, Environment, Analysis*, Volume 7, pages 139-151.

Monteiro, L.V.S., Bettencourt, J.S., Spiro, B., Graça, R. and Oliveira, T.F. (1999): The Vazante zinc mine, MG, Brazil: constraints on fluid evolution and willemitic mineralization; *Exploration and Mining Geology*, Volume 8, pages 21-42.

Monteiro, L.V.S., Bettencourt, J.S., Juliani, C. and Oliveira, T.F. (2006): Geology, petrography, and mineral chemistry of the Vazante non-sulphide and Ambrosia and Fagundes sulphide-rich carbonate-hosted Zn-(Pb) deposits, Minas Gerais, Brazil; *Ore Geology Reviews*, Volume 28, pages 201-234.

Paradis, S. and Simandl, G.J. (2011): Carbonate-hosted, Nonsulphide Zn-Pb (supergene) Mineral Deposit Profile B09; in Geological Fieldwork 2010, *BC Ministry of Energy, Mines, and Petroleum Resources*, Paper 2011-1, pages 189-193; http://www.empr.gov.bc. ca/Mining/Geoscience/PublicationsCatalogue/Fieldwork.

Peck, W.H., Volkert, R.A., Mansur, A.T. and Doverspike, B.A. (2009): Stable isotope and petrologic evidence for the origin of regional marble-hosed magnetite deposits and the zinc deposits at Franklin and Sterling Hill, New Jersey Highlands, United States; *Economic Geology*, Volume 104, pages 1037-1054.

Sangster, D.F. (2003): A special issue devoted to nonsulfide zinc deposits: a new look; *Economic Geology*, Volume 98, Number 4, pages 683-684.

Schneider, J., Boni, M., Laukamp, C., Bechstädt, T. and Petzel V. (2008): Willemite (Zn_2SiO_4) as a possible Ribs geochronometer for dating nonsulfide Zn-Pb mineralization: Examples from the Otavi Mountainland (Namibia); *Ore Geology Reviews*, Volume 33, pages 152-167.

Simandl, G.J., Paradis, S., Fajber, R., and Rogers, N. (2011): Hand-held, portable XRF in exploration for carbonate-hosted sulphide and nonsulphide Pb-Zn deposits; Geofile 2011-6, *BC Ministry of Energy, Mines, and Petroleum Resources*; http://www.empr.gov.bc.ca/ Mining/ Geoscience/PublicationsCatalogue/GeoFiles.

Sedimentary Phosphate Deposits
Mineral Deposit Profile F07

by G.J. Simandl[1,2], S. Paradis[2,3] and R. Fajber[1]

IDENTIFICATION

SYNONYMS

Upwelling phosphate deposits, phosphorite or stratiform phosphate deposits

COMMODITIES (*BYPRODUCTS*)

Phosphate ± *F, ± rare earth elements (REE including Y), ± V, ± U, ± gypsum (phosphogypsum)*

EXAMPLES

(British Columbia (MINFILE #) – *Canada/International*): Crow (082GNE025), Cabin Creek (CS) (082GSE055), Bighorn (082GSE060), Ram 1 (082GSE056), Wapiti (093I 008) and Wapiti East (093I 022); *Athabaska Basin (Saskatchewan, Canada)*, *Bone Valley and Hawthorn Formations (Florida, U.S.A.), Phosphoria Formation (Idaho, Montana and Wyoming, U.S.A.); Ganntour deposit (Morocco).*

GEOLOGICAL CHARACTERISTICS

CAPSULE DESCRIPTION

Sedimentary phosphate deposits are stratiform or lens-shaped, measuring from less than 1 metre to tens of metres in thickness. They extend for tens to hundreds of kilometres in their longest dimension. Mineralized zones consist of phosphorites (≥18% P_2O_5) or phosphate rocks (<18% P_2O_5). These rocks are bedded. They may be primary or reworked (secondary). The main ore mineral is microcrystalline francolite, commonly in form of laminae, pellets, oolites, nodules and fragments of bones or shells (Figure 1). This mineral may be also present within the rock matrix.

[1] *British Columbia Geological Survey, Victoria, BC*
[2] *School of Earth and Ocean Sciences, University of Victoria, Victoria, BC*
[3] *Geological Survey of Canada, Sidney, BC*

This publication is also available, free of charge, as colour digital files in Adobe Acrobat® PDF format from the BC Ministry of Energy and Mines website at http://www.empr.gov.bc.ca/Mining/Geoscience/PublicationsCatalogue/Fieldwork.

Figure 1. Typical appearance of phosphate rock containing a fragment of a crinoid (Fernie Formation, southeastern British Columbia).

TECTONIC SETTING(S)

The most favourable tectonic settings for larger deposits are passive continental shelves and adjacent sag basins; some sedimentary phosphate deposits formed at active continental margins, intracontinental basins and even lacustrine environments.

DEPOSITIONAL ENVIRONMENT / GEOLOGICAL SETTING

Deposition usually occurred in areas of warm paleoclimate, mostly between the 40th parallels. The most common depositional environment for sedimentary phosphate deposits is a marine sedimentary basin with a good connection to the open sea (commonly west-facing at the time of phosphate deposition), and upwelling areas with high plankton productivity.

AGE OF MINERALIZATION

Deposits range in age from Proterozoic to Holocene. Phosphate deposits are particularly abundant in Cambrian, Permian, Jurassic, Cretaceous, Eocene and Miocene times (Cook and McElhinny, 1979). In terms of inferred resources (tonnage), the Eocene, Miocene and Permian are the most important time intervals. In British Columbia, the majority of phosphate occurrences are located in rocks of Jurassic and Triassic age.

HOST / ASSOCIATED ROCK TYPES

Hostrocks are phosphorites (≥18% P_2O_5) and phosphate rocks (<18% P_2O_5). Associated rock types are typically sedimentary rocks including marl, black shale, chert, limestone, dolostone, and in some cases lava flows, tuffs and diatomite-bearing rocks. Figure 2 shows conceptual vertical section of the platform perpendicular to the shoreline.

DEPOSIT FORM

Phosphate-bearing rocks are generally stratiform; bed thicknesses range from less than 1 metre to tens of metres and may extend for distances up to several hundreds of kilometres in their longest dimension. The thickest deposits are amalgamated/condensed beds (tabular units) reflecting variations in upwelling intensity and storm frequency through time. Individual phosphorite deposits delimited by drilling may measure from a few hundreds of metres to tens of kilometres in their longest dimension. Phosphorite deposits commonly occur in belts.

TEXTURE / STRUCTURE

Phosphorite deposits commonly contain phosphate pellets and nodules as well as phosphatized shells and bones; ooids (Figure 3), intraformational rip-up breccias, clasts, concretions, phosphatic stromatolite mounds (or their fragments), crossbeds, hardgrounds and burrows. Phosphatic minerals may also form the matrix. Gangue mineralogy and textures in phosphorites are determined partially by the depositional environment at the time of phosphogenesis and partially by the environment that prevailed during reworking and winnowing (natural P_2O_5 upgrading) of the original phosphate rocks and during diagenesis. Phosphorites formed by replacement (during diagenesis) may be paler buff, tan and/or macroscopically featureless.

"Pristine" phosphate accumulations (one cycle of phosphogenesis) are characterized by phosphatised laminae and lenses, coated grains, coprolites, peloids and fossils. Allochthonous phosphate accumulations show sharp and erosive lower boundary, assemblages of phosphatic and non-phosphatic particles and internal grading, accreted grains, minor unconformities, scour marks and bed truncations, and heterogeneous phosphate particles. Condensed phosphates represent an intermediate stage between pristine and allochthonous phosphate deposits (Föllmi, 1996).

ORE MINERALOGY (Principal and *subordinate*)

Francolite (carbonate-rich fluorapatite), s*econdary minerals derived by the weathering of francolite: millisite, Fe-pallite, crandalite, wavellite and other Al-phosphates*. Secondary minerals are not desirable from the metallurgical point of view.

GANGUE MINERALOGY (Principal and *subordinate*)

Dolomite, calcite, quartz, montmorillonite or illite ±*chert*, ±*halite*, ±*gypsum*, ±*iron oxides*, ±*siderite*, ±*pyrite*, ±*carnotite*, ±glauconite,±sphalerite, ±zeolites*.

*Carnotite is a potassium uranium vanadate radioactive mineral with chemical formula: $K_2(UO_2)_2(VO_4)_2 \cdot 3H_2O$. It is commonly considered as a gangue mineral; however, if present in high concentrations it becomes an ore mineral.

ALTERATION MINERALOGY

Dahllite is believed to form during late diagenesis (Trappe, 1998).

WEATHERING

Lateritic alteration of francolite results in the formation of millisite, Fe-pallite, crandalite, wavellite and other aluminum-phosphates. Turquoise may form if copper is present. Weathering decreases concentrations of pyrite and sphalerite and may result in the release of selenium.

ORE CONTROLS

Phosphorites are stratigraphically and spatially linked to paleodepositional environments favourable for phosphogenesis (high bio-productivity and phosphorus flux, stratification within water/unconsolidated sediment column, and a moderate to low supply of allogenic sediment). Phosphorite deposits are spatially related to multiple cycles of regression-transgression. Phosphate facies commonly rest on, or are associated with, erosional surfaces (unconformities) and/or start with phosphatic lag concentrates. Entrapment basins (zones) characterized by a low influx of continent-derived sediments are required for the deposition of phosphorites.

GENETIC MODEL

Seawater averages 0.071 ppm phosphorous (Redfield, 1958) and may contain as much as 0.372 ppm phosphorus (Gulbradsen and Robertson, 1973). Warm surface waters typically contain less than 0.0033 ppm phosphorus (McKelvey, 1973). Phosphate rocks and primary phosphorites form in or laterally adjacent to organic-rich sediments beneath regions where upwelling, nutrient-rich, cold waters interact with a warm sunlit surface seawater layer, creating favourable conditions for intense algal bloom. Algae die, or are eaten by other life forms, then accumulate on the seafloor as fecal pellets and/or organic debris beneath sites of active coastal upwelling. Decomposition of organic debris in an oxygen-deprived environment by bacteria and dissolution of fish bones and scales are linked to precipitation of phosphate minerals (phosphogenesis) near the sediment-water interface. Precipitation of apatite within intergranular spaces during diagenesis and through non-biological chemical processes may also contribute to formation of phosphate rocks.

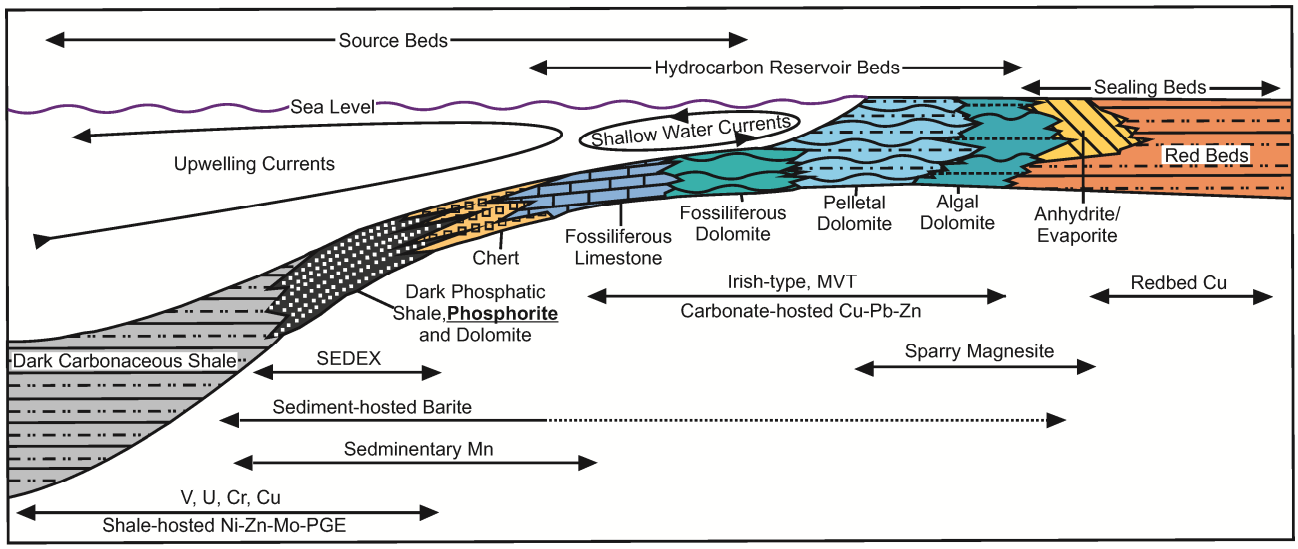

Figure 2. Schematic vertical section across continental platform, showing key lithologies and spatial relationship between phosphorites and other deposit types and hydrocarbons (modified from Sheldon, 1963; Hein *et al.*, 2004).

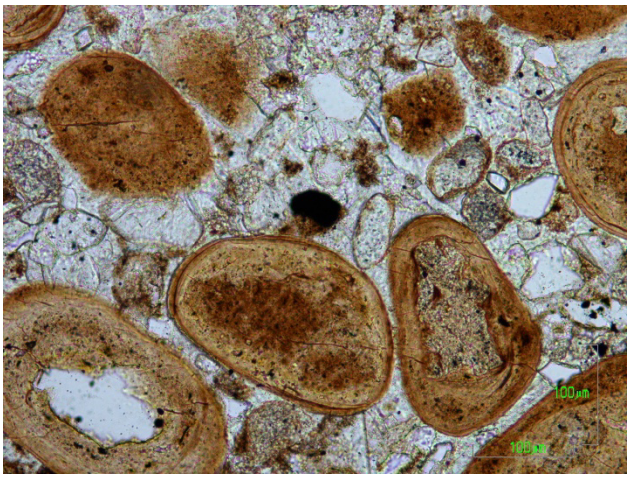

Figure 3. Phosphorite of Sulphur Mountain Formation, northeast British Columbia. Phosphate ooids in carbonate matrix (plane-polarized light; shorter margin of the photograph equals 500 microns). This phosphorite contains 23.6% P_2O_5, 1167.4 ppm of rare earth elements (including 227 ppm La, 122.5 ppm Ce, 45.4 ppm Pr, 186 ppm Nd, 35.7 ppm Sm, 8.75 ppm Eu, 43.5 ppm Gd, 8.4 ppm Ho, 23.7 ppm Er, 3.0 ppm Tm, 15.2 ppm Yb, 2.1 Lu and 399 ppm Y).

Most phosphorites were enriched by the reworking, winnowing (concentration) and accumulation of the above described phosphorus-bearing sediments.

ASSOCIATED DEPOSIT TYPES

Sedimentary manganese deposits (F01), evaporites (gypsum-anhydrite, F02), SEDEX deposits (E14), coal deposits (A03 and A04), hydrocarbon reservoirs, Mississippi Valley-type Pb-Zn deposits (E12), sparry magnesite deposits (E09) and red bed Cu deposits (E04) are spatially associated with the phosphate deposits. See Figure 2.

COMMENTS

The high trace element content of some phosphorites may limit their suitability for agricultural applications. Repetitive fertilizing of agricultural fields over several decades may result in unacceptable concentrations of potentially harmful elements in soils. For example, elevated concentrations of uranium, thorium, lead, cadmium, selenium and chromium in fertilizer are not desirable.

Phosphorite deposits can supply several by-products, such as fluorine (Simandl, 2009). Uranium and vanadium were extracted from phosphate deposits in United States. Phosphate deposits also have the potential to produce yttrium (Pell, 1991) and other rare earth elements as byproducts (Simandl *et al.*, 2011a, b). Synthetic gypsum (phosphogypsum) can also be a byproduct of phosphoric acid production; however, its use is typically limited because it incorporates unwanted trace elements.

EXPLORATION GUIDES

GEOCHEMICAL SIGNATURE

Phosphorous and in some cases rare earth elements, fluorine, and uranium can be used as pathfinders. Since phosphogenesis is commonly associated with organic-rich sediments, nitrogen and carbon may be considered as part of the signature; however, in practice these elements are not part of standard analytical packages used in exploration. Rapid ammonium molybdate – nitric acid field method can be used for field identification of phosphate (Swanson, 1981); however, this method is generally considered as over sensitive. A portable, hand-held XRF is an effective tool in determining the concentrations of phosphorus, light rare earth elements,

yttrium, and a number of other trace elements commonly contained in phosphate rocks (Fajber and Simandl, 2012).

GEOPHYSICAL SIGNATURE

Radiometric surveys could be an effective exploration tool if the deposit contains above background concentrations of radioactive elements.

OTHER EXPLORATION GUIDES

Phosphate deposits are expected to occur mostly in favourable paleolatitudes (between the 40th parallels). Remote sensing (spectral analysis) is also showing some promise. Conceptual vertical section showing spatial distribution of the associated deposit types (Figure 2) may be used as a guide in early stages of exploration.

Phosphatic and glauconitic facies are commonly spatially related (Odin and Letolle, 1980). In those settings, glauconite, characterized by its green colour (easily recognizable by prospector), may be used as an indirect guide to mineralization.

ECONOMIC FACTORS

TYPICAL GRADE AND TONNAGE

According to the United States Geological Survey grade and tonnage model, 90% of the sedimentary phosphate deposits contain more than 26 million tonnes, 50% of them contain 330 million tonnes or more, and less than 10% of these deposits contain more than 4200 million tonnes (Mosier, 1992). According to the same model, 90% of these deposits grade more than 15% P_2O_5, 50% of them grade more than 25% P_2O_5 and less than 10% grade more than 32% P_2O_5 (Mosier, 1992).

Historically only deposits with grades exceeding 25% P_2O_5 were considered of economic interest. As these deposits are being depleted, lower ore grades are becoming acceptable and upgrading has become common practice. For example, in Idaho companies use high-grade ore (or acid grade >31% P_2O_5) directly in fertilizer plants, while medium grade (or furnace grade) rock (24 to 31% P_2O_5) can be used as feed for elemental phosphorus plants. Lower grade rocks (15 to 24% P_2O_5) are also mined but they have to beneficiated to meet the above requirements.

Under favourable conditions (*i.e.* near existing flotation plants, as in Florida), even phosphate rocks grading as low as 3% P_2O_5 may be of economic interest (Zhang *et al.*, 2006). Furthermore, a small proportion of mined phosphate rock is simply ground and sold to growers of organic products as "natural rock phosphate". Such products work reasonably well in acidic soils; however, most of the phosphorus contained in these products is not readily available for plant use in neutral or alkaline soils (pH ≥7).

ECONOMIC LIMITATIONS

Most of the deposits are being mined using open-pit methods or drag lines; however, under exceptional circumstances, high-grade deposits may be mined by underground methods.

Phosphatic rocks may be enriched in REE, V, U, F, Ag, Cd, Cr, Mo, As, Se, Sr, Te, Zn and other elements. Elements such as U, Th and their decay products, Cd, Tl, Se and Hg are closely monitored. If found in excessive concentrations these elements are recovered to mitigate environmental risks linked to fertilizer use or phosphate tailings disposal (Laznicka, 1985; Northolt, 1994; Trappe, 1998).

High concentrations of certain elements other than P can cause problems during processing. High CaO/P_2O_5 ratios result in an increase in sulfuric acid consumption during phosphoric acid production; high concentrations of Mg and SiO_2 cause filtration problems; high concentrations of Na and K results in scaling; organic matter causes foaming during production of phosphoric acid; high Cl concentrations cause premature corrosion. High levels of relatively toxic elements (*e.g.* Cd, Se and As) may make a phosphorite unsuitable for fertilizer production.

IMPORTANCE

World phosphate production for 2011 is estimated at 176 million tonnes. Sedimentary phosphate deposits account for 80% of the world phosphate production. Morocco and the Western Sahara (administered by Morocco) accounted for 50 million tonnes. Other North African countries, China, U.S.A. and Russia are also major producers (Jasinski, 2011). Other sources of phosphorus include apatite concentrate produced from some carbonatite deposits (N01) and peralkaline intrusions (Brazil, Canada, Russia and South Africa), guano deposits (small and only of local importance) and also apatite produced as a by-product of iron extraction from some of iron oxide copper gold (IOCG) deposits (D07).

Phosphorus is an essential element for plant and animal life. There are no substitutes for phosphorus in agricultural applications. Elemental phosphorus is used in production of variety of intermediate products that are consumed in the manufacturing of detergents, matches, fireworks, pesticides, toothpastes and explosives. Phosphorus compounds may also be used as gasoline additives, in some plastics, fire retardants, *etc.*

The recovery of phosphate from waste waters is technically possible; however, the economics of the process remain challenging at current prices of phosphate fertilisers (Parson and Smith, 2008).

ACKNOWLEDGMENTS

The document benefitted from the reviews by David Lefebure currently with Lefebure GeoLogic Ltd., Salt

Spring Island, British Columbia, Canada and former Chief Geologist of the British Columbia Geological Survey.

SELECTED BIBLIOGRAPHY

Butrenchuk, S. (1996): Phosphate deposits in British Columbia; *BC Ministry of Employment and Investment*, British Columbia Geological Survey, Bulletin 98, 126 pages.

Cook, P.J. and McElhinny, M.W,(1979): A re-evaluation of the spatial and temporal distribution of sedimentary phosphate deposits in the light of plate tectonics; *Economic Geology*, Volume 74, pages 315-330.

Fajber, R. and Simandl, G.J. (2012): Portable X-ray fluorescence (XRF) instrument use in evaluation of rare earth element containing sedimentary phosphate deposits; *BC Ministry of Energy and Mines*; Geological Fieldwork 2011 (this volume).

Föllmi, K.B. (1996): The Phosphorus cycle, phosphogenesis and marine phosphate-rich deposits; *Earth Sciences Reviews*, Volume 40, pages 55-124.

Gulbrandsen, R.A. and Roberson, C.E. (1973): Inorganic phosphorus in seawater; in Griffith, E.J., Beeton, A., Spencer, J.M. and Mitchell, D.T. (Eds.), *Environmental Phosphorus Handbook;* John Wiley & Sons, New York, pages 117–140.

Hein, J.R., Perkins, R.B. and McIntyre, B.R. (2004): Evolution of thought concerning the origin of the Phosphoria Formation, Western US phosphate field; in Life cycle of the Phosphoria Formation; Hein, J.R., Editor, Elsevier, Amsterdam, *Handbook of Exploration and Environmental Geochemistry,* pages 19-42.

Jasinski, S.M. (2004): Societal relevance, processing, and material flow of western phosphate – refreshments, fertilizer, and weed killer; in Life cycle of the Phosphoria Formation; Hein, J.R., Editor, Elsevier, Amsterdam, *Handbook of Exploration and Environmental Geochemistry*, Volume 8, pages 599-610.

Jasinski, S.M. (2011): Phosphate rock; Commodity Summaries; *US Geological Survey*, pages 118-119.

Laznicka, P. (1985): Empirical metallogeny; depositional environments, Lithologic Associations and Deposits; Volume 1, *Phanerozoic Environments, Associations and Deposits*; Elsevier, Amsterdam, pages 482-488.

McKelvey, V.E. (1973): Abundance and distribution of phosphorus in the lithosphere; in Griffith, E.J., Beeton, A., Spencer, J.M. and Mitchell, D.T. (Eds.), *Environmental Phosphorus Handbook;* John Wiley & Sons, New York, pages 13–31.

Mosier, D.L. (1992): Descriptive model of upwelling type phosphate deposits; Mineral Deposit Models; in Cox, D.P. and Singer D.A., Mineral Deposit Models, *US Geological Survey*, Bulletin 1693, pages 234-236.

Moyle, P.R. and Piper, D.Z. (2004): Western phosphate field – depositional and economic deposit models; in Life cycle of the Phosphoria Formation; Hein, J.R., Editor, Elsevier, Amsterdam, *Handbook of Exploration and Environmental Geochemistry*, Volume 8, pages 575-598.

Notholt, A.J.G. (1994): Phosphate rocks: factors in economic and technical evaluation; in Whateley, M.K.G. and Harvey, P.K. editors; Mineral Resource Evaluation II; Methods and Case Histories, *Geological Society Special Publication No. 79*, pages 53-65.

Odin, G.S. and Letolle, R. (1980): Glauconitization and phosphatization environments: a tentative comparison, SEPM Special Publication No.29; *The Society of Economic Paleontologists and Mineralogists*, pages 227-237.

Orris, G.J. and Chernoff, C.B. (2004): Review of world sedimentary phosphate deposits and occurrences; in Life cycle of the Phosphoria Formation; Hein, J.R., Editor, Elsevier, Amsterdam; *Handbook of Exploration and Environmental Geochemistry*, Volume 8, pages 550-573.

Parsons, S.A. and Smith, J.A. (2008): Phosphorus removal and recovery from municipal wastewaters; *Elements*, Volume 4, pages 109-112.

Pell, J. (1991): Yttrium-enriched phosphorites in the Fernie Basin, Southeastern British Columbia; in Hora, Z.D., Hamilton, W.N., Grant, K. and Kelly, P.D. eds., Industrial Minerals of Alberta and British Columbia, Canada, Proceedings of the 27th Forum on the Geology of Industrial Minerals, *BC Ministry of Energy, Mines and Petroleum Resources*, Open File 1991-23, pages 117-124.

Poulton, T.P. and Aitken, J.D. (1989): The Lower Jurassic phosphorites of southeastern British Columbia and terrane accretion to western North America; *Canadian Journal of Earth Sciences*, Volume 26, issue 8, pages 1612-1616.

Prévôt, L. (1990): Geochemistry, Petrography, genesis of Cretaceous-Eocene phosphorites - TheGanntour Deposit (Morocco): a type example; Mémoires de la Société Géologique de France, *Société Géologique de France, Paris*, Mémoire 158, 232 pages.

Redfield, A.C. (1958): The biological control on the chemical factors in the environment; *American Journal of Science*; Volume 46, pages 205-221.

Rogers, M.C. (1995): Phosphorite; in Rogers, M.C., Thurston, P.C., Fyon, J.A., Kelly, R.I. and Breaks, F.W.(comps.), Descriptive Mineral Deposit Models of Metallic and Industrial Deposit Types and Related Mineral Potential Assessment Criteria, *Ontario Geological Survey*, Open File Report 5916, pages 155-158.

Simandl, G.J. (2009): World fluorspar resources, market and deposit examples from British Columbia, Canada; *BC Geological Survey*, Information Circular 2009-4, 16 pages.

Simandl, G.J., Fajber, R. and Grieve, D. (2011): Rare Earth concentrations in phosphate deposits, Fernie Formation, South-Eastern British Columbia, Canada; *BC Ministry of Energy and Mines*; Geofile 2011-08.

Simandl, G.J., Fajber, R. and Ferri, F. (2011): Rare earth concentrations in phosphate deposits, Sulphur Mountain Formation, Northeastern British Columbia, Canada; *BC Ministry of Energy and Mines*; Geofile 2011-09.

Sheldon, R.P. (1963): Physical stratigraphy and mineral resources of Permian rocks in western Wyoming; *US Geological Survey*, Professional Paper, 313-B, 273 pages.

Slansky, M. (1980): Géologie des phosphates sedimentaires; *Mémoire B.R.G.M. 114*; 92 pages.

Swanson, R.G. (1981): Sample examination manual; *American Association of Petroleum Geologists*, Methods in Exploration Series; No. 1, 117 pages.

Trappe, J. (1998): Phanerozoic phosphorite depositional systems–A Dynamic Model for a Sedimentary Resource System; *Spinger Verlag*, Berlin-Heidelberg, Germany, 256 pages.

Zhang, P., Weigel, R. and El-Shall, H. (2006): Phosphate Rock; in Industrial Minerals & Rocks; Commodities, Markets, and Uses, Kogel, J.E., Trivedi, N.C., Barker, J.M. and Krukowski, S.T., eds., *Society for Mining, Metallurgy, and Exploration, Inc. (SME)*, Littleton, Colorado, U.S.A.; pages 703-722.